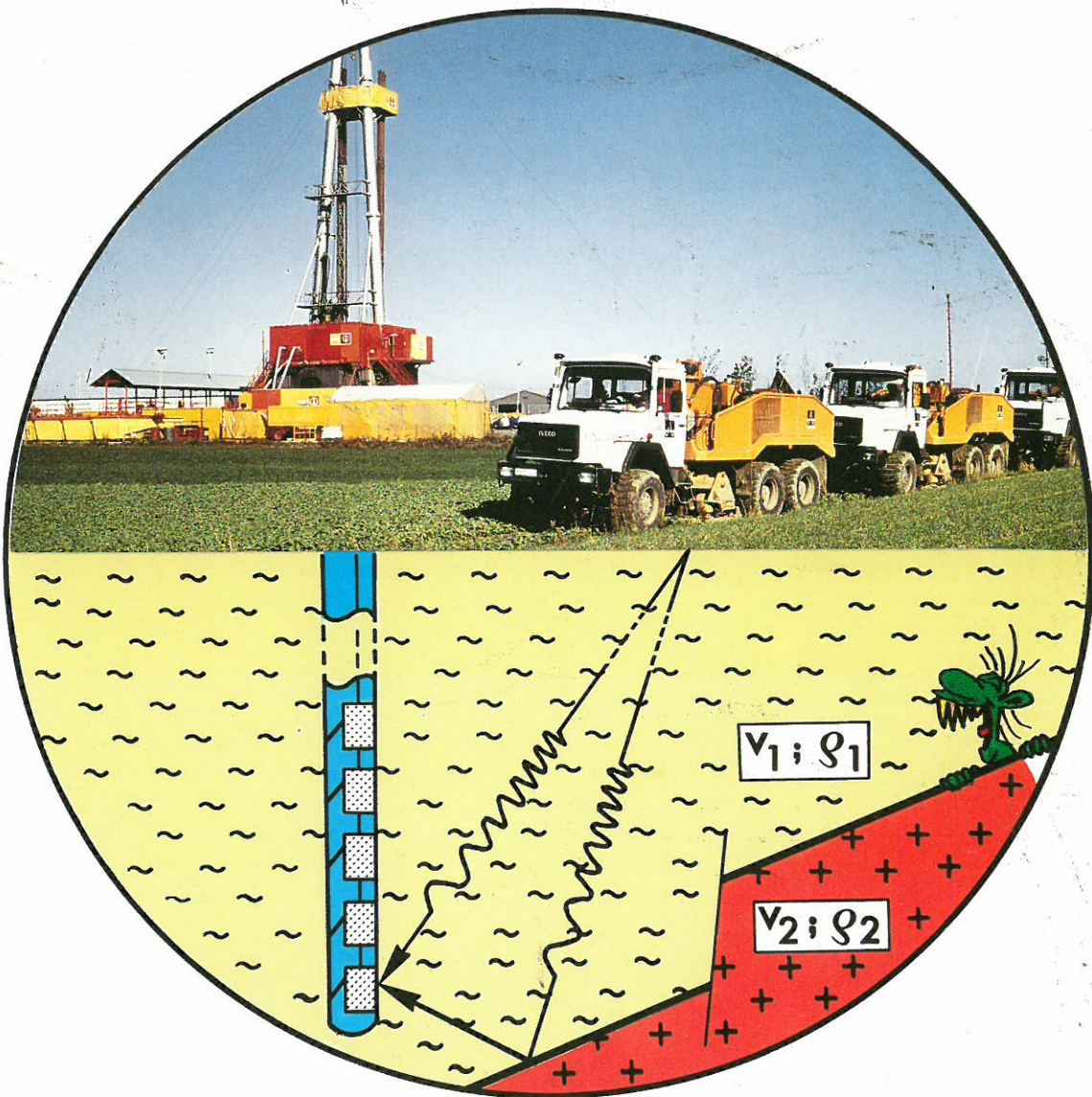


# KTB REPORT 92-5

# DEKORP REPORT

Integrated Seismics Oberpfalz 1989

Data evaluation and interpretation as of October 1992



Edited by  
Projektleitung Deutsches Kontinentales Reflexionsseismisches Programm  
and  
Projektleitung Kontinentales Tiefbohrprogramm der Bundesrepublik Deutschland  
im Niedersächsischen Landesamt für Bodenforschung

H.-J. Dürbaum, Ch. Reichert, P. Sadowiak, K. Bram

Editors: Dr. H.-J. Dürbaum, Dr. Ch. Reichert,  
Dr. P. Sadowiak, Dr. K. Bram

Printed by: Wittmann & Wäsch, D-3007 Gehrden

Distribution: E. Schweitzerbart'sche Verlagsbuchhandlung

Orders: E. Schweitzerbart'sche Verlagsbuchhandlung  
Johannesstr. 3A  
D-7000 Stuttgart

Front cover: Vibrator trucks in operation close to the KTB pilot hole. The emitted compressional and shear wave energy is detected by a chain of borehole geophones. Partly the seismic energy travels directly to the receivers, partly it is reflected from geological structures in the surroundings.

All projects reported hereafter are entirely funded by the Bundesministerium für Forschung und Technologie. The Editors cannot be held responsible for the opinions given and statements made in the articles published, the responsibility resting with the authors.

© Niedersächsisches Landesamt für Bodenforschung  
Hannover 1992

Reprinting, copying and translations, broadcasting, reproduction by photomechanical or in other ways as well as storage in databases - even in parts - are subject to prior permission.

All rights are reserved.

Editors' address: Niedersächsisches Landesamt für Bodenforschung, POB 51 01 53, D-3000 Hannover 51  
Phone: 0511/643-2675

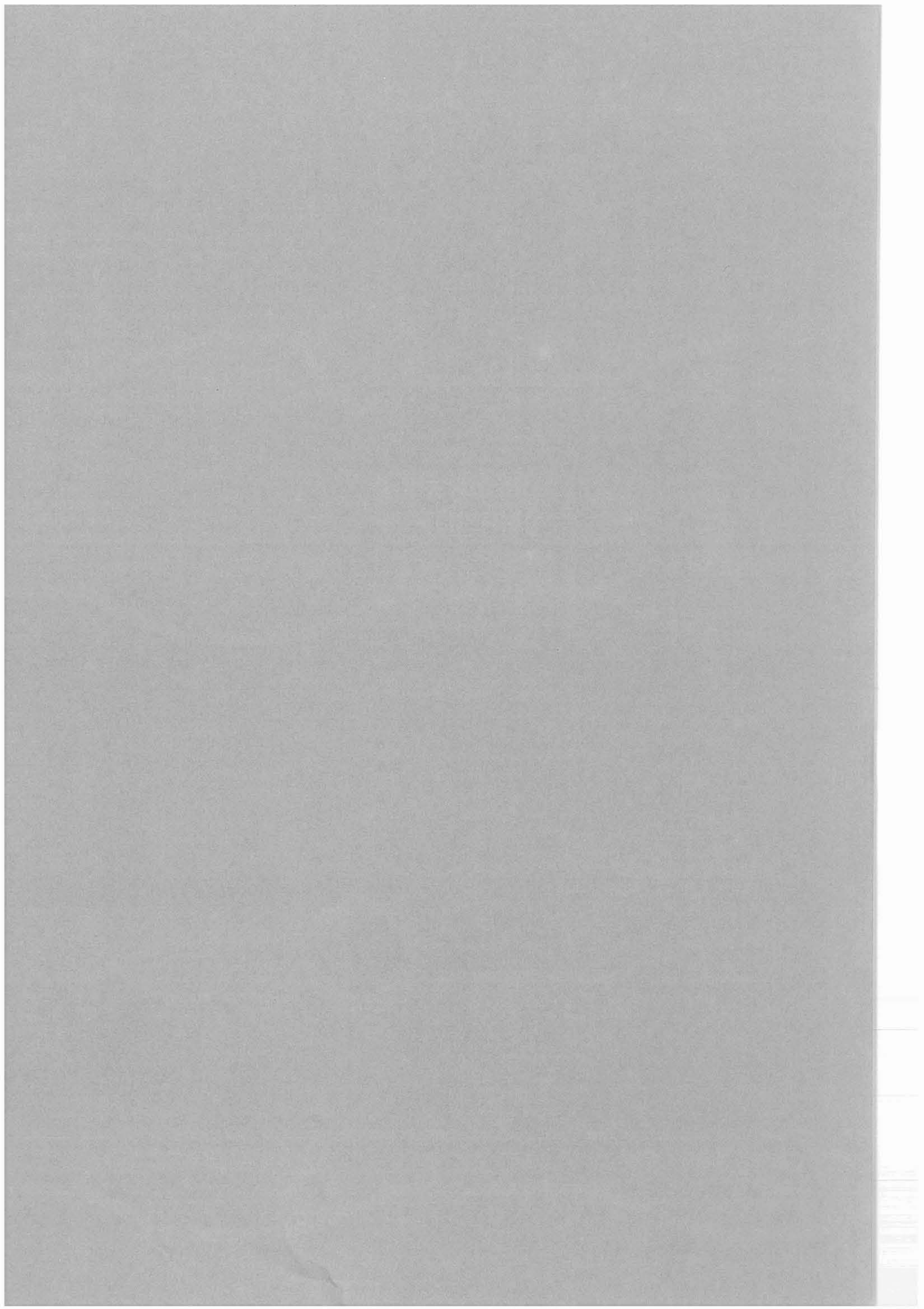
ISSN 0939-8732  
ISBN 3-928559-08-7

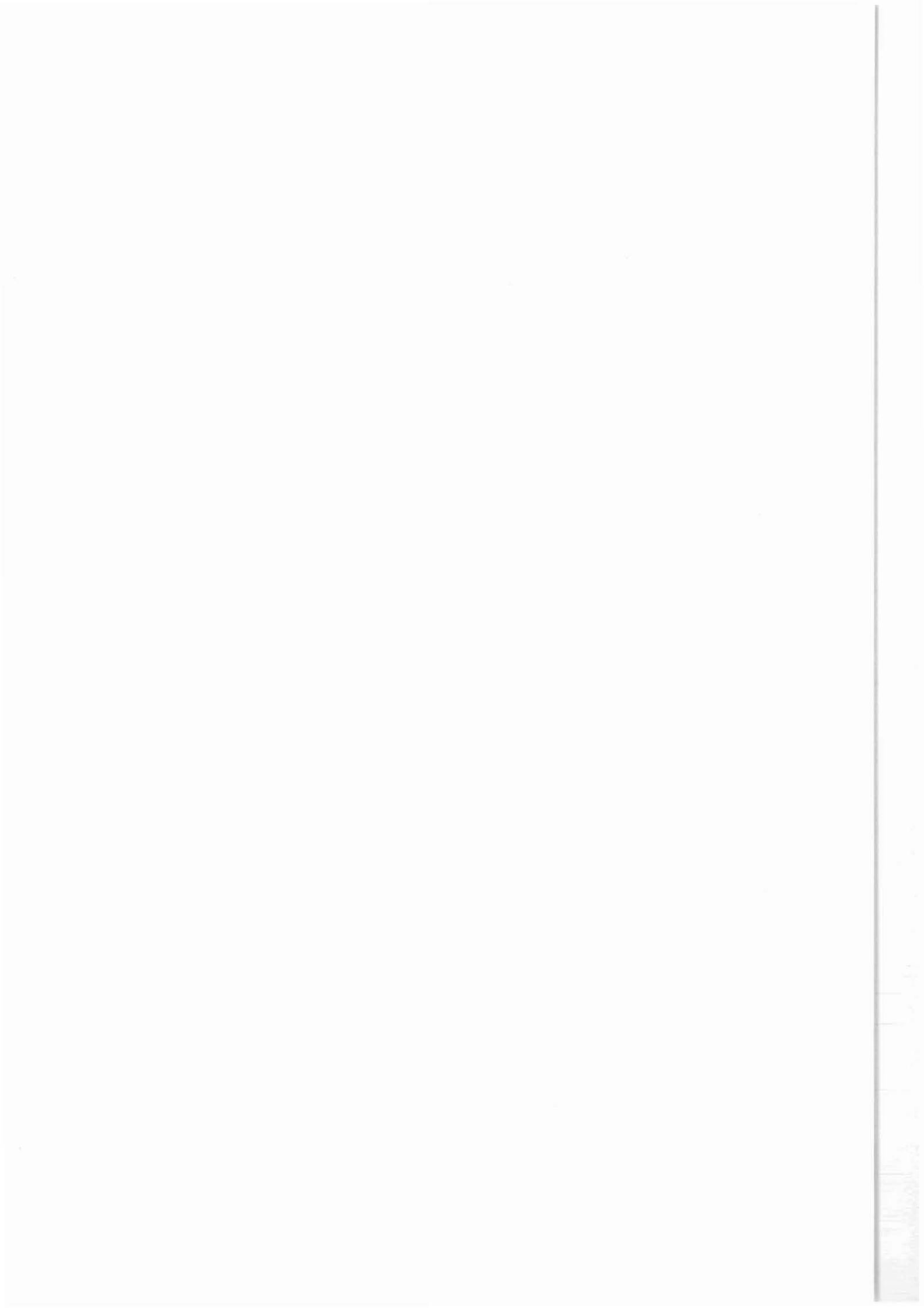
CONTENTS

	Page
Dürbaum, H.-J.: Introduction . . . . .	1
Stiller, M.: Preliminary Generation of a Stacked Data Volume of the Entire ISO'89-3D Data Set Using an Envelope Technique . .	3
Hluchy, P., Körbe, M., Thomas, R.: Preliminary Interpretation of the 3D-Seismic Survey at the KTB Location . . . . .	31
Stiller, M., Tormann, M.: Application of a Simplified Horizon Migration Process to the Data of the 3D-Seismics ISO'89 . . . . .	53
Wiederhold, H.: Interpretation of Envelope-Stacked 3D Seismic Data and its Migration - Another Approach . . . . .	67
Körbe, M., Reichert, C.: On the Character of "Steep Event SE-1" - Reflected Energy, Reflected Refraction, Diffraction or Any Artifact? . . .	115
Janik, M., Harjes, H.-P.: Structural Interpretation of the MSP - Experiment . . . . .	133
DEKORP Research Group: Depth Determination of Prominent Seismic Structures beneath the KTB Main Drillhole KTB-HB . . . . .	149
Simon, M.: Structural Images from 3D-Isochron Migration of Wide- Angle Data in the Surroundings of KTB . . . . .	161
Söllner, W., Lüschen, E., Li, X.-P., Hubral, P., Gut, T.W., Widmaier, M.: VSP - A Link between Reflection Seismic Profiling and Lithology . . . . .	169

	Page
Rühl, T., Hanitzsch, C.: Average and Interval Velocities Derived from First Breaks of Vertical Seismic Profiles at the KTB Pilot Hole . . . . .	201
Bönnemann, C., Buttkus, B.: Results of the 3-D Expanding Spread Experiment . . . . .	221
Martini, N., Stiller, M.: Results of the ISO'89 Experiment "Durchschallung": Recording of the Vibrator Sweeps of the 3D-Seismics in the KTB Borehole . . . . .	233
Lüschen, E., Werner, U.: Fluid/Gas Indications in 8 km Depth beneath the KTB and Rock Anisotropy From Shear-Wave Reflection Surveys . . . . .	247
Rabbel, W.: Seismic Anisotropy at the KTB Deep Drilling Site . . . . .	275
Gut, T.W., Söllner, W., Lueschen, E., Edelmann, H.A.K.: More Reliable Shear-Wave Data from VSP by Using CIPHER-Technique . . . . .	291
Bopp, M.: Shear-Wave Splitting Observed by Wide-Angle Measurement . . . . .	297
Hanitzsch, C., Rühl, T., Heinemann, B.B.: Detection of Permeable Fracture Zones by Tube Waves in the KTB Pilot Hole . . . . .	309
Hanitzsch, C., Hubral, P., Rühl, T., Söllner, W.: Migration of Steeply Dipping Reflectors at the KTB Site: Depth Errors Caused by Inaccurate Velocity Models . . . . .	333
Stettner, G.: Zur Korrelation des tektonischen Baues mit den seis- mischen Strukturen im Raum KTB-Oberpfalz - Münchberger Gneismasse . . . . .	343
Hirschmann, G.: On the Geological Interpretation of the 3D-Seismic Data with Special Regard to the Information from the KTB Boreholes . . . . .	351

Annex





## Introduction

Hans-Jürgen Dürbaum

From July until November 1989 the so-called Integrated Seismic Experiment Oberpfalz (ISO89) had been carried out in the area around the KTB-well in a cooperative effort by the contractor PRAKLA-SEISMOS and a large number of university institutes for geophysics under the DEKORP project management. The major part consisted of a 3D reflection seismic survey in a square area of 19 x 19 km with the KTB at its center.

The signals of the 3D survey were recorded in the depth range of 3220 to 3420 m in the KTB-pilot hole (experiment "Durchschallung") and by an additional reflection recording equipment for the experiment "3D-expanding spread". Further wide-angle reflection experiments were carried out in order to extend the area of information on the highly reflective Erbendorf structure. VSPs with various offsets were carried out between 710 and 3660 m and two orthogonal moving source profiles (MSP) with geophones between 3310 and 3690 m. Two orthogonal common midpoint profiles were recorded with shear waves (SCMP experiment), and p- and s-waves were recorded in the well from various azimuths and distances (experiment MASE).

The technical details of the experiments and first results have been published in the first joint KTB/DEKORP report 90-6b in 1990. This second report of this kind gives the results derived from the ISO89-data so far. Still the results are preliminary to a certain extent. This mainly concerns the work on the 3D-reflection seismic data. The reasons for the

---

Author's address: DEKORP Project Management, Nieders. Landesamt für Bodenforschung, Stilleweg 2, D-W 3000 Hannover 51

difficulties are the complicated 3-dimensional velocity structure including the anisotropy of the rocks and the steep dip of many reflecting elements. New ways had to be found to stack and migrate the data set. A "true-phase" stacking, therefore, is only now under way, and it is anticipated that the migration of the stacked data set may run into difficulties due to the steepness of dip of some structures.

In this report the results of a procedure of "envelope-stacking" are presented from which the reflecting elements were picked and then migrated. Moreover so far we have only a very approximate idea about the velocity distribution as a function of space coordinates and direction because the seismic data does not allow mapping the subvertical boundaries between granites, gneisses and amphibolites. Finally, we are still in the process of learning what the major causes of the reflection of the seismic energy are: boundaries between lithological or tectonic units? It seems to be that the tectonic structures are of the greatest importance, but we have to learn about the corresponding changes of the physical properties to understand the observations.



Preliminary generation of a stacked data volume of the entire  
ISO'89-3D data set using an envelope technique

Manfred Stiller<sup>1</sup>

Abstract

The first attempts of azimuth-dependent normal moveout correction and subsequent phase-consistent stacking resulted in unsatisfying quality in the crystalline part of the ISO'89-3D survey area - especially for the extremely dipping elements in the first few km. One decisive observation is the different reflectivity (i. e. traveltimes and amplitude of events) for different azimuth ranges, so that no constructive, phase-consistent 3D-stack with all traces of each bin was attainable. Thus, another stacking method using not the seismic traces themselves but their envelopes was worked out to produce the first stack of the entire 3D data cube. This technique reacts more tolerantly towards inaccurate travel-time corrections, but of course it cannot yield the high resolution of phase-consistently stacked data. The procedure for the envelope stacking method is described in detail and many of the resulting sections are depicted in different slice directions.

A variety of recognizable horizons within the envelope-stacked data set was evaluated with an interactive 3D-seismic interpretation system. The dip information contained in the resulting traveltimes maps was used to perform horizon migrations and to control directly the azimuth-dependency of the stacking velocity for a new and improved phase-consistent stack. Therefore, the close connection of processing and interpretation is of high advantage. Another efficient process, developed at the DEKORP Processing Center in Clausthal, is also presented - a true spatially operating coherency enhancement method leading to a clearly increased perceptibility of all events correlating within larger areas. As a by-product additional coherency-dependent dominant dip values are attained in a very high spatial density. They can be used again for a control of the azimuth-dependency of the dynamic corrections for the final, phase-consistent and migratable 3D-stack of the ISO'89-3D data volume.

---

<sup>1</sup> Author's address: DEKORP Processing Center, Inst.f.Geophys.d.  
TU CLZ, Arnold-Sommerfeld-Str.1, 3392 Clausthal-Zfd., Germany

### Problems of conventional 3D-processing in crystalline setting

The location and the topography of the survey area are shown in figures 1a and b. Due to geological and hardware-technical aspects it was necessary to divide the 20 km \* 20 km survey plane into four subareas A, B, C, and D. The processing is completely performed at the DEKORP Processing Center (DPC) at Clausthal. A detailed description of the acquisition geometry of the ISO'89-3D reflection seismics has already been given by Rehling and Stiller (1990). The aims and the recording configuration resulting from this have been discussed as well as the problems and solutions with its transposition into the field. In addition, all survey parameters, the subsurface coverage-, offset-, and azimuth distributions have been summarized. That publication ended with the description of the extensive and careful checking of geometry- and seismic data (quality control, conformity between geometry-, static- and trace-data bases). A detailed flow chart was given as an overview of the processing- and interpretation sequence planned at that stage.

The probably most important procedure to obtain a phase-consistent, high-resolution 3D-stack is the determination of appropriate normal moveout (NMO) correction velocities specified in detail in time and space. On the one hand, the stacking velocities depend on the respective location in the area, on the respective horizon depth, on the actual subsurface velocity and on the respective source-receiver distance (offset). But on the other hand, they depend predominantly on the apparent reflector dip and dip direction, measured against the direction of the respective source-receiver configuration.

In 2D-seismics with linear geophone arrangement the source-receiver-azimuths generally do not vary (or only for the near-offset traces in the case of lateral source offsets, which commonly neglected). In 3D-seismics, however, a well-balanced offset- and azimuth distribution of the source-receiver combinations is intended to collect reflection information from different directions and distances for each bin. This is a prerequisite to investigate the true, spatial position (amount and direction of dip) of all reflecting elements with certainty. Thus, for dipping layers the stacking velocities must be determined and applied strictly with respect to their azimuth-dependency. A more detailed representation of the theoretical background is given by Stiller (1991).

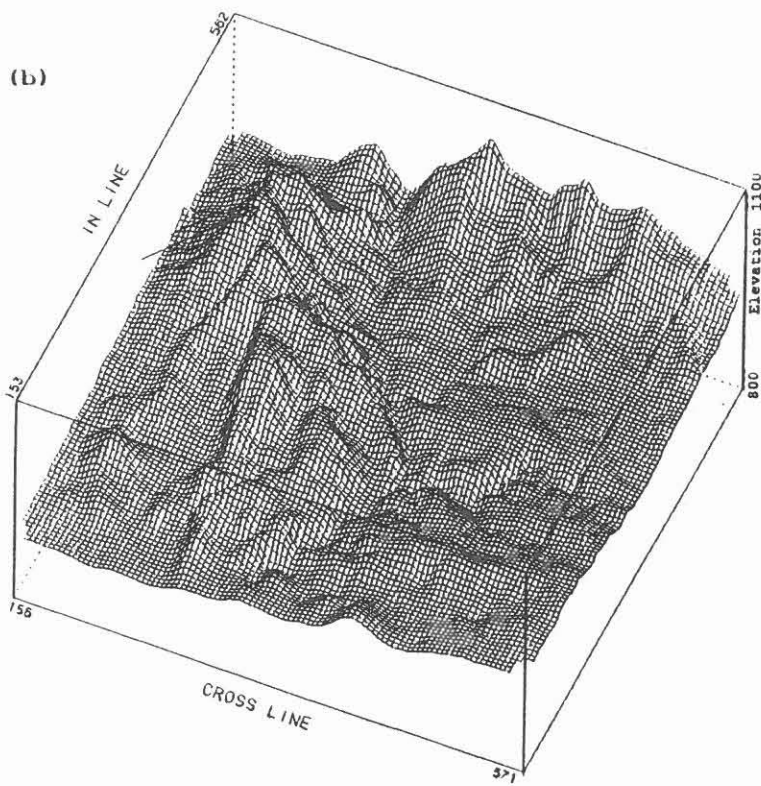
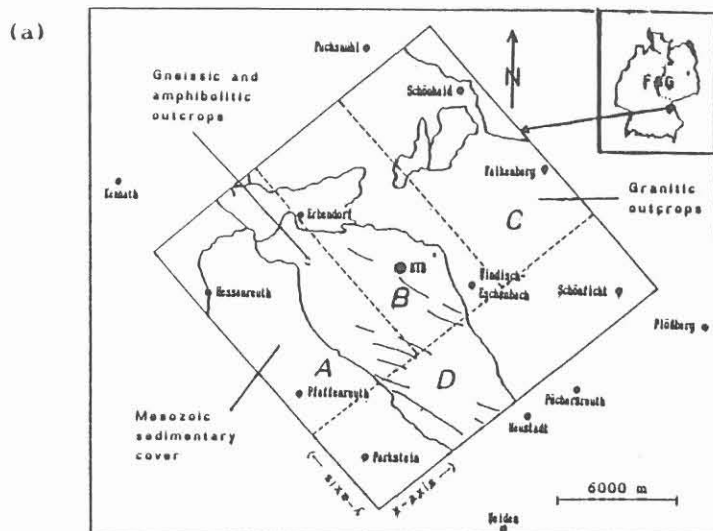


Fig. 1: (a) Location map of the survey area (partitioned into subareas A, B, C, and D for processing purposes).  
(b) Topography of the survey area (elevations between 400 and 800 m).

Actually, all attempts of azimuth-dependent velocity analyses with subsequent, conventional azimuth-dependent phase-consistent 3D-stack, as well as azimuth-restricted test stacks, yielded only unsatisfying results so far. This occurred most strongly in the crystalline part of the study with its extremely inclined reflectors. It was an unexpected observation, because the conventional 3D-processing method described above is well-suited for exploration tasks in sedimentary areas even in the presence of dipping layers. At first sight, azimuth-restricted stacks with balanced and optimized selection of correction parameters have led to satisfactory results in the beginning of the ISO'89-3D processing. Actually, however, the reflectivity (time position and strength of events) for different azimuth ranges appears sufficiently different, so that no constructive, phase-consistent 3D-stack using all traces of each bin is attainable.

Especially, when performing azimuth-restricted stacks (to overcome the problem of azimuth-dependent variation of the NMO-velocities), the subsurface coverage is severely reduced. This implies an insufficient improvement of the signal/noise (S/N) ratio, so that several adjacent vertical slices had to be summed up perpendicularly to the respective slice direction. This process of horizontal mixing, however, works as a wavelength filter which perfectly suppresses those reflections dipping steeply in summation direction, so that a continuous, spatial and reliable interpretation is no longer guaranteed. Figures 2 and 3 illustrate the variation of information content in azimuth-restricted stacks by the opposition of two inline- and two crossline sections, showing the same CDPs respectively, however for two different 45°-azimuth ranges. Figure 4 shows the improvement of S/N-ratio by horizontal mixing perpendicularly to the slice direction followed by 2D coherency filtering in slice direction.

Some possible reasons for the observed phenomena preventing a conventional phase-consistent stack can be summarized as follows:

- poorness and discontinuity of reflections in crystalline setting unlike to those in sediments,
- very steep reflector dips in the first few km of the crust,
- probably considerable and irregular anisotropy of the subsurface,
- usage of vibroseis-method with a vertical stacking rate of only 5- to 8-fold,
- just 15-fold subsurface coverage (with 45°-azimuth-restriction even only 4-fold).

SW - NE INLINE SECTION / 350 m NW TO KTB - HOLE

4 - FOLD STACK / 7 - FOLD YBIN MIX / COFILT

ONLY SOURCE - RECEIVER AZIMUTHS  $\pm 22.5^\circ$  TO  
SHOTPOINT LINE DIRECTION

ONLY SOURCE - RECEIVER AZIMUTHS  $\pm 22.5^\circ$  TO  
GEOPHONE LINE DIRECTION

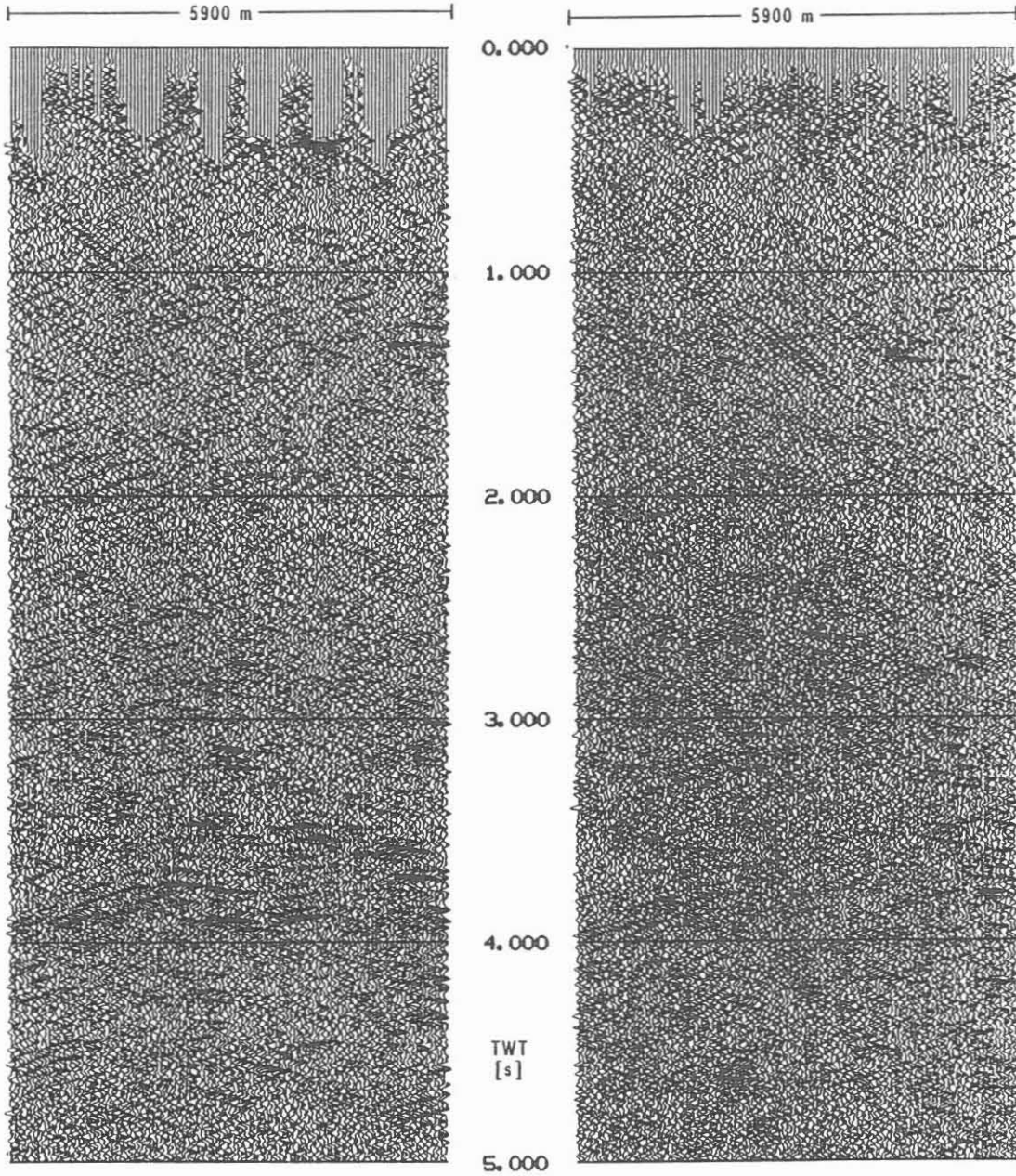


Fig. 2: Azimuth-restricted stacks (inline sections, subarea B): comparison of different azimuth ranges used for stacking the same CDP line.

NW - SE CROSSLINE SECTION / 600 m NE TO KTB - HOLE

4 - FOLD STACK / 7 - FOLD XBIN MIX / COFILT

ONLY SOURCE - RECEIVER AZIMUTH  $\pm 22.5^\circ$  TO  
SHOTPOINT LINE DIRECTION

ONLY SOURCE - RECEIVER AZIMUTHS  $\pm 22.5^\circ$  TO  
GEOPHONE LINE DIRECTION

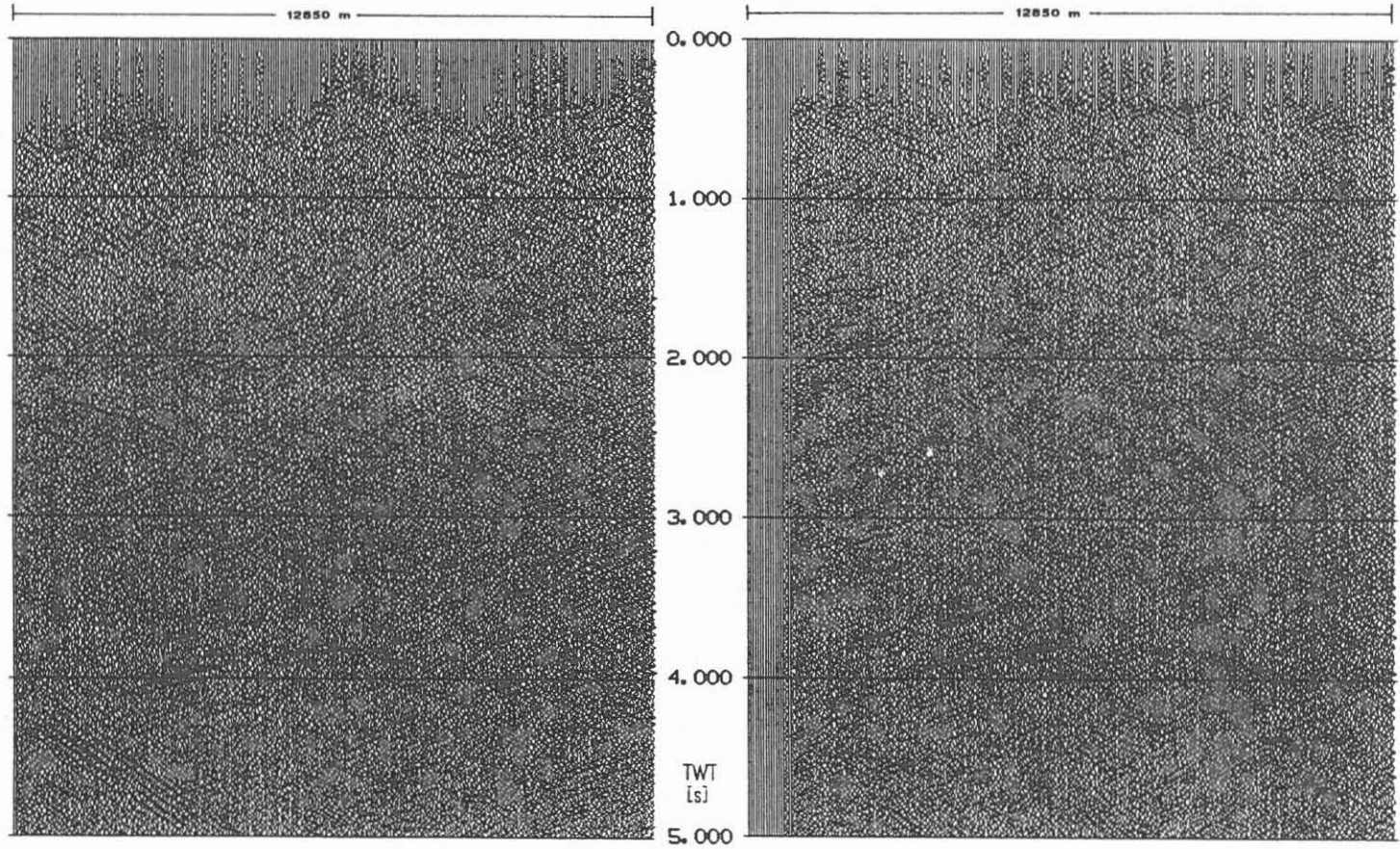


Fig. 3: Azimuth-restricted stacks (crossline sections, subarea B): comparison of different azimuth ranges used for stacking the same CDP line.

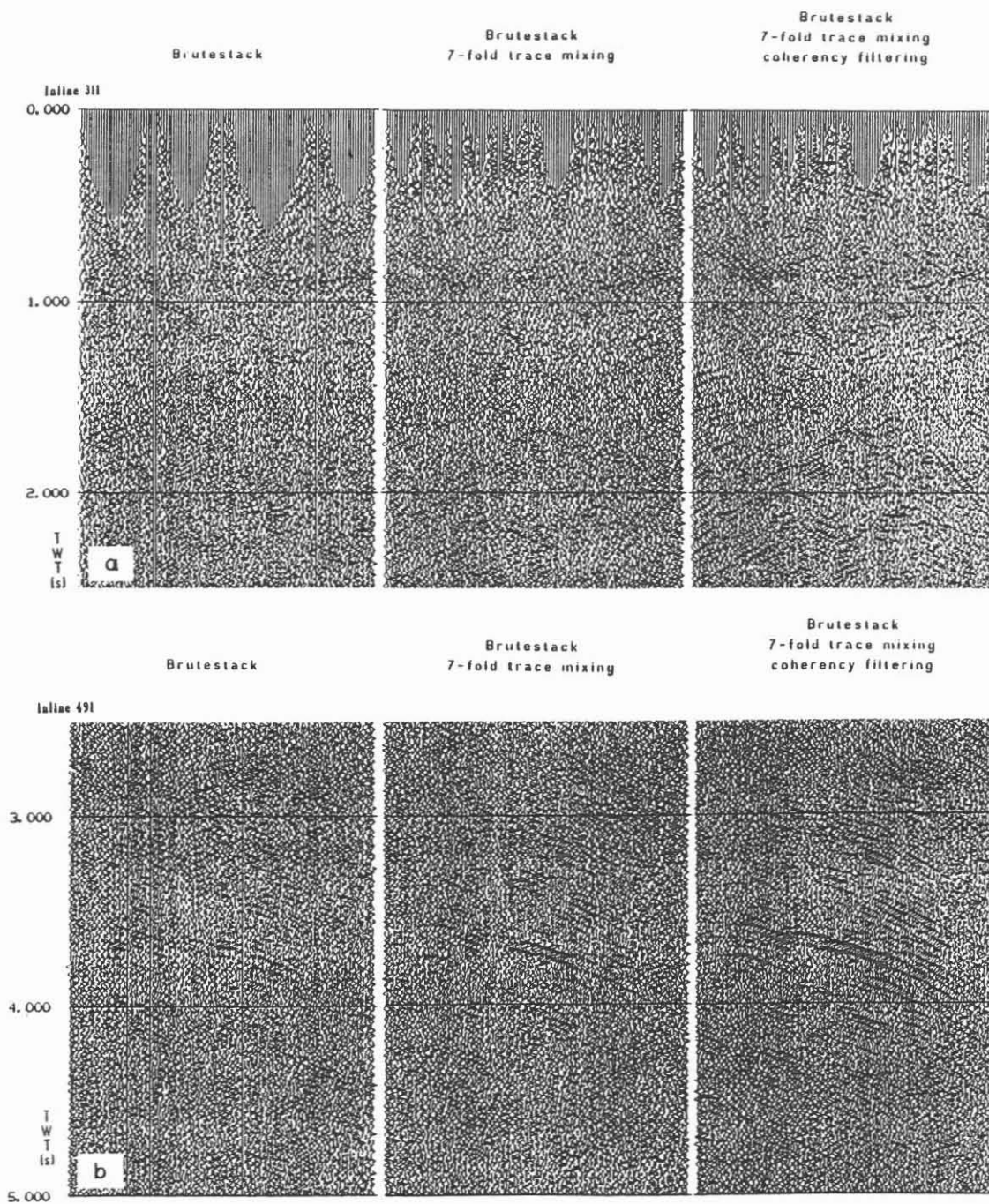


Fig. 4: Improvement of signal/noise-ratio by horizontal mixing and 2D coherency filtering. (a): for steep events, (b): for 'Erbendorf' events.

This situation suggests the testing and development of alternative processing concepts like application of automatic residual-dynamic corrections, modification of the NMO to allow for consideration of anisotropy, 3D-DMO stacking, diffraction stacking theory, prestack migration etc. For sure, this would be an extremely lengthy attempt with certainly arising new problems.

#### **A fast approach to stacking laterally inhomogeneous 3D-data**

In order to obtain relatively fast and with reasonable efforts a nevertheless (at least simplified) spatial image of the main subsurface structures, an envelope stacking technique was developed at the DPC Clausthal and successfully applied. By this method, simply spoken, the envelopes of the absolute amplitudes of all traces of a bin are azimuth-independently summed up to form a stacked trace. The summation of those (only positive) envelope values, as well as the lowpass-effect of the envelope generation process, prevent destructive stacking rather efficiently. Subsequently, the result is squared to enhance the dynamics and to obtain an 'energy section'. Table 1 shows the processing sequence used for envelope stacking at the DPC.

The envelope stacking technique reacts much more insensibly against errors in the stacking velocities which can be determined only roughly and azimuth-independently due to the not yet exactly known spatial position of the subsurface structures. But the use of the envelopes instead of the data itself implies the loss of any phase-consistence and diminishes considerably the time resolution. These disadvantages are clearly compensated, however, by the increased S/N-ratio, yielded by the stacking of all traces within each bin. Thus, the horizontal trace-mixing of adjacent slices can be avoided preserving all dips equivalently. In other words, the reflection information concerning the spatial position of horizons is almost completely maintained enabling a spatially continuous interpretation for the first time.

In contrast to 3D exploration seismics, where the study region usually is rather known by previous 2D-surveys and drillholes, the crystalline subsurface around the KTB is nearly unknown. Thus, it is quite advisable to detect and map large-scaled structures in a first, coarse step (e. g. by an envelope stack), and then exactly evaluate single phases of defined horizons in a second step (by a final phase-consistent stack).



TABLE 1  
PROCESSING SEQUENCE OF ISO 89 / KTB 3D - ENVELOPE STACKS

EDITING AND SORTING INTO COMMON DEPTH POINT ORDER

ANALYTICAL SCALING FOR AMPLITUDE DECAY COMPENSATION  
FULL STATIC CORRECTIONS  
MUTING OF FIRST ARRIVALS AND WIDE ANGLE EVENTS  
RANDOM WINDOW SCALING  
BAND PASS FILTERING TO ELIMINATE UNUSEFUL FREQUENCIES  
AGC SCALING

ROUGH DYNAMIC CORRECTIONS  
BUILDING OF THE TRACE ENVELOPES  
STACKING (FULL 15-FOLD COVERAGE)

HORIZONTAL EQUALIZATION  
SPATIAL MIXING (EACH TRACE WITH ALL 8 DIRECT NEIGHBOURS)  
BUILDING OF THE TRACE ENERGIES  
PROGRAMMED SCALING FOR COVERAGE COMPENSATION  
LOW PASS FILTERING FOR SMOOTHING

SORTING INTO INLINE, CROSSLINE OR TIME SLICE ORDER  
AREA-DISPLAY WITH BIAS

Due to the good results of the envelope stacking procedure achieved in one subarea all other subareas of the survey have been processed in this manner. Thereby a preliminary synopsis over most of the fundamental reflection information contained in the 3D-data set is now at hand by:

- 357 vertical sections in inline direction (SW-NE, parallel one to another with a slice distance of 50 m),
- 382 vertical sections in crossline direction (NW-SE, parallel one to another with a slice distance of 50 m),
- 750 horizontal sections (6 sec, parallel one to another with a time slice distance of 8 ms).

The double-faced figures 5, 6, and 7 show exemplarily 24 sections of the three slice types respectively, at about equal spacing through the entire data volume (see Fig. 8 for the location of the several sections within the survey area).

Furthermore, the envelope-stacked data set was, after compressing the amplitude dynamics, transferred into a microcomputer system. A program was written enabling the user to let series of vertical sections or time slices of the 3D-volume run on the screen (with up to 25 pictures/sec) like a 'movie'. This 'animation' of the ISO'89-3D data allows to identify spatially correlating events by another method and provides an amazing visualization of many reflection elements and their respective position, especially in the coloured version. Another advantage of this computer animation is, that not only a few sample sections (like the use of common paper displays) but all existing sections in all three space directions are accessible in this compact way.

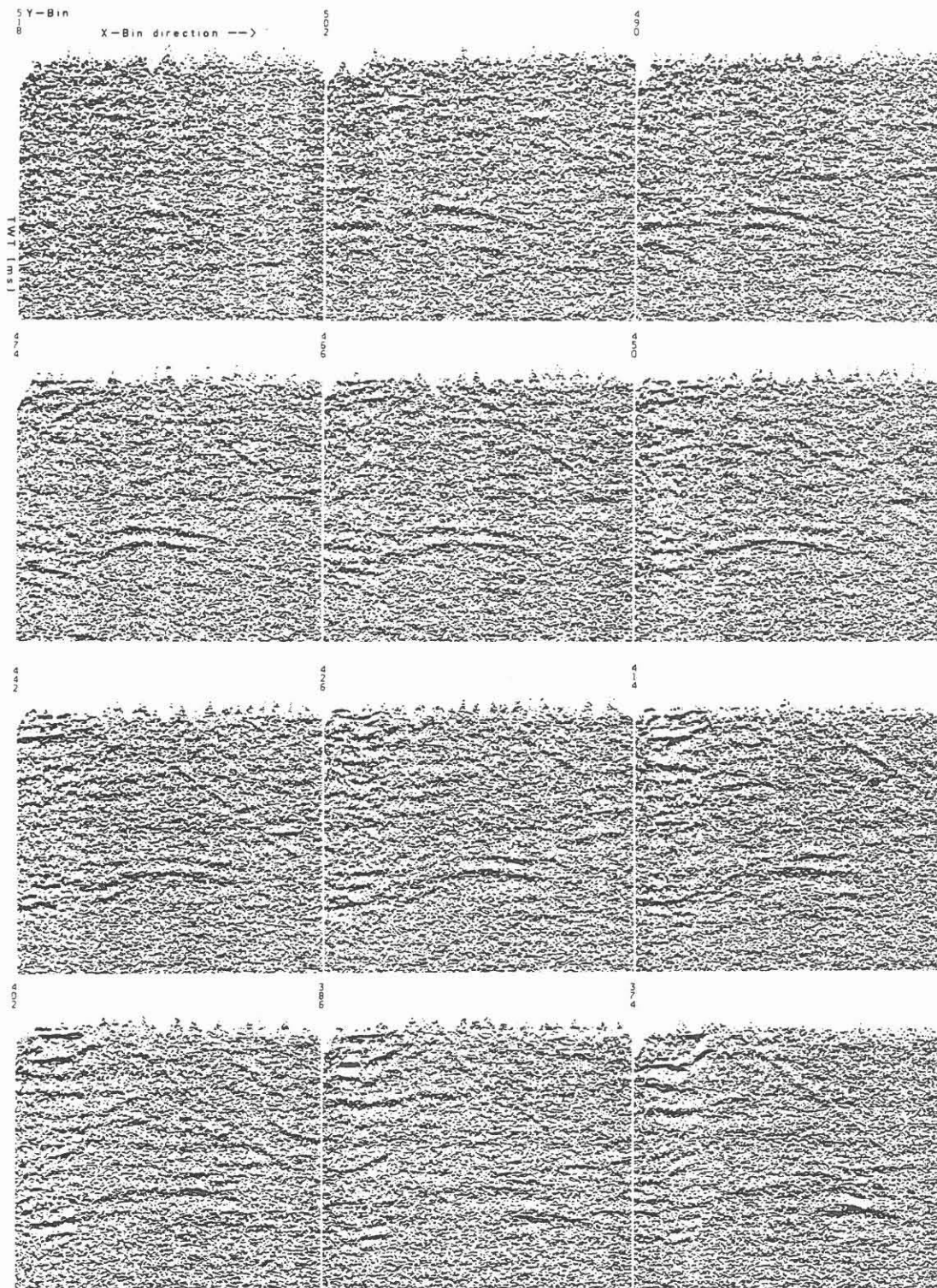


Fig. 5: Selection of 24 envelope-stacked inline sections (each SW-NE, 18.2 km long, 6 s TWT). See Fig. 8 for position of the respective Y-bin numbers within the data volume.

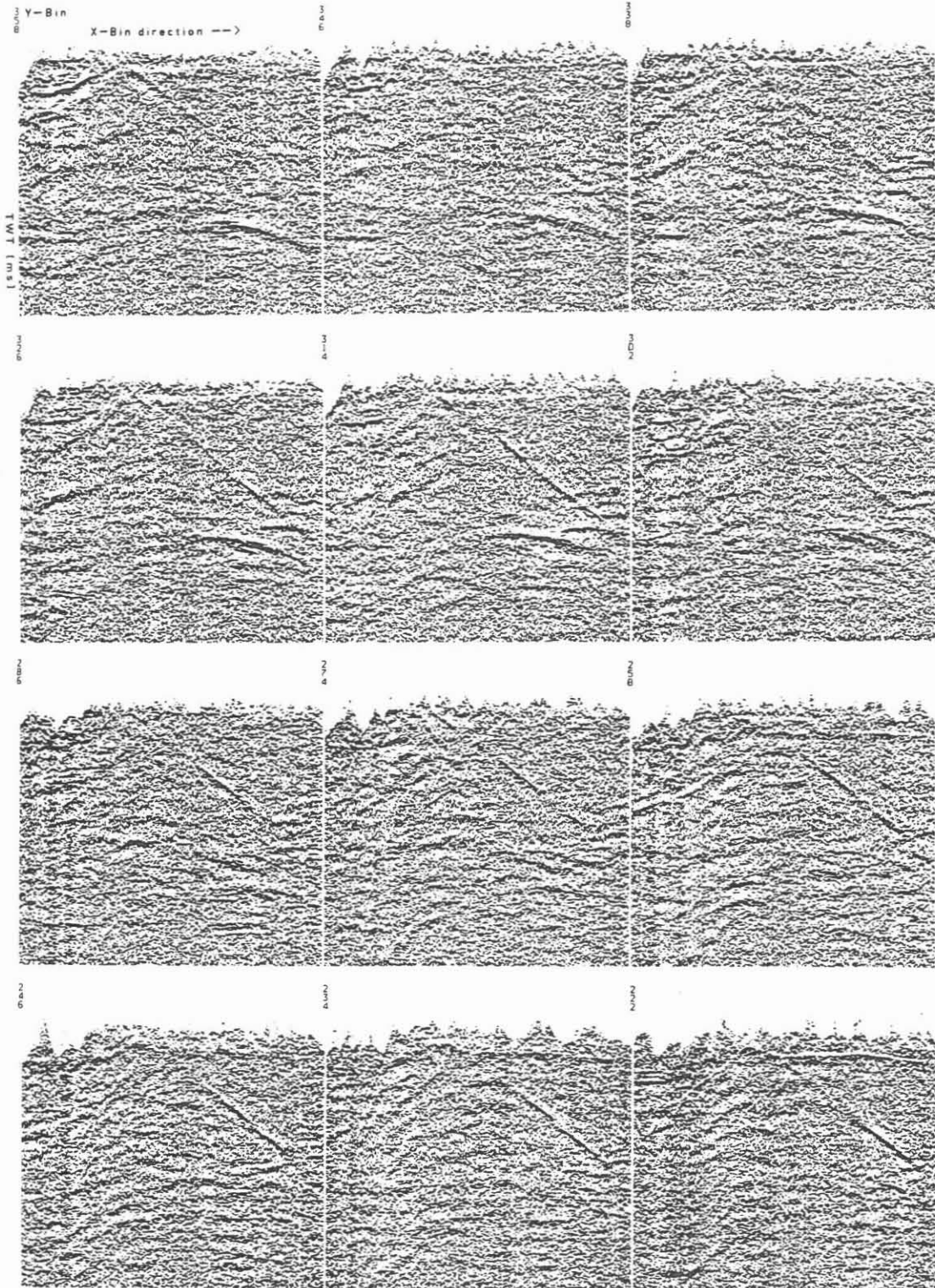


Fig. 5 (continued)

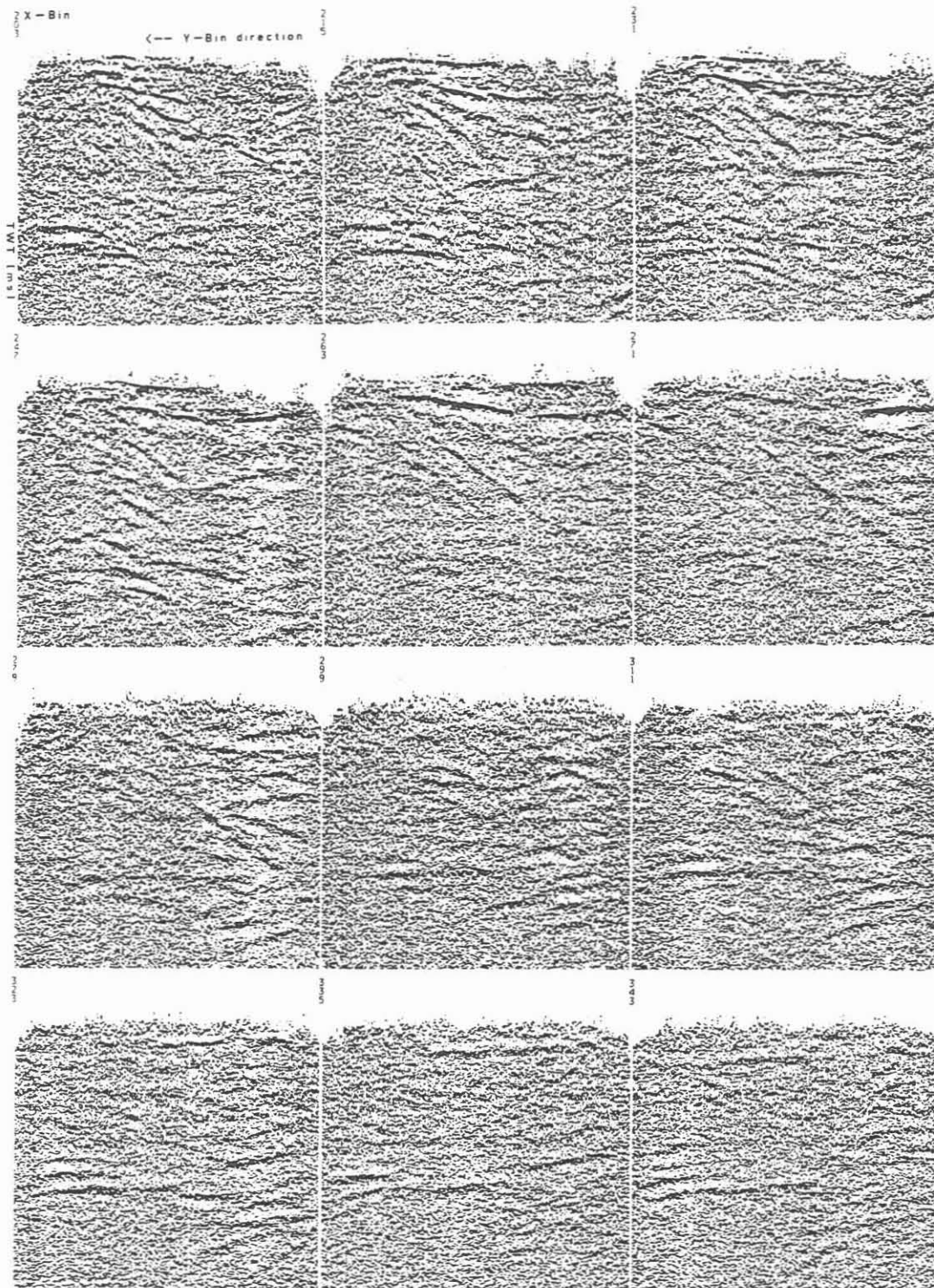


Fig. 6: Selection of 24 envelope-stacked crossline sections (each SW-NE, 17.4 km long, 6 s TWT). See Fig. 8 for position of the respective X-bin numbers within the data volume.

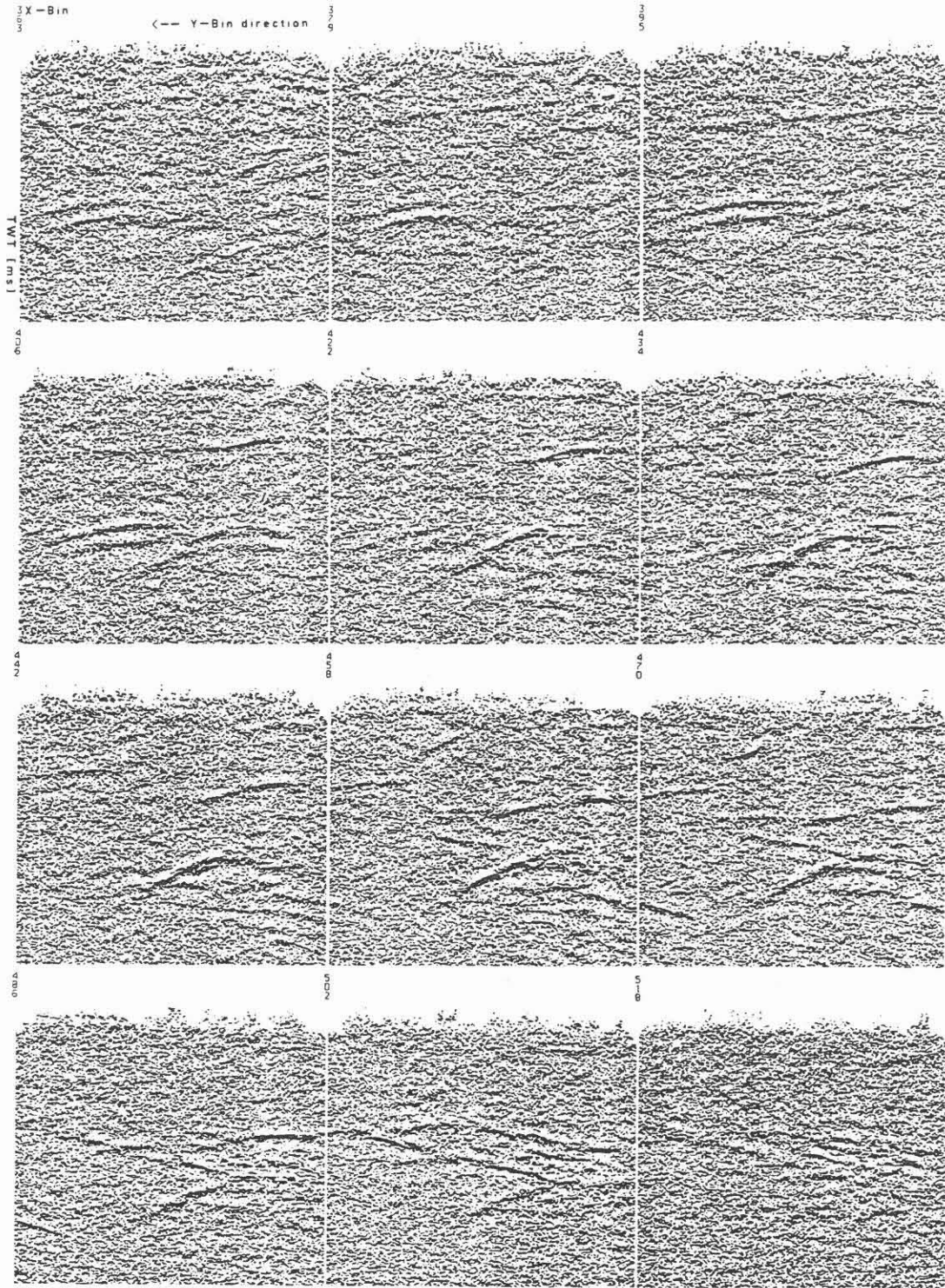


Fig. 6 (continued)

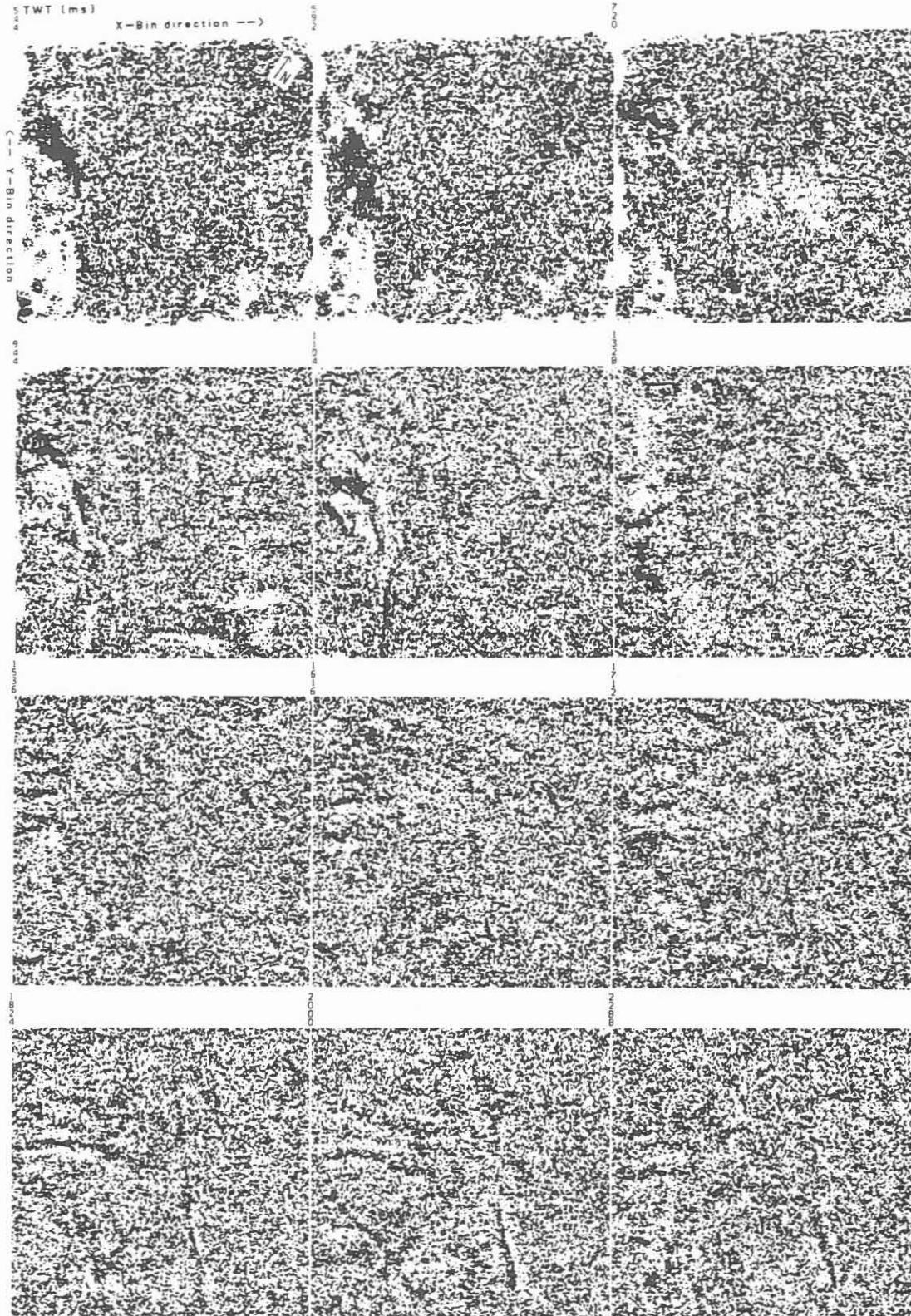


Fig. 7: Selection of 24 envelope-stacked time slices (each 18.2 km \* 17.8 km). See Fig. 8 for position of the respective TWT in ms within the data volume.

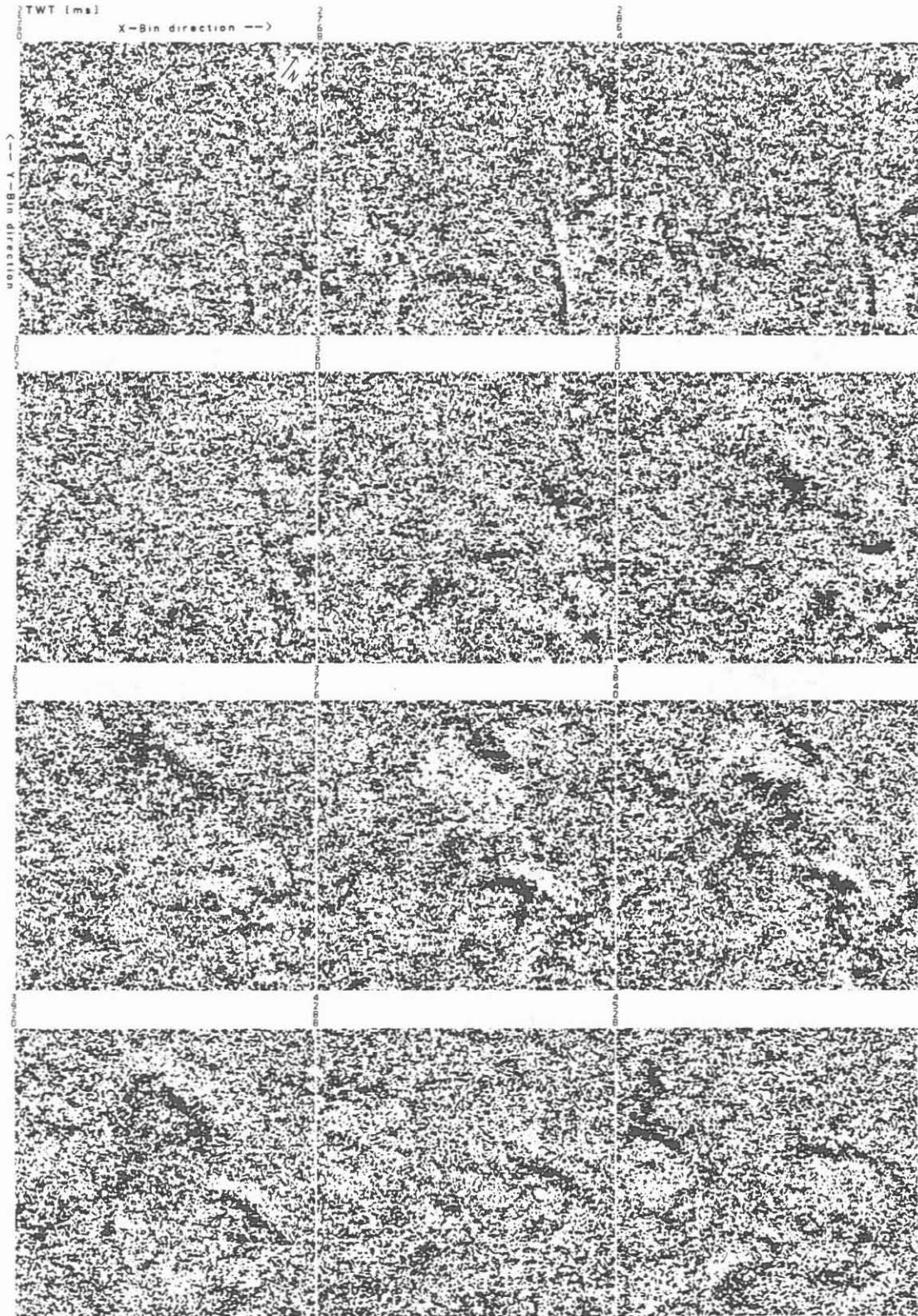


Fig. 7 (continued)

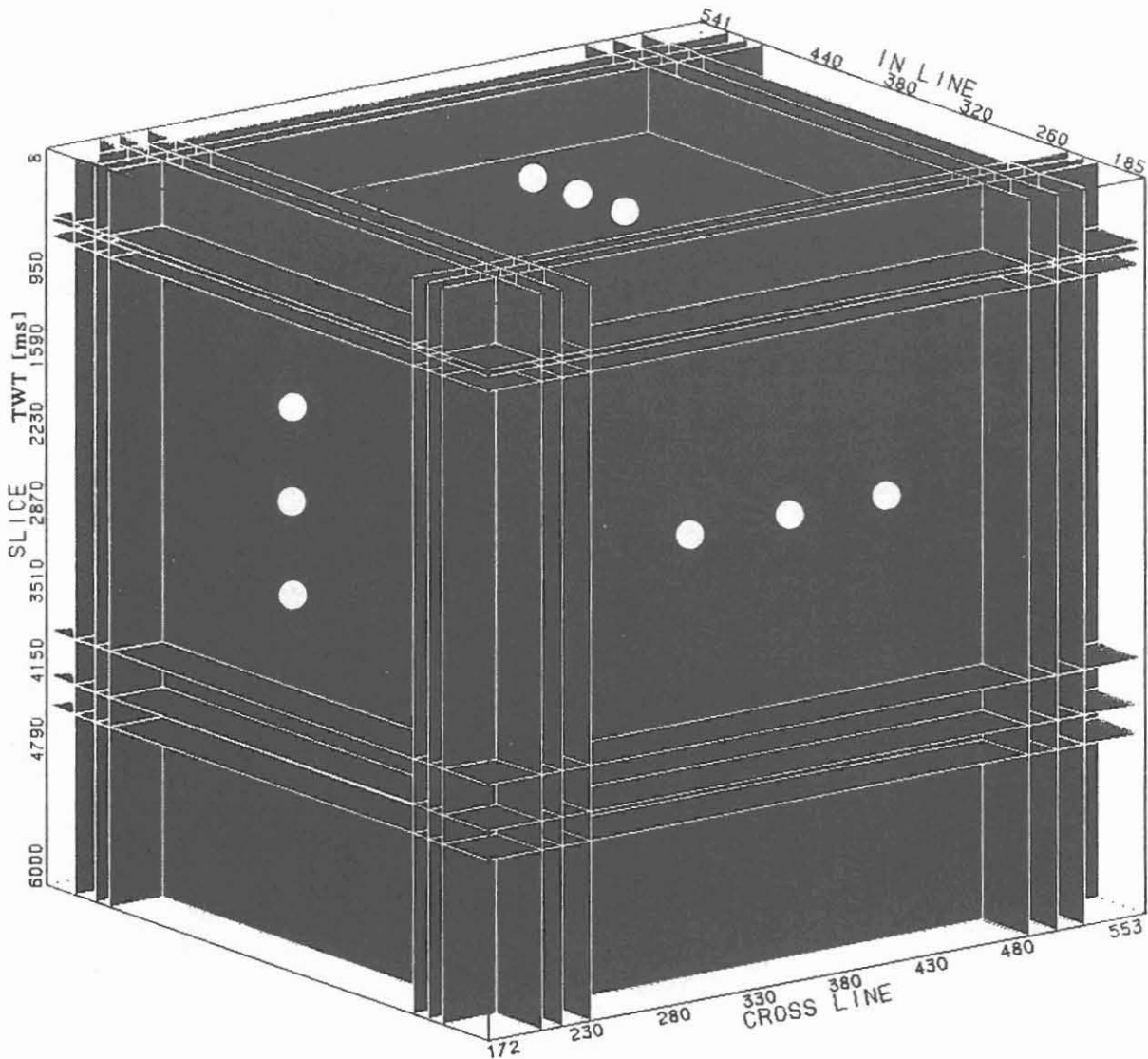


Fig. 8: Position of the vertical and horizontal section series of Fig. 6, 7 and 8 within the ISO'89 data cube.

**Description, rating, and application of some major results**

Quite good visible in the here depicted sample sections are the strongly NE-dipping reflection events at about 0.4 to 3.5 s TWT which pass through nearly the entire survey area. In the inline sections they appear with about their maximum apparent dip and in the crosslines nearly horizontally (i. e. in about their strike direction). Since doubts existed initially, whether these steeply dipping events were true reflections or only reflected refractions (e. g. caused by the Franconian Line (FL) striking in crossline direction), extensive modelling has been carried out to clarify this question (Koerbe and Reichert, this volume).



In the same context another seismic data set must be regarded which is also figured in Koerbe and Reichert (this volume) - the reprocessing of the 2D-profile KTB 8502, passing in inline direction through the survey area. In the first processing of 1985 the main emphasis was laid upon subhorizontal events. Therefore, steeply dipping events, which are now approved as real features, could be recognized only weakly. However, they appear very clearly in the reprocessed version of 1991, after adaption of the processing parameters to the steep dips (especially the NMO-velocities and the migration method used). Meanwhile the 2D-profile KTB 8502, especially in its migrated version, has turned out to be a valuable help with regard to a depth and dip prediction for important key horizons reachable by the KTB.

Already during the 3D-data processing several horizon planes, recognizable over larger areas within the whole data volume (subsets A, B, C and D), have been evaluated at the DPC section by section and spatially consistently with the help of an interactive, graphic interpretation system for 3D-seismic data (COMSEIS). In the crystalline part east of the FL a total of 13 events could be detected and evaluated over larger areas, in the sedimentary part west of the FL further three events have been selected in the upper and four in the lower time range. Hluchy et al. (this volume) denote and describe all horizons interpreted so far. Moreover, they value the suitability of the ISO'89-3D envelope stack for an exact and reliable interpretation.

It turned out, that a connection of processing and interpretation already in an early stage is of high advantage. For example the perspective colour-displays of coherent events generated after horizon-oriented evaluation of envelope sections are much more instructive than the common plot series of black and white (2D) paper sections. The figures 9a, b, and c show such 3D-arrangements of combined vertical and horizontal slices as so-called 'skeleton'-, 'chair'-display, or 'flying carpet'.

But the main objective of the interpretation of unmigrated envelope stacks is the generation of travelttime maps for a lot of important reflectors in the survey area. These enable the determination of amount and direction of the local, apparent dips. With those parameters a certainly simplified, but nevertheless spatially correct image of the actual subsurface structures can be calculated using an appropriate horizon migration algorithm. Especially the multiplicity and variety of the parameters

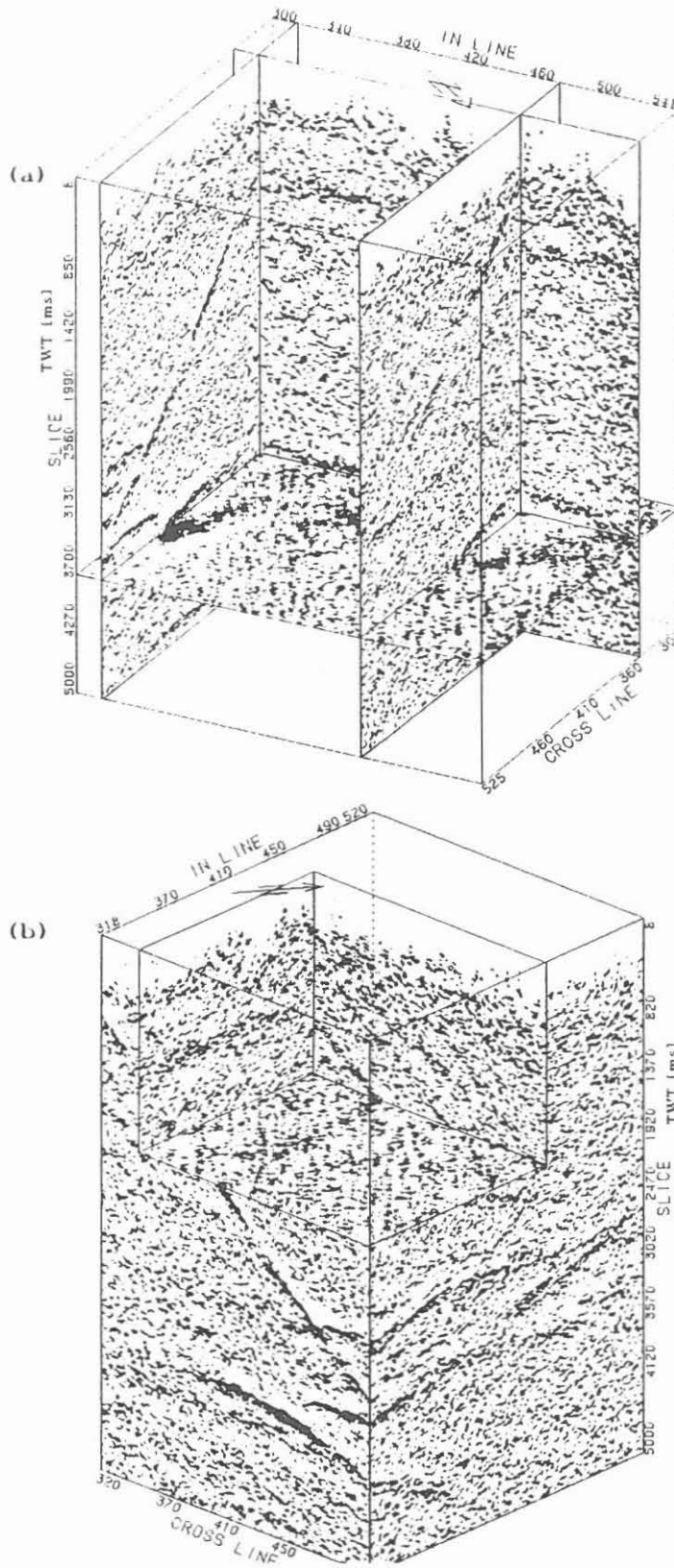


Fig. 9

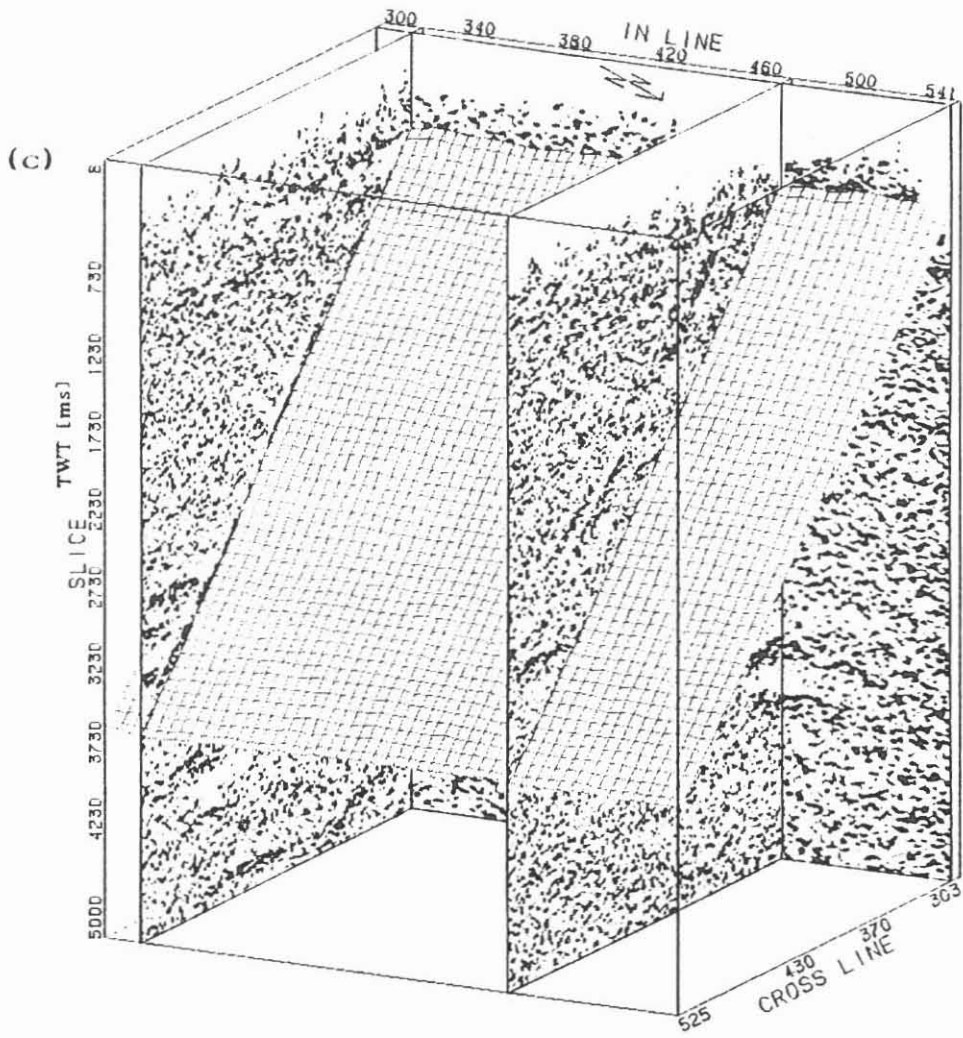


Fig. 9: Perspective views of combined envelope-stacked sections (for subareas B + C):  
(a) 'Skeleton': 2 inlines, 1 crossline, 1 time slice.  
(b) 'Chair': data cube cut open to provide an inner view.  
(c) 'Flying carpet': evaluated horizon between 2 inlines and 1 crossline.

for the azimuth-dependent velocity analyses of the unstacked data, yet lying ahead, can be considerably reduced. Thus, the generation of a phase-consistent stack with the expected high time resolution and accuracy is for the first time possible with reasonable efforts. Apparent dip and dip direction of reflectors, namely, are two important quantities absolutely necessary for phase-consistent stacking in the presence of greater dips. Commonly, these unknown quantities are to be determined by lots of painstaking and time-consuming azimuth-dependent velocity analyses as described in the beginning of this contribution. Now, however, they are directly accessible after the COMSEIS-interpretation of envelope stacks.

Therefore, FORTRAN-programs have been developed at the DPC CLAUS-thal providing:

- the data transfer between COMSEIS-system and SSL 3D-processing software,
- the manipulation (gridding, interpolation, smoothing etc.) of horizon time picks,
- the calculation and preparation of dips and dip directions based on horizon times,
- a simplified 3D horizon migration using constant velocity,
- the generation of azimuth-dependent velocity analysis data bases based on the migrated dips.

By using the horizon planes interpreted with COMSEIS, the horizon migration procedure yields approximately the true spatial horizon positions and, thus, allows for a more precise depth and dip prediction for reflectors in the range accessible by the KTB borehole. The technical background and the migration results for selected horizons are described in detail in another contribution of this volume (Stiller and Tormann, this volume). All 13 travelttime maps east of the FL, interpreted with COMSEIS have been migrated meanwhile in this manner.

#### **Phase-consistent stacking and further improvements**

It should be clearly emphasized, that the actual sequence of final processing and horizon interpretation as performed so far is upside-down due to immense difficulties encountered in the study area. Correctly and commonly, all evaluation and interpretation is to be based on a true wavefield migration calculated from phase-consistently stacked 3D-data. The approach described here consists of a horizon migration of COMSEIS-evaluations yielded from an unmigrated envelope stack (due to the lack of a satisfying phase-consistent stack of the whole 3D-data set so far). The decisive advantage of this reverse sequence is, however, that (based on the COMSEIS-time picks) within each affected bin of each interpretable horizon amount and direction of the local apparent dip are simultaneously provided - two decisive parameters for the necessary consideration of the azimuth-dependency of the NMO-velocities. By this, laborious azimuth-restricted velocity analyses can be omitted. Thus, the subsequent phase-consistent 3D-stack is now attainable by a considerably smaller time effort, maybe comparable with the requirements for a 2D-profile of the same data amount.

Consequently, the main objective is at present directed progressively towards the realization of a phase-consistent stack for the entire ISO'89-3D data set in a quality which is common in 2D deep seismics and which is a precondition for an exact 3D-migration of the stacked data. Certain problems, however, with destructive stacking effects occurring due to insufficiently determinable NMO-velocities for steeply inclined reflectors in anisotropic settings will probably still remain.

The first phase-consistent stack was performed for the subset B. The unmigrated traveltime information of four key horizons (SE1, SE2, B1, B2) recognizable within the whole block B was used. As outlined in Stiller (1991) an elliptical dependency of the stacking velocities on azimuth was assumed and the ellipse parameters were derived from the dip information calculated from the time picks of the COMSEIS envelope interpretation. Compared to the previous envelope stack this first phase-consistent stack with the full subsurface coverage shows a remarkably high time resolution and accuracy even without any poststack 'cosmetics' (like horizontal summing of adjacent slices, coherency filtering etc.).

Further improvements will be probably gained by an inclusion of additional 'COMSEIS-dips' for those horizons being only detectable within smaller areas. However, certain limits will be reached in any case with regard to a correct handling of 'crossing' or 'ending' horizons.

Another extensive and efficient new development at the DPC Clausthal was the realization and successful application of a program to produce a true spatial coherency enhancement of phase-consistently stacked 3D-data with tolerable computer runtimes.

The 2D coherency filtering is used since years as a standard for stacked sections in 2D deep seismics. This efficient process enhances the S/N-ratio by emphasizing events which correlate over a number of CDPs (even if the amplitude is low) and by attenuating non-correlating events (even those with higher amplitudes). It is based on an automatic execution and rating of test stacks of adjacent CDPs along user-defined dips and time windows and results in an enhancement of those dip portions, for which the stacking amplitudes become maximum. For a more detailed description see Stiller and Thomas (1989).

Of course, it is possible to apply this 2D-procedure on 3D-data as well by treating each in- or crossline slice as a single 2D-section. However, when performing coherency filtering in inline direction for example, it is not guaranteed at all, that in adjacent inline slices always the same dominant dips are detected and enhanced to obtain a sufficient coherency filtering in crossline or any other direction as well and to result finally in a continuous coherency-filtered 3D horizon plane again. Especially for 3D-data with poor and discontinuous reflectivity a coherency filtering in only one specific direction can lead to unclear, ambiguous and possibly deteriorated results in all other directions. In order to overcome these shortcomings with certainty, the DPC approach is based on a spatial concept and comprises the following steps:

- already for the coherency analysis a number of CDPs lying in an area (e.g. 5\*5 bins) are taken as a basis (instead of a number of CDPs lying on a line as in the 2D-case),
- for these bin areas test stackings along planes of different dips and dip directions are then performed and rated over appropriate time windows
- that plane position in space is to be found, along which the stacking amplitudes become maximum (which should happen exactly when the related dip parameters coincide with the actual position of the reflector plane).
- the center traces of the analysed bin areas are weighed with coherency factors derived from the maximum stacking amplitudes in the respective time windows.

This proceeding guarantees that in adjacent slices of any direction always the same horizons are recognized and intensified resulting in a spatially enhanced S/N-ratio of the complete 3D-data set. DPCs corresponding computer program meets all these requirements. In addition, it makes use of data base- and data formats of the SSL 3D-processing software enabling data in- and output without any difficulties. The computer runtime depends to a high degree upon the number of different plane positions in space to be analysed. With appropriate parameters it amounts to about 1.5 min/CDP, i. e. 750 hours or 30 days for one of the four 3D-subsets (using a VAX 11/750 system). Subset B was spatially coherency-enhanced so far in the way described above. The figures 10, 11 and 12 show a comparison of two inline section (ca. 2.5 km SE of the KTB) in the processing stages envelope stack and phase-consistent stack, the latter with and without spatial coherency enhancement to illustrate the efficiency of this new tool.

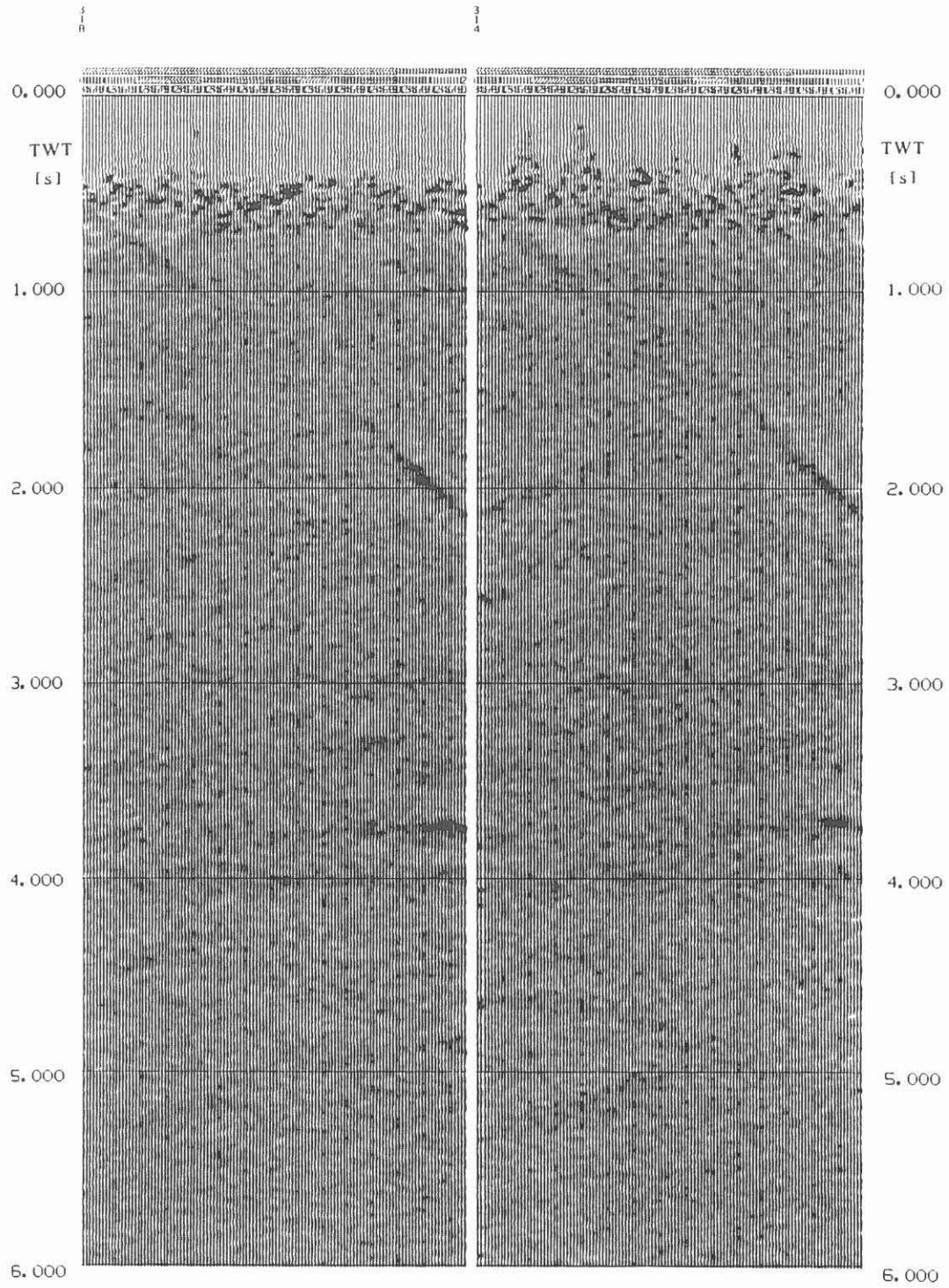


Fig. 10: Envelope stack of two inline sections (subarea B), each 5.9 km long).

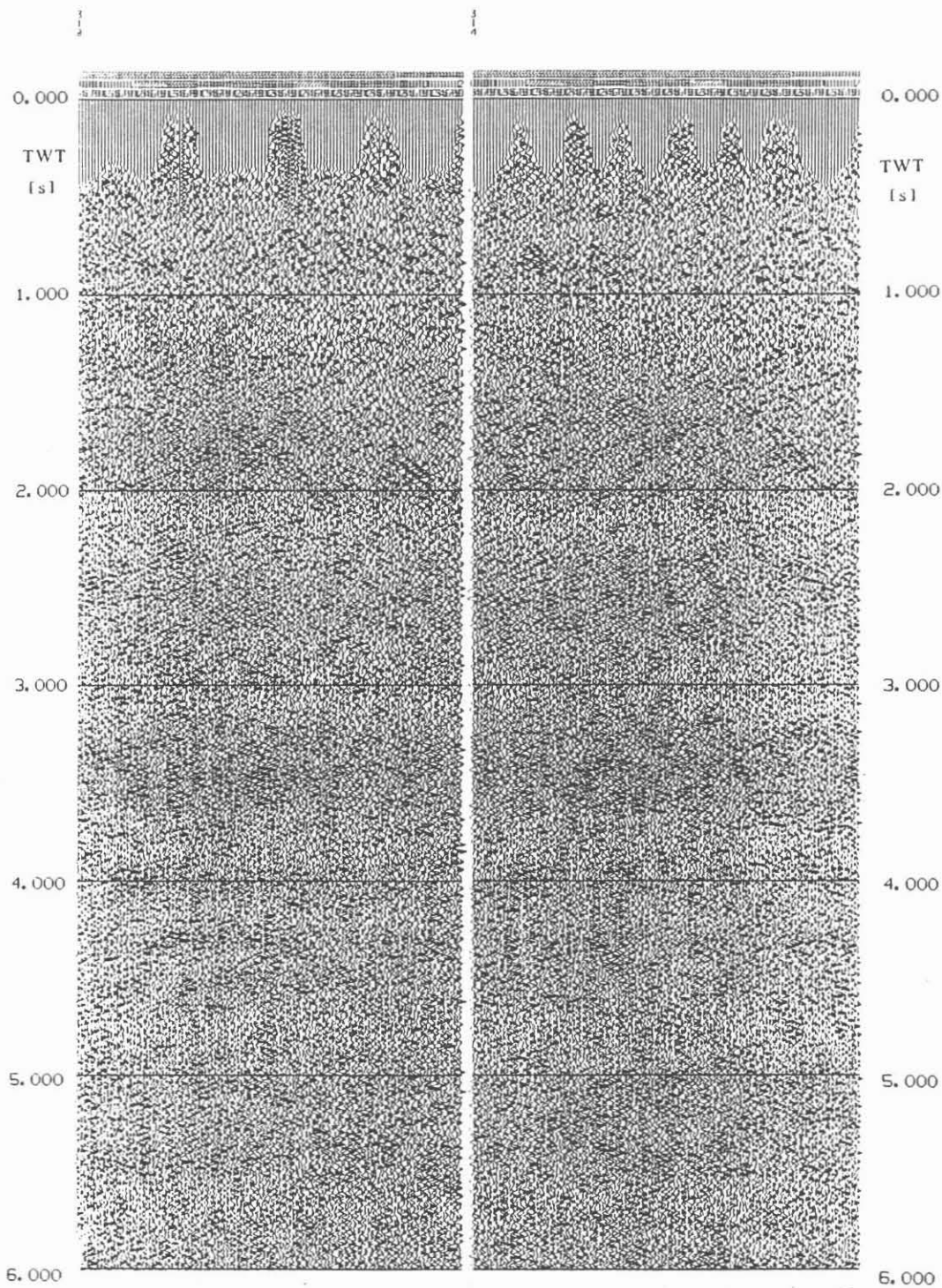


Fig. 11: Phase-consistent stack of two inline sections (see Fig. 10 for comparison).



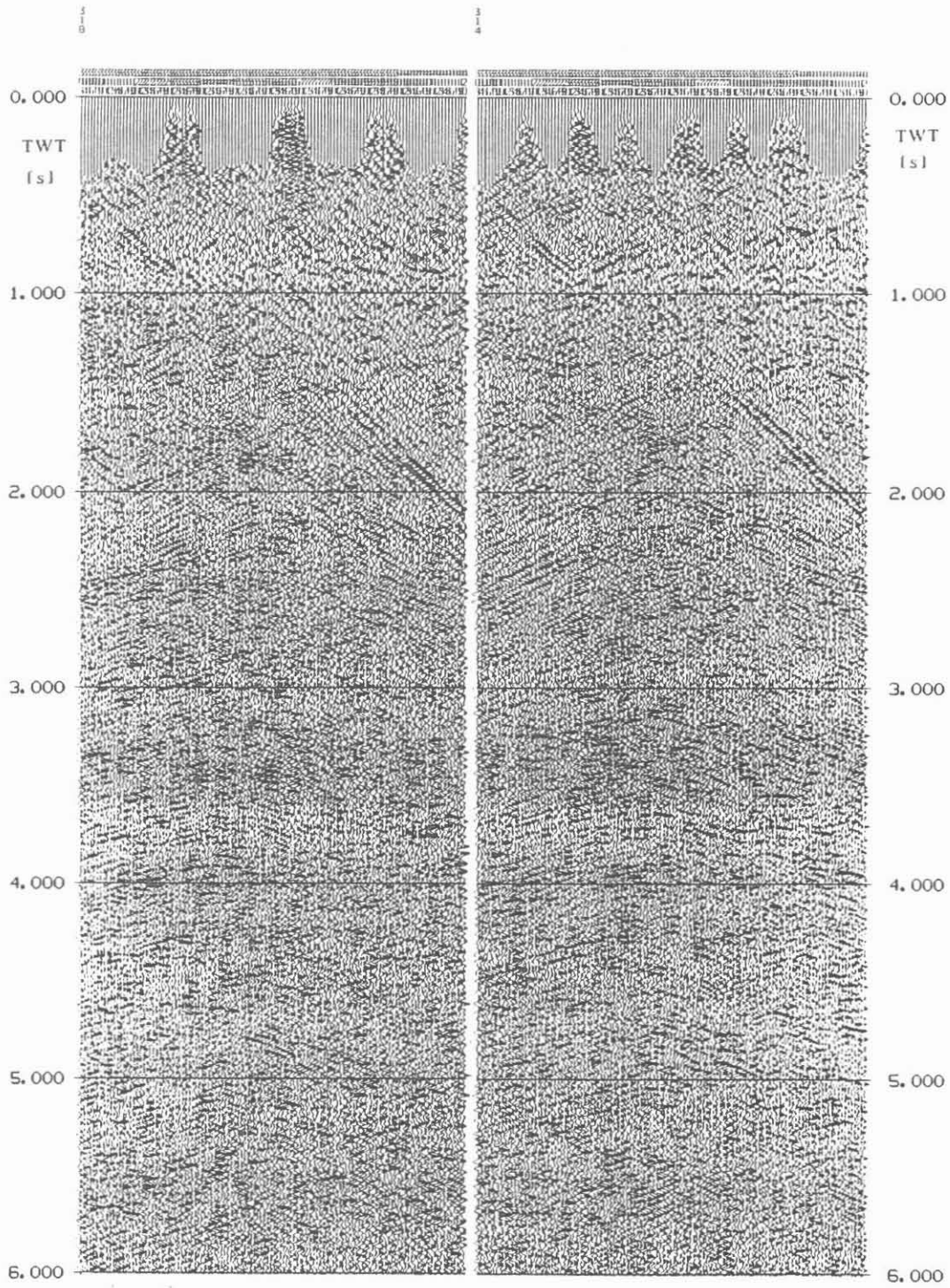


Fig. 12: Phase-consistent stack of two inline sections with subsequent spatial coherency enhancement (see Fig. 10 and 11 for comparison).

A 'by-product' of this spatially operating coherency procedure turned out to be of very high advantage: inclination and azimuth of the respective dominant dip for each bin in each time window are automatically determined and written to a data base. Thereby, additional NMO-correction parameters are provided with a very high density automatically and independently from the COMSEIS-based dips mentioned before. They can be used (after editing and smoothing if necessary) to attain a second, improved phase-consistent stack. By this, also an iterative approach is easily realizable consisting of several alternating repetitions of stacks with dip-controlled NMO and improved dip determinations by coherency analyses of these stacks.

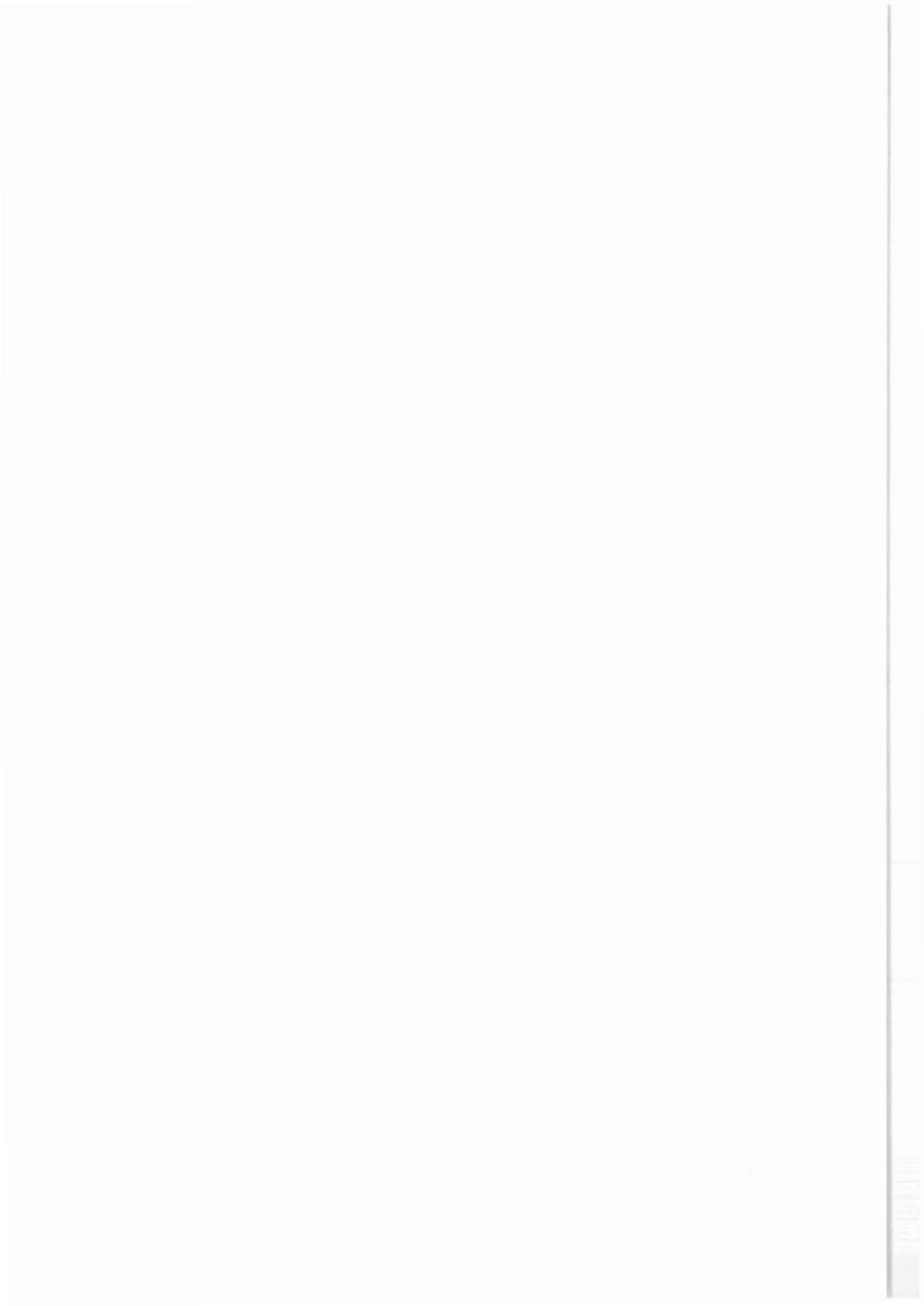
The methods described in this contribution open up a variety of possibilities to produce a high resolution final data cube of the entire ISO'89-3D data set within an acceptable time schedule providing a suitable basis for the 3D wave-field migration of the phase-consistently stacked data and a spatially consistent geological interpretation.

#### References:

- Hluchy, P., Koerbe, M., Thomas, R., 1992. Preliminary results of the interpretation of the 3D-seismic survey at the KTB location, KTB Report 92-5, DEKORP Report (this volume), Nieders. Landesamt f. Bodenforschung, Hannover.
- Koerbe, M., Reichert, C., 1992. On the character of 'Steep Event SE-1' - reflected energy, reflected refraction, diffraction or any artifact, KTB Report 92-5, DEKORP Report (this volume), Nieders. Landesamt f. Bodenforschung, Hannover.
- Rehling, J. G., Stiller, M., 1990. 3-D Reflection Seismic Survey of the Area around the KTB Drilling Site, KTB Report 90-6b, DEKORP Report, Nieders. Landesamt f. Bodenforschung, Hannover.
- Stiller, M., Thomas, R., 1989. Processing of Reflection-Seismic Data in the DEKORP Processing Center Clausthal, in: Emmermann, R., Wohlenberg, J., (Eds.), The German Continental Deep Drilling Program (KTB), Springer, Berlin, Heidelberg.

Stiller, M., 1991. 3-D vertical incidence seismic reflection survey at the KTB location, in: Continental Lithosphere - Deep Seismic Reflections, Geodynamics 22, American Geophysical Union.

Stiller, M., Tormann, M., 1992. Application of a simplified horizon migration process on the data volume of the 3D-seismics ISO'89, KTB Report 92-5, DEKORP Report (this volume), Nieders. Landesamt f. Bodenforschung, Hannover.



# Preliminary Interpretation of the 3D-Seismic Survey at the KTB Location

P. Hluchy, M. Körbe, R. Thomas \*

## Summary

A preliminary interpretation has been done on an envelope stack of the three-dimensional seismic survey of the ISO 89 experiment. This kind of stack is interpretable as well as a normal stack with some restrictions, but all major elements are detectable. The major structural elements, which have been the target of the interpretation in this special case, can be divided into five groups. The three most important groups are a bundle of steeply northeast dipping reflections with outcrops in the area of the outcrop of the Franconian Line, a zone of high reflectivity with five reflections named Erbsdorf body and two curved interfaces at the time range 3.5 to 4.5 s TWT. The results of this interpretation are in good correspondence to the former interpretations done on the two-dimensional seismic lines in the survey area.

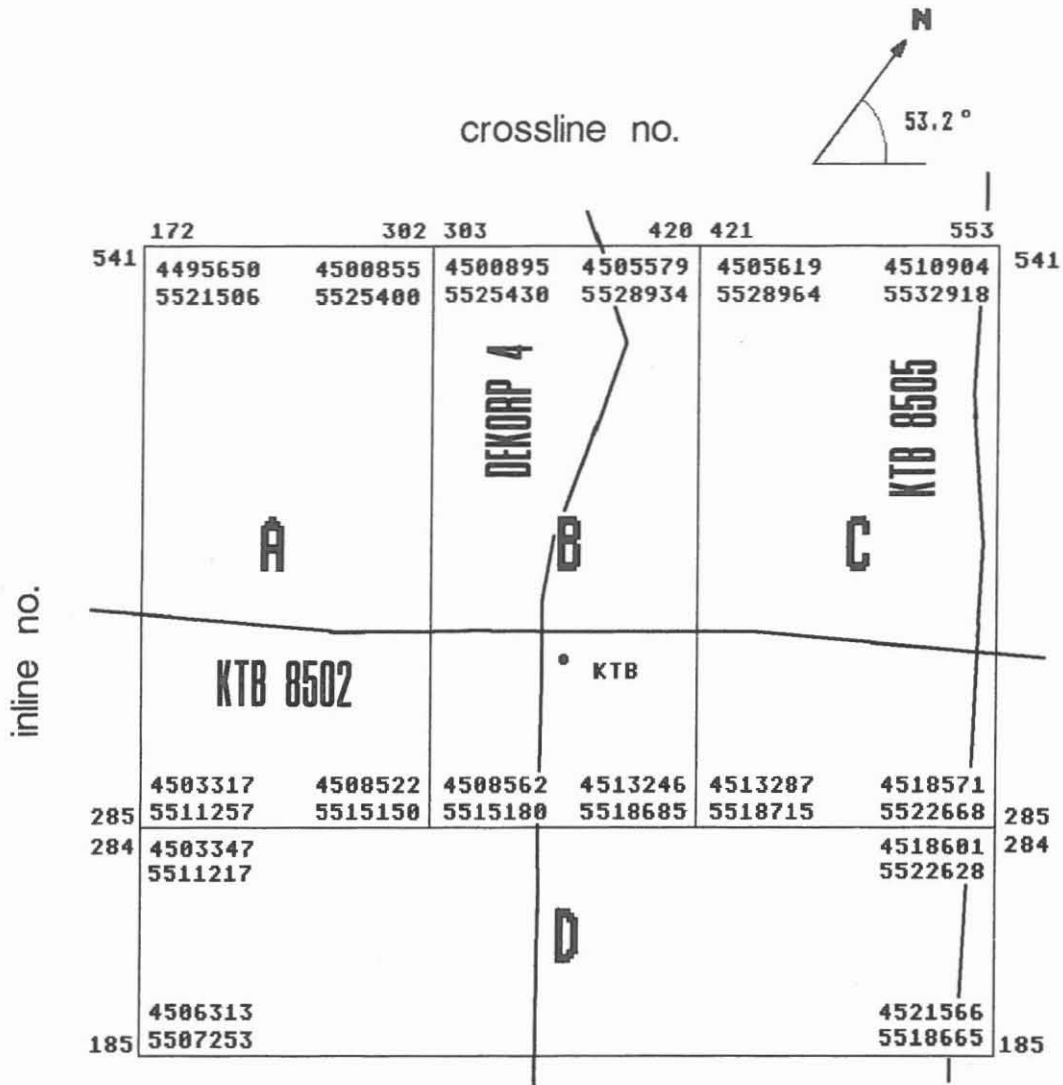
## 1 Introduction

One, maybe the biggest, part of the experiment **Integrated Seismics Oberpfalz 1989** (ISO 89) was the measurement of a 3D steep-angle, deep-seismic survey at the KTB location. An area of 17.85 km x 19.1 km was covered by this survey. The average coverage in the center of the survey is 15-fold. For a more detailed description of the survey and its acquisition see Rehling and Stiller (1990).

In a first step the first seven seconds of the recorded twelve seconds reflection time have been processed at the DEKORP Processing Center (DPC) at the Institute for Geophysics of the Technical University Clausthal. In the sketch of the survey area (Fig. 1) the Gauß-Krüger-coordinates related to the 12th meridian are quoted at the corners of the four subareas. The division into these subareas was necessary because of the restricted volume of disk storage at the DPC. The numbering of the inlines (I 185 - I 541) and the crosslines (C 172 - C 553) is shown at the outside of the area. The inline direction SW - NE is parallel to the geophone lines. The crossline direction NW - SE is parallel to the shotpoint lines that means they are almost parallel to the strike direction of the Franconian Line, which separates a crystalline basement area in the northeast from an smaller area covered with Mesozoic and Paleozoic sediments in the southwest.

---

\*Authors' address : DEKORP Processing Center, Institut für Geophysik, TU Clausthal, Arnold-Sommerfeld-Str. 1, 3392 Clausthal-Zellerfeld



**Figure 1:** The 3D-survey area at the KTB location. The coordinates of the super deep borehole are 4508790/5519880. This location is almost crossed by inline 357 and crossline 363 (further details see text).

The processing of the seismic data showed that the conventional three-dimensional processing scheme based on seismics in sedimentary areas failed in such a complicated crystalline area as it was found around the KTB drill site. Therefore, the first and up to now the only stack of the whole survey has been done as an envelope stack. More details of this processing procedure can be found by Stiller (1992) in this volume.

This envelope stack of the three-dimensional survey has been interpreted with three main aims:

- Firstly, the interpretation should give support to the drilling crew at the KTB. There should be hints for zones critical for drilling as well as information about the possible casing emplacement in the deeper part of the drill hole.

- Besides the special informations about the close surrounding of the KTB the structure of the whole area covered by the survey should be evaluated. These results should be reconciled with the results of the interpretation of the two-dimensional seismic lines in this area (Schmoll, et al., 1989) or should correct the interpretations done earlier.
- Last but not least the interpretation should give support to the processing of the 3D-survey to achieve the aim of a stack with improved quality which includes informations about the phase of the signals.

## 2 Interpretation of an envelope stack — possibilities and problems

First of all it had to be proved that events which can be detected in a standard stack (with phase information) can be seen in a corresponding envelope stack. The necessary tests have been done with approximately 300 CMP's of the two-dimensional line KTB 8502, because there occur the same structures as they can be found in the 3D-survey.

The line KTB 8502 has an average coverage of 80-fold. The standard stack with this coverage is displayed in Figure 2. This stack has been processed with very high stacking velocities to image the steep dipping events in that area (Körbe and Reichert, this volume). A coherency filter has been used to improve the signal/noise ratio. Figure 3 shows the corresponding envelope stack. The velocities used for this stack were the same as used for the standard stack. The envelope stack was filtered with a high-cut filter with a cut-off frequency of 30 Hz to get a smoother image of the data. In this first test it can be seen that the main interpretable structures of the standard stack can be found in the envelope stack, too. Even adjacent signals can be separated satisfactorily and diffraction-like structures underneath 3 s TWT are clearly displayed.

Then the coverage was reduced to 15-fold to get a comparison with the data of the 3D-survey. At first sight there is a great loss of information in the data of the normal stack (Fig. 4). Even the coherency filtering cannot really improve the result. The reflections with steep dip are no longer continuous and it will be very difficult to interpret them. The diffraction like events underneath 3 s TWT can be hardly determined as such events, too. In contrast to this these events are still interpretable in the envelope stack with this very low coverage (Fig. 5). The steep dipping events seem to be more continuous as in the standard stack and are interpretable as well.

As results of these tests it can be summarized:

- The steeply dipping events can still be interpreted in the envelope stack, even if they are almost invisible in the normal stack. The structure of diffraction like events can be determined with some restrictions (e.g. if the hyperbola branch crosses other events this cannot be resolved).
- In general it can be said that events located separately in the data can be determined in an envelope stack even if the coverage is very poor. Events which crosses each

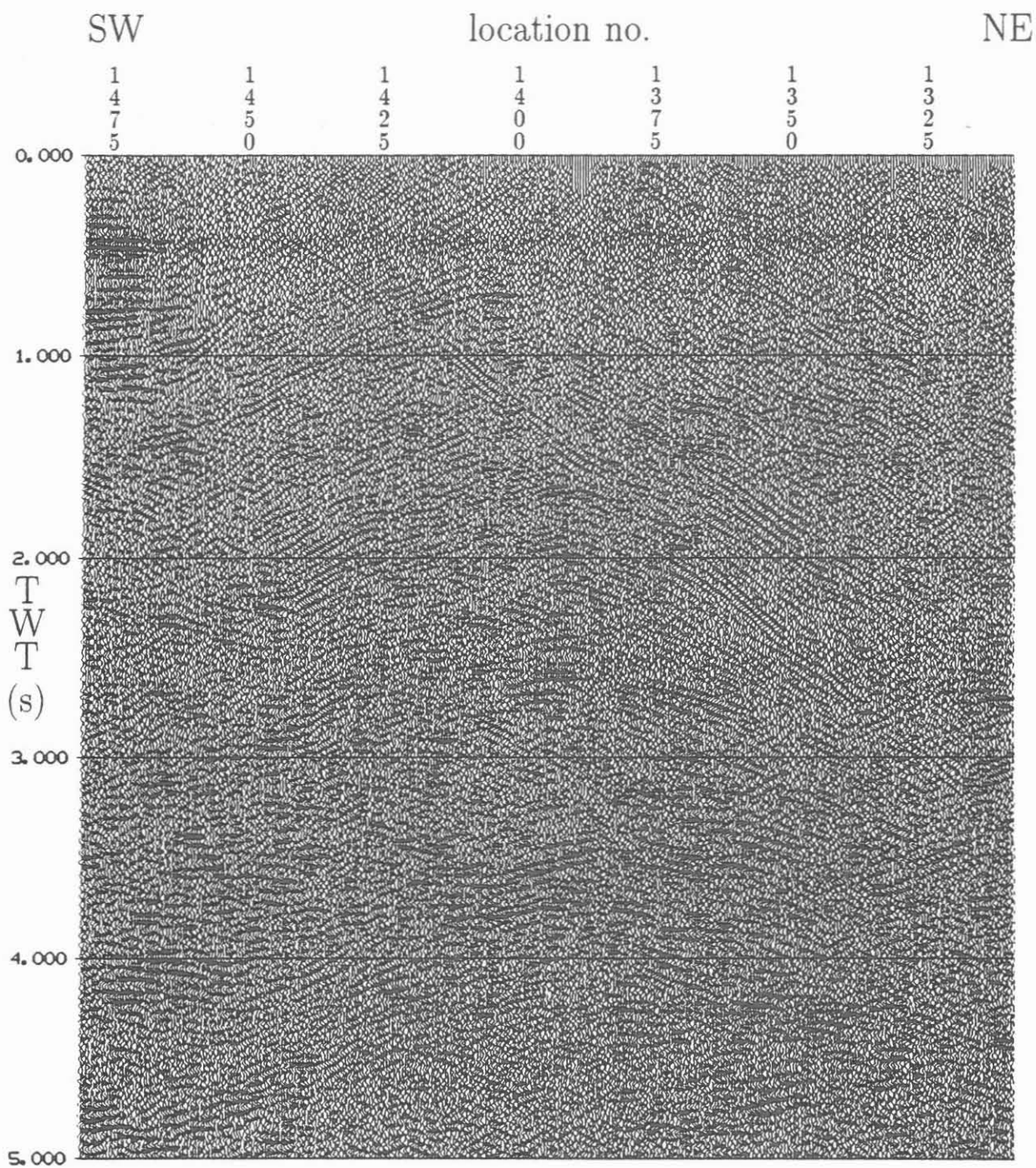
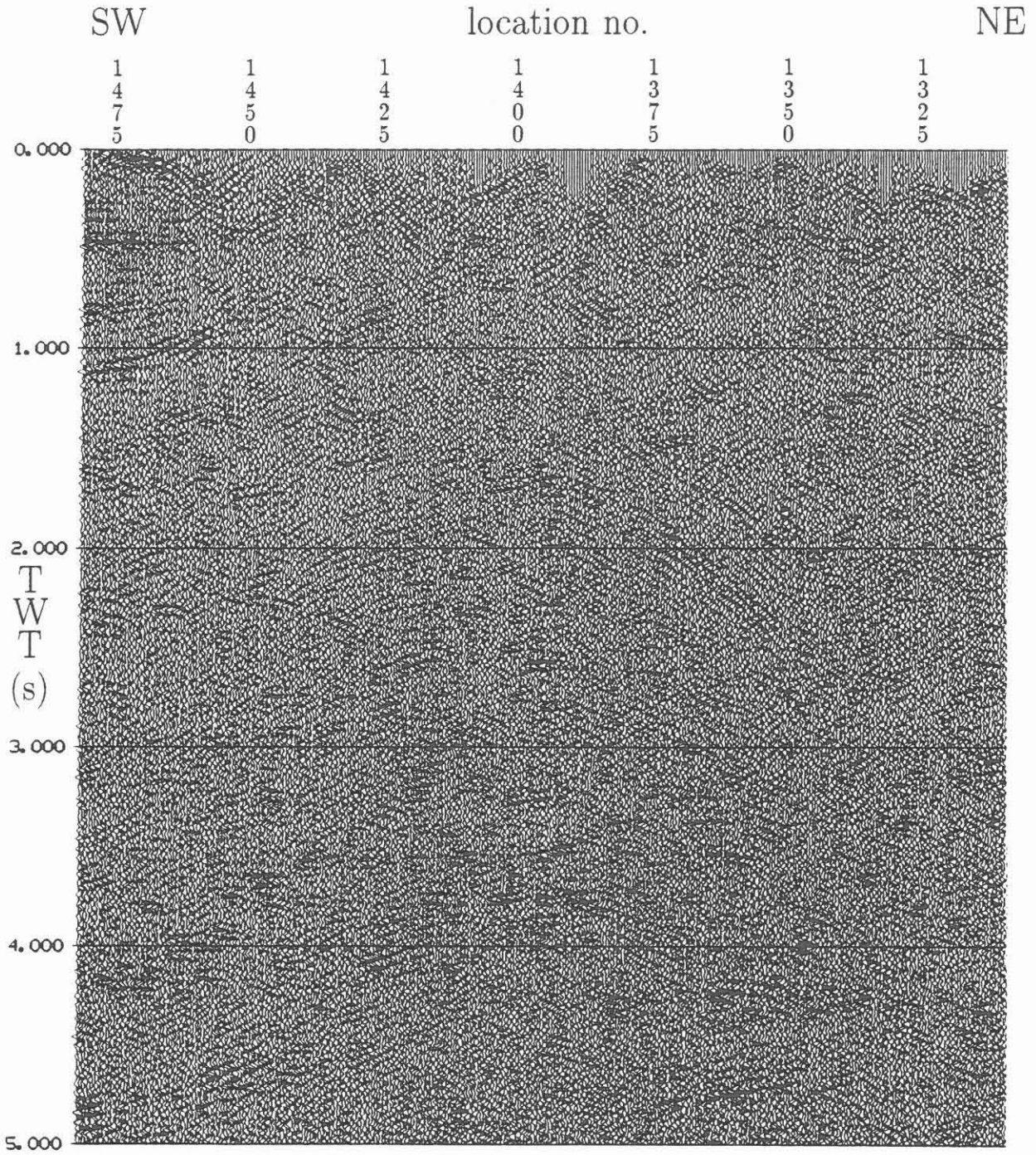


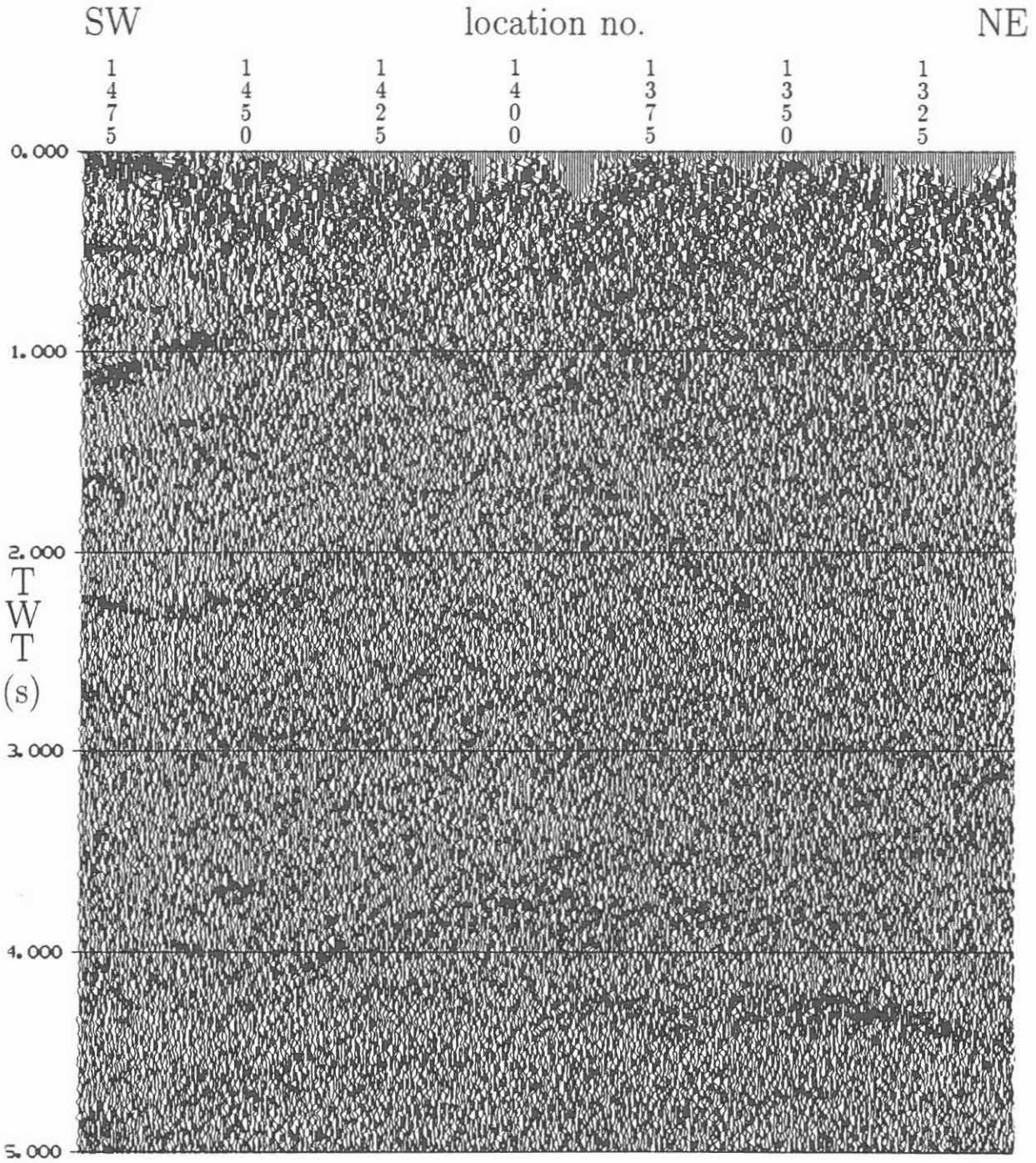
Figure 2: Part of line KTB 8502 crossing the 3D-survey. Coherency stack with 80-fold coverage. The horizontal scale is 1:100000.







**Figure 4:** Part of line KTB 8502 crossing the 3D-survey. Coherency stack with 15-fold coverage. The horizontal scale is 1:100 000.



**Figure 5:** Part of line KTB 8502 crossing the 3D-survey. Envelope stack with 15-fold coverage. The horizontal scale is 1:100000.

other or are adjacent in the duration of the signal cannot be resolved in such a stack, but it is possible to notice them.

- It is quite clear that such an envelope stack cannot replace a standard stack with phase information. But an interpretation made on the basis of an envelope stack will get all main structures. However the resolving of the events is not as high as in a normal stack. In this special case the reliability of the interpretation will be improved because it is a 3D-survey. Thus the interpretation must fit the data in the adjacent in- and crosslines. This will help to avoid severe misinterpretations.

After the proof of making sense to interpret such an envelope stack it is necessary to describe the considerations made for this interpretation.

The targets of this first interpretation have been the major events occurring in great parts of the area due to the nature of the envelope data. These events have been picked at the relative maximum of amplitude and not only in parts of the area where they show a very high absolute amplitude. So it has been tried to get a close interpretation of continuous events, because this has been necessary for the processing of the 3D-data. Therefore the interpretation of the inlines was transferred by its tie-points to the crosslines and reverse. So it was possible to reduce the scattering of the interpretation-picks between inlines and crosslines caused by the long duration of the signal of the envelope (30 – 70 ms). These tie-points can help to extend the interpretation to an area in which only very weak amplitudes occur, too. The interpretation has mainly been carried out in the in- and crosslines. The slices have been used to control the results of these interpretation, because a reflection of an undulating surface causes a smearing of the reflection in the slices. So the slices are not interpretable in a clear way.

### 3 Interpretation of the three-dimensional data

The interpretation of the survey, which has been done on a COMSEIS-system of Prakla-Seismos (now Geco-Prakla), included the results of the two-dimensional seismic lines DEKORP 4, KTB 8502 and KTB 8505, which cross the 3D-survey (for a sketch of the 3D-survey and these lines see Fig. 1). Further information on these lines can be found by Schmoll, et al. (1989).

It was necessary to do the interpretation in two blocks. The first block contains the crystalline area northeast of the Franconian Line, the second block is the area in the southwest covered with sediments. This division into two blocks is necessary because of the seismic pull-down effect caused by the sediments, which show a thickness of up to 3000 m. This effect of about 700 ms here can only be removed from the data by a depth migration, but at this time the data are still unmigrated and so the events underneath the sediments have to be considered separately.

Figures 6 to 8 show examples for the interpretation of the three-dimensional data. There are only some of the interpretations displayed to keep the clearness of the picture.

Figure 6 shows the inline 291 located almost in the center of the survey. The line is displayed in the direction SW – NE. In the sedimentary area the horizons A-1 (the lower one) and A-4 are marked. Underneath the sediments there are two horizons marked which

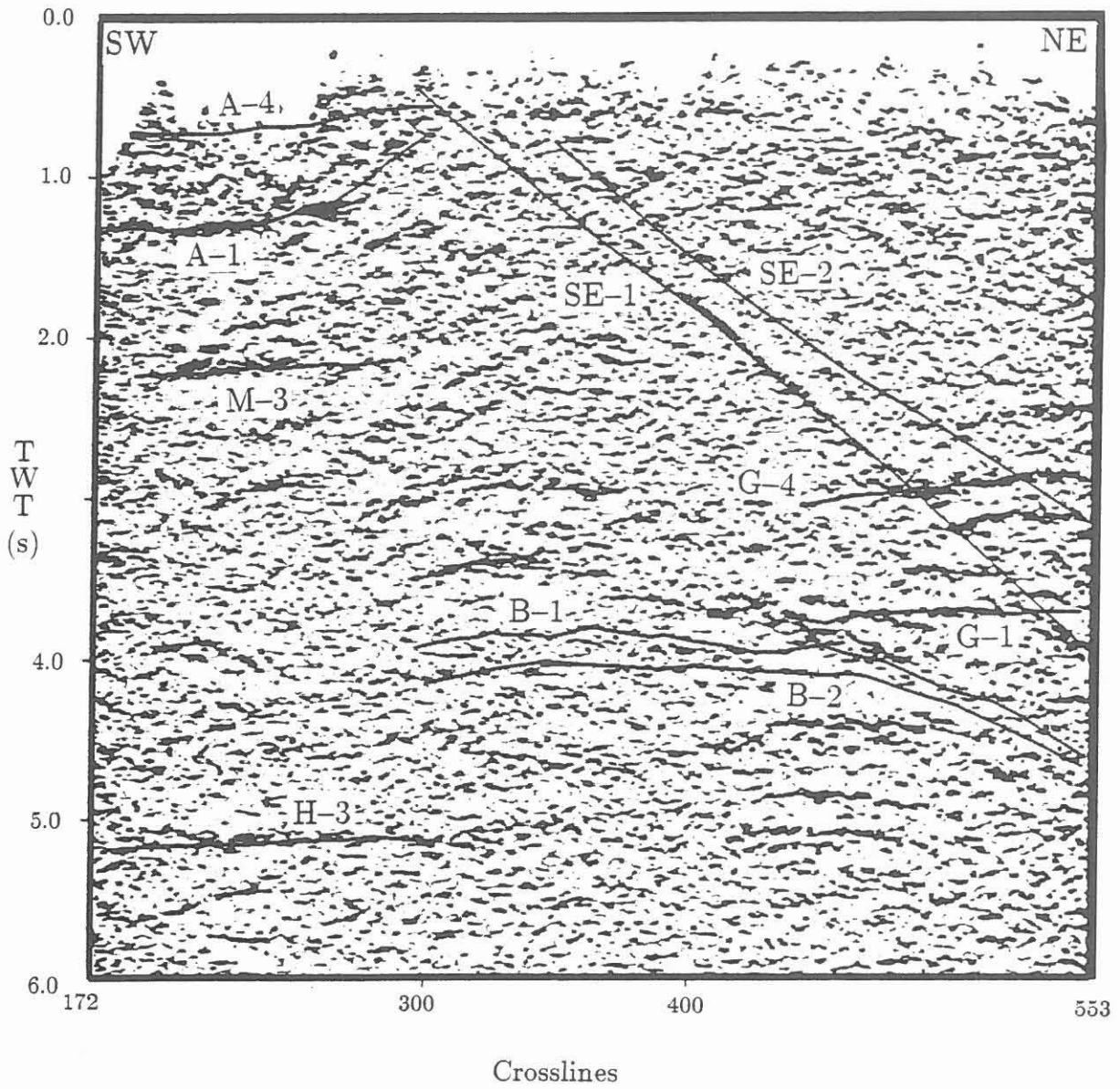
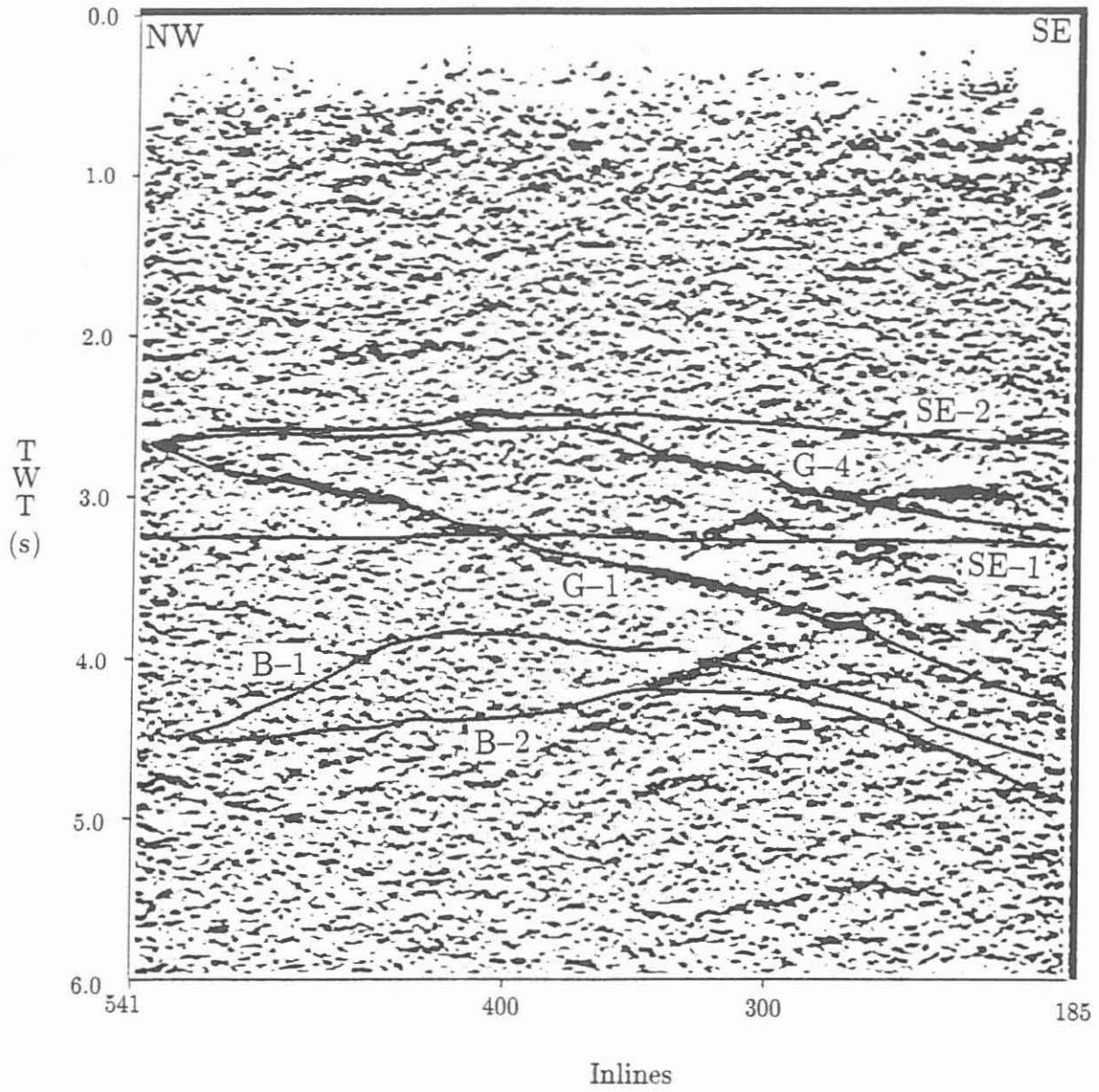
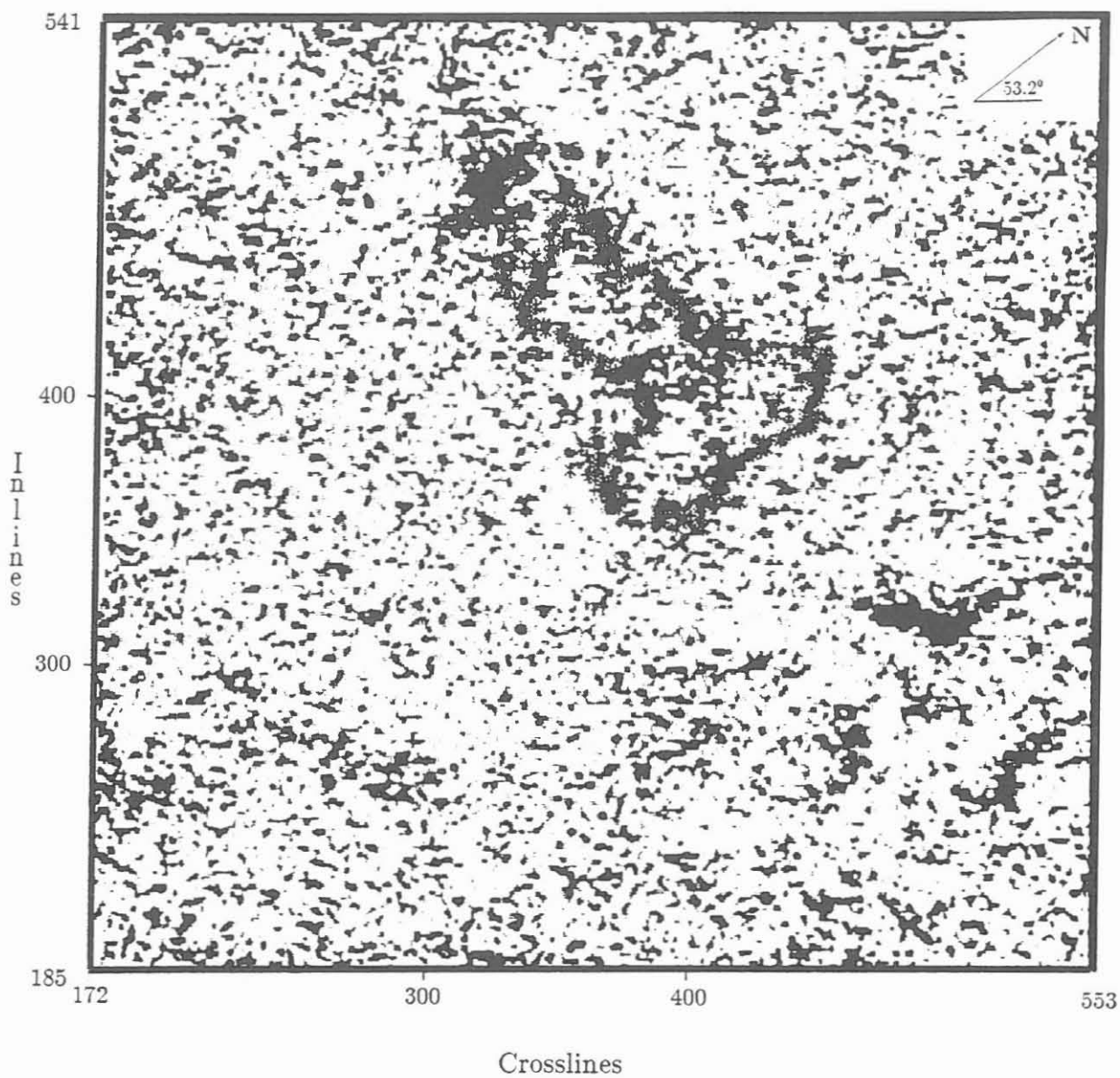


Figure 6: Inline 291 with some interpreted horizons marked (more details in the text).



**Figure 7:** Crossline 494 with some interpreted horizons marked (more details in the text).



**Figure 8:** Time slice at 3576 ms of the 3D-survey. The tie-points of horizon B-1 are displayed.

are each an example for a number of similar horizons. The upper one (M-3) belongs to a group of southeast dipping elements which can be detected only underneath the sediments. The lower one (H-3) is one of three horizons which occur almost horizontally in the area of 5 s TWT. The connection with the horizons in the crystalline part of the survey area is not clear, yet.

In the part northeast of the Franconian Line there are two steep dipping elements (SE-1, SE-2) marked. They are the lower and upper bound of a bundle of similar elements. Besides these horizons the elements B-1, B-2, G-1 and G-4 are marked. These horizons will be described and explained below.

In Figure 7 the crossline 494 located at the northeastern edge of the survey is displayed in NW -SE direction . In this crossline the same elements are marked as in the inline as far as they can be seen here. The rhomboid structure formed by the horizons G-1 and G-4 can be seen clearly. This picture gives an impression of the complexity of the interpretation work which has to be done on this data. The complexity is mainly caused by a number of crossing elements especially the SE-horizons.

The 3576 ms slice displayed in Figure 8 has been used to control the interpretation done in the in- and crosslines. This controlling has been done with the tie-points which are displayed for horizon B-1 in this Figure. The horizon with the shape of a pear can be detected in the northwestern part of the survey area. But it can also be seen that there is no clear and sharp signal which can be interpreted in an unambiguous way.

The results of the preliminary interpretation can be summarized in five main groups:

- The first group consists of steeply dipping events with a true dip up to 65 degrees to northeast. These events, which have partially a parallel, partially a split structure (s. Fig. 6), are named SE (steep event)-1, SE-2, SE-3 and SE-5. The origin of those reflections may be overthrust planes, which reach the surface in the area of the Franconian Line.
- The second group contains two slightly curved, almost parallel major events and a diffraction like event in the time range 3.5 - 5.0 s TWT. These reflections seems to be continuous in the envelope stack, but there are severe hints that these events consist of a number of overlapping diffractions. This can be caused by a very rough or broken surface of a body. The elements of this group are named B-1, B-2 and R-1.
- The third group consists of five reflections interpretable in block C in the time range 2.5 - 4.0 s TWT. These reflections are well known as the rhomboid structure named Erbendorf body in the two-dimensional line KTB 8505 (Schmoll, et al., 1989). These reflections are named G-1 to G-5.
- The fourth group is composed of the reflections of the sediments in the southwest. In the envelope stack five horizons named A-1 to A-5 are interpretable.
- The events underneath the sediments form the fifth group. In the envelope stack it is quite difficult to decide which one is a multiple of the sediments and which one is a true reflection. It is quite difficult to interpret the connection of these events with the events in the crystalline block, too. So these events are not interpreted clearly,



yet. There is the need for a normal stack with the informations on the phase of the signals.

Besides these five groups there are many small reflections and remarkable diffraction like events, which can be interpreted only in some parts of the area.

Some remarkable reflections shall be described in more detail in the following. The Figures 9 to 15 display the orientation in space of these events.

**SE-1:** It is a steeply northeast-dipping event with a partially split structure, which is recognizable only in the normal stack. This event shows a very poor amplitude in the northeastern part of the survey area. In contrast there are strong amplitudes in the near surrounding of the KTB well. In the area of block D (s. Fig. 1) it is quite difficult to detect this event. The extrapolated outcrops of this structure will be some ten meters west of the Franconian Line. The true dip varies between 40 and 65 degrees. The reflection SE-1 seems to be the lower boundary of a bundle of events steeply dipping to northeast. The KTB well will hit this structure as a zone of fractures. A so called "flying carpet" of horizon SE-1 is displayed in Figure 9.

**SE-2:** This event (Fig. 10) is a steep dipping event, too. It belongs to the above mentioned bundle of steep events and it seems to be the upper boundary of it. The reflection shows strong amplitudes mainly in the northwestern part of the survey area. The dip of this event is some degrees lower than that of SE-1. The extrapolated outcrops of this structure will be some ten meters east of the Franconian Line. The KTB well will hit this reflection as a zone of fractures, too.

**SE-3:** At about 900 ms TWT this event (Fig. 11) splits off from reflection SE-1. Because of this its dip is lower than that of SE-1. The reflection can be seen in the whole survey only fragmentarily. The KTB well will hit this structure, but it will be very difficult to identify this structure in the borehole beneath a number of similar zones of fractures in that depth.

**B-1:** It is a curved diffraction-like event between 3.5 and 4.5 s TWT. This event is interpretable in the whole survey area. The undulations, which are recognizable in the three-dimensional display of the horizon (Fig. 12), lead to the presumption that this is not a continuous reflection. It seems that there are broken reflectors, which occur in the seismic section mainly as diffractions. Thus the interpretation of this event can be understood as an envelope of some single events located at a surface. The structure will be hit, if the KTB well can be deepened down to 11 km depth.

**B-2:** This event is quite similar to event B-1 (Fig. 13). It is located deeper than B-1. It seems to be possible that both events have the same origin because of their almost parallel course. Event B-1 can be the upper boundary and event B-2 can be the lower boundary of a very rough or broken body. It seems to be doubtful if the KTB well will be able to reach this lower boundary B-2 because of the greater depth.

- G-1:** This event is the lower boundary of a zone of high reflectivity, which occurs in the northeast of the survey area. It is quite possible that this event will continue in block B, but at the moment it can only be said for sure that it occurs in block C. Its prolongation into Block B can only be decided by the knowledge of the standard stack that means by the knowledge of the phase informations. This event dominates together with reflection G-4 in this zone.
- G-4:** This upper boundary of the zone with high reflectivity converges with the reflection G-1 in the northeast of the survey area. So this event intercepts the horizons G-2 and G-3 (s. Fig. 7). The rhomboid structure formed by the reflections G-1 and G-4 can be seen in Figure 14. In the two-dimensional seismic line KTB 8505 this structure is called Erbandorf body (Schmoll, et al., 1989). The seismic wide-angle measurements yielded to the result that this structure is a high velocity zone (Gebrande, et al., 1990).
- A-1:** The reflection A-1 (Fig. 15) is, from the actual state of the interpretation, the deepest reflection horizon of the sediments in the southwest of the survey area. The horizon shows a flat syncline, which traces in the higher horizons. The interface shows a dragging in the direction of the Franconian Line. It seems that the interface is broken because of that dragging, but this can only be decided in a standard stack, because fault zones are not recognizable in the envelope stack for sure.

The depth of the interpreted events can only be evaluated by a migration of the data or by a map migration of the interpreted horizons due to the very steep dips. Up to now the only migration which exist is a map migration of some selected reflections (Stiller and Tormann (1992) and Wiederhold (1992), this volume).

## 4 Conclusion

There are some major reflections in the three-dimensional survey of great importance for the structural image of the subsurface. The most problematic reflections are the steeply dipping reflections, because the true orientation in space of this events is very sensitive to the velocity model deduced for this area due to their steep dip. So there is the need for very careful investigations on the velocity model. It is also quite necessary to get a migrated data set to maintain more knowledge of the homogeneity of reflections cut by the steeply dipping overthrust planes (SE-\*) (Hirschmann (1992), this volume). But it seems to be sure that some structural elements of that area cannot be reached by the KTB well. It will be difficult to integrate the interpretation into the results of the drilling, because these results show a lot of small fracture zones, which cannot be resolved by the envelope stack. A preliminary interpretation and a comparison of well data, lithology and seismic results is given by Hirschmann (this volume).

The results of the two-dimensional seismic lines could be corroborated, especially the rhomboid structure named Erbandorf body. But to achieve a resolution like the interpretations of these two-dimensional lines it is necessary to prepare a stack which shows all

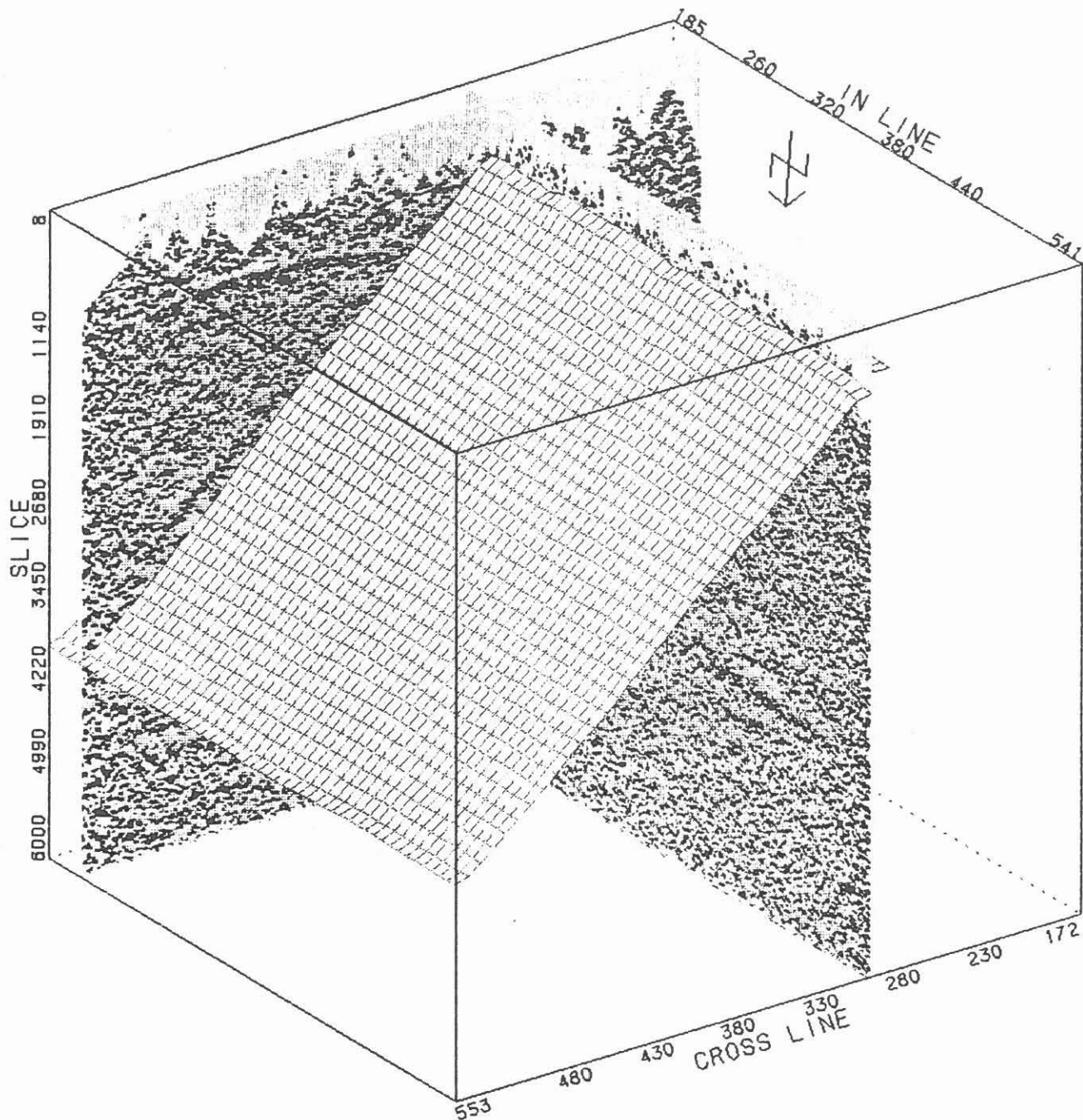


Figure 9: Horizon SE-1 displayed as a "flying carpet". The displayed data belongs to inline 210 and crossline 300. The line of sight is from the north.

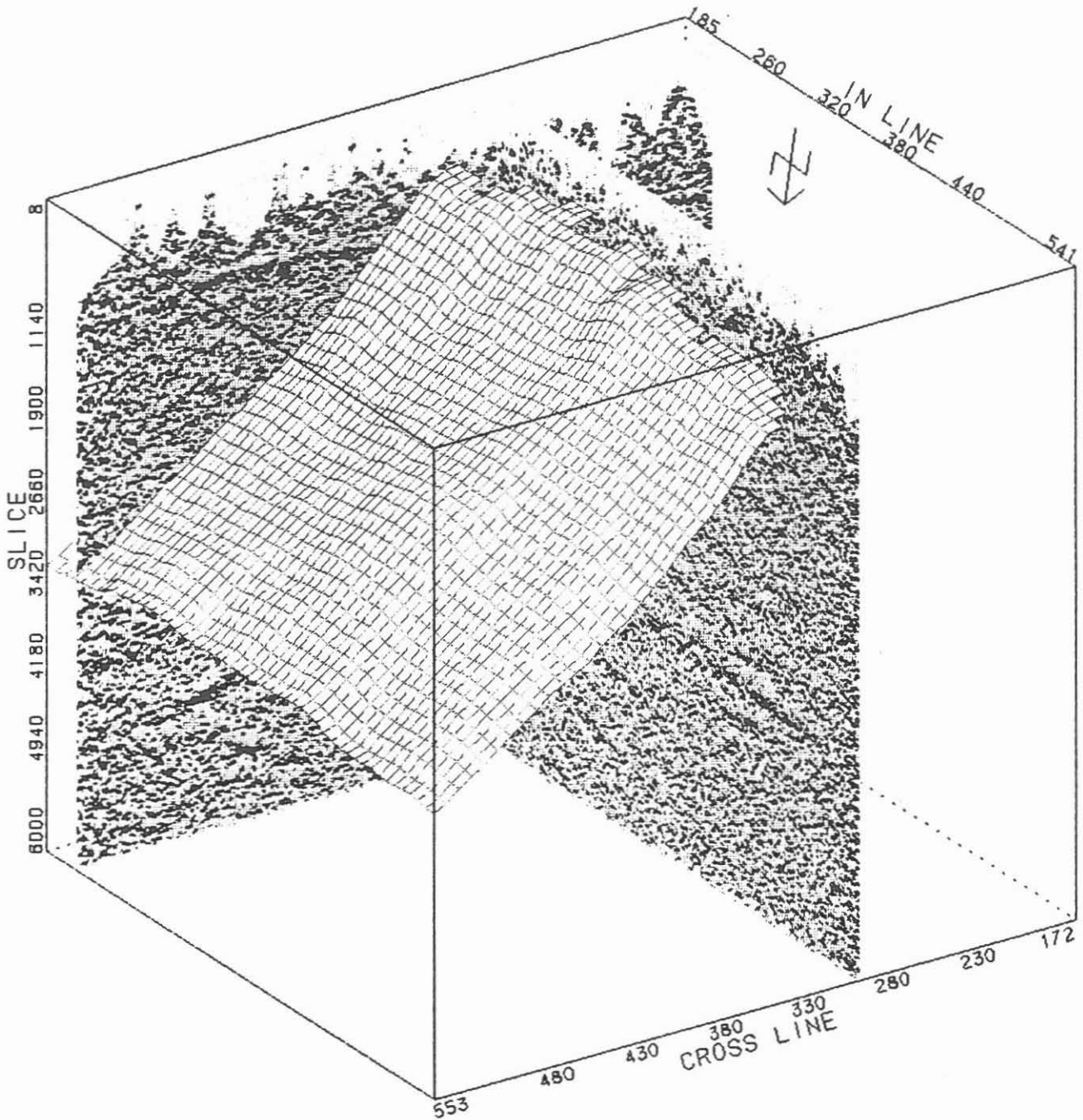


Figure 10: Horizon SE-2 displayed as a "flying carpet". The depicted data belongs to inline 210 and crossline 300. The direction of view is from the north.

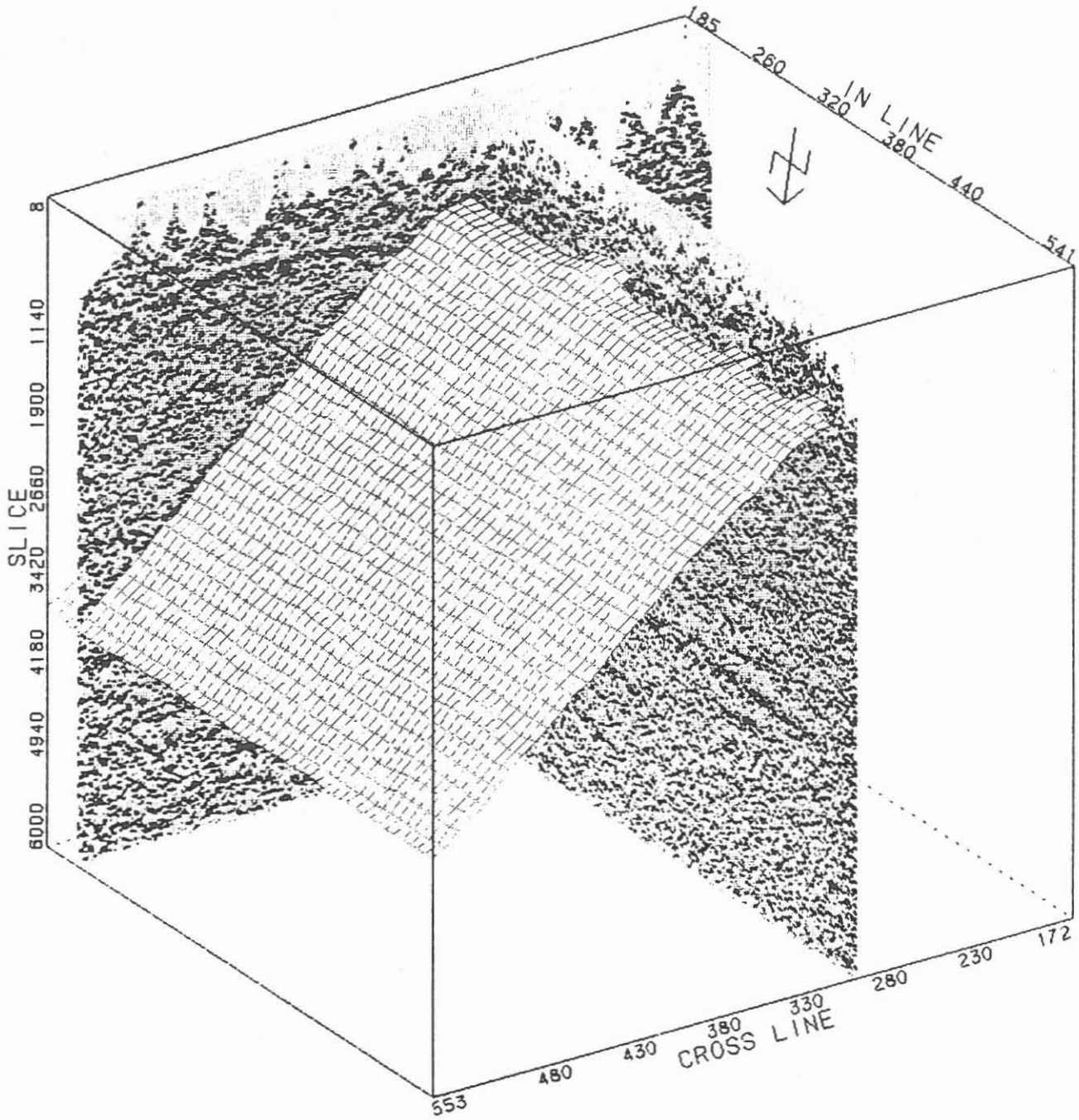
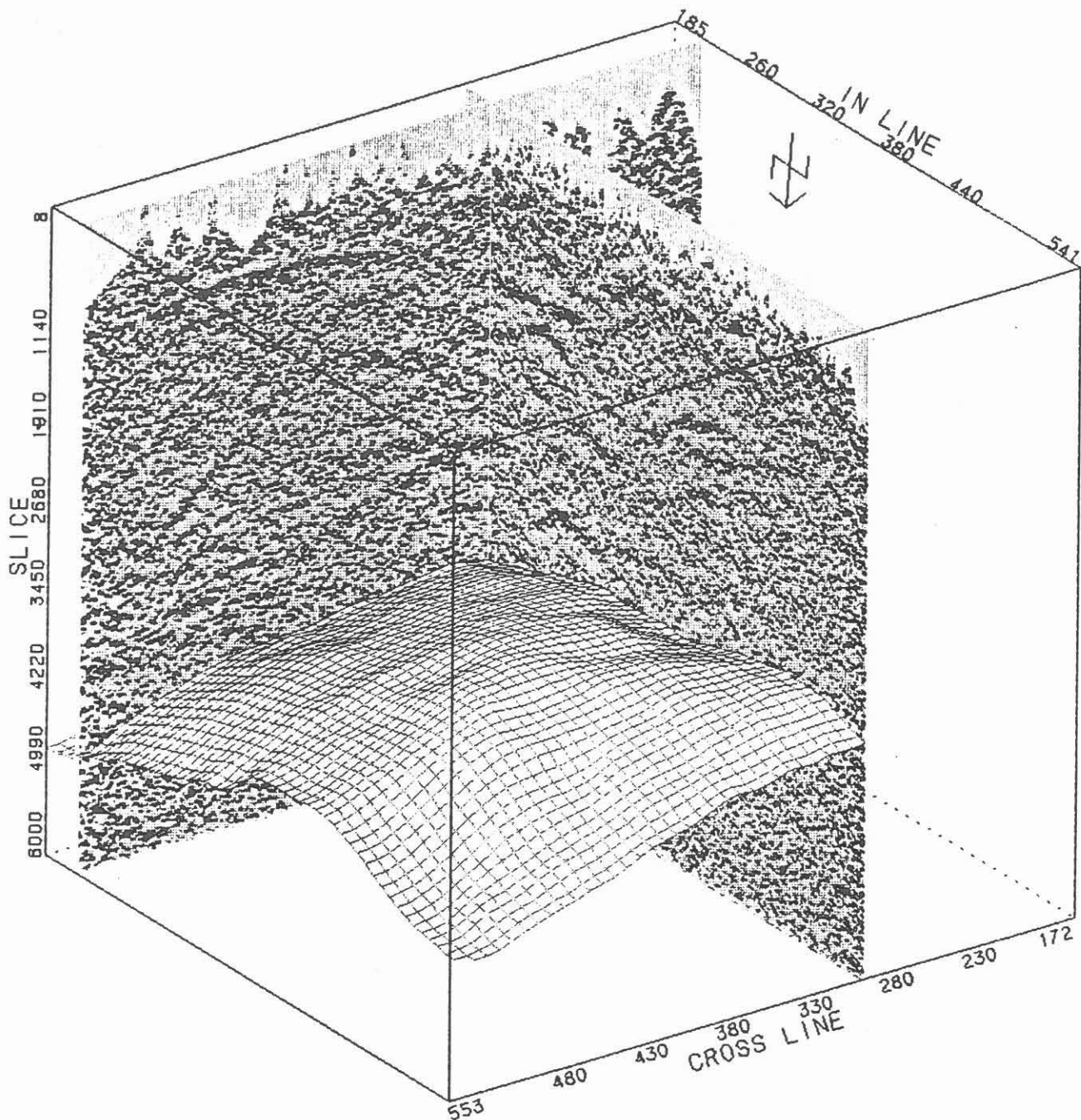


Figure 11: Horizon SE-3 displayed as a "flying carpet". The depicted data belongs to inline 210 and crossline 300. The data is viewed from the north.



**Figure 12:** Horizon B-1 displayed as a "flying carpet". The depicted data belongs to inline 210 and crossline 300. The direction of view is from the north.

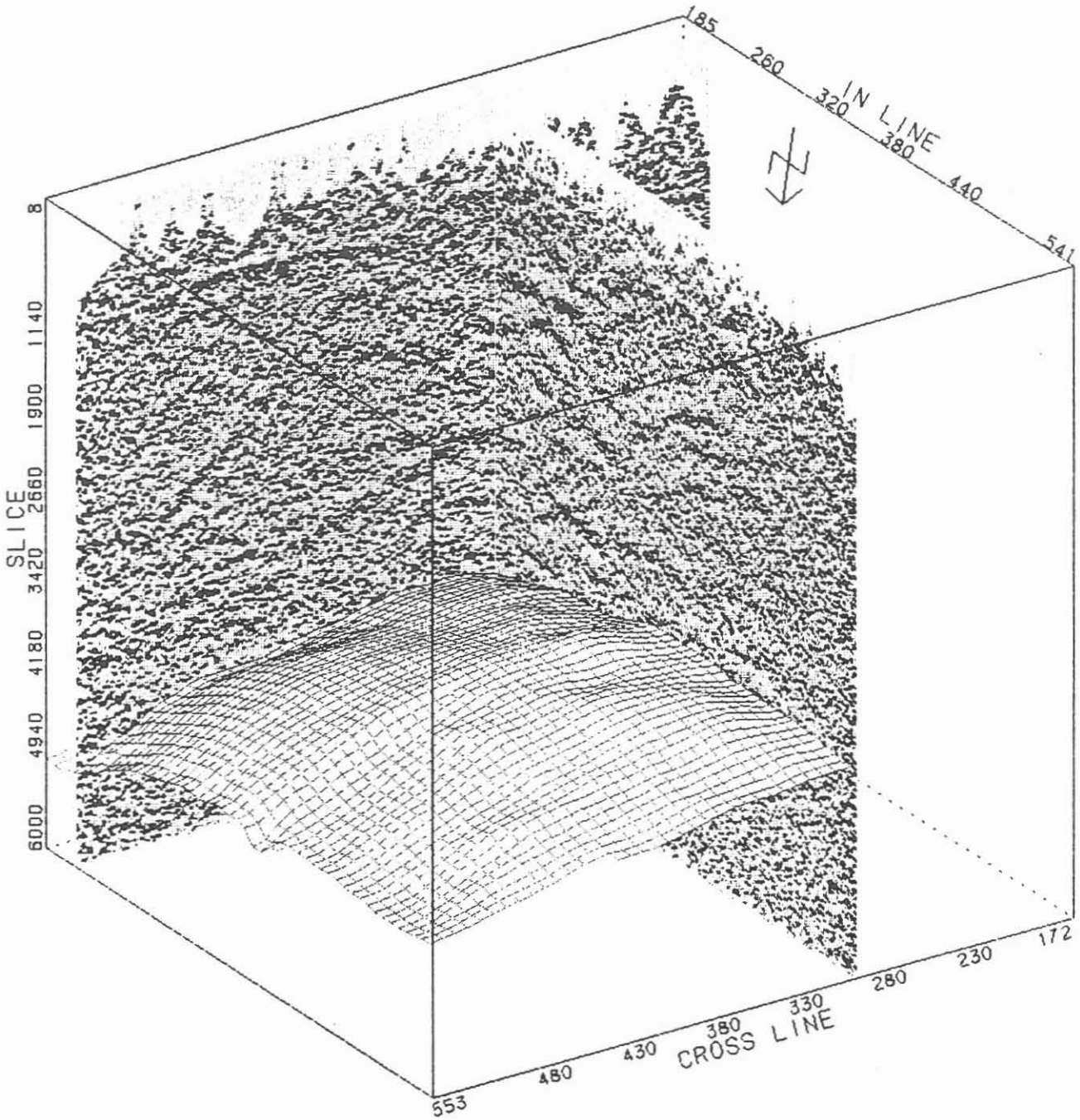
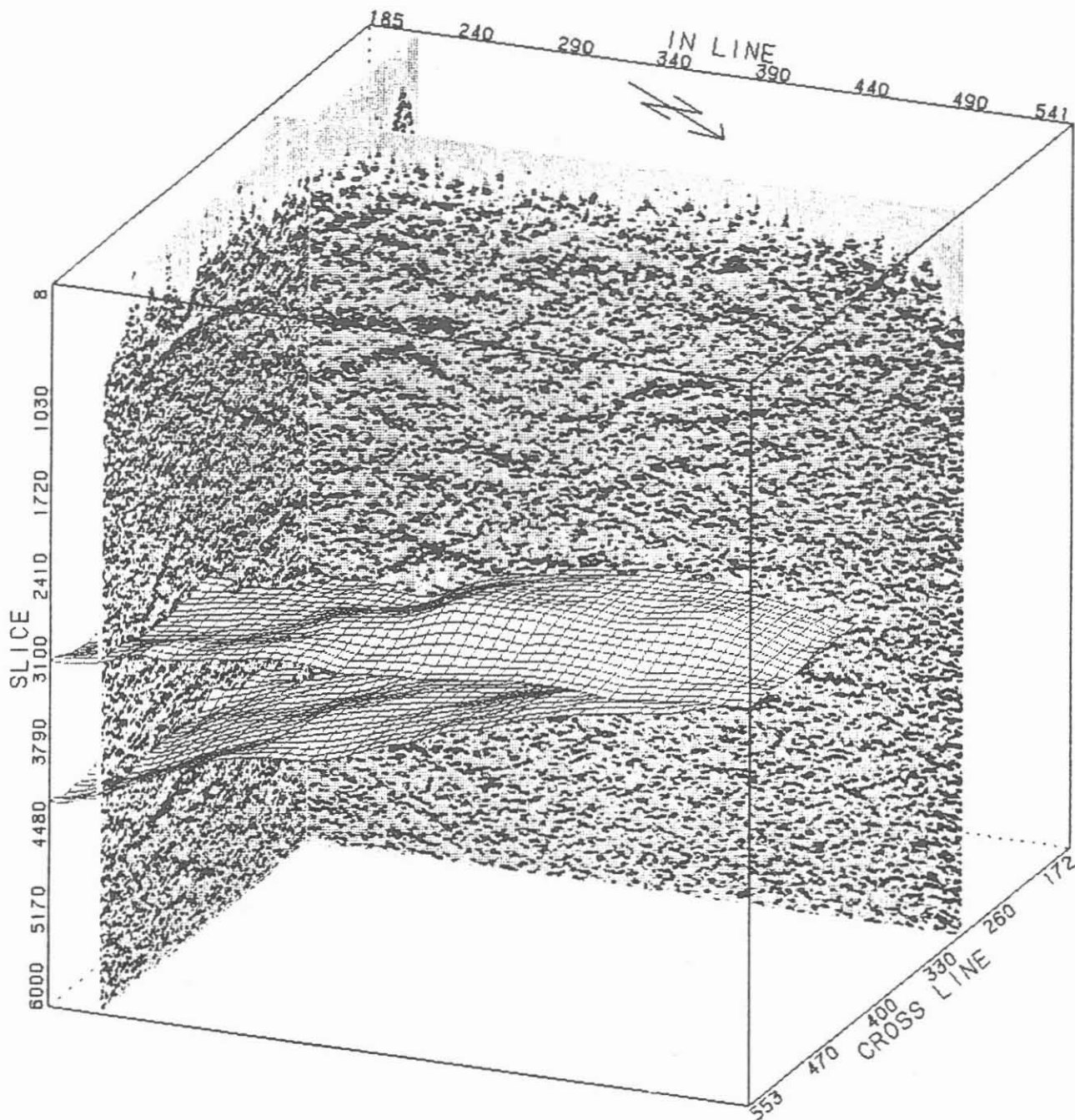
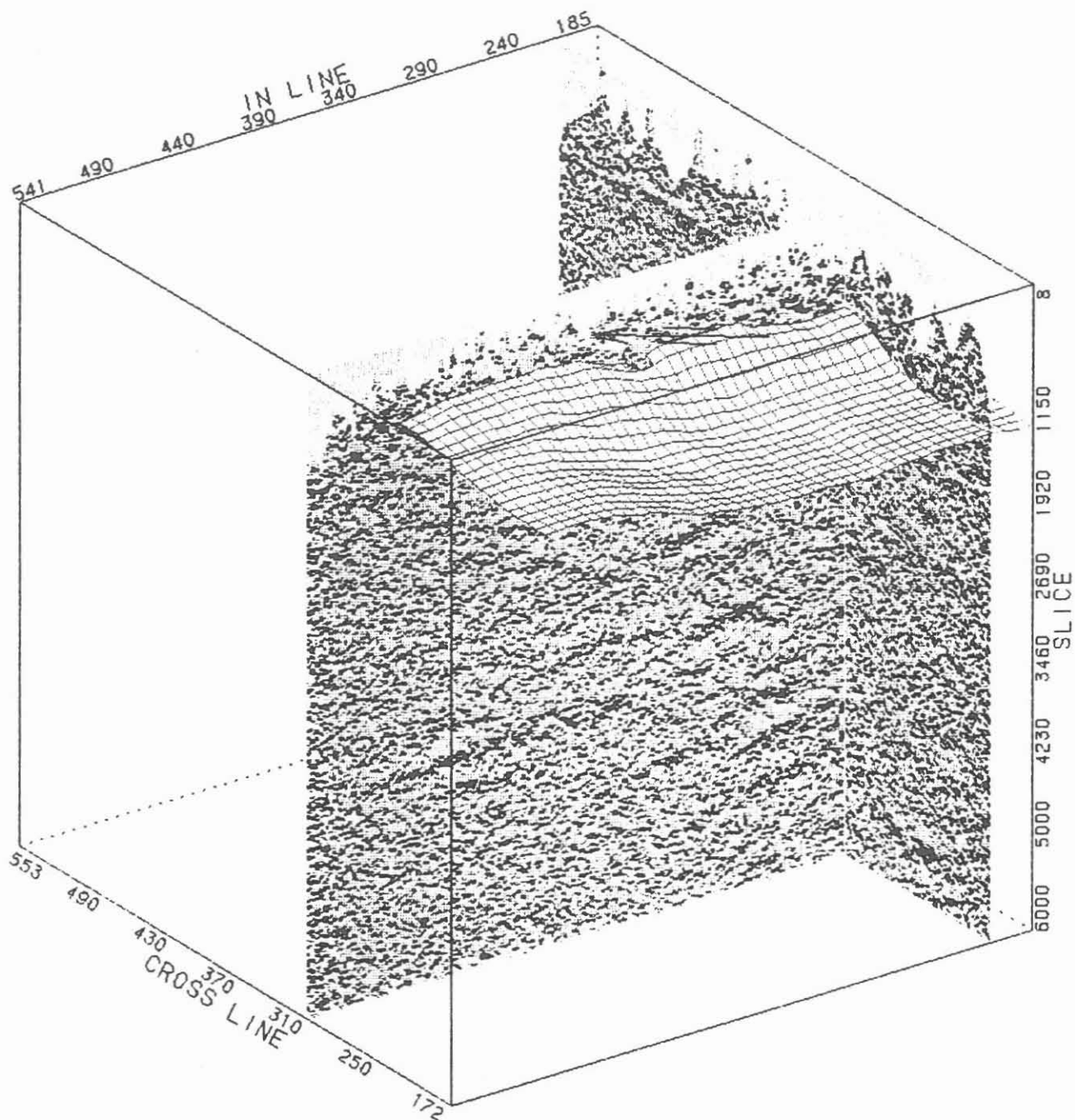


Figure 13: Horizon B-2 displayed as a "flying carpet". The depicted data belongs to inline 210 and crossline 300. The line of sight is from the north.



**Figure 14:** The horizons G-1 (the lower one) and G-4 both displayed as a "flying carpet". The depicted data belongs to inline 210 and crossline 300. The data is viewed from NNE.





**Figure 15:** Horizon A-1 displayed as a "flying carpet". The depicted data belongs to inline 210 and crossline 300. The direction of view is from the west.

events and has in addition the information of phase. To reach that aim this preliminary interpretation can help in some way, because of the horizon orientated velocity description in the three-dimensional data processing. If there will be a better stack all interpretation must be revisited and maybe changed.

## Literature

- Gebrande, H., Bopp, M., Meichelböck, M., Neurieder, P.** , 1990: 3D Wide-Angle Investigations in the KTB Surroundings as Part of the "Integrated Seismics Oberpfalz 1989 (ISO 89)". In: Dürbaum, H.-J., Reichert, C., Bram, K. (eds): KTB Report 90-6b, DEKORP Report, Integrated Seismics Oberpfalz 1989, NLfB, Hannover.
- Hirschmann, G.** , 1992, On the Geological Interpretation of the 3D-Seismic Data with Special Regard to the Informations from the KTB Boreholes. In: KTB Report 92-5 DEKORP Report, this volume.
- Körbe, M., Reichert, C.** , 1992, On the Character of "Steep Event SE-1" — Reflected Energy, Reflected Refraction, Diffraction or any Artifact. In: KTB Report 92-5, DEKORP Report, this volume.
- Rehling, J., Stiller, M.** , 1990, 3D Reflection Seismic Survey of the Area around the KTB Drilling Site., In: Dürbaum, H.-J., Reichert, C., Bram, K. (eds): KTB Report 90-6b, DEKORP Report, Integrated Seismics Oberpfalz 1989, NLfB, Hannover.
- Schmoll, J., Bittner, R., Dürbaum, H.-J., Heinrichs, T., Meißner, R., Reichert, C., Rühl, T., Wiederhold, H.**, 1989: Oberpfalz Deep Seismic Reflection Survey and Velocity Studies. In: Emmermann, R., Wohlenberg, J. (eds): The German Continental Depp Drilling Program (KTB). Springer, Heidelberg.
- Stiller, M.** , 1992, Preliminary Generation of a Stacked Data Volume of the Entire ISO 89 3D-Reflection Data Set Using an Envelope Technique. In: KTB Report 92-5, DEKORP Report, this volume.
- Stiller, M., Tormann, M.** , 1992, Application of a Simplified Horizon Migration Process on the Data of 3D-Seismics ISO 89. In: KTB Report 92-5, DEKORP Report, this volume.
- Wiederhold, H.** , 1992, Interpretation of Envelope-Stacked 3D-Seismic Data and its Migration — Another Approach. In: KTB Report 92-5, DEKORP Report, this volume.

Application of a simplified horizon migration process to the data  
of the 3D-seismics ISO'89

Manfred Stiller, Martin Tormann<sup>1</sup>

Abstract

For several reasons the ISO'89 3D-seismic data are at hand not as conventional, phase-consistent stack so far but as 'envelope stack' only. Therefore, the common wave-field migration procedures cannot be applied to attain information on the spatially correct position of the particular reflector elements. To cope with this problem a simplified 3D-horizon migration program was developed at the DEKORP Processing Center Clausthal. It allows to migrate not the seismic traces of the ISO'89-3D survey themselves but the traveltimes values for specific horizons derived by interactive picking with a 3D-seismic interpretation system on the basis of an envelope stack. The motivation, the basic assumptions and the principles of this procedure are outlined as well as the mathematical background and the particular processing steps. The migration results of some selected key horizons in the area of the KTB are depicted by isochrone maps and 3D-views. By this, a preliminary geological interpretation based upon the true position and shape of several detected seismic surfaces is enabled although the final processing, i. e. a phase-consistent stack of the entire 3D-dataset (and its subsequent wave-field migration), has not been finished yet.

Problem

For a reliable geological interpretation of seismic data it is indispensable to transform the traveltimes information of the stacked zero-offset data into a migrated depth version which should represent a true image of the surveyed subsurface structures as much as possible. Since the process of seismic migration, realized by solving the plane wave equation, requires quite large computer run times, it is commonly carried out only once, i. e. after finishing all other processing steps with final

---

<sup>1</sup> Authors' address: DEKORP Processing Center, Inst.f.Geophys.d.  
TU CLZ, Arnold-Sommerfeld-Str.1, 3392 Clausthal-Zfd., Germany

parameters. If this particular final processing is already very time-consuming, e. g. handling a large 3D-survey, it is considered very helpful to attain a migrated image of particular horizons already at an earlier stage to enable a preliminary geological interpretation. This is possible by migrating the picked horizon time field instead of the original seismic traces. As described in another contribution of this volume (Stiller, this volume) the conventional 3D-processing scheme, approved in sedimentary areas, failed in the complicated crystalline area surrounding the KTB drill site where extremely steep dips and a considerable amount of anisotropy dominate. Therefore, the first and up to now only stack of the whole ISO'89-3D seismic data set of sufficient quality was based on an envelope stacking technique which avoids destructive stacking by summing up only positive amplitudes. It offers, however, an evidently poorer time resolution combined with a complete loss of the phase information. Since it does not represent the complete wave field, the common migration procedures such as Finite differences-, Frequency-wavenumber-, or Kirchhoff summation method are not applicable. A migration method which nevertheless allows a rough estimation of the true spatial position of particular horizons already in the present processing stage has only to fulfill the following basic conditions:

- use of picked horizon times instead of the original seismic traces
- full 3D-ability and exact treatment of extreme horizon dips
- acceptable processing times and compatibility to existing data formats (SSL processing system, COMSEIS interpretation system).

Considering the aim of a merely rough imaging of the shape and spatial position of a few important key horizons as well as the relatively poor velocity contrasts in a crystalline area the simplification of a constant velocity model down to the respective horizon, i.e. the neglecting of refraction, seems to be adequate.

#### Method

A software package which is able to transform unmigrated travel-time surfaces into migrated horizon surfaces, according to the conditions mentioned above, was developed, implemented and successfully tested at the DEKORP Processing Center Clausthal. The principles and the proceeding will be described more detailed in the following:

Starting point is the horizon-oriented picking process of travel-times with the aid of the interactive seismic interpretation system COMSEIS based on the ISO'89 3D-envelope stack. From these irregularly distributed time picks (on average each 10th bin in each cross- and inline section has been evaluated for each of the horizons detected so far) closed travelttime planes are to be constructed by spatial interpolation. For that, several processes of input data reduction beforehand and horizon smoothing afterwards are necessary to avoid excessive local dips due to picking inaccuracies between adjacent bins. Moreover, small-scale effects are suppressed by this which cannot be imaged at all according to the low resolution of the envelope method.

Bin ranges with insufficient density of input picks or doubtfully inter- or extrapolated time values may adulterate the migration results for bin ranges of ensured horizon interpretation severely. Thus, it is recommendable in any case to edit (and disregard) the former ones before the migration is applied.

If a horizon surface is given by time picks within a closed XY-bin area the instantaneous apparent dip  $dt/ds$  follows immediately by amount and direction for each bin. After selection of a suitable migration velocity the local true horizon dip can be calculated (see Fig. 1 and Table 1 for nomenclature) by

$$\frac{dr}{ds} = \frac{v}{2} \frac{dt}{ds} = \sin \alpha$$

The dip angle  $\alpha$  appears again as  $\sin \alpha = S_{mig}/r_{mig} = S_{mig}/(v t/2)$ . Hence, the horizontal shift during migration is

$$S_{mig} = v \frac{t}{2} \left( \frac{dt}{ds} \frac{v}{2} \right)$$

The horizon depth after migration follows from  $\cos \alpha = z_{mig}/r_{mig}$ , and with  $z_{mig} = (v/2) t_{mig}$  the migrated travelttime is

$$t_{mig} = t \sqrt{1 - \left( \frac{dt}{ds} \frac{v}{2} \right)^2}$$

$$\frac{dt}{ds} \frac{v}{2} = \frac{dr}{ds} = \sin \alpha$$

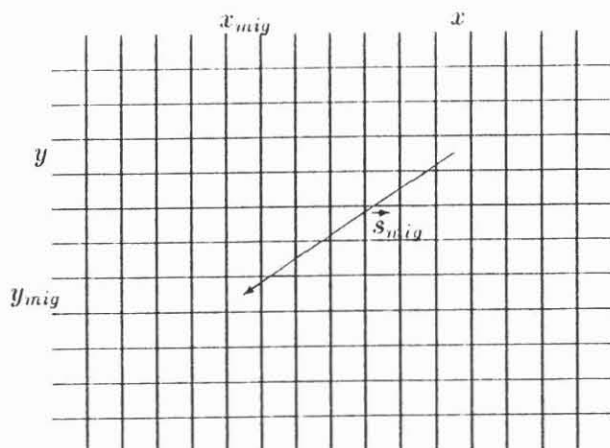
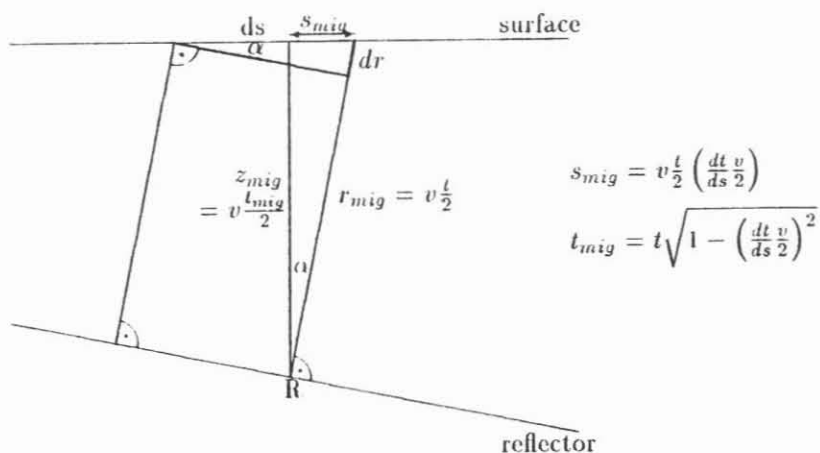


Fig. 1: Coordinate system and basic formulae for the horizon migration algorithm. Top: vertical plane along  $\vec{s}_{mig}$ , bottom: horizontal plane containing  $\vec{s}_{mig}$ .

TABLE 1: Nomenclature for the migration formulae

t:	zero offset twoway travelttime
v:	migration velocity
$\alpha$ :	true dip angle against surface
dt:	time interval
dr:	distance interval along zero offset ray
ds:	distance interval along surface (in dip direction)
$r_{mig}$ :	distance to reflector along zero offset ray
$s_{mig}$ :	horizontal distance to reflection point
$z_{mig}$ :	vertical distance to reflection point
$t_{mig}$ :	migrated travelttime (TWT)

The direction of the true dip is identical with the direction of the apparent dip. With this relation now all parameters are known to find a migrated traveltime and a corresponding new XY-bin for every horizon traveltime pick of each CMP-bin.

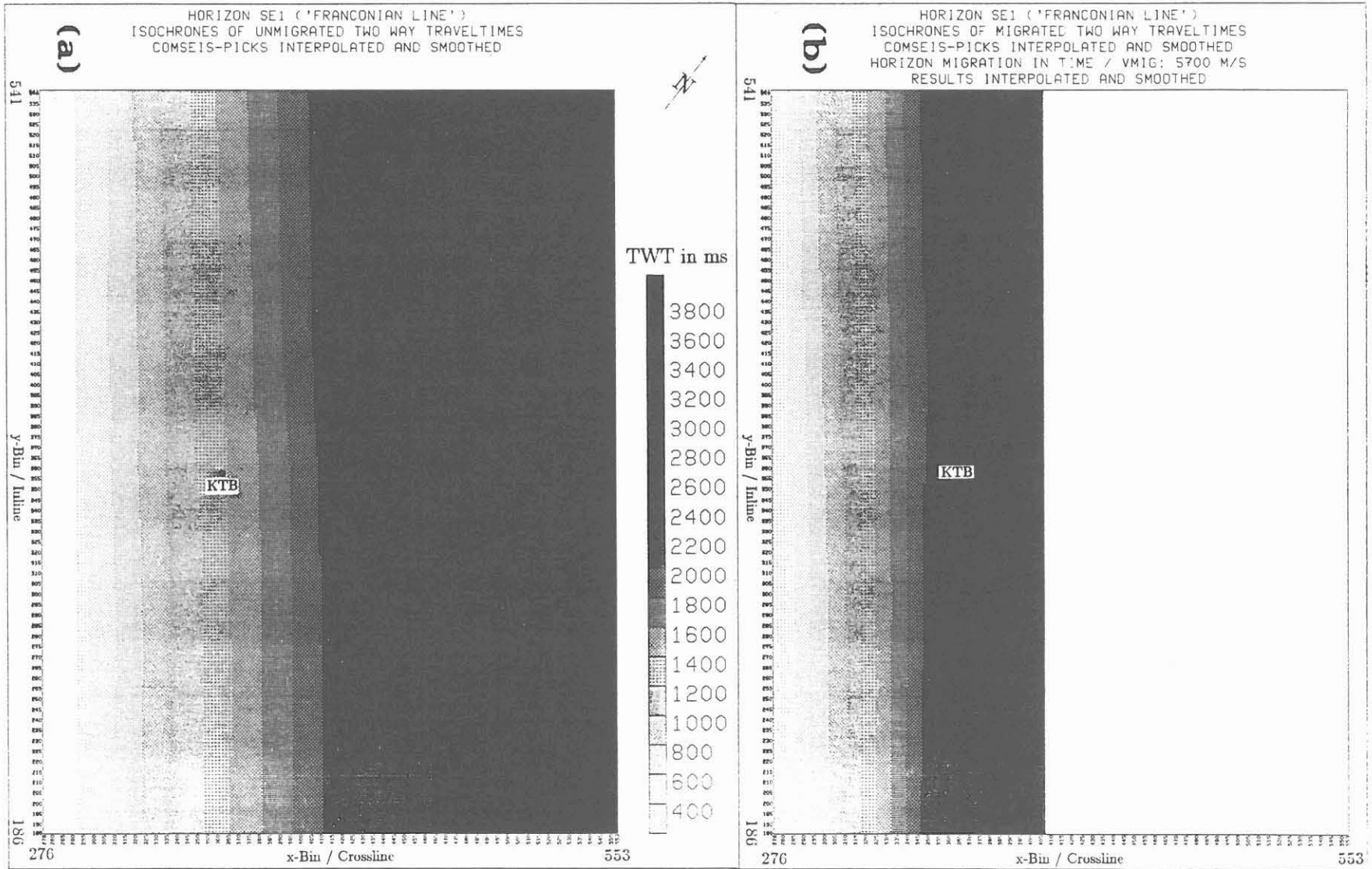
Often, however, more than one migrated point fall into the same bin, e. g. when diffractions or steep dips are encountered. In practice, they will not have necessarily the same migrated traveltime, then. For these cases an average time value, weighted with the migration shift, is advisable to be used. Especially if the picked horizon surface lacks planarity, the migrated points may strongly scatter within the bin area. After migration it is therefore necessary to perform again a spatial interpolation with similar parameters as for the unmigrated points to obtain a closed, migrated horizon surface again. Of course, it has to be taken care that only ranges which are verified by a sufficient density of migrated points may be used to construct the migrated horizon plane. In addition, uncertain migration ranges, e. g. margins, are to be disregarded.

## Results

Finally, some of the migration results obtained so far are presented as isoline maps and 3D-views. Concerning the nomenclature and description of the particular horizons it is referred to another contribution in this volume (Hluchy et al., this volume). The presentation is restricted to the part east of the Franconian Line (FL) only. On each figure the exact position of the KTB is marked by a thick black dot. After an appropriate editing, only those parts of the horizon surfaces are left which comprise reliably picked or migrated data.

Figure 2a shows isochrones for the SE1 horizon approaching the surface close the FL. The data are based on unmigrated two-way traveltimes (TWT) picked interactively by the aid of a 3D-seismic interpretation system (COMSEIS) and interpolated to form a continuous horizon surface. The display is given in variable grey density shading. Figure 2b shows the same target after application of the horizon migration with a constant velocity of 5700 m/s. As expected the dip becomes much steeper and, finally, shows nearly doubled depth values compared to the unmigrated version. Figure 3 gives a 3D-perspective view of the SE1 horizon before and after migration.

Fig. 2: Isochrone maps of the SE1 horizon (variable grey density).  
 (a) unmigrated and (b) migrated TWT.





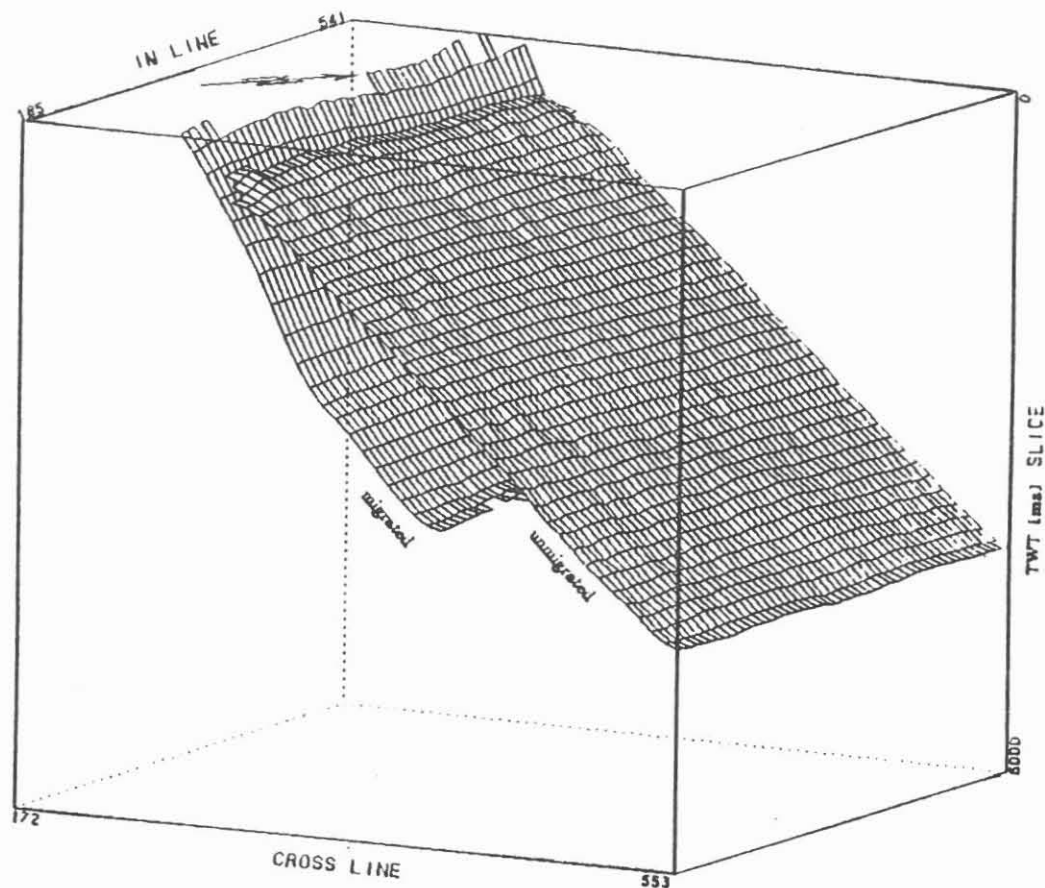


Fig. 3: Perspective view of the SE1 horizon before and after horizon migration.

A similar situation is encountered regarding the even steeper, north dipping SE4 horizon approximately approaching the Fichtelnaab Fault in its western part and the boundary between the Falkenberger and Friedenfelser Granite in its eastern part. Figure 4a and b show the unmigrated and migrated TWT isoline maps ( $v_{mig} = 5000$  m/s).

The B1 horizon is ascribed to the top range of the Erbdorf reflectivity zone (Fig. 5a and b). Its domed structure appearing in the unmigrated TWT distribution is contracted towards the center after migration ( $v_{mig} = 6000$  m/s).

The R1 horizon in the range of the Erbdorf reflectivity zone appears like an image of a point-like diffractor in the unmigrated isochrone map (Fig. 6a). After migration, however, it does not form a small-scaled diffraction element as expected, but a clearly synformal structure (Fig. 6b). This situation does not change even if the migration velocity of 5000 m/s is varied within larger limits. Thus, a diffraction can be excluded rather definitely.

Fig. 4: Isochrone maps of the SE4 horizon (variable grey density).  
(a) unmigrated and (b) migrated TWT.

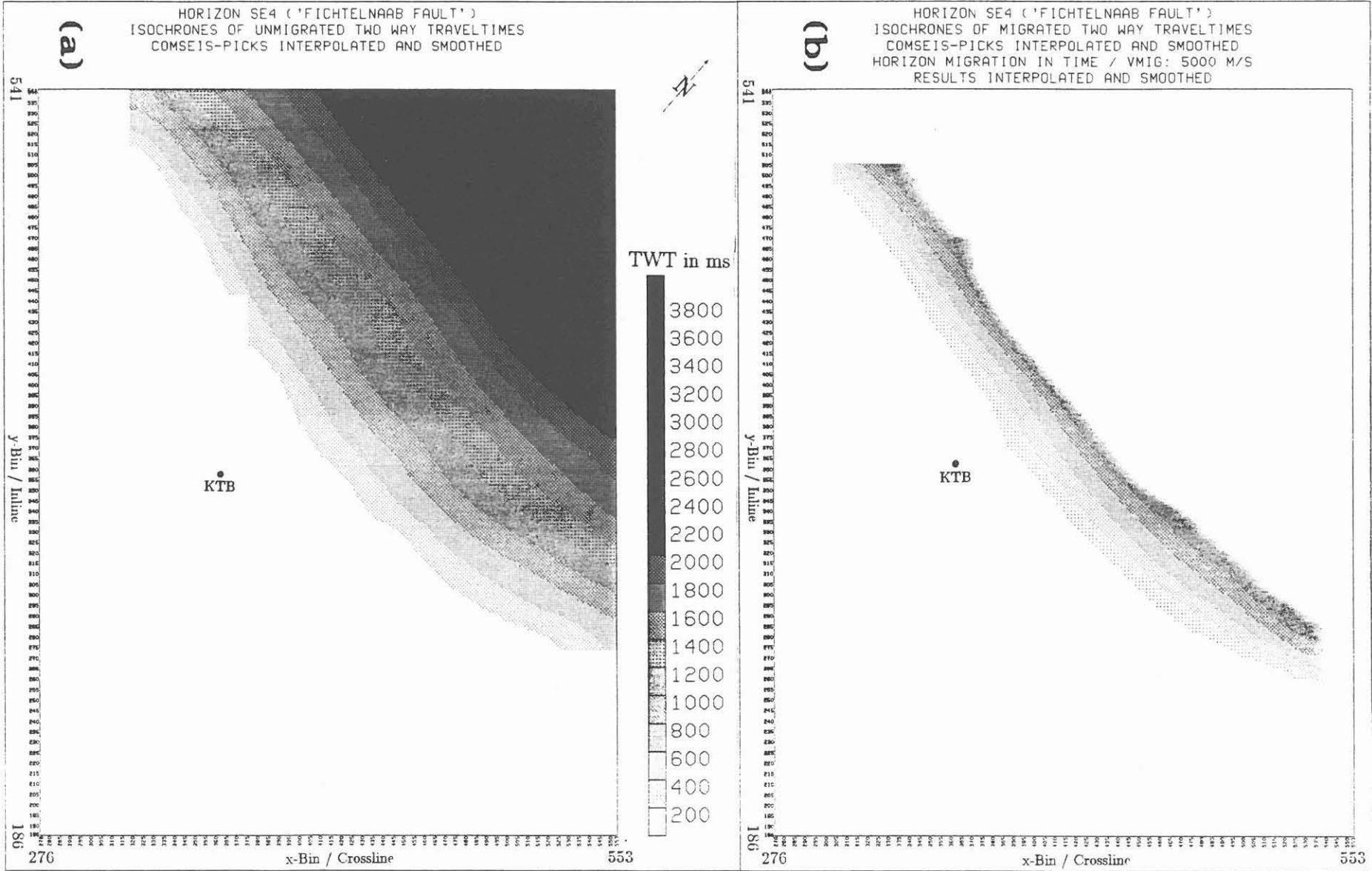


Fig. 5: Isochrone maps of the B1 horizon (variable grey density).  
 (a) unmigrated and (b) migrated TWT.

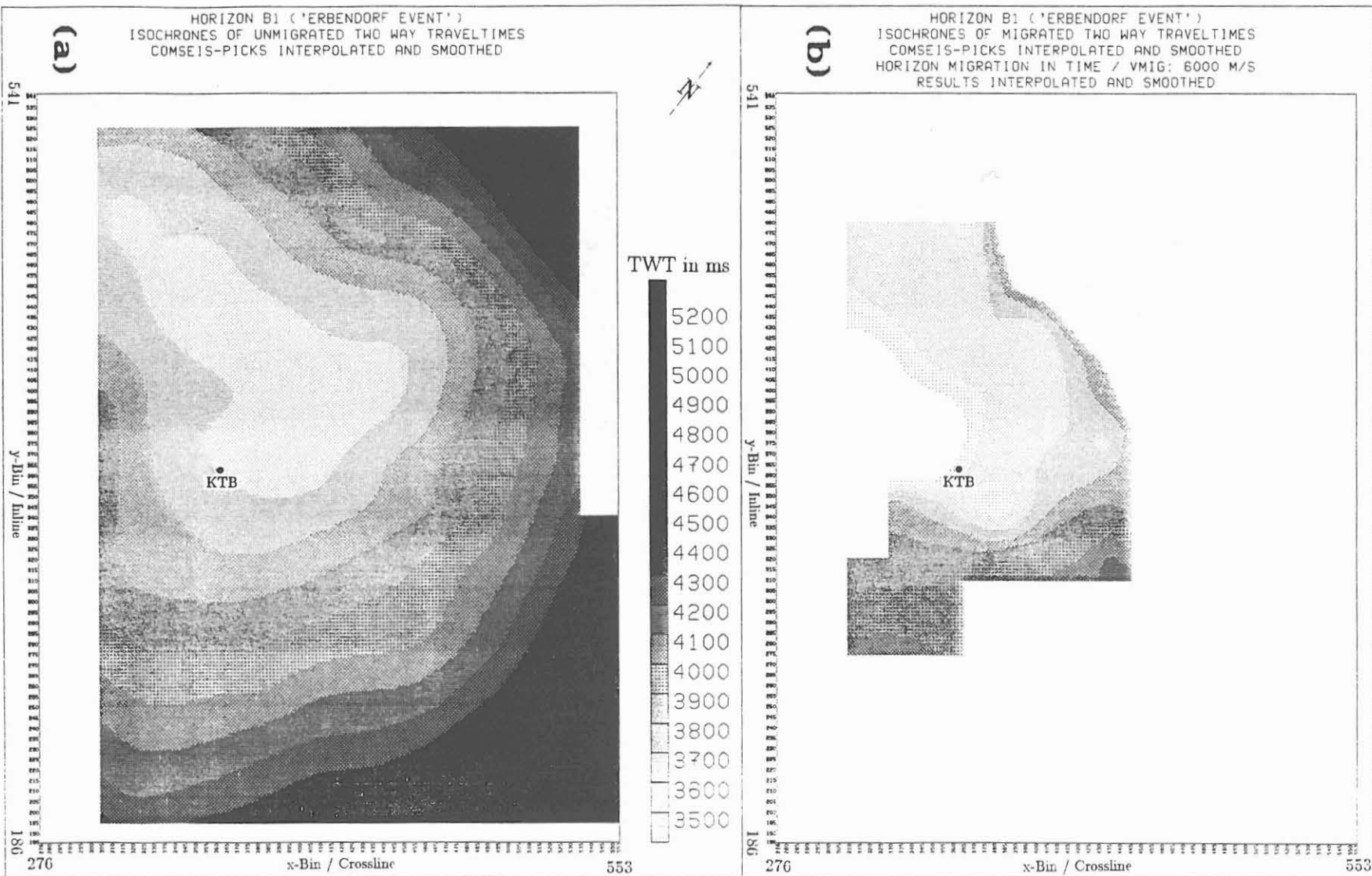
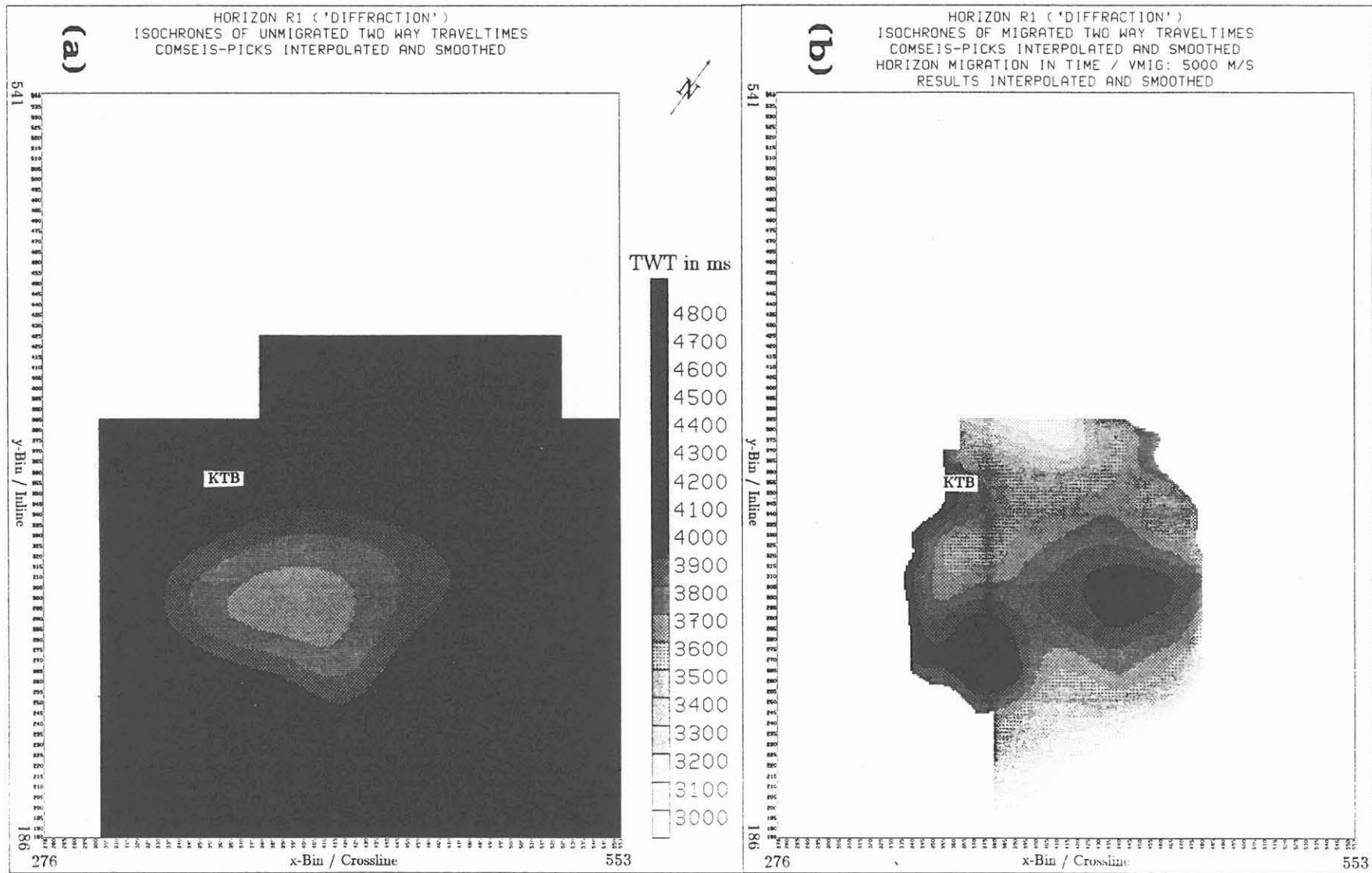


Fig. 6: Isochrone maps of the R1 horizon (variable grey density).  
 (a) unmigrated and (b) migrated TWT.



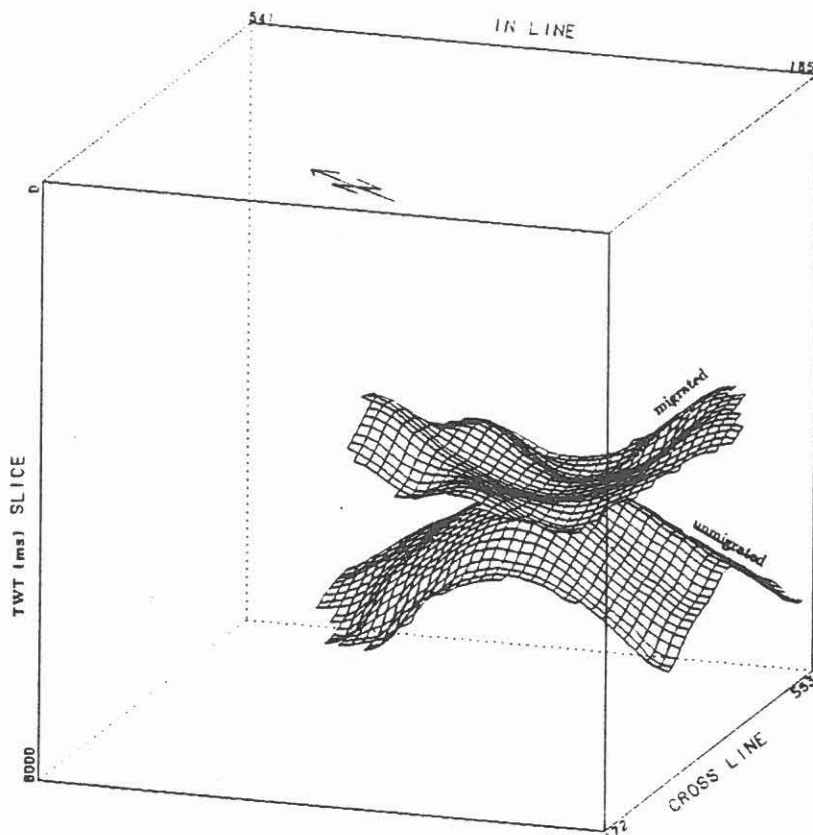


Fig. 7: Perspective view of the R1 horizon before and after horizon migration.

Figure 7 shows once more the position and shape of the R1 horizon again before and after horizon migration as a 3D view. This migration result, however, should be interpreted only carefully because a synformal structure actually would appear as a more complicated reflection response bearing additional TWT-branches. Therefore, the COMSEIS-picked migration input data might be incomplete in this case.

In the described manner 13 horizons have been evaluated over larger areas and migrated so far. A conversion of the migrated TWT into true horizon depth values is too inaccurate without exact velocity information and implies an error bar of at least +300 m. This is dramatically illustrated in Fig. 8 where the SE1 horizon has been migrated with only  $v_{mig}=5200$  m/s, a velocity which yielded plausible results for the SE1 on the 2D-migrated profile KTB 8502. The isoline map of Fig. 8 should be compared with that one of Fig. 2b showing the horizon migration with  $v_{mig} = 5700$  m/s. This more realistic velocity was derived from first break pickings within the ISO'89-experiment 'Durchschallung' which is described in another contribution of this volume (Martini und Stiller, this volume). This experiment yields more reliable large-scale average velocities than others, at least for the range above of the respective depth of the borehole geophone.

## Conclusions

The expected depth of SE1 below the KTB location calculated from the migrated TWT using the above mentioned velocities, is 5300 m for the lower (and certainly wrong) migration velocity and 6600 m for the higher, more realistic one. Regarding the problem of migration velocity and horizon depth prediction it is also referred to another contribution in this volume (Wiederhold, this volume).

In any case, it must be emphasized clearly that the high velocities obtained by bore-hole logging in the KTB are useless for migration purposes for several reasons. Besides other aspects, the main point is that the reflections from those steeply dipping horizons must be considered in a three-dimensional way of viewing. Therefore, seismic rays having their reflection points just below the KTB location start in their majority from distant areas at the surface with different geology. Concerning the steeply NE-dipping SE 1 horizon the corresponding rays start from granitic material of lower velocity several km NE of the bore-hole, for instance. Thus, the average velocities for the whole ray paths cannot be compared to the micro-scale velocities investigated by well-logging.

Generally, a detailed 3D velocity model is indispensable for accurate depth calculations which requires, however, arbitrarily high efforts when suitable subsurface velocity distributions are not at hand, directly. Thus, for the area surrounding the KTB reasonable compromises must be intended approaching the real nature of the subsurface in the most reliable manner.

In this context certain simplifications have been made: constant subsurface velocity, smoothing of small-scale structures by envelope stacking technique and TWT picking with subsequent interpolation. Having this in mind the 3D horizon migration process yields a preliminary migrated image of many detected and evaluated seismic surfaces, nevertheless. It allows the extraction of basic parameters for the further 3D-processing of the seismic data (e. g. true dip and azimuth of reflectors which influence the NMO-velocities severely) and makes an earlier and more reliable geological interpretation possible by moving the major events to their approximately correct spatial position. Moreover, it allows for a (more or less) precise depth and dip prediction for reflectors in the range accessible by the KTB borehole.

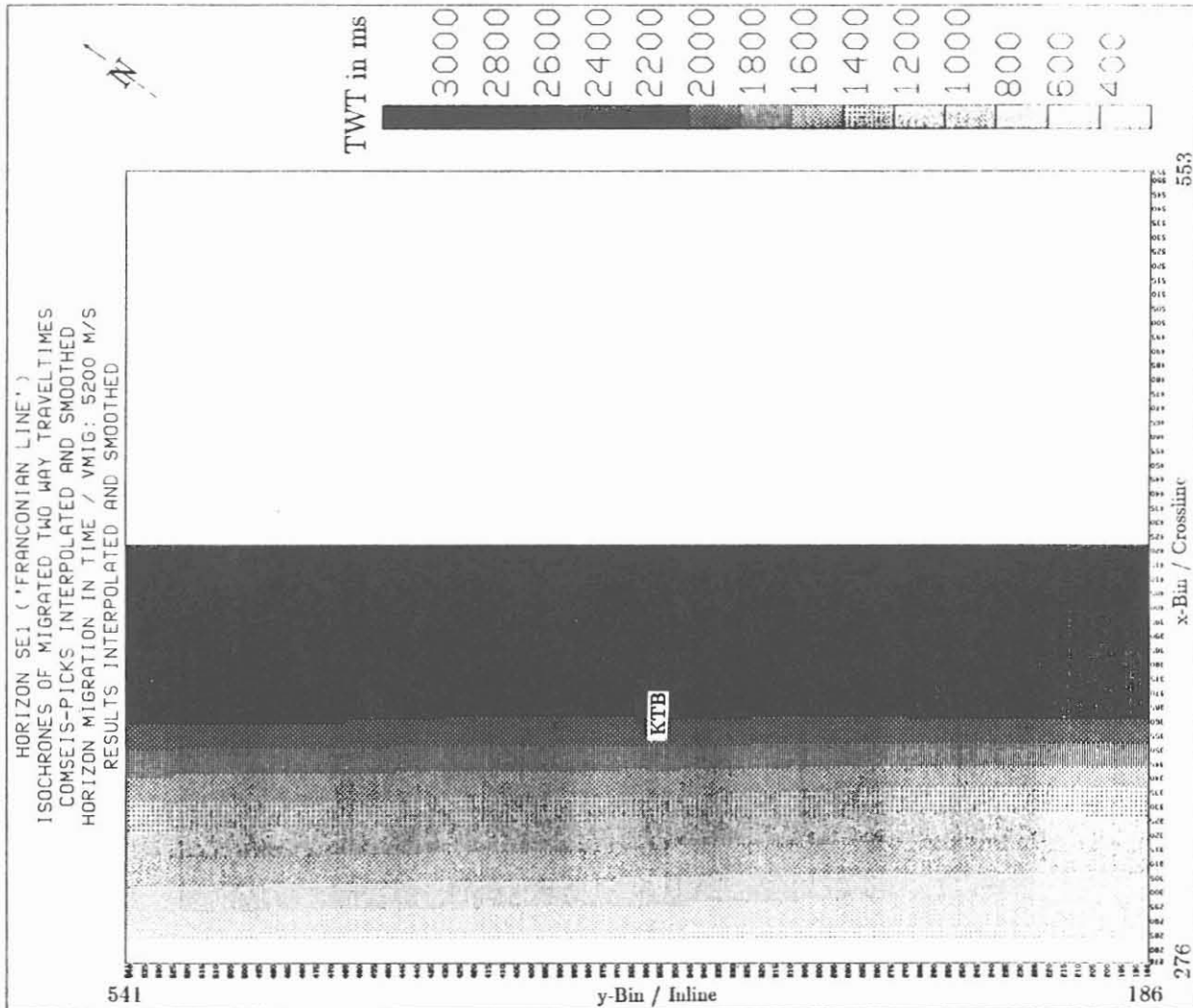
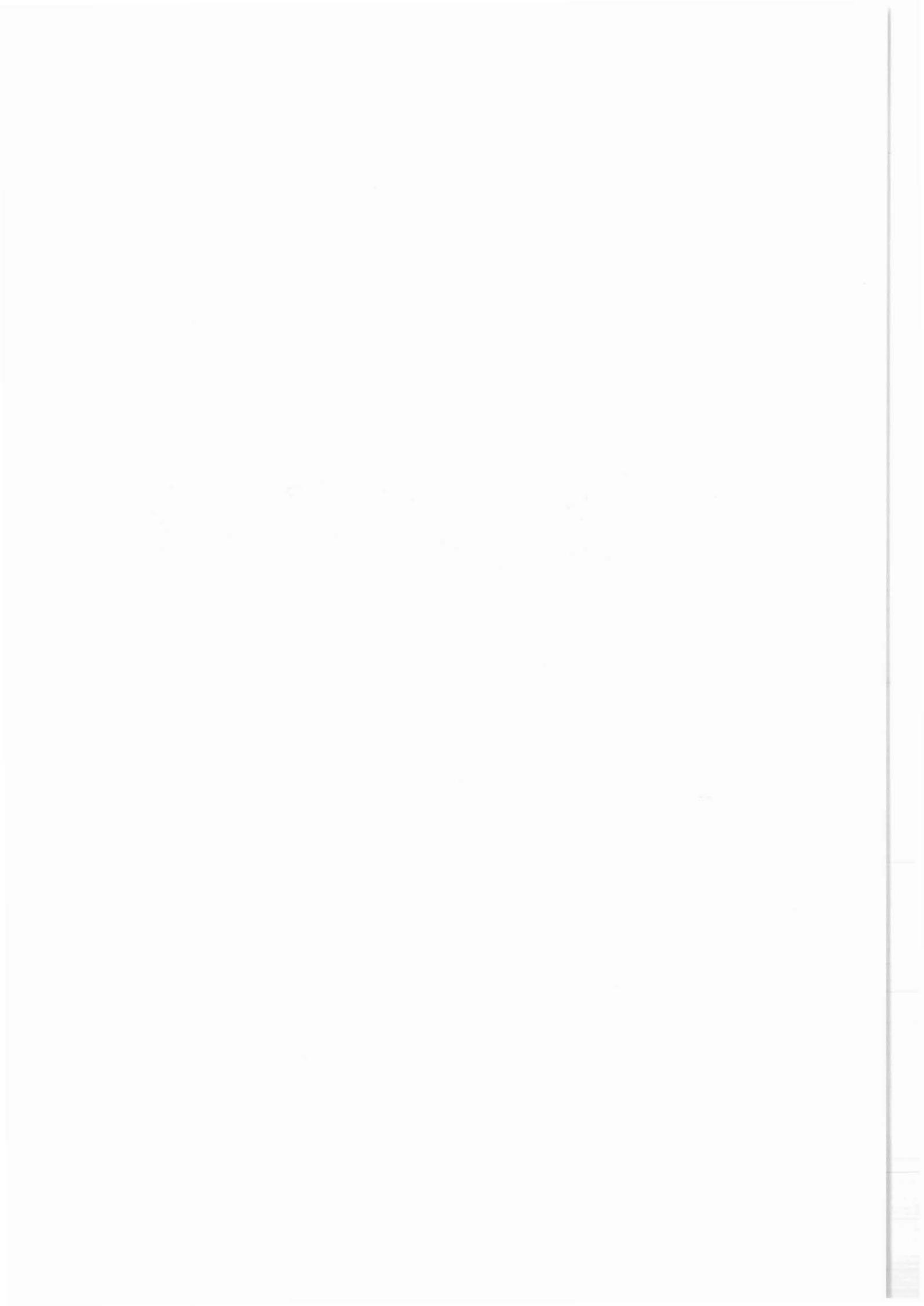


Fig. 8: Isochrone map of the SE1 horizon after horizon migration using too low velocity (variable grey density). Compare with Fig. 2b.

References:

- Hluchy, P., Koerbe, M., Thomas, R., 1992. Preliminary results of the interpretation of the 3D-seismic survey at the KTB location, KTB Report 92-5, DEKORP Report (this volume), Niedersaechs. Landesamt f. Bodenforsch., Hannover.
- Stiller, M., 1992. Preliminary generation of a stacked data volume of the entire ISO'89 3D-reflection dataset using an envelope technique, KTB Report 92-5, DEKORP Report, (this volume), Niedersaechs. Landesamt f. Bodenforsch., Hannover.
- Stiller, M., Martini, N., 1992. Results of the ISO'89 experiment 'Durchschallung' - recording of the vibrator sweeps of the 3D-seismics in the KTB bore-hole, KTB Report 92-5, DEKORP Report, (this volume), Niedersaechs. Landesamt f. Bodenforsch., Hannover.
- Wiederhold, H., 1992. Interpretation of Envelope-Stacked 3D-Seismic Data and its Migration - Another Approach, KTB Report 92-5, DEKORP Report (this volume), Niedersaechs. Landesamt f. Bodenforsch., Hannover.





INTERPRETATION OF ENVELOPE-STACKED 3D SEISMIC DATA AND ITS  
MIGRATION - ANOTHER APPROACH

Helga Wiederhold

ABSTRACT

The heart of the Integrated Seismics Oberpfalz 1989 experiment (ISO89) is a 3D seismic survey with a subsurface covered area of 19.1 km \* 17.85 km and the KTB borehole at its centre. The brute processing by the DEKORP Processing Center (DPC) at Clausthal resulted in an envelope-stacked data set that is used for a preliminary interpretation. Several strong reflections are addressed and mapped in 3D. The results are presented in form of time contour maps. For the depth conversion several velocity models are discussed and compared. The depth conversion itself is realized by a map migration of the interpreted horizons (SATTLEGGER 1986). The true 3D geometry for several horizons is presented as well as the depth they will be encountered in the KTB borehole.

## INTRODUCTION

The complete data set of the 3D seismic survey ISO89 (REHLING and STILLER 1990, STILLER 1991) was made available from the DEKORP Processing Center (DPC) Clausthal as envelope-stacked data (STILLER, this volume) and was loaded into an interactive seismic interpretation system (Interactive Exploration System, GeoQuest Systems) installed at the Niedersächsische Landesamt für Bodenforschung (NLfB) in Hannover. The reason for a further interpretation of the data in addition to that one done at the DPC at Clausthal (HLUCHY et al., this volume) was seen in the complexity of the data and was supported by the possibility to use the GeoQuest system at the NLfB. The work in Hannover is another approach in interpretation. The data volume is so spacious and ambiguous that there will not be a unique solution. Interpretation in this paper means picking, tracking, mapping and migration of strong events. For a further geological interpretation see e.g. the papers of HIRSCHMANN and STETTNER in this volume but also the paper of SCHMOLL et al. (1989) with the interpretation of the 2D seismic network of 1985.

## INTERPRETATION OF THE ENVELOPE-STACKED DATA

The 3D data volume loaded into the GeoQuest system includes all 357 inline sections (numbered 185 to 541) with 382 traces each (see Fig. A0 in the appendix and Fig. 1 in HLUCHY et al., this volume). The trace spacing as well as the inline spacing is 50 m, i.e. a trace exists for every bin and from these inline sections crossline sections may be calculated (numbered 172 to 553). This is done for every 5th crossline. The trace length is 6 s and the sampling interval is 8 ms; timeslices are calculated every 40 ms. With this it is possible to go through the data on inlines, crosslines and timeslices, but it is also possible to create any arbitrary profile (reconstruction cuts). Picking is possible on any of these lines and the advantage of such an interpretation system is that on each crossing section the point of penetration is marked by a small circle (e.g. Figs. 1-7) and helps to track the event seen e.g. on inline also on crossline and vice versa.

Several strong and also less strong events were addressed and could be followed by inlines, crosslines and timeslices in large areas and are presented in two-way-traveltime (TWT) in the following (Figs. 1-7). Time contour maps of all these horizons are shown in the appendix (Figs. A1-A30). The true strike and true dip (after migration) of the horizons is given - if possible - in Table 2.

These horizons can be classified into several groups (see also HLUCHY et al., this volume):

- Steeply north-east-dipping events (SE1, SE2, SE3, SE12); inline sections nearly match the dip (e.g. Figs. 1-4) and crossline sections nearly match the strike direction (e.g. Figs. 5-7). The strongest event that is also the deepest one (SE1) nearly corresponds with the strike of the Franconian Line (FL) if elongated linearly to the surface

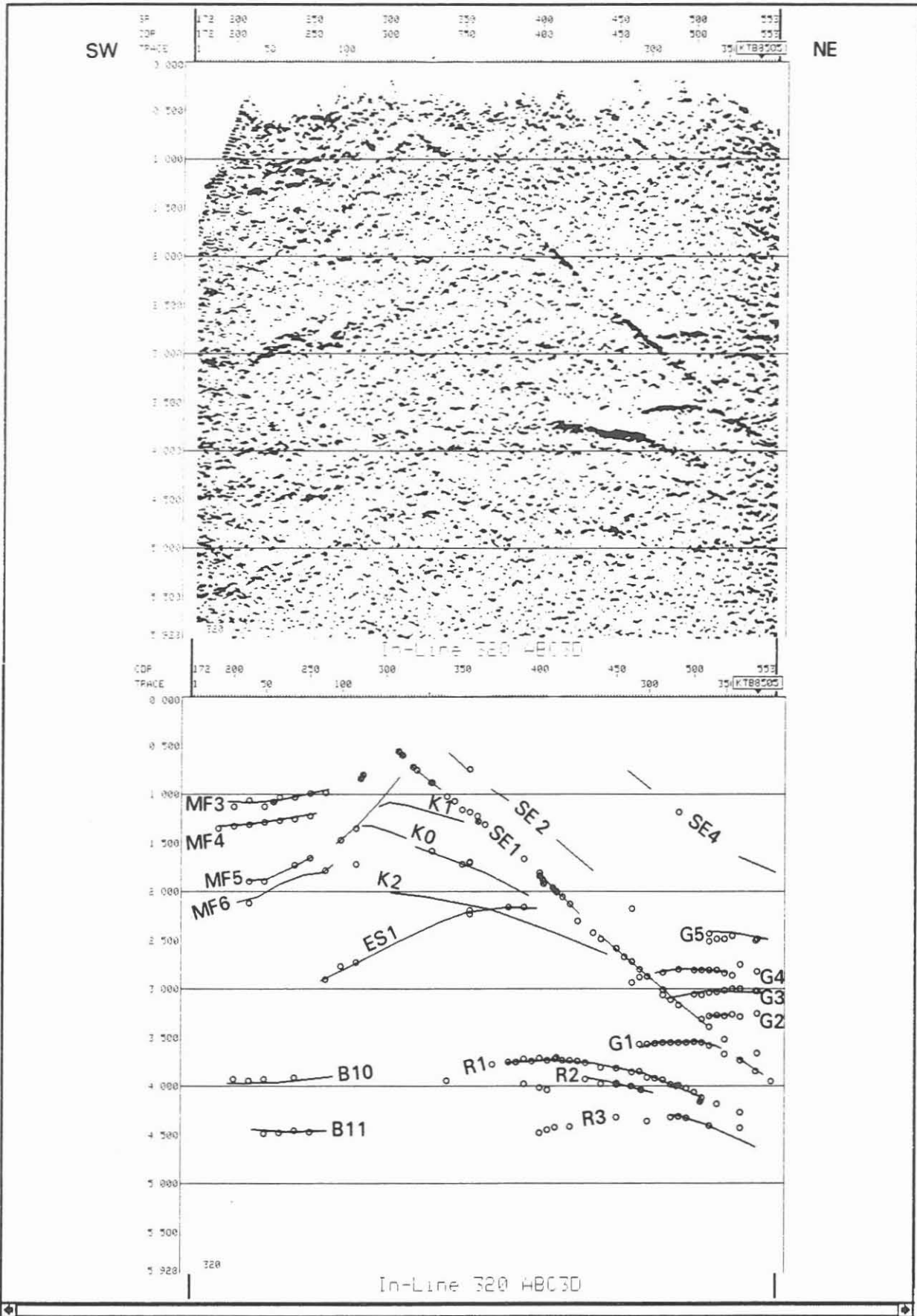


Fig. 1: Inline 320; envelope-stacked 3D seismic data and interpretation.

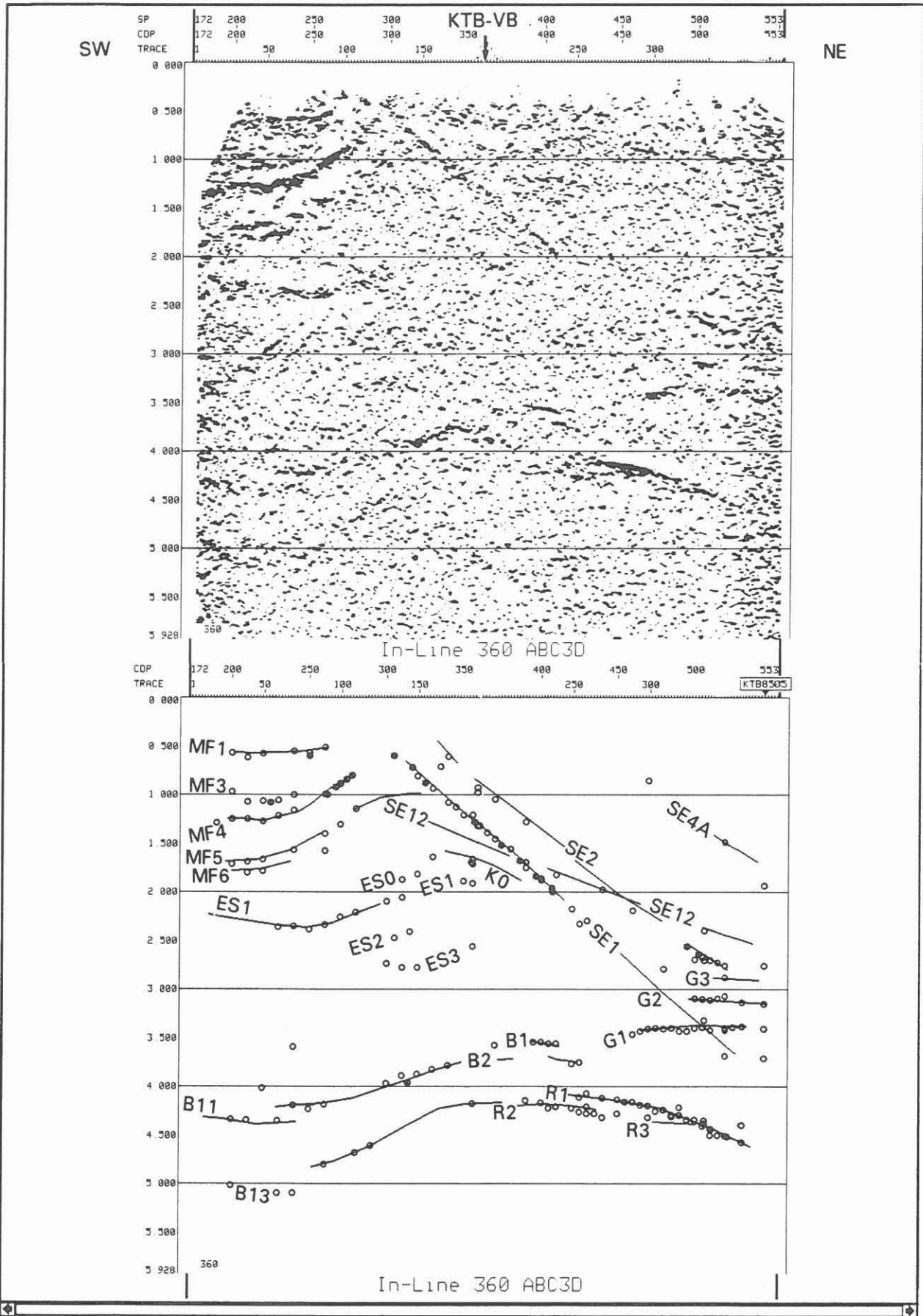


Fig. 2: Inline 360; envelope-stacked 3D seismic data and interpretation.

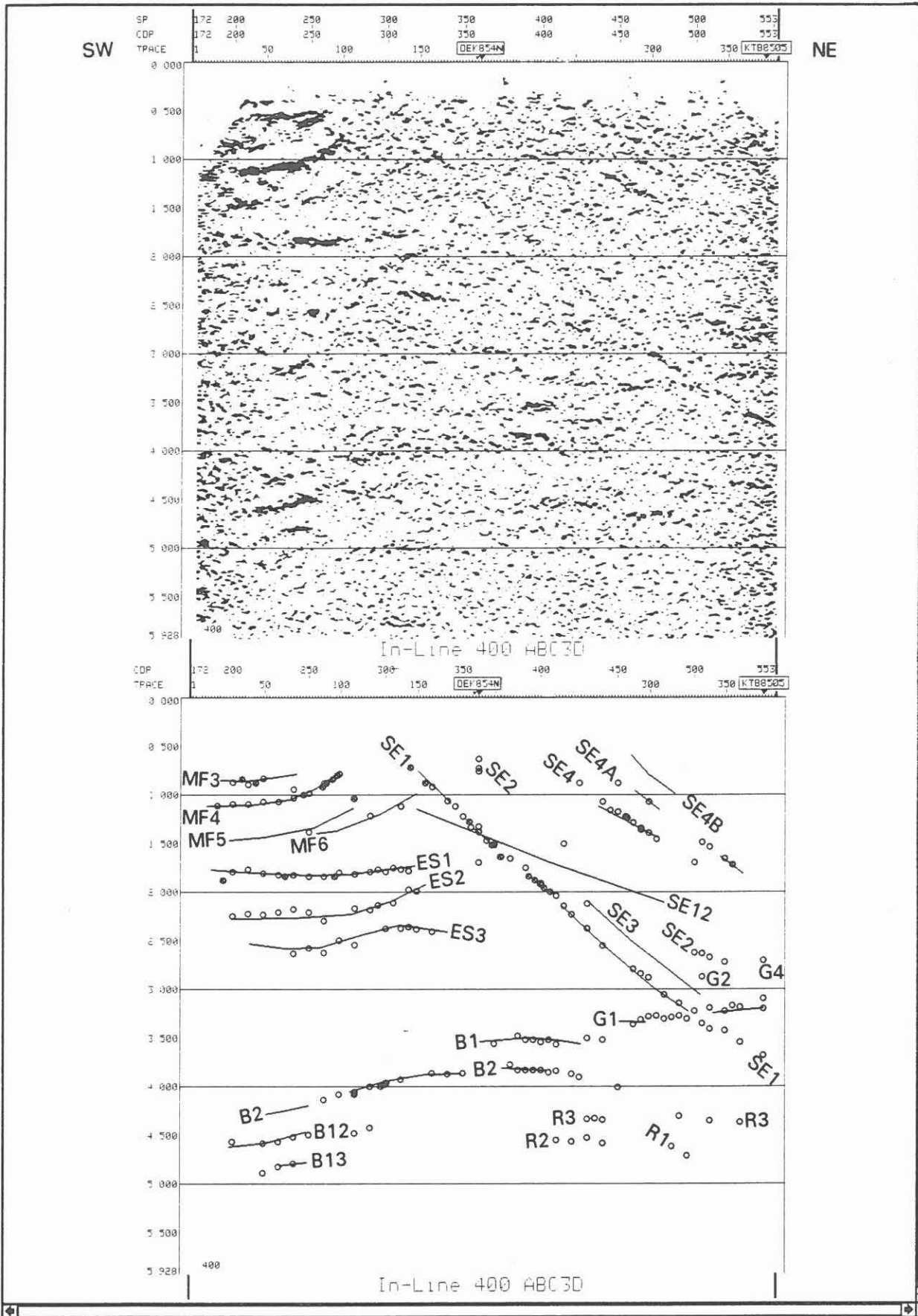


Fig. 3: Inline 400; envelope-stacked 3D seismic data and interpretation.

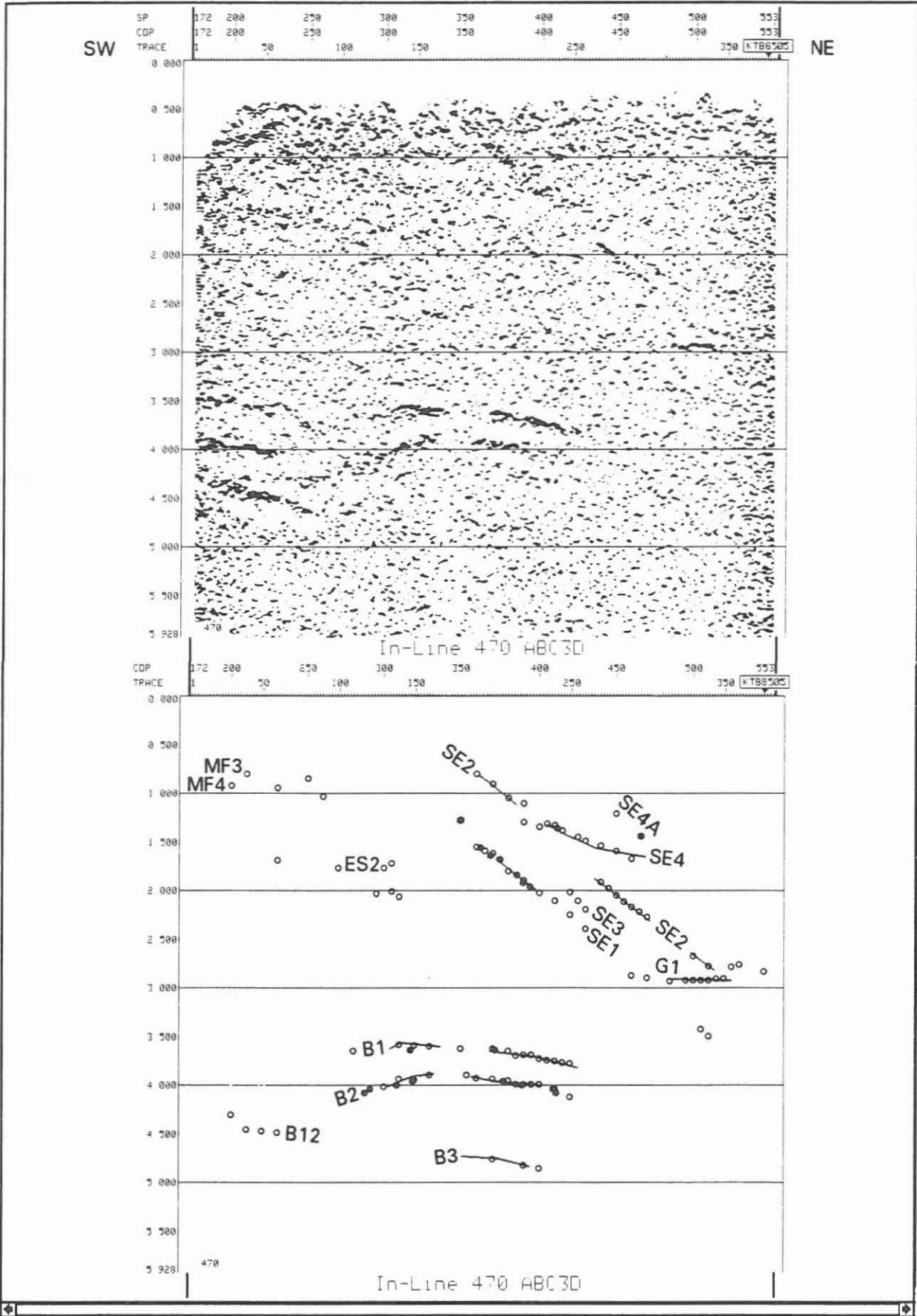


Fig. 4: Inline 470; envelope-stacked 3D seismic data and interpretation.

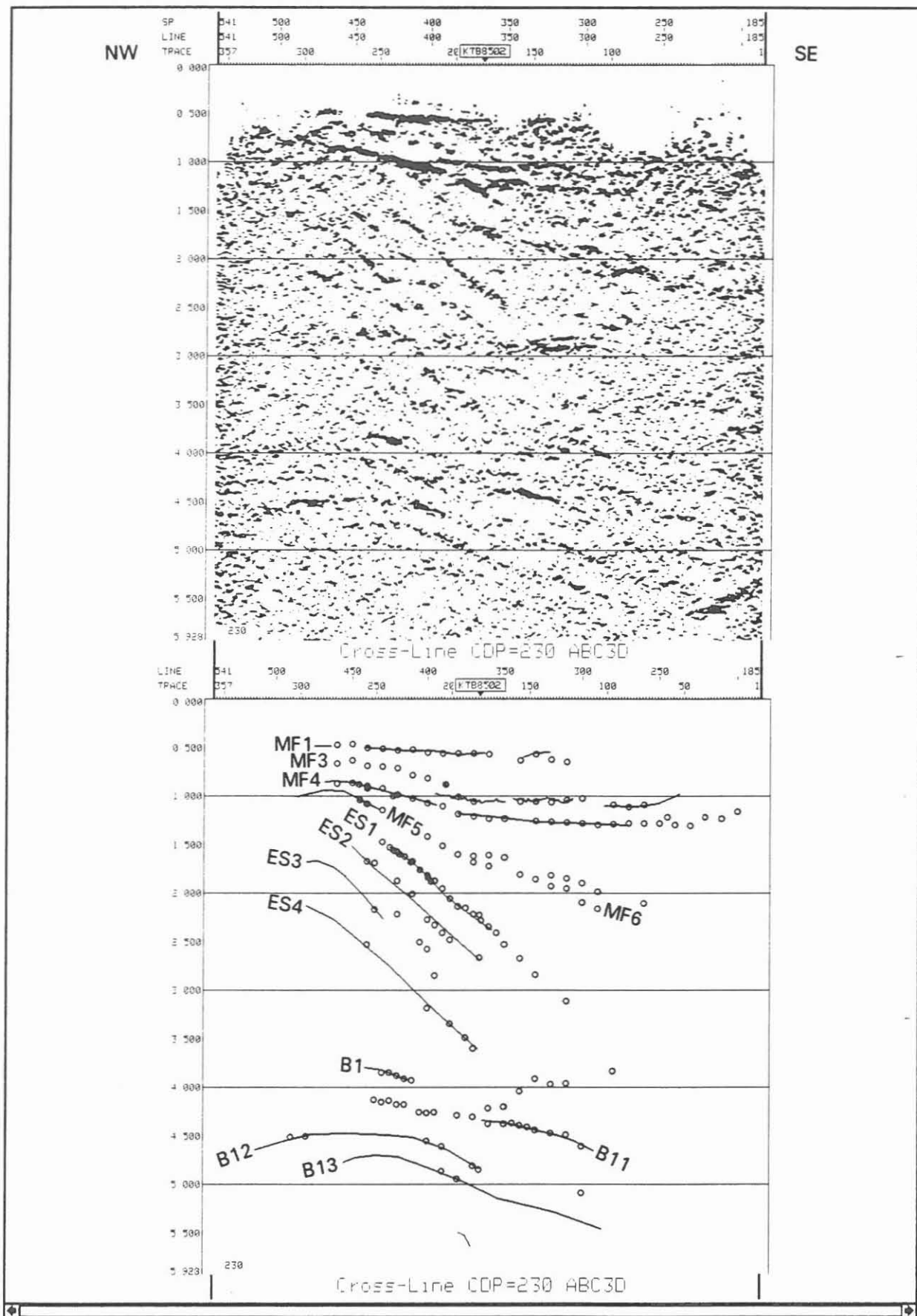


Fig. 5: Crossline 230; envelope-stacked 3D seismic data and interpretation.

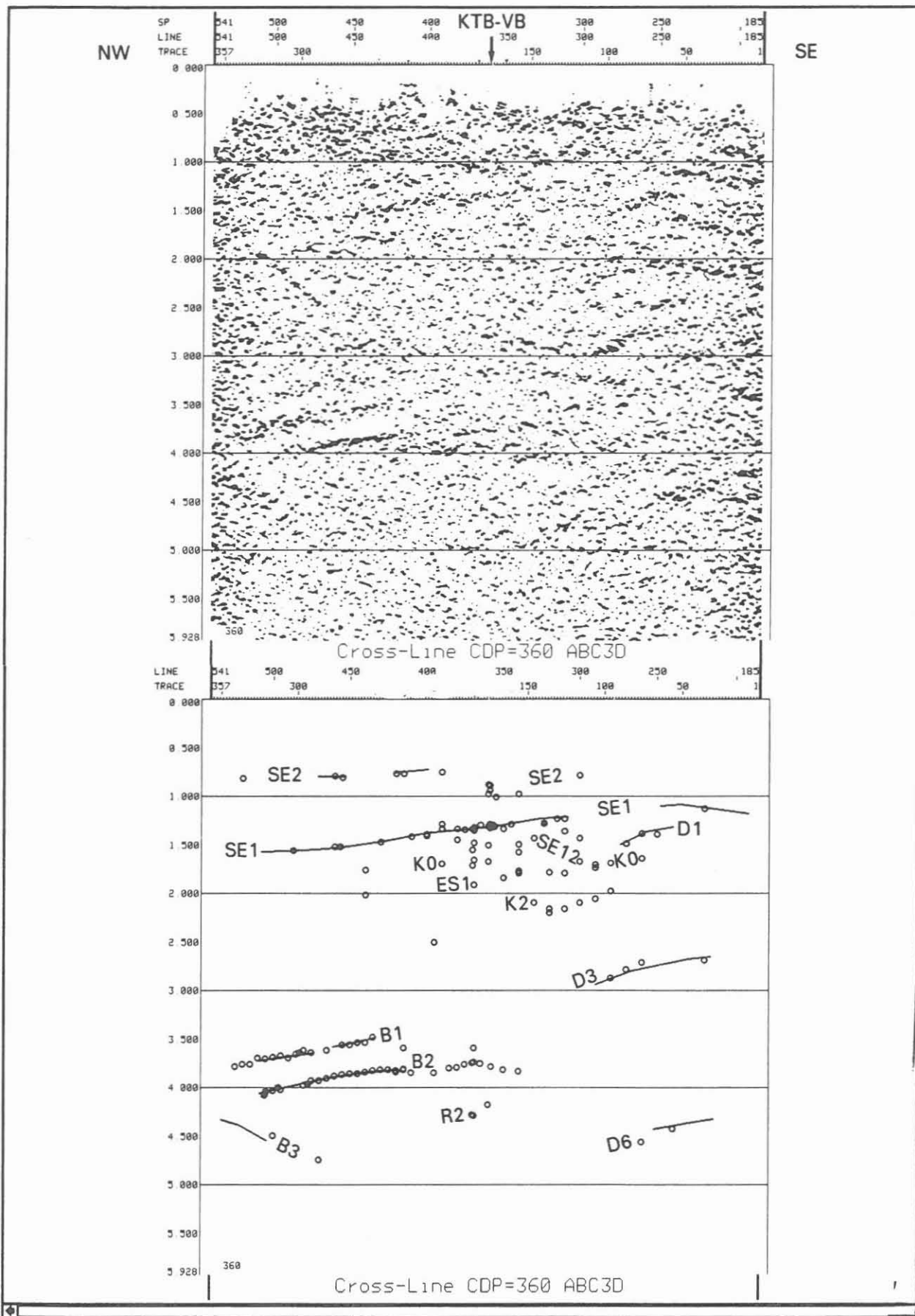


Fig. 6: Crossline 360; envelope-stacked 3D seismic data and interpretation.



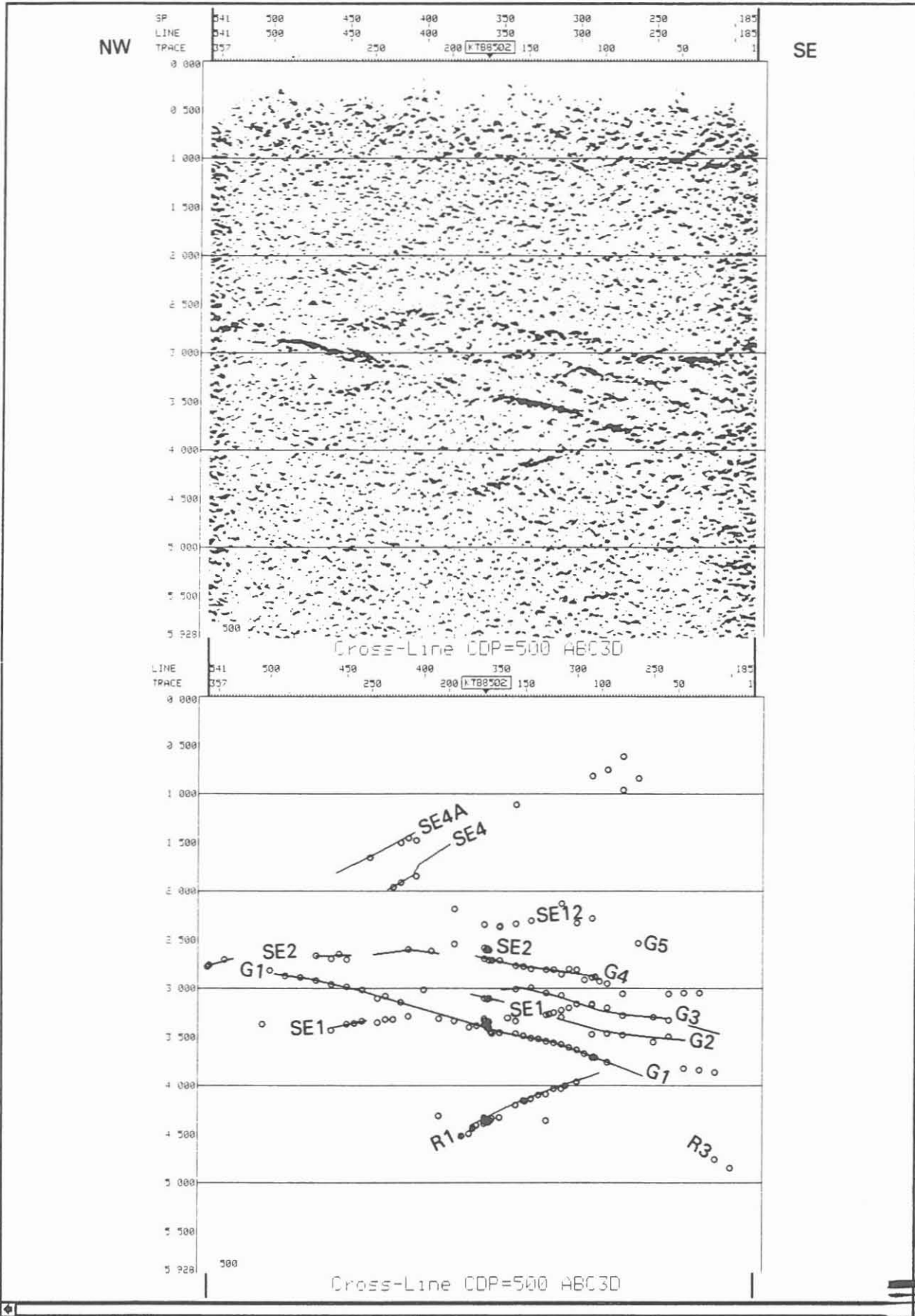


Fig. 7: Crossline 500; envelope-stacked 3D seismic data and interpretation.

- (Figs. 1-4 and Fig. A1). Parallel to this further but less energetic events follow upwards (SE3 and SE2, Figs. A2, A3). SE12 seems to split off from SE1 with decreasing dip (e.g. Fig. 3 and Fig. A5).
- Steeply north-north-east-dipping events (SE4 and SE4A, Figs. 1-4) that differ in strike from the preceding group (Figs. A6 and A7) and correspond at the surface with the Fichtelnaab-fault (HIRSCHMANN, this volume).
  - Strong, slightly convex shaped horizons in the TWT range from 3.5 to 4.5 s (B1, B2, R1, R2, R3 see Figs. 1-4 and Figs. A8-A12) and also up to 5 s (R10, Fig. A13).
  - A series of 5 more or less parallel reflectors in the TWT range from 2.5 to 4 s. The deepest and also strongest of them is south-east-dipping (G1). The upward following reflectors have less dip (G2-G5). These reflectors appear only in the north-eastern part of the surveyed area (Figs. 1,2 and 7 and Figs. A14-A18).
  - West of the outcrop of the FL at surface the reflections of the Mesozoic foreland sediments (MF1, MF3, MF4) dominate the range of the first 1.5 s TWT (Figs. 1-3 and 5, A19, A20). And below these the events MF5 and MF6 follow with similar basin shape (Figs. A21 and A22).
  - Below the sediments a series of strong, south-east to south-dipping reflections occurs (ES1, ES2, ES3). ES1 is the topmost and can be followed best (Figs. 3 and 5, A23-A25).
  - Not too strong and widespread but also worth mentioning are the events K0 and K2 (Fig.1 and Figs. A26, A27). They dip slightly to the north-east and seem to converge on SE1.
  - In the area south and south-east of KTB the reflections D3, D4 and D6 are worth mentioning, that show a slight increase to the south/south-east/east (Figs. 6, A28-A30).

#### COMPARISON WITH RESULTS OF THE 2D SEISMIC PROFILES

The 3D seismic data can be combined with the large-scale geology by a network of 2D seismic profiles that was surveyed in 1985 (DEKORP RESEARCH GROUP 1988, SCHMOLL et al. 1989). These data have a considerably higher degree of coverage than the 3D seismic data, i.e. 80-fold against 15-fold, and show a much better resolution and thus are of great importance for the structural relations. Three of these profiles - DEKORP 4, KTB 8502 and KTB 8505 - cross the area of the 3D seismic survey. The stacked version of these data was also loaded into the GeoQuest System and with the help of the points of penetration a fair relation between all the data is possible.

Already the test stacks of the central part of the 3D seismic data exhibited the steep event SE1 in the inline direction (STILLER 1991) while the corresponding 2D profile KTB 8502 showed only little indication of this event (DEKORP Research Group 1988, SCHMOLL et al. 1989). However, the reprocessing of this 2D line with especially high stacking velocities improved the appearance of this reflection tremendously (e.g. KÖRBE and REICHERT, this volume). The interpretation of the 2D network by SCHMOLL et al. suspected already a series of north-east-dipping events that were interpreted - at that

time a little bit speculative - as overthrusts. This interpretation is confirmed more or less by the reprocessing of KTB 8502 and the 3D seismic data that agree so far, but the 2D profile exhibits much more reflectivity and a higher resolution than the 3D data volume.

Very good coincidence occurs between the KTB 8505 profile and the corresponding crossline 540. The events G1 to G5 reflect parts of the wedge-shaped imbricate structure that is known as the Erbenhof body (EB) (DEKORP RESEARCH GROUP 1988, SCHMOLL et al. 1989). G1 represents the basis. This part is excellently wedge-shaped and can be traced excellently in 3D - including its internal structure -; its occurrence is limited to the north-eastern part of the 3D area.

The correlation with the DEKORP 4 profile (crossline 360) is not so easy. The events B1 and B2 also belong to the EB but to another block than the G-reflections. The wedge-shape of the EB in 3D data is not seen as clearly as on the DEKORP 4 profile by SCHMOLL et al. (1989). The continuation of the B-reflections to the south/south-east is uncertain. But a slight rise in that direction is demonstrated by the D-reflections (e.g. D3 in Fig. 6). There may be a relation between B and D reflections. The basis of the zone of Erbenhof-Vohenstrauß (ZEV) defined on the DEKORP 4 profile by SCHMOLL et al. (1989) cannot be followed in the 3D data and in the south-east it was apparently mixed with energy of the SE1 event.

The horizons MF1, MF3 and MF4 represent sediments of the mesozoic foreland west of the FL. MF4 was regarded as basis of the Permo-Carboniferous by SCHMOLL et al. (1989).

The 3D seismic data reveal the spatial arrangement of the reflectors. Therefore it becomes obvious that some reflections on the 2D profiles lie not in the 2D plane but come from the side and are not truly taken into account by the 2D migration process. This is especially valid for the steep events that occur on DEKORP 4 and KTB 8505 more or less horizontally. The 2D migration had no severe influence on these reflections, but true 3D migration will shift them parallel to greater traveltimes or depths respectively (see below).

It is noteworthy that the static corrections on the KTB 8502 profile west of the FL are calculated with a slightly higher velocity ( $\approx 4.2$  km/s) than used with the 3D data. The maximum inline geophone offset of 12 km on the 2D line enabled the use of a deeper refraction horizon than in 3D data. The discrepancy results in a time difference of about 130 ms TWT, i.e. in the stacked seismic section KTB 8502 the onset of reflections is about 130 ms earlier than the corresponding onset in the 3D seismic. This concerns only the part west of the FL.

#### MIGRATION AND DEPTH ESTIMATION

The interpreted horizons were transferred to the Sattlegger ISP003 software for map migration (SATTLEGER 1986). The main

problem with the migration is the choice of the proper velocity distribution.

At the KTB location and for the depth of the pilot hole, a lot of velocity information exist from vertical seismic profilings (VSP) (RÜHL and HANITZSCH 1992), sonic logs and core analyses (LIPPMANN et al. 1989, KERN et al. 1991). But how can this information be extrapolated to the 3D area? A constant velocity distribution certainly does not match the requirements of the complex geology. Other velocity data acquired within ISO 89 are related to large offsets (wide-angle observations) and thus are ambiguous in the near-surface domains where velocity changes significantly with depth. Moreover, these data do not cover the entire 3D area. The most obvious procedure seems to start at the datum level (500 m a.s.l.) with subweathering velocities used for static corrections (LENGELING 1991, SCHWANITZ et al. 1990), and available for the whole area. The subweathering velocity is the velocity of the wave that is refracted by the not weathered rock. In the area of crystalline rocks east of the FL these refractor velocities are in the range from 5 to 6 km/s, with the 6 km/s correlating well with amphibolite areas and the 5 km/s correlating well with the Steinwald granite area. West of the FL the velocities vary in the range from 2.8 to 3.8 km/s due to the underlying Mesozoic sediments.

For the depth continuation several models have been tested and are discussed in the following.

After LIPPMANN et al. (1989) and KERN et al. (1991) it is conspicuous that the sonic log velocities are lower than the laboratory velocities. LIPPMANN et al. (1989) refer to the different geometry of both measurements and the presence of anisotropy: the sonic log determines the velocity of sound-waves travelling parallel to the borehole, whereas their laboratory measurements are obtained perpendicular to the axis of the cores. KERN et al. (1991) measure the velocity with respect to the foliation, i.e. parallel and normal to the foliation plane. Generally the fastest and slowest velocities are measured parallel and normal to this plane, respectively. The velocities of KERN et al. (1991) represent inherent or quasi in-situ velocities. They are determined under in-situ pressure- and temperature-conditions on sample cubes of dry rocks. Velocity model 1007 in Table 1 represents a rough approximation of this velocity-depth profile.

Laboratory measurements are done in the MHz-range, sonic logs in the kHz-range, but the frequencies for seismic prospecting are less than 100 Hz. Taking into account the behaviour of velocity as a function of frequency in a viscoelastic material, that is the most realistic approach (e.g. AKI and RICHARDS 1980), the difference in laboratory and sonic velocities could also be explained by dispersion of seismic velocities.

Fig. 8 after LIU et al. (1976) shows the velocity and attenuation behaviour of a standard linear solid - a material including linear elasticity and viscosity and therewith attenuation - with several relaxation peaks superimposed.

Through this procedure any frequency behaviour of the quality factor  $Q$  - that describes the reciprocal value of attenuation - may be modelled as shown in the example in Fig. 8. The dependence of velocity with frequency is linear. Evidence for this velocity function we find for example in CHENG and JOHNSTON (1981) who have measured the static and dynamic bulk moduli as continuous functions of pressure for several materials moreover a granite. The low velocity level in Fig. 8 is comparable with the static bulk modulus ( $K$ ). The high velocity level is comparable with the dynamic bulk modulus ( $K_d$ , measured at 1MHz). CHENG and JOHNSTON (1981) show that for a Westerly Granite the  $K/K_d$  ratio at atmospheric pressure is 0.5 but at a pressure of 300 MPa still is 0.9 i.e. 10%. The dependence of the  $K/K_d$  ratio with pressure is explainable by the closing of microcracks.

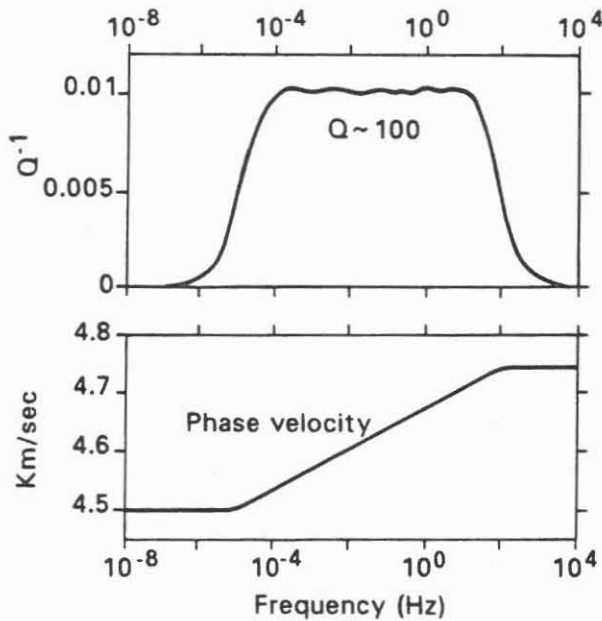


Fig. 8: Internal friction ( $1/Q$ ) (top) and phase velocities (bottom) as a function of frequency in a standard linear solid with 12 different relaxation peaks superimposed (after LIU et al. 1976).

With this in mind the difference in sonic and laboratory velocities found in the KTB borehole is acceptable and an analysis of attenuation of seismic waves seems to be fruitful, but cannot be the subject of this paper.

A problem now arises with the velocities resulting from the VSP. The interval velocities as well as the average velocities are shown in RÜHL and HANITZSCH (1992, this volume) and are compared to the sonic velocities. Surprising is the result that the sonic velocities are in several depth ranges smaller than the interval velocities. This is not compatible with the theory above and other observations (e.g. GOETZ et al. 1979). RÜHL and HANITZSCH (1992) are also aware of this problem. They try to explain this discrepancy by geometric effects and a possibly wrong geometric correction. Indeed their results don't look very reliable. Especially the interval velocities of VSP 101 oscillate between 5 km/s and more than 8 km/s. This seems to be unrealistically high. They estimate the mean value of all interval velocities to be 6 km/s.

HANITZSCH et al. (1992) give the following simplified velocity model for the VSP measurement: starting with 5.4 km/s at the surface - that correlates well with the velocities from surface refraction measurements -, increasing to 6 km/s in 2.5 km depth and a constant velocity of 6 km/s below 2.5 km depth. In my opinion this simplified model seems to be a compromise of all mentioned facts and a fair approximation of the real complicated situation.

Thus for the area east of the FL the following velocity models were used: starting with the velocities used for static corrections, assuming a linear velocity gradient up to 6 km/s in 2.5 km depth and continuing with a constant velocity of 6 km/s (model 1000). For another model the depth extension of the granitic area north-east of the KTB drill site is taken into consideration by decreasing the gradient so that the 6 km/s velocity is reached at 4 km depth east of crossline 400 and north of 5526000 North (model 1005). An alternative model (1004) assumes a step by step transition between the 2.5 km depth of the 6 km/s velocity to the 4 km depth north-east of the KTB location. With reference to the laboratory measurements models with higher velocities were also tested (see Table 1, models 1002, 1001, 1007) as well as models with a constant velocity or a constant velocity gradient (Table 1, models 1003, 1007, 1007).

All these models have been tested in migrating horizon SE1. The results are presented in Table 1 as depths of the reflector SE1 to be found in the KTB borehole. According to the above discussion respecting dispersion the high velocity models (1002, 1001, 1007) as well as the extreme low velocity model (1006) can be ignored. Model 1003 has no convincing basis. Most reliance is given to models 1000, 1004 and 1005. The considerable difference in depth of 400 m can be explained in that way that most rays that are reflected at the steep event SE1 below the KTB location originate in the area of the granites and thus a decrease in velocity gives rise to a less steep dip of the reflector.

From geological aspects as well as from gravimetric measurements (BEHR et al. 1989, SOFFEL et al. 1989) a certain depth continuation of the granites down to approximately 4 km is expected. This means that the velocity contrast granite against gneiss/amphibolite will exist down to that depth. This fact is taken into consideration in models 1004 and 1005. Velocity model 1005 was chosen for migration of all other horizons.

The results of migration are shown in Figs. A31-A47 in the appendix. In Table 2 the true strike and dip values of several reflectors are listed as well as the depth they are likely to be intersected by the KTB borehole. Not all picked horizons are migrated yet.

TABLE 1. Result of migration of event SE1 with different velocity models.

velocity model	description	depth of reflector SE1 in KTB in m
1000	refractor velocities, linear gradient to 6 km/s in 2.5 km depth, constant 6 km/s.	7000
1005	same as 1000, but east of crossline 400 and north of 5526000 North gradient to 6 km/s in 4.0 km depth, constant 6 km/s.	6600
1004	same as 1000, but east of crossline 400 and north 5526000 North gradient to 6 km/s in 3 km and east of crossline 440 in 4 km depth, constant 6 km/s.	6600
1002	refractor velocities, linear gradient to 6 km/s in 1.2 km and 4 km depth respectively (see 1004), linear gradient to 6.2 km/s in 4 km and 6.8 km depth respectively.	6900
1001	same as 1002, but east of crossline 400 gradient to 6 km/s in 2 km, east of crossline 440 in 3 km and east of crossline 480 in 4 km depth and the gradient to 6.2 km/s in 4.8 km, 5.8 km and 6.8 km respectively.	6700
1003	refractor velocity and constant velocity gradient of 0.2.	7700
1006	refractor velocity, constant depth continuation.	5900
1007	constant velocity function with 2 linear gradients: $V_0 = 5.4$ km/s, gradient to 6 km/s in 1.2 km depth ( $=0.4s^{-1}$ ) and to 6.2 km/s in 4 km depth ( $=0.07s^{-1}$ ).	8400

TABLE 2. Result of migration with velocity model 1005. The value in parentheses results from a slightly different interpretation.

reflector	depth of reflector in KTB-HB in m	dip/strike of reflector
SE2	3700 (- 4200)	40°-45°NE / 320°
SE12	4700	20°NE / 330°
SE3	5800	50°NE / 330°
SE1	6600	55°NE / 320°
SE4	---	50°NE / 290°
SE4A	---	45°NE / 300°
B1	10700	---
B2	11400	---
R2	13150	---
R10	---	10°SE / 45°
G5	---	10°SE / ≈45°
G4	---	≈8°SE / ≈45°
G3	---	20°S / 100°
G2	---	15°SE / 55°
G1	---	≈15°SE / 40°-70°

#### ERRORS IN DEPTH ESTIMATION

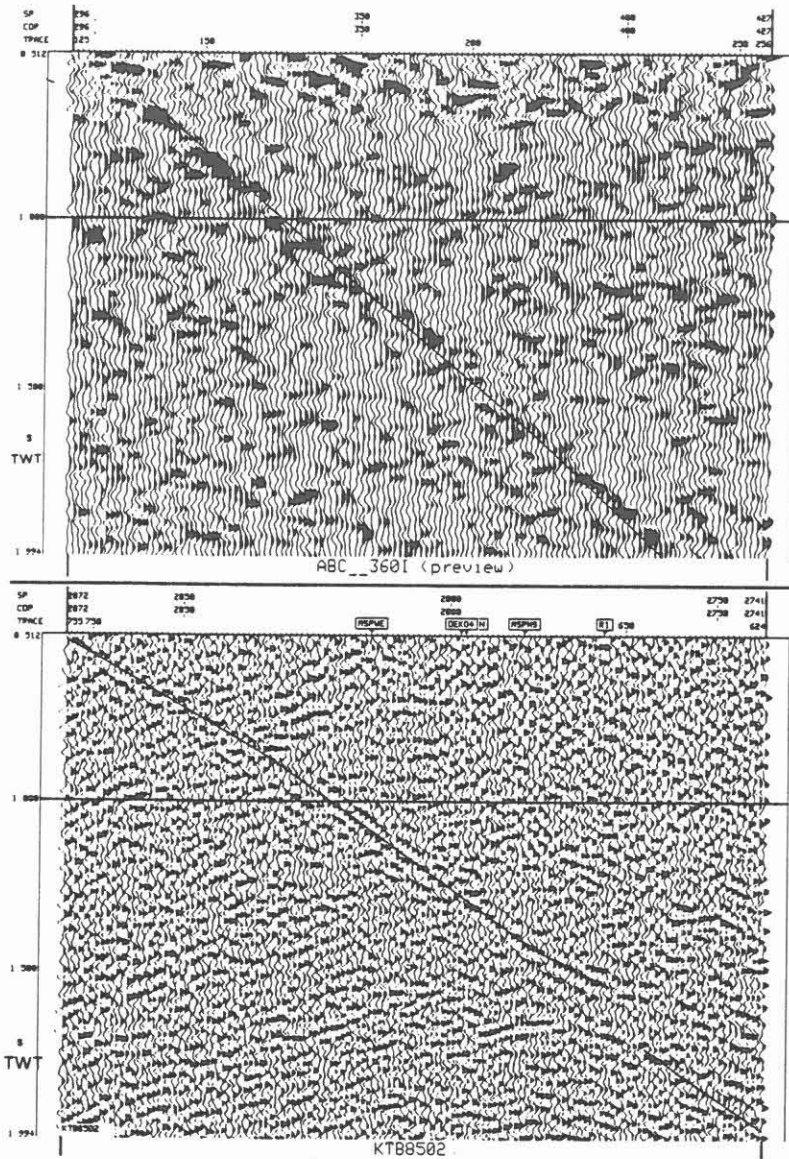
Two different error sources result in relatively high inaccuracy of depth estimations: The velocities used for migration of the events and the picking of arrival times in the broad signal of the envelope-stacked seismic data.

The result of an envelope-stacked seismic data set is a relatively broad seismic signal with only positive amplitudes and a high low frequency content that gives much less guidance in picking than a phase-stacked signal. An example for this is shown in Fig. 9 in which signals of the SE1 event from envelope-stacked data (inline 360, Fig. 9a) and from phase-stacked data (KTB 8502 profile, Fig. 9b) are shown.

On the screen an attempt is made to pick the envelope in its maximum energy. The average length of an envelope-stacked signal is about 80 ms. An uncertainty in picking in this range must be taken into account. By 2D gridding and interpolation large deviations in the picked data are smoothed. The standard deviation between data points and grid values can be given for each horizon and should be a criterion for an error estimation.

This error must be applied in direction of the raypaths. The consequence for the steeply dipping events is that the value for the vertical depth error must be divided by the cosine of the dip angle. In Table 3 the standard deviations and vertical depth errors are listed for several horizons. For the SE1 event with a dip angle of 55° and a standard deviation of ±27 ms the vertical depth error is about ±47 ms, ±140 m respectively; thus the minimum depth the reflector will be met in the KTB is 6460 m (velocity model 1005).





a)

b)

Fig. 9: Examples of envelope-stacked signals from inline 360 (a) and phase-stacked signals from profile KTB 8502 (b). The windows of the seismic sections are not exactly identical and the trace spacing is different (Fig 9a: 50 m, Fig. 9b: 80 m).

Table 3. Standard deviation of residual between picked data and gridded data and resulting vertical depth error.

horizon	dip	standard dev. sd	vertical travel- time error $t=(sd/\cos(\text{dip}))$	vertical depth error ( $s=\frac{1}{2}vt$ ) ( $v=6000\text{m/s}$ )
SE2	43°	+47 ms	+64 ms	+200 m
SE12	20°	+59 ms	+63 ms	+190 m
SE3	50°	+23 ms	+36 ms	+110 m
SE1	55°	+27 ms	+47 ms	+140 m
SE4	50°	+29 ms	+45 ms	+135 m
SE4A	45°	+29 ms	+41 ms	+125 m
B1	--	+57 ms	+57 ms	+160 m
B2	--	+25 ms	+25 ms	+ 75 m
R2	--	+37 ms	+37 ms	+115 m

The vertical depth error by the uncertainty in velocities used for migration is discussed already in the above chapter and shown in Table 1 for quite different velocity models. For the most reliable velocity models (1000, 1004 and 1005) a vertical depth difference of 400 m must be taken into account.

A further uncertainty in depth statements results from the interpretation itself. Fig. A4 shows a second interpretation of the horizon SE2. The only difference to Fig. A3 is that the SE2 is also fixed in the area marked (Fig A4) where the occurrence of SE2 is doubtful. A slight difference in the contourlines is seen. But the depth difference for SE2 in KTB is important: 4200 m instead of 3700m.

#### DISCUSSION OF RESULTS AND PREDICTION FOR THE KTB BOREHOLE

The interpretation of the ISO89 3D seismic data presented above results from a first but time consuming review of the data. It represents the momentary state but certainly not the final state of interpretation. Also this 'brute' envelope-stack contains much more information than has been extracted up to now. A careful correlation with results from measurements in the borehole itself will give impulses for further interpretation of the data.

But what are now the conclusions from this interpretation for the KTB borehole? The result of this 3D seismic interpretation is shown in Fig. 10 where the true situation of the horizons migrated up to now is sketched. Down to a depth of at most 8 km, the SE horizons (SE1, SE2, SE3, SE12) dominate the seismic section and should be drilled through. Dip, strike and depth are listed in Table 2. SE2 seems to be the upper limitation of a bundle of north-west/south-east-striking, steeply dipping horizons whereas SE1 represents the lower limitation. Between these reflections several further events occur with more or less the same dip and strike but with less energy. One attempt in picking these events is demonstrated by the SE3 reflection. Already Fig. A2 shows that there are only a few lines where this reflection could be picked. Another attempt is given by SE12. This reflector differs from the other SE events by a lesser dip. It should be noted that also the SE2 reflector is less prominent than the SE1 reflector and SE2, SE3 and SE12 are subject to greater uncertainty than SE1.

An often asked question concerns the nature of reflections. This cannot be answered here. But a relation of the steeply dipping events (SE1, SE2, SE3) with the FL is obvious and a nice correlation occurs with results from seismology. In April 1991 a small earthquake - magnitude 0.5 - was recorded in the surroundings of the KTB location. The focus was situated about 6 km north of the drill site (ca. inline 445/crossline 450 in 3D seismic data) in a depth of 7 km and the focal solution points to a dextral fault (DAHLHEIM et al. 1992). The focus correlates well with the SE2 event in that

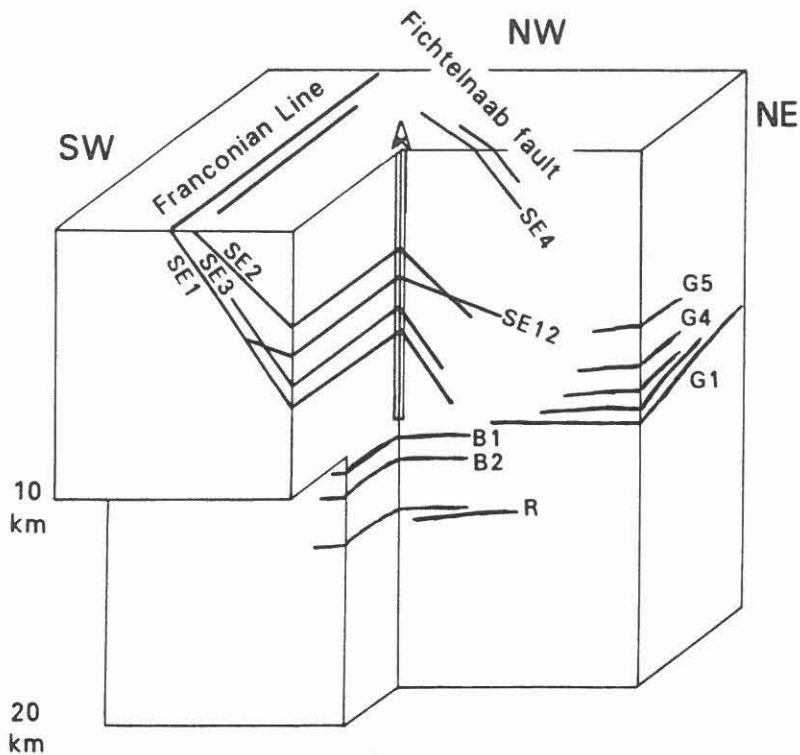


Fig. 10: Result of 3D seismic interpretation after depth migration. For depth values see Table 2.

area and thus gives indications that the SE-events reflect fault planes. The events SE4 and SE4A differ from the other SE-events by a slightly different strike direction. Their strike correlates quite well with the Fichtelnaab-fault (HIRSCHMANN, this volume).

In greater depths, i.e. below 10 km, reflections of the EB will come ahead of the bit. The EB complex consists of several events, i.e. the B- and G-reflections, that are probably displaced by a fault plane that probably is represented by the SE1 event. A look on to the depth contour maps of B2 and G1 (Figs. A38 and A43) which may correspond with each other clearly shows the separation of these horizons. The throw is about 1-3 km. The SE1 horizon (Fig. A1) excellently fits into this picture as fault plane. This is a further indication that the SE-events reflect fault planes. The nature of the EB and whether the R-reflections also belong to the EB are still open questions that must be answered by the KTB borehole.

Disregarded up to now are several events that are not yet migrated in the depth domain (e.g. ES1, ES2, ES3, K0, K2 in Figs. A23-A27).

The errors and uncertainties in depth estimation given in this paper are frightening. However, the accuracy of 3D seismic data in a crystalline area certainly cannot be compared with the accuracy we are used to in oil and gas

exploration. The latter refers to a substantially denser network of seismic profiles (2D as well as 3D) and boreholes and experience in fitting reflections, velocities and logging information. With only one borehole the tolerances in depth estimations of the oil companies would be the same as it is in our case.

#### ACKNOWLEDGEMENT

This work was supported by the Bundesministerium für Forschung und Technologie (BMFT). Special thanks are due to Dres. C. Reichert, R. Kirsch and H.-J. Dürbaum for discussions and critical review of the manuscript.

#### REFERENCES:

- AKI, K., P.G. RICHARDS, 1980. Quantitative Seismology, Theory and Methods, Volume 1, W.H. Freeman and Co., San Francisco.
- BEHR, H.J., S. GROSSE, T. HEINRICHS, U. WOLF, 1989. A reinterpretation of the gravity field in the surroundings of the KTB drill site - implications for granite plutonism and terrane tectonics in the Variscan, in: The German continental deep drilling program (KTB), EMMERMANN, R. and J. WOHLBERG (eds.), Springer Verlag, Berlin Heidelberg, 501-525.
- CHENG, C.H., D.H. JOHNSTON, 1981. Dynamic and static moduli, Geophysical Research Letters, 8, 39-42.
- DAHLHEIM, H.A., H. GEBRANDE, E. SCHMEDES, H. SOFFEL, 1992. The KTB seismological network, KTB Report 92-3, NLfB, Hannover, 167-204.
- DEKORP RESEARCH GROUP, 1988. Results of the DEKORP 4/KTB Oberpfalz deep seismic reflection investigations, J. Geophys., 62, 69-101.
- GOETZ, J.F., L.L. DUPAL, J. BOWLER, 1979. An investigation into the discrepancies between sonic log and seismic check shot velocities, J. Austral. Petr. Explor. Assoc., 19, 131-141.
- HANITZSCH, CH., P. HUBRAL, TH. RÜHL, W. SÖLLNER, 1992. Migration of steep dipping reflectors at the KTB site: Depth errors caused by inaccurate velocity models, KTB Report 92-5, NLfB, Hannover.
- HIRSCHMANN, G., 1992. On the geological interpretation of the 3D-seismic data with special regard to the information from the KTB boreholes, KTB Report 92-5, NLfB, Hannover.
- HLUCHY, P., M. KÖRBE, R. THOMAS, 1992. Preliminary results of the interpretation of the 3D-seismic survey at the KTB location, KTB Report 92-5, NLfB, Hannover.
- KERN, H., R. SCHMIDT, T. POPP, 1991. The velocity and density structure of the 4000 m crustal segment at the KTB drilling site and their relationship to lithological and microstructural characteristics of the rocks: an experimental approach, Scientific Drilling, 2, 130-145.
- KÖRBE, M., C. REICHERT, 1992. On the character of "Steep Event SE-1" - reflected energy, reflected refraction, diffraction or any artifact, KTB Report 92-5, NLfB, Hannover.

- LENGELING, R., 1991. Bewertung eines Inversionsverfahrens zur Berechnung statischer Korrekturen in der 3D-Seismik und seine Anwendung auf reflexionsseismische DEKORP-Messungen in der Oberpfalz 1989, Dissertation, Universität Karlsruhe.
- LIPPMANN, E., CH. BÜCKER, E. HUENGES, A. RAUEN, J. WIENAND, K. WOLTER, H.C. SOFFEL, 1989. Rock physical properties: first results of the KTB-field-laboratory, Scientific Drilling, 1, 143-149.
- LIU, H.P., D.L. ANDERSON, H. KANAMORI, 1976. Velocity dispersion due to anelasticity; implications for seismology and mantle composition, Geophys. J. R. astr. Soc., 47, 41-58.
- REHLING, J.G., M. STILLER, 1990. 3D reflection seismic survey of the area around the KTB drilling site, KTB Report 90-6b, NLfB, Hannover.
- RÜHL, TH., HANITZSCH, CH., 1992. Average and interval velocities derived from first breaks of vertical seismic profiles at the KTB deep drilling site, KTB Report 92-5, NLfB, Hannover.
- SATTLEGGGER, J., 1986. Three-dimensional map migration and modeling algorithm, Sattlegger Ingenieurbüro für angewandte Geophysik, Meppen.
- SCHWANITZ, H., J. MYLIUS, R. LENGELING, H. ARNETZL, 1990. DEKORP - Integrierte Seismik Oberpfalz 1989 (ISO'89), Bericht, PRAKLA-SEISMOS AG, Hannover.
- SCHMOLL, J., R. BITTNER, H.J. DÜRBAUM, T. HEINRICHS, R. MEISSNER, C. REICHERT, T. RÜHL, H. WIEDERHOLD, 1989. Oberpfalz deep seismic reflection survey and velocity studies, in: The German continental deep drilling program (KTB), EMMERMANN, R. and J. WOHLLENBERG (eds.), Springer-Verlag, Berlin Heidelberg, 99-149.
- SOFFEL, H.C., S. PLAUMANN, R. PUCHER, C. BÜCKER, H.J. GÖTZE, M. WAGENER, V. HAAK, 1989. Gravity and magnetic investigations at the KTB locations Schwarzwald and Oberpfalz, in: The German continental deep drilling program (KTB), EMMERMANN, R. and J. WOHLLENBERG (eds.), Springer-Verlag, Berlin Heidelberg, 409-431.
- STILLER, M., 1991. 3D vertical incidence seismic reflection survey at the KTB location, Oberpfalz, in: Continental Lithosphere: Deep Seismic Reflections, MEISSNER et al. (eds.), Geodynamics Series Vol. 22, Am. Geophys. Union, Washington D.C., 101-113.
- STILLER, M., 1992. Preliminary generation of a stacked data volume of the entire ISO89 3D-reflection data set using an envelope technique, KTB Report 92-5, NLfB, Hannover.
- STETTNER, G., 1992. Zur Korrelation des tektonischen Baues mit den seismischen Strukturen im Raum KTB-Oberpfalz - Münchberger Gneismasse, KTB Report 92-5, NLfB, Hannover.

APPENDIX

Figs. A1 - A30: Two-way-travel-time contour maps [ms] of interpreted horizons. The profiles the reflections are picked on are marked by bars; the darker the colour the greater the traveltime.

Figs. A31 - A47: Depth contour maps [m] obtained by map migration using the velocity model 1005. The 0-contour-line refers to sea-level.

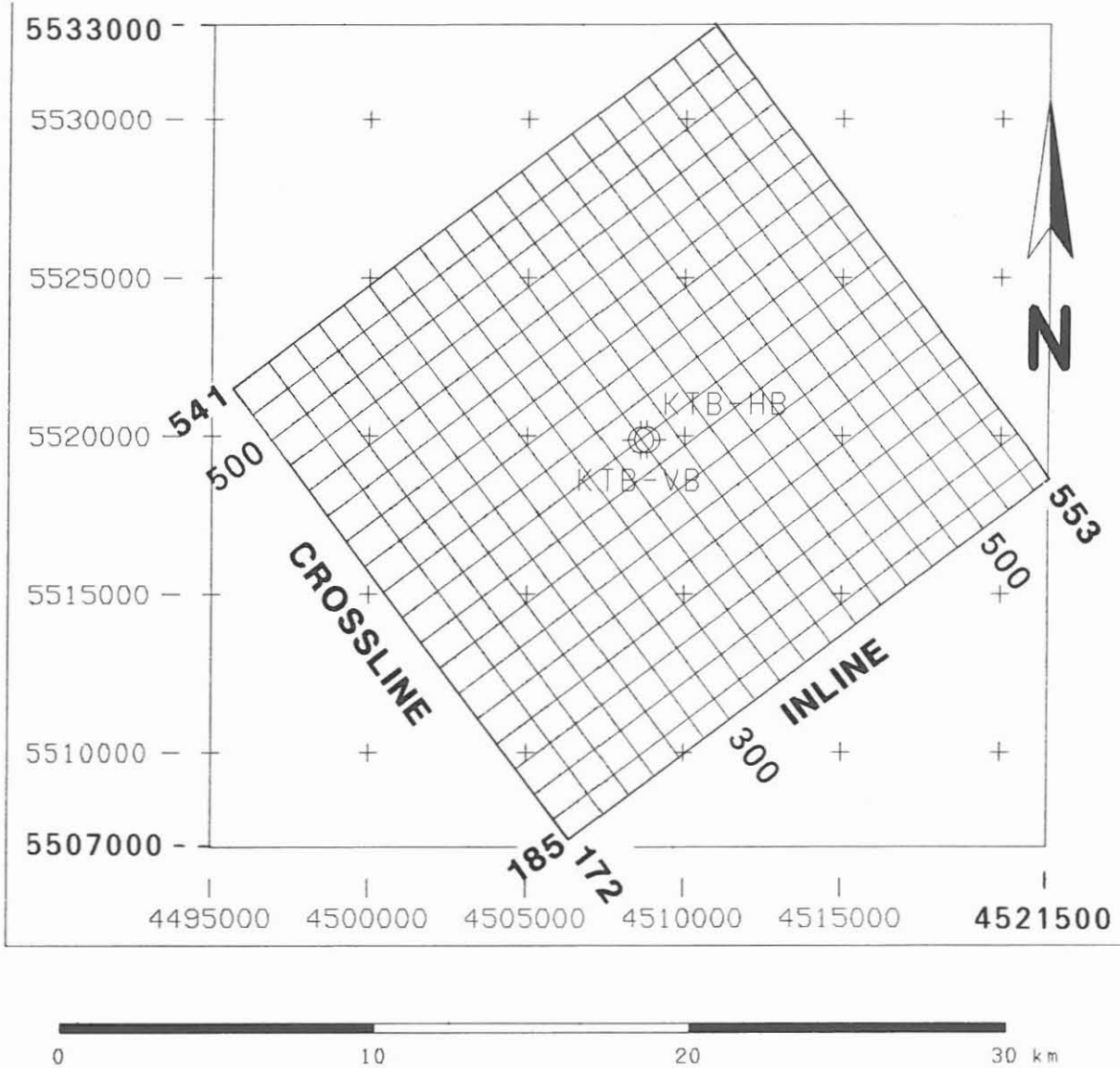


Fig. A0: Map window for figures in appendix.

Coordinates of KTB:	Gauß-Krüger	Crossline/Inline
KTB-VB (pilot hole):	4508590 E/5519865 N	CDP 360/Inline 360
KTB-HB (main hole):	4508790 E/5519880 N	CDP 363/Inline 357

Height above sea-level: 513 m.

The pilot hole (KTB-VB) and main hole (KTB-HB) are marked or only the main hole.

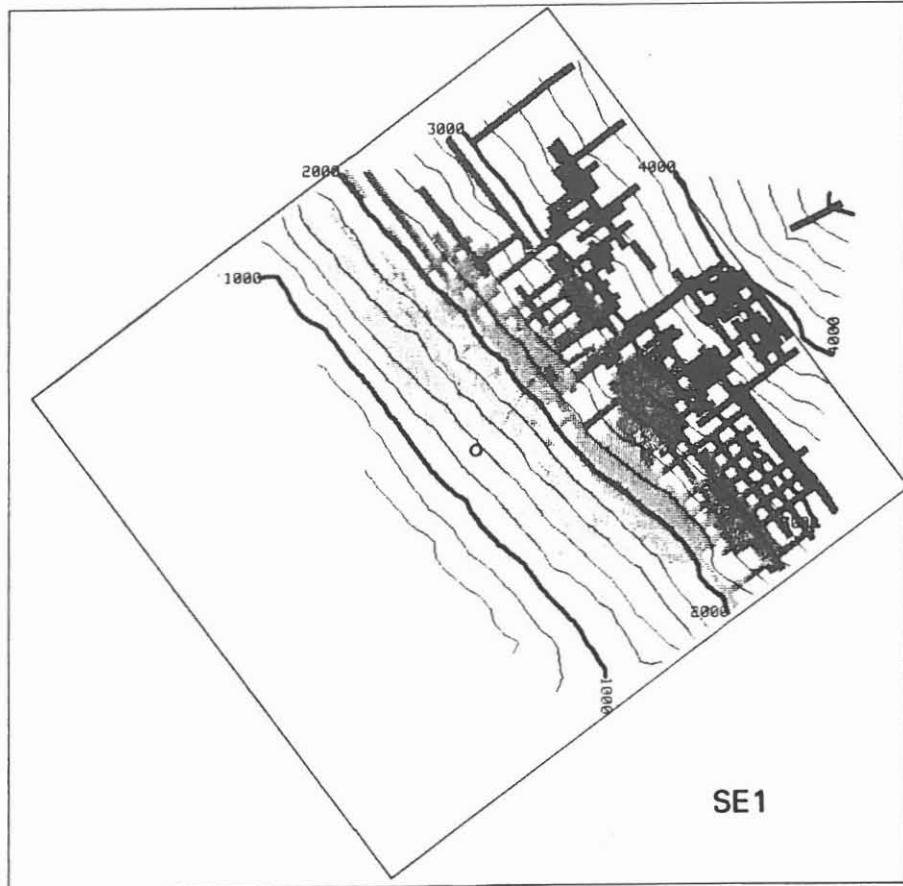


Fig. A1

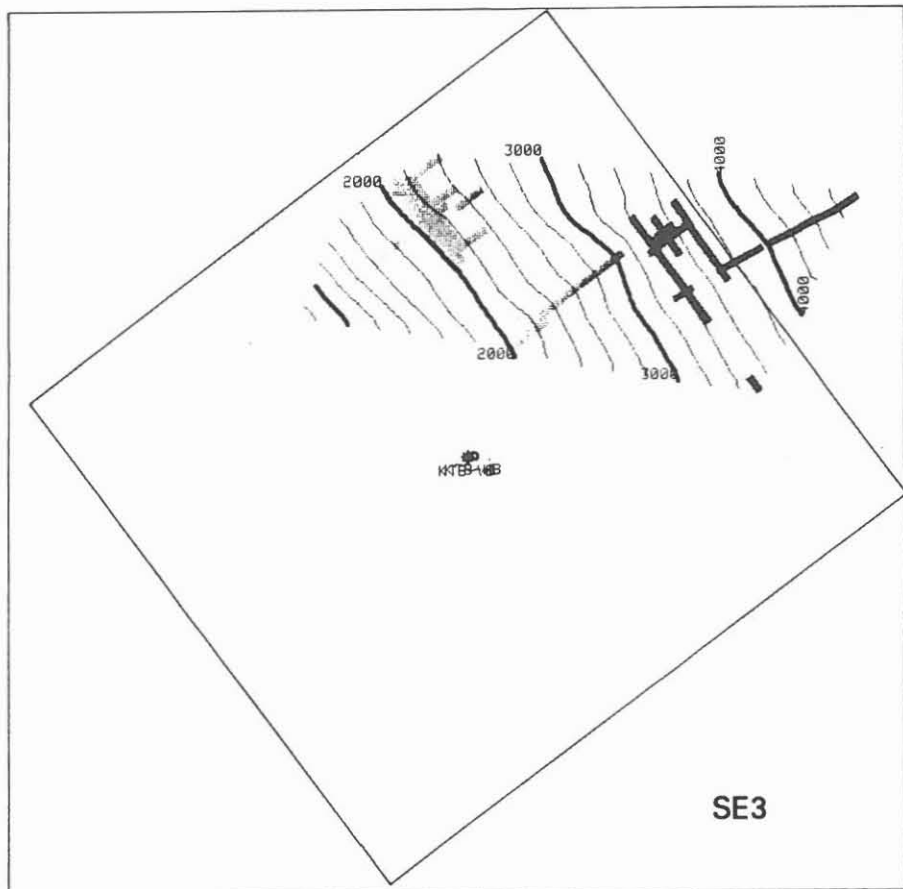


Fig. A2

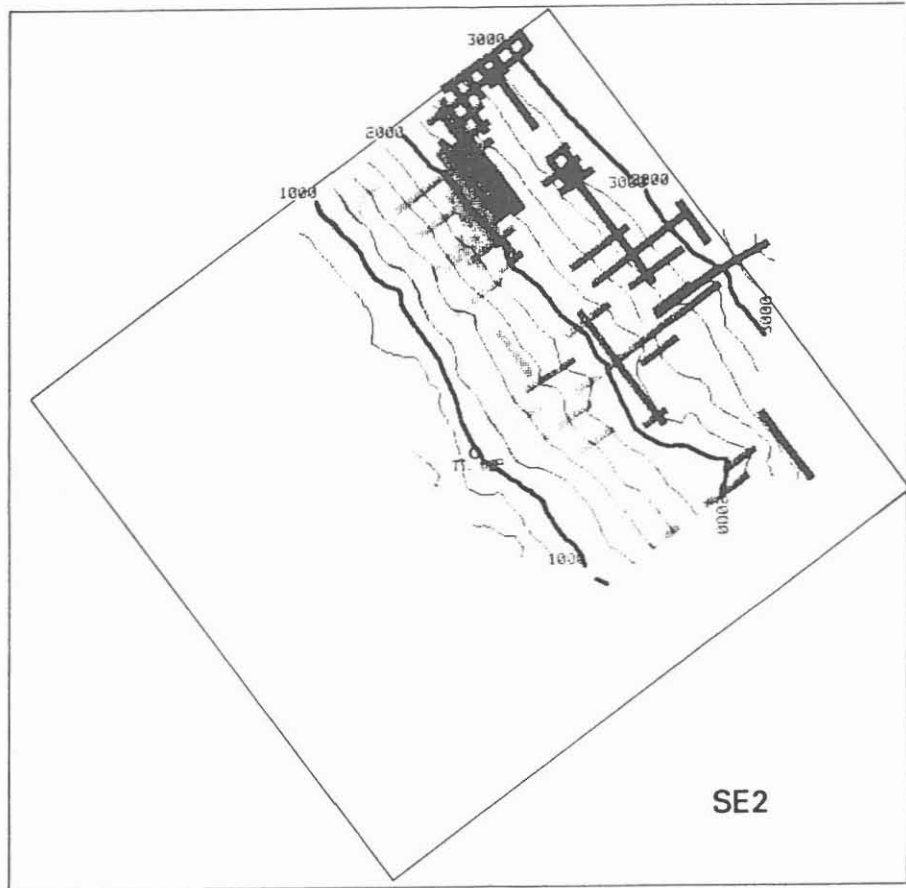


Fig. A3



Fig. A4:  
The area of  
interpretation  
that differs  
from Fig. A3  
is marked by  
dots.



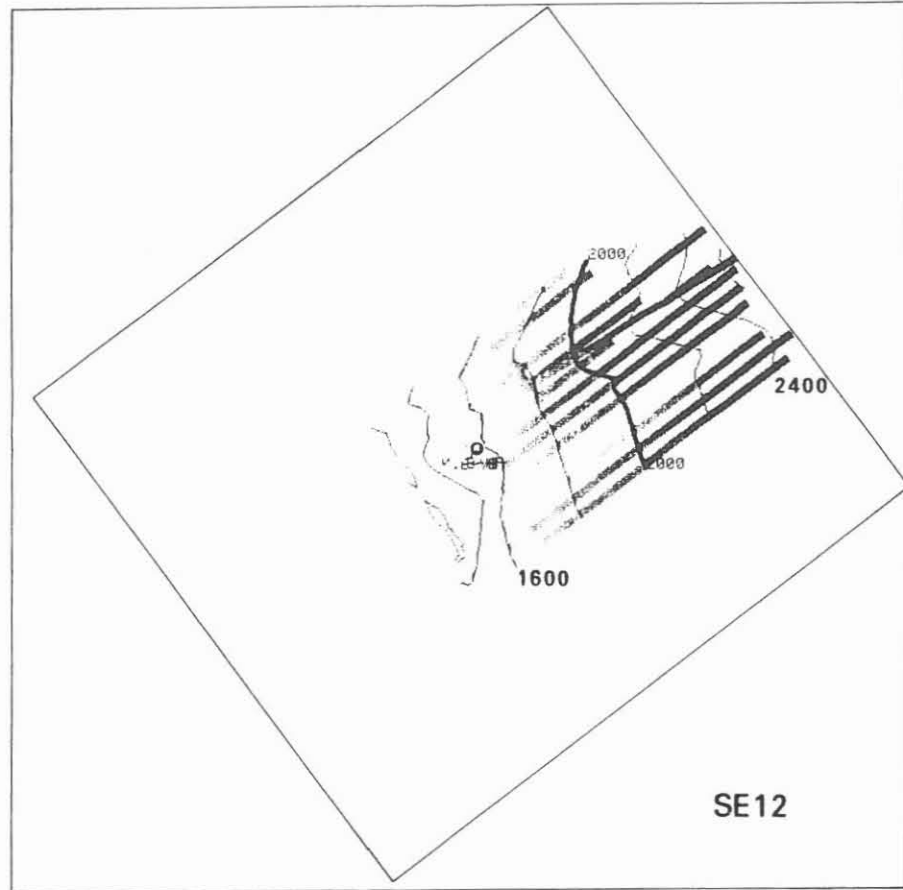


Fig. A5

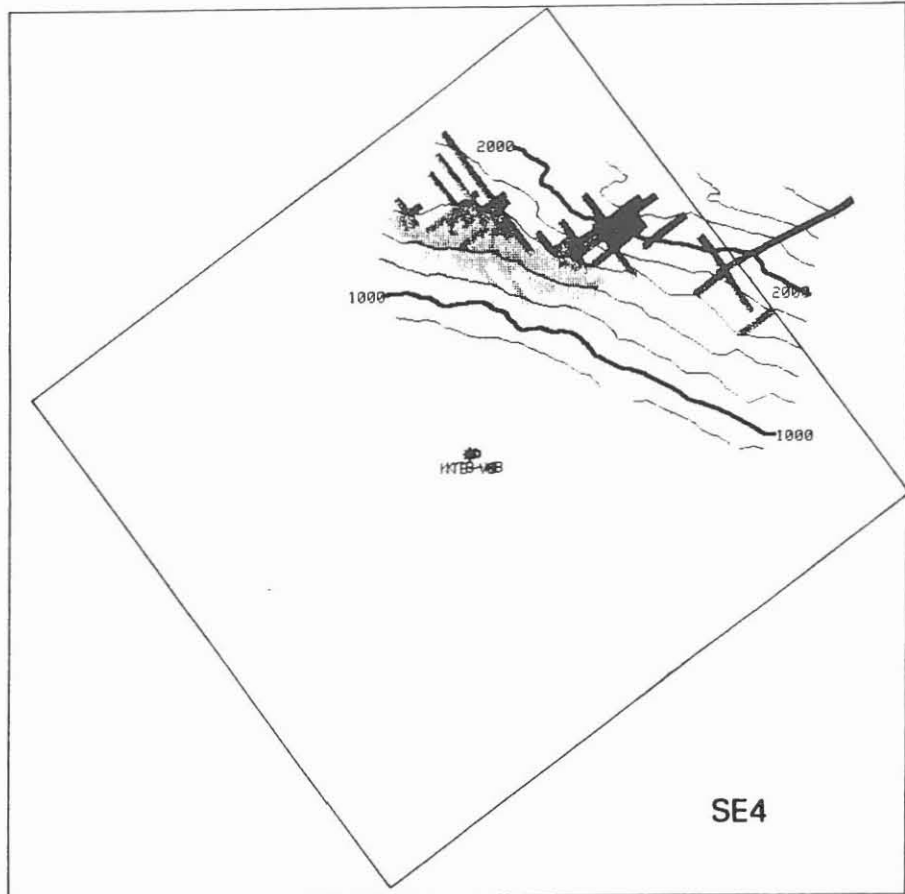


Fig. A6

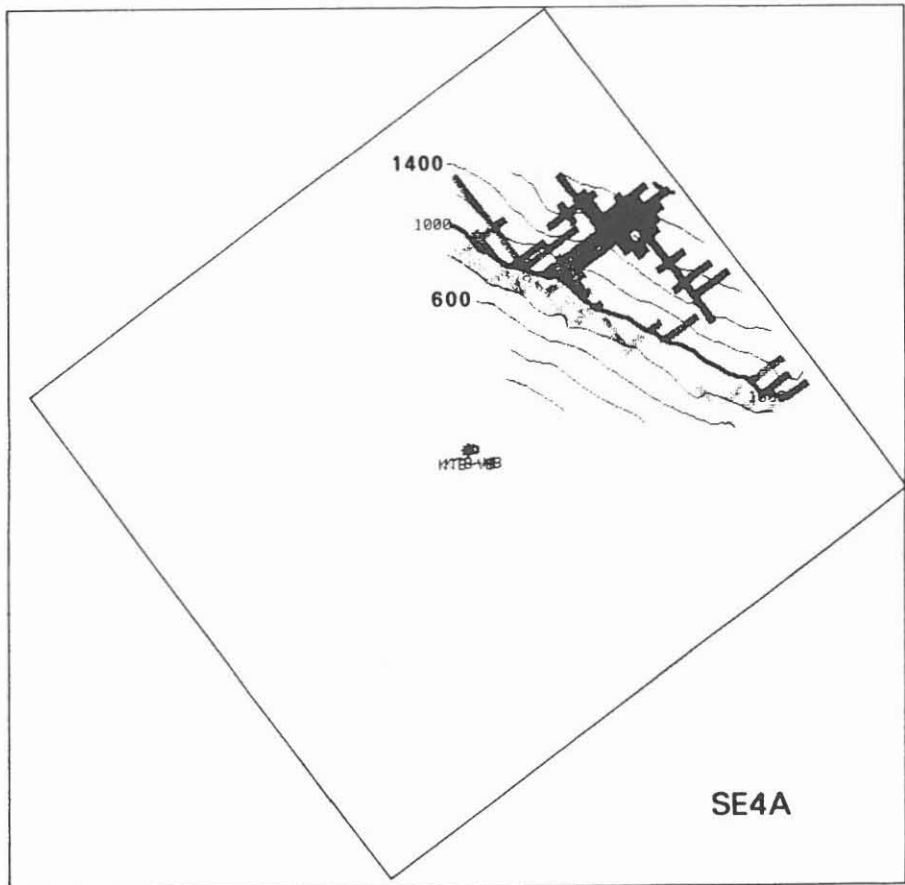


Fig. A7

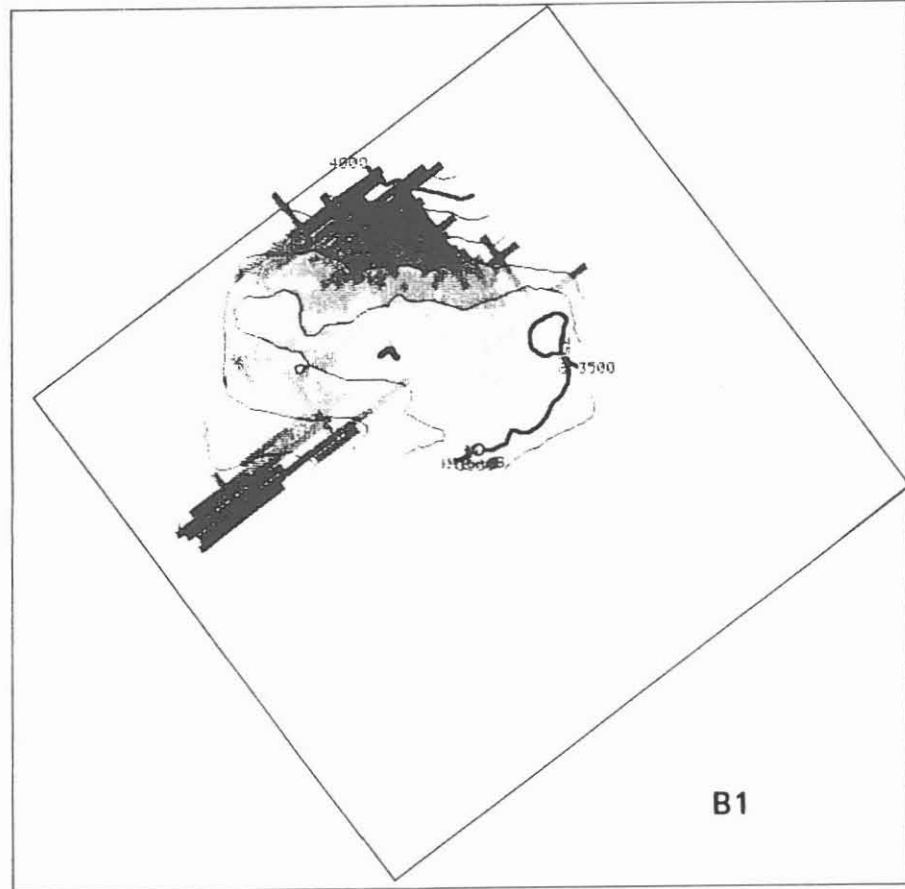


Fig. A8

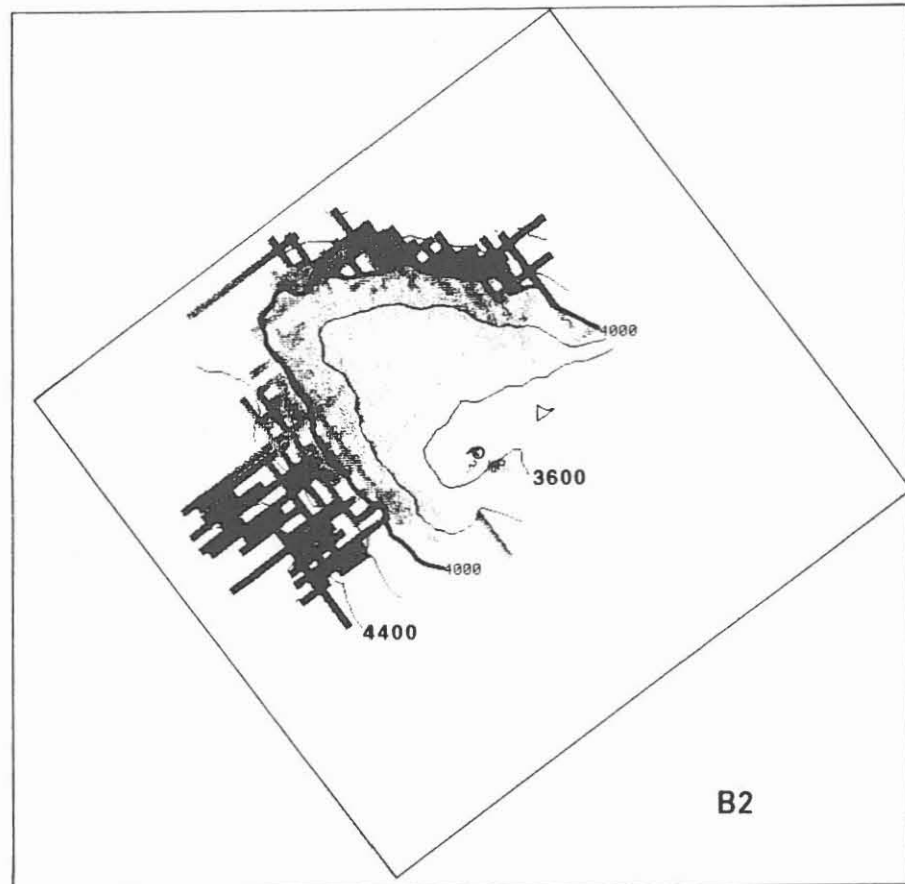


Fig. A9

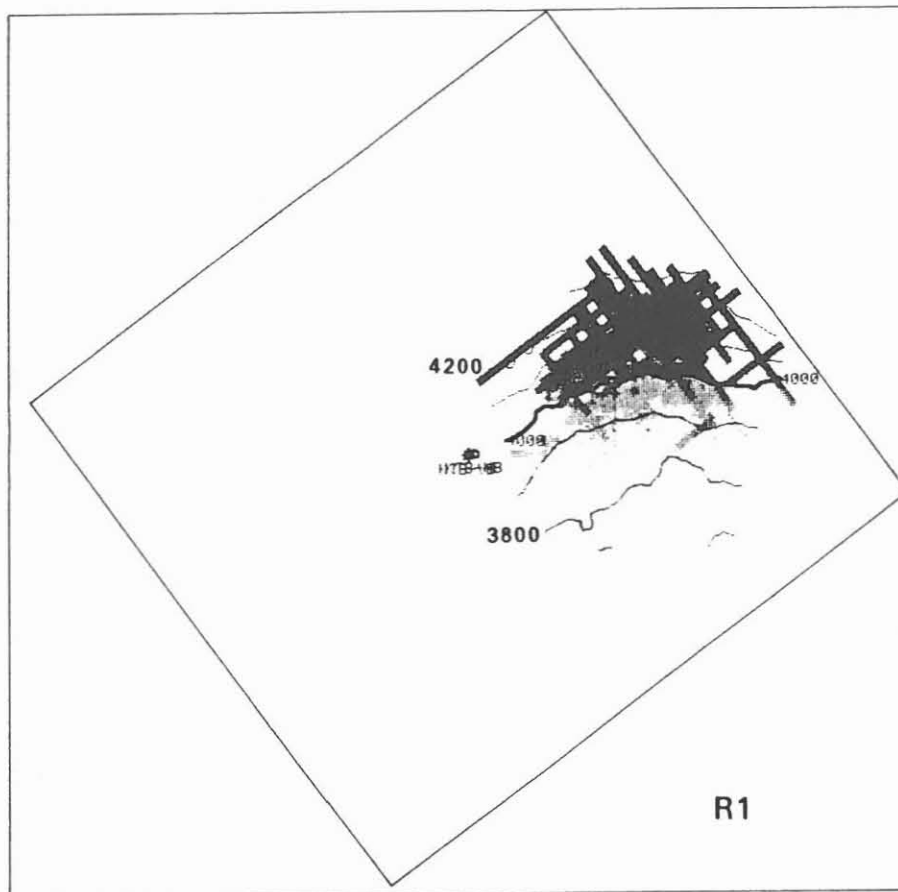


Fig. A10

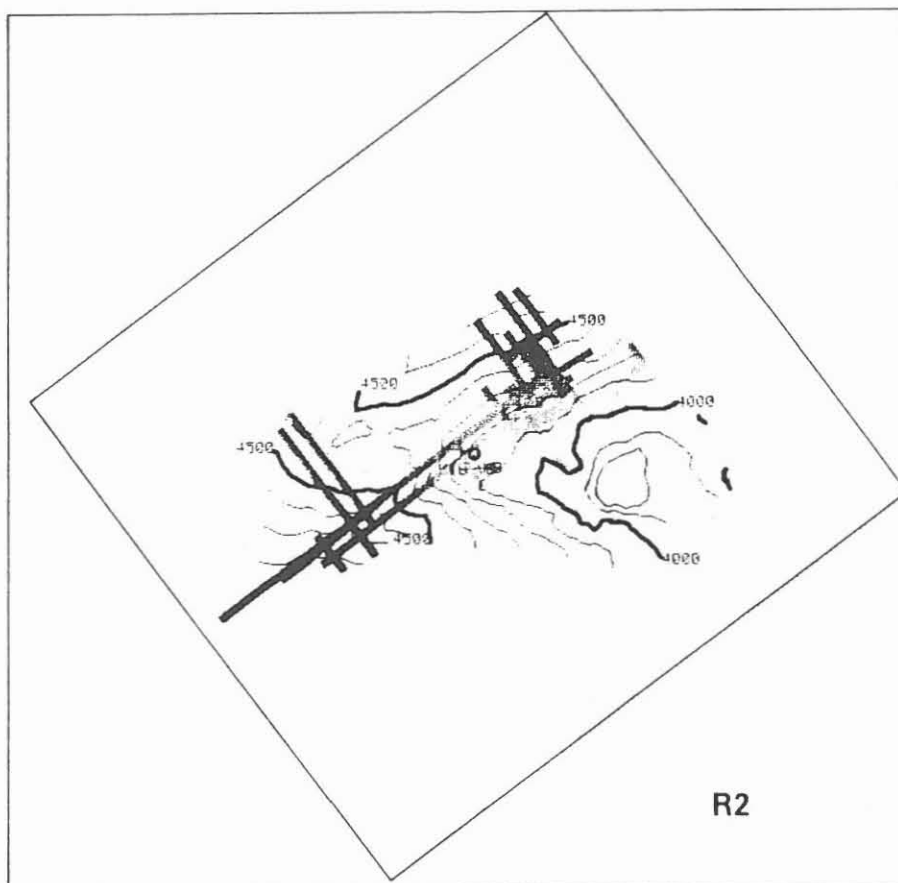


Fig. A11

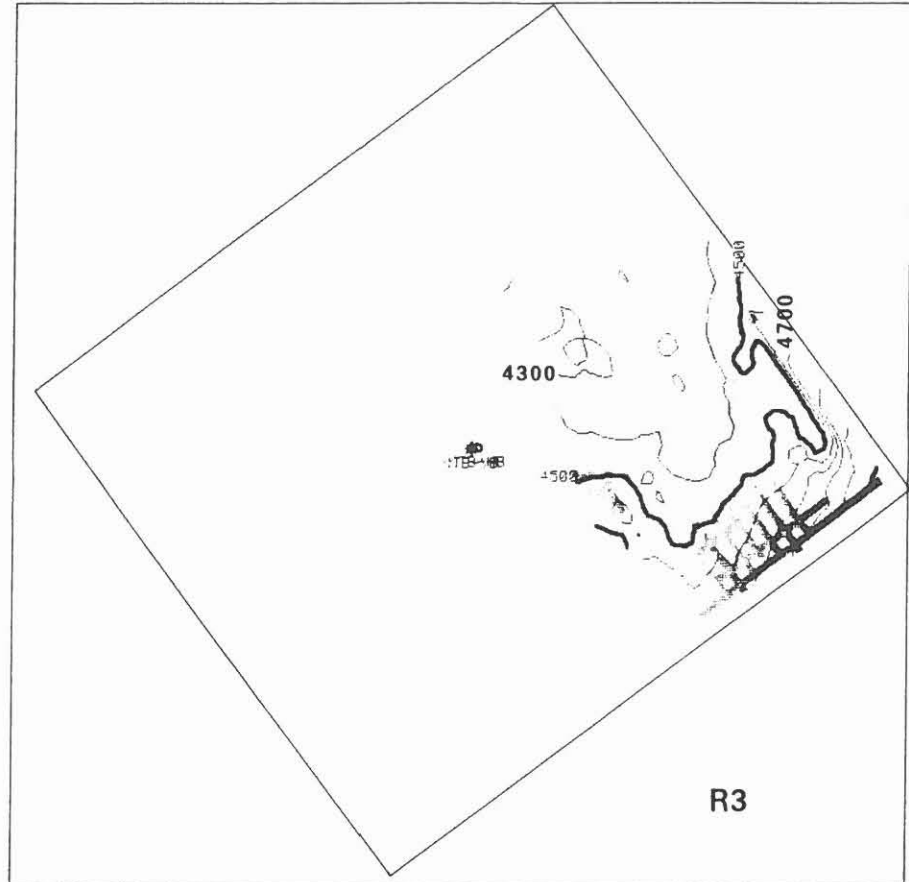


Fig. A12

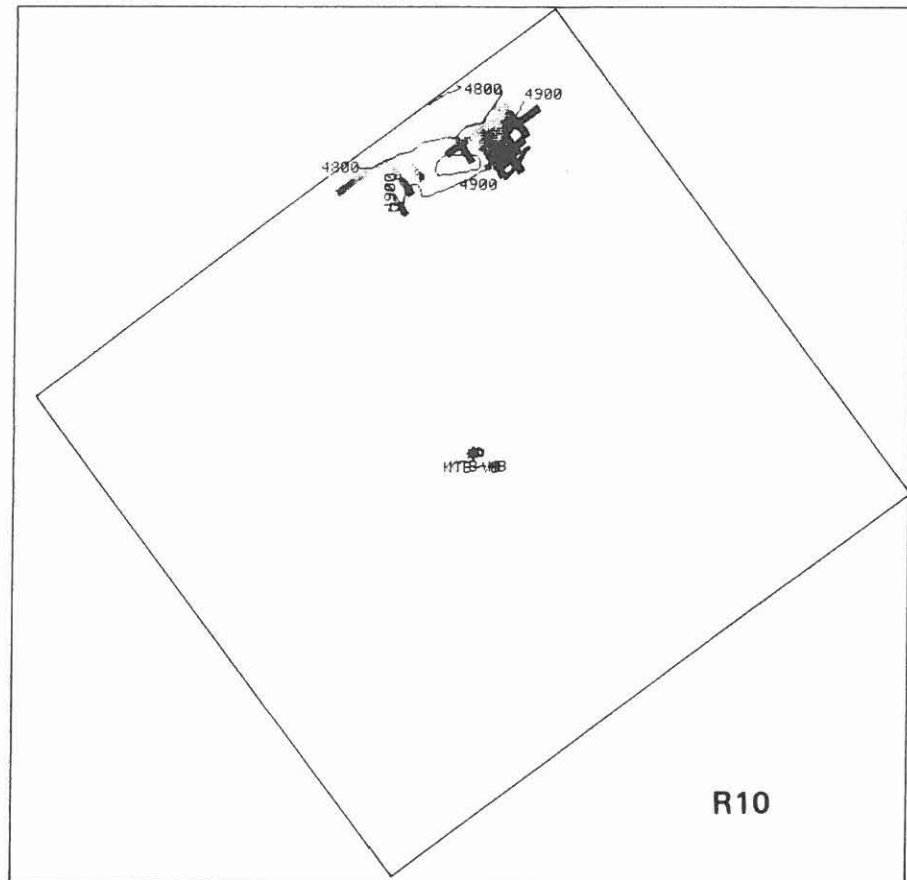


Fig. A13

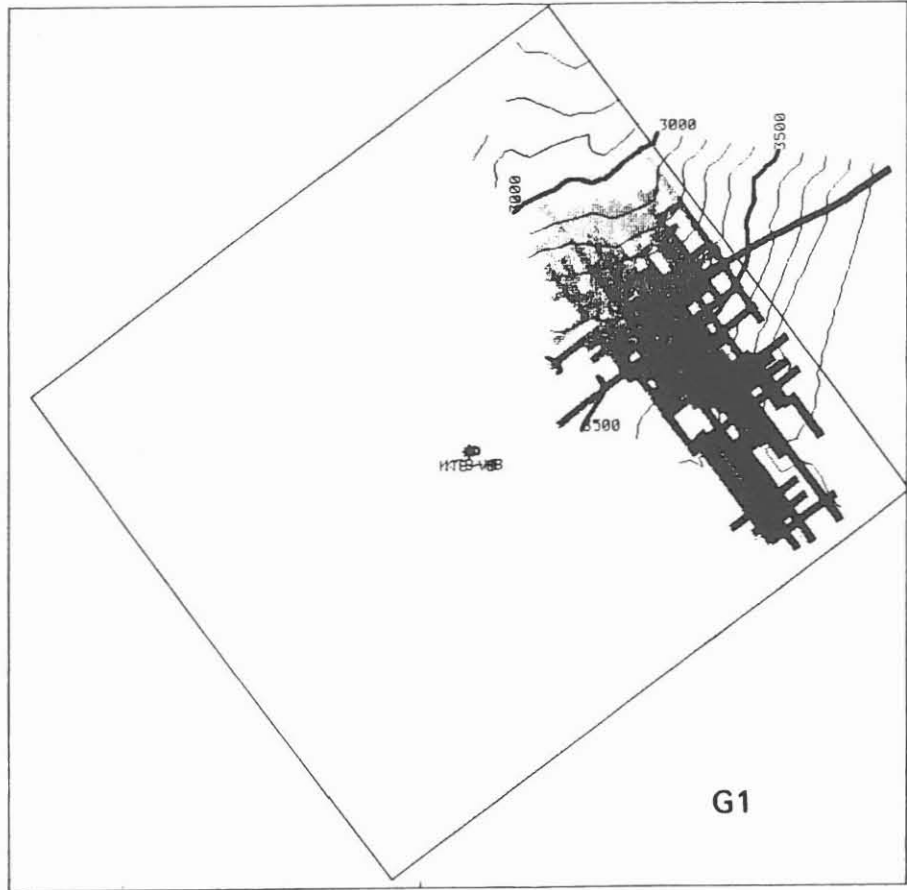


Fig. A14

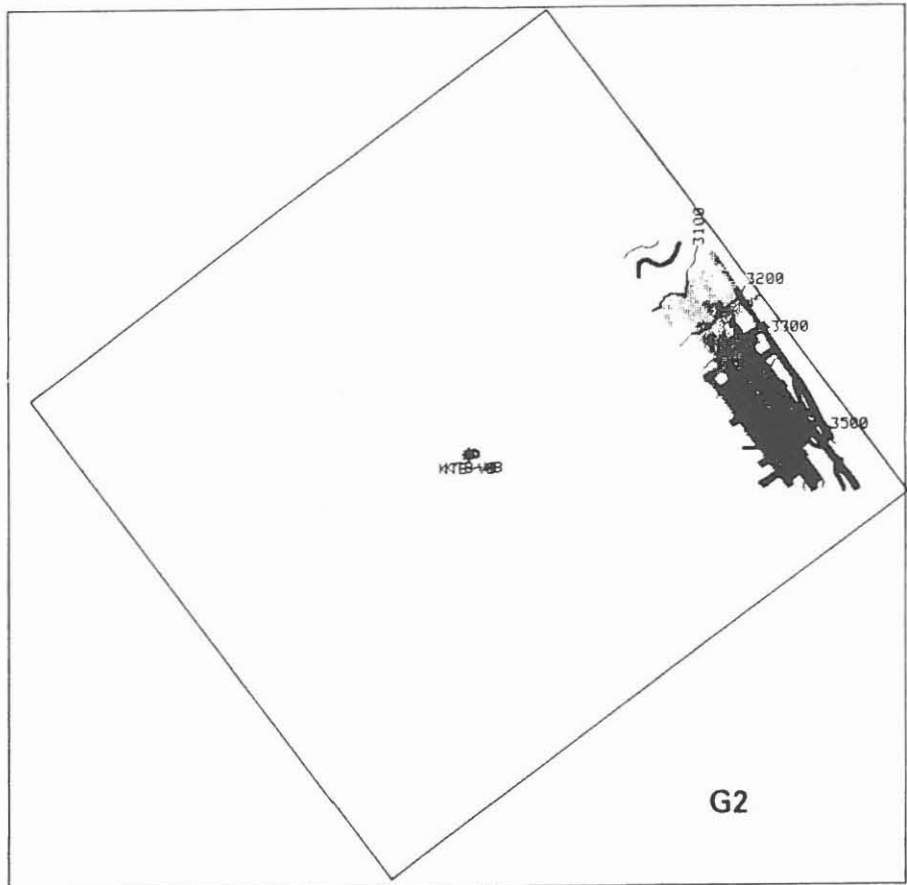


Fig. A15

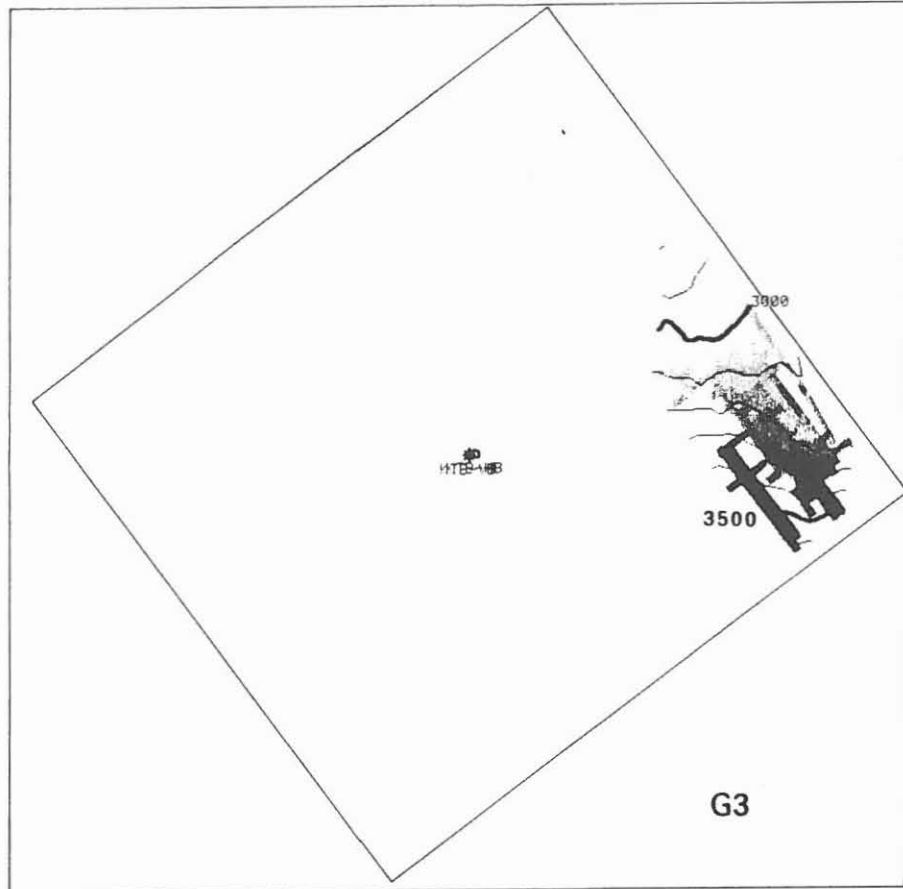


Fig. A16

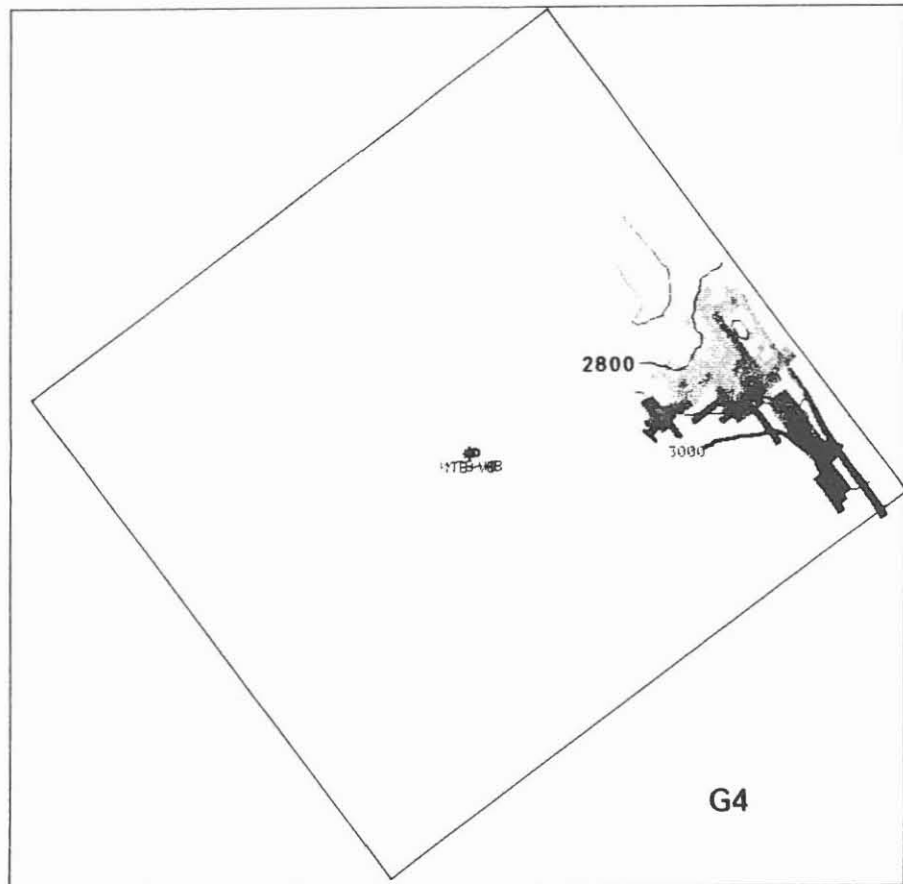


Fig. A17

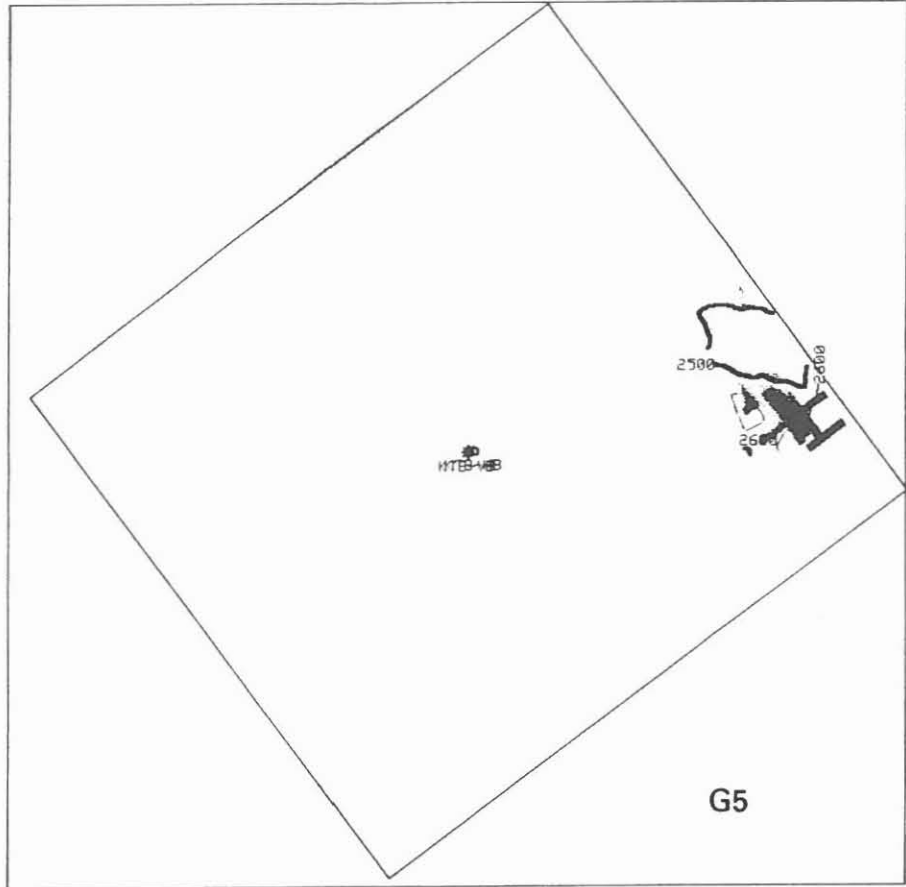


Fig. A18

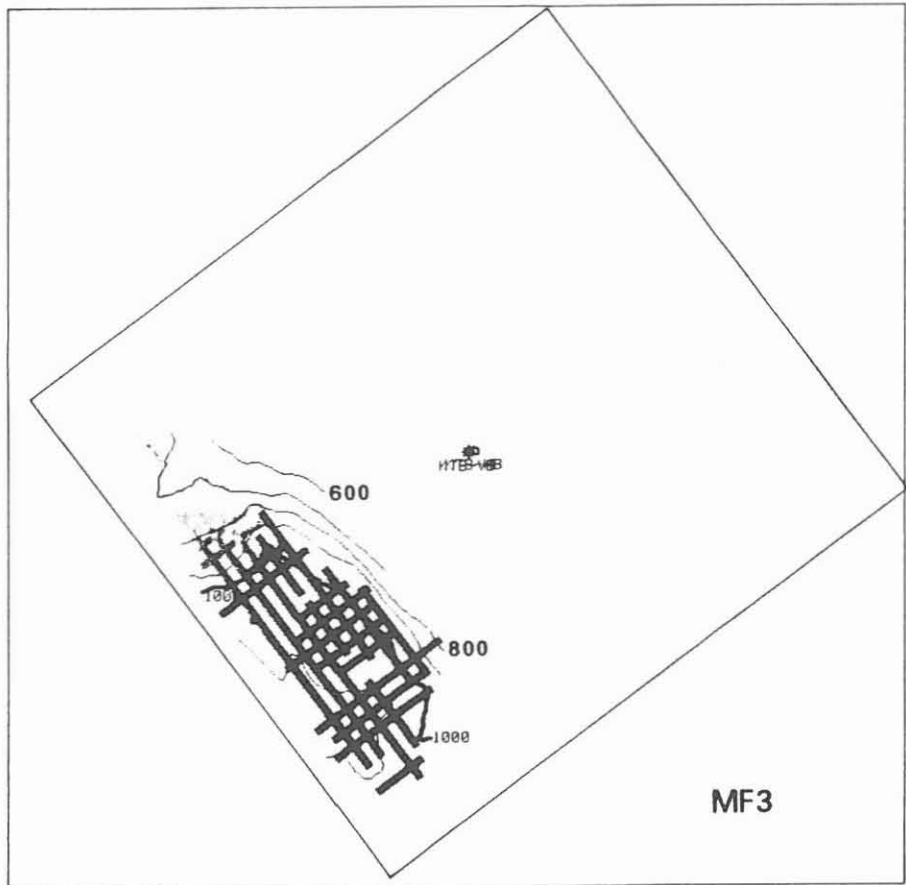


Fig. A19



Fig. A20

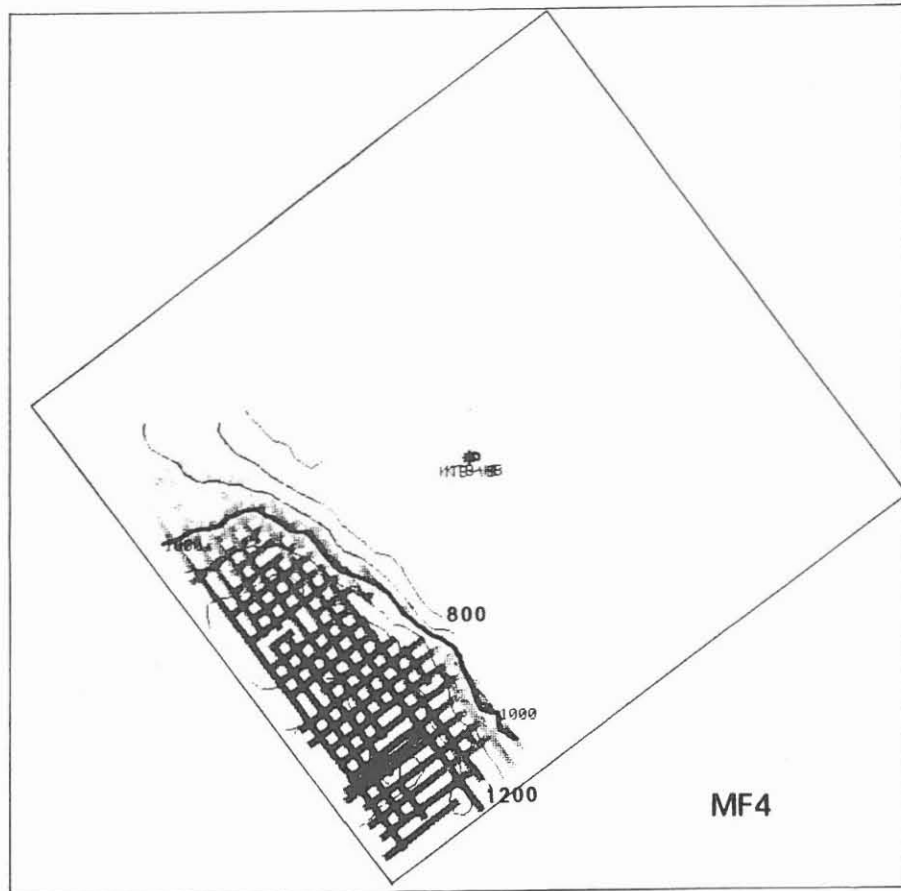
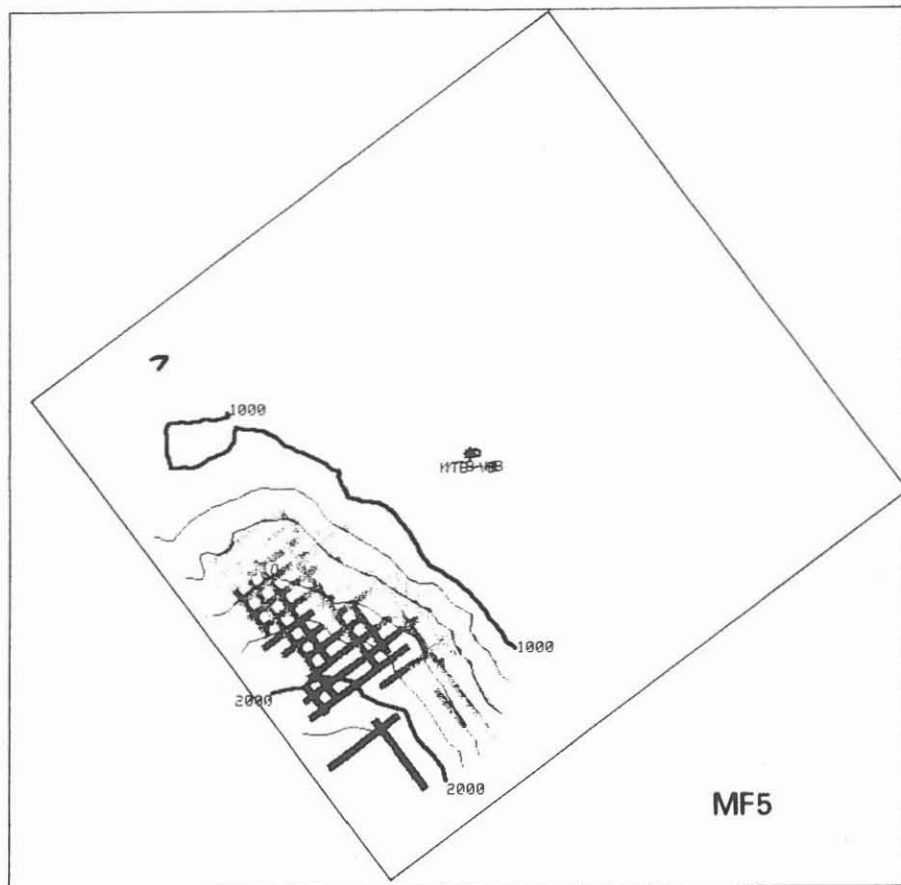


Fig. A21



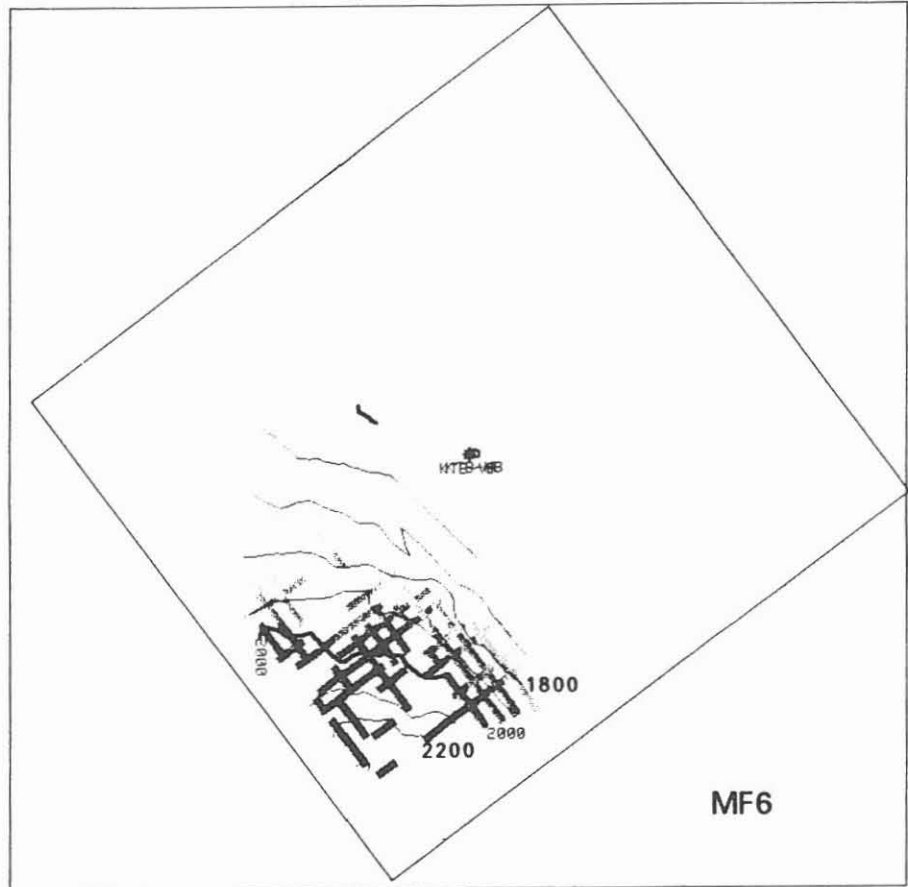


Fig. A22

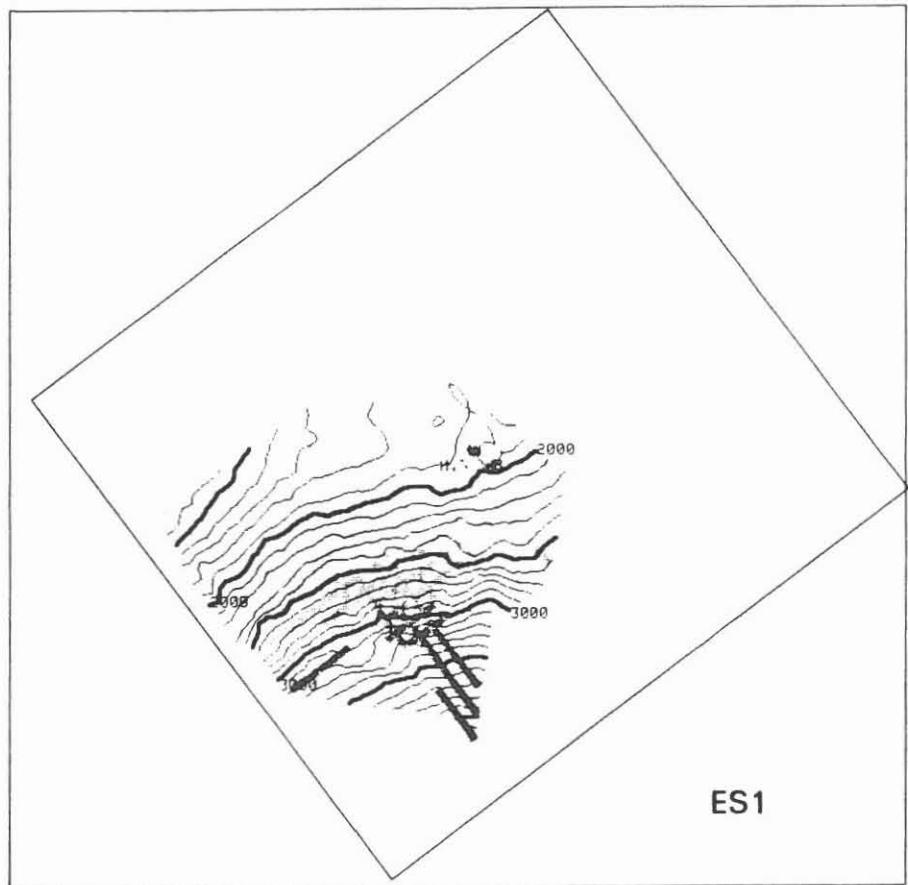


Fig. A23

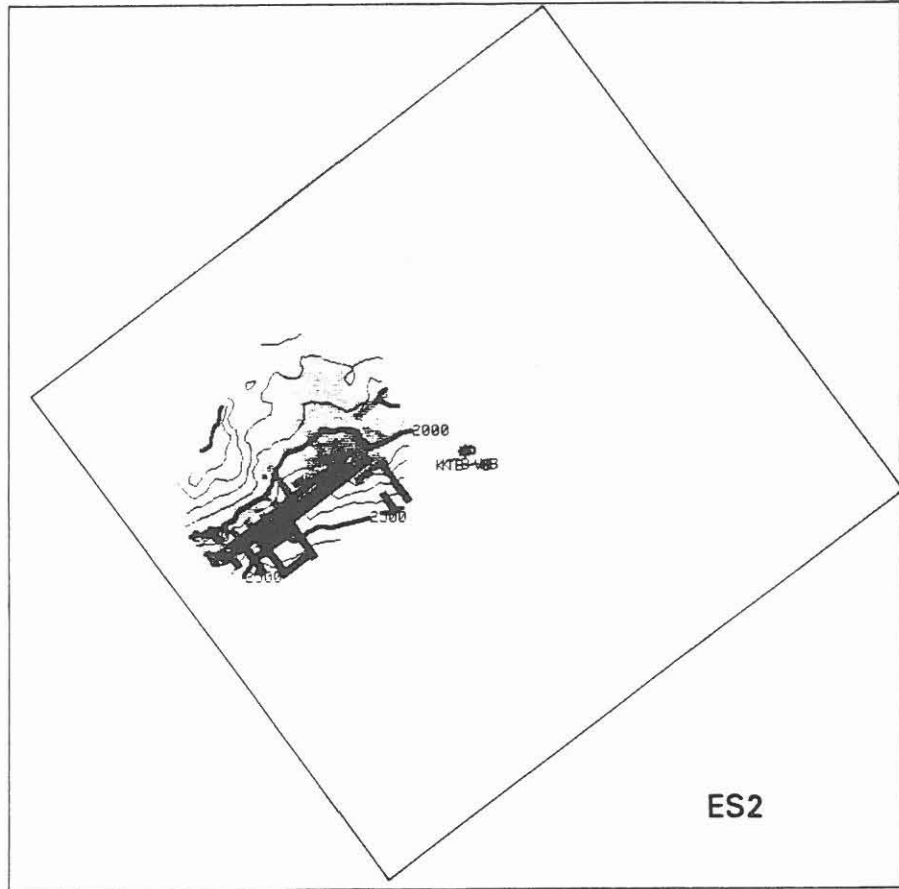


Fig. A24

ES2

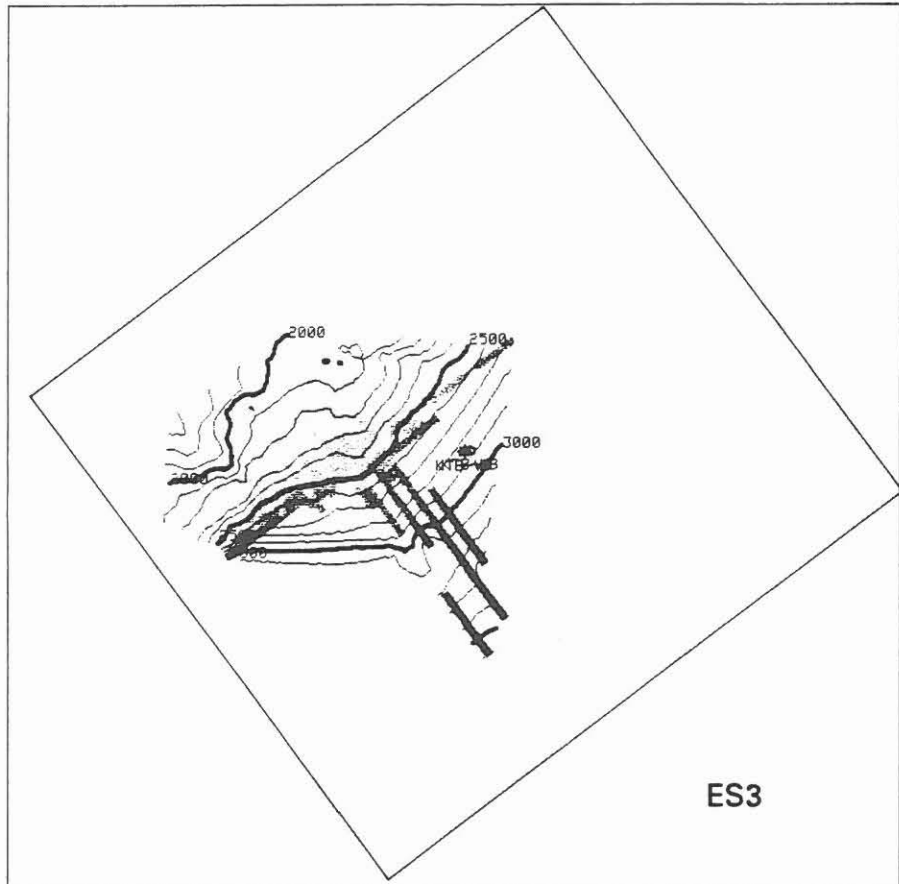


Fig. A25

ES3

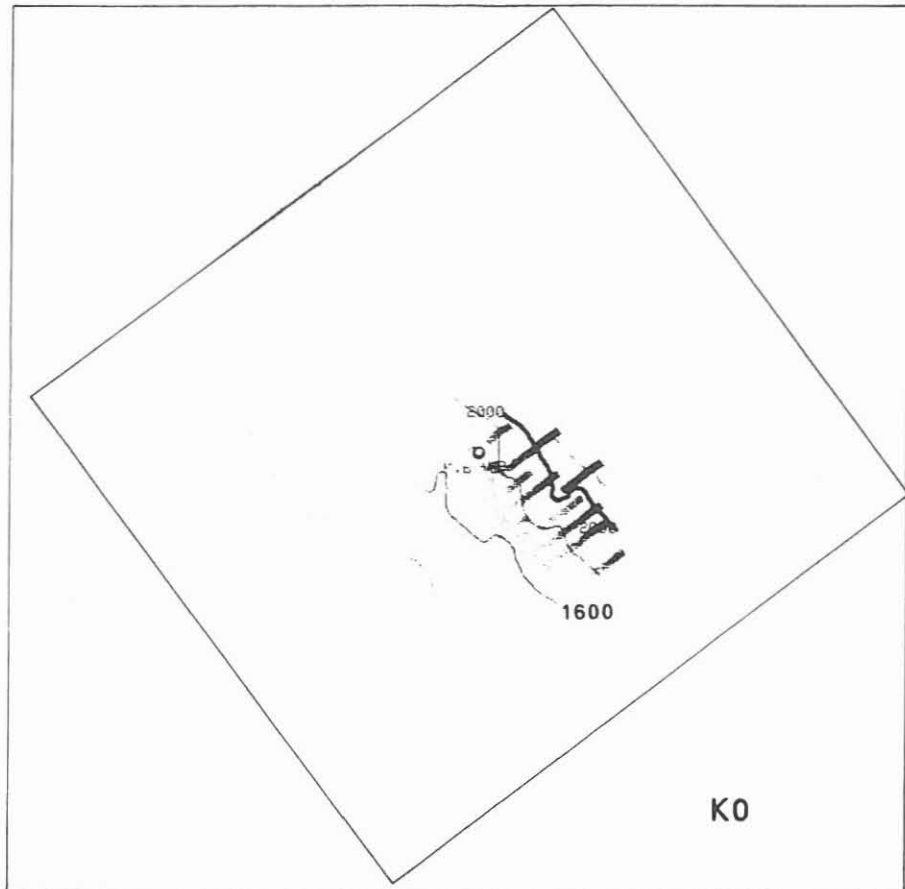


Fig. A26

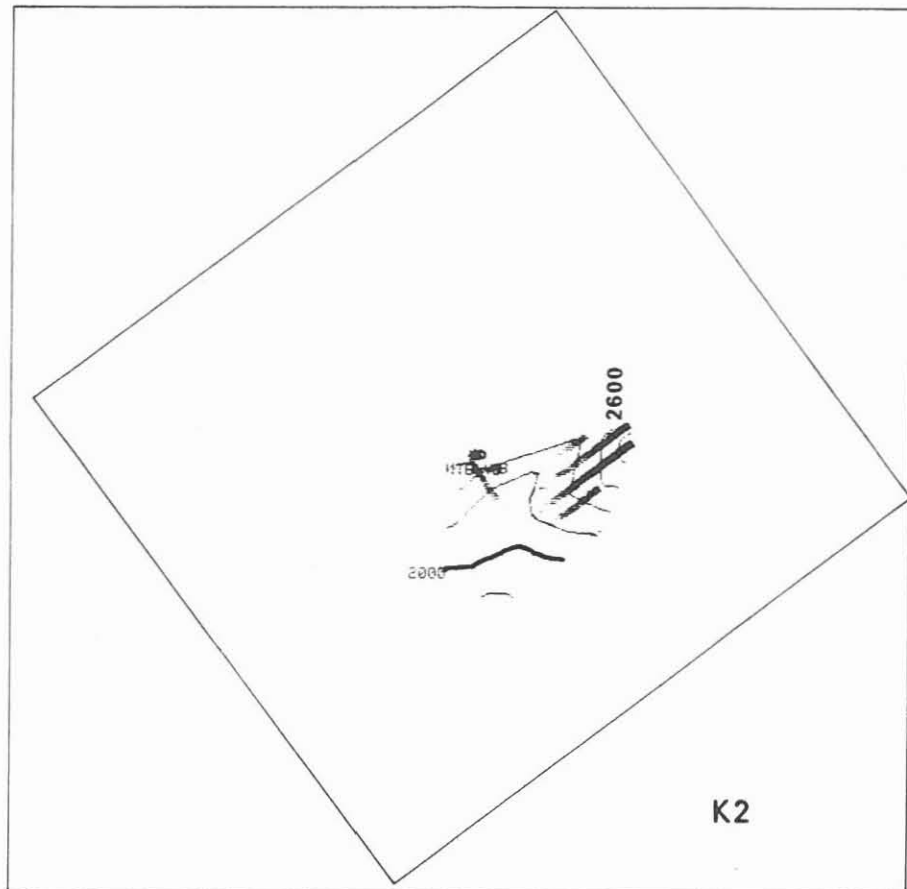


Fig. A27

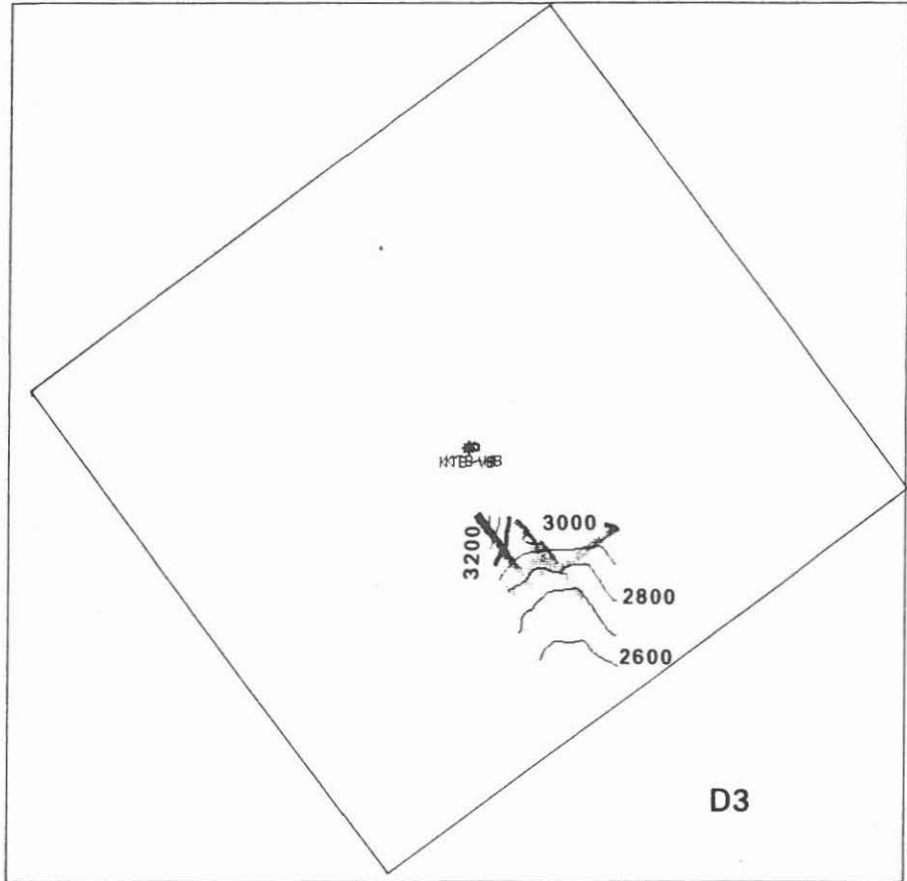


Fig. A28

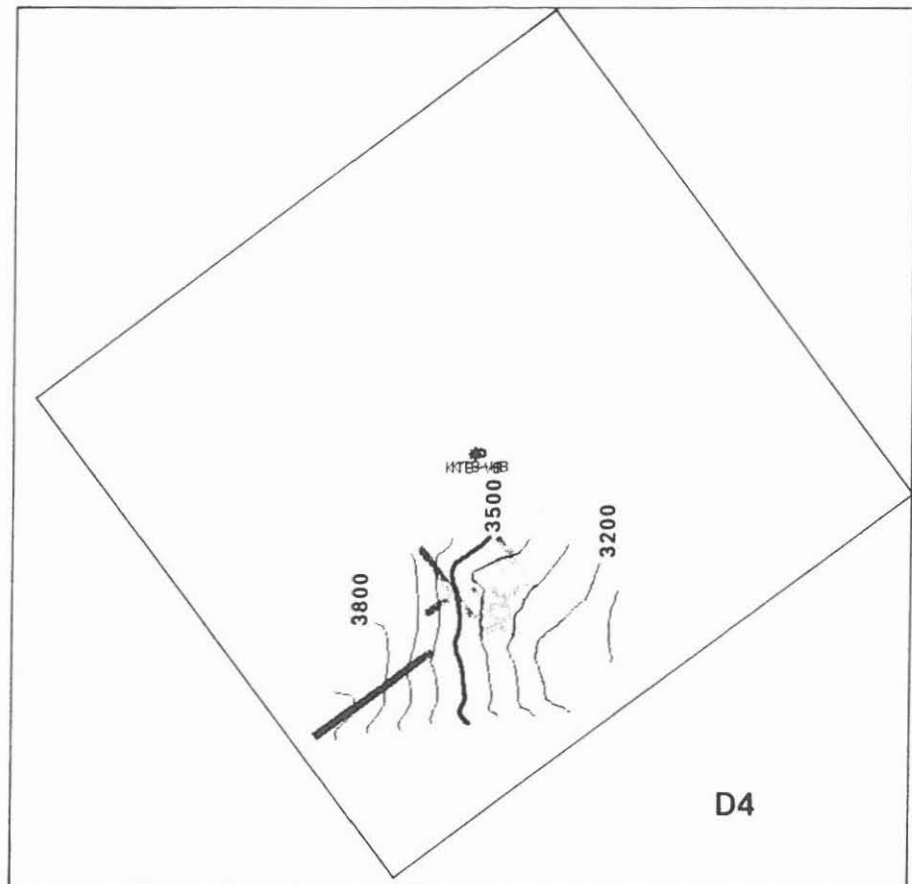


Fig. A29

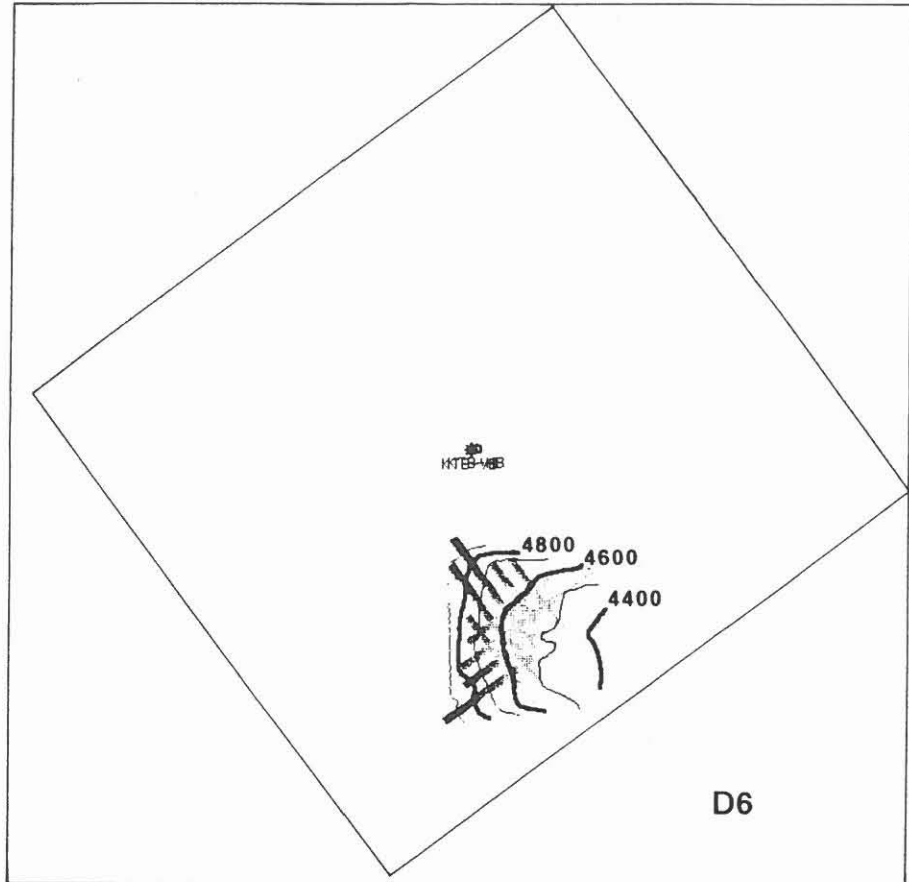


Fig. A30

4495000 4500000 4505000 4510000 4515000 4520000

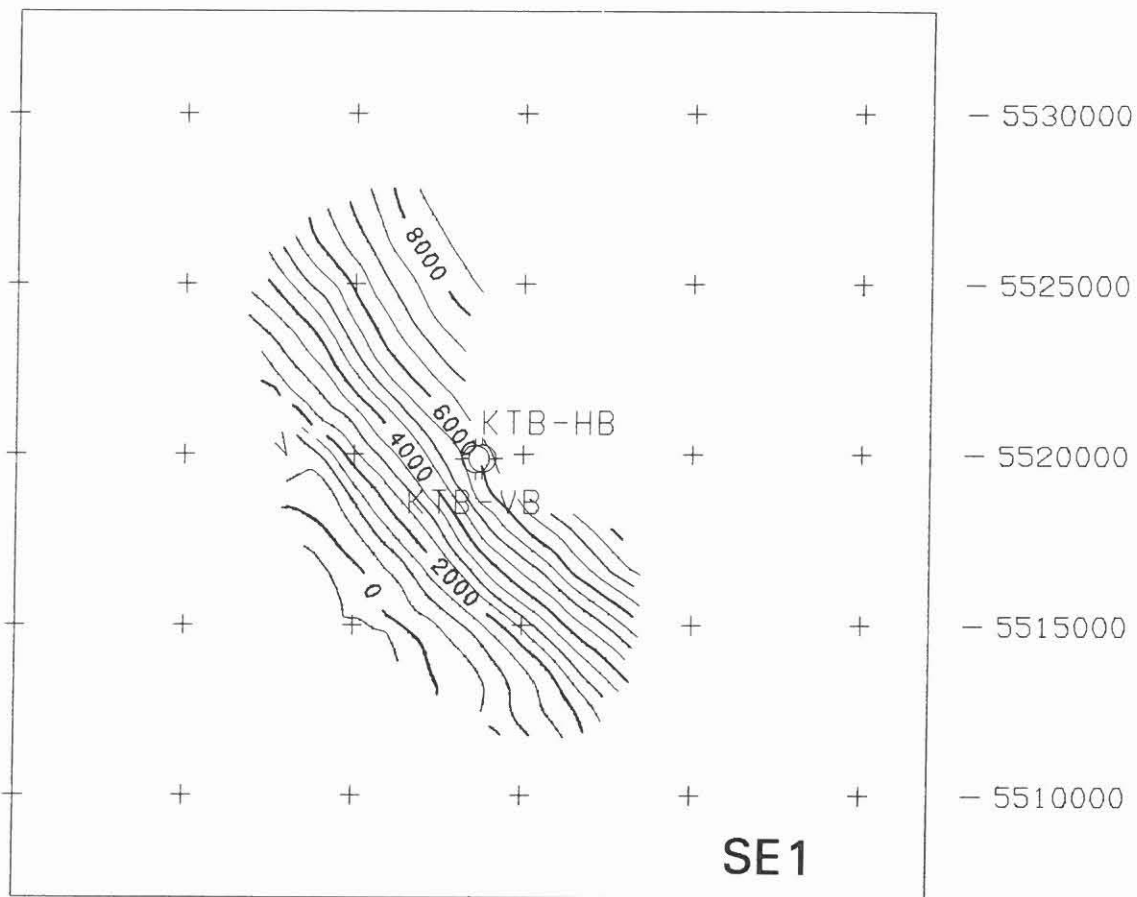


Fig. A31

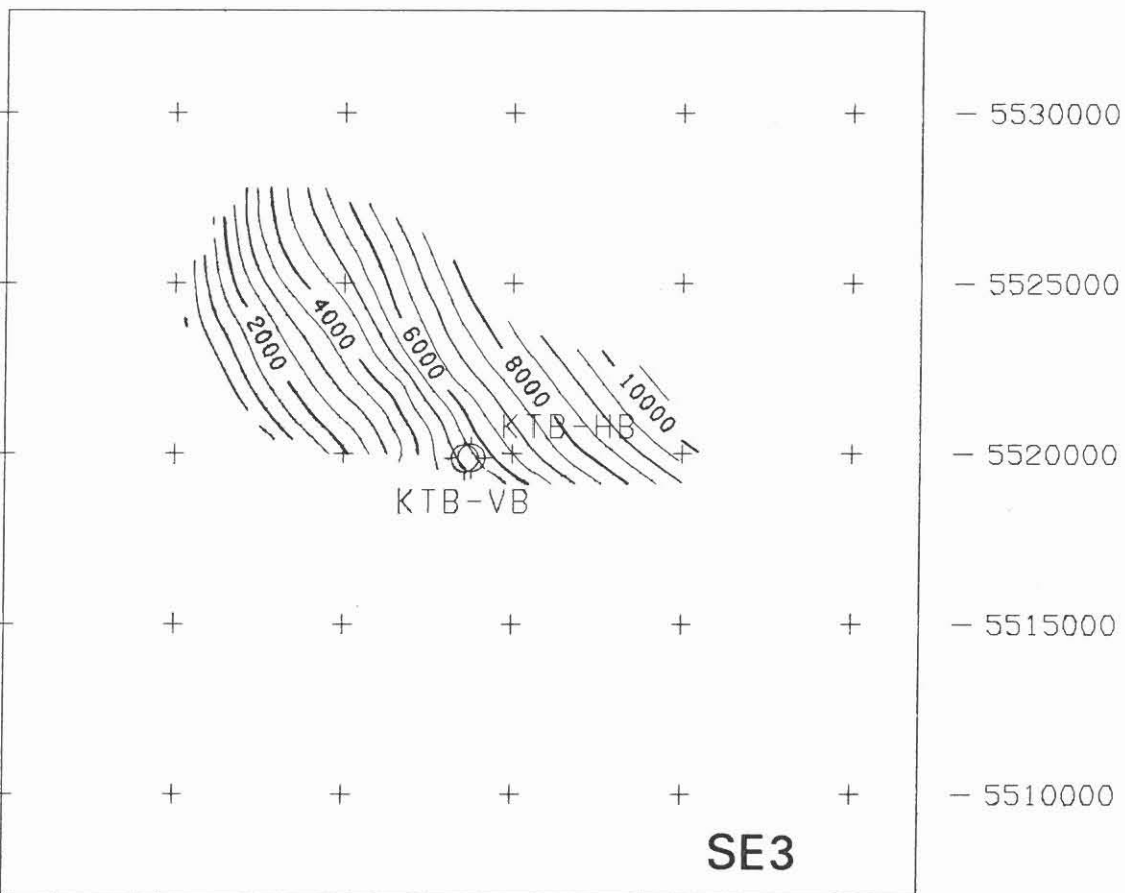


Fig. A32

4495000 4500000 4505000 4510000 4515000 4520000

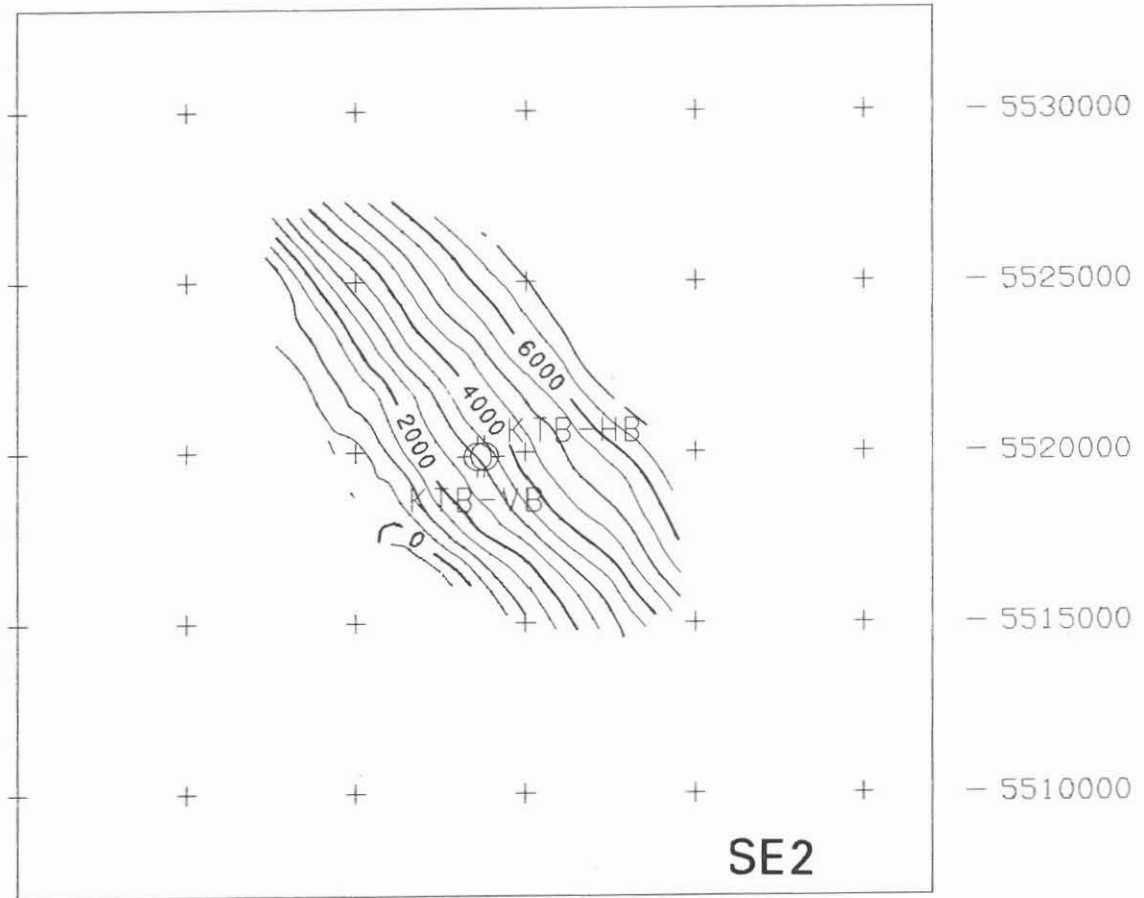


Fig. A33

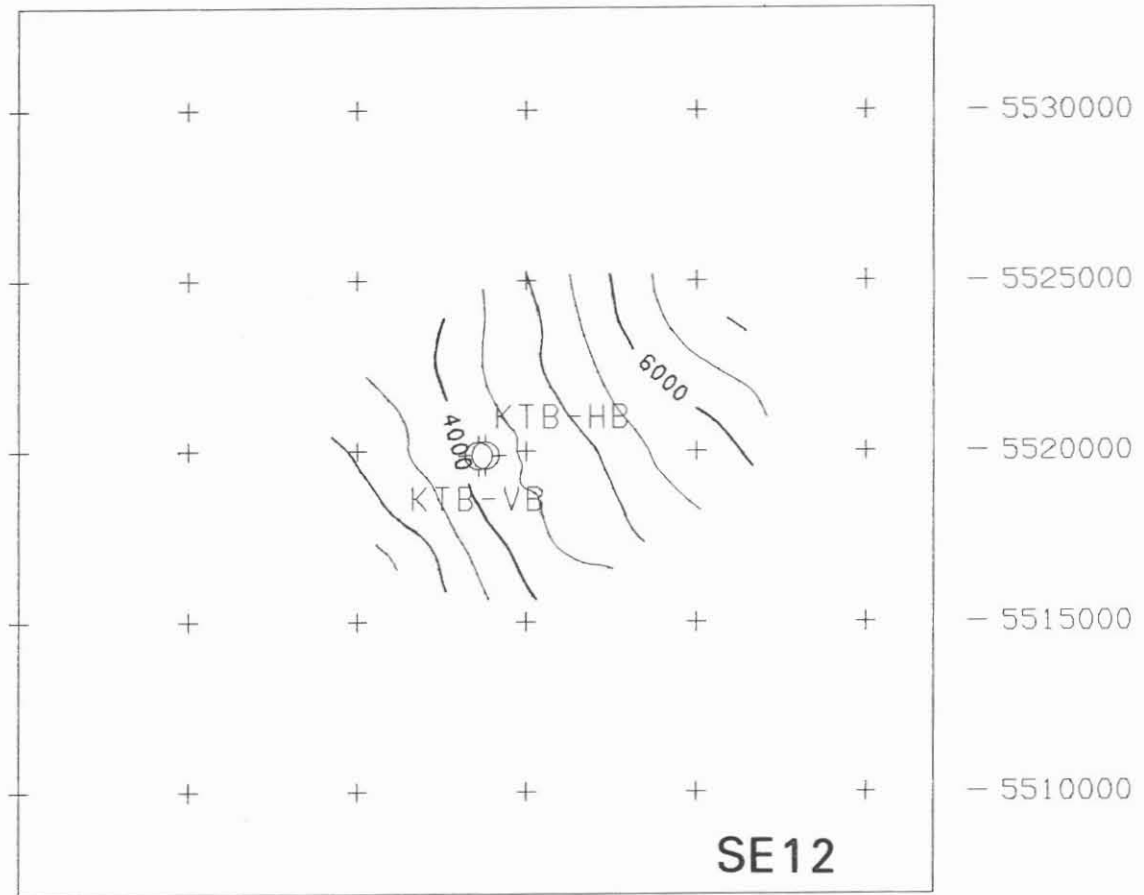


Fig. A34

4495000 4500000 4505000 4510000 4515000 4520000



4495000 4500000 4505000 4510000 4515000 4520000

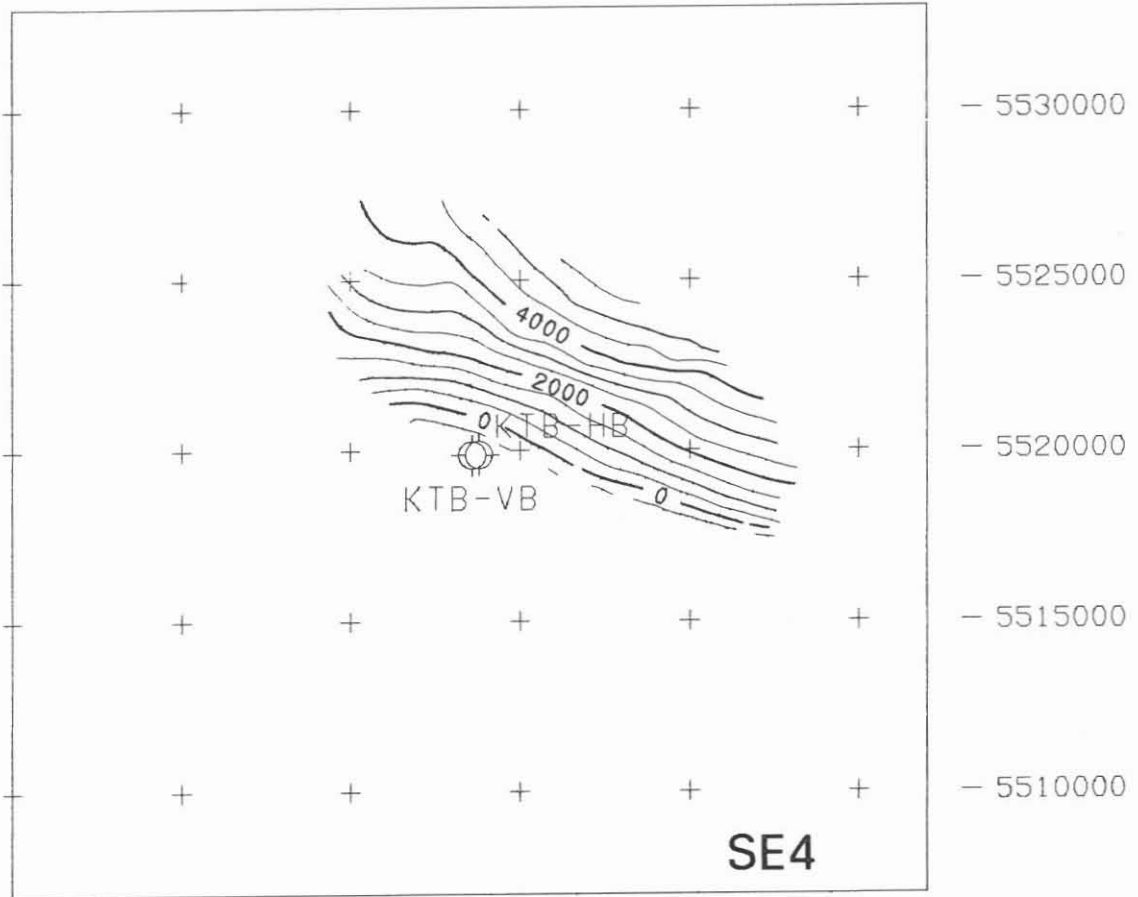


Fig. A35

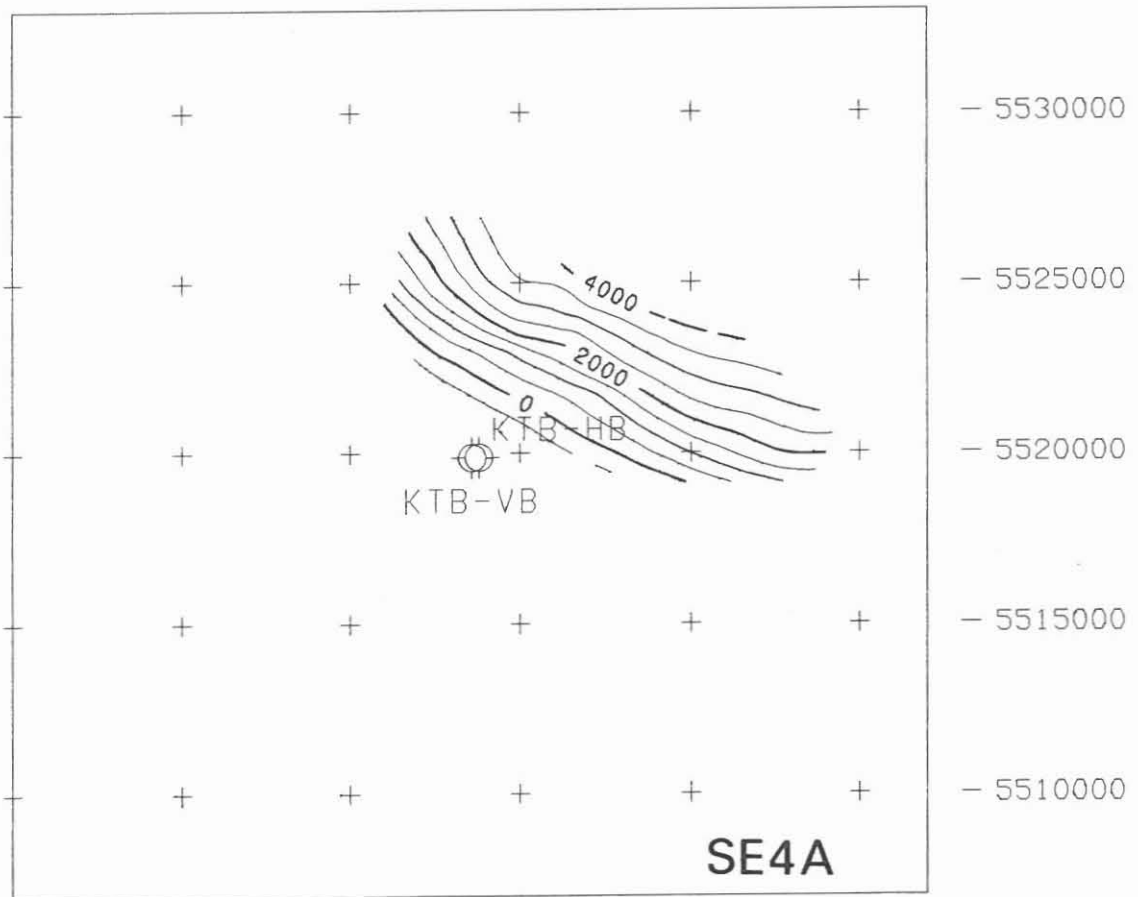


Fig. A36

4495000 4500000 4505000 4510000 4515000 4520000

4495000 4500000 4505000 4510000 4515000 4520000

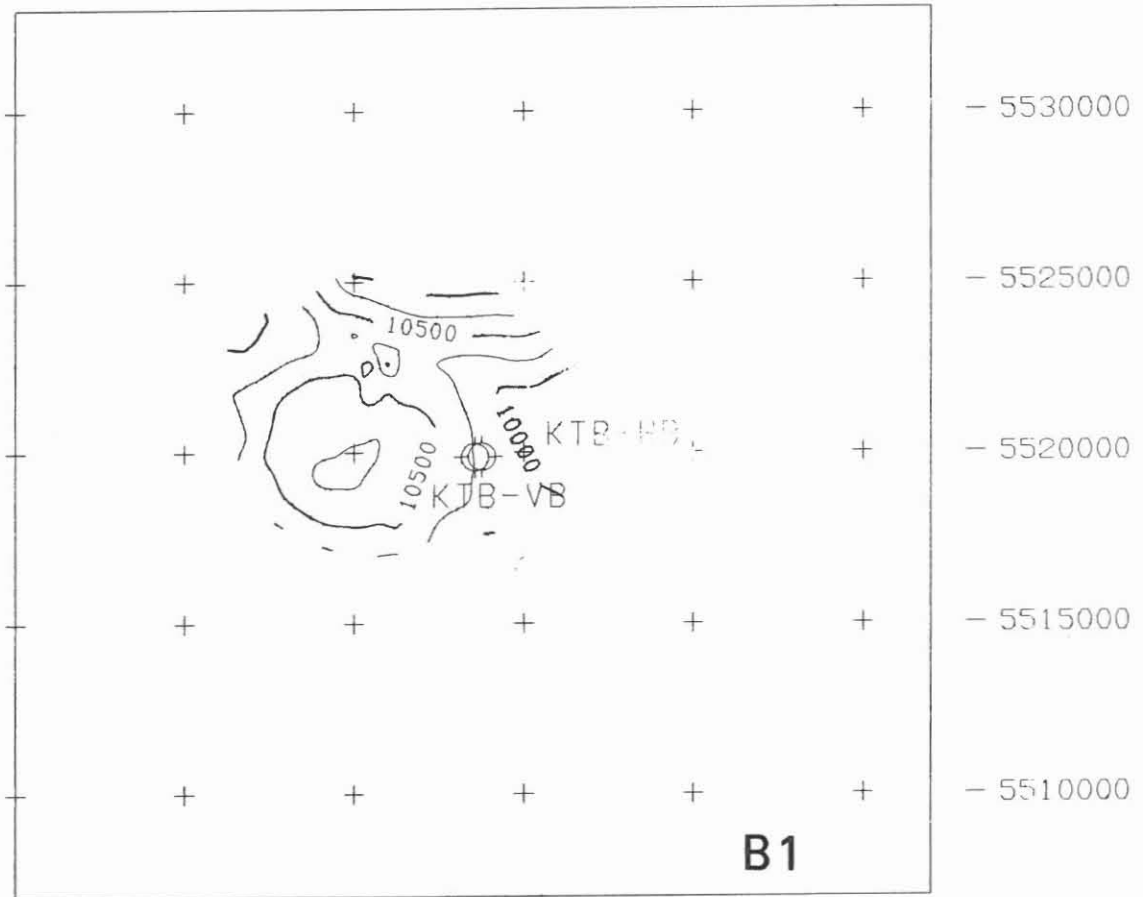


Fig. A37

B1

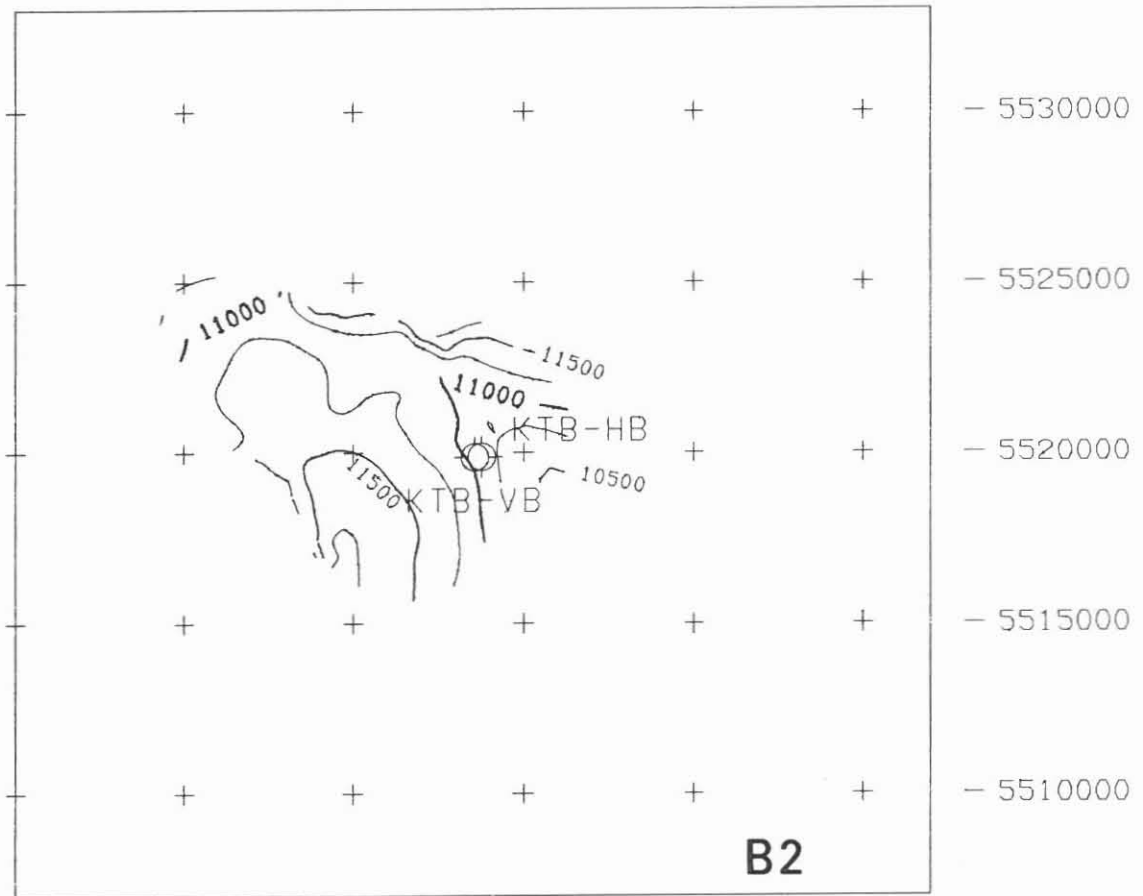


Fig. A38

B2

4495000 4500000 4505000 4510000 4515000 4520000

4495000 4500000 4505000 4510000 4515000 4520000

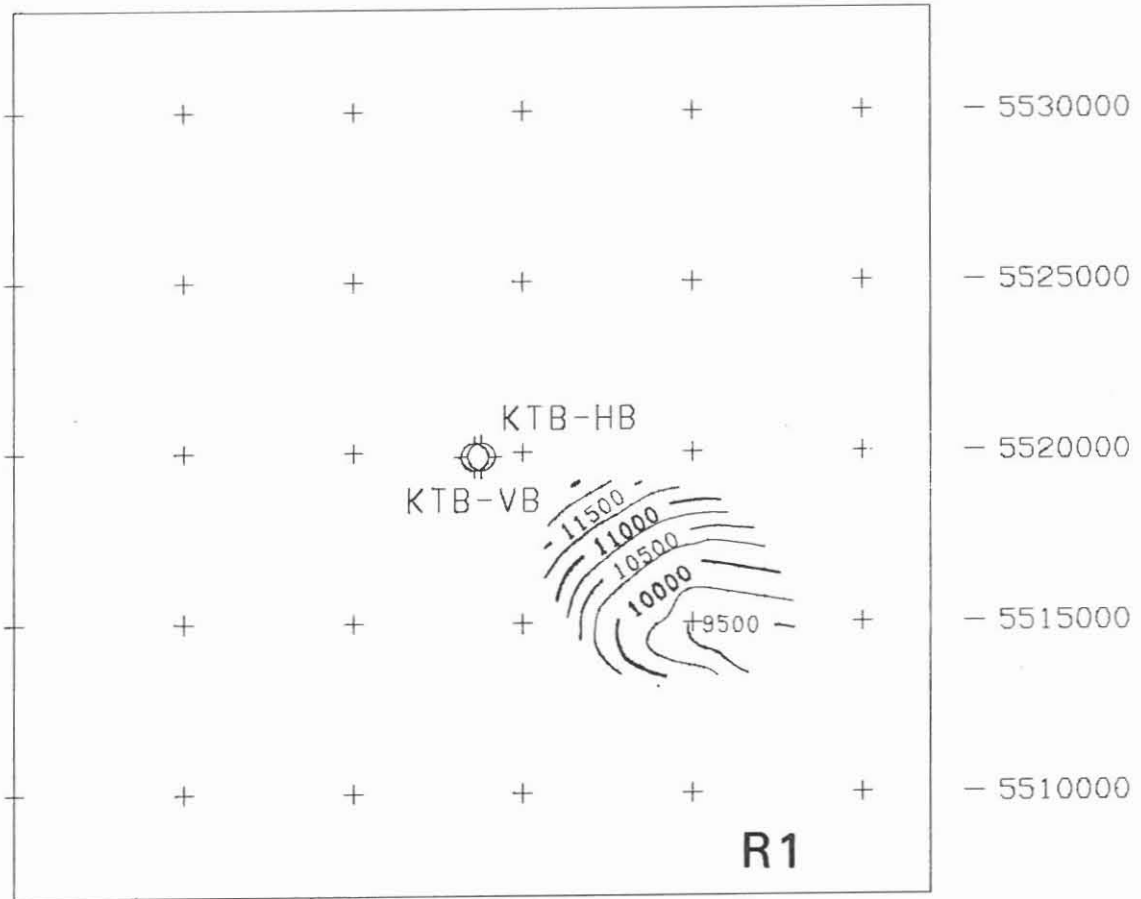


Fig. A39

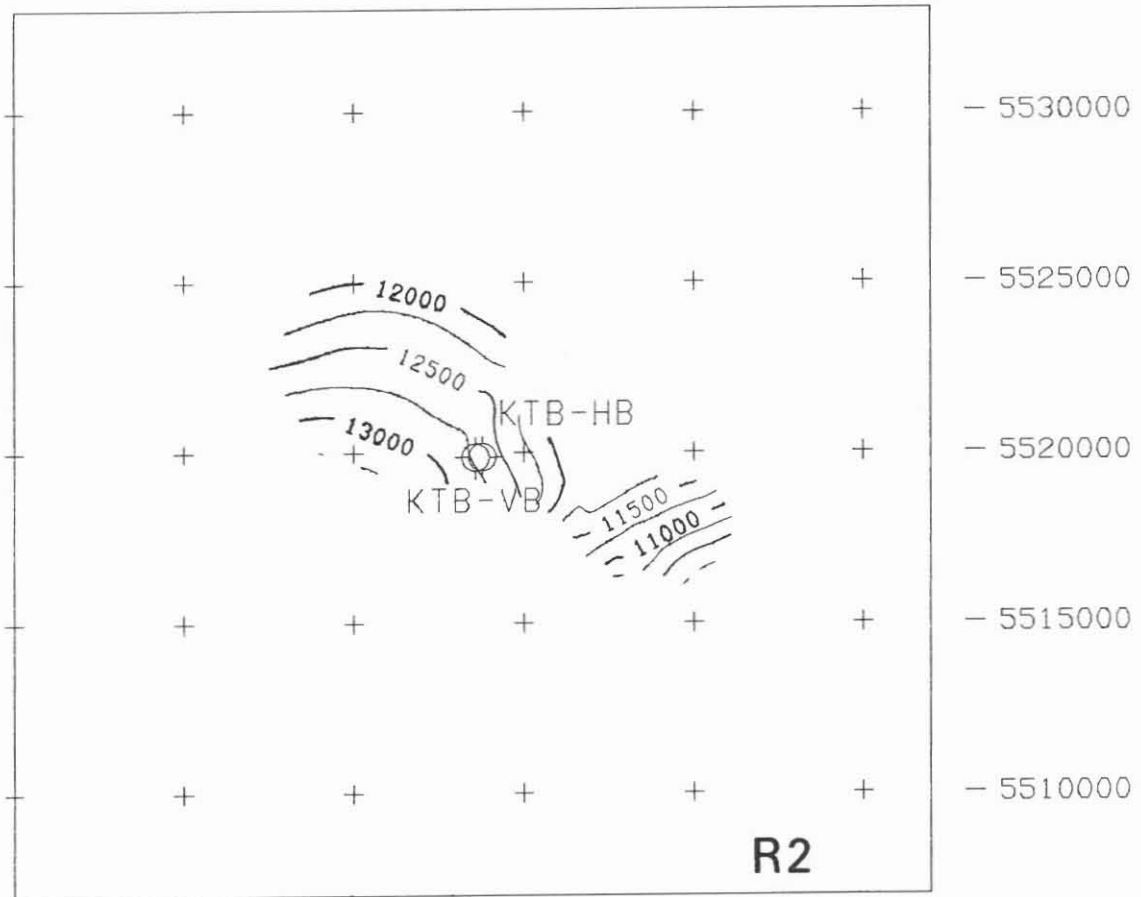


Fig. A40

4495000 4500000 4505000 4510000 4515000 4520000

4495000 4500000 4505000 4510000 4515000 4520000

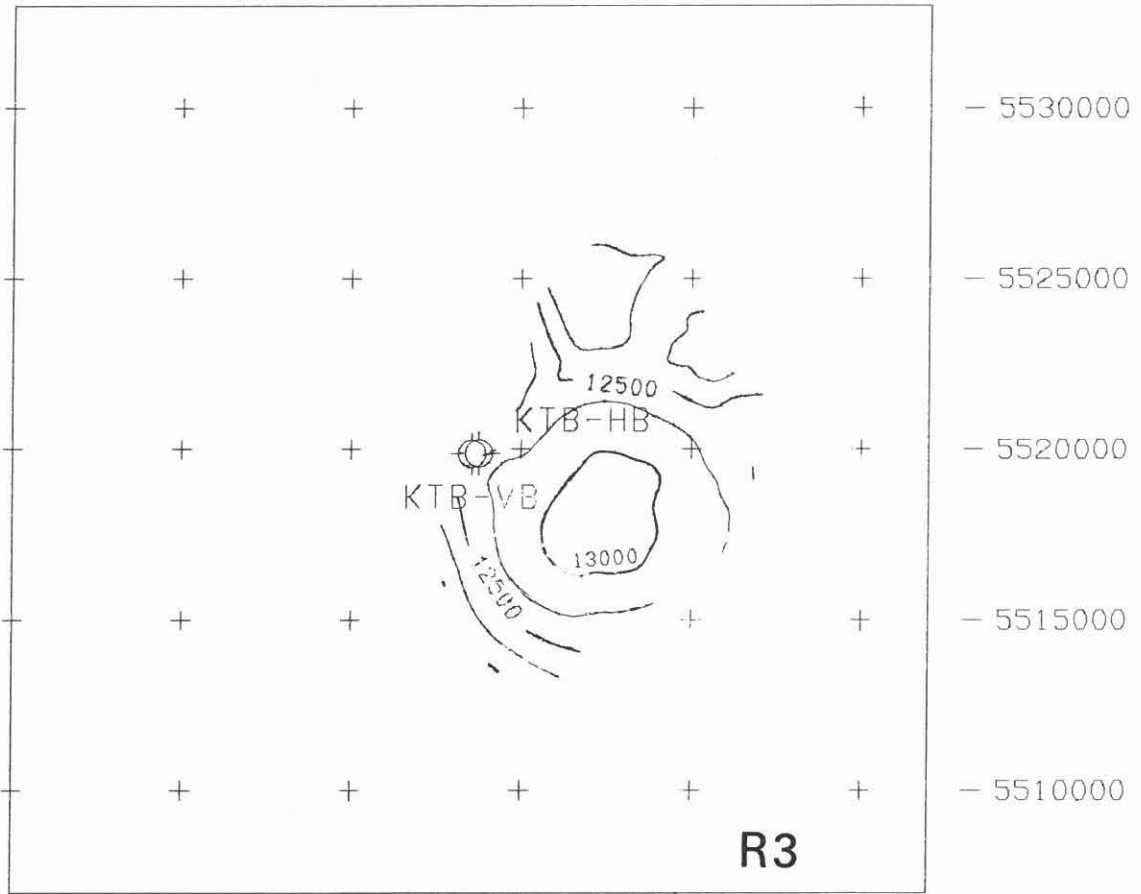


Fig. A41

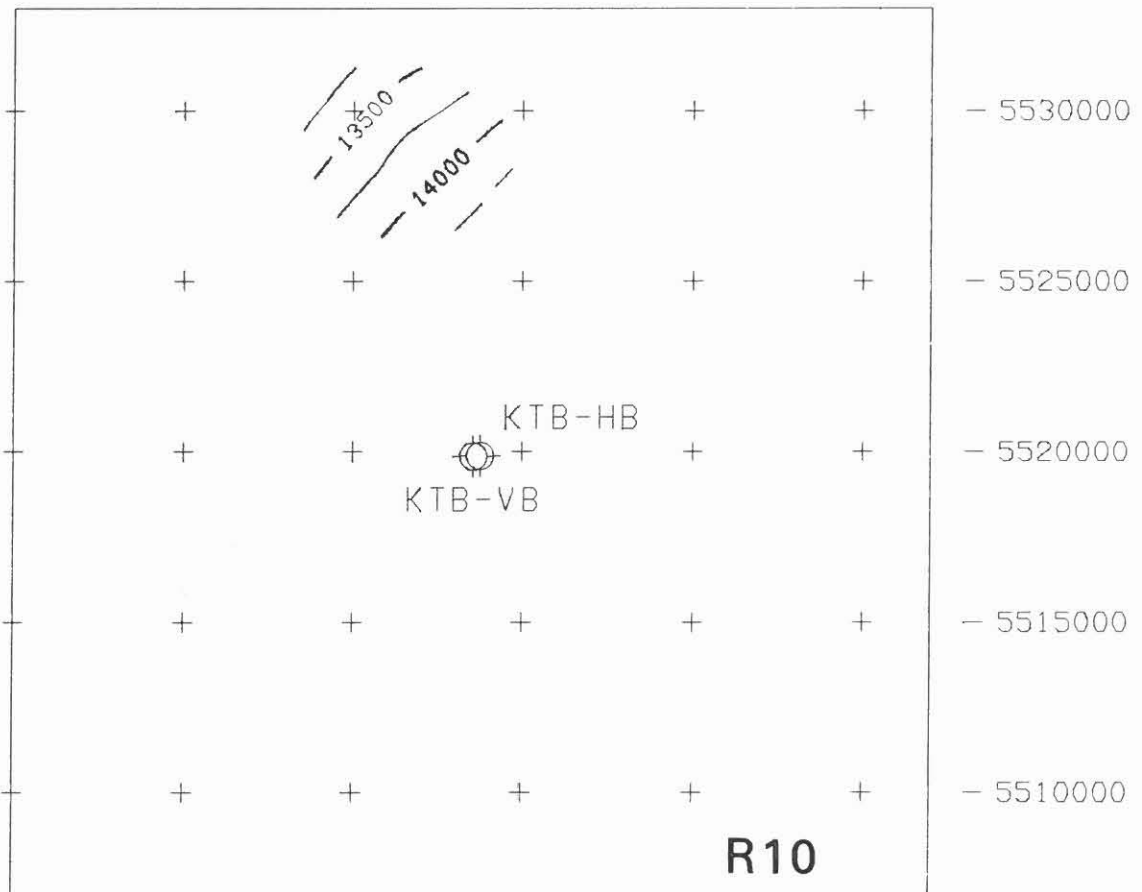
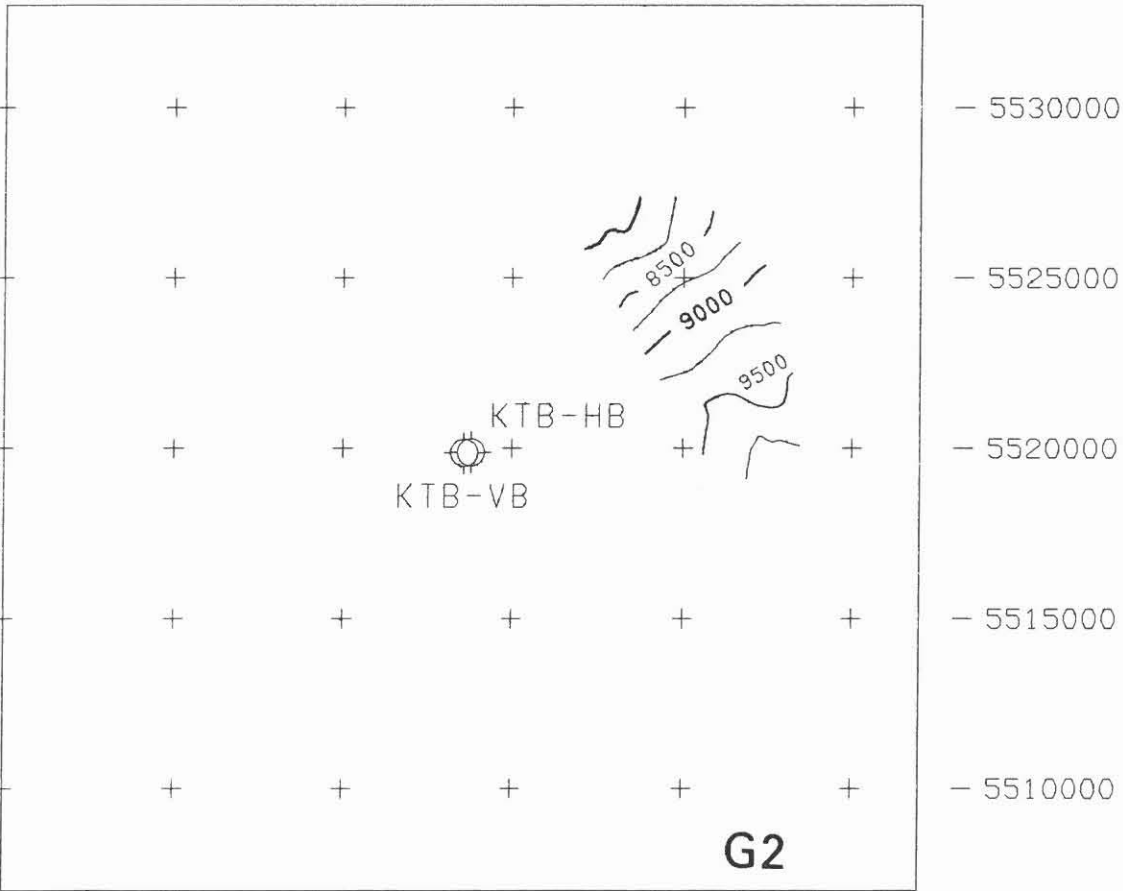
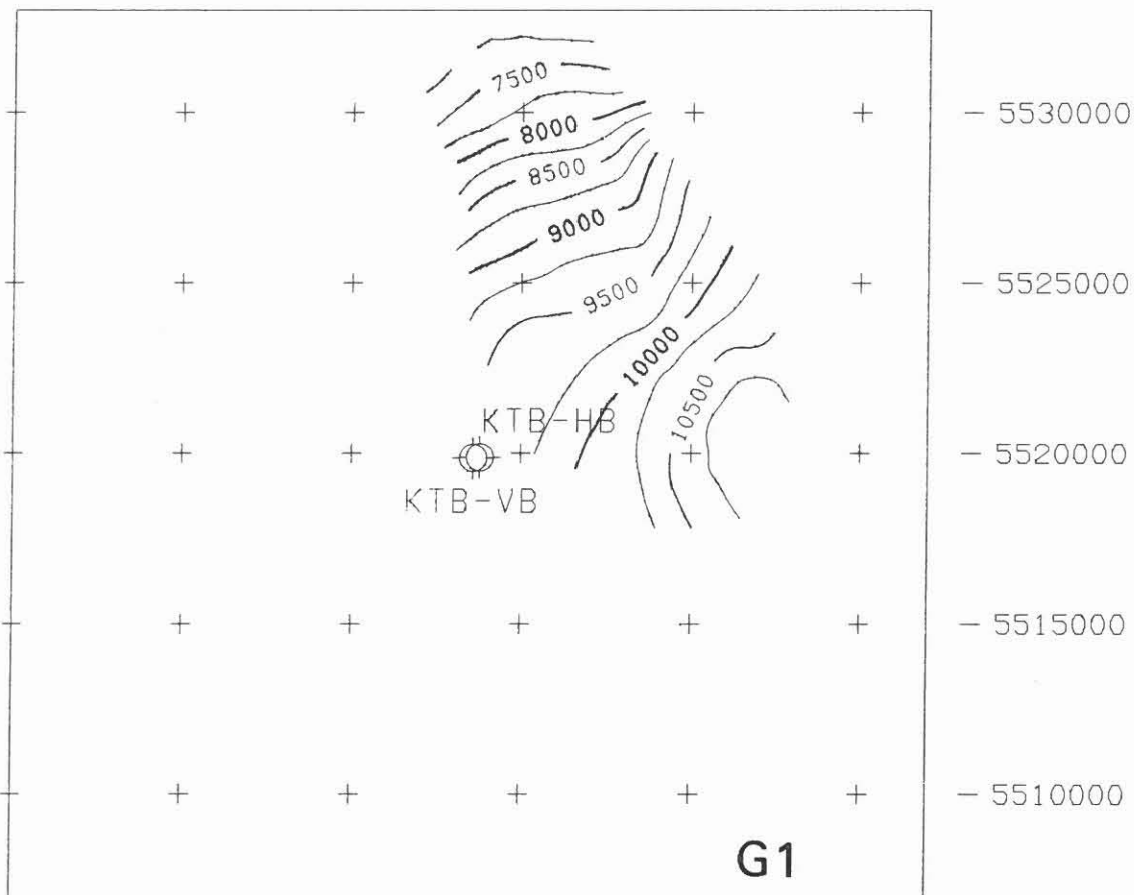


Fig. A42

4495000 4500000 4505000 4510000 4515000 4520000

4495000 4500000 4505000 4510000 4515000 4520000



4495000 4500000 4505000 4510000 4515000 4520000

4495000 4500000 4505000 4510000 4515000 4520000

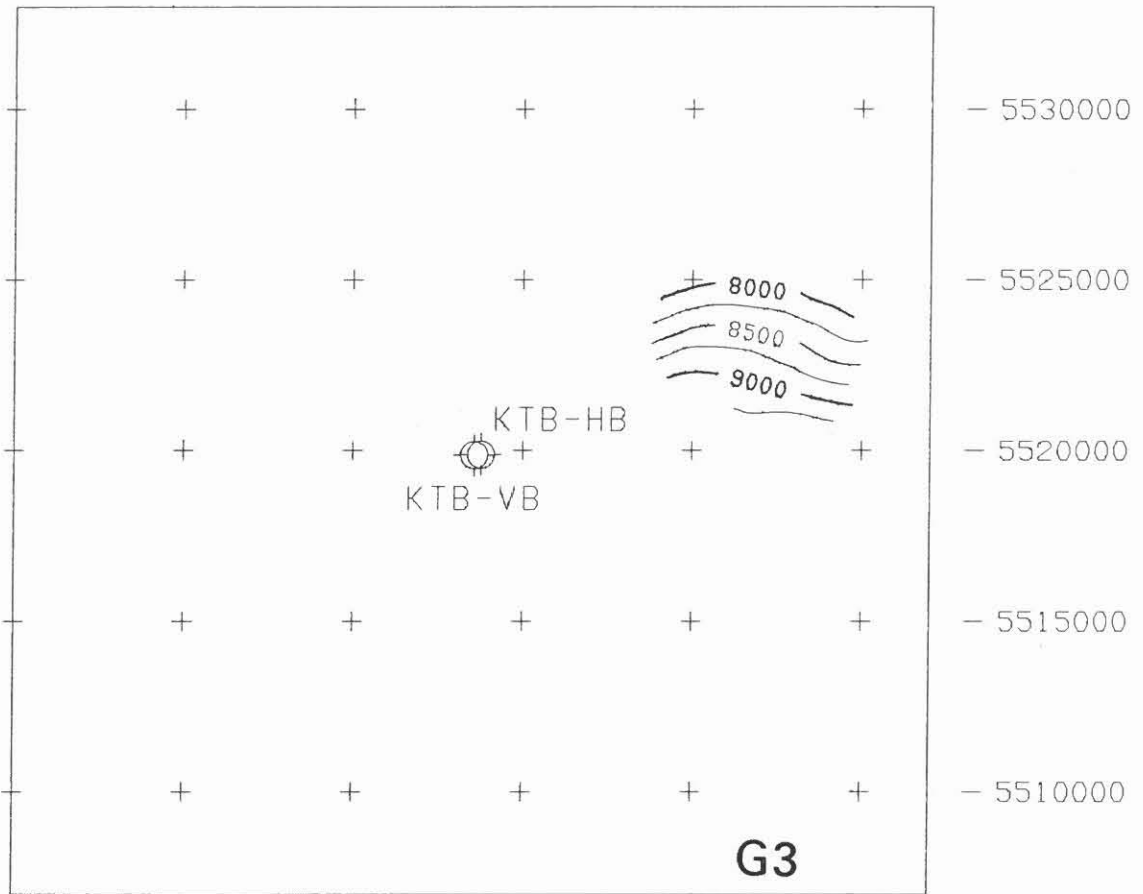


Fig. A45

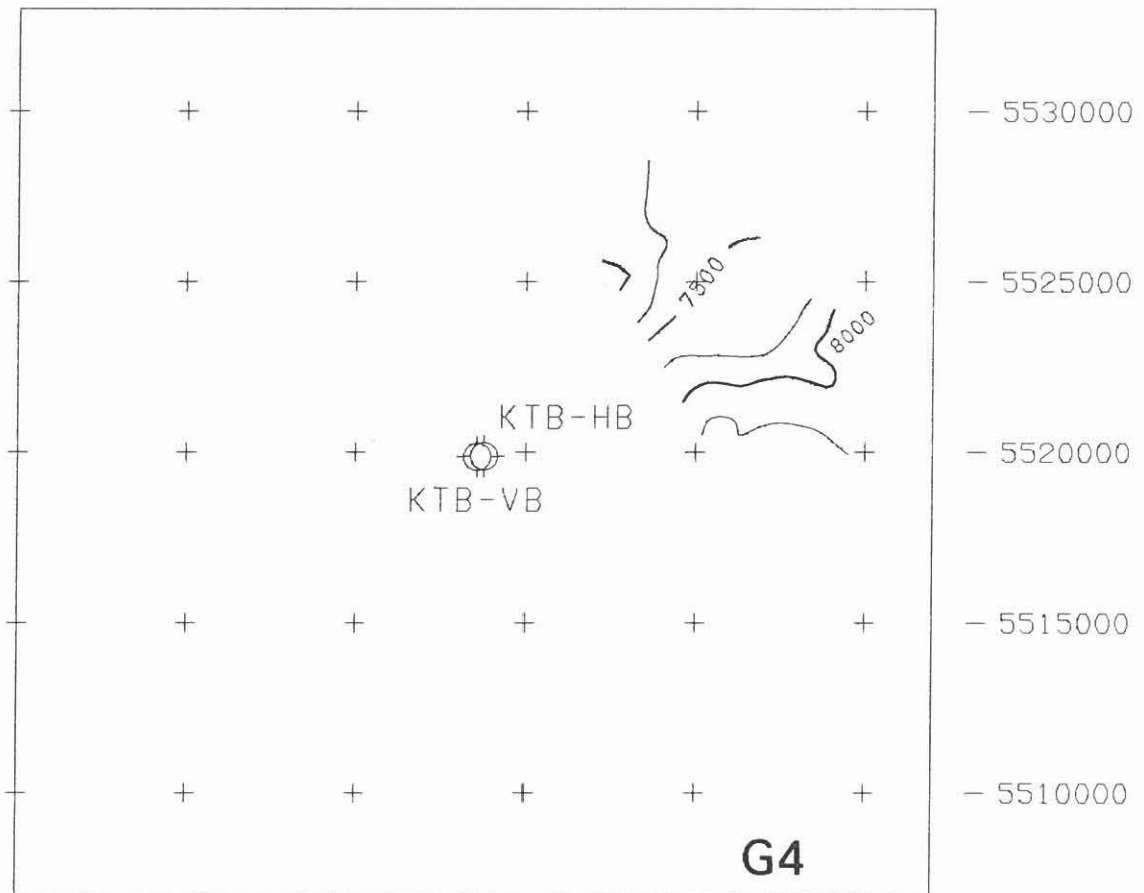


Fig. A46

4495000 4500000 4505000 4510000 4515000 4520000

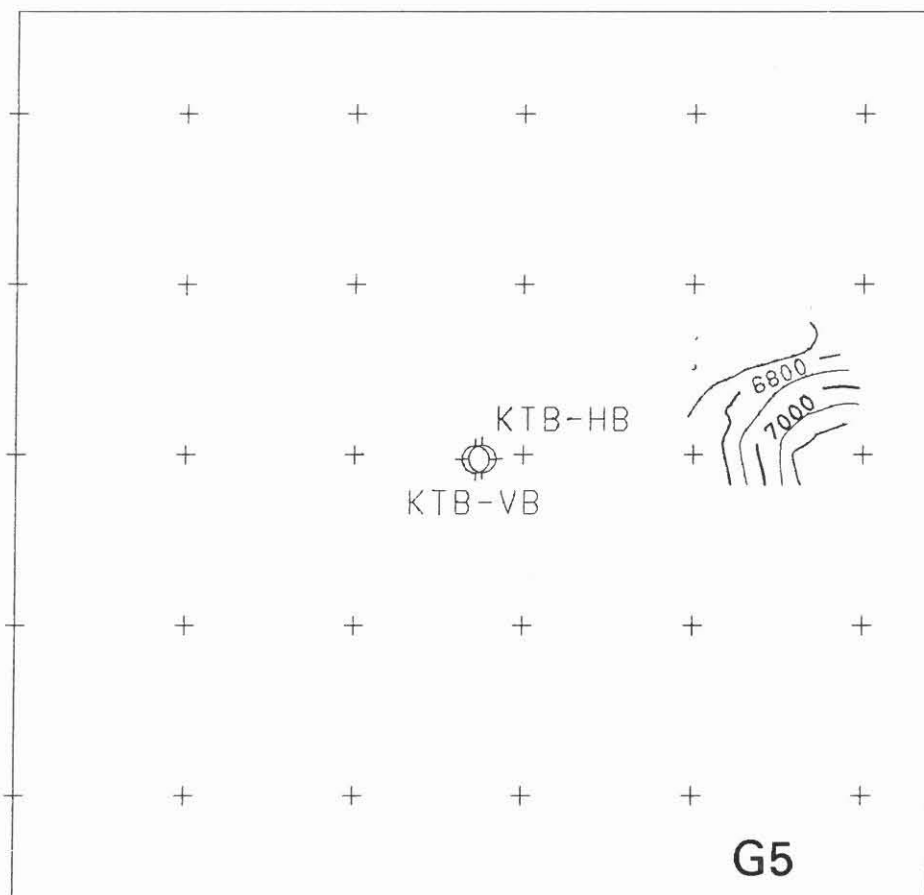


Fig. A47

4495000 4500000 4505000 4510000 4515000 4520000





# On the character of "Steep Event SE-1" — reflected energy, reflected refraction, diffraction or any artifact ?

M. Körbe\*, C. Reichert†

## Summary

The three-dimensional seismic survey within the ISO 89 program revealed the wide-spread extent of a seismic event denoted as SE-1 (steep event no. 1). This phenomenon was observed previously in two-dimensional seismic sections, already, but its energy was rather faint due to conventional processing procedures and its character was unclear. Its widely extended presence in the 3D-data emphasizes its great importance and thus provoked special investigations to detect the meaning of this event. From careful analysis of 2D and 3D-data as well as basic considerations it could be inferred that we are dealing with a true seismic reflection with NE dip of some  $55^{\circ}$  on average after migration. Its prolongation hits the surface very close to the outcrop of the Franconian Line within the range of some 100 m.

## 1 Introduction

From the very beginning of the processing of the three-dimensional seismic data of the Integrated Seismics Oberpfalz 1989 (ISO 89) at the DEKORP Processing Center (DPC) at the Technical University of Clausthal a steeply northeast dipping event was found as one of the most remarkable events in the data. This event could be seen in a great number of in-lines and cross-lines around the location of the KTB. At that early stage of data processing this event raised a lot of questions. To ensure a reliable interpretation different possible explanations had to be checked:

- A true reflection,
- a reflected refraction (Brauch, 1958; Dürbaum, H.-J., 1961; Fitch, 1976; Day, Edwards, 1983) caused by a reflector located in vicinity of the Franconian Line,

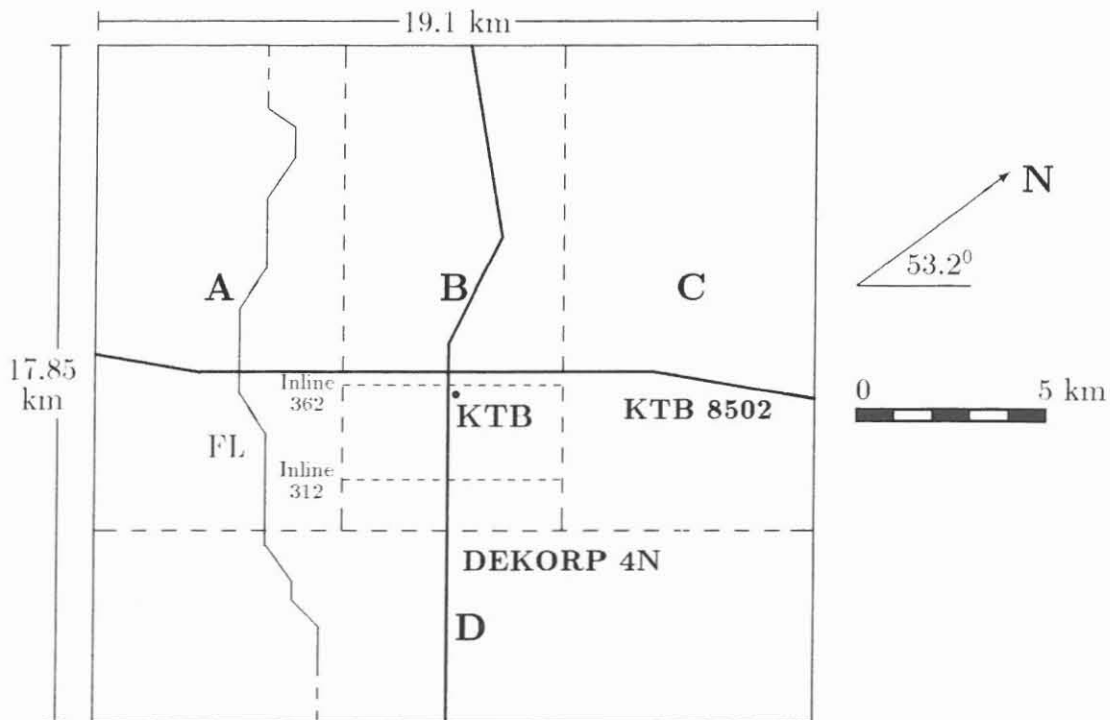
---

\*Institut für Geophysik, TU Clausthal, Arnold-Sommerfeld-Str. 1, 3392 Clausthal-Zellerfeld

†Niedersächsisches Landesamt für Bodenforschung, Stilleweg 2, 3000 Hannover 51

- a diffraction,
- or some other kind of artifact.

It was quite necessary for the further processing of the data to clarify the presumptions mentioned above. If it is a real reflection there will be the need for very high stacking velocities in the direction of dip of the steep event. But if it is not a true event it has to be suppressed in the data processing. These two main possibilities are quite different and need almost opposite processing steps from the very beginning of processing. The investigations on this problem were made regarding the seismic data of the 3D-survey and the seismic lines DEKORP 4 and KTB 8502. These lines cross each other almost at the location of the KTB. The mentioned 2D-lines and the geological border called Franconian Line (FL) which separates the crystalline area in the northeast from an area covered with Mesozoic and Paleozoic sediments in the southwest are marked in the sketch (s. Fig. 1) of the three-dimensional survey area.



**Figure 1:** Sketch of the area covered by the three-dimensional seismic subsurface data. The abbreviation FL stands for "Franconian Line". The broken lines indicate the subdivision of the data set for processing purposes at the DEKORP Processing Center (DPC).

## 2 Check for possible artifacts

Seismic observations can be disturbed by several artifacts some of which especially apply for the study area:

1. Supersonic bursts from aircrafts,
2. coherent noise from industrial plants and machineries,
3. noise from shell explosions at the Grafenwöhr military training area,
4. quarry blasts,
5. malfunction of the recording equipment including induced electromagnetic noise.

All these phenomena show particular features enabling the detection of their occurrence. Item 1 produces linear events in single source gathers with apparent velocities ranging from values greater than sound velocity up to infinity. Items 2 through 4 are point sources exhibiting the related curved traveltime curves in the single source gathers. Item 5 normally shows up by spikes occurring coincidentally on a greater number of traces, i.e. with an infinite apparent velocity.

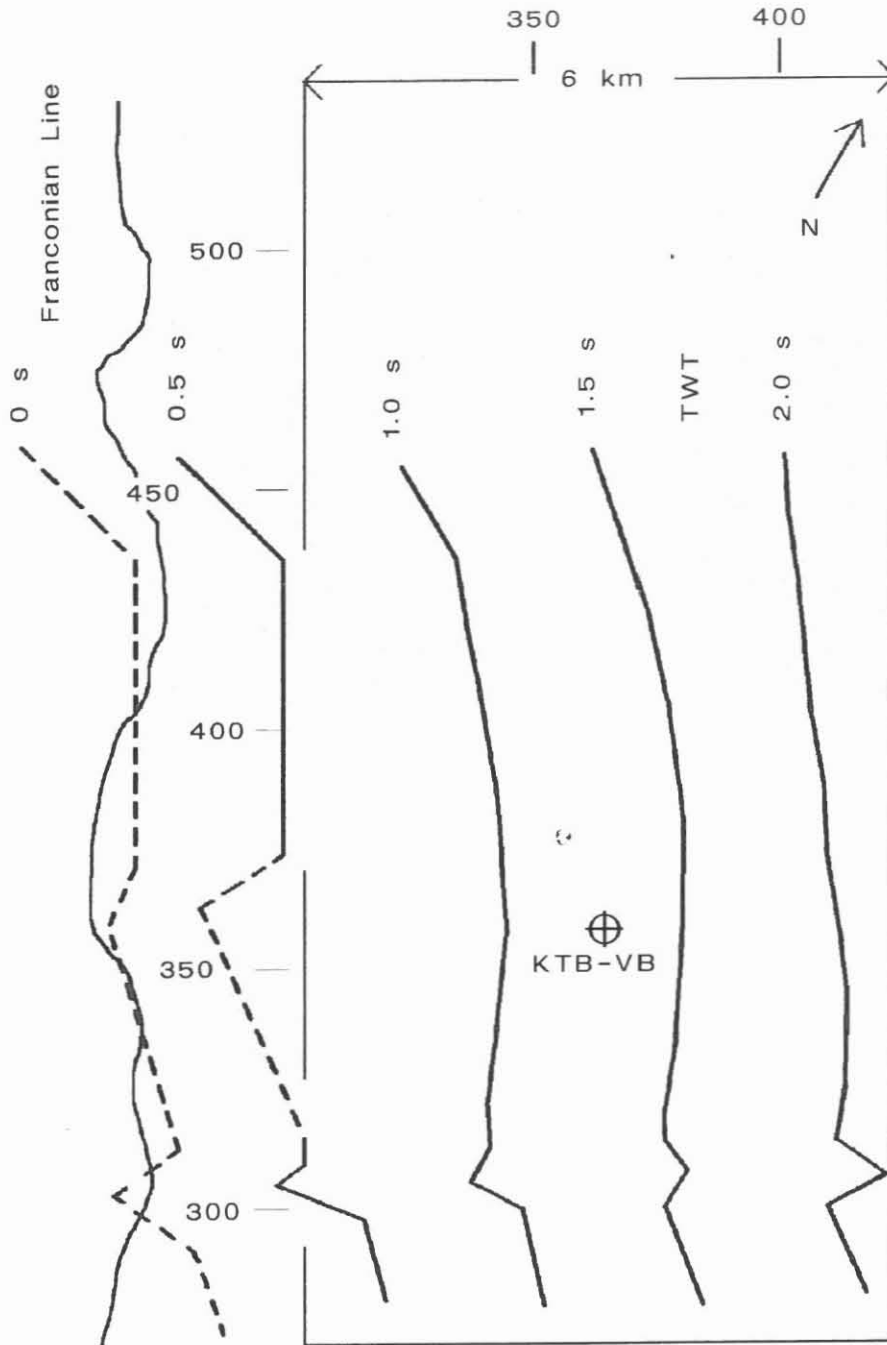
On profiles observed at different times in the same area items 1, 3, 4 and 5 cannot appear in a coherent manner such that they could be confused with true reflections. Actually, they are not observed in the seismic reflection Oberpfalz data discussed in this paper, i.e. DEKORP 4, KTB 8502 and 3D-seismic reflection, and can therefore be ruled out. This is illustrated by examples from the DEKORP 4 line which extends from NW to SE almost parallel to the Franconian Line.

Inspection revealed that the steep event could be seen only in very few records in the area of the location of the KTB. An example is shown in Figure 2. In the case of a true reflection the event must have been imaged almost in strike direction due to the azimuth of DEKORP 4. In record 823 SE-1 can be found at about 1.2 s but only at short offsets. Figure 3 shows the same data after application of a preliminary normal moveout correction of 5250 m/s in this case.

In the field records of KTB 8502 extending from SW to NE almost parallelly to the in-lines of the three-dimensional seismic, the steep event was observed at a large offset range up to the Franconian Line. It was found in a remarkable number of shots but the best quality was encountered in the area of the borehole location again. In Figure 4 which shows the record 304 in this area, SE-1 can be seen starting at 1.4 s down to 2.6 s. In its upper part the event shows a clear curvature. The crossing of the receivers over the Franconian Line can be seen in the first breaks as well.

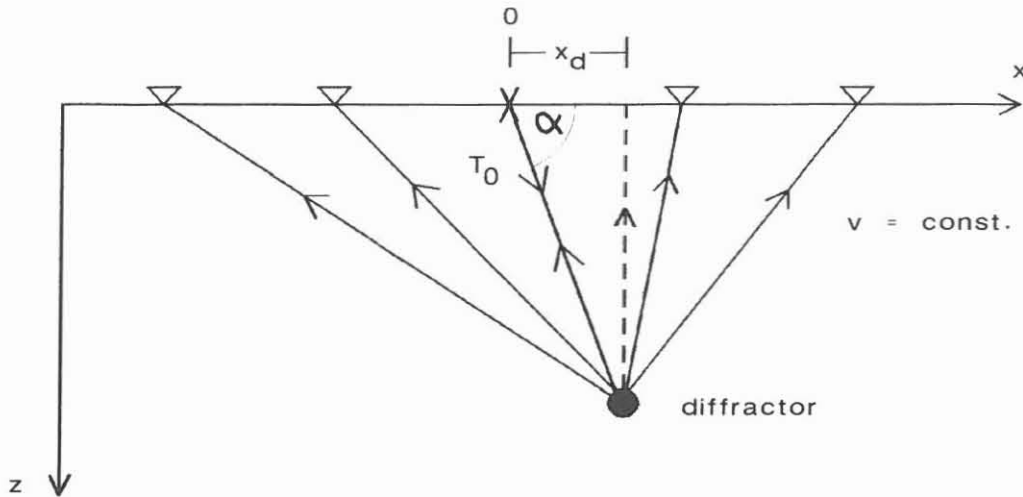
Item 2 if applicable corresponds to the signals generated by a point diffractor. This case can simply be excluded by inspection of the 3D-data showing sublinear and parallel isochrons for SE-1 event (Fig. 5). Figure 6a and 6b show different in-lines about 2.5 km apart where the event under study appears nearly at the same position. Its image is not





**Figure 5:** Isochron map of picked in-line events belonging to SE-1 (unmigrated) in block B. Numbers at the block margin indicate in-line and cross-line numbers. Isochron interval: 0.5 s. Dashed lines denote linearly interpolated values.





**Figure 7:** Modell of a diffractor located with lateral offset to the source. Dashed line: ray path of the hyperbola apex.

- $x_d$  : Horizontal distance between source point and diffractor (i.e. apex of the hyperbola).
- $\alpha$  : Incidence angle of ray from source point to diffractor.
- $T_0$  : Two-way-time from the source point to the diffractor.
- $T_d$  : Traveltime from source point to diffractor to receiver at position  $x_d$ .
- $v$  : Velocity of the overburden.

The parameters horizontal shift of the apex  $x_d$  and traveltime at the apex  $T_d$  are determined from the observed data in record 304. Then it was tried to model the observed traveltime curve by the diffractor model. It was impossible, however, to match the shape of the curve and the position of the apex simultaneously. That means if the  $T_d$ -time fits, the curvature of the traveltime curve is too strong and if the curvature fits, the calculated  $T_d$ -time is much too high. Therefore neither the point diffractor nor the line diffractor model apply for the observed data.

## 4 Check for reflected refraction

An effort was made to model the event as shown in Figure 4 by a reflected refraction. Figure 8a shows the velocities extracted out of record 304 and Figure 8b displays the corresponding subsurface model. Against this model there are two very important objections:

- On the one side it could not explain the curvature of the event. At the point where the refracted wave hits the reflector always a diffraction is caused but with reasonable velocities ( e.g. from the borehole data) the curvature of this diffraction is much stronger than observed in Figure 4.

- The second point and maybe the most important one is the missing of any hint for this model in the seismic data. There could not be found any dipping refractor with a velocity of more than 6000 m/s.

In order to avoid cross dip effects the 3D-seismic data had to be inspected. To get pure information about the origin of the SE-1 event it was necessary to look at the single source gathers because this data is nearly undisturbed by processing effects and based on a quite simple geometry. The steep event was found only in some suitable records. Even there it could be recognised only in some of the ten geophone lines belonging to each record. Figure 9 shows an example for a record located in block B, but there are source points located in block A and C on which SE-1 could be seen, too. For three selected records its apparent velocity was determined (Tab. 1). These velocities are much higher than the velocities of the first arrivals which were determined approximately to 5400 m/s.

record number	time range	apparent velocity
2003	1.8 – 2.5 s	6700 m/s
1925	2.0 – 2.5 s	7000 m/s
1893	2.5 – 3.0 s	7500 m/s

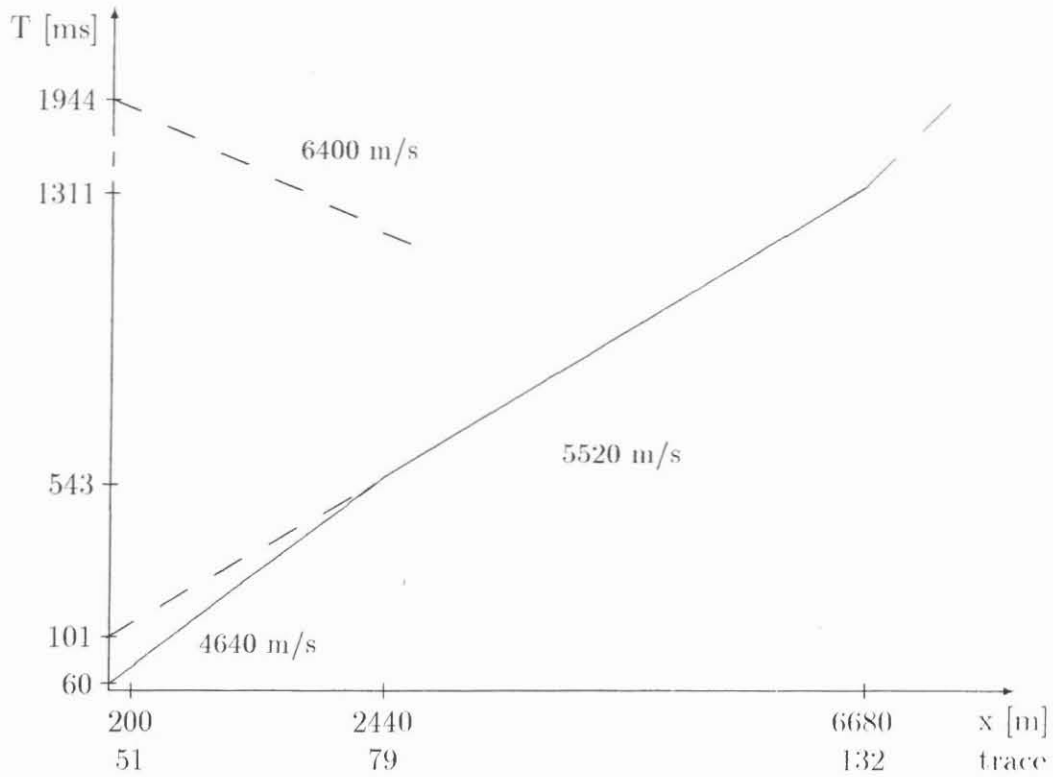
**Table 1:** Apparent velocity of steep event SE-1.

If the steep event is, as supposed, a reflected refraction there is the need for another high-velocity-refractor or a refractor with a remarkable dip. But except of the main refractor determined by the contractor with some 5000 m/s below the weathering zone there could not be found any other refractor in the 3D-data. Nevertheless calculations were made for a high-velocity-refractor with the appropriate apparent velocity found in the records and for the determined main refractor close to the surface. In this case the outcrop of the Franconian Line at surface is regarded as reflector. The results of these calculations presented in Table 2 differ ca. 100–150 milliseconds from the measured traveltimes.

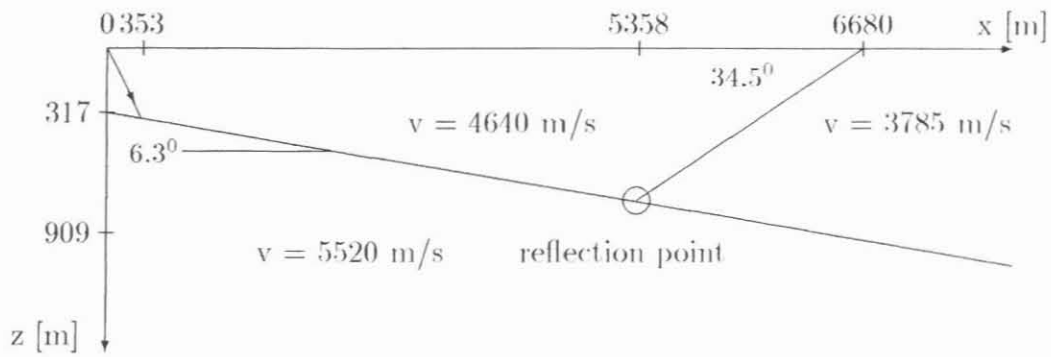
record 1		record 2	
two-way distance to FL		two-way distance to FL	
13.225 km		13.875 km	
velocity	traveltime	velocity	traveltime
5000 m/s	2.645 s	5000 m/s	2.725 s
6700 m/s	1.974 s	6600 m/s	2.102 s
measured traveltime		measured traveltime	
1.800 s		1.985 s	

**Table 2:** Calculations for a reflected refraction. The first velocity used here is the velocity of the main refractor in the survey area, the second is the apparent velocity of the steep event in the respective shot. The distance between surface and refractor can be regarded as neglectable.

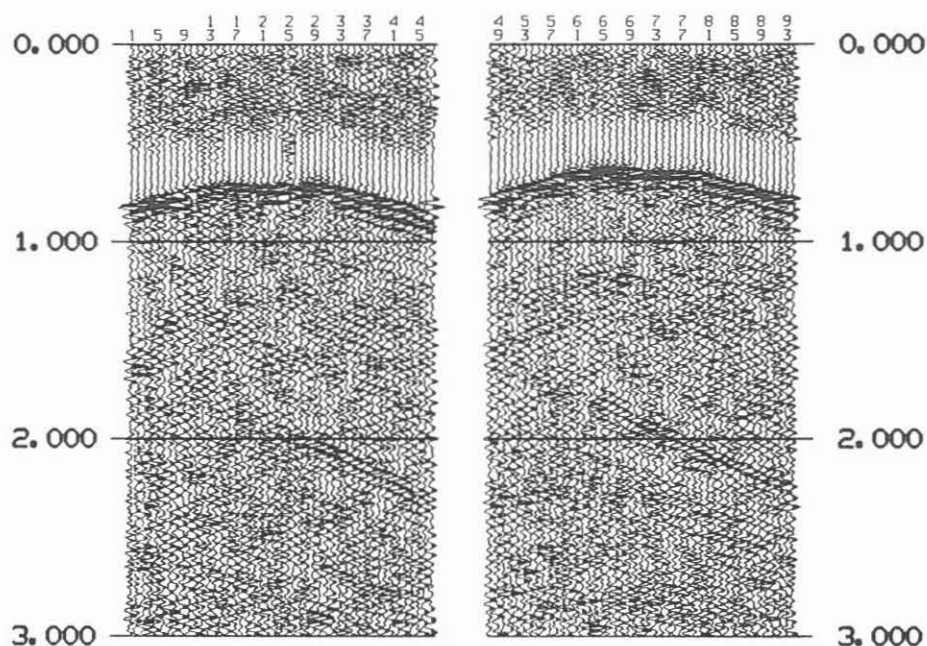




**Figure 8a:** Schematic travelttime diagram of record 304. Solid line: velocities extracted out of the first breaks; dashed line: apparent velocity of event SE-1.



**Figure 8b:** A possible model of the subsurface for a reflected refraction determined from the above velocity distribution.



**Figure 9:** Two geophone lines of record 2003 located in block B. The plot is bandpass-filtered and scaled by an AGC.

Simple considerations on traveltimes and apparent or true velocities, respectively, illuminate the above studies. Figure 10a presents the results of a simplified model calculation regarding a NE dipping refractor. A dip of  $10^\circ$  was chosen arbitrarily just to demonstrate the effect. A reflected refraction wave yields traveltimes with large deviations from the observed ones provided an overburden velocity of 4000 m/s and a refractor velocity of 7000 m/s. The deviation decreases by a small amount if the difference between overburden velocity and refractor velocity diminishes (e.g. 6000 m/s and 6200 m/s resp.). But this effect is quite small and in both cases the slope of the calculated traveltimes clearly differs from the observed one. Decreasing refractor dip would yield a closer fit but then an unreasonably high refractor velocity must be provided, since it has to be 7000 m/s in the case of a horizontal refractor (observed velocity = 3500 m/s). Every overburden velocity less than this value produces a traveltime delay so that only very small overburden thickness can be present in this case.

In the case of a SW dipping refractor (s. Fig. 10b) basically the same arguments are valid. Even the small velocity contrast of 6000 m/s against 6200 m/s produces too large traveltime deviations which could be detected easily in the observed data set (up to 300 ms). If the refractor dip is decreased for this velocity contrast then the calculated traveltime in the far distance from the reflecting point remains nearly the same whereas the traveltime close to the reflecting point decreases, i.e. the slope of the calculated traveltime provides increasing mismatch to the observed one.

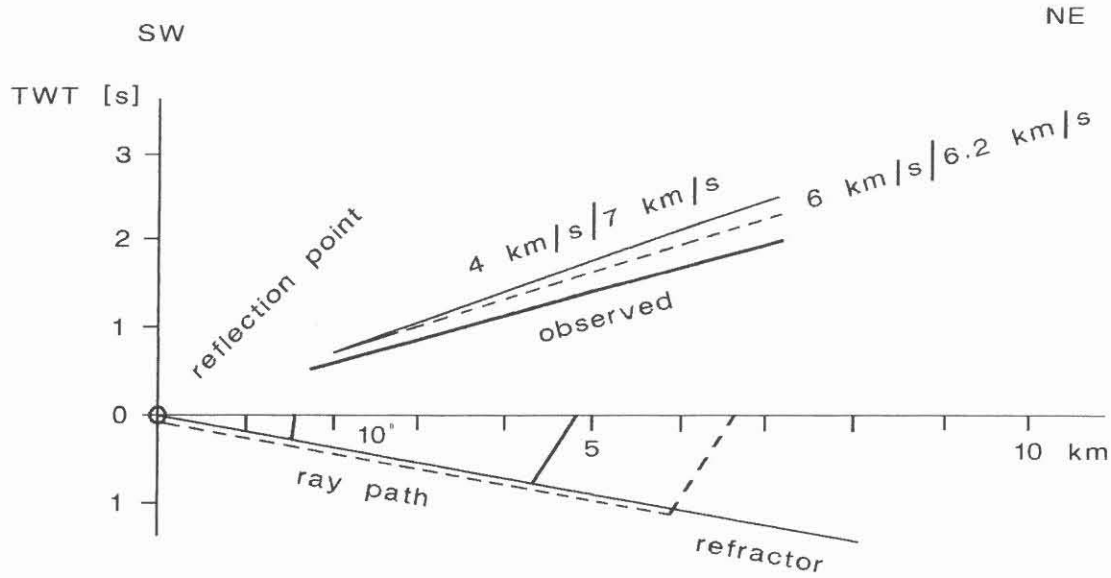


Figure 10a: Basic calculations on a reflected refractor model with NE dip. Thick line: observed data; thin line (calculated): overburden velocity = 4 km/s, refractor velocity = 7 km/s; dashed line (calculated): overburden velocity = 6 km/s, refractor velocity = 6.2 km/s. Traveltime in seconds TWT.

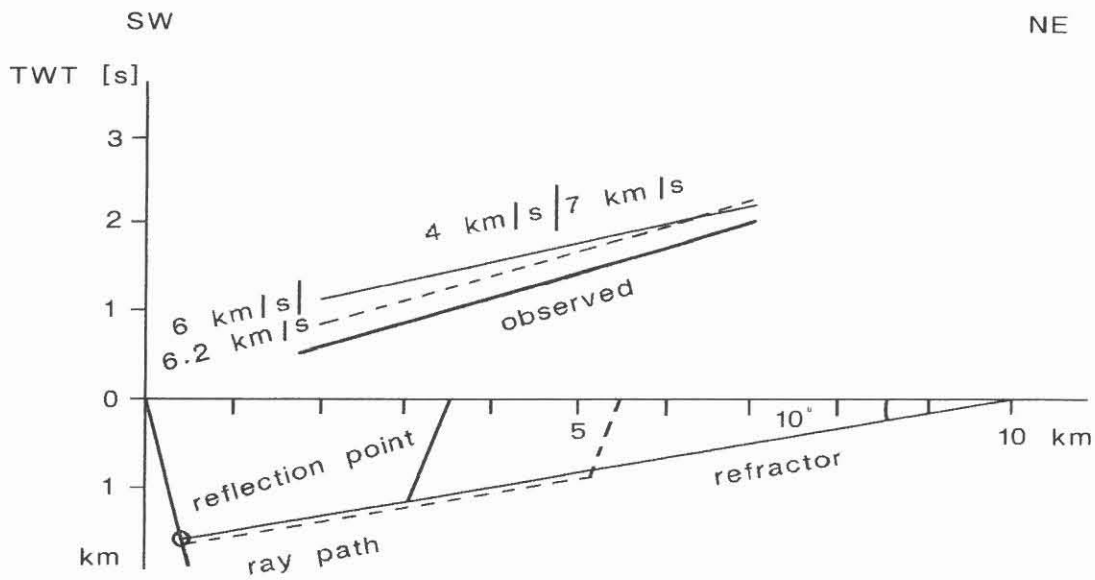


Figure 10b: Same as Figure 10a but refractor dipping SW.

Thus it can be deduced:

1. To match the observed data the reflected refractor model implies very high velocities of some 7000 m/s very close to the surface. Other model values can be excluded within the travelttime resolution of the given data set (20 – 30 ms).
2. Such high velocities close to the surface are observed only at very particular places world-wide. They definitely do not exist in the area under investigation according to KTB drilling results (Emmermann, 1989), wide-angle investigations (DEKORP Research Group, 1988; Gebrande, et al., 1990) and static corrections (Lengeling, 1991).
3. The reflected refractor model definitely does not apply to the SE-1 steep event!

## 5 Check for true reflection

After ruling out artifacts, diffractions and reflected refractions as possible explanations for the SE-1 only the true reflection alternative remains to be studied. For this purpose 2D-model calculations were carried out on the basis of the record 304 belonging to the KTB 8502 profile. In the case of a true reflection the horizontal shift of the observed travelttime hyperbola apex is related to the dip of the corresponding reflector element (Fig. 11). The appropriate equations read as follows:

$$x_a = vT_0 \sin \alpha \qquad T_a = T_0 \cos \alpha$$

$x_a$  : Horizontal distance between source point and apex of the travelttime hyperbola.

$\alpha$  : Dip angle of the reflector.

$T_0$  : Two-way-time for normal incidence

$T_a$  : Reflectiontime from the source point to the receiver at position  $x_a$ .

The best fitting reflection-travelttime curve is shown in Figure 12. The reflector has a dip of 43 degrees and the overburden velocity is 5000 m/s. The  $T_0$ -travelttime is 1.92 s. The velocity is within the range used for the normal moveout correction on line DEKORP 4. Small differences in the upper part of the travelttime curve occur in the order of a reflector with slightly varying dip ( $\approx 25$  ms per degree).

## 6 Conclusions

Analysis of two-dimensional data, especially of the KTB 8502 profile, gave strong evidence against the reflected refractor model already. Moreover the model of an extended line diffractor could definitely be ruled out by numerical calculations. Inspection of isochron maps of the SE-1 event from three-dimensional data excluded man-made artifacts and the point diffractor model. Further calculations and basic considerations on travelttimes,

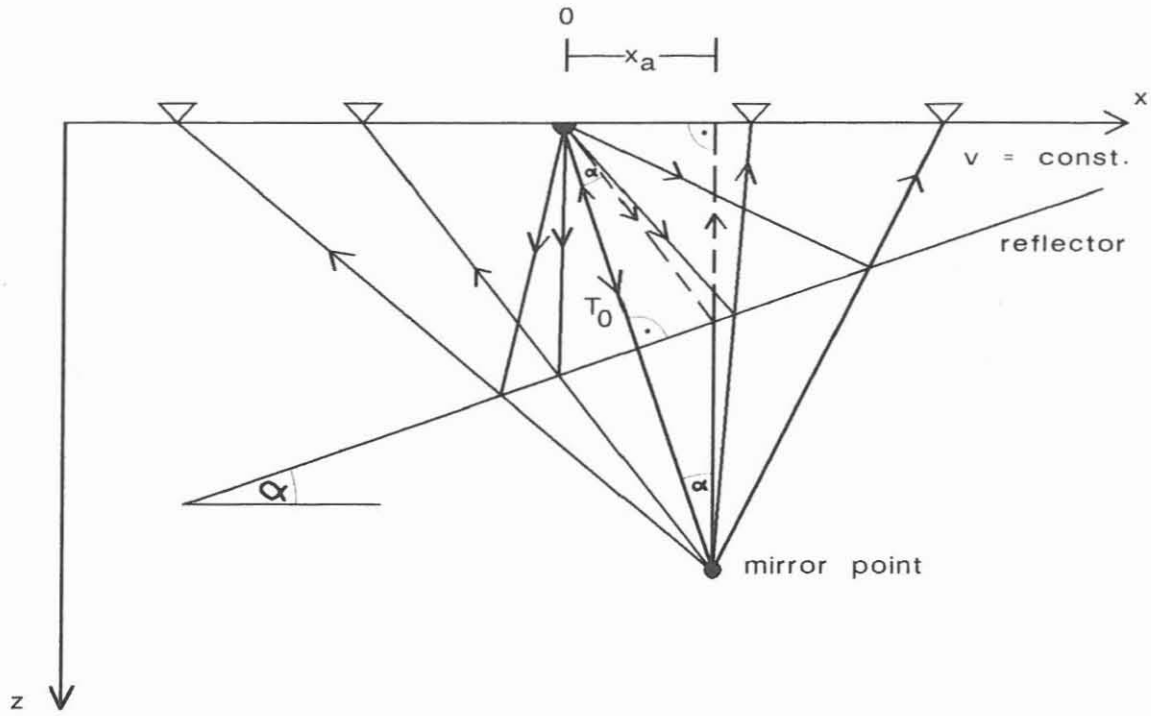


Figure 11: Model of a dipping reflector. Dashed line: ray path of the hyperbola apex.

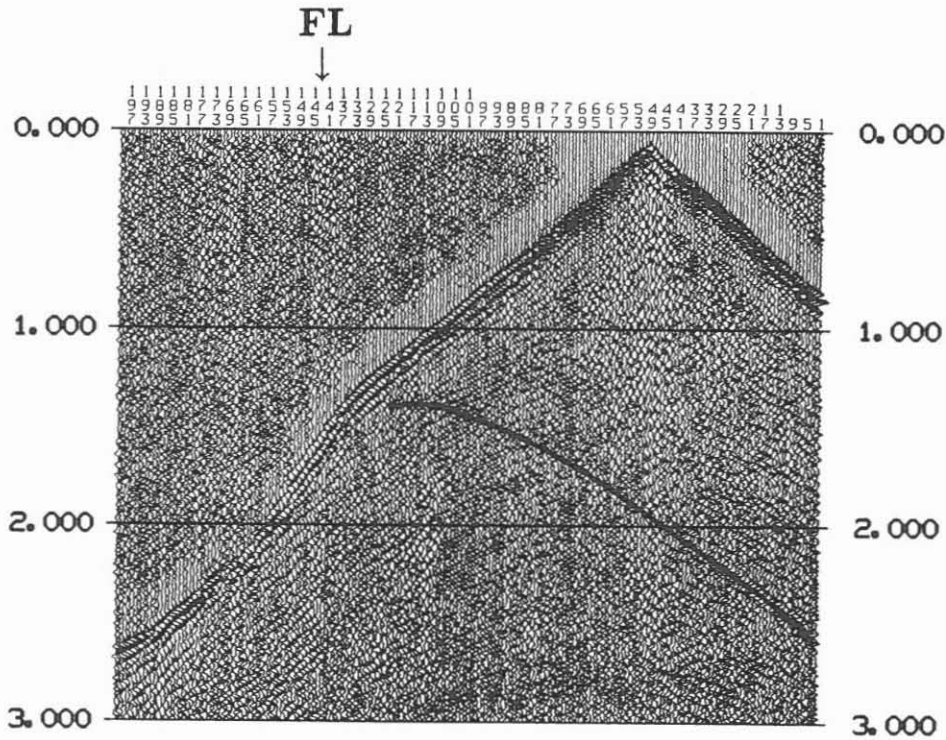


Figure 12: Record 304 of line KTB 8502 with the modelled traveltime curve of a steeply dipping reflector (more details in the text).

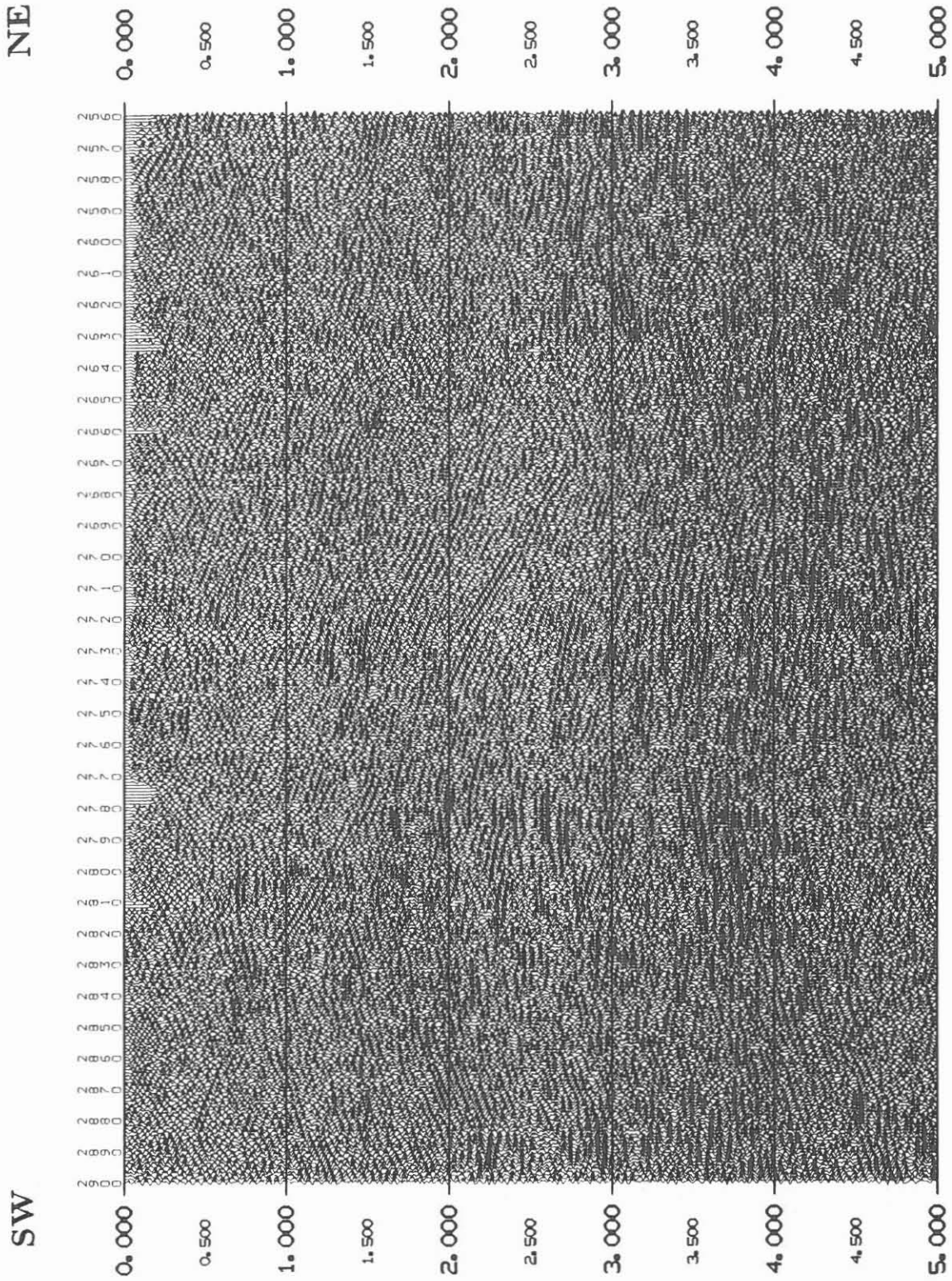


Figure 13: Result of the reprocessing: Coherency stack of the part of line KTB 8502 crossing the 3D-survey.

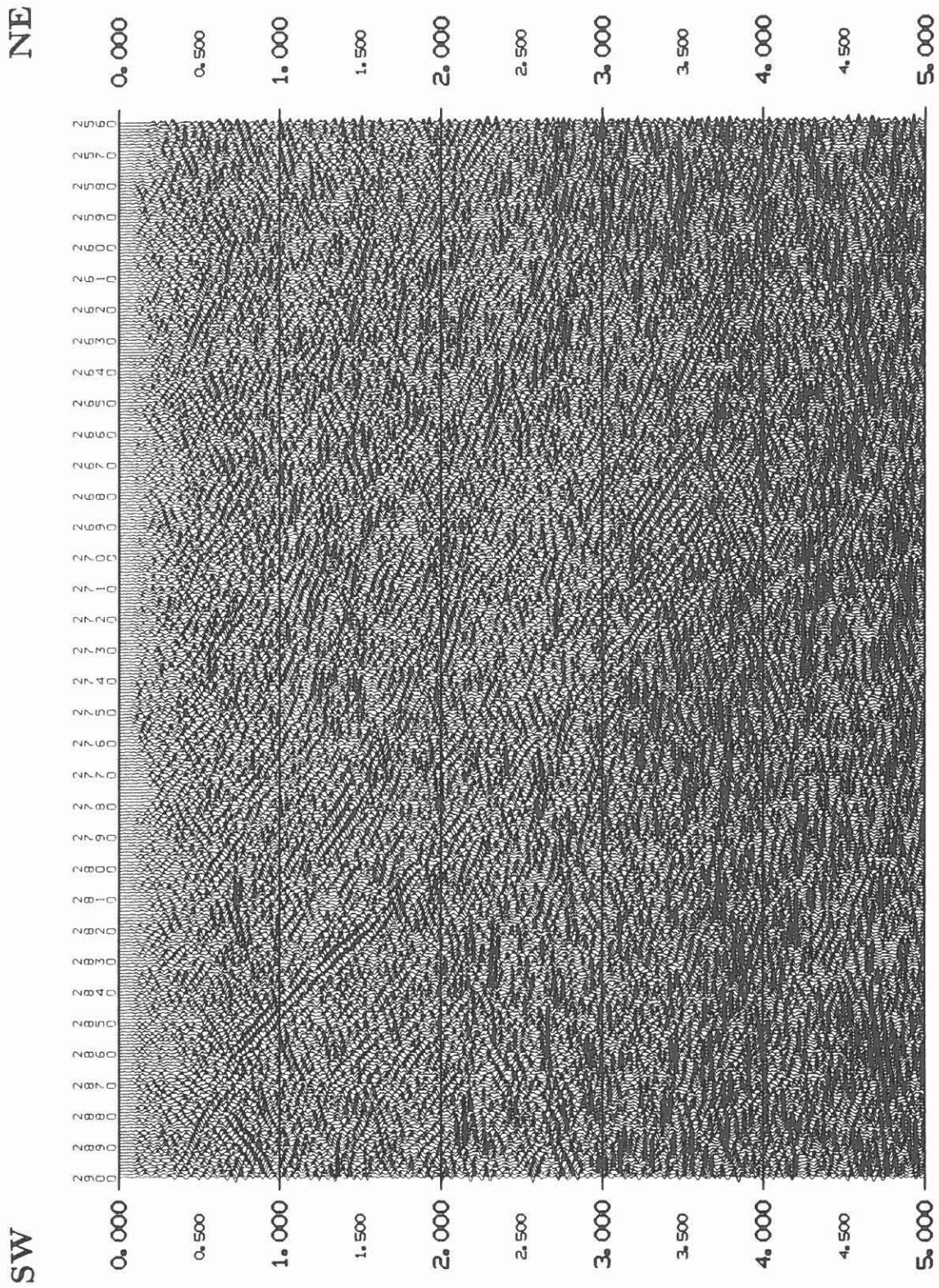


Figure 14: Result of the reprocessing: Coherency migration of the part of line KTB 8502 crossing the 3D-survey.

slopes, velocities and dip angles enabled us to rule out the reflected refractor model, too. Thus it can be stated definitely that the SE-1 event represents reflected energy related to a reflector with some  $55^{\circ}$  dip on average and intersecting the surface close to the Franconian Line (Hluchy, et al., this volume).

## 7 Two-dimensional reprocessing initiated by the conclusions

The first processing of the two-dimensional line KTB 8502 considered only moderate stacking velocities for the final stack but such a steep dipping reflector needs very high stacking velocities. The steep event was already observed in the velocity analyses during the first processing of KTB 8502 (Stiller and Thomas, 1989), and in the final stack, too (Schmoll et al., 1989). However, the quality of seismic data was not so strong that the objections against a steep dipping reflector in the vicinity of the Franconian Line could be refused completely at that time. Nevertheless, the most favoured interpretation of the two-dimensional lines in the KTB area incorporated the presence of steeply dipping reflectors, already (Schmoll et al., 1989). By the aid of the three-dimensional data and from the studies presented in this paper the steeply dipping element SE-1 can be considered proven. This result provoked a reprocessing of the two-dimensional lines in this area.

These considerations made it advisable to reprocess KTB 8502 and DEKORP 4 as well in the vicinity of the KTB with special focus on dipping elements (i.e. preference of high stacking velocities). On DEKORP 4 this was done already at a very early stage of the processing in 1985/86. Unfortunately, due to some technical insufficiencies the result was not very convincing.

Again, the reprocessing of DEKORP 4 showed no better results than the processing with "normal" velocities (i.e. adapted to subhorizontal reflections) because the line is almost in the strike direction of SE-1. A second reason is the unfortunately high scattering of the subsurface reflection points in the area around the KTB caused by the field layout. All points being more than about 150 m apart from the ideal line could not be used. Traces from points with a greater distance have a delay of more than half of the wavelength due to the steep reflector dip, even if the normal moveout correction was exact. These traces would cause destructive interference in the stacking process. Thus the coverage is not very high in the area of the KTB. Contrary to DEKORP 4 the reprocessing of line KTB 8502 (Fig. 13) showed much better results. Besides the single event SE-1 a bundle of steep SE dipping reflections was found. The reflection SE-1 seems to be the lower bound of this bundle. To achieve this result it was necessary to use stacking velocities up to 11 000 m/s, quite unusual in normal processing. The Kirchhoff migration (Fig. 14) showed the true dip of the reflection SE-1, it varies between  $45^{\circ}$  in its upper part and  $60^{\circ}$  in the lower part. The reflector reaches the surface close to the Franconian Line but it is not unambiguously ensured yet that it represents its extension into depth. However, since the Franconian Line consists of a bundle of subparallel thrusts there is strong evidence that the observed reflections are closely related to this structure.



## Literature

- Brauch, W.** , 1958: On reflected refraction waves. *Geophysical Prospecting* 6, 365–381.
- Emmermann, R.** , 1989: The KTB Pilot Hole: Tectonic Setting, Technical Data and First Results. In: Emmermann, R., Wohlenberg, J. (eds): *The German Continental Deep Drilling Program (KTB)*. Springer, Heidelberg.
- Day, G. A., Edwards, J. W. F.** , 1983: Reflected refracted events on seismic sections. *First Break* 1, no. 9, 14–17.
- Dürbaum, H.-J.** , 1961: On Reflected Refractions, Their Identification and Construction. *Bull. Iranian Petr. Inst.*, 3, 47–62, Teheran.
- Fitch, A. A.** , 1976: *Seismic reflection interpretation*. Gebrüder Borntraeger, Berlin.
- Gebrande, H., Bopp, M., Meichelböck, M., Neurieder, P.** , 1990: 3D Wide-Angle Investigations in the KTB Surroundings as Part of the "Integrated Seismics Oberpfalz 1989 (ISO 89)". In: Dürbaum, H.-J., Reichert, C., Bram, K. (eds): *KTB Report 90-6b, DEKORP Report, Integrated Seismics Oberpfalz 1989*, NLFB, Hannover.
- Hluchy, P., Körbe, M., Thomas, R.** , 1992: Preliminary Interpretations of the 3D-Seismic Survey at the KTB Location. In: *KTB Report 92-5, DEKORP Report*, this volume.
- Lengeling, R.** , 1991: Bewertung eines Inversionsverfahrens zur Berechnung statischer Korrekturen in der 3D-Seismik und seine Anwendung auf reflexionseismische DEKORP-Messungen in der Oberpfalz 1989. Dissertation, Universität Karlsruhe.
- Schmoll, J., Bittner, R., Dürbaum, H.-J., Heinrichs, T., Meißner, R., Reichert, C., Rühl, T., Wiederhold, H.** , 1989: Oberpfalz Deep Seismic Reflection Survey and Velocity Studies. In: Emmermann, R., Wohlenberg, J. (eds): *The German Continental Deep Drilling Program (KTB)*. Springer, Heidelberg.
- Stiller, M., Thomas, R.** , 1989: Processing of reflection-seismic data in the DEKORP Processing Center, Clausthal. In: Emmermann, R., Wohlenberg, J. (eds): *The German Continental Deep Drilling Program (KTB)*. Springer, Heidelberg.



## STRUCTURAL INTERPRETATION OF THE MSP - EXPERIMENT

M. Janik\* and H.-P. Harjes\*

**Abstract.** For the first time, a "Moving Source Profiling" (MSP) experiment or walk-away VSP - a seismic technique widely used in oil and gas exploration - was carried out in crystalline rock at the KTB pilot borehole. The main goal was to predict structural elements to be hit by the ultradeep hole of the KTB project. Despite of limited aperture and little velocity information, several reflections can be located after application of a special migration algorithm. Of particular interest are NE dipping elements at 5000 m and 8000 m depth. Further, the reflections of the so called Erbendorf body can be detected. It is demonstrated that the MSP technique is a useful supplement to surface seismic experiments in the crystalline environment.

### Introduction

A "Moving Source Profiling" (MSP) experiment was conducted within the "Integrated Seismics Oberpfalz 1989" (ISO 89) project at the KTB drill site (Harjes et al., 1990). This seismic borehole measurement technique comprises not only the variation of geophone depth as in the conventional VSP, but also includes the generation of energy at many source locations along a line at the surface (Fig. 1a).

The MSP-profile directly crosses the location of the KTB - pilot borehole and runs from there 7 km to the NE and 3 km to the SW (Fig. 1b). Along this profile Vibroseis sources generated sweeps from 10 Hz to 80 Hz at 50 m interval. Signals were recorded by three-component geophones deployed along the borehole at twenty equidistant (25 m) depth positions between 3685 m and 3210 m. After correlation, listening time was 12 s with a sampling interval of 2 ms.

---

\* Authors' address: Institut für Geophysik der Ruhr-Universität Bochum,  
Postfach 102148, 4630 Bochum, FRG

The main objective of an MSP survey is to collect structural information in the vicinity of the borehole. Besides, structural prediction ahead of the drill bit plays a major role. With the spread of source locations at the surface it is possible to calculate the dip of a structure. Usually the experiments are target oriented, which means that a reflection horizon identified by surface seismics is examined by an MSP with high resolution in the area to be drilled through.

Moreover, the ISO 89 MSP was expected to answer the question, whether this seismic technique, developed for sediments, is suitable for a crystalline environment at all.

## Method

In this article, a structural interpretation of the experiment with the objective of prediction ahead of the bit at the KTB main drill site will be discussed.

Therefore, special migration techniques were applied to the processed data. This report contains the results of a ray theoretical method. It is an extension of the well known wavefront migration with respect to arbitrary source and receiver configurations. The velocity distribution has to be predefined within an arbitrary two-dimensional shape.

The migration algorithm uses a ray-equation based extrapolation and a generalized Kirchhoff summation. A two-dimensional grid is laid over the area to be imaged. The traveltimes from the source and receiver positions to each grid point are calculated. Then all traces are "smeared out" along curves of constant traveltime i.e. isochrones. In case of constant velocity, these are ellipses. The form of the isochrones becomes more complicated if the velocities vary in the medium. Interference of all smeared traces enhances coherent reflections at their true migrated positions by eliminating non-coherent events and random noise. Position and dip of the reflections are thus determined by the constructive interference of the signals. The phase defines areas of coherency and incoherency and therefore mostly contains the structural information.

Figure 2 shows how the method works. Synthetic traces, calculated from a simple model, are migrated one by one. In Fig. 2a, one can identify the elliptic shape of the isochrone along which the signal is smeared out. Doing this for all traces (Fig. 2d) the envelope is formed and the reflector is imaged at its true position, where the signal portions of all traces combine by constructive interference.

In detail, the method has been described and tested with synthetic data by Janik (1990). The algorithm is based on a publication by Hu and McMechan (1986).

### Synthetic example

Another synthetic example is presented in order to verify the suitability of that method for the conditions at the KTB location, especially varying depth positions of the receivers, low S/N ratio and high velocities which have not been determined exactly up to now. Additionally, we want to illustrate the image properties of an MSP (Fig. 3).

Three reflectors with different dips ( $15^\circ$ ,  $45^\circ$  and  $60^\circ$ ) and a point diffractor are embedded in a half space with constant velocity 5900 m/s. Figure 3 presents the model and the synthetic data without (b) and with random noise (c). The results of migrating a single profile and stacking five migrated profiles acquired at 100 m depth intervals between 3500 m and 3100 m are shown in Fig. 4. The accurate and a deliberately inaccurate (10% too slow) migration velocity were used for comparison.

As expected, only those parts of the reflectors are imaged, which were illuminated by the measurement configuration. Additionally it should be mentioned that certain possible reflection elements within the image area are not seen by the MSP configuration at all, because of their dip and position. One example is indicated by a dash-dotted line in Fig. 3a. The structures are migrated to the correct depth position if the assumed velocity is accurate (Fig. 4, left). If the velocity is too small, the general shape of the image does not change, but depth and horizontal position of the elements are biased (Fig. 4, right).

The fact that only parts of the underground can be imaged is caused by the limited aperture of the MSP experiment. The effect of limited aperture is illustrated by Fig. 5. Here a method of Carrion et al. (1991) is applied, who demonstrated that just those points of the medium can be imaged at which a normal to the interface is enclosed by a normal bundle. A normal bundle is defined by the gradients in a point of all isochrones going through that point.

A point, at which the normal to the interface is directed outwards the bundle, cannot be recovered. There the aperture of the measurement configuration is not sufficient for imaging the interface. In relation to the configuration, this point has to be viewed as a diffraction point. So one can prove analytically on one side, that only parts of an existing reflector are illuminated by a limited aperture, and on the other side, that interfaces cannot be recovered at all although they are in the area of the experiment.

In the figure the correct velocities were used with the intention to present just the effects of limited aperture. The additional effect of velocity fluctuations has to be taken into account. This mainly causes the inaccurate location of interfaces.

Before applying the migration process to the data, the development of artifacts must be considered. In general, artifacts are of elliptic shape due to the principle of wavefront migration. They are caused by coherent noise energy in the section. One single high

amplitude may also cause an artifact if it is smeared out across the whole section. Furthermore, at profile ends these so-called "smiles" are visible because no destructive interference is possible. Recognizing the aperture of the measurement configuration, artifacts and true reflections can be distinguished.

### **Structural interpretation of the MSP**

The MSP-experiment and preliminary data processing have been presented by Kemper and Harjes (1990). In this paper, only the results of migrating the upgoing wavefield, measured by the Z-component of the borehole geophones, are presented. To reduce artifacts, each profile input to migration was prepared as shown in Fig. 6. The remaining parts of direct P- and S-arrivals have been muted and the edges were tapered to reduce the margin effects. To focus on the area to be drilled through, only the first 4 sec of the MSP data have been considered.

Geophones between 3685 m and 3585 m depth were not correctly coupled to the formation and not well oriented. Therefore these depth positions require special processing and will not be considered further in this context.

The structural interpretation will be restricted to interfaces which can be reached by the KTB main drill hole. All those events are identified as interfaces which stand out against the background noise by energy and coherency. There is no sufficient S/N ratio for a detailed polarization analysis.

In total, 15 processed profiles (common receiver gathers) of the MSP recorded between 3560 m and 3210 m depth were processed as in Fig. 6. Then they were migrated and stacked by the method described above. To take into account the uncertainty of velocity distribution in that area, Fig. 7 shows the results of using three different migration velocities.

Generally, the image is superimposed by elliptic shaped segments because of the limited aperture of the MSP experiment. Only those events are of special interest whose shape contrasts with the elliptic arcs. The events in the upper part are imaged stronger when using the lower velocity. The interfaces in the lower part come out at a higher velocity. The uncertainty in velocity introduces an uncertainty in depth of  $\pm 300$  m depending on dip and depth position of each event.

The image illustrates the complex crystalline environment of the KTB site. There are no strong, continuous discontinuities. All reflecting elements are of weak energy. Only events of more than 1 km lateral extension have been interpreted.

In view of the low S/N ratio, this interpretation should be done with caution. It is based on the energy and coherency of the prominent events. The interpretation is also founded

on comparable events detected in 3D seismics and the surface profile KTB 8502, as demonstrated below.

Among others, four remarkable reflecting elements were mapped within the region to be drilled through:

- (i) A bundle of  $10^\circ$  to  $30^\circ$  NE dipping reflectors starts at around 5000 m depth. This region extends to about 5500 m although no single reflecting element has a longer lateral extension than 1 km.
- (ii) Another interesting area of short reflectors which dip at about  $30^\circ$  to the SW starts at 6500 m depth. In the migrated section these reflectors are several hundred meters offset to the east from the borehole position.
- (iii) The clearest reflections can be seen at 8000 m depth in the vicinity of the borehole; they are again dipping to the NE similarly to the reflection bundle at 5000 m.
- (iv) Finally, the most remarkable reflecting area begins at about 9500 m with short elements east of the borehole which then continue between 10 km and 11 km in the direct neighborhood of the borehole, whereas the reflector with the largest lateral extension appears at a depth of 13 km NE of the borehole. The whole reflection zone - occasionally named the "Erbendorf body" - is certainly not a homogeneous geological unit but rather a scaly and laminated complex of acoustic impedance contrasts.

The structures mentioned are located in the area to be drilled through and therefore of special interest. Altering the velocities within a realistic range between 5500 m/s and 6000 m/s does not change the total shape of the image but introduces the mentioned uncertainty of  $\pm 300$  m for the depth values (Fig. 8).

Figure 9 shows the interpretation in relation to the surface seismic profile KTB 8502<sup>1</sup> (Fig. 10) which parallels the MSP line. Only a small portion of the steep event "SE 1", which is the dominant feature of the re-processed KTB 8502 profile (Fig. 10b) and the 3D-seismics, is seen by the MSP at the western margin of the imaged area. This segment would have to be extrapolated to get a depth value at the drill site. Such an extrapolation cannot be attempted, because close to the borehole neither dip nor continuity of this structure can be derived from the MSP experiment.

---

<sup>1</sup> The processing of KTB 8502 was done by the DEKORP Processing Center in Clausthal.

The other structures mentioned above are also visible in the KTB 8502 surface seismic profile. They are marked by dotted lines in Fig. 9. Comparing both profiles, it is evident that the MSP illuminates only parts of the underground. The structures imaged by the MSP possibly are seismic discontinuities within the subsurface, but there could be other reflectors within the area which are not revealed by this particular MSP-configuration.

### Summary and Conclusions

The Moving Source Profiling experiment was designed to facilitate a prediction of structural or lithological changes ahead of the drill bit. Several remarkable reflecting elements were mapped within the region to be drilled through like a bundle of  $10^\circ$  to  $30^\circ$  NE dipping reflectors at around 5000 m depth and reflections at 8000 m depth also dipping to the NE.

A further region of reflecting elements dips at about  $30^\circ$  to the SW at 6500 m depth. But these reflectors are mapped in several hundred meters offset to the east from the borehole position. The most remarkable reflecting area is the so called "Erbendorf body". The region of these reflectors begins at about 9500 m with some short elements east of the borehole and continues between 10 km and 11 km with reflections in the direct neighborhood of the borehole. The element with the largest lateral extension appears at a depth of about 13 km.

The result demonstrates for the first time that MSP experiments can be used to resolve fine structures of target areas around the borehole even in crystalline environment. The MSP technique can therefore be regarded as an essential extension of surface seismic profiles. At this time, the MSP does not allow a geological or petrological interpretation. If the imaged elements will be drilled through and verified, there will be a unique opportunity to compare petrophysical parameters determined from borehole measurements with the reflection attributes derived from seismic methods.

### References

- Carrion, P. M., Sato, H. K. and Buono, A. V. D., 1991. Wavefront sets analysis of limited aperture migration sections, *Geophysics*, 56, 778-781.
- Harjes, H.-P., Janik, M. and Kemper, M., 1990. Moving Source Profiling - A Link between KTB-Borehole Data and Seismic Surface Measurements, KTB Report 90-6b, DEKORP Report, Nieders.Landesamt für Bodenforschung, Hannover, 135-155.
- Hu, L. Z. and McMechan, G. A., 1986. Migration of VSP data by ray equation extrapolation in 2-D variable velocity media, *Geophysical Prospecting*, 34, 704-734.



- Janik, M., 1990. Die strahlentheoretische Wellenfrontenmigration und ihre Anwendbarkeit auf MSP-Sektionen aus kristallinen Regionen, Diplomarbeit, Institut für Geophysik, Ruhr-Universität Bochum.
- Kemper, M. and Harjes H.-P., 1991. Processing and analysis of MSP - experiments within the KTB-project, in: Continental Lithosphere: Deep Seismic Reflections, R. Meissner, L. Brown, H.-J. Dürbaum, W. Franke, K. Fuchs and F. Seifert (eds.), Geodyn. Series, 22, AGU, Wash. DC., 135-145.

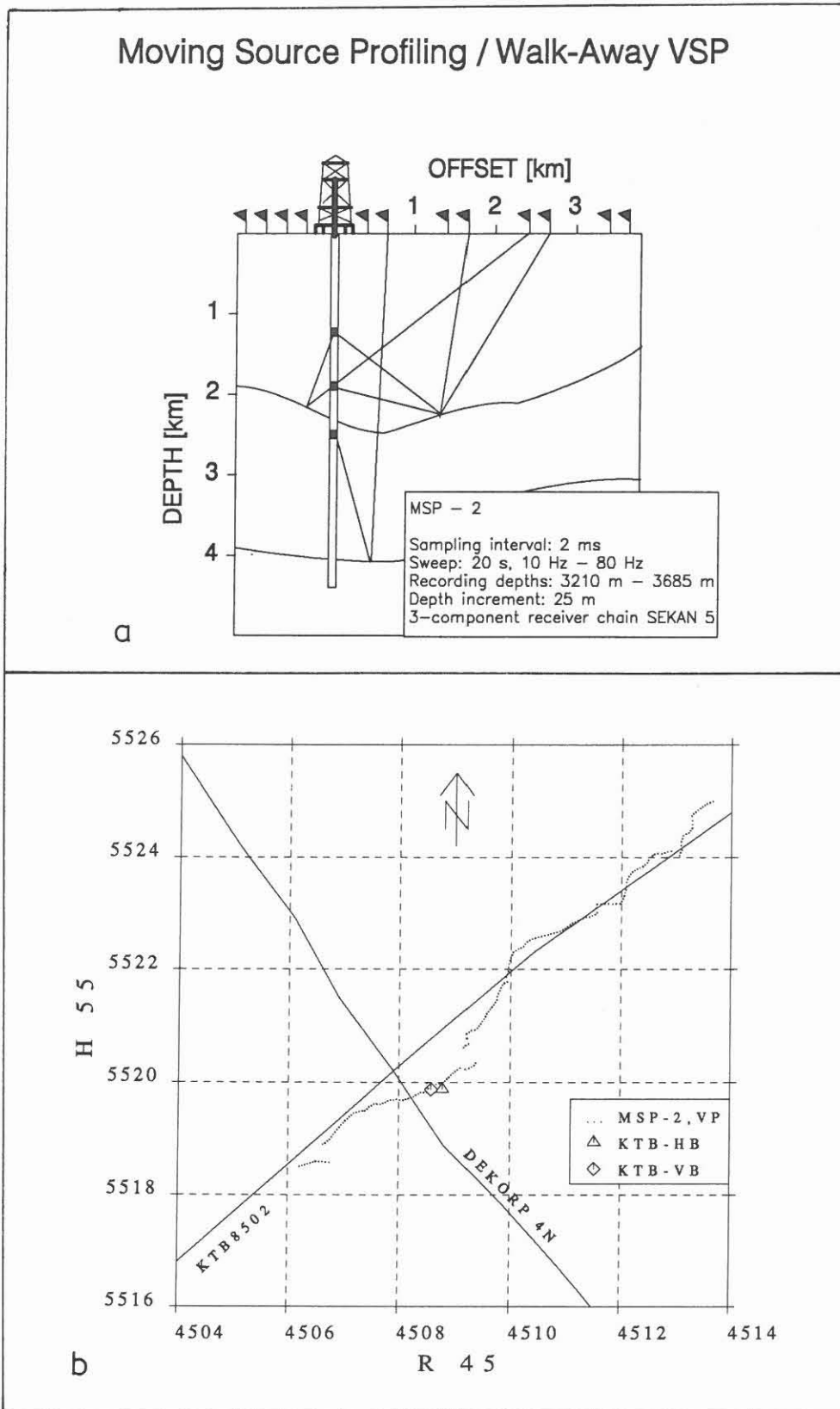


Figure 1: a) Principle of an MSP survey and some information about the MSP survey within the ISO 89 project. b) Map of seismic lines at the KTB-location. Note that the MSP lies alongside the KTB 8502 surface seismic profile. (VP: vibrator position, KTB-VB: pilot borehole, KTB-HB: main hole).

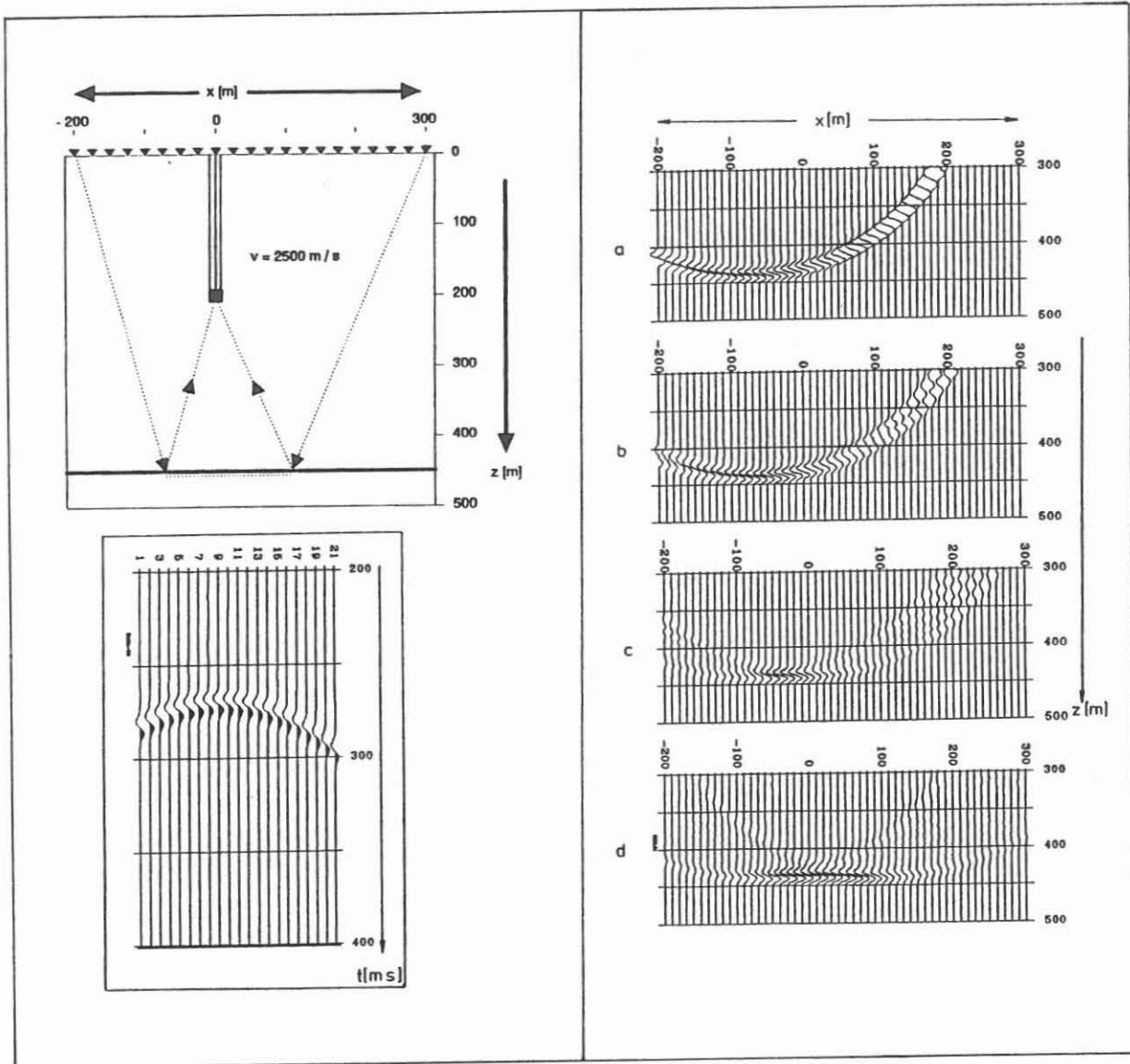


Figure 2: Principle of wavefront migration. The envelope of the isochrones defines the reflector. On the left, the model and the data, on the right the result of migrating a) trace 1, b) traces 1 and 5, c) traces 1, 5, 9, 13 and 17, d) all 21 traces.

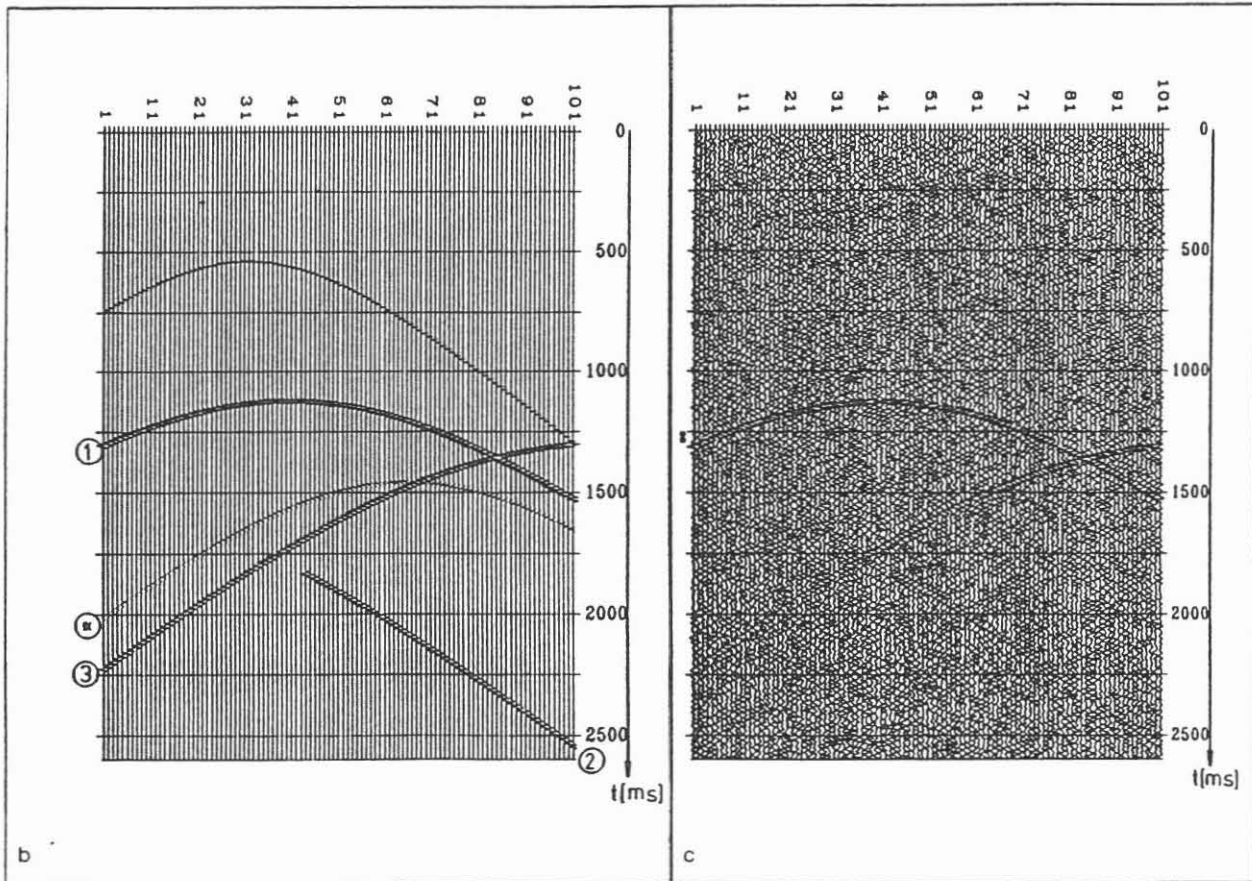
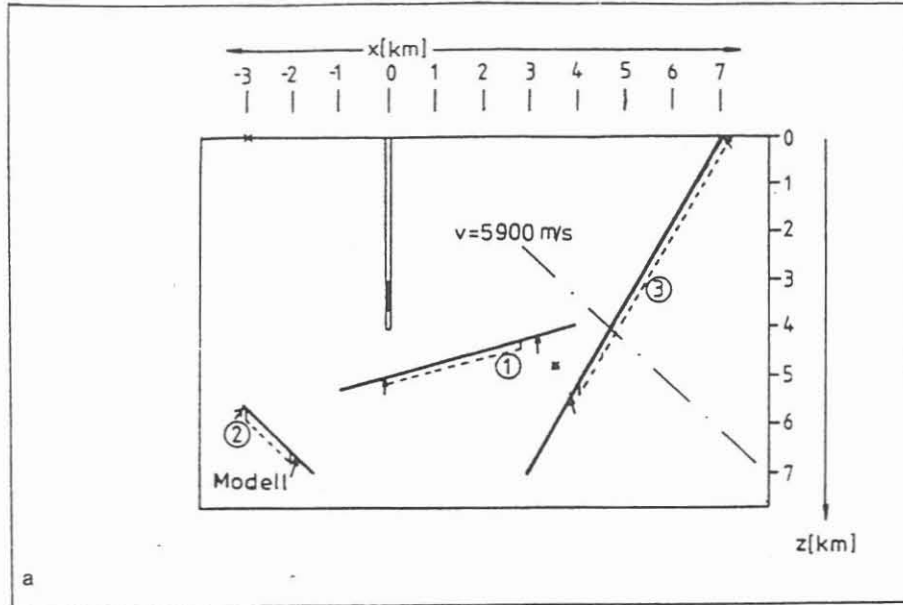


Figure 3: Synthetic example. a) Model, the dash-dotted line marks a reflector which is not detected by this specific measurement configuration. b) Synthetic data generated from model (a). c) Same data as (b) with random noise added.

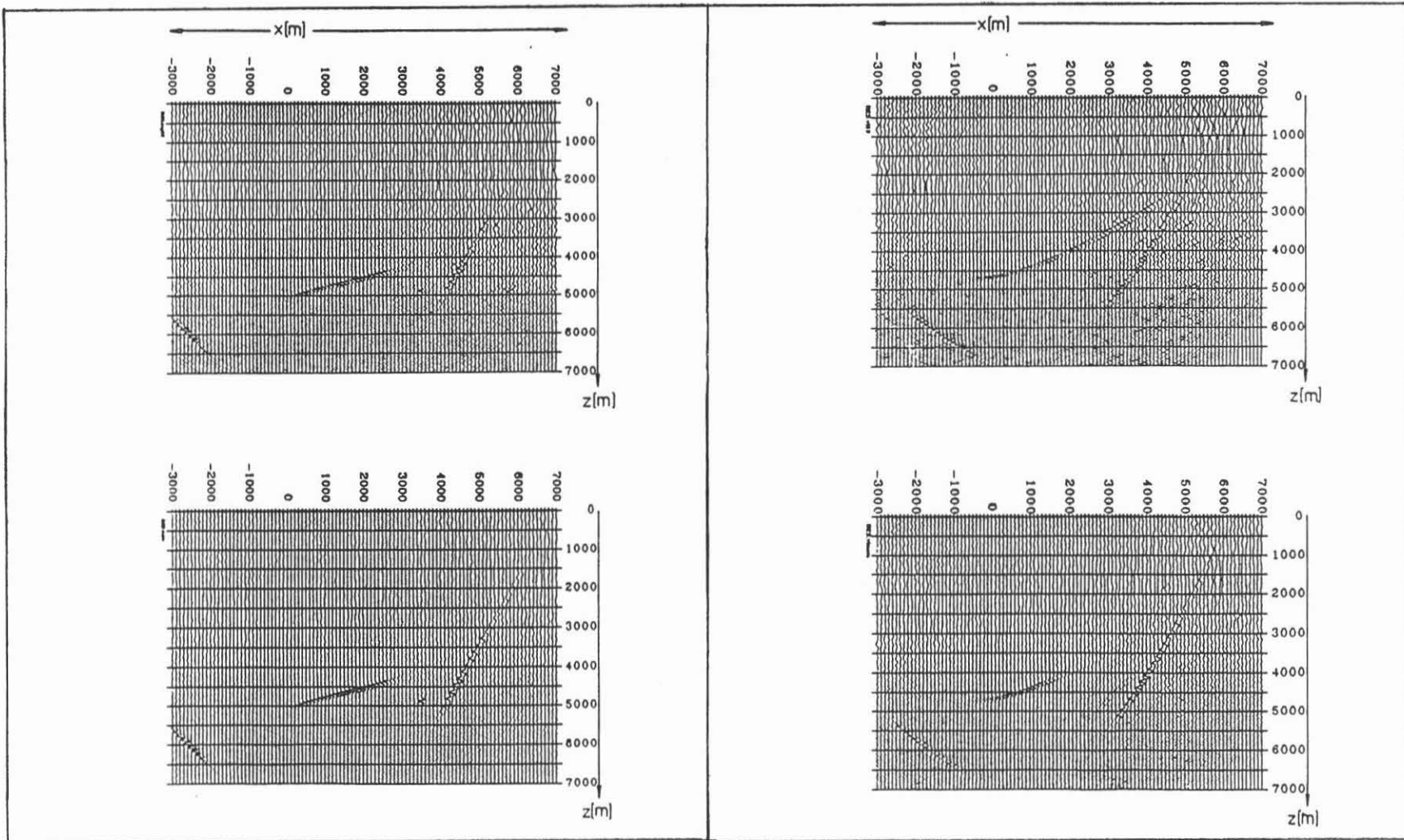


Figure 4: Result of migration: 5 profiles as in (3c) were calculated for different geophone depths (3500 m up to 3100 m). On the left the result of migration with velocity 5900 m/s, one single profile (upper) and the stack (lower). On the right the same for migration velocity 5310 m/s (10% too low).

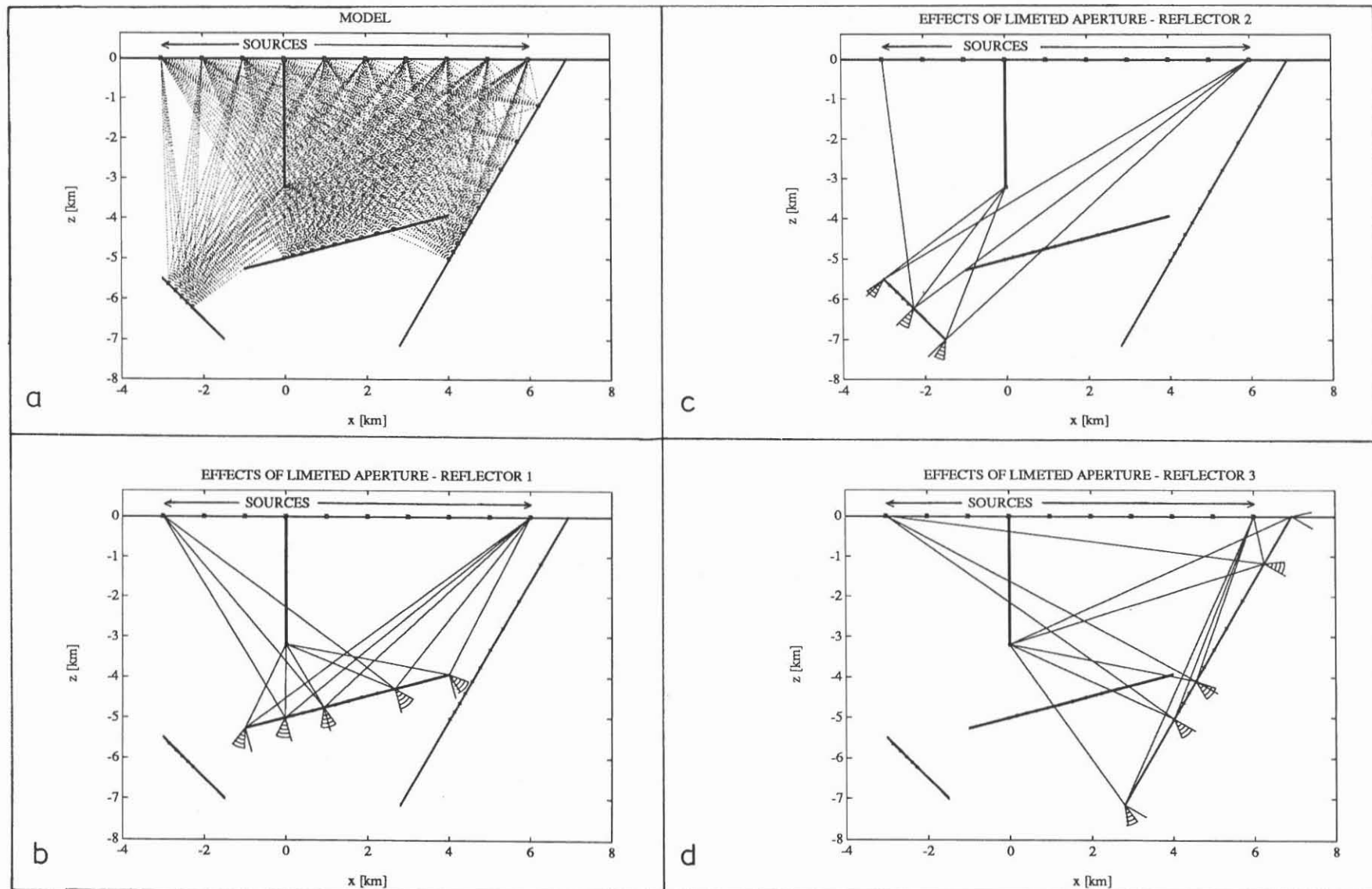


Figure 5: Limited aperture of the MSP experiment: The normal bundles show the limits of reconstruction of each reflector element (b-d). Figure (a) presents the model with every tenth source position only.

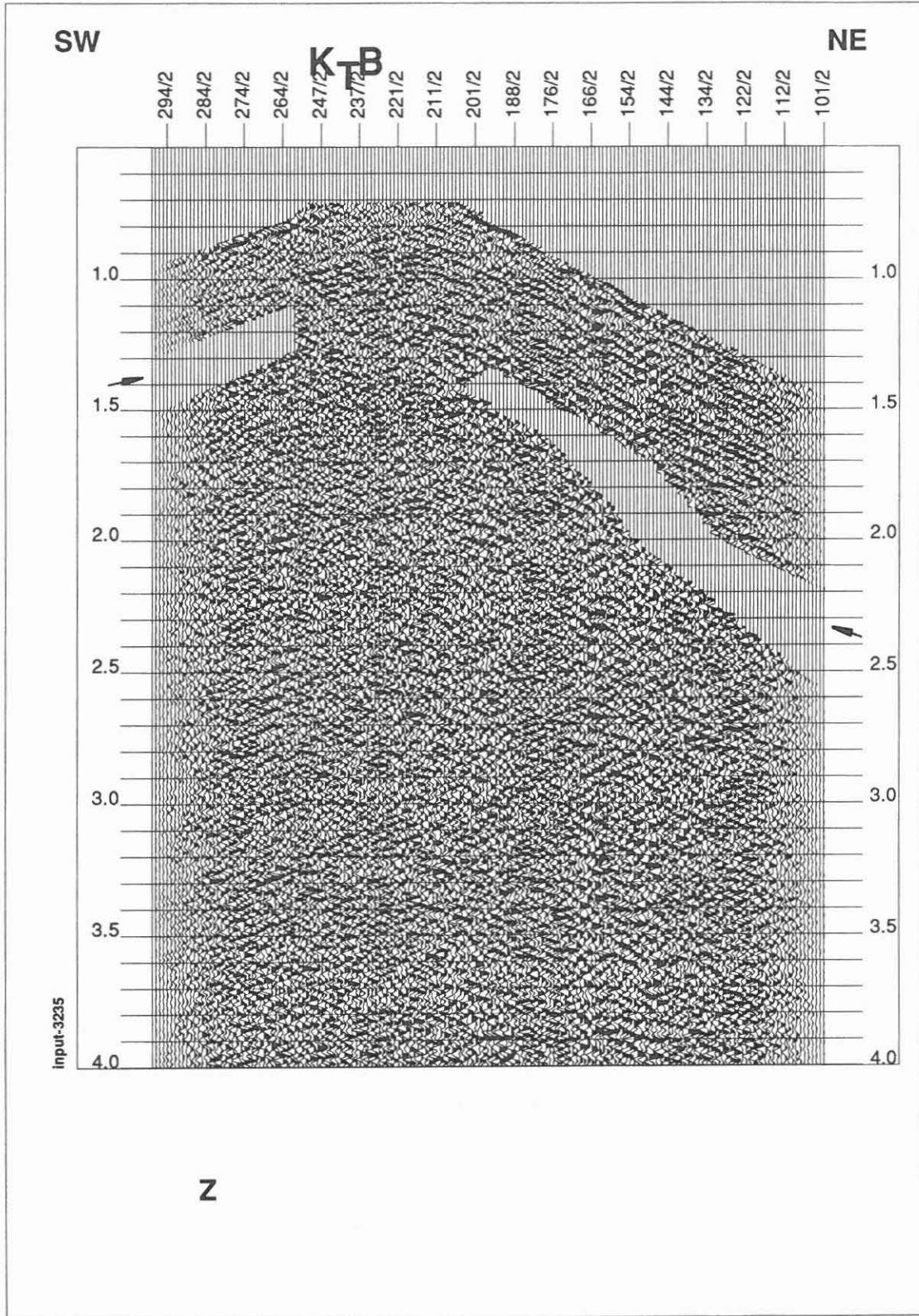


Figure 6: Example of input data to migration, i.e. the upgoing part of the Z-component registration of the geophone at 3235 m depth. Remaining parts of the downgoing wavefield have been muted and the margins of the section have been tapered. The mute of the S-arrival causes the gap in the data (arrows).

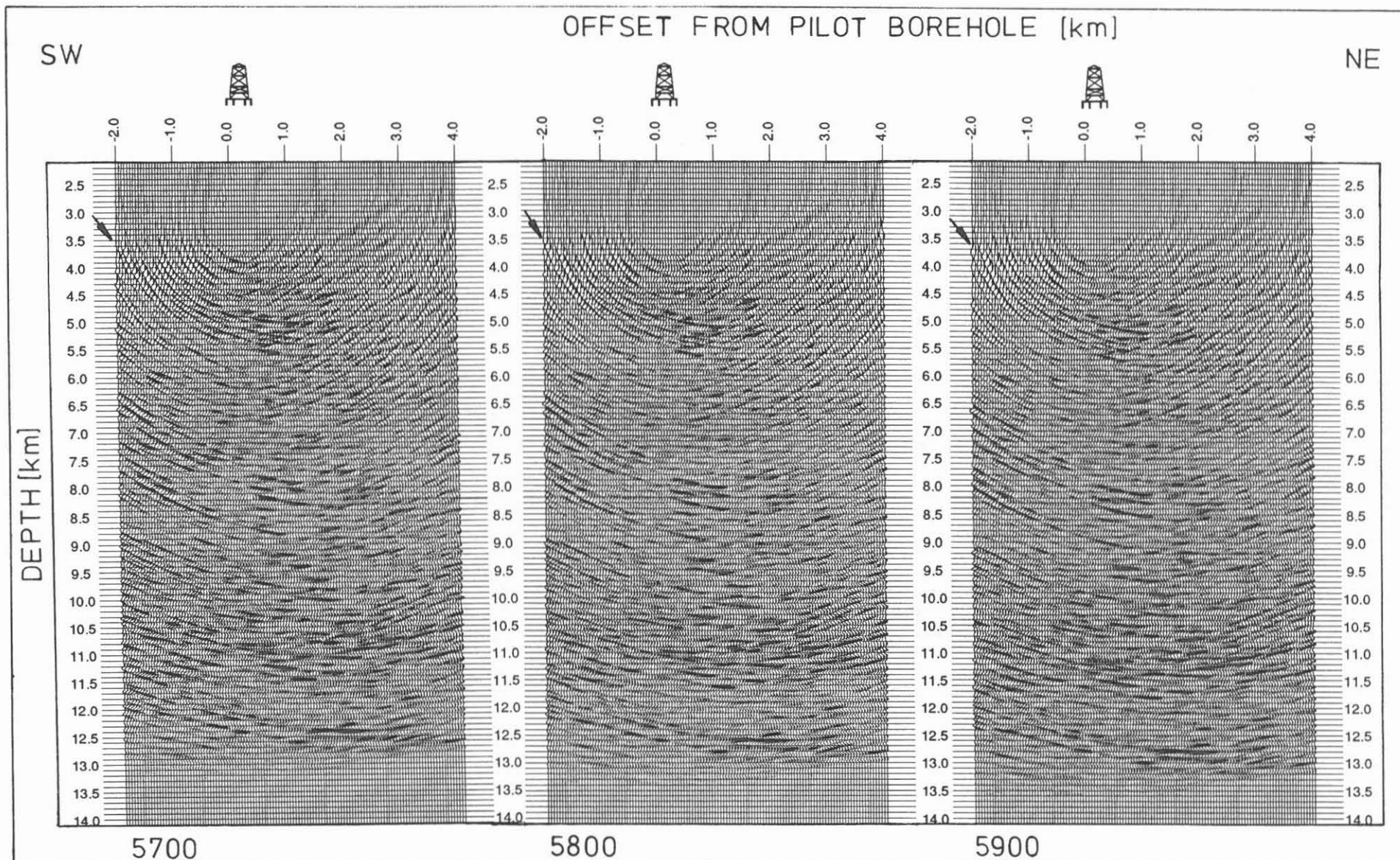


Figure 7: Result of migration and stack of 15 ISO 89 MSP common receiver gathers recorded between 3560 m and 3210 m, using three different migration velocities 5700 m/s, 5800 m/s and 5900 m/s (from left to right). Remarkable structures at 5 km, at 8 km and the "Erbendorf event" below 10 km depth. Note the steeply dipping event at the SW - margin of the image beginning at about 4 km depth (marked by the arrows).



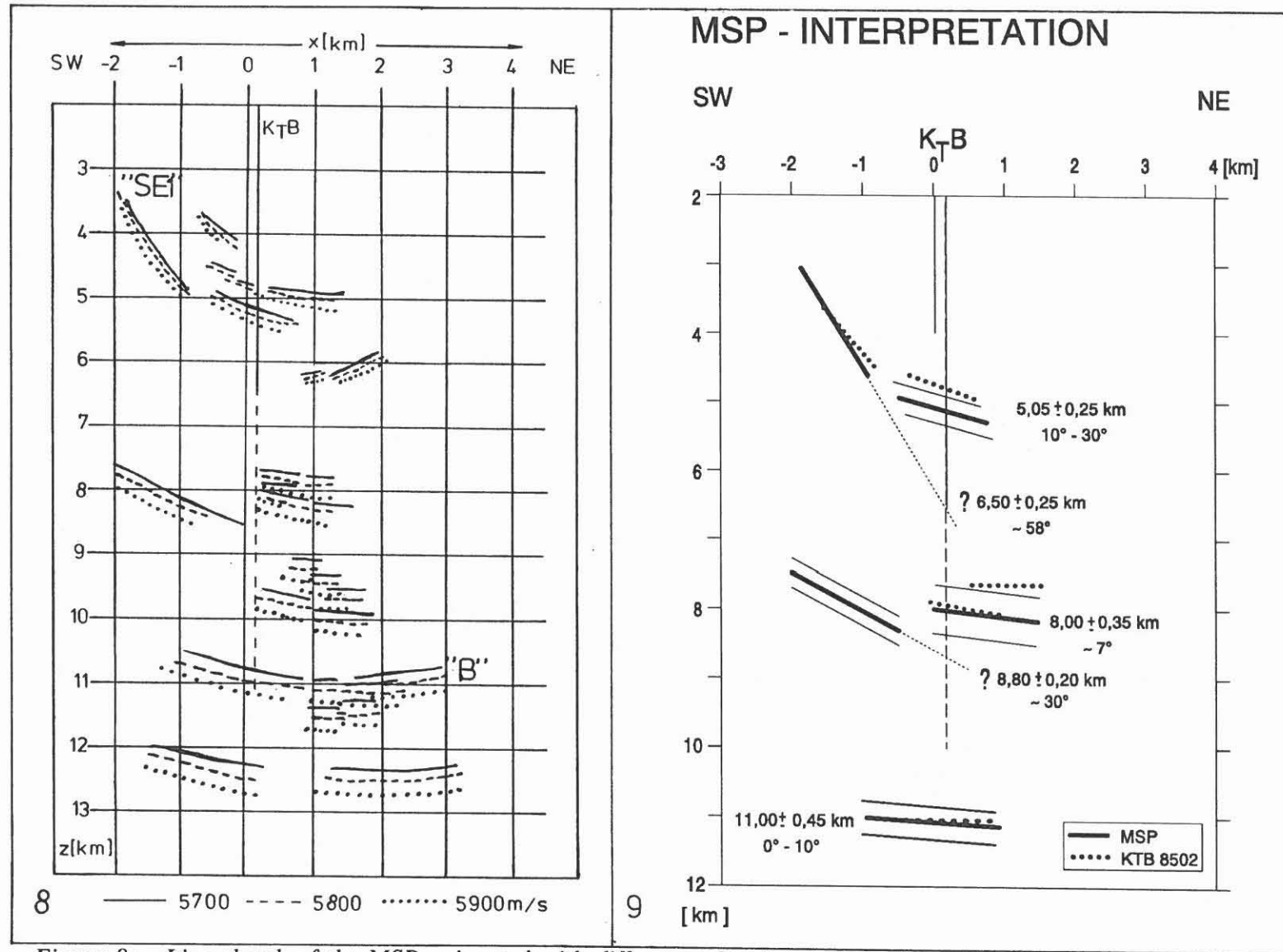


Figure 8: Line sketch of the MSP, migrated with different velocities, indicated by different line types. "SE I" is the dominant steep event detected by 3D-seismics and KTB 8502. "B" is one of the structures of the "Erbendorf-event".

Figure 9: Schematics of the interpretation of the MSP experiment with special reference to elements which can be hit by the drill bit. The elements are marked by thick black lines, dotted lines mark corresponding elements picked from the KTB 8502 profile. The thin lines bound the uncertainty of the depth values.

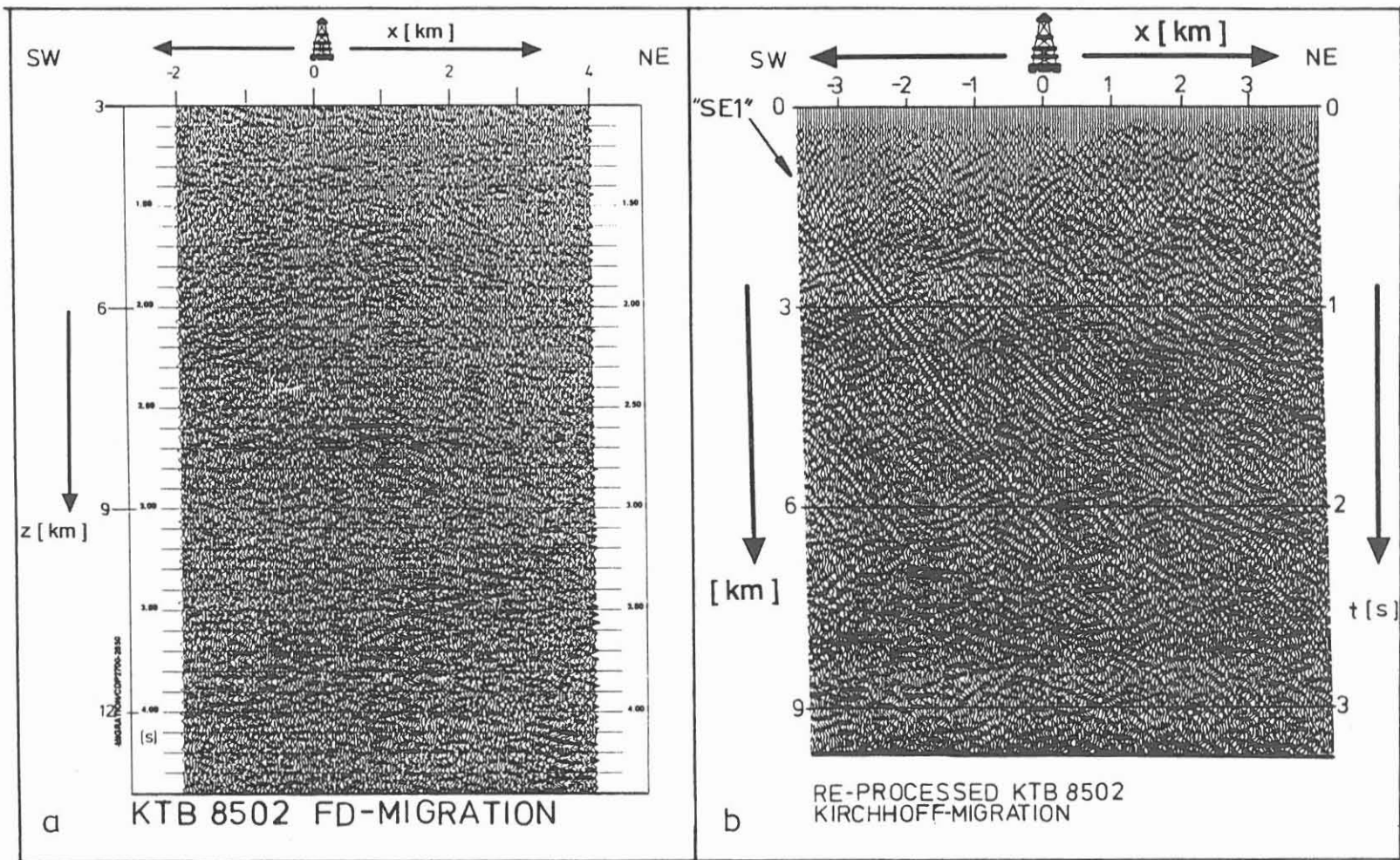


Figure 10: a) Part of the FD-migrated KTB 8502 profile. b) Part of the Kirchhoff-migration of the re-processed KTB 8502 profile. Re-processing was done specially to image the steeply dipping elements like "SE 1".

## **Depth determination of prominent seismic structures beneath the KTB main drillhole KTB-HB**

**DEKORP Research Group\***

### **Summary**

Within the framework of the Integrated Seismic Survey Oberpfalz 1989 (ISO89) different methods were used to study the seismic structures and properties of the surroundings of the KTB drilling location Oberpfalz/Bavaria. A main target was the determination of those structures which are to be penetrated by the drillhole and will enable direct correlation to the geological and lithological results of the drilling. Therefore, they will play a key role in the interpretation of reflections found in this area and, moreover, provide important clues to deep crustal studies in other regions as well.

A number of dominant seismic reflections was detected beneath the KTB by the different seismic methods. However, depth determination is very critical in this spatially inhomogeneous environment since the exact 3D velocity distribution is a pre-requisite for this purpose. Because there is no depth nor velocity control by other deep wells in the study area the velocity distribution can be derived only from surface observations and within narrow limits from seismic observations within the KTB pilot hole. In this paper the structural results obtained from the different seismic studies are compiled and their related depths and the confidence levels are given relying on a most probable 3D velocity distribution which was derived from all seismic information accessible so far.

### **Introduction**

Comprehensive seismic investigations using different methods were carried out in 1989 in the surroundings of the KTB scientific drilling location Oberpfalz/Bavaria. Initial results and technical reports on the conduction of the field work are published in KTB Report 90-6b and in Meissner et al. (1991). The results presented in this paper are a compressed outline of the particular results and analyses elaborated by the different working groups partaking in this project. It deals only with the prominent reflections present in the close surroundings of the KTB, their depths and the 3D p-wave velocity distribution necessary for spatial depth determination. Reliable statements on drilling relevant structures could be inferred essentially from the interpretation of the 3D seismic observations (Hluchy et al., this volume; Wiederhold, this volume) and from the MSP experiment (Janik and Harjes, this volume), only.

---

\* Correspondence to: C. Reichert, Niedersächsisches Landesamt für Bodenforschung, Stilleweg 2, W-3000 Hannover 51, Germany

## Review of seismic elements picked beneath the KTB location

The DEKORP Processing Center (DPC) at Clausthal provided a 3D unmigrated data set stacked by a simplified envelope method (Stiller, this volume). This set was interpreted simultaneously at the DPC (Hluchy et al., this volume) and at Hannover (Wiederhold, this volume) using 3D working stations to obtain two independent views of the data enabling greater reliability. A number of different reflection elements was picked and mapped in space. The results of both interpretations were compared and the reliable elements were compiled.

Fig. 1 presents the spatial arrangement of the picked elements in a two-way travel-time unmigrated display. A bunch of subparallel reflections striking NW/SE with relatively steep NE dip ( $40^\circ - 60^\circ$ ) is most conspicuous. The lowermost and strongest group is called SE1 (Hluchy et al, this volume; Körbe and Reichert, this volume; Wiederhold, this volume). The uppermost one is denoted by SE2 and the one in the centre by SE3. A rather weak element named SE12 ties up SE1 and SE2 and bends listrically. At the intersection with the drillhole it shows a rather weak dip of about  $20^\circ$ . This is revealed very clearly on the KTB8502 profile (Fig. 2). SE3 is the faintest element of this group providing a high degree of uncertainty.

Extrapolating SE1 linearly it hits the surface very closely to the fault system of the Franconian Lineament (FL) consisting in that area of the Waldeck-Klotzenreuth and Atzmannsberg-Altenparkstein fault zones (Hirschmann, 1992). Two other similarly steeply dipping reflectors SE4 and SE4A exhibit a different strike direction and can be correlated rather well at the surface with the Fichtelnaab fault. However, both horizons are outside the reach of the drillhole.

Another element denoted by BS is expected below the group of the SE horizons at about 8 km depth but its spatial position is still unclear. At depths greater than 10 km the subhorizontal reflections of the Erbdorf structure appear (B1, B2, R1, R2). The depths and spatial characteristics of the reflectors to be encountered by the deep drilling are compiled in Table 1.

The accuracy of the given depth values is generally affected by two sources of inaccuracy:

- the assessed 3D velocity model necessary for the depth migration
- the error limits when picking reflections in the present data set

Different velocity models will be discussed in detail in the next chapter.

Uncertainties when picking reflections on 'envelope'-stacked data are essentially stronger than on phase-consistent data. Producing the latter in crystalline setting brought about several difficulties discussed by Stiller (this volume) and is still in preparation. Particular events of the 'envelope'-stacked data exhibit a typical length of some 80 ms implying a picking error of the same order. However, larger deviations are compensated by the spatially correlated picks and planar interpolation before mi-

gration. Error bounds can be determined by standard deviation between particular picked data points and the fitted surface. The resulting error must be adjusted to the direction of the respective ray path. This was achieved by dividing the vertical error by the cosine of the dip angle (Wiederhold, this volume).

### Migration of time horizons into depth

P-wave velocities are absolutely essential for the conversion of the seismically observed (p-wave) structures from the two-way time domain into the depth domain. Within ISO89 numerous efforts were made by different field arrangements to investigate the 3D velocity field in the area of the 3D seismic survey. Due to limited budget these approaches have always their shortcomings. Most reliable results were obtained, of course, along the drilling path by sonic logs and core analyses. Since the ray paths of the 3D seismic study transect nearly the entire 3D volume below the 2D surface field arrangement such precise velocity information should be at hand analogously, especially for greater depth ranges. This condition should be met especially in a tectonically as well as geologically so complex setting as the area under study.

The 'envelope'-stacked data of the 3D seismic survey provided by DPC were impossible to undergo a wavefield migration and, thus, were transformed into depths using different map migration programmes basing on various velocity models: at the DPC a map migration programme was developed migrating the data in the time domain (Stiller and Tormann, this volume). Constant velocities are used in this approach, i.e. for each horizon an optimal velocity was selected as listed in Table 1. The depth conversion was accomplished using a constant velocity of 6.0 km/s. At Hannover a 'map migration' algorithm after Sattlegger (1986) was used incorporating also more complicated velocity models which are presented in the following. In Fig. 3 the most prominent reflection elements in the area of the 3D seismic survey of ISO89 are displayed at correct spatial position.

A compilation of the various velocity data determined for the 3D seismic relevant space is given in Table 2. Regarding the near-surface range a dense network of velocity data is at hand resulting from first breaks of the 3D seismic data and from short refraction lines (Lengeling 1991). Formerly, these data were used to calculate static corrections for the 3D seismic processing. They provide sound information on the velocity of the solid rocks below the weathering horizon (i.e. at datum level) and correspond quite well with the alternating geological situation found at the surface. Especially the areas of gneissic, granitic and metabasitic rocks as well as the sediments west of the FL show up clearly in these velocity data.

The VSP results at the drillhole provide velocities of some 6.0 km/s at depths greater than 2.5 km (Hanitzsch et al., this volume). This value was used as basic limit when establishing the spatial velocity model. Between the refractor velocities at datum level (500 m a.m.s.l.) and the fixed value of 6.0 km/s at 2.5 km depth a constant vertical velocity gradient was assumed and its value was calculated depending on its horizontal position (velocity model no. 1000 in Table 1).

Another velocity model (1005) was developed attempting to accommodate to the border between the gneisses and Falkenberg granites. This border was modeled as a step assuming the bottom of the granites at 4 km depth. This depth was determined from gravity modeling (Soffel et al., 1989) and, therefore, provides the related uncertainties. Velocity model 1005 uses the correction velocities at datum level and an appropriate constant velocity gradient so that the velocity of 6.0 km/s is fitted at 4 km depth in the Falkenberg area. The results of these depth migrations are listed in Table 1. A related graphic display of the most prominent reflection is given in Fig. 3.

In order to diminish the uncertainties of the selected velocity models the depths of the steeply dipping reflectors SE1, SE2, SE3 and SE12 were also calculated by using the results of the 'Durchschallungs-' experiment DUSCH (Albrecht and Teichert, 1990). These data provide traveltime values from the surface (source points of the 3D seismic survey) to a borehole geophone at 3.22 km and 3.42 km depth, respectively, located in the KTB pilot hole. For the depth calculation the data set for geophone depth of 3.42 km was used in order to comprehend ray paths reaching as deep as possible. The DUSCH data are related to 500 m a.m.s.l datum level and the height of the well head was accounted for. Moreover, the depth dependent geometrical drilling deviation was considered when calculating the average velocity along the respective ray path. However, due to missing details the refraction effect of the rays penetrating different rocks was not accounted for.

At first, the source points at the surface related to the reflection points beneath the drilling location were determined using the ray paths obtained from migration results. The traveltimes from these surface points to the geophone at 3.42 km depth are provided by the DUSCH experiment. Neglecting the presumably small deviations of the straight ray path from the actual one all velocity effects above 3.42 km affecting the average velocity are ruled out. Only the range below this depth still contributes to velocity uncertainties. In order to assess this residual effect the depth differences to 3.42 km were calculated using different plausible velocities. The related depth variations - depending on the depth difference - amount up to 175 m maximum only. The results are given in Table 1.

### Results of the MSP experiment

The MSP experiment only provides results within the closest vicinity of the drillhole (Janik and Harjes, this volume). Dips of up to 40° are observed. The spatial position of these elements, however, cannot be determined. The SE1 reflector is observed also in these data but only beyond the extrapolated drilling path. At 5 km depth a reflector with 30° dip is detected which might correlate with the SE12 element found in the 3D seismic data. Another subhorizontal reflector (7° dip) appears at 8 km depth (cf. Table 1).

## Conclusions

All information available up to now was compiled in order to calculate the depth values of the seismic elements detected in the ISO89 experiments as precisely as possible. It should be mentioned that this work was done already before the drilling reached the depth of 6,750 m and got stuck. A reliable 3D velocity model still remains the most crucial point. However, strong efforts were made to cope with this problem and the data of the DUSCH experiment were extremely helpful for this purpose. Indeed, from the calculated depth values it could be inferred that the SE2 reflection is related to a fault and SE3 probably to a change in rock foliation (Hirschmann, this volume). At the depth of about 6.700 m a strongly cataclastic zone was encountered which is most probably related to the SE1 reflector. However, these results still have to be confirmed by additional structural information from appropriate logs. Furthermore, the continuation of the drilling will reveal if we are dealing already with the SE1 reflector at 6,700 m depth and if there perhaps might follow a lithological change in the footwall.

## References

- Albrecht, J., D. Teichert (1990): Experiment 'Durchschallung' - Calculation of Static Corrections from Seismic Borehole Records Using the Vibrator Signals of the 3D Seismic Reflection Survey within ISO89.- KTB Report 90-6b, DEKORP Report, Hannover.
- Hanitzsch, Ch., P. Hubral, Th. Rühl, W. Söllner (1992): Migration of Steep Dipping Reflectors at the KTB Site: Depth Errors Caused by Inaccurate Velocity Models.- KTB Report 92-5, DEKORP Report, Hannover.
- Hirschmann, G. (1992): Preliminary Interpretation of the 3D-Seismic Survey at the KTB location.-KTB Report 92-5, DEKORP Report, Hannover.
- Hluchy, P., M. Körbe, R. Thomas (1992): Interpretation of Envelope-Stacked Data of the 3D Seismic Survey at the KTB Location.- KTB Report 92-5, DEKORP Report, Hannover.
- Janik, M., H.-P. Harjes (1992): Structural Interpretation of the MSP-Experiment.- KTB Report 92-5, DEKORP Report, Hannover.
- Körbe, M., C. Reichert (1992): On the character of 'Steep Event SE-1' - Reflected Energy, Reflected Refraction, Diffraction or Any Artifact? - KTB Report 92-5, DEKORP Report, Hannover.
- Lengeling, R. (1991): Bewertung eines Inversionsverfahrens zur Berechnung statischer Korrekturen in der 3D-Seismik und seine Anwendung auf reflexionsseismische DEKORP-Messungen in der Oberpfalz 1989. - Diss., TH Karlsruhe.

- Meissner, R., L. Brown, H.-J. Dürbaum, W. Franke, K. Fuchs, F. Seifert (eds.) (1991): Continental Lithosphere: Deep Seismic Reflections.- AGU - Geodynamic Series, v. 22, Washington D.C.
- Sattlegger, J. (1986): Three-Dimensional Map Migration and Modeling Algorithm.- Sattlegger Ingenieurbüro für angewandte Geophysik, Meppen.
- Soffel, H. C., S. Plaumann, R. Pucher, C. Bucker, H.-J. Götze, M. Wagener, V. Haak (1989): Gravity and Magnetic Investigations at the KTB Locations Schwarzwald and Oberpfalz.-In: Emmermann,R.,J.Wohlenberg (eds.) (1989): The German Continental Deep Drilling Program (KTB).- Springer Verlag, Berlin-Heidelberg, pp.409-431.
- Stiller, M. (1992): Preliminary Generation of a Stacked Data Volume of the Entire ISO89-3D Data Set Using an Envelope Technique.- KTB Report 92-5, DEKORP Report, Hannover.
- Stiller, M., M. Tormann (1992): Application of a Simplified Horizon Migration Process to the Data of the 3D-Seismics ISO89.- KTB Report 92-5, DEKORP Report, Hannover.
- Wiederhold, H. (1992): Interpretation of Envelope-stacked 3D Seismic Data and Its Migration - Another Approach.-KTB Report 92-5, DEKORP Report, Hannover.



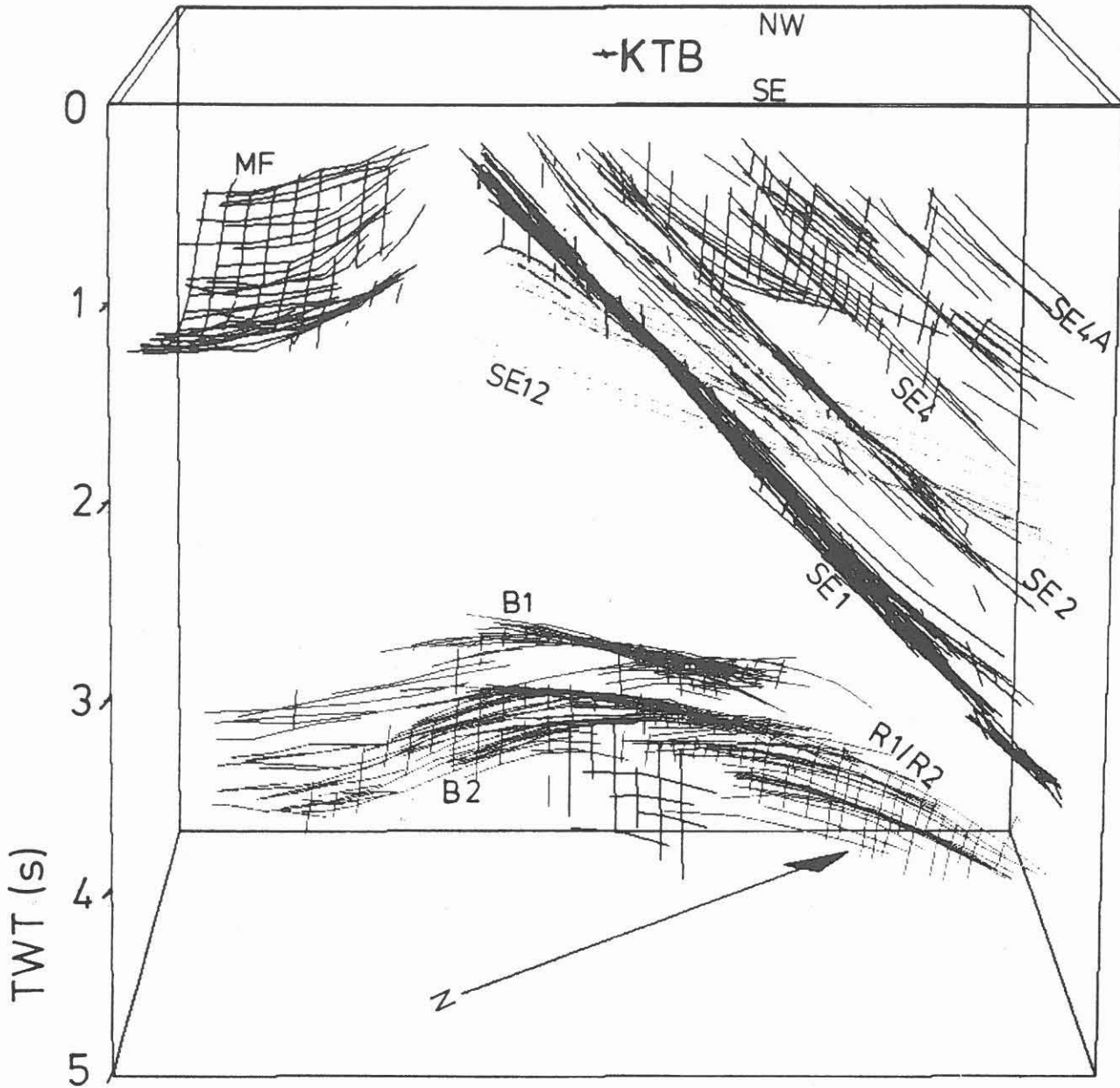


Figure 1: 3D block of the mapped horizons. The display presents unmigrated two-way traveltimes (MF = base of ?Permo-Carboniferous). The position of the KTB is indicated on the top of the block (=datum level). From Wiederhold 1992.

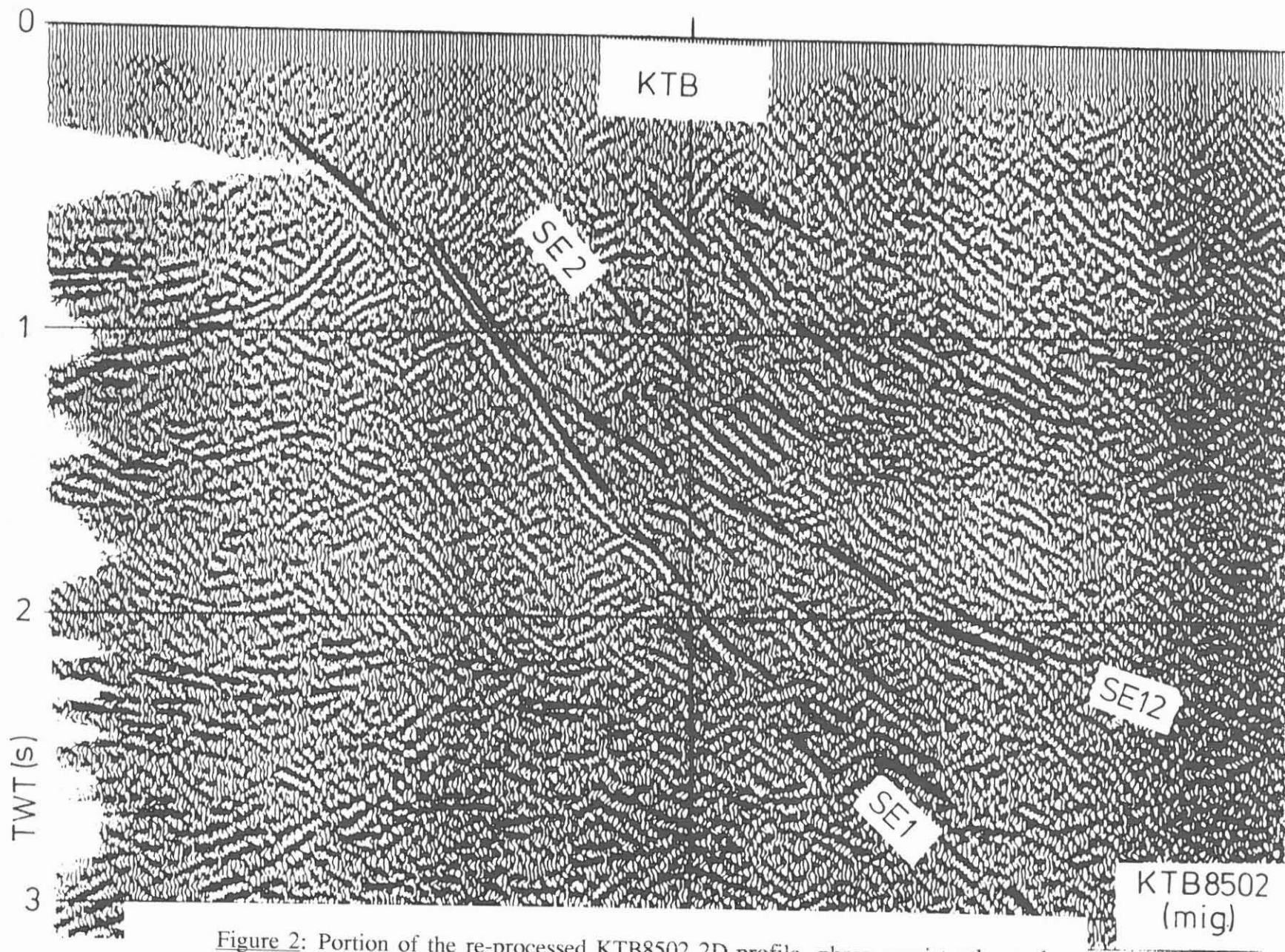


Figure 2: Portion of the re-processed KTB8502 2D-profile, phase consistently stacked, migrated and coherency filtered. From DPC, Clausthal.

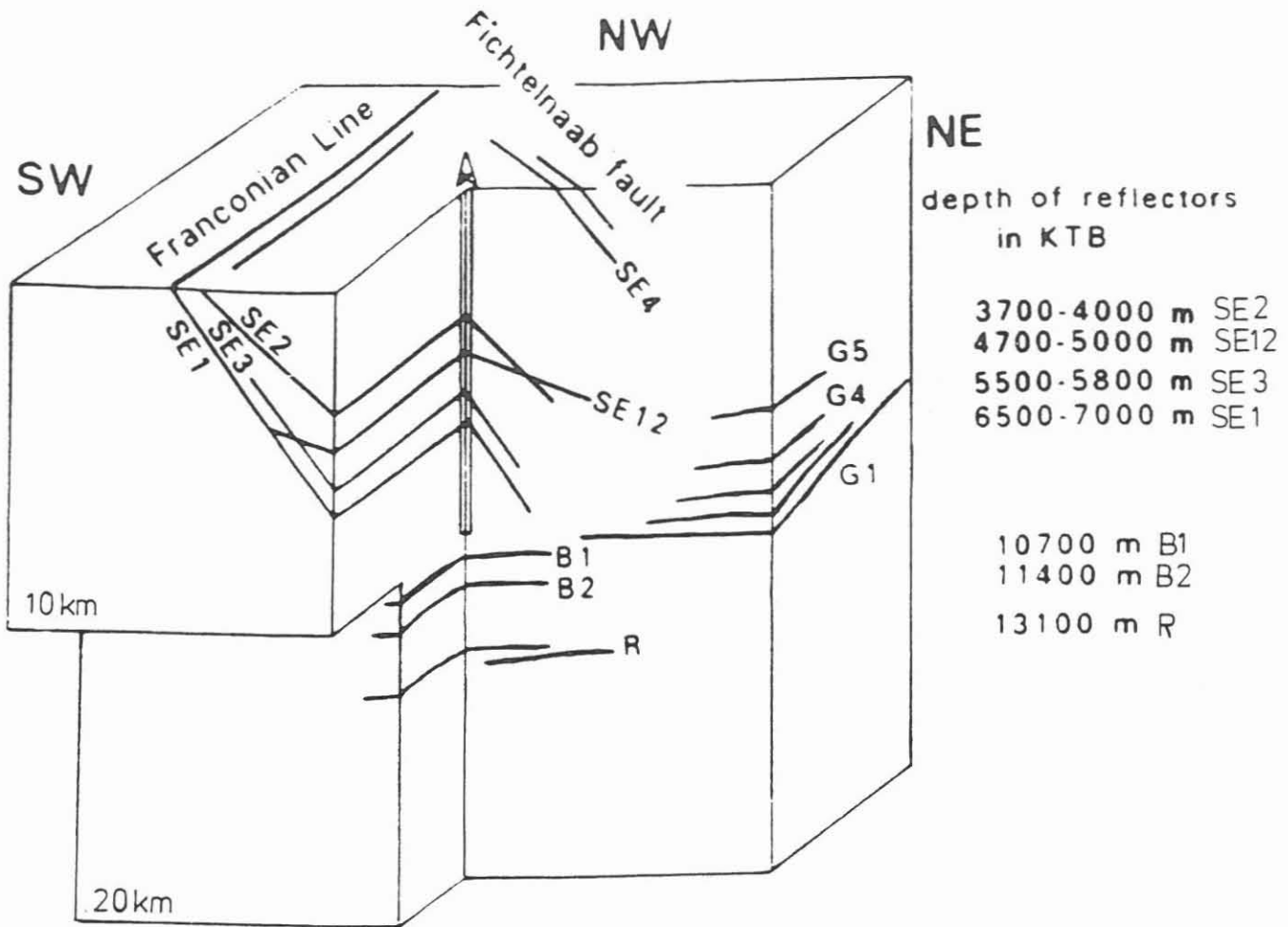


Figure 3: True spatial location of the most prominent reflecting elements in the area of the 3D seismic survey (ISO89) after depth migration. From Wiederhold 1992.

Interpretation: 3D-Seismik:		depths of reflectors in KTB-HB in m				MSP: Janik & Harjes (1992)
Reflector	Dip/Strike	Stiller & Tormann (1992)	Wiederhold (1992)		depth-estimation with exper. "Durchschallung" (after Reichert)	Moving Source Profiling MSP
		velocity= $v$ = constant depth conversion with $v=6$ km/s	velocity-model 1000	velocity-model 1005		
SE2	40°-45° / 320°	4000 ±200 ( $v_{mig}=5.2$ km/s)	3700 ±200	3700 ±200	3775±200 ( $v=6$ km/s) 3770 " ( $v=5.875$ "") 3790 " ( $v=6.4$ ")	----
SE12	20° / 330°	4750 ±200 ( $v_{mig}=5.2$ km/s)	4700 ±190	4700 ±190	4875±190 ( $v=6$ km/s) 4845 " ( $v=5.875$ "") 4930 " ( $v=6.25$ ")	5050 ±250 (30°)
SE3	50° / 330°	5500 ±300 ( $v_{mig}=5.2$ km/s)	----	5800 ±110	5940±110 ( $v=6$ km/s) 5900 " ( $v=5.875$ "") 6025 " ( $v=6.25$ ")	----
SE1	55° / 320°	6500 ±200 ( $v_{mig}=5.2$ km/s)	7000 ±140	6600 ±140	7025±140 ( $v=6$ km/s) 6965 " ( $v=5.875$ "") 7140 " ( $v=6.250$ "")	----
BS		7850 ±200 ( $v_{mig}=5.9$ km/s)	----	----	----	8000 ±350 (7°)
B1		10600 ±200 ( $v_{mig}=6.0$ km/s)	10700	10700		
B2		11550 ±200 ( $v_{mig}=6.0$ km/s)	11400	11400		
R1		11250 ±200 ( $v_{mig}=6.0$ km/s)	----	----	----	
R2		----	13150	13150		
SE4	50° / 290°	----	----	----	----	
SE4A	45° / 300°	----	----	----	----	

Table 1: Reflector depths and related dip angles along the drillhole trajectory calculated on the basis of different models.

Table 2: Compilation of seismic velocities observed at the KTB drilling location as of March 1992.

1. Closest vicinity of the KTB pilot hole and main hole

a) Sonic-Log (available)

b) VSP

0 km 5.4 km/s  
from 2.5 km 6.0 km/s

c) Laboratory data (Kiel) (available)

d) Laboratory data (KTB-Feldlabor) (available)

e) Wide-angle seismics ( $\tau$ -p-method)

Reflex2 SW-NE (ISO89)			DEKORP4 NW-SE (CMP96)		
depth	velocity		depth	velocity	
0 km	5.0 km/s		0 km	5.0 km/s	
0.6 km	5.2/5.7 km/s		1.0 km	6.0 km/s	
3.0 km	5.8/5.9 km/s		5.0 km	6.05/6.1 km/s	
6.0 km	6.25/5.5 km/s		7.25 km	6.12/5.75 km/s	
8.0 km	5.5/5.7 km/s		8.4 km	5.85/6.15 km/s	
8.4 km	5.7/5.5 km/s		9.5 km	6.16/6.20 km/s	
8.8 km	5.5/6.5 km/s		10.0 km	6.20/6.35 km/s	
10.2 km	6.85/6.6 km/s		10.5 km	6.35/6.40 km/s	
11.8 km	6.6/7.0 km/s		11.1 km	6.40/6.45 km/s	
13.4 km	7.25/6.5 km/s		11.6 km	6.55/6.60 km/s	
			12.0 km	6.75 km/s	
			12.25 km	6.75/6.85 km/s	
			13.1 km	6.85/7.05 km/s	
			13.75 km	7.15/7.25 km/s	
			14.1 km	7.30/7.25 km/s	
			15.0 km	7.50/6.50 km/s	

f) 3D-ESP (NMO velocities)

depth	velocity	azimuth: N 80° - 110° E
0 km	5.42 km/s	
1.29 km	5.75 km/s	
1.82 km	6.04 km/s	
2.45 km	5.75 km/s	
3.9 km	6.0 km/s	
5.08 km	6.5 km/s	

- Compiled from a), c) and d) by E. Huenges:

depth range/domin. lithology	velocity range	anisotropy
0 - 1.6 km gneiss/metabasite	5.8 - 6.4 km/s	5 - 10%
- 3.6 km gneiss	6.0 - 6.2 km/s	10%
- 6.0 km metabasite	6.4 - 6.6 km/s	5%

velocity gradient

dominantly gneissic depth range 0-4 km: 0.26 s<sup>-1</sup>  
dominantly metabasitic depth range 4-6 km: 0.4 s<sup>-1</sup>

Table 2 (continued)

2. Surroundings of the KTB location

a) COMSTAT (two-dimensional velocity distribution on top of the unweathered crystalline, available)

b) MSP amphibolite (gneiss): 5.95 km/s  
granite: 5.55 km/s

c) wide-angle seismics (ISO89)

- migration velocities:

	SP 101-120	SP 201-220
at surface	5.46 km/s	5.8 km/s
at 6 s TWT	5.97 km/s	6.04 km/s

- Reflex2 (area of Falkenberg granite, x-t-v method)

depth	velocity
0.0 km	4.8 km/s
0.5 km	5.2/5.3 km/s
1.6 km	5.85/5.87 km/s
2.9 km	6.15/5.8 km/s

d) wide-angle seismics (DEKORP4; ray tracing, 1988)

CMP 90 Erbendorf		CMP 95 Windisch-Eschenbach	
depth	velocity	depth	velocity
0 km	5.46 km/s	0 km	5.25 km/s
0.63 km	5.85 km/s	0.65 km	5.75 km/s
0.88 km	5.96 km/s		
3.96 km	5.96/5.77 km/s	3.75 km	6.06/5.85 km/s
7.0 km	5.96/6.06 km/s	7.5 km	5.90/6.06 km/s
8.0 km	6.32 km/s	10.5 km	6.33 km/s

e) ESP2 (DEKORP4, Vohenstrauß)

depth	velocity
0 km	4.8 km/s
1.46 km	5.69 km/s
1.86 km	5.76 km/s
3.51 km	5.83 km/s
4.23 km	6.0 km/s
5.94 km	6.08 km/s
9.51 km	5.83/6.0 km/s

f) MASE 6.1 km/s (average value)

g) DUSCH (Durchschallung) (available)

h) Earthquake monitoring (available)

## STRUCTURAL IMAGES FROM 3-D-ISOCHRON MIGRATION OF WIDE-ANGLE DATA IN THE SURROUNDINGS OF KTB

Michael Simon \*)

### Summary

As part of the program "Integrated Seismics Oberpfalz 1989" a specially designed wide-angle 3D-survey was carried out to investigate the velocity distribution and structural features beneath the KTB site. The so-called Erbendorf Body in about 11 - 14 km depth with its strong wide-angle reflectivity and unusual high P-wave velocities (over 7 km/s) was the main target of this measurements.

After careful true amplitude preprocessing a 3D-isochron prestack migration was applied to image vertical and horizontal sections. The Erbendorf Body is shown to exist in the whole northwestern part of surveyed area and its top forms a smooth syncline. Some reflectors known from steep-angle seismics are also visible.

### Layout of Measurements

The layout of the 3D-wide-angle measurements (Gebrande et al. 1991) was optimized for good resolution in the middle crust beneath KTB. This was obtained by two sets of dynamite shots, each registered among others by a 312 channel receiver spread in an offset range of 25 to 50 km (Fig. 1). This geometry provides a two-fold coverage in an area of  $10 \times 12.5 \text{ km}^2$  around the KTB site.

For the ease of comparison, the same symbols (SE, B, G) are used for reflection groups as in IS089 steep-angle seismics (Stiller, this volume). Also the bin numbers of inline (I...) and crossline (C...) sections are the same, but inlines are extended to NE by about 2 km compared with steep-angle seismics. The seismic datum for all velocity functions and migrations in this paper is 500 m above sea level.

### Concept of 3D-Isochron Migration

Isochron-migration is a migration method which produces an image of the underground by adding every sample of each seismogram to all places on a grid of the underground, from where it could have been reflected or diffracted. A 2D-version developed by Schmidt (1991) has recently been extended to the 3D-case (Simon, 1992).

---

\*) Author's address: Institut für Allg. u. Angew. Geophysik,  
Theresienstr. 41, IV  
W-8000 München 2,  
Germany

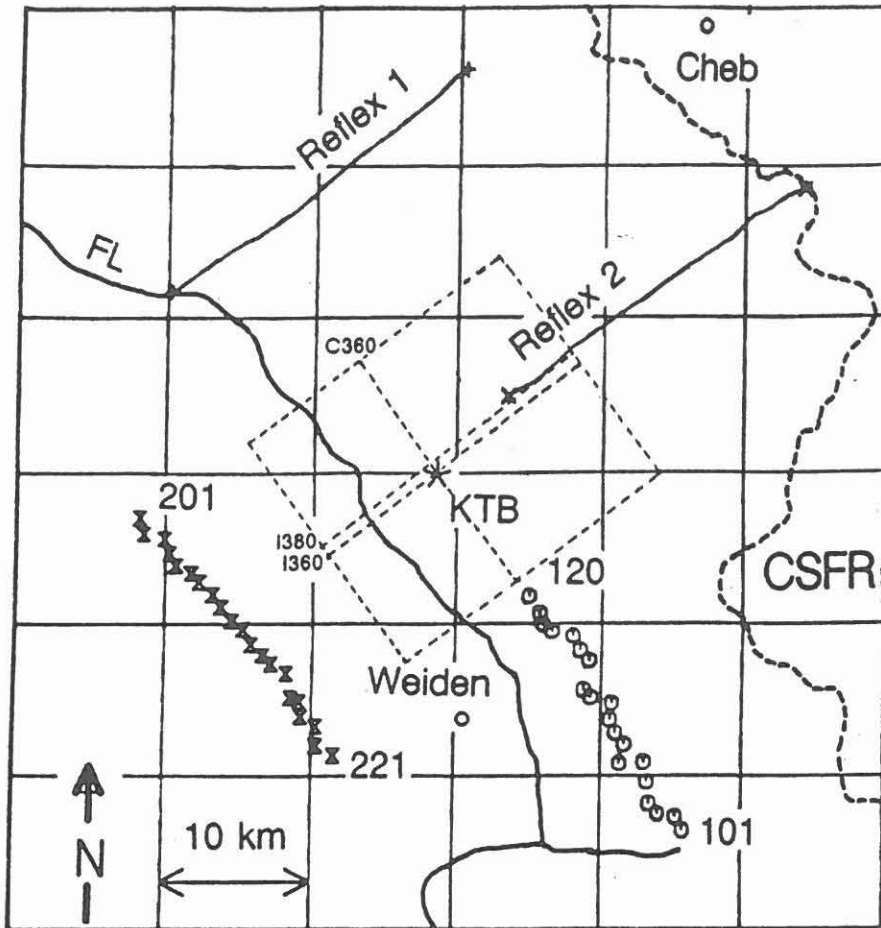


Fig. 1: Location map of ISO89 wide-angle measurements discussed in this paper; shotpoints 101-120 registered by 312 channels of receiver spread Reflex1 and shotpoints 201-221 by receiver spread Reflex2. (I360 and I380 = "inline" sections 360 and 380, C360 = "crossline" section 360, FL = Franconian line)

Input to this migration are normally shot-ensembles, which can have irregular receiver spacing. Migration then will be performed into a migration array which represents either an arbitrary oriented vertical time (or depth) section or a time (or depth) slice. For each input shot-ensemble there is an output of a migrated section or slice which then may be processed further before it is stacked vertically with other single shot migrations. A migrated 3D-block is build up by many parallel sections or slices.

The method handles migration velocity functions which can depend on depth or TWT and on common midpoint (CMP) coordinates. Furthermore, an offset-dependent correction can be applied. The migration velocity function is calculated by raytracing from independently derived velocity models and stored in a seismic data base.

#### Limitations

To avoid overinterpretations it is important to keep a few points in mind. Due to the field set-up some reflectors, depending on their position, strike and dip, may be well illuminated by the



rays of a specific shot, and by others not at all. Therefore, in addition to the reflectors visible in the sections, others may exist in the underground that are not imaged by the actual geometry. There is, e.g., the chance to get reflections from a steeply NE-dipping reflector parallel to the Franconian Line by the shots 101-120 but not by the shots 201-221.

Furthermore, there may be some algorithmic noise in the form of elliptic events ("smiles") especially near the edge of the sections where coverage decreases. They can be identified by their elliptic appearance.

### **Preprocessing**

Through the whole preprocessing true amplitudes were preserved (e.g. no AGC!). Prior to the migration the samples were multiplied by time to correct for spherical divergence, and individual shot intensities were equalized. Although isochron migration is based on kinematic principles, the amplitudes may be regarded qualitatively as an image of the reflectivity distribution. In the preprocessing the wavelets were equalized and contracted by a predictive deconvolution to about two maxima. Therefore, a single reflector appears in the contour plots of this paper as two or three parallel lines, because positive and negative amplitudes are darkened but with different hatching.

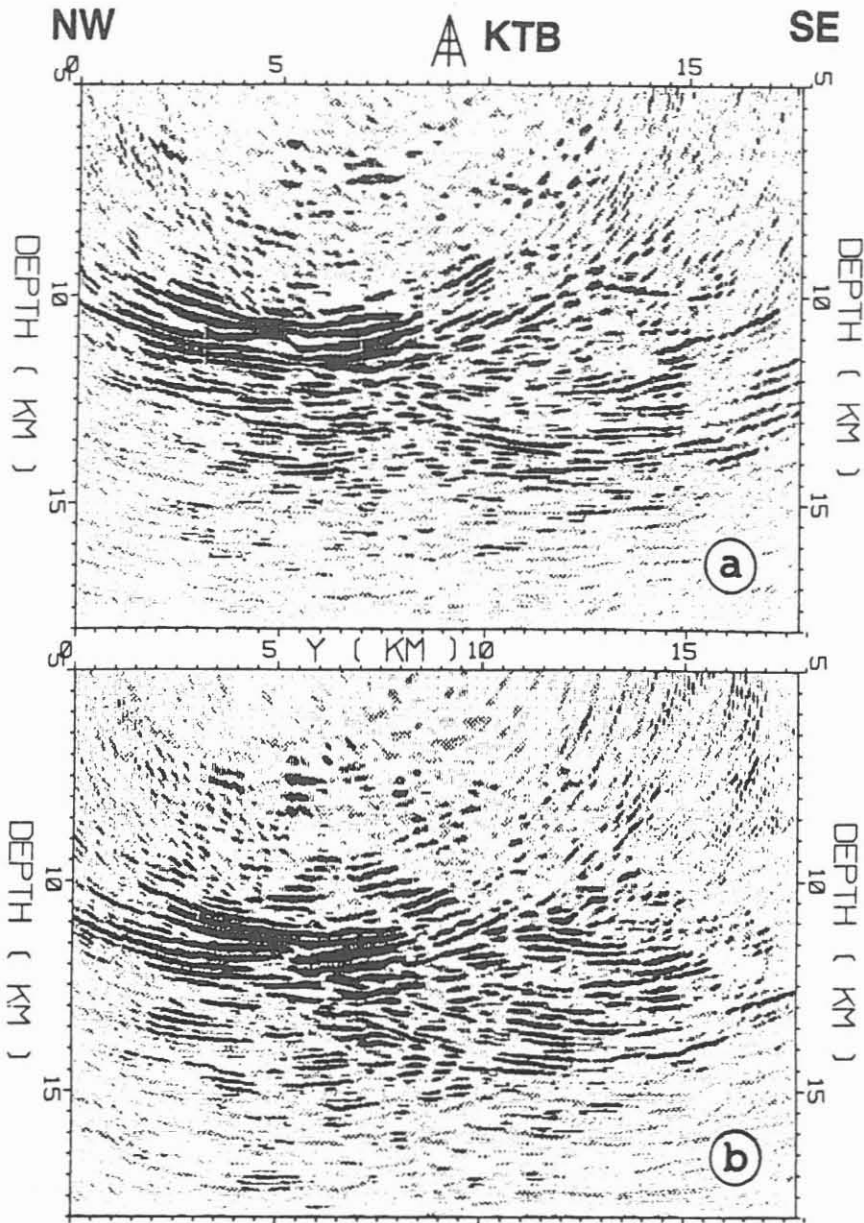
### **Migration Velocity Functions**

The migration velocity functions (Fig. 2) for the profiles Reflex1 and Reflex2 were calculated by raytracing from 2D-models. Offset dependent effects are included and therefore they are not to be identified with zero-offset migration velocities. Moreover, migration velocities for profile Reflex2 are much smaller than for Reflex1 because shots 201 - 221 are located within a thick sedimentary cover west of the Franconian Line. Representing average velocities for the whole ray path, the migration velocities differ even for the same CMP for the different field setups. Such differences are also a consequence of azimuthal velocity anisotropy.

Migration velocity errors are estimated to be in the order of about +/- 0.5 %. In Fig. 3a shots 201-221 were migrated with 99.5 % of the calculated migration velocity, in Fig. 3b with 100.5 %. In spite of the minute velocity differences, the migration results differ significantly and position errors of about +/- 500 m occur.

### **Results**

The I360 section of Fig. 4 crosses the KTB-location from SW to NE. The upper part of the section to about 5 km depth must be interpreted very carefully, because effects of the direct waves are superimposed, which were not muted prior to migration. Nevertheless, a group of NE dipping reflectors in the upper part of the section is very dominant and may be identified with the SE-reflectors of steep-angle seismics (Stiller, this volume).



**Fig. 3:** Migrated section C360 of shots 201-221 with a) 99.5% and b) 100.5% of migration velocity function given in Fig. 2.

I380 (Fig. 6) from shots 201-221 shows a section 1 km further to the NW of the former one. The waves of the shots, used for this migration, have travelled more or less perpendicularly to the waves of shots 101-120 used for the migrations in Fig. 4 and 5. Therefore, reflectors were illuminated differently. Especially the B-group (10 - 14 km), which may be identified with the Erben-dorf Body, is built up by strong reflections in this migration.

Fig. 7 shows section C360 derived from shots 201-221, again with very strong B-reflectors forming a wedge structure around 11 km depth and a reflector around 14 km depth in the right part of the section.

Fig. 8 shows a depth slice at  $z = 11$  km generated from the same shots as in Fig. 6 and 7. Again, very strong amplitudes of the B-reflectors - forming a smooth syncline - are visible north of the KTB location. It is the top of the so-called Erben-dorf high velocity body.

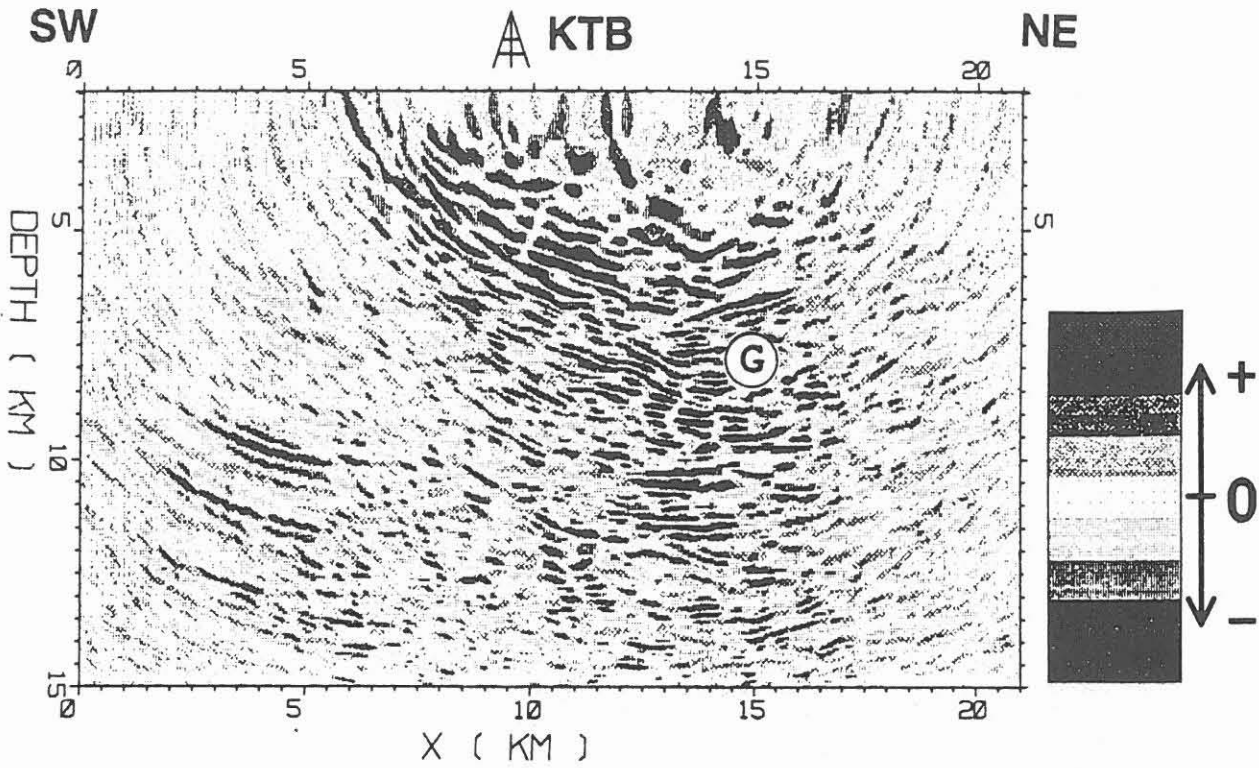


Fig. 4: Migrated section I360 of shots 101-120 (G = G-reflectors)

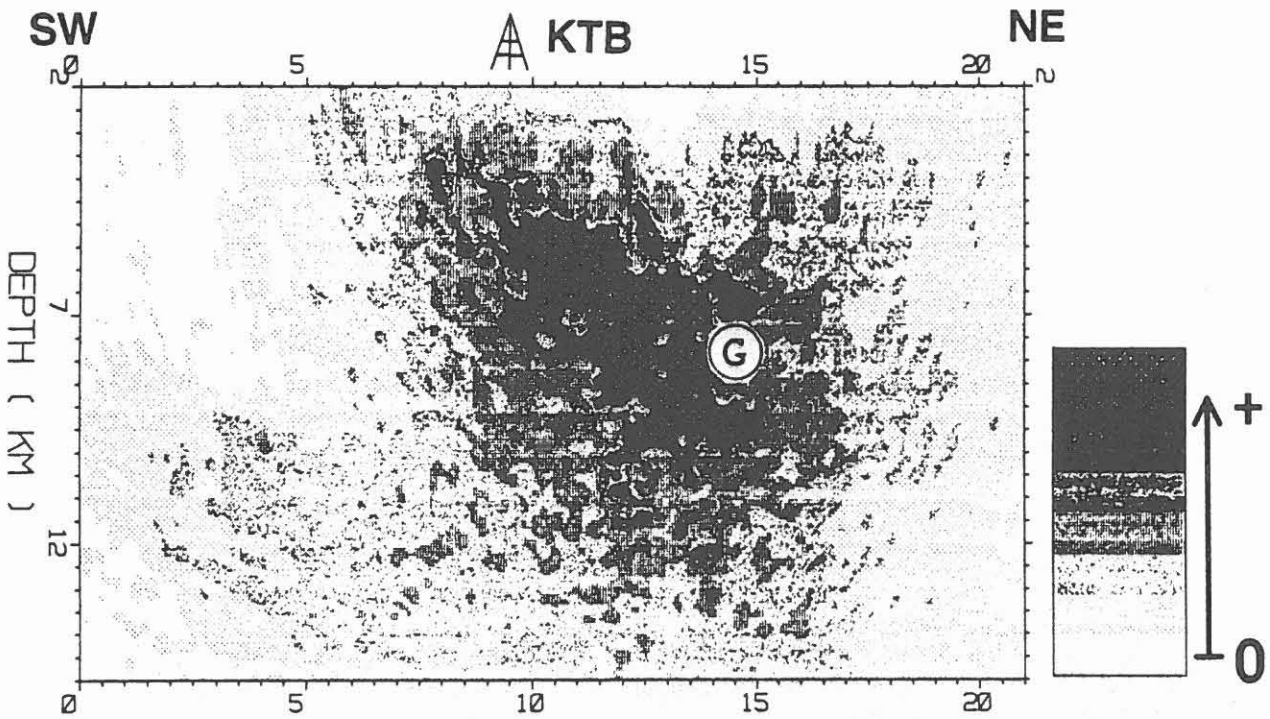


Fig. 5: Migrated section I360 of shots 101-120; envelopes of single shot migrations have been stacked (G = G-reflectors).

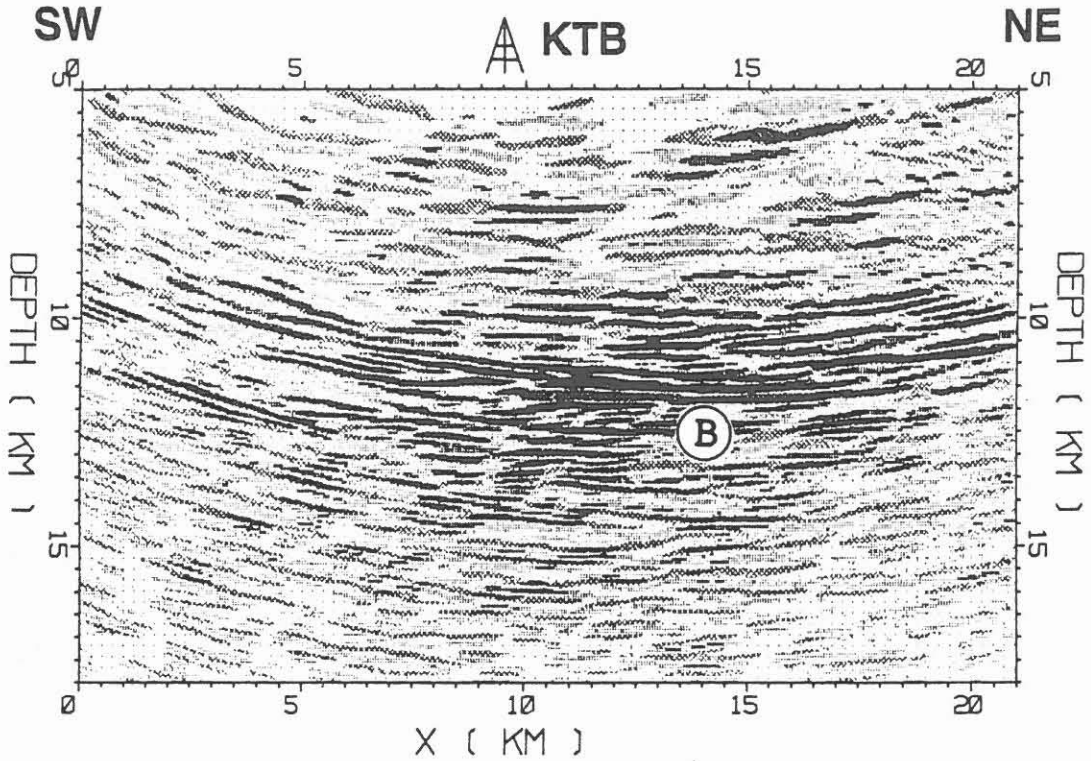


Fig. 6: Migrated section I380 of shots 201-221 ( KTB = projection of KTB-location into this section, B = B-reflectors).

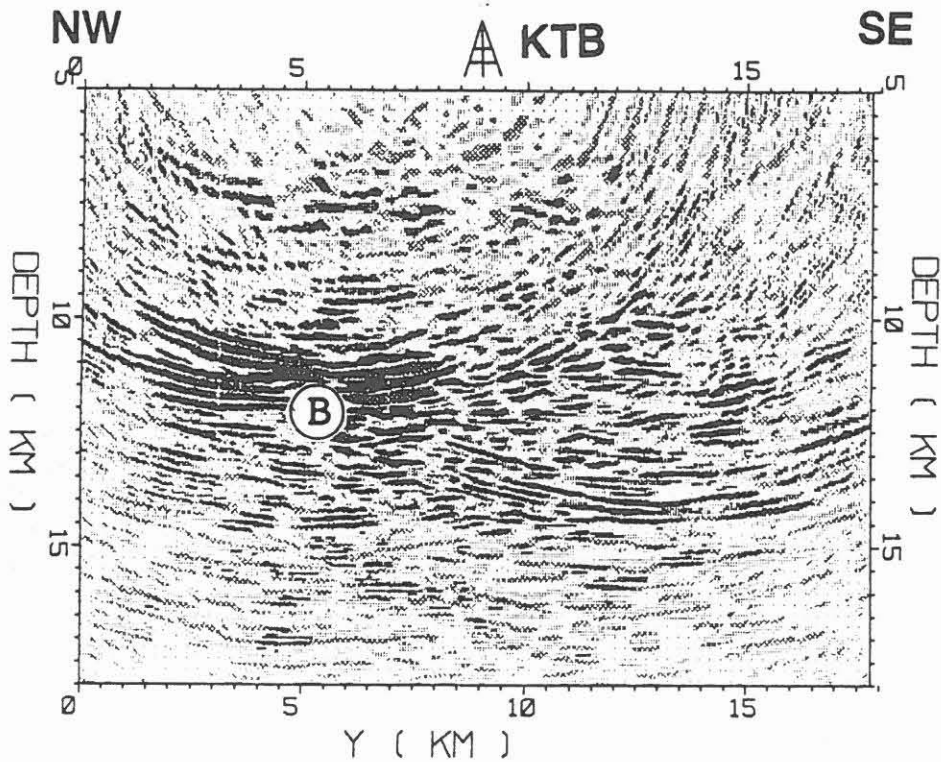


Fig. 7: Migrated section C360 of shots 201-221 (B = B-reflectors).

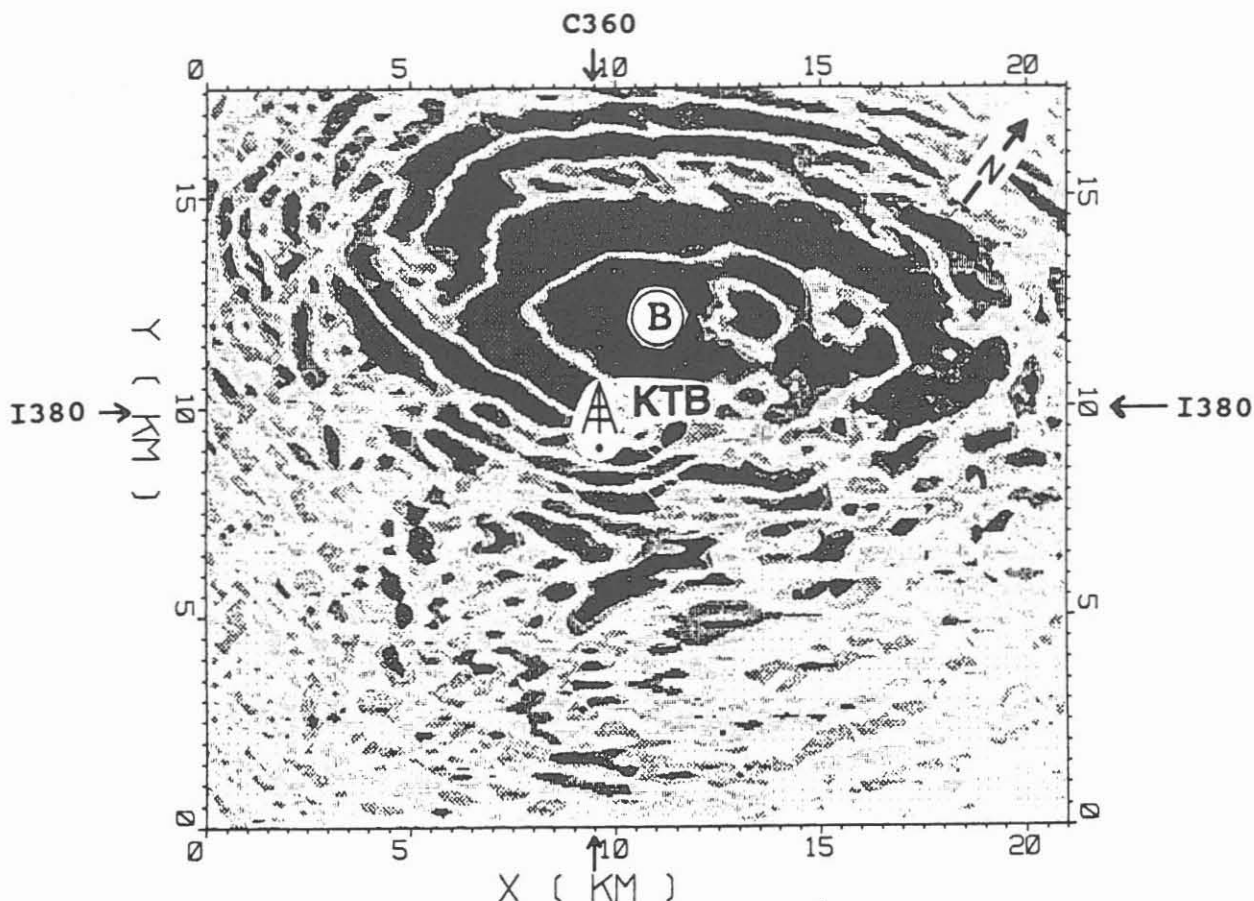


Fig. 8: Depth slice at  $z = 11$  km of migrated shots 201-221 (B = B-reflectors).

### Conclusions

In principle, a perfect agreement of steep- and wide-angle images is not to be expected since the illumination of reflectors depends on azimuth and incidence angles of wave propagation and the reflection coefficients are angle-dependent. Nevertheless, typical reflector groups of IS089 steep-angle reflection seismics are also visible in migrated wide-angle sections.

Wide-angle migrations depend very sensitively on migration velocities and further efforts have to be made to refine the velocity model. This requires, necessarily, an iterative procedure in which the comparison of wide-angle and steep-angle migration results will be of crucial importance.

### References

- Gebrande, H., M. Bopp, M. Meichelböck and P. Neurieder, 1991, 3-D Wide-angle Investigations in the KTB Surroundings as Part of the "Integrated Seismics Oberpfalz 1989 (IS089)", First results, in Continental Lithosphere: Deep Seismic Reflections, Meissner, R., Brown, L., Dürbaum, H-J., Franke, W., Fuchs, K., Seifert, F. (Eds.), Geodyn. Ser. 22, AGU, Washington, D.C., 147-160.

- Schmidt, T., 1991, Seismisches Abbilden durch 2D-Isochronen-Migration von Weitwinkeldaten am Beispiel des DEKORP4-Profiles, Diss. Ludwig-Maximilians-Universität München, pp. 125.
- Simon, M., 1992, Entwicklung eines 3D-Migrationsverfahrens mit Anwendungen auf das KTB-Umfeld, Diss. Ludwig-Maximilians-Universität München, in preparation, pp 150.
- Stiller, M., Preliminary Generation of a Stacked Data Volume of the Entire ISO89 3D-Reflection Dataset Using an Envelope Technique, KTB Report 92-5, DEKORP Report, Nieders. Landesamt für Bodenforschung, Hannover.

# VSP - A Link between Reflection Seismic Profiling and Lithology

W. Söllner\*, E. Lüschen\*, X.-P. Li\*, P. Hubral\*,  
T.W. Gut\*, M. Widmaier\*

## Abstract

VSP investigations offer a link between the reflectors observed in surface seismic profiles (2D, 3D) and the highly detailed informations from borehole measurements. There is a high number of correlations with impedance contrasts seen in the sonic log and the lithological description (metabasites, paragneisses), but most of the VSP reflection elements appears to be caused by structural features (fractures, faults). Strongly dipping features (up to 90 degrees) are dominant in the VSP. Horizontal elements correlate well with surface reflection sections. With appropriate VSP processing even very steeply dipping structures were imaged which could not be seen in other experiments. Shear wave splitting is restricted to the upper 3 km and is caused by seismic anisotropy of the order of 10 % due to rock foliation.

## Introduction

Vertical seismic profiling (VSP) provides the closest interpretational link between reflection events observed in 2D/3D surface seismic profiling and lithology. This is well known from many applications in sedimentary basins (Gal'perin, 1974; Balch and Lee, 1984; Hardage, 1985). One of the main objectives of VSP measurements at the KTB is to explain the nature of reflections in a crystalline medium.

In the framework of ISO 89 (Integrated Seismics Oberpfalz 1989) an extensive programme of VSP-measurements using different offsets, source types and azimuths was performed. For technical details and first results see Lüschen et al. (1990, 1991). Interpretations of the first near-offset VSP (VSP 3600, explosive source) measured in 1988 were published by Kästner et al. (1989), Hohrath et al. (1992) and by Rühl and Hanitzsch (1992). Recently, this VSP has been extended to 6000 m depth using a vibrator source (8-123 Hz, 20 s length, 6 s listening time) and 12.5 m geophone spacing with three components.

---

\* Authors' address: Geophysikalisches Institut, Universität Karlsruhe, Hertzstr. 16, W-7500 Karlsruhe 21, F.R. Germany

In this study we used P-wave data of the combined VSPs particularly for velocity estimation and structural imaging and S-wave data including the horizontal components to analyze the seismic anisotropy. For the imaging we used two different approaches: firstly, structural imaging near the borehole by applying standard imaging and processing routines based on constrained model assumptions, and secondly, we studied a larger volume of the crystalline basement by a special imaging technique. In this paper we give a short description of the applied methods and an outline of the main results.

Data has been acquired by SCHLUMBERGER in March-April 1992 and by contract with the KTB-Project Management which made the field data (correlated and uncorrelated, stacked and unstacked) available to us.

## 1 Velocity evaluation

The preprocessing of the extended VSP field data (3000-6000 m) consisted of editing, selecting and vertical stacking (7-fold) of correlated field records. Fig. 1 shows the combined VSPs with its downgoing (original) wavefield.

The first P-wave arrivals (zero-phase Vibroseis signal) have been calibrated with the previously existing dynamite profiles (to 3600 m depth) and then picked using an automatic picking algorithm. Fig. 2 shows the traveltimes and the average velocity versus depth. The average velocity increases continuously to 6.15 km/s at 6 km depth. Its dependence on depth can be well approximated by the following analytical function, which also can be used for depth predictions ahead of the drillbit:

$$V = 2.5 v_0 \left( 1 - \frac{1}{bz} \right), \quad (1)$$

where

$V$  is the average velocity,

$v_0$  is the start value for average velocity ( $v_0 = 2500$  m/s),

$b$  is a parameter which describes the physical character of the medium and ( $b = 0.099$ )

$z$  is the receiver depth.

The traveltimes in Fig. 1 and 2 appear to be aligned perfectly along a straight line. Fig. 3 presents the data of the new VSP with a higher velocity resolution and demonstrates that there are well pronounced variations of the interval velocity. The first arrivals have been deconvolved (spike deconvolution), plotted with a reduced time scale ( $T_{red} = T_{obs} - z/V_{red}$ ), and shifted by a constant of +500 ms. This procedure is well known from refraction seismics and was used for a better estimation of the apparent velocity. The arrivals appear to be aligned horizontally along the timing line of 500 ms which represents an average velocity of 6000 m/s. Intervals were determined based on this plot, resulting in error bars of approx. 100 m, which are caused by the sampling interval of 2 ms. These intervals and the errors were confirmed by cross-checking with the sonic log. Average velocities for these intervals were computed and marked in the figure. Sonic log velocities



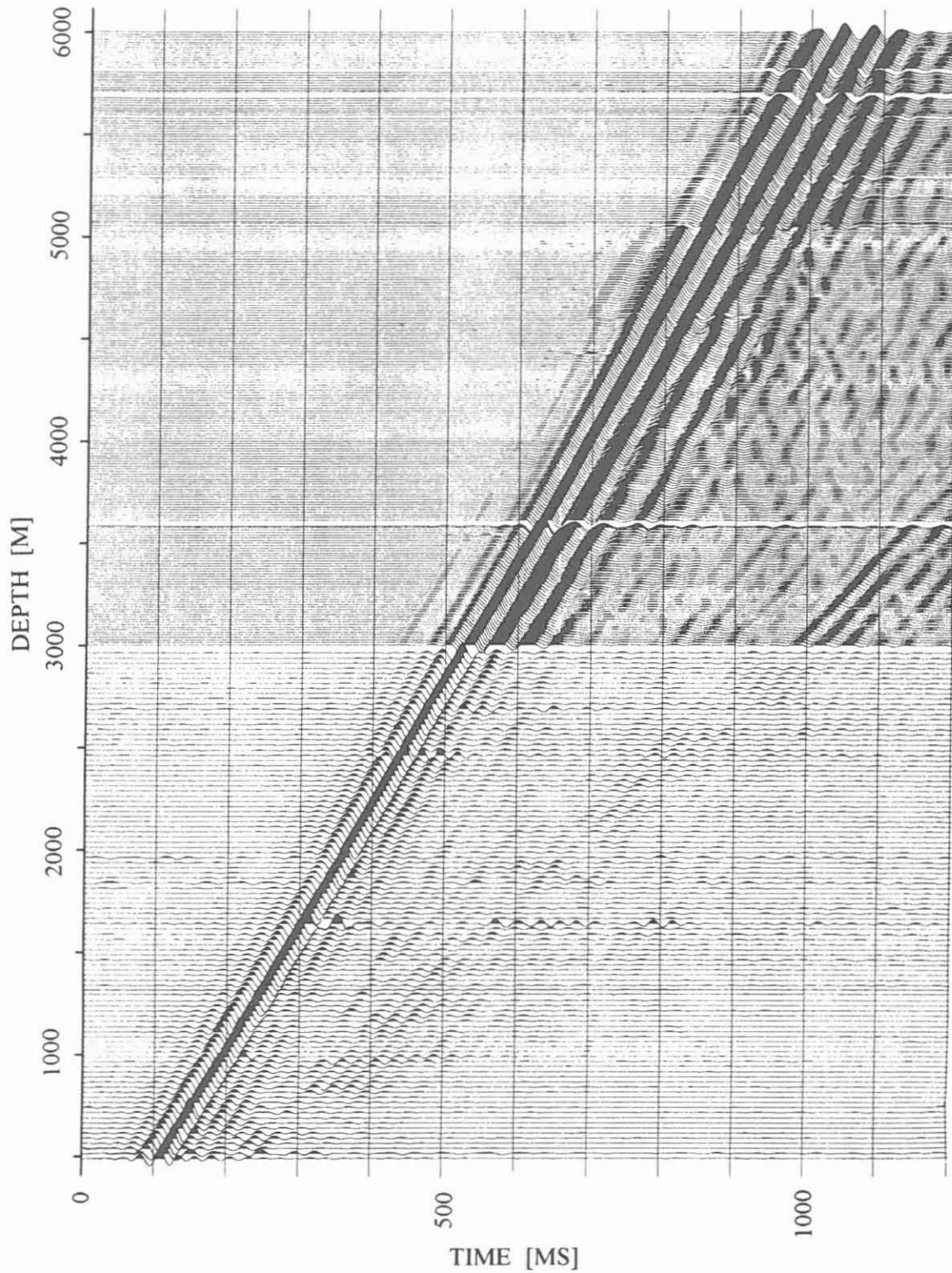


Fig. 1: Original wavefield of the Vertical Seismic Profile from 0 to 6000 m depth, composed of the VSP VP101P (Lüschen et al., 1990; Vibroseis 10-80 Hz) and the new extension from 3000 to 6000 m depth. Raw data after editing, selecting, vertical stacking and balancing of correlated field records.

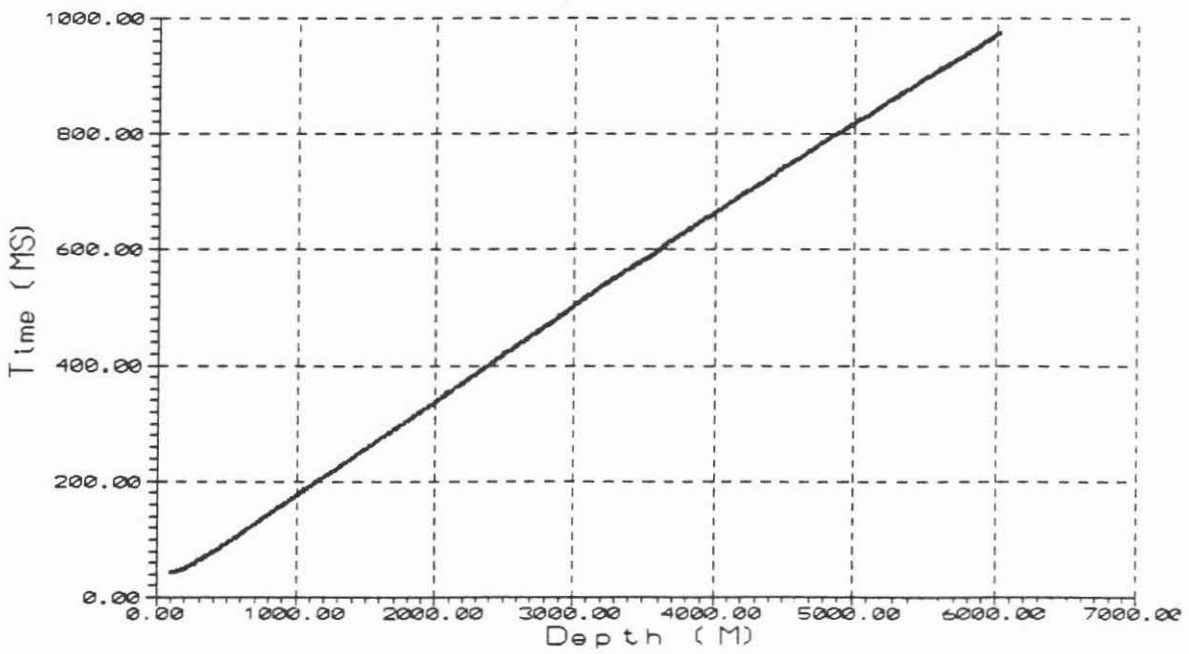
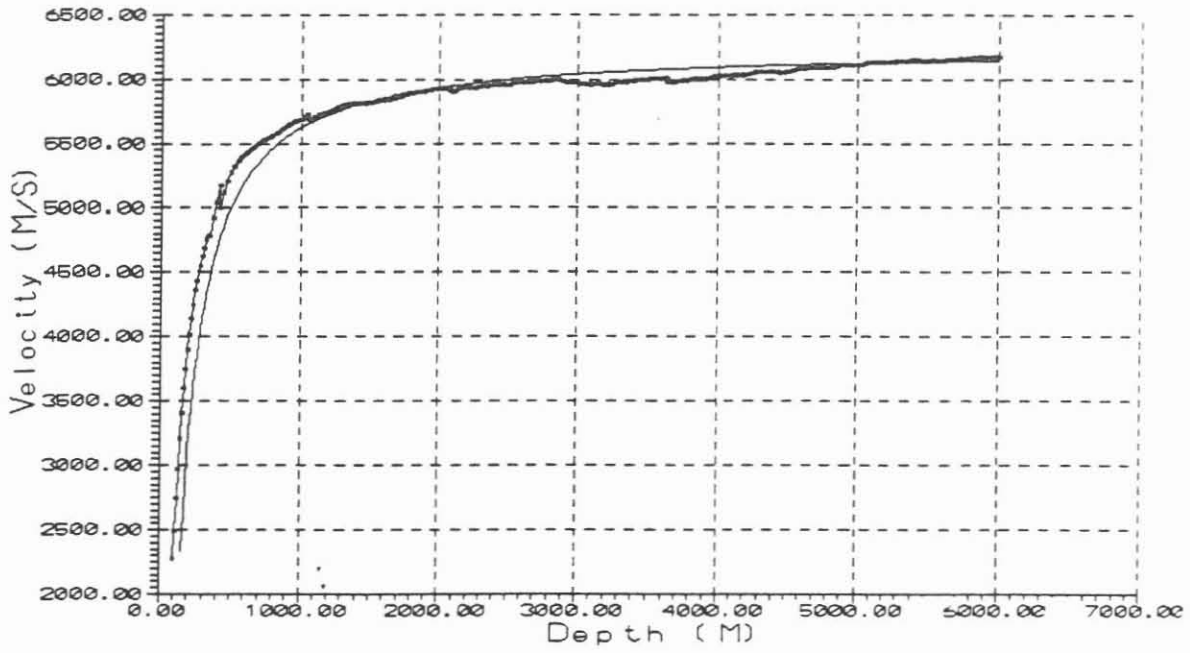


Fig. 2: Automatically picked P-wave traveltimes versus depth (bottom) and computed average velocities versus depth (top).

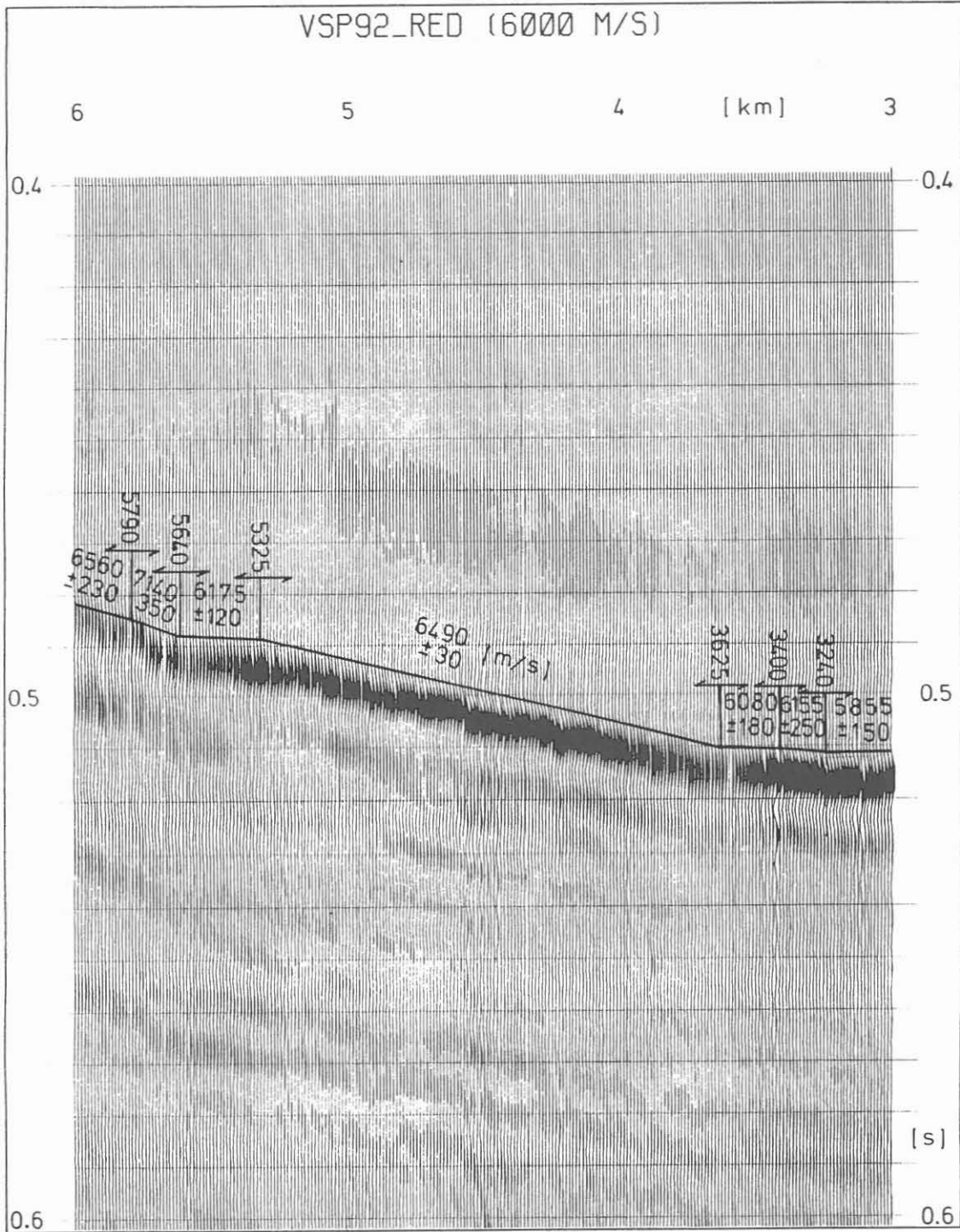


Fig. 3: Plot of the P-wave first arrivals after deconvolution. Time scale is reduced by reduction velocity of 6 km/s (see text for explanation), traces have been shifted by 500 ms. Interval velocity with their corresponding errors are plotted above.

and their intervals generally agree well with the VSP interval velocities, except for certain depth ranges where deviations can be explained by variations in foliation and seismic anisotropy. This has been noted already for the depth range from 0 to 3600 m by Hohrath et al. (1992) who presented a comparison of interval velocities and acoustic log velocities for this depth range.

The new VSP between 3000 m and 6000 m has been acquired in the KTB main hole (Hauptbohrung) which is located 200 m off the pilot hole (4000 m depth). Maximum horizontal deviation of the main hole is of the order of 10 m, therefore no corrections for deviation were necessary for the new VSP, in contrast to the former VSP (Hohrath et al., 1992).

## 2 VSP-CDP Conversion

One of the main objectives of VSP interpretation in a crystalline media is to provide the best possible link between the surface CDP reflection data and the lithology. The interpretation of VSP data as well as the interpretation of surface CDP data is strongly related to the processing parameters and the underlying model assumptions. In order to obtain a good correlation these assumptions must be accommodated.

### 2.1 Processing of VSP data

The most important assumptions in processing VSP data are that a plane wave propagates vertically in a homogeneous or horizontally layered medium and the internal multiples are negligible. If these conditions are reasonably satisfied the recorded seismic trace can be written as a superposition of downgoing and upgoing wave fields:

$$S(f, z) = D(f, z) - U(f, z) \quad (2)$$

$S(f, z)$  is the recorded seismic trace in the frequency domain at depth position  $z$ .  $D(f, z)$  and  $U(f, z)$  are the down and upgoing wave fields. The upgoing wave field can be described as a convolution of the downgoing wave with the series of reflection coefficients. In frequency domain representation, we obtain:

$$U(f, z) = -[D(f, z) \cdot R(f, z)] \quad (3)$$

where  $R(f, z)$  is the spectrum of the reflection coefficient series at receiver depth  $z$ . These relations above determine the theoretical background for the most important processing steps (wave field separation, wavelet deconvolution, geometrical divergence correction, etc.).

We do know that these assumptions are strongly violated in crystalline media. This implies to act very cautiously and to make many tests before performing each processing step. Fig. 4 shows a flowchart with the main processing steps we applied in processing the VSP data. A detailed description of preprocessing including demultiplexing, trace editing, vertical stacking, correlation of vibroseis data, component rotation, etc., is given in Lüschen et al. (1990).

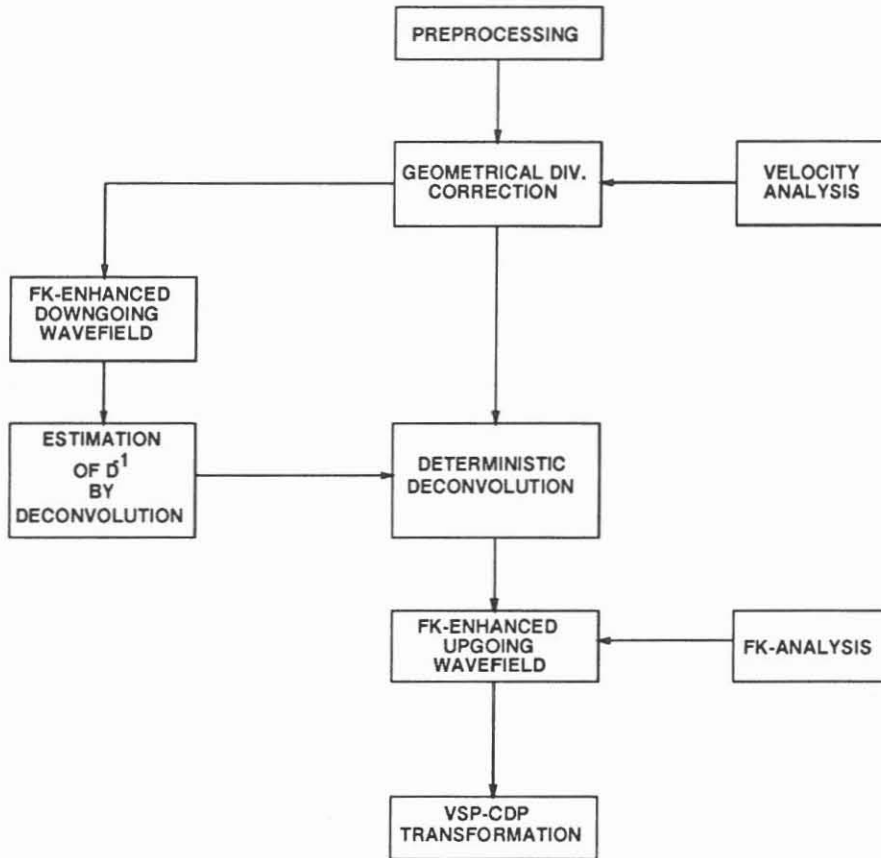


Fig. 4: Flowchart of standard VSP processing.

### 2.1.1 Geometrical Divergence Correction

In order to compensate the amplitude decay in a VSP record due to geometrical divergence we proceed as described by O'Brien and Lucas (1971), and multiply each trace by

$$\frac{t(z)V(z)_{RMS}^2}{v_1}, \quad (4)$$

the divergence factor for the downgoing wave field. It is a function of the one way travelttime  $t(z)$  and the RMS-velocity  $V(z)_{RMS}$  and is equivalent to the 'Newman-factor' for the case of normal incidence up to a constant factor.  $v_1$  is the velocity of the first layer. For application of a geometrical divergence correction a RMS-velocity estimation is needed. Interval velocities can be directly computed from the first arrivals of the downgoing wave field (see section 1), and RMS-velocities are obtained with help of the Dix formula.

To apply the geometrical divergence correction we used an analytical function, which fits the RMS-velocities. After the geometrical divergence correction (Fig. 5) we observe a coherent downgoing P-wave over the whole depth range with small amplitude fluctuations. The amplitude fluctuations can be explained by superposition of direct and reflected waves.

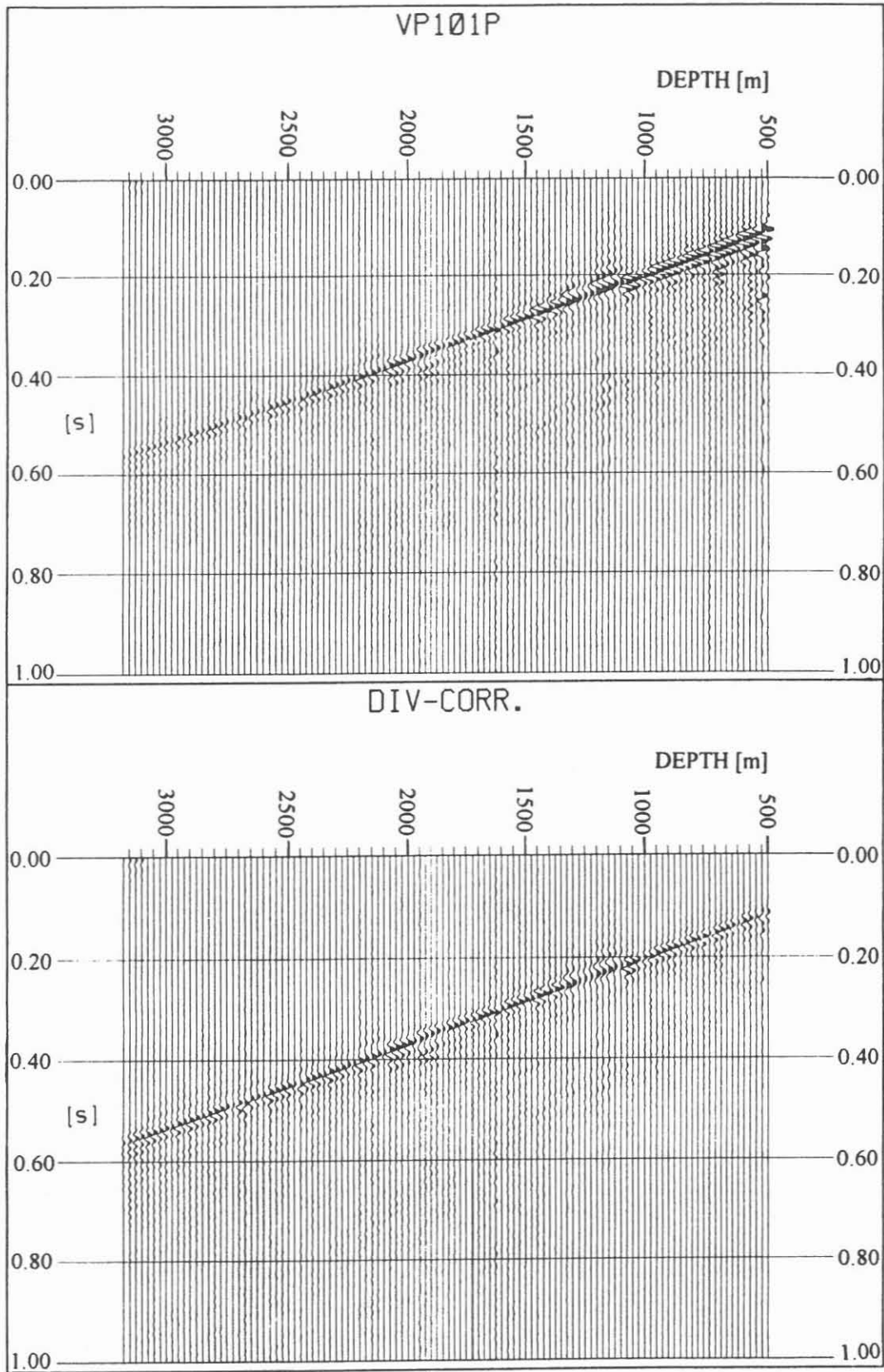


Fig. 5: Vertical component of VSP VP101P without (top) and with geometrical divergence correction applied (bottom).

### 2.1.2 Deconvolution

Usually we apply a deterministic deconvolution in processing VSP data (Gaiser et al.,1982). This means that for each recorded direct arrival the inverse transfer function is estimated and multiplied with the corresponding seismic trace in the frequency domain. The needed time signal to determine the antifilter  $D^{-1}(f, z)$  for each receiver depth is extracted by f-k-filtering from the downgoing wave field of the entire dataset. From equation (3) we obtain the reflection coefficient series  $R(f, z)$  after applying  $D^{-1}(f, z)$ :

$$U_d(f, z) = D^{-1}(f, z) \cdot D(f, z) \cdot R(f, z) \quad . \quad (5)$$

An important aspect of this processing scheme is that an accurate estimation of  $D(f, z)$  can be obtained. A critical recording parameter may be the depth sampling rate. The 25 m depth interval for zero distance VSP SP101 with dynamite source was too large, and we had some problems because the direct S-wave was aliased. Fig. 6 shows an example of typical VSP wavelet deconvolution. In contrast to unfiltered data a sharp coherent first arrival from the top to the borehole bottom can be observed. A reduced direct S-wave crosses the much weaker reflection events near the borehole. In the deeper part of the borehole a strong, very steep reflection event is marked.

### 2.1.3 Wave Field Separation

For better identification of reflection events a separation of the downgoing direct wave field and the upgoing reflected wave field is performed. This separation is usually done by f-k-filtering. Fig. 7 shows the f-k-analysis before and after rejection the downgoing wave field. In Fig. 7a (f-k-analysis of near offset VSP SP101 with dynamite source) dominating frequencies are relatively high (80–120 Hz). The dominating frequencies of VSP6000 (vibrois source) are between 20 Hz and 50 Hz (Fig. 7b). In both f-k-plots a strong higher harmonic can be recognized. After rejection the direct wave, a large number of reflection events can be seen (Fig. 8). The reflected wave field consists of weak events with different dips. The reflection events are much more disturbed by interferences compared to the direct wave.

As a last step and only for presentation we applied a bandpass frequency filter and trace equalization or automatic gain control (AGC) with a window length of 750 ms. The parameters for frequency filtering were established after filter tests. During the testing phase for VSPs with dynamite source we made the following observations:

- the identification of reflection events is better in the very high frequency range (100–150 Hz),
- several reflection events (e.g. reflections of different dip) show their best correlation in different frequency ranges (Fig. 9).

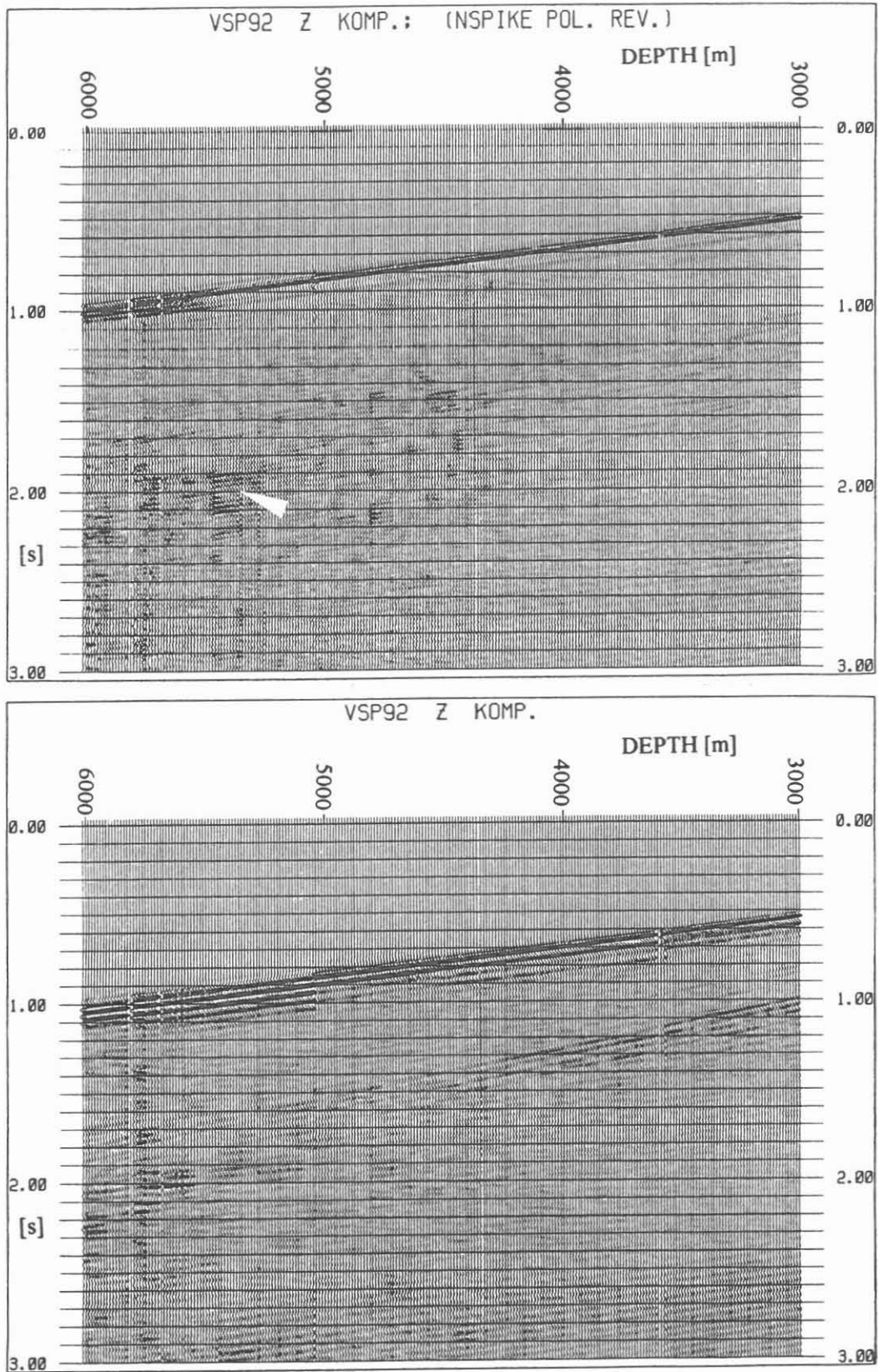


Fig. 6: VSP6000 (bottom) and the same section with deconvolution applied (top). A steep reflection element is marked.



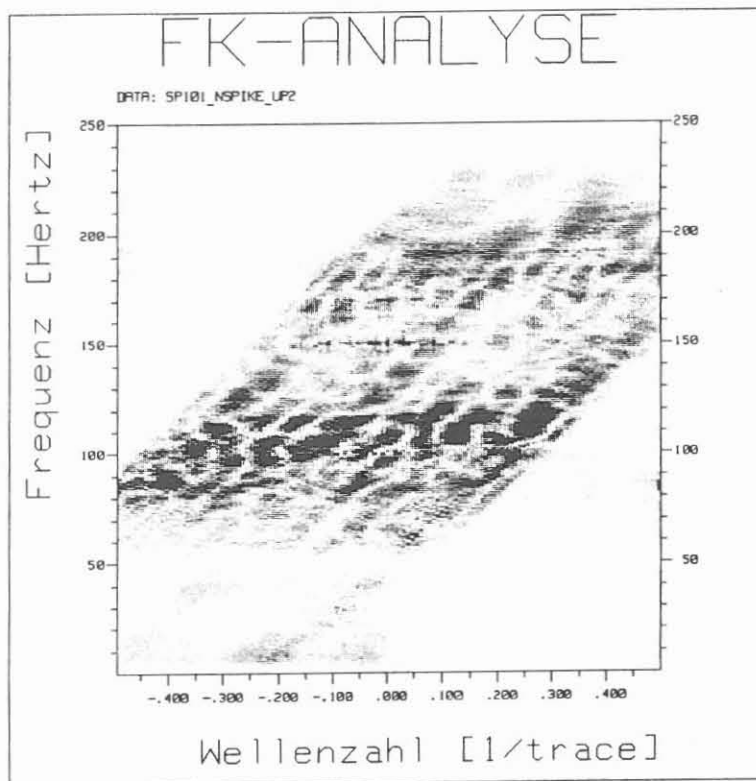
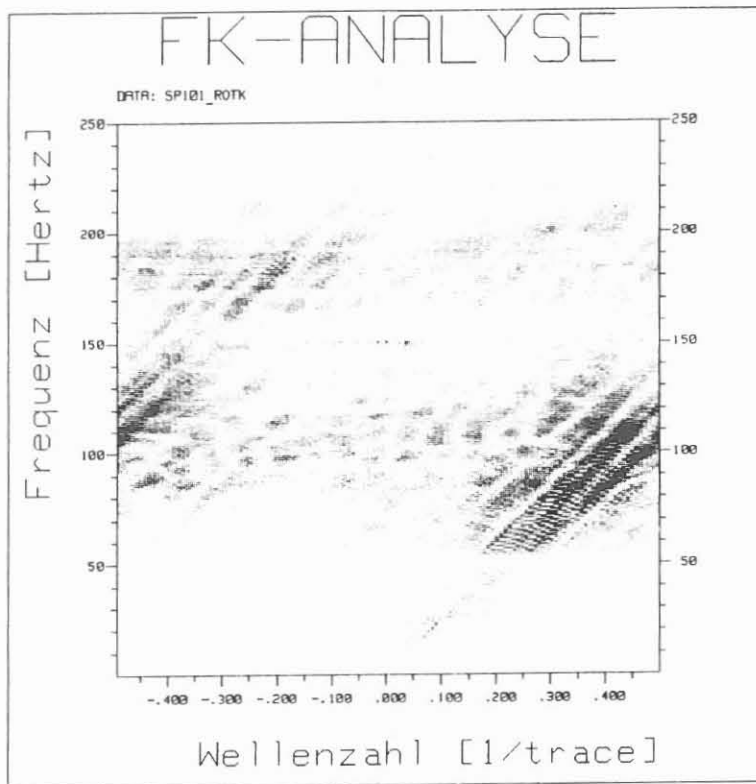


Fig. 7a: Spectrum of VSP SP101 before (top) and after rejection the downgoing wave field (bottom). Dominating frequencies: 80-120 Hz.

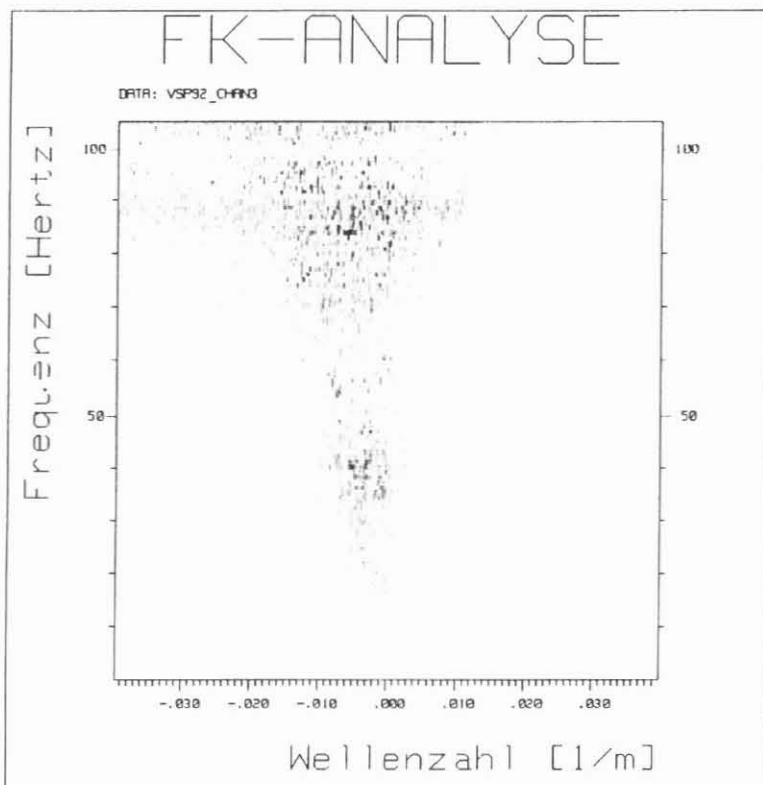
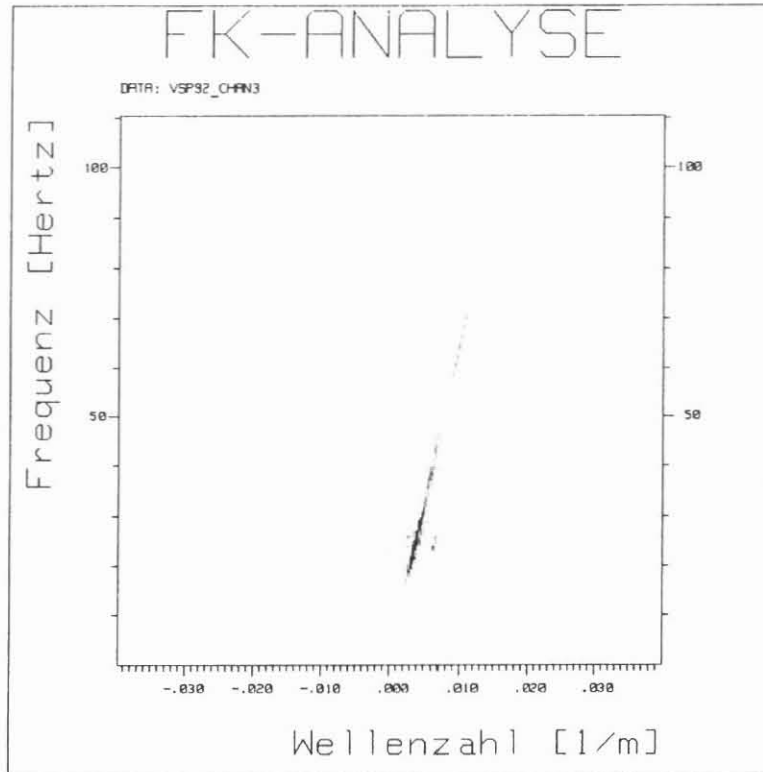


Fig. 7b: Spectrum of VSP6000 before (top) and after rejection the downgoing wave field (bottom). Dominating frequencies: 20-50 Hz.

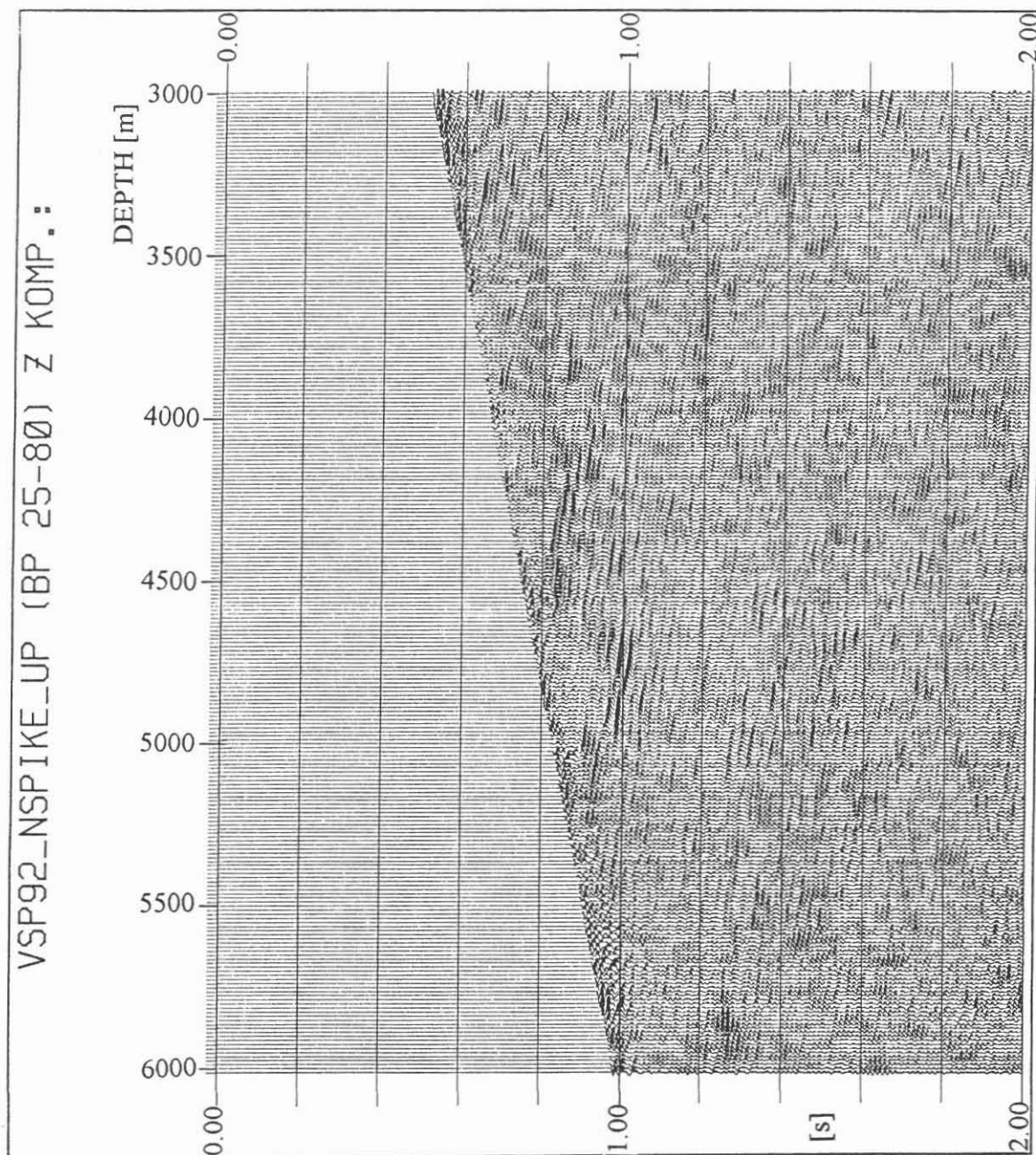


Fig. 8: Upgoing wave field of VSP6000 (f-k-filter applied as shown in Fig. 7b).

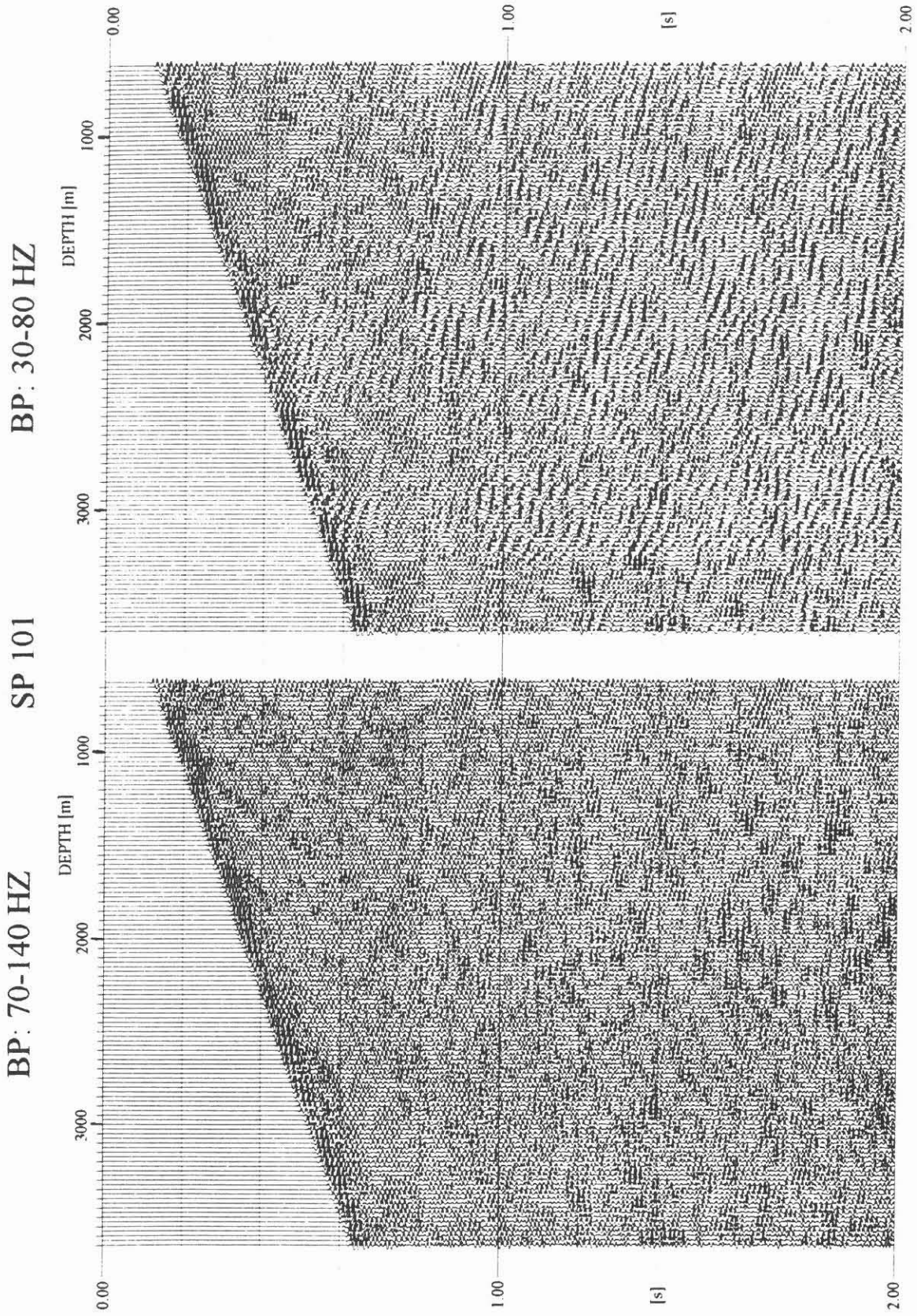


Fig. 9: Low and high frequency range of VSP SP101.

By reflection event we mean a sharp (Dirac-impulse like) reflection wave. Slow variations in velocity can disturb the event character mainly in the low frequency range. Taking these observations into account we made the interpretation of dynamite source VSPs in different frequency ranges.

## 2.2 Imaging and Interpretation

In a first step we identified the characteristic reflection events in the VSP section, correlated them with downhole measurements (log-data, lithology) and with surface seismic profiles after VSP-CDP conversion. Fig. 10 shows the upgoing wave field of the two combined zero-offset VSPs (VP101P and VSP6000), from 485 m up to 6000 m depth. The characteristic reflection events are marked by an overlaid linedrawing. Log-data and lithological column are attached to provide a comparison between reflection events and borehole information. Fig. 10 displays a remarkable matching between reflection events and lithology, but a significant portion of the reflections can not be explained by lithological changes.

The VSP-CDP conversion (VSP mapping) is a geometrical operation which allows a direct comparison of surface seismic data with a VSP section. A detailed description of VSP-CDP conversion is given in Dillon and Thomson (1984). This operation holds for a homogeneous medium above a horizontal layer boundary and any distance between source and wellhead. In the case of a zero offset VSP a simple addition of reflected traveltimes and first arrival time transforms the recorded data into a two way traveltimes corrected VSP section (Fig. 11). By stacking over the whole depth range the badly corrected events from dipping reflectors are suppressed and the result can be viewed as a normal incidence trace of nearly horizontal reflectors. In Fig. 12 the stacked converted trace from VSP6000 is displayed within the surface seismic section KTB8502 (DEKORP Research Group, 1988). We find a remarkable correlation mainly for horizontal events (e.g. "Erbendorf-body" at 3.8 s TWT).

## 3 Vertical Zero-Offset Conversion

Up to now we used the seismic reflection events from VSP data to obtain a more correct determination of the depth of a priori defined seismic events from surface data and to identify their nature by calibration with other borehole measurements. By VSP-CDP conversion we focused on nearly horizontal events and suppressed all events from steeply dipping reflectors after two way traveltimes correction and stacking.

During the processing phase we observed, that the strongest reflection events are from nearly vertical structures (e.g. the marked events in Fig. 6). This observation was made in raw data and after some processing steps (e.g. after deconvolution) in several VSP sections. The VSP configuration offers the unique possibility to image nearly vertical reflectors.

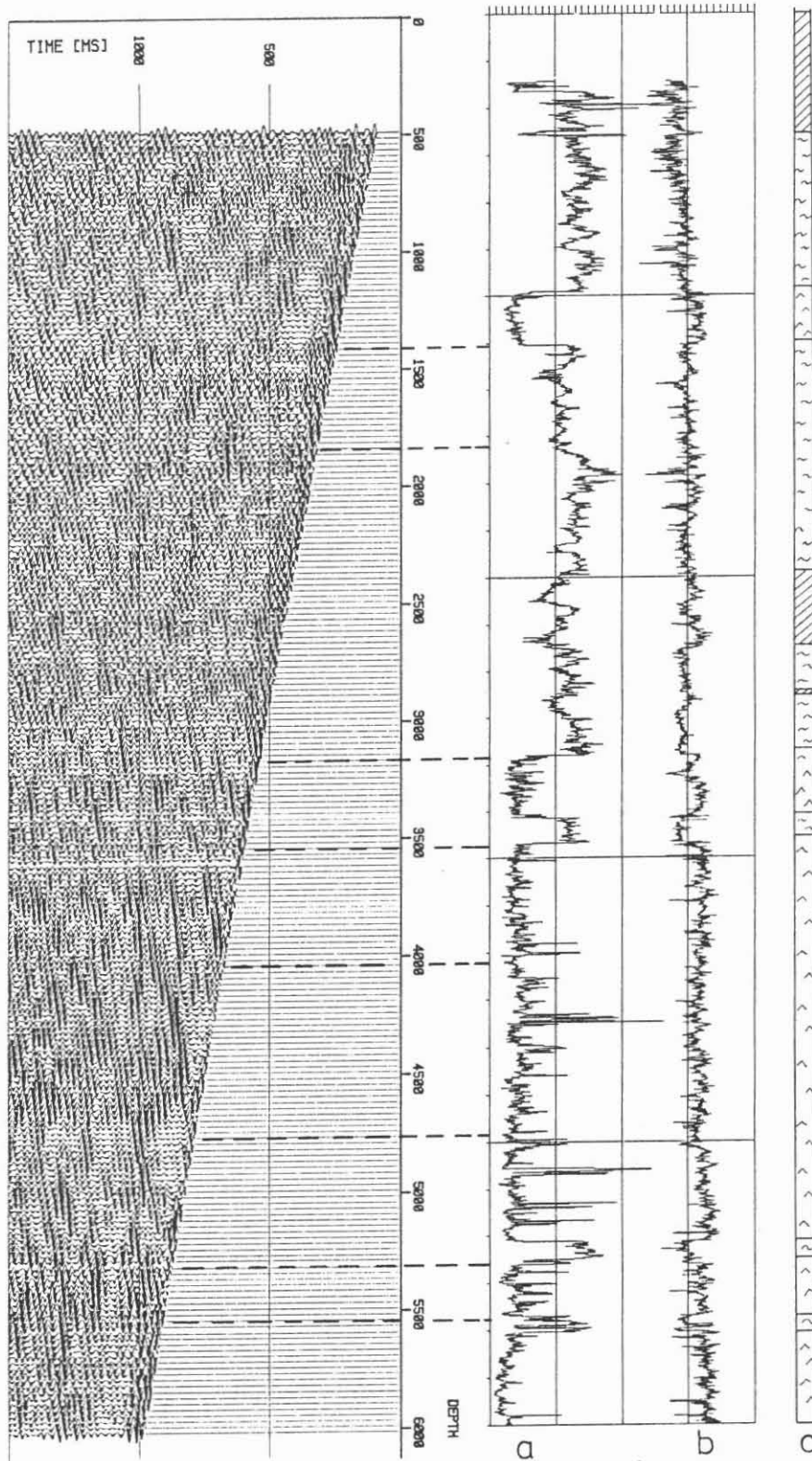


Fig. 10: Link between borehole measurements and combined VSP section. Left: Upgoing wave field of VP101P and VSP6000. Right: (a) gamma-log; (b) sonic-log P-wave; (c) simplified lithology. Log-data by KTB Referat Bohrlochmessungen.

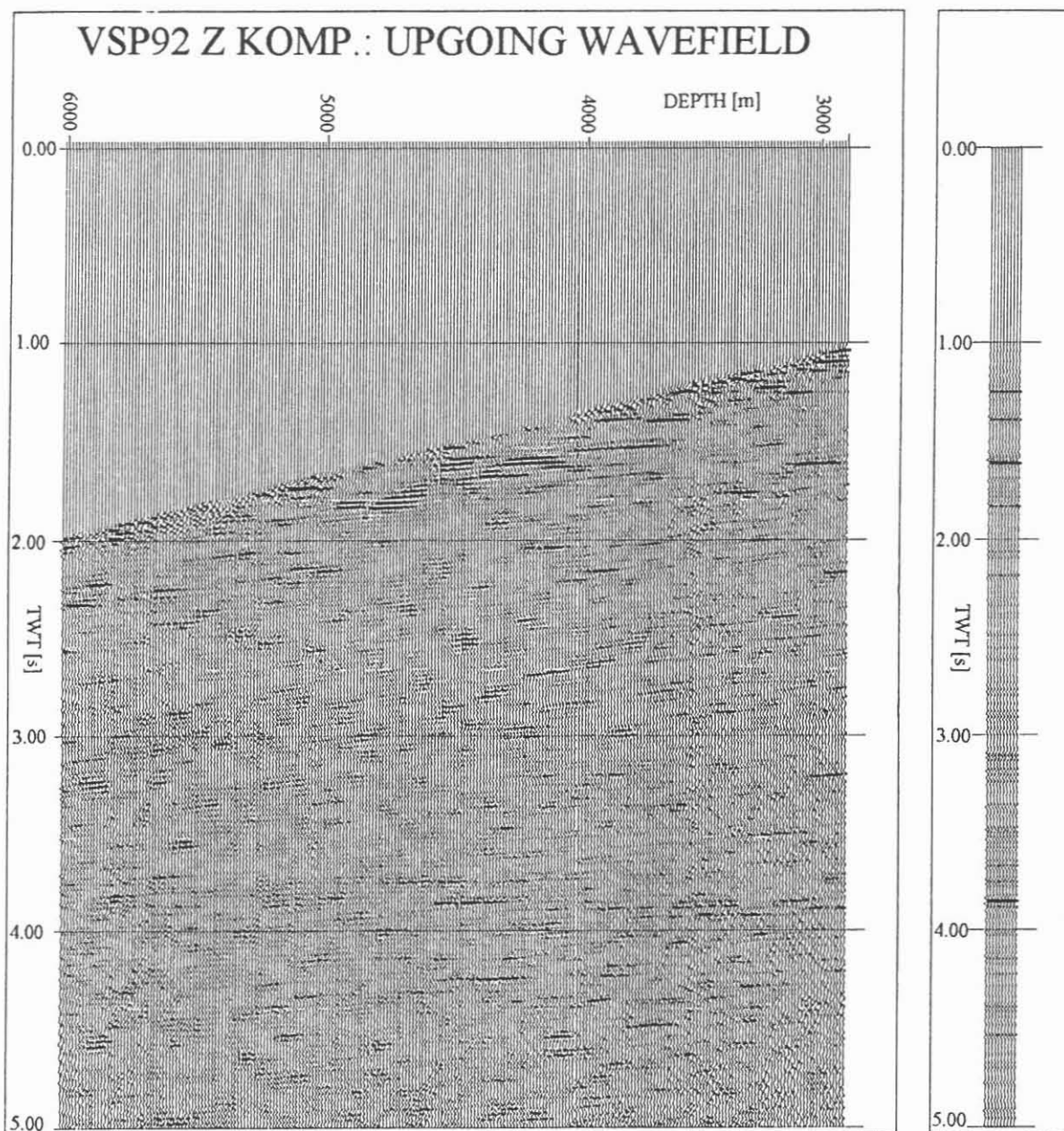
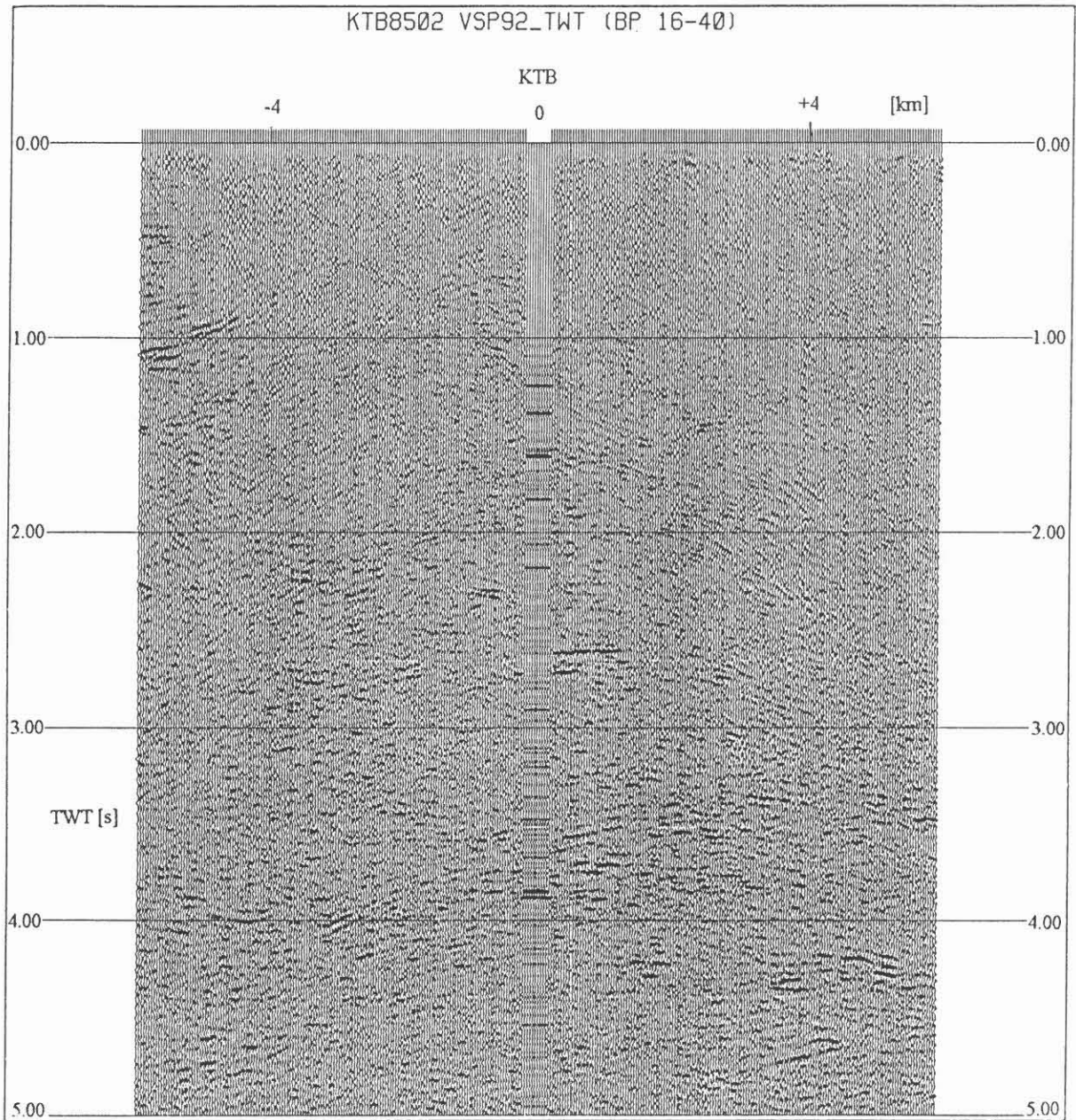


Fig. 11: Upgoing wavefield of VSP6000 after application of two way traveltime correction (left) corresponding stack of all traces (right).



*Fig. 12: Link between VSP6000 (stack of all traces) and surface seismic section KTB8502 (final stack) by DEKORP Research Group.*



### 3.1 Rotated Layered System

We introduce a medium which consists of an arbitrary number of homogeneous layers separated by vertical interfaces (vertically stratified medium), embedded in a global coordinate system, as indicated in Fig. 13. The origin of the coordinate system is the source position at the wellhead. The  $z$ -axis is the recording line and points in depth direction whereas the  $x$ -axis is perpendicular to the  $z$ -axis. This new situation is obtained after rotating a surface seismic profile (horizontally layered medium) into the global coordinate system.

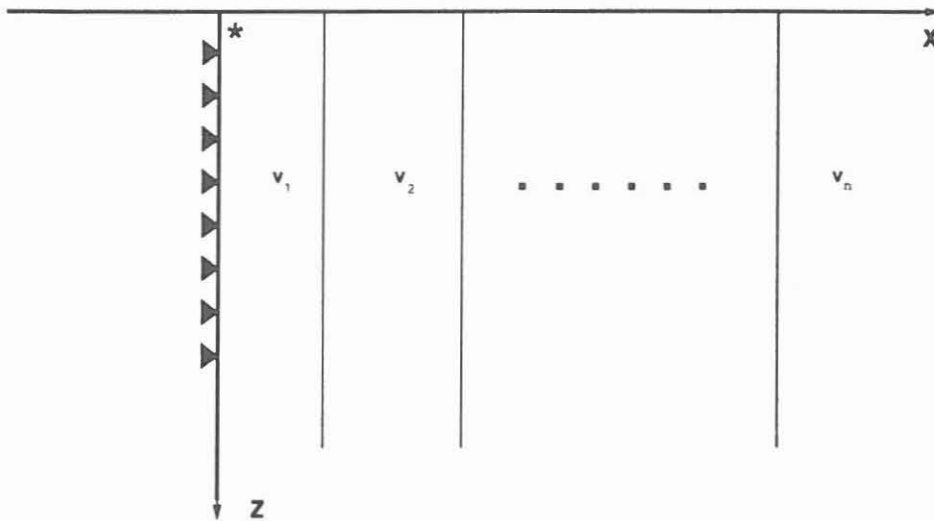


Fig. 13: Vertically stratified medium:  $z$ -axis represents the recording line in the borehole. The  $x$ -axis is perpendicular to the  $z$ -axis. The layers are separated by plane interfaces.

Using the laws of geometrical seismics (straight-line propagation in homogeneous regions, the rule for refraction and the rule for reflection) the traveltimes along the rays passing through this seismic system are given by

$$T^2 = T_0^2 + \frac{z^2}{V_{RMS}^2} \quad (6)$$

for small depth.  $T$  is the traveltime of the reflection event,  $T_0$  is the traveltime along the normal incidence ray and  $V_{RMS}$  is the RMS-velocity of the vertically stratified medium.

This rotated layered system has several drastic implications for VSP processing. The conditions for wavefield separation are not satisfied anymore. The typical VSP deconvolution has to be replaced by a statistical or source signal deconvolution (Ziolkowski, 1991). For this changed situation we used a new processing sequence (Fig. 14).

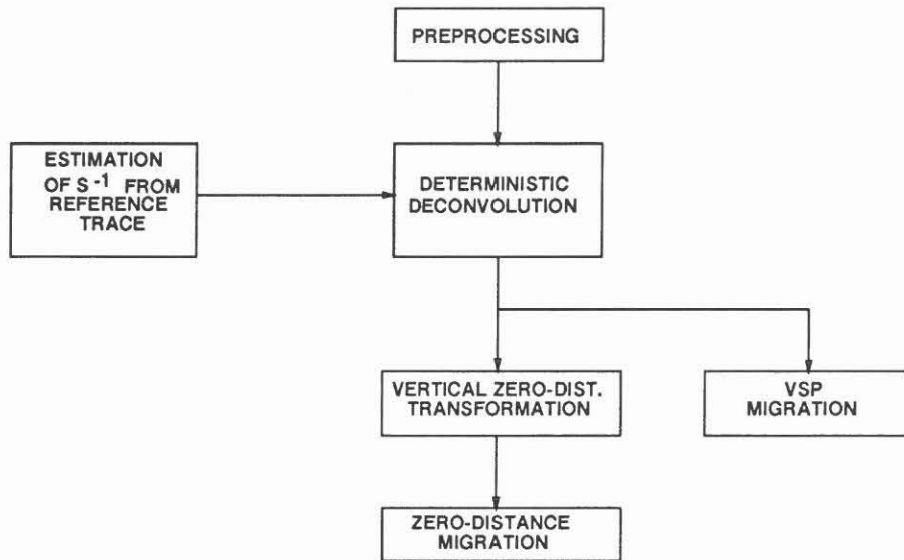


Fig. 14: Flowchart of the modified VSP processing sequence.

### 3.2 Imaging of Vertical Structures

The imaging of a rotated system consists of two steps: the dynamic (NMO) corrections and the zero distance migration. The NMO-correction is obtained by subtraction of

$$\frac{1}{2} \frac{z^2}{t_0 V_{RMS}^2} \quad (7)$$

from the traveltimes of the reflected ray at each receiver position and transforms the traveltimes to zero-offset times at the position  $z/2$ . The dynamic correction depends only on the receiver depth for a defined reflection event. It is valid in the same order of approximation as the corresponding process for surface seismic data and can be extended to a more general model (curved interfaces of different dip) as described by Hubral and Krey (1980) and Bortfeld (1989). We do not know whether a similar model extension is possible for standard VSP configuration.

Fig. 15 shows a vertical zero-distance conversion of VSP6000. This result has to be interpreted as a seismic section where the midpoint positions  $z/2$  are in the borehole. Many steeply dipping events can be recognized (nearly horizontal in our representation). The real position of these events can be determined by using the information of three component data (angle of incidence). The strong seismic event we marked in the raw data section (Fig. 6) is again identified as a nearly vertical structure with 1.7 s two way traveltime. The corresponding distance to the borehole is 5 km. At this distance, the SE border of the Bohemian crystalline massif against a mesozoic sedimentary basin is observed in geological maps ("Franconian Line"). The strength of the reflection amplitude indicates a high impedance contrast caused by such a change from a crystalline to a sedimentary medium.

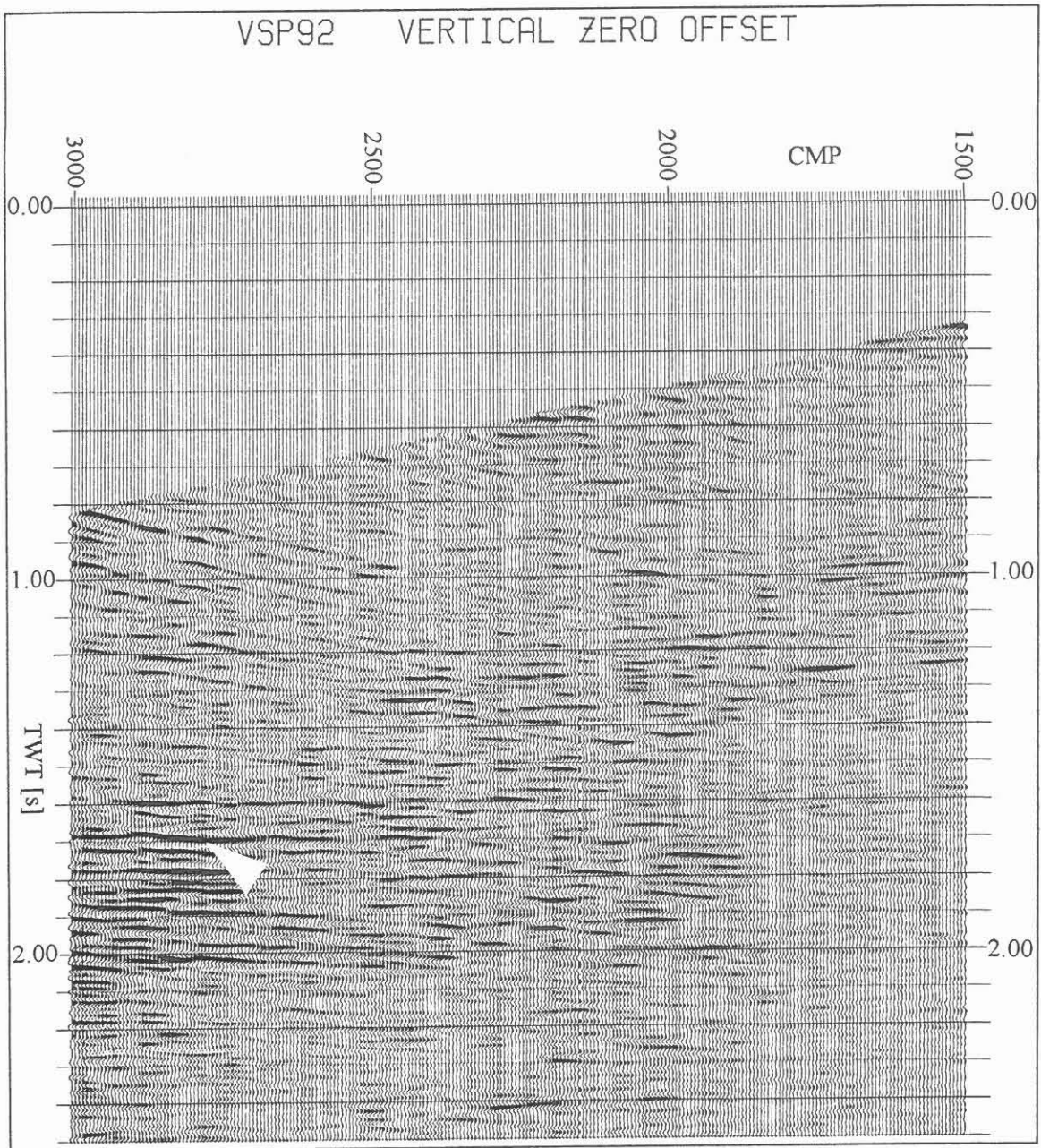


Fig. 15: Vertical zero-distance conversion of VSP6000.

## 4 VSP-Migration

The most direct use of the migration principle is the classical diffraction stack (Hagedoorn, 1954). The diffraction stack is a summation of recorded amplitudes along curves of maximum convexity (diffraction curves). The diffraction time is obtained by the traveltimes summation of the following two transmitted events:  $t(\vec{x}, \vec{s})$  from the source position  $\vec{s}$  to a fixed image point  $\vec{x}$  and  $t(\vec{r}, \vec{x})$  from any receiver position  $\vec{r}$  to the same image position  $\vec{x}$ , whereas the diffraction curve  $d_x$  can be described as a set of those data points  $u(\vec{r}, \vec{s}, t)$  in which the time corresponds to the diffraction time:

$$d_x = \{u : t_d = t(\vec{r}, \vec{x}) + t(\vec{x}, \vec{s})\}. \quad (8)$$

The summation along diffraction curves is computed for each image point and provides finally the migrated section. Fig. 16 shows the migrated section of the far offset VSP (SP401, 4 km NE from the KTB) and Fig. 17 the corresponding reflection seismic profile KTB8502. The dynamite source of SP 401 is located 4 km NE from the KTB site. In each section the corresponding reflection events are marked. Due to aperture limitation the VSP migration is not suitable for providing a structural image for a single shot position.

## 5 Shearwave Splitting in Near Offset VSPs

The most suitable and direct way to study and analyze seismic anisotropy is the near-offset shear-wave VSP experiment. Shear-wave splitting (Crampin, 1986) as a direct indicator of seismic anisotropy can be identified by traveltimes divergence (different velocities) and orthogonal polarization of two direct S-wave phases and can be related to the lithology or to structural elements. The polarization analysis was carried out with the aid of the Covariance Method introduced by Benhama et al. (1988). The covariance matrix is computed over a well defined time window, with a window length depending on the signal period. This method works accurately, if the time delay between the different S-wave phases is greater than the window length.

In the depth range of 0–3500 m the S-wave splitting has been discussed by Lüschen et al. (1990, 1991) based on VSPs acquired in the KTB pilot hole using different source techniques, among them standard dynamite and vertical vibrator sources, a horizontal vibrator, a horizontal hammer source (Marthor) and a newly developed circular horizontal vibrator source (CIPHER, Edelmann, 1992; Gut et al., 1992). These different sources provided a wide range of frequencies and will be studied for frequency-dependent signal characteristics, e.g. attenuation and anisotropy.

Fig. 18 presents the main result concerning anisotropy. A continuous diverging of two S-wave phases and their orthogonal polarization were indicative for such a symmetry system that shows NW (fast) and NE (slow) preferred orientations for vertical raypaths. This system represents the average anisotropy in the upper 3 km

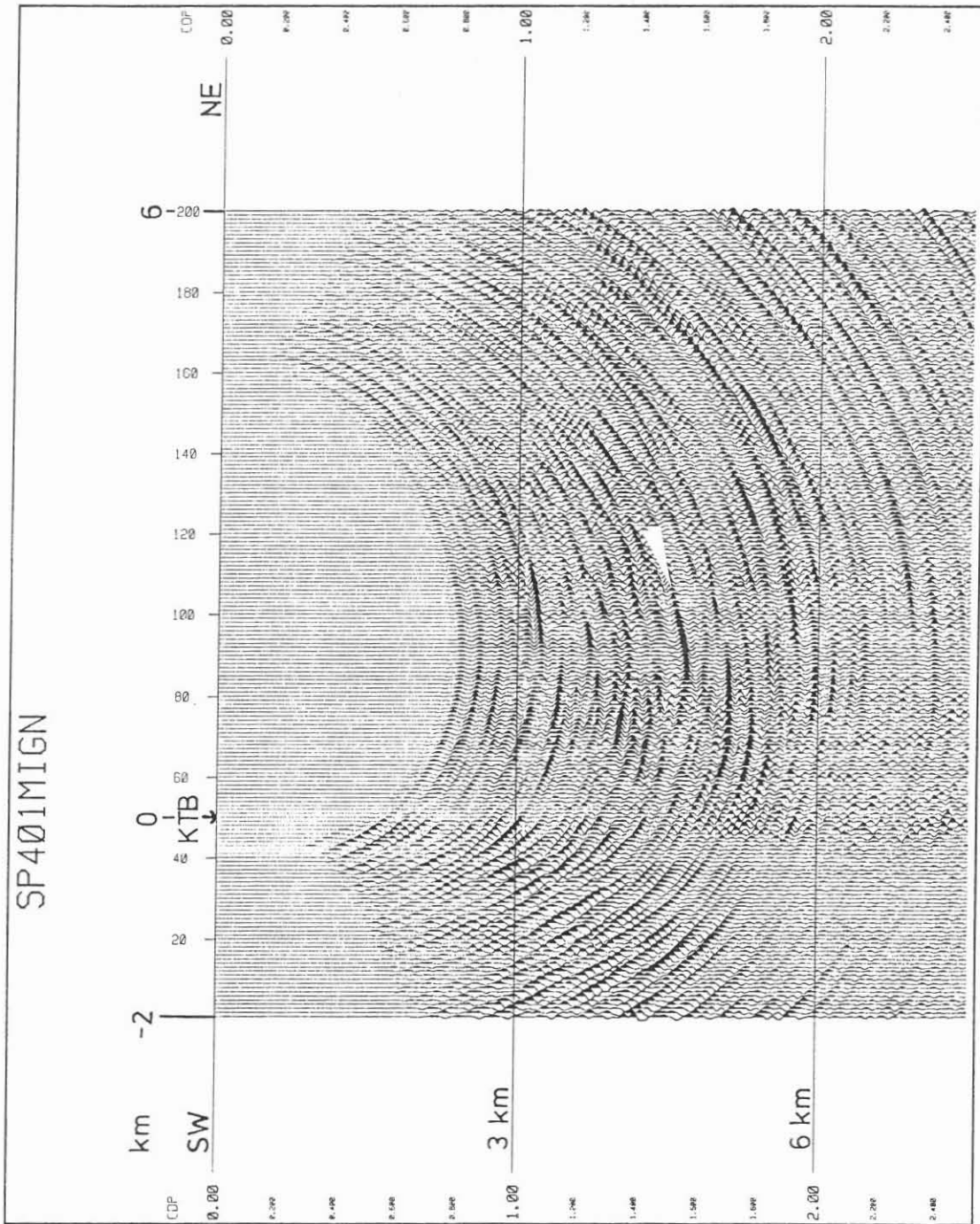


Fig. 16: Migrated section of far offset VSP SP401, corresponding to surface profile KTB8502 (Fig. 17). Marked is a dominant reflection event.

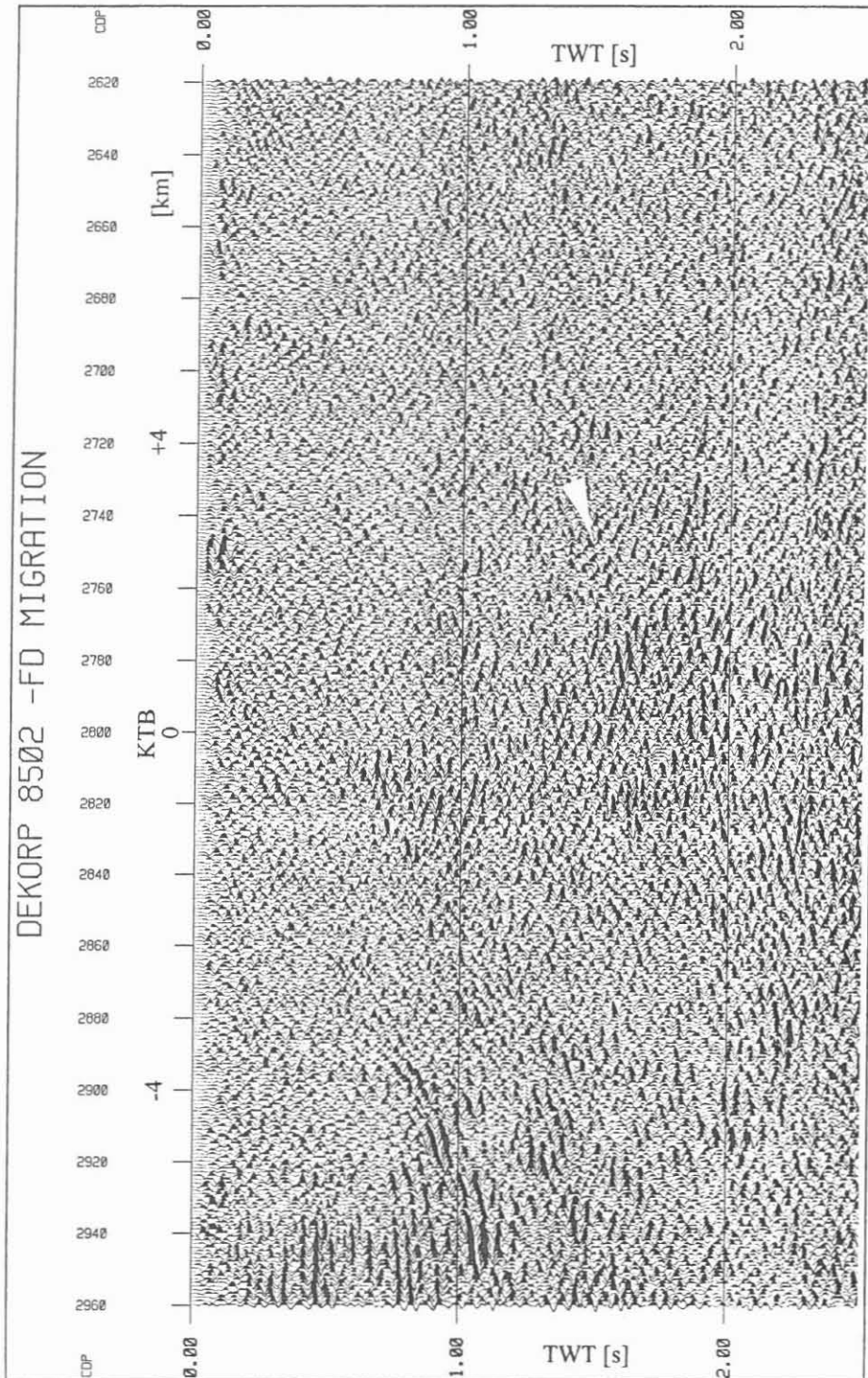


Fig. 17: Migration of surface seismic profile KTB8502 by DEKORP Research Group. Marked is the same reflector as in Fig. 16.)

about 10 %. Fig. 19 shows the preferred orientations based on a polarization analysis. The two orientations of the predominating linearly polarized S-wave phases are visible because of a sufficiently large time delay between them.

The magnitude of the anisotropy as well as the preferred orientations fit well to results obtained from systematic core sampling and corresponding laboratory experiments (Kern et al., 1991) which indicate that the seismic anisotropy is mainly caused by the rock microtexture (foliation). Lüschen and Werner (1992) determined the same preferred orientations from S-wave reflections of the "Erbendorf-Body" (11-12 km), but the particle motions of the fast and slow phases have changed their directions. This indicates that the anisotropy symmetry system (foliation and lineation) is rotated by 90 degrees somewhere between 3 and 11 km. This will be studied directly by the recently acquired VSP from 3 to 6 km. Strong shear-waves are again visible on the horizontal components, although the source was a vertical vibrator (Fig. 20).

The rotation of the symmetry system, if it occurs between 3 and 6 km, should be indicated by a crossing of the previously diverging split S-wave phases. A preliminary analysis of Fig. 20 shows that this depth range behaves rather isotropically. All S-phases propagate with the same velocity. The crossing of these phases and the postulated rotation of the symmetry system should therefore occur below 6 km depth.

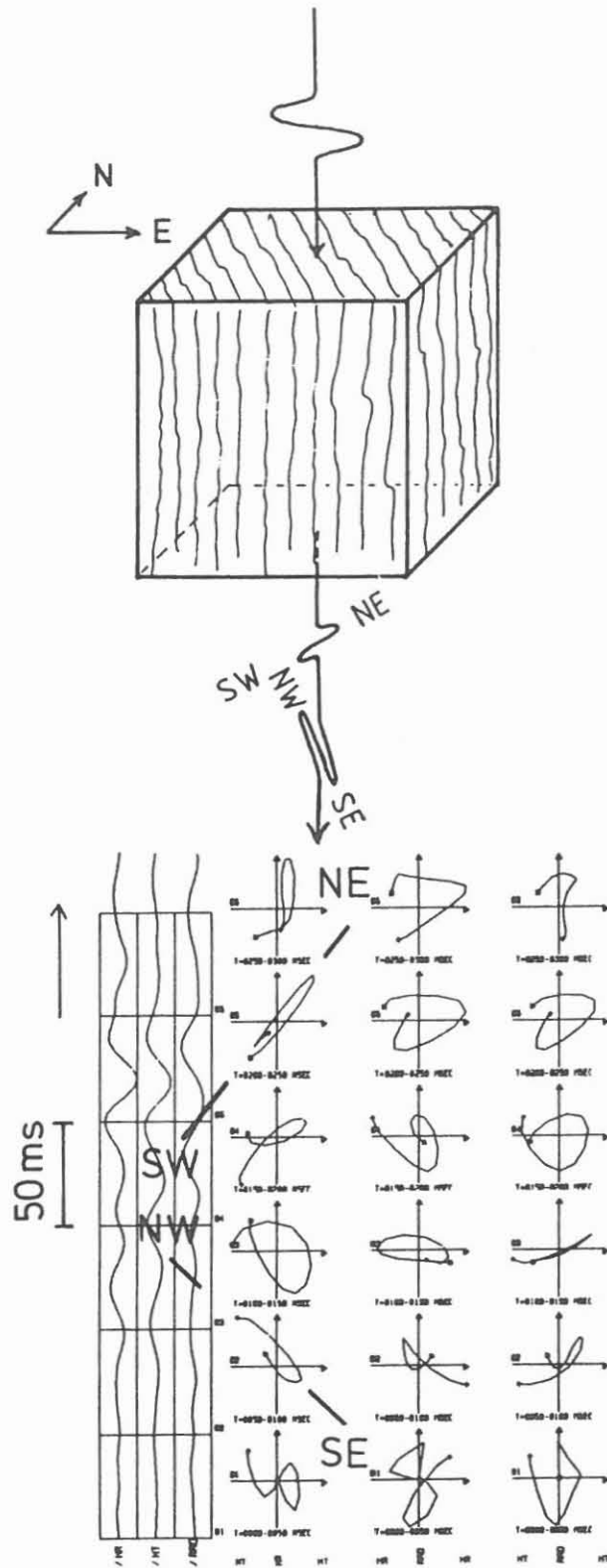
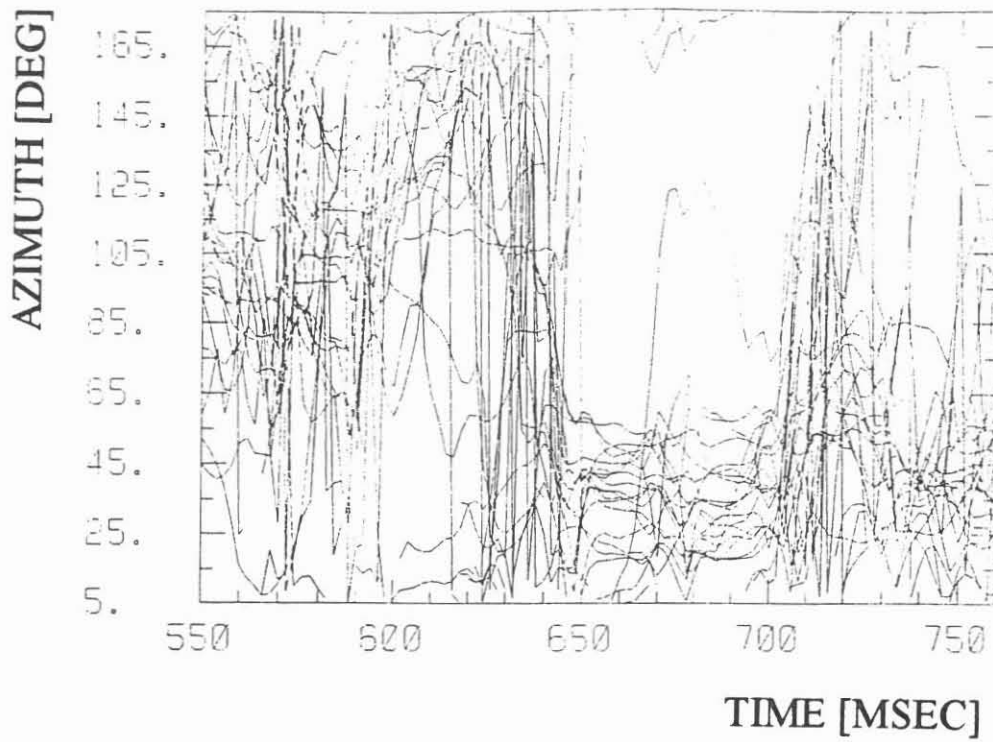


Fig. 18: Schematic diagram demonstrating the suggested effect of rock foliation on shear-wave splitting. Lower part shows an example of the effect seen in particle motion diagrams of shearwave direct arrivals of VSP VP101S at 3200 m depth. Motion is first in NW-SE, then in SW-NE direction with a delay of about 100 ms (Lüschen et al., 1991).



### AZIMUTH OF VP101 P



### AZIMUTH OF VP101 S

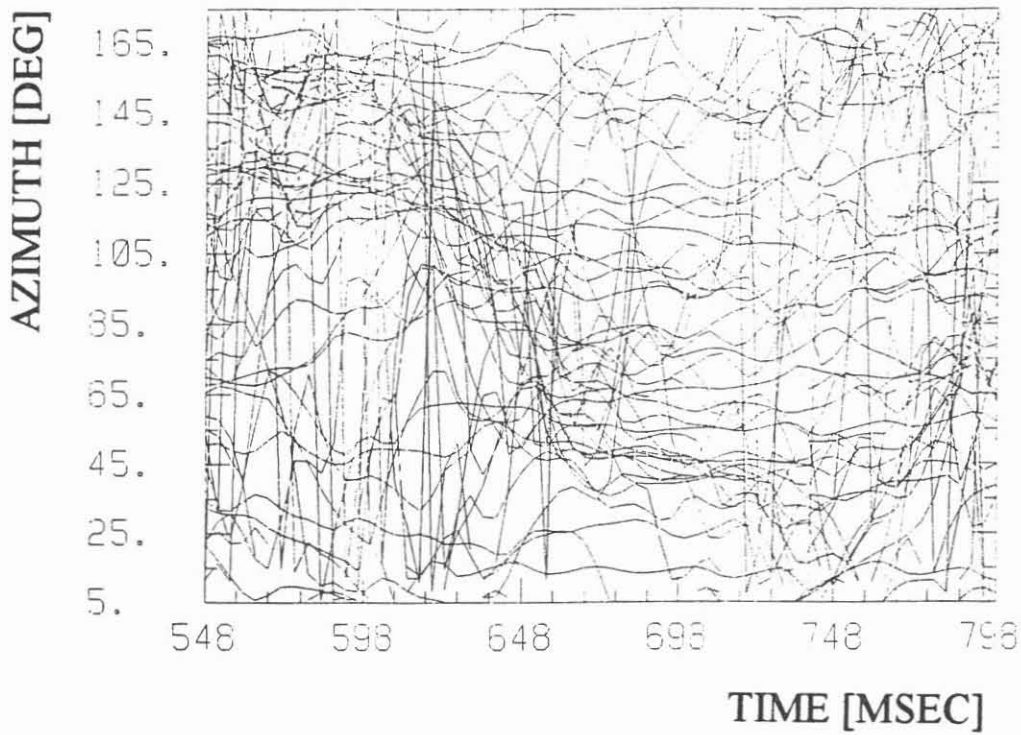


Fig. 19: Polarization direction versus time: VP101P with P-wave source and VP101S with S-wave source (Vibroseis).

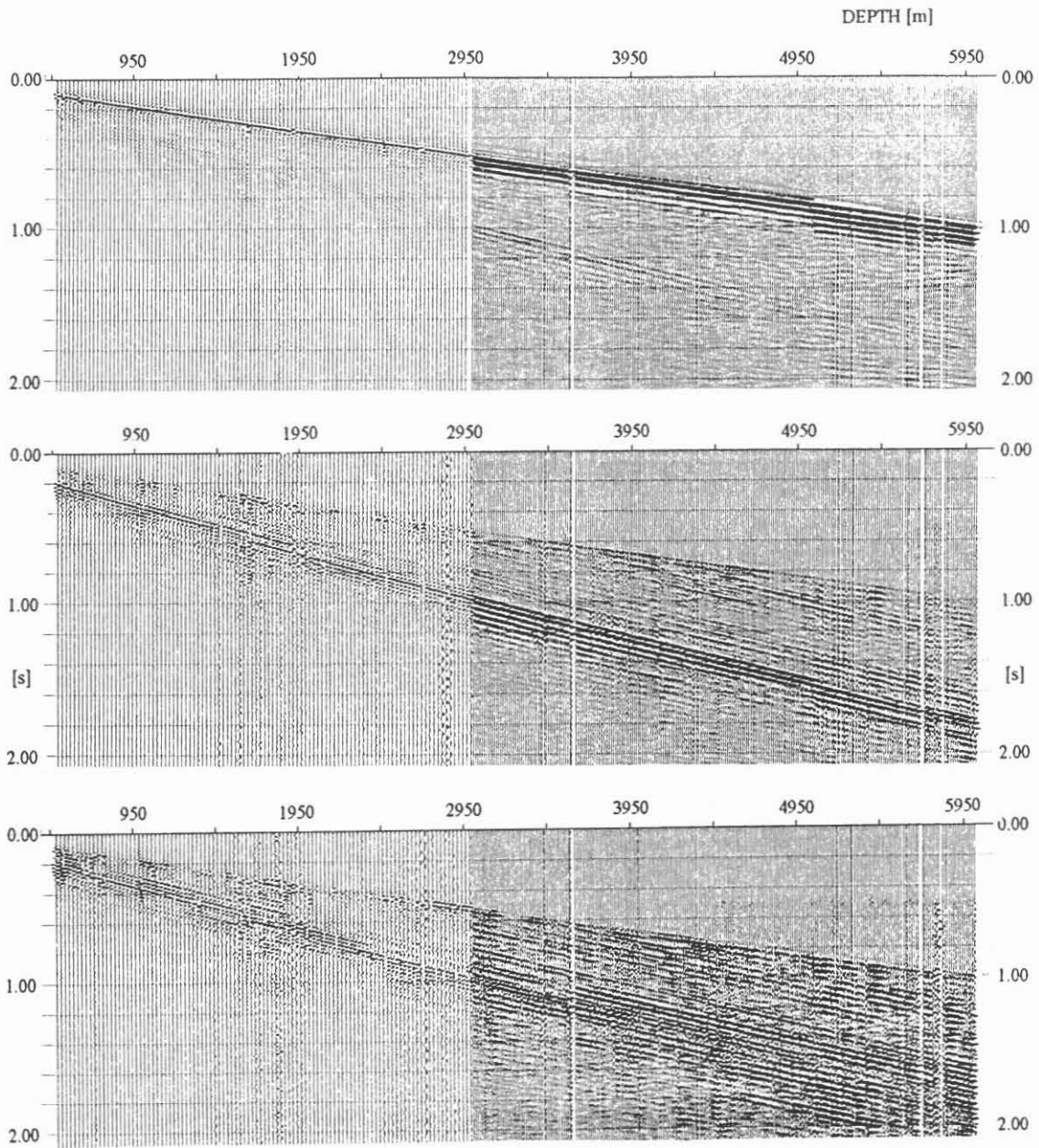


Fig. 20: Combination of VSP VP101P and VSP6000 (downgoing wave field), vertical component (top) and the two horizontal components.

## 6 Conclusions

The combination of near offset VSPs offers a link between the reflectors observed in surface seismic profiles (2D, 3D) and the highly detailed informations from borehole measurements. There is a high number of correlations with impedance contrasts seen in the sonic log and the lithological description (metabasites, paragneisses), but a significant portion of the VSP reflection elements appear to be caused by structural features (fractures, faults). Horizontal elements correlate well with surface reflection sections. Strongly dipping features (up to 90 degrees) are dominating the VSPs. With appropriate VSP processing even very steeply dipping structures were imaged which can not be seen by other experiments. Shear wave splitting is restricted to the upper 3 km and is caused by seismic anisotropy of the order of 10 % due to rock foliation. The average velocity increases continuously to 6.15 km/s at 6 km depth and its dependence on depth can be well approximated by a two parameter function. This function can be used for depth predictions of reflection events.

## 7 Acknowledgements

We are grateful to the Deutsche Forschungsgemeinschaft (DFG, Bonn) for funding through grant No. Hu 413/3-1 within the KTB priority program. We thank the logging section of the KTB (KTB management, Hannover) for administrative support and data transfer of the VSP6000. Geophysical Institute Karlsruhe contribution No. 570.

## References

- Balch, A.H. and Lee, Myung W., 1984, Vertical Seismic Profiling. Technique, Applications and Case Histories: D. Reidel Publishing Company, Holland.
- Benhama, A., Cllet, C., and Dubesset, M., 1988, Study and applications of spatial directional filtering in three-component recordings: *Geophysical Prospecting*, **36**, 591-613.
- Bortfeld, R., 1989, Geometrical ray theory: Rays and traveltimes in seismic systems (second-order approximations of the traveltimes): *Geophysics*, **54**, 342-349.
- Crampin, S., 1986, Anisotropy and transverse isotropy: *Geophysical Prospecting*, **28**, 541-549.
- DEKORP Research Group, 1988, Results of the DEKORP4/KTB Oberpfalz deep seismic reflection investigations: *Journal of Geophysics*, **62**, 69-101.
- Dillon, P.B. and Thompson, R.C., 1984, Offset source VSP surveys and their image construction: *Geophysical Prospecting*, **32**, 790-811.

- Edelmann, H.A.K., 1992, Circularly polarized shear waves used for VSP measurements: *Geophysics*, **57**, 643-646.
- Gaiser, J.E., Ward, R.W., and DiSiena, J.P., 1982. Three component vertical seismic profiles: Polarization measurements of p-wave particle motion for velocity analysis: Proc. 52nd Annual SEG Meeting, Dallas, Texas.
- Gal'perin, E.I., 1974, Vertical Seismic Profiling: Society of Exploration Geophysicists.
- Gut, T.W., Söllner, W., Lüschen, E., and Edelmann, H.A.K.. 1992, More reliable shear-wave data from VSP by using CIPHER-technique. *in* Dürbaum, H.-J., Reichert, C., and Bram, K., Eds., KTB Report 92-5: Niedersächsisches Landesamt für Bodenforschung.
- Hagedoorn, J.G., 1954, A process of seismic reflection interpretation: *Geophysical Prospecting*, **2**, 85-127.
- Hardage, B.A., 1985, Vertical Seismic Profiling, part A: Principles: Handbook of Geophysical Exploration, **14A**, Geophysical Press, London.
- Hohrath, A., Bram, K., Hanitzsch, C., Hubral, P., Kästner, U., Lüschen, E., Rühl, T., Schruth, P.K., and Söllner, W., 1992, Evaluation and interpretation of VSP-measurements in the KTB-Oberpfalz pilot borehole: *Scientific Drilling*, **3**, 89-99.
- Hubral, P. and Krey, Th., 1980, Interval velocities from seismic reflection time measurements: *Soc. Explor. Geophys.*
- Kästner, U., Bram, K., Hubral, P., Kiefer, W., Köninger, C., Macdonald, C., Merz, J., Rühl, T., and Sandmeier, K.-J., 1989, Seismische Untersuchungen an der KTB-Lokation, *in* Dürbaum, H.-J., Reichert, C., and Bram, K., Eds.. KTB Report 89-1: Niedersächsisches Landesamt für Bodenforschung.
- Kern, H., Schmidt, R., and Popp, T., 1991, The velocity and density structure of the 4000m crustal segment at the KTB drilling site and their relationship to lithological and microstructural characteristics of the rocks: an experimental approach: *Scientific Drilling*, **2**, 130-145.
- Lüschen, E., Söllner, W., Hohrath, A., and Rabbel, W., 1990. Integrated p- and s-wave borehole experiments at the KTB-deep drilling site, *in* Dürbaum, H.-J., Reichert, C., and Bram, K., Eds., KTB Report 90-6b: Niedersächsisches Landesamt für Bodenforschung.
- Lüschen, E., Söllner, W., Hohrath, A., and Rabbel, W., 1991. Integrated p- and s-wave borehole experiments at the KTB-deep drilling site in the Oberpfalz area (SE Germany), *in* Meissner, R., Brown, L., Dürbaum, H.-J., Franke, W., Fuchs, K., and Seifert, F., Eds., *Continental Lithosphere: Deep Seismic Reflections*: American Geophysical Union, Washington, D.C., 121-133.
- Lüschen, E. and Werner, U., 1992, Indications for a fluid/gas reservoir in 8 km depth beneath the KTB and rock anisotropy from shear-wave reflection surveys, *in* Dürbaum, H.-J., Reichert, C., and Bram, K., Eds., KTB Report 92-5: Niedersächsisches Landesamt für Bodenforschung.

- O'Brien, P.N.S. and Lucas, A.L., 1971, Velocity dispersion of seismic waves: *Geophysical Prospecting*, **19**, 1-26.
- Rühl, T. and Hanitzsch, C., 1992, Average and interval velocities derived from first breaks of vertical seismic profiles at the KTB deep drilling site, *in* Dürbaum, H.-J., Reichert, C., and Bram, K., Eds., KTB Report (this volume): Niedersächsisches Landesamt für Bodenforschung.
- Ziolkowski, A., 1991, Why don't we measure seismic signatures?: *Geophysics*, **56**, 190-201.



# Average and interval velocities derived from first breaks of vertical seismic profiles at the KTB pilot hole

T. Rühl\* and C. Hanitzsch†

## Abstract

A kinematic evaluation of first breaks of the direct P-wave in several VSPs, carried out at the KTB pilot hole in 1988 and 1989, is presented. After picking and correction to vertical traveltimes, average and interval velocities were computed.

The average velocity increases with depth caused by the successive closing of microcracks under increasing confining pressure. This average velocity-depth curve is the most accurate velocity information at the KTB site and can be used in migration and time-depth conversion problems in 2D- and 3D reflection surveys.

---

\*Geophysikalisches Institut, Universität Karlsruhe, Hertzstr. 16, W 7500 Karlsruhe 21, Germany; now at: GEOMAR, Wischofstr. 1-3, W 2300 Kiel 21, Germany

†Geophysikalisches Institut, Universität Karlsruhe; now at: ELF UK, Geoscience Research Centre, 114A Cromwell Road, London SW7 4EU, UK

## Introduction

In this paper we report about a kinematic investigation of vertical seismic profiles (VSP) conducted at the KTB pilot hole.

In a vertical seismic profile a hydrophone or a geophone (sometimes an array of them) is lowered into a borehole. Seismic sources (shots or vibrators) are placed at the Earth's surface at some distance from the borehole. The seismic energy released by these sources propagates through the medium in the vicinity of the borehole. It is reflected and diffracted at seismic interfaces and inhomogeneities. The upgoing reflected wavefield is recorded by borehole geophones in addition to the downgoing transmitted wavefield.

VSP-measurements can be evaluated under different aspects. The seismic structures can be imaged with high accuracy and resolution. Using shear-wave sources (shear-wave vibrators or even shots) and three-component geophones the shear-wave response of the medium can be investigated. This was done at the KTB pilot hole [Lüschen et al., 1990]. The authors found some evidence of shear-wave splitting indicative of seismic anisotropy.

Another aspect of VSPs is the determination of the velocity–depth function using traveltimes of direct transmitted waves. Average velocities from VSPs can be used in migration and time–depth conversion problems in surface reflection surveys. They are more suited than velocities derived by other methods (e.g. sonic log), because the VSP raypaths are very similar to those of surface seismic experiments. Several VSPs were carried out in 1988 and 1989 at the KTB pilot hole [Hohrath et al., 1992; Lüschen et al., 1990]. VSPs with different offsets from the borehole (up to 8 km) and two orthogonal azimuths are available. In contrast to a usual check-shot survey for velocity determination, a VSP has often a much smaller depth spacing of the receivers. For the KTB experiment the spacing is 12.5 or 25 m respectively and can be regarded as a high resolution check-shot survey.

Our kinematic investigation is restricted to the first breaks of the direct compressional wave because it is hardly possible to pick the onset times of the shear wave, at least with the same accuracy as for the compressional wave. Another reason is that we often see two or more shear-wave phases with different phase velocities. This is due to P–S-conversion and shear-wave splitting phenomena as mentioned above. Therefore a shear-wave velocity analysis should be done in conjunction with an anisotropy investigation.

The next chapter represents the data investigated here. The picking and traveltime correction is described as well as the computation of average and interval velocities.

In the third chapter the results are presented. The average velocity is important in migration and inversion problems. This velocity is the most accurate one for time–depth conversion of all seismic measurements for the depth range 500–3600 m.

The interval velocities are important for the determination and classification of different lithological units. The interval velocities can be compared with velocity measurements of core samples [Lippmann et al., 1989; Nover et al., 1989; Kern and Siegesmund, 1989] and with sonic logs [Stewart et al., 1984]. Effects causing deviations between both measurements are discussed as for example different frequencies used, scanning of different parts of the formation, intrinsic absorption and dispersion and dispersion due to scattering.

## Data processing of first breaks of VSP

Several VSPs with different types of sources were conducted at the KTB drilling site which are now available for traveltime analysis.



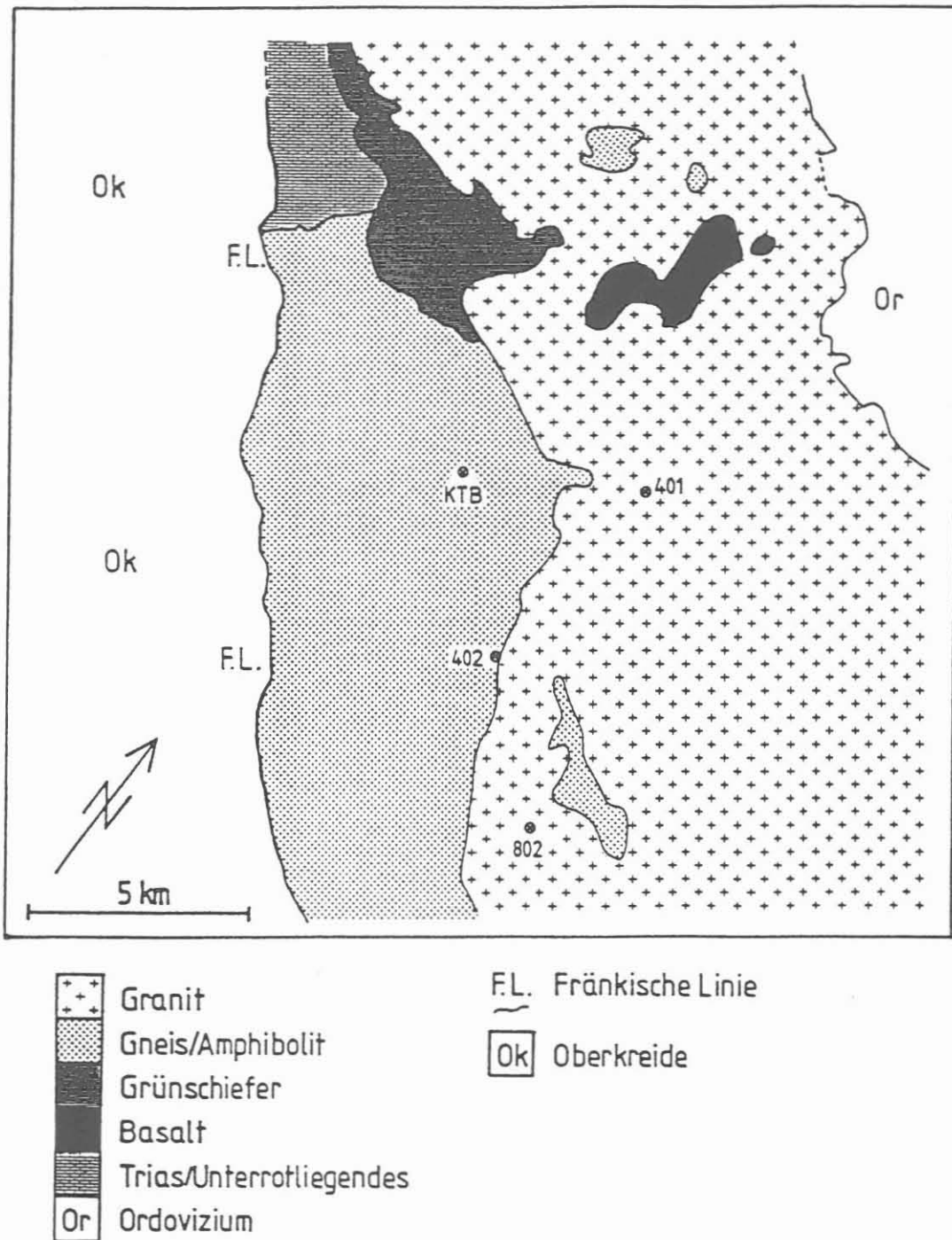


Figure 1: Geologic map of the region of the KTB deep drilling site. The square with approximately 22 km length covers the area of a 3D seismic survey conducted in 1989. The main geologic units are: granite, gneisses and amphibolites, green schist zone, basalt, Trias and Unterrotliegendes, and Ordovician. The Franconian Line (F.L.) separates the crystalline area in the north-east from the Upper Cretaceous sediments in the south-west. Note the location of the KTB where the VSP 100 and 101 are situated and the locations of the far-offset VSP 401, 402 and 802.

A zero-offset VSP (actual offset 200 m) was recorded in 1988 [Schruth et al., 1991] and is labeled here VSP 100. This corresponds to VSP 3600 in Lüschen et al. [1990]. The dataset with a dense receiver spacing of 12.5 m consists of two overlapping datasets measured at different times. This combination of two datasets causes problems concerning different wavelet signature and also small static time-delays have to be corrected for.

In 1989 several VSPs and other borehole and surface seismic surveys were conducted during the ISO 89 (integrated seismic survey Oberpfalz) [Lüschen et al., 1990]. Different types of sources (shots, vibrators, Marthor) were used. Several offsets were realized, one zero-offset VSP (VSP 101) and three far-offset VSPs with 4 km offset (VSP 401 and 402) and 8 km offset (VSP 802). These VSPs correspond to those named SP with the same location number as in Lüschen et al. [1990].

The source locations are shown on a simplified geologic map (Fig. 1). For a detailed description of the geologic and tectonic framework of the KTB drill site see papers in Emmermann and Wohlenberg [1989]. The KTB-location is situated in a gneiss and amphibolite area in the so called ZEV-zone (zone of Erbdorf-Vohenstrauss). The location 401 is situated in the Falkenberg granite. The location 402 is in an amphibolite, very close to the border of the Friedenfels granite. The location 802 is contained in the Friedenfels granite. Both granites are not differentiated in the map.

From the available data sets only VSPs with impulse excitations (shots) were used in this investigation, because of their larger signal- to -noise ratio and to avoid problems of zero-phase signals. The geophone spacing was 25 m (except VSP 100: 12.5 m).

The traveltimes of the compressional first-arrivals were picked manually on a digitizing table. Each dataset was picked several times in order to check the accuracy of the time picks. Deviations of several pickings amount up to 2 ms.

The traveltimes between source and borehole-geophone must be corrected in order to be able to compare with each other and with the sonic log (Fig. 2). The effects of the deviated borehole, the difference in elevation between source and wellhead, the source-hole depth and the weathering layer must be taken into account. The reference level is the elevation of the well head. The correction formula is:

$$t = t_o \cos \beta - t_w + t_c \quad (1)$$

with

$$\begin{aligned} t_w &= \frac{z_w - z_s}{v_w} \\ t_c &= \frac{z_w - z_h}{v_c} \\ \cos \beta &= \frac{z_g}{l} \\ l &= \sqrt{z_g^2 + x_g^2} \\ z_g &= z + z_h - z_s \end{aligned}$$

The quantities have the following meaning (see also Fig. 2):

- $t_o$  measured traveltime
- $t$  corrected traveltime
- $\beta$  angle between ray and the vertical
- $z_w$  thickness of weathering layer
- $z_s$  depth of source hole

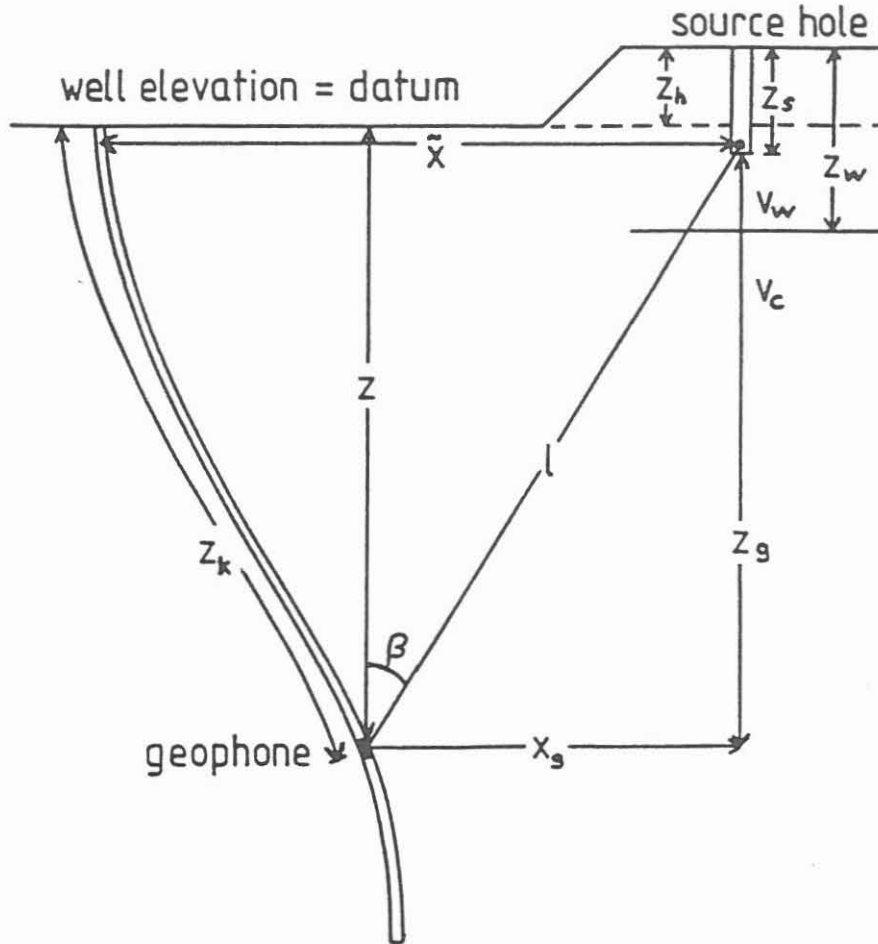


Figure 2: Correction of the measured traveltime to the vertical traveltime. Effects of the deviated borehole, the elevation differences, source hole depth and weathering layer must be considered (see text).

- $z_h$  elevation difference between source surface and wellhead surface
- $v_w$  velocity of the weathering layer
- $v_c$  correction velocity (equal to the computed average velocity)

In case that the source hole is deeper than the weathering layer,  $z_w$  must be set equal to  $z_s$ . Then the second term cancels. The values for the quantities necessary for the time correction are summarized in Table 1.

The depth of the source borehole is estimated to be 20 m. The depths and velocities of the weathering layer are estimated and extrapolated from results of short refraction profiling during the 3D-seismic survey. The coordinates of the borehole are computed from values of azimuth and dip in 20 m intervals. Values in between are linearly interpolated.

The corrected traveltimes are the basis for the computation of velocities. In principle the average velocity  $v_{ave}$  is given by

$$v_{ave} = \frac{z}{t} \quad (2)$$

After inserting (1) into (2) and equating the correction velocity  $v_c$  to the average velocity  $v_{ave}$ , the average velocity is calculated as

$$v_{ave} = \frac{z + z_h - z_w}{t_o \cos \beta - \frac{z_w - z_s}{v_w}} \quad (3)$$

Table 1: Values needed for the travelttime correction (see text).  $\Delta E$  ( $\Delta N$ ) is the source offset from the wellhead in east-west (north-south) direction. The other abbreviations are explained in Fig. 2.

VSP	100	101	401	402	802
$\Delta E$	191	-50	3513	3011	5936
$\Delta N$	77	-7	2058	-2872	-5472
$\tilde{x}$	206	51	4071	4161	8073
$z_h$	0	0	-24	-69	-58
$z_s$	20	20	20	20	20
$z_w$	15	15	65	47	17
$v_w$	1100	1100	2550	2400	950

In case the source hole is deeper than the weathering layer, (3) simplifies to

$$v_{ave} = \frac{z + z_h - z_s}{t_o \cos \beta} = \frac{l}{t_o} \quad (4)$$

The interval velocity is generally calculated as

$$v_{int,i} = \frac{\Delta z}{\Delta t} \quad (5)$$

with  $\Delta z = z_{i+1} - z_i$  and  $\Delta t = t_{i+1} - t_i$ .

In order to get reliable values for the interval velocities, we use the linear regression method. After some tests, we chose an averaging interval of 200 m, i.e. 8 (VSP 100: 16) adjacent time values are taken for the determination of one velocity value. The averaging window is moved along the whole travelttime curve. The computed velocity value was put into the middle of the averaging window.

In order to get an idea about the errors in the velocity depth curve we estimate a travelttime picking error of 2 ms and an error of source coordinates of 10 or 25 m and  $\delta z_s = 5$  m. We use the Gaussian error propagation method for computing the error bounds of the velocities. In case of the average velocity we chose the maximum error propagation method, which yields larger errors.

## Results

### Average velocities

Average velocity-depth curves for VSP 100, 101, 401 and 402 are presented in Fig. 3. The gaps in the curves are due to bad data quality. The left and right curves indicate the error bounds of the average velocity (center curve), computed with the maximum error propagation method.

All curves show a continuous increase of average velocity with depth. This can be explained by the influence of microcracking. In the low-pressure range, velocities of measured gneisses and amphibolites increase very rapidly with increasing confining pressure, i.e. depth, effectively closing most of the microcracks. Above about 150-200 MPa (below 5.-6.5 km depth)

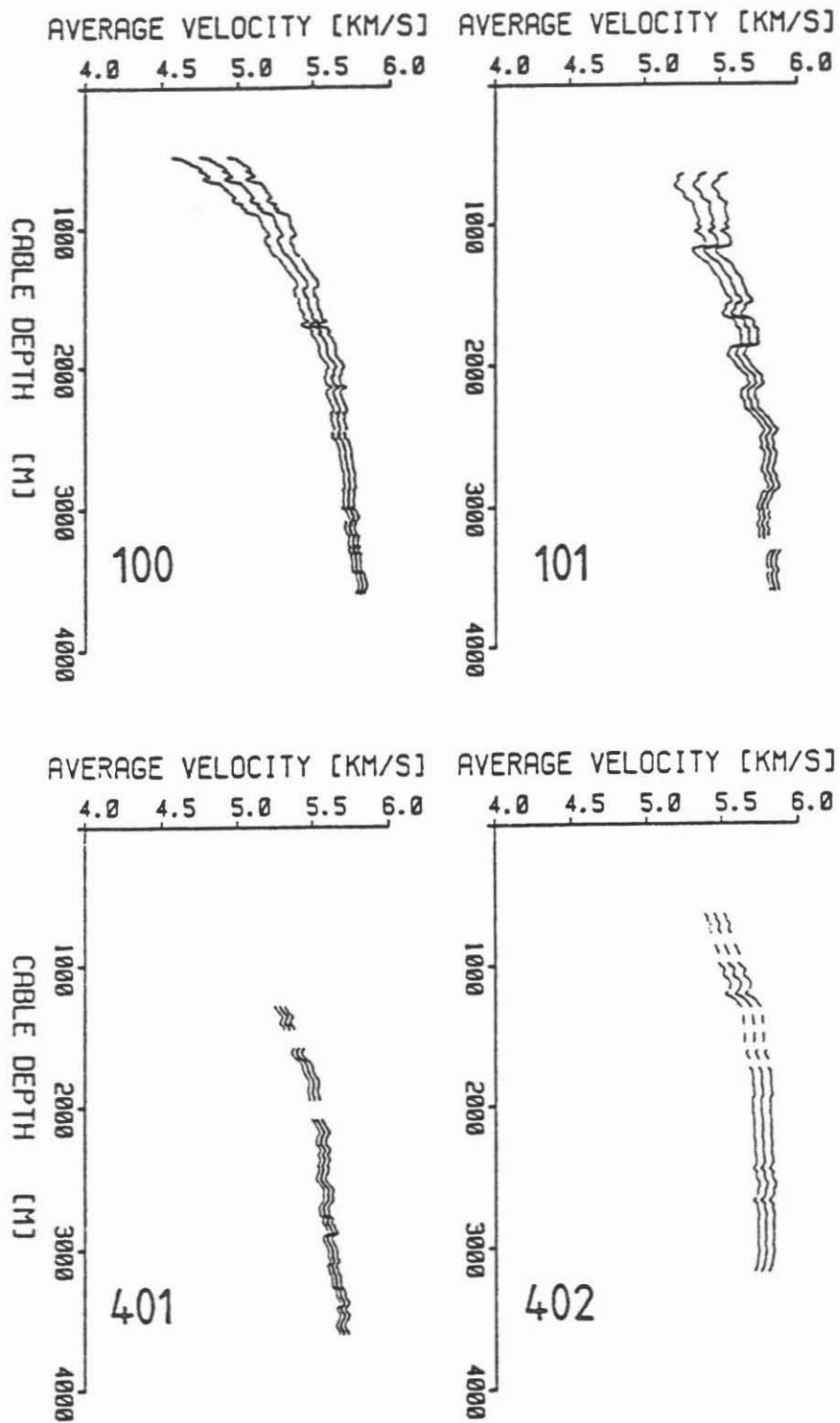


Figure 3: Average velocity - depth curves for VSP 100, 101, 401 and 402 (see Fig. 1 for locations). The gaps in the curves are due to bad data quality. The left and right curves mark the error bounds.

when nearly all microcracks are closed the pressure derivative gets smaller showing only the intrinsic dependence of velocity on pressure [Kern and Siegesmund, 1989].

VSP 100 shows a very pronounced increase of velocity, from 4780 m/s at 500 m depth to 5800 m/s at 3640 m depth.

In VSP 101 the velocity increases more gently, from 5380 m/s at 640 m depth to nearly the value as in VSP 100. Velocities are slightly higher especially above 2000 m depth. It is remarkable that both zero-offset VSPs show such a deviation in velocity in the upper part (see Tab. 1 for actual non-zero offsets from the well-head, both shots were separated by nearly 250 m). It is evident, that the medium parameters vary on this length scale.

Velocities in VSP 401 (offset: 4 km) increase with the same gradient as the zero-offset VSP, but they are shifted to lower values. Compared to VSP 100 (101) velocities are lower by 80–150 m/s (150–250 m/s). We explain this difference with a lower velocity in the granite of Falkenberg on which the source site is located (see Fig. 1).

In VSP 402 (offset: 4 km) the average velocity shows a gentle increase from 5460 m/s (650 m) to 5750 m/s (2000 m). It is nearly constant below 2000 m depth. Therefore in comparison to VSP 401, VSP 402 has a totally different character in the upper depth range. Velocities in VSP 401 are lower than in VSP 402, but the velocity converges towards a common value below 2500 m.

### Interval velocities

Fig. 4 shows the interval velocity–depth curves for VSPs 100, 101, 401 and 402. The error bounds are computed with the Gaussian error propagation method based on the estimated errors of traveltimes and source coordinates.

In VSP 101 we recognize strong oscillations in interval velocities reaching unreasonably high values up to 8500 m/s. This is due to bad data quality and changes in the source signature. Also static effects due to different shot statics play an important role.

The mean value of all interval velocity curves is about  $6000 \text{ ms}^{-1}$ . The mean value in VSP 100 seems to increase slightly with depth while the other curves deviate from a constant depth-independent mean value. The velocity jump at 1160 m depth which correlates with an amphibolite body (see Fig. 11) is seen in all curves. The velocity increase below 3000 m depth is obvious in VSP 100 and 401.

One can argue that the calculation of interval velocities from traveltimes of far-offset VSPs and a comparison with the sonic log is not allowed. This is certainly true in a strict sense. But the application on different far-offset VSPs and the comparison with zero-offset VSPs can yield interesting features.

In Fig. 5 and 6 the interval velocities are compared with the P-wave sonic-log velocities (continuous heavy line). Because of the strong oscillations of the interval velocities of VSP 101 this dataset was not used in the comparison. The first observation is that the sonic velocities are in general smaller than the interval velocities. This result is surprising because it is well known that in most cases the opposite is true (see Fig. 9). Only in very limited depth ranges, sonic velocities are higher than interval velocities, e.g. in VSP 100 between 1300–1600 m and 2000–2150 m.

Many features agree quite well in both datasets. The velocity jump at 1160 m, caused by an amphibolite as mentioned above, is clearly reproduced in all interval velocity curves. Another feature is the low-velocity anomaly between 2600–2800 m which is seen in VSP 401 and 402 but neither in the other VSP nor in the sonic log. The most remarkable deviation of sonic and interval velocity is found below 2900–3000 m. The sonic velocity is decreasing whereas

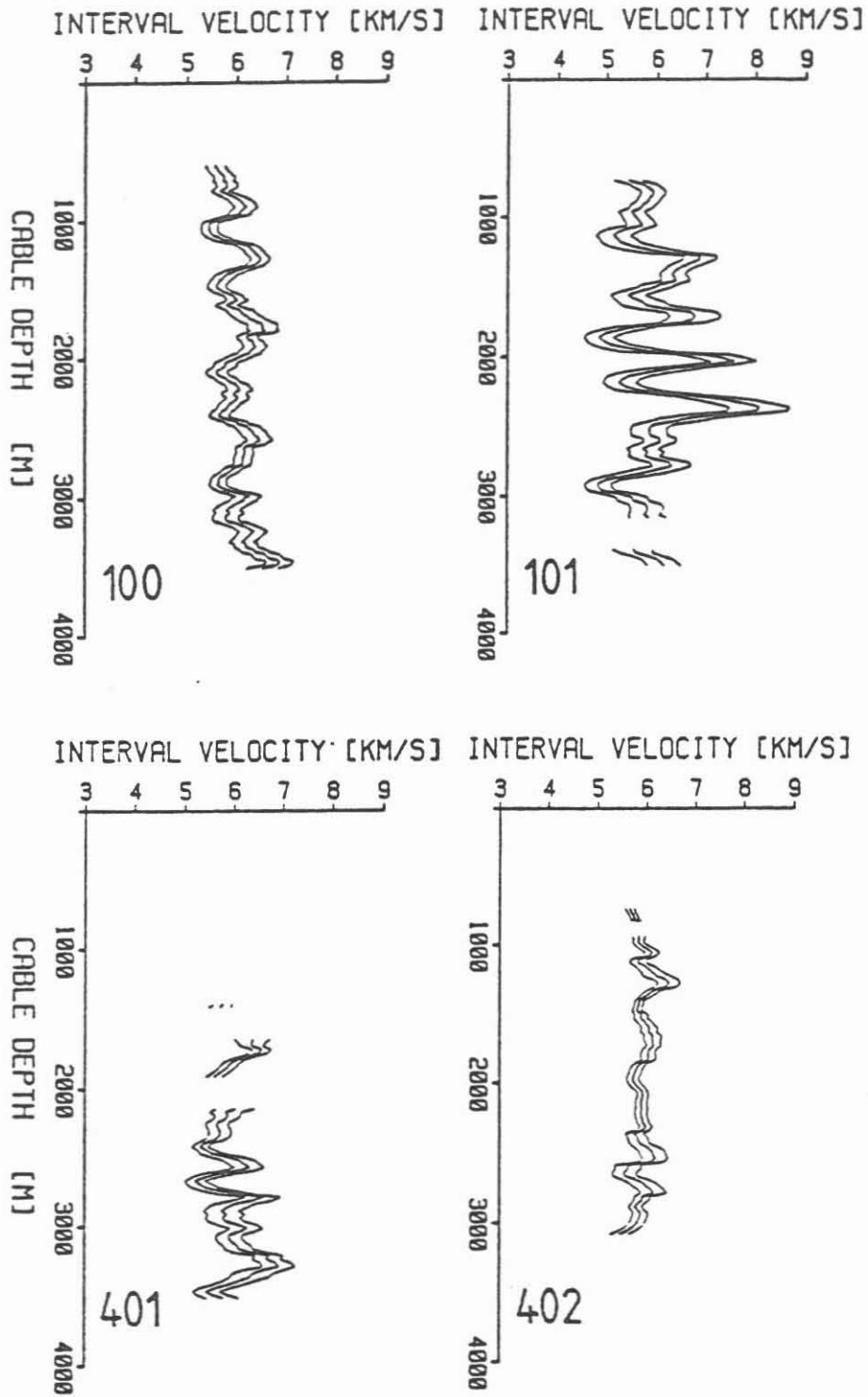


Figure 4: Interval velocity - depth curves for VSP 100, 101, 401 and 402 (see Fig. 1 for locations). The gaps in the curves are due to bad data quality. The left and right curves mark error bounds.

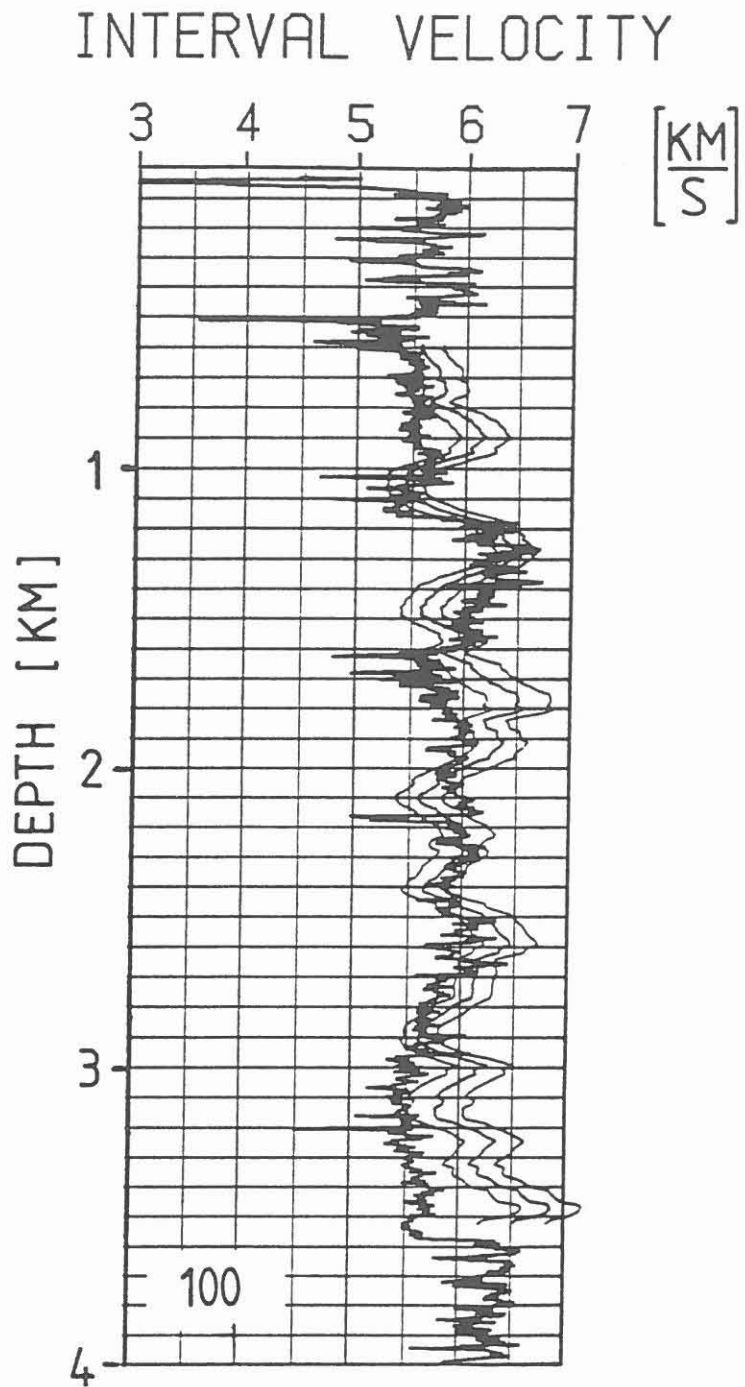


Figure 5: Comparison of VSP interval velocities (3 light lines, see Fig. 4) with P-wave sonic log velocities (heavy line) for VSP 100.



# INTERVAL VELOCITY INTERVAL VELOCITY

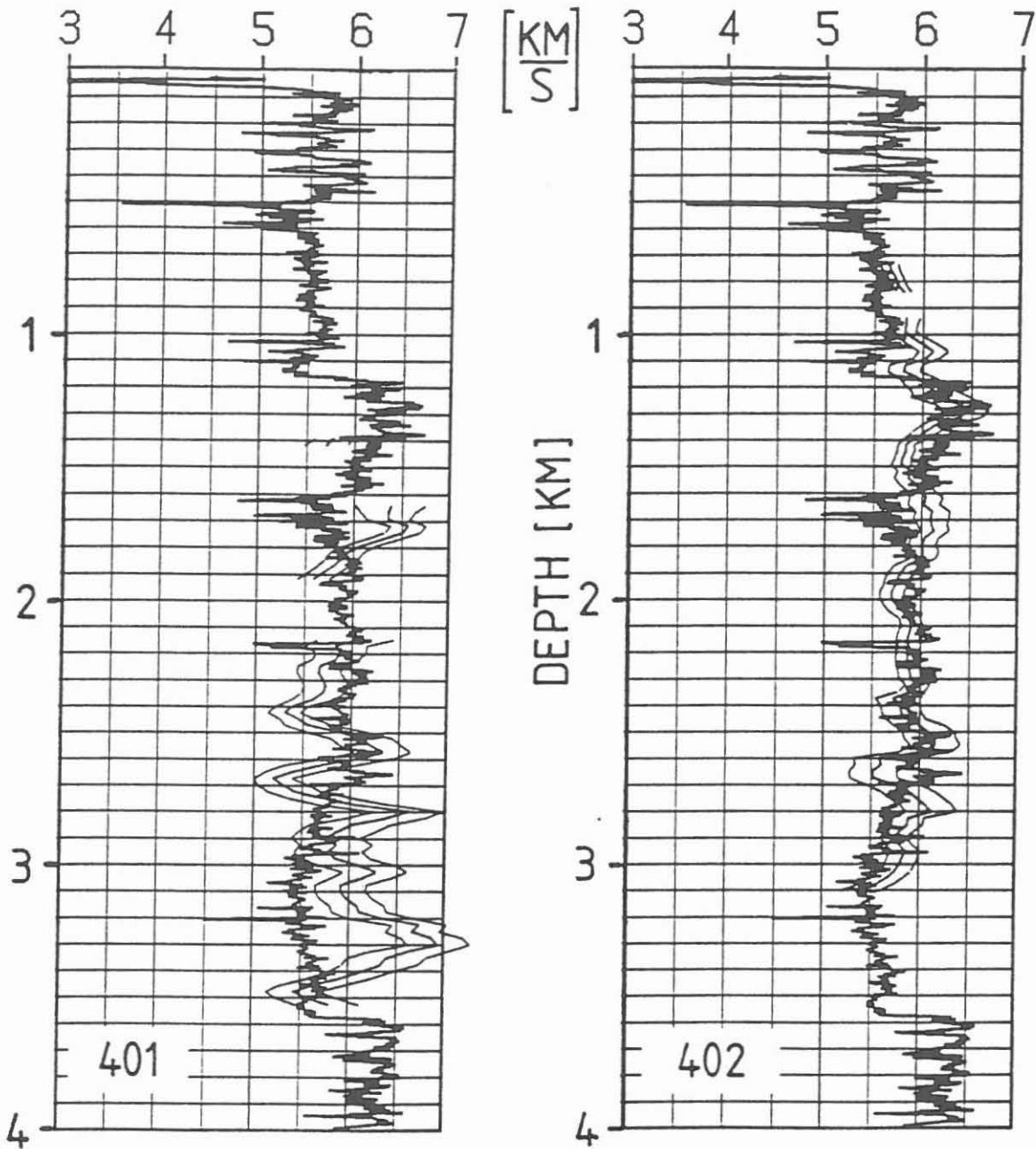


Figure 6: Comparison of VSP interval velocities (3 light lines, see Fig. 4) with P-wave sonic log velocities (heavy line) for VSP 401 (left) and 402 (right).

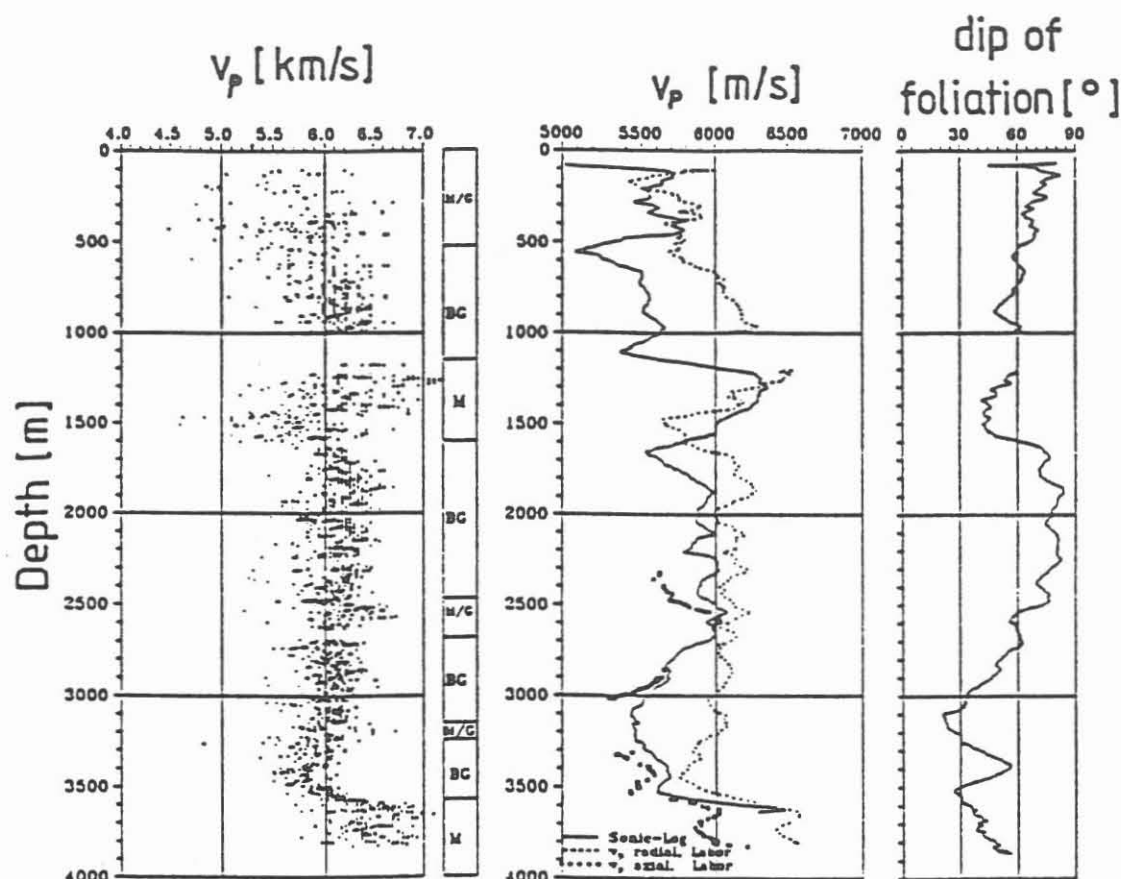


Figure 7: Compilation of P-wave velocities measured at core samples in the KTB field laboratory [Lippmann et al., 1989]. The maximum values of P-wave velocities perpendicular to the core axis are plotted (left) and averaged (moving averaging window 100 m, dotted line in the middle part). The solid line represents the averaged sonic log, the black dots are measured velocities parallel to the core axis. Note the dip of foliation (right). Lithologic column: M = metabasite, G = gneiss, BG = biotite gneiss

the interval velocity is increasing. Considering the shapes of both curves it is remarkable that they fit quite well in the case of VSP 402, but for the other far-offset VSP 401 the correspondence is bad. To be able to discuss possible explanations which are given in the last chapter we first compare these results with velocities from core samples.

### Comparison with velocities from core samples

Velocity measurements at core samples were performed in the KTB-field laboratory [Lippmann et al., 1989]. Below 2300 m depth the P-wave velocity was determined in radial direction (perpendicular to the core axis) and in axial direction (parallel to the core axis).

The maximum values of velocities are presented in Fig. 7. The minimum and also the average velocities show an even larger scattering about the mean value [Lippmann et al., 1989]. Therefore the maximum values are more meaningful. The maximum velocities are always measured parallel to the foliation plane of the gneisses and amphibolites. In the middle part of Fig. 7 the sonic and core sample velocities (axial and radial) averaged in a moving window of 100 m are compared. The maximum radial velocity is nearly always higher than the sonic velocity. The radial velocities do not show the same pronounced velocity decrease as the sonic log. In contrast, the axial velocities are always smaller than the sonic velocities

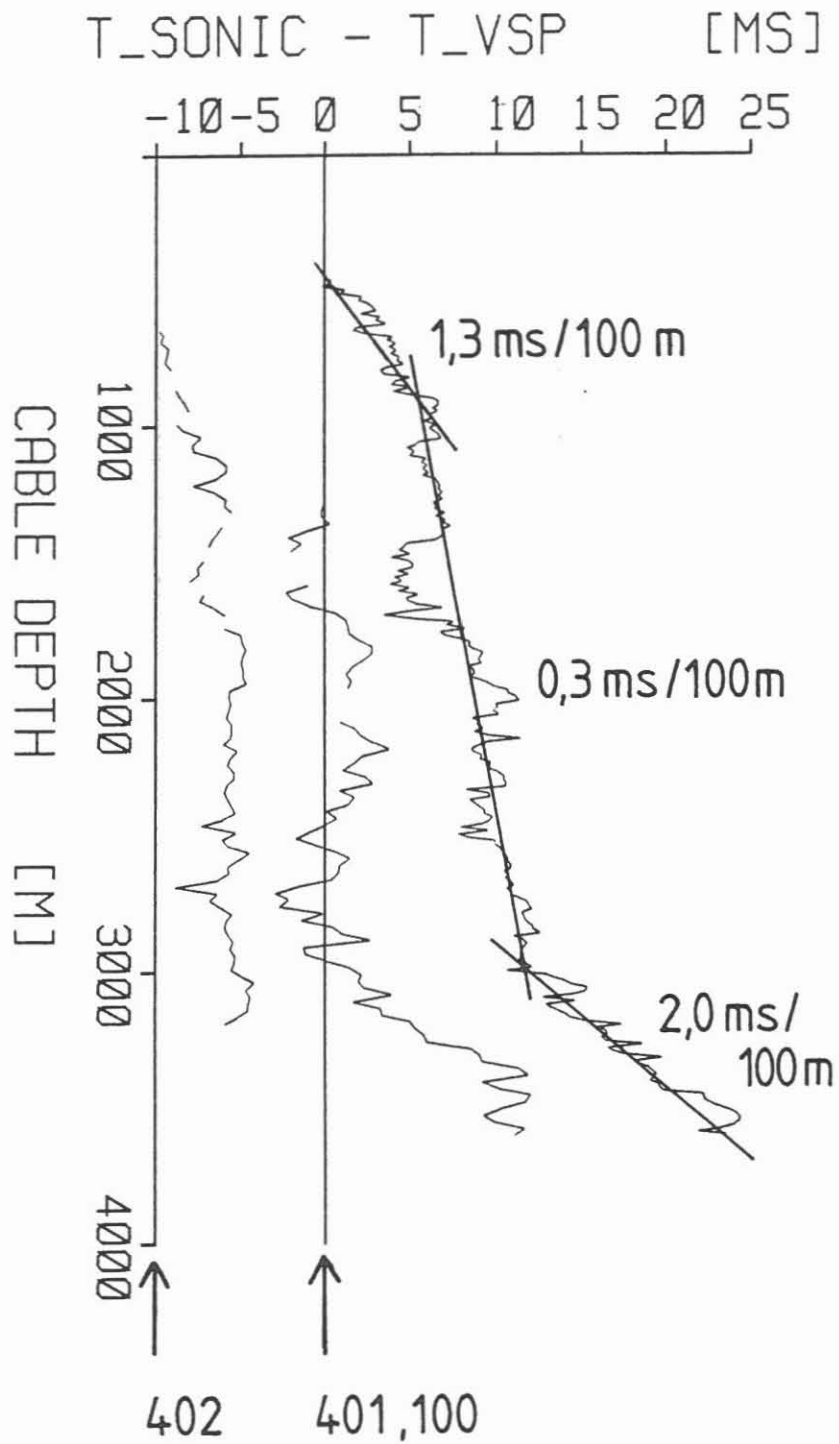


Figure 8: Difference of integrated sonic traveltime and check shot (VSP) traveltime (both corrected to the vertical). The drifts (time difference in a certain depth interval) are indicated. Note also the different depths of points where the time difference starts from a zero value. The origin of the curve for VSP 402 is shifted to -10 ms.

and reproduce very well this low-velocity anomaly between 2700 and 3500 m depth. This is explained by the change of dip of foliation in this depth range (see Fig. 7, right panel). The foliation changes from  $70^\circ$  to less than  $30^\circ$  at the point of minimal sonic velocity. Lippmann et al. (1989) estimate the in-situ anisotropy of the gneisses to be 10%.

### Comparison of VSP traveltimes and integrated sonic traveltimes

Another method to detect discrepancies between a VSP survey and a sonic log is to integrate the sonic log interval transit time and to compare it with the VSP traveltimes. This is the usual way to calibrate the sonic log. The integrated sonic log traveltime curve is fitted into the check shot traveltime curve and then the sonic log traveltime curve is differentiated to give the now calibrated sonic velocity curve. This is not done here as we only want to see whether the results of the last section can be confirmed with another approach in order to get confidence in the results.

In Fig. 8 the difference between the integrated sonic traveltimes and the check shot (VSP) traveltimes are shown for VSP 100, 401 and 402. The origin of the curve for VSP 402 is time-shifted by -10 ms. Note that the point where the time difference starts from zero is situated at different depths.

All curves are quite similar. This confirms again the similarity of the interval velocity curves. The time difference is always positive which means that the sonic velocities are smaller than the VSP interval velocities. The mentioned anomaly at 2600–2800 m depth is present in the far-offset VSP but not in VSP 100. The difference curve can be divided into three ranges with different drifts, i.e. time differences over a certain depth interval. Above 1000 m the drift is 1.3 ms/100 m whereas in the depth range 1000–3000 m the drift is very small (0.3 ms/100 m). Below 3000 m the drift is large again (2.0 ms/100 m). This confirms the great discrepancy at this depth again.

## Discussion

The most surprising result of this investigation is the observation that the sonic velocity is in general lower than the check shot interval velocity. This was also seen in a comparison of integrated sonic traveltime and VSP traveltime. Usually the difference  $t_{VSP} - t_{IntSonic}$  is plotted (in contrast to Fig. 8). With this convention our time differences are negative.

Negative drifts are not very common. Stewart et al. (1984) report about some results published in the literature concerning this topic. Only in a few cases negative drifts were found in the uppermost depth range. Goetz et al. (1979) showed a histogram of drifts based on results of 159 wells from depths greater than 3000 ft. The maximum lies at +2 ms / 1000 ft. The average drift at the KTB pilot hole is -2.3 ms / 1000 ft (-0.75 ms / 100 m).

Fig. 9 shows a comparison of sonic velocities (left) and VSP velocities (right) in the 1500 m deep borehole Böttstein in North-Switzerland [Nagra, 1985]. The hole is also situated in a crystalline environment, in this case granite. The average velocity ( $V_A$ ) is always smaller than the interval velocity ( $V_I$ ) as it is the case at the KTB pilot hole. But in the Böttstein borehole the sonic velocities are generally higher than the interval velocities which is the usual case. This is in contrast to our investigation.

How can we explain such negative drifts like those found at the KTB pilot hole? The sonic log operates in the kilohertz range and its penetration depth lies in the range of a few cm's. In this part of the formation, the velocities can be influenced by a mud cake or by borehole

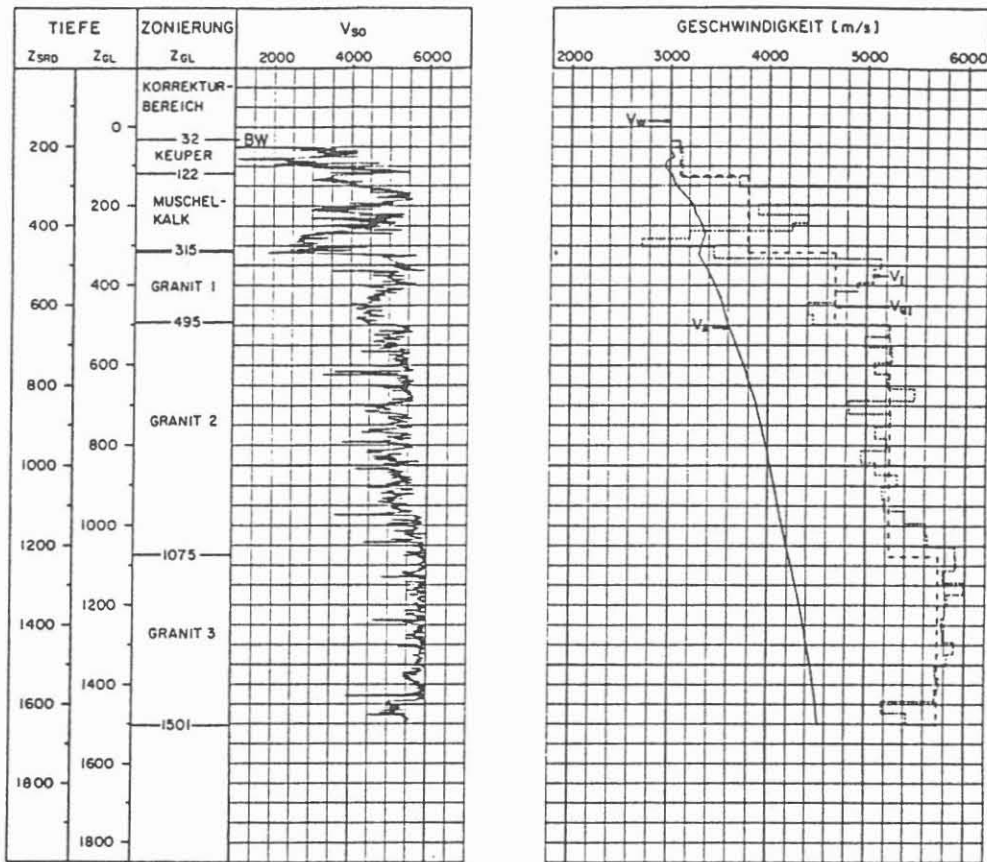


Figure 9: Comparison of sonic velocities ( $V_{so}$ ) and check shot velocities ( $V_A$  average velocity,  $V_I$  interval velocity) in a 1500 m deep borehole (mainly through granite) in North-Switzerland [Nagra, 1985]. Sonic velocities are generally higher than interval velocities.

damage due to drilling. Probably these effects only play a minor role in the KTB pilot hole because mud cake is not known so far.

Three possible explanations for the check shot traveltimes being smaller than expected are given in Fig. 10. The time correction described in the second chapter assumes straight rays and a homogeneous isotropic medium. In case of a vertical velocity gradient, the rays are no longer straight, but they are continuously refracted (see also Fig. 12). A high velocity refractor in the vicinity of the borehole can produce shorter traveltimes than expected for the straight ray. A possible candidate for a good refractor is the dipping high velocity amphibolite body at 3575 m which might be responsible for the increase of interval velocity below 3000 m.

As mentioned above, laboratory measurements and other investigations have shown that seismic and even nonseismic parameters have an anisotropic behaviour. In metamorphic areas the anisotropy is mostly caused by foliation and orientation of microcracks. The velocity parallel to the foliation plane is always higher than perpendicular to it. Depending on the orientation of the foliation planes the VSP-traveltime can appear too small in comparison to the sonic log which measures partly in a direction perpendicular to foliation.

Fig. 11 gives a model of the structural geologic situation at the KTB site [Müller et al., 1989]. It is seen that dip and strike of the foliation planes and folded gneiss-series change

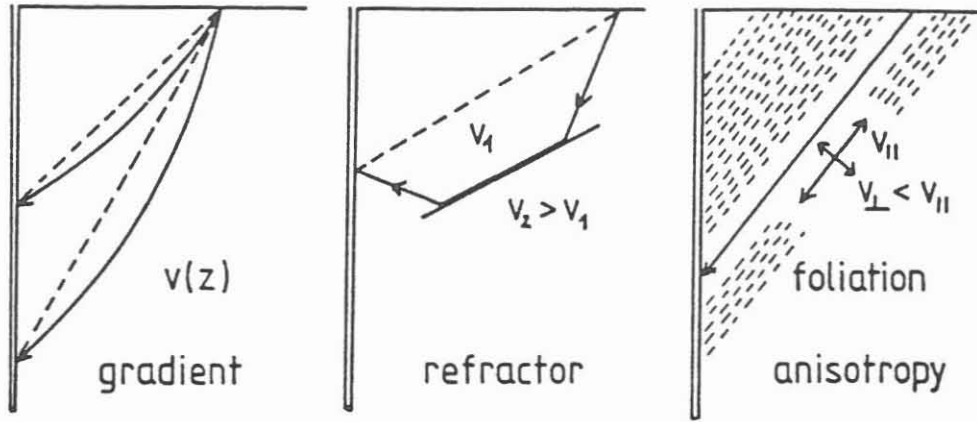


Figure 10: Three possible explanations for the check shot traveltimes being smaller than expected. The time correction assumes straight rays (dotted) and a homogeneous isotropic medium. In all these cases the “corrected traveltimes” are falsely corrected and too small (see Fig. 12)

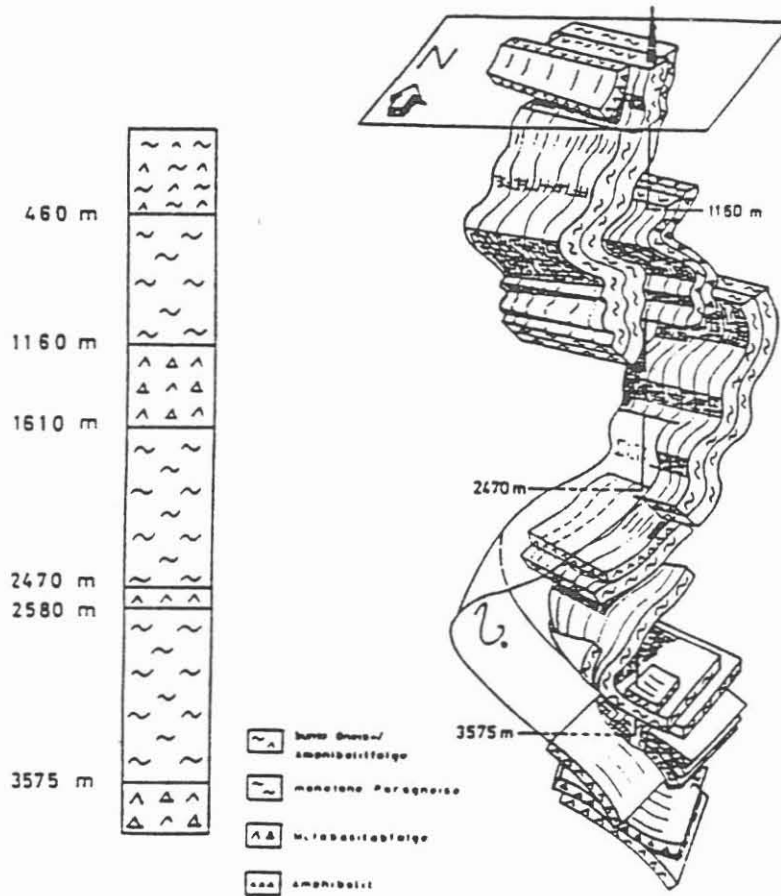


Figure 11: Simplified lithological column (left) and model of the structural geologic situation (right) after Müller et al. (1989).

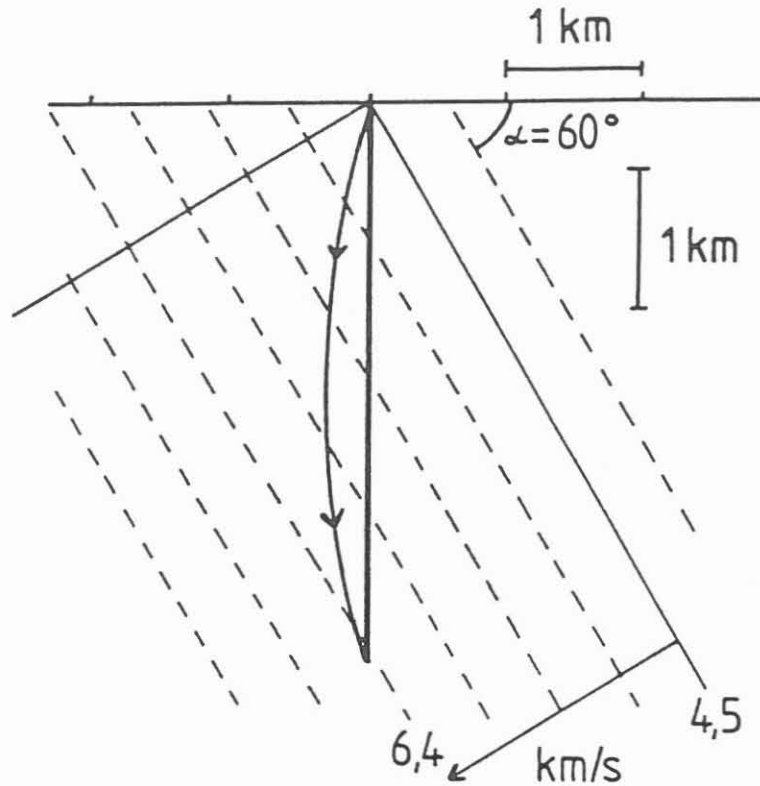


Figure 12: A simple model shows that the refracted ray is faster than the "borehole ray". Typical values for the KTB site of borehole depth, velocity gradient and dip of gradient are chosen. The analytically computed time difference is 5 ms. This agrees well in order of magnitude with the observed difference (see Fig. 8).

dramatically below 2700 m.

In a medium with a velocity gradient, it is known that the actual refracted ray is faster than the "borehole ray" (Fig. 12). A velocity gradient is likely to be existent at the KTB site (see average velocities in Fig. 3). Typical values for the KTB site of borehole depth, velocity gradient and dip of gradient were chosen. The analytically computed time difference is 5 ms. This agrees well in an order of magnitude with the observed difference (see Fig. 8).

In all three cases of Fig. 10 the "corrected traveltimes" are falsely corrected and too small. It is not possible to explain the observed drifts with only one model. Probably, the drift above 1000 m (Fig. 8) is caused by the velocity gradient which is very prominent in this depth range. The drift below 3000 m is likely to be produced by a combination of refractor and anisotropy.

In the case of VSP 402 the curves of the check shot interval velocity and of the sonic log velocities (see Fig. 6) show a good conformity. This is surprising because, in a strict sense, the computation of interval velocities from far-offset VSPs is only allowed if in between the medium is homogeneous. The geologic map (Fig. 1) shows that both the KTB pilot hole and the source location of VSP 402 (in the southeast) are situated in the same main geologic unit (gneisses and amphibolites). In the case of VSP 401 the correspondence of both curves is bad. The source of VSP 401 is located in granite northeast of the KTB pilot hole. It is obvious

that significant differences must exist between the raypaths of both far-offset experiments. One possible explanation is that the medium at the KTB site is dipping from southwest to northeast. In that case the raypaths from VSP 402 to the KTB pilot hole should be quite straight but those of VSP 401 must transmit at least one interface between two major geologic units.

## Conclusions

The evaluation of first breaks of VSP surveys yields a very accurate average velocity-depth function which is indispensable to migration and time-depth conversion problems in seismics.

The interval velocity curves for the different VSPs show similar features. The comparison with the sonic log reveals that sonic velocities are lower than the VSP interval-velocities. This surprising effect can be explained in several ways. A vertical velocity-gradient in the formation, a refractor near the borehole or velocity anisotropy can make direct traveltimes shorter than assumed in a homogeneous, isotropic medium. It is likely that above 1000 m depth, a vertical velocity-gradient is responsible for this effect. Below 3000 m depth, a pronounced discrepancy between sonic log and VSP velocities correlates with a region where dip and strike of the foliation change dramatically. Therefore, either anisotropy or a dipping refractor produces the effect. In this work it was not possible to use modeling (anisotropic ray tracing) for a simulation of the observed effects. This remains as an interesting task especially if the results of the 3D seismic survey are taken into account.

## Acknowledgements

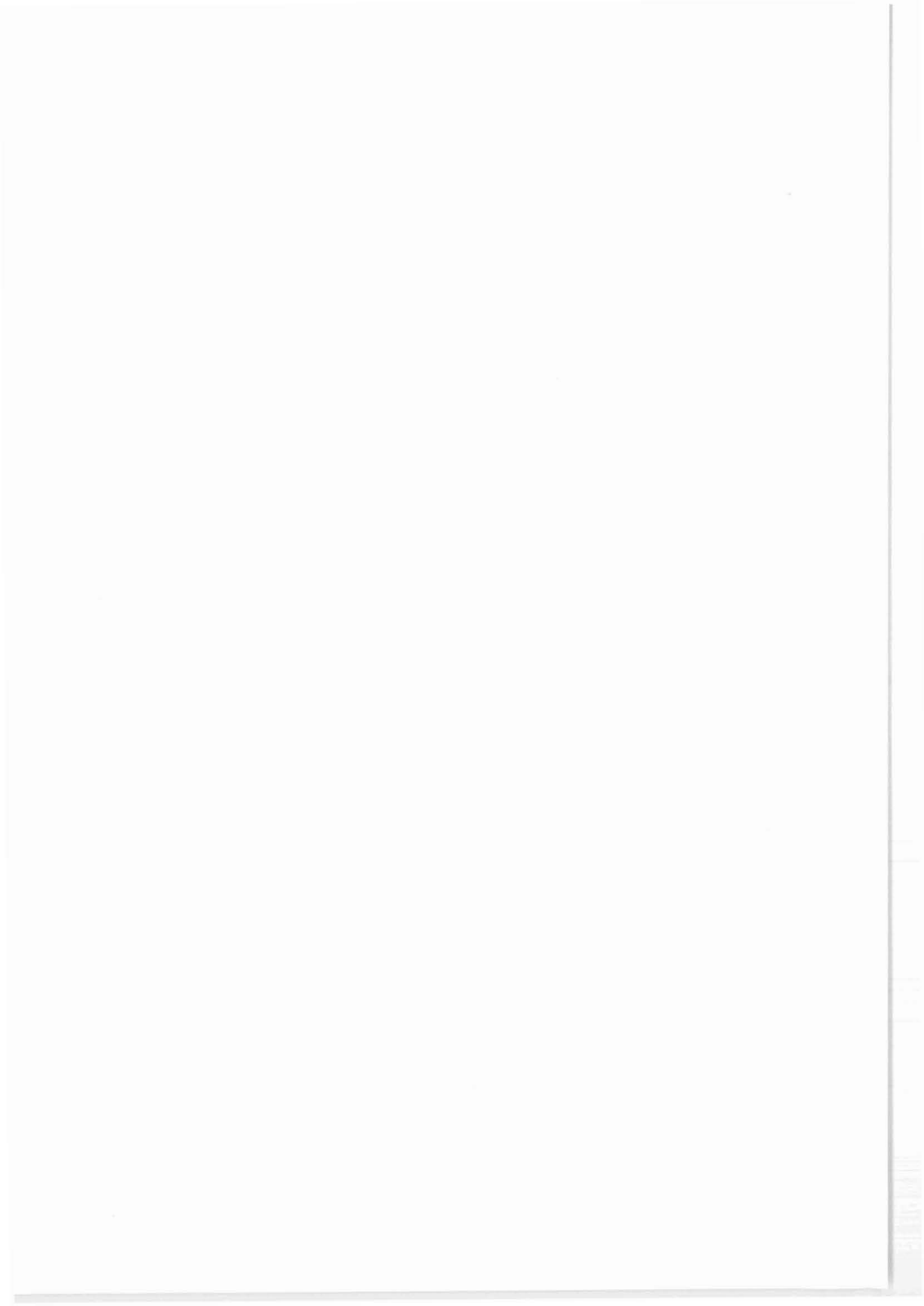
We like to thank C. Reichert and H. Wiederhold (NLFb), who made available to us a geologic map of the area covered by the 3D survey at the KTB drilling site. We thank W. Söllner and E. Lüschen who did the data preprocessing necessary for picking. Sonic and VSP 3600 data were provided by KTB project management, other data of ISO 89 (DEKORP). We thank I. Bush, K. Bram, J. Draxler and E. Lüschen for carefully reading the manuscript. We are grateful to the Deutsche Forschungsgemeinschaft (DFG, Bonn) for funding grant No. HU 413/2-1 within the KTB priority program.

## References

- Balch, A.H. and Lee, M.W., 1984, Vertical Seismic Profiling: Technique, applications and case histories: D. Reidel Publishing Comp.
- Emmermann, R. and J. Wohlenberg, Eds., 1989, The German Continental Deep Drilling Program KTB - Site selection studies in the Oberpfalz and Schwarzwald: Springer Verlag.
- Goetz, J.F., Dupal, L., and Bowles, J., 1979, An investigation into discrepancies between sonic log and seismic check shot velocities: Australian Petrol. Explor. Assoc. Jour., **19**, 131-141.
- Hohrath, A., Bram, K., Hanitzsch, C., Hubral, P., Kästner, U., Lüschen, E., Rühl, T., Schruth, P.K., and Söllner, W., 1992, Evaluation and interpretation of VSP-measurements in the KTB-Oberpfalz pilot borehole: Scientific Drilling, **3**, 89-99.
- Kern, H. and Siegesmund, S., 1989, Elastic wave velocities, anisotropy and density of KTB core samples at PT conditions: 2. KTB Kolloquium, KTB-Report 89-3, 406.



- Lippmann, E., Bücken, C., Rauen, E., Wienand, J., and Wolter, K.E., 1989, Gesteinsphysik im KTB-Feldlabor: Messungen und Ergebnisse: 2. KTB-Kolloquium, KTB-Report 89-3, 120-129.
- Lüschen, E., Söllner, W., Hohrath, A., and Rabbel, W., 1990, Integrated P- and S-wave borehole experiments at the KTB-deep drilling site: KTB-Report 90-6b, 85-136.
- Müller, H., Tapfer, M., Emmermann, R., and Wimmenauer, W., 1989, Die Paragneise im Profil der KTB-Vorbohrung: 2. KTB Kolloquium, KTB-Report 89-3, 61-66.
- Nagra, 1985, Sondierbohrung Böttstein - Untersuchungsbericht: Technical Report 85-01, Nagra.
- Nover, G., Buntebarth, G., Kern, H., Pusch, G., Pohl, I., Schopper, J.R., Schult, A., and Will, G., 1989, Ergebnisse gesteinsphysikalischer Untersuchungen an Bohrkernen und ihre Bedeutung für das KTB: 2. KTB Kolloquium, KTB-Report 89-3, 130-140.
- Stewart, R.R., Huddleston, P.D., and Kan, T.K., 1984, Seismic versus sonic velocities: A vertical seismic profiling study, *in* Balch, A.H. and Lee, M.W., Eds., Vertical seismic profiling: D. Reidel Publishing Comp., 385-423.



## Results of the 3-D Expanding Spread Experiment

C. BÖNNEMANN<sup>1</sup>, B. BUTTKUS<sup>1</sup>

### Abstract

The 3-D expanding spread experiment, performed within ISO 89 at the KTB site, has been evaluated under two aspects. The first aspect was the estimation of velocity-depth functions. Due to the limited reflection strength, estimating NMO velocities as a function of two-way traveltimes was possible in east-west direction only. Thus the calculation of interval velocities, requiring the correction of 3D effects, was not possible.

The second aspect was the directional dependency of the P-wave velocity at the top of the crystalline by evaluating the direct waves. After eliminating the effects of the lithology, a least-mean-squares anisotropy-velocity ellipse was fitted to the data with WSW as the direction of the maximum velocity and a velocity contrast of about 6%.

A 3-D expanding spread experiment was performed around the KTB site within the scope of the Integrated Seismics Oberpfalz 1989 project (ISO 89) to estimate the three-dimensional velocity distribution. Using the source signals of the 3-D seismic survey and additional geophone spreads, a 4 km × 4 km common-midpoint area around the KTB site has been covered for the whole azimuthal range with offsets ranging up to 24 km (WIEDERHOLD, 1990.) In a first processing step the data were sorted into 50 m × 50 m bins. After gathering nine neighbouring bins to form related macro bins all traces of the 150 m × 150 m macro-bin with the KTB location in its center are displayed in Figures 1 and 2.

The data have been evaluated under two aspects: the NMO (Normal Move Out) velocities were estimated as a function of two-way traveltimes and direction and the first breaks were analysed to study directional dependency of the velocities and whether there at the top of crystalline basement. The first breaks could only be picked for offsets up to 14 km due to the relative weak source signal used for the 3-D seismic survey. The azimuth is measured relative to the inline direction, bearing +53.2° against north. Thus, an angle of +126.8° against the inline direction represents south bearing. All directions given in this paper refer to inline direction, i.e. a correction of -126.8° must be applied to obtain geographic directions.

---

<sup>1</sup>Bundesanstalt für Geowissenschaften und Rohstoffe, P.O. Box 510153, Hannover, Fed. Rep. of Germany

## Velocity-Depth Determination

To estimate the velocity in different azimuth directions, special methods for signal enhancement and velocity analysis in the  $\tau - p$  domain, developed within the DEKORP Project (BÖNNEMANN and BUTTKUS, 1990), were applied to  $30^\circ$  azimuth ranges of the macro bin from Figures 1 and 2. Due to the source-receiver geometry, these azimuth ranges are only very sparsely covered with traces, making the extraction of reflections very difficult. Therefore, it is impossible to apply conventional velocity analysis methods. With the  $\tau - p$  method time-distance gathers are transformed into the intercept-time ray-parameter domain. Reflection hyperbolae map into ellipses. NMO corrections can be calculated in the  $\tau - p$  domain using the equation of the ellipse and the correct NMO velocities (Figure 3).

Regarding deep seismic studies the most important advantage of this method is provided by the compression of the whole shot record or CMP gather into a limited  $p$ -range. This effect, which can be considered as a first stack, becomes particularly effective for deep reflections. A second advantage of the  $\tau - p$  transform is the option to incorporate the hyperbolic velocity filter introduced by TATHAM et al. (1983), resulting in a drastic improvement of the data quality in the  $\tau - p$  domain. By this filter the mapping from the  $x - t$  domain to the  $\tau - p$  domain can be limited by a physically reasonable range of NMO velocities.

After the  $\tau - p$  transform, reflection hyperbolae from the bin-sorted data are mapped into ellipses. If no ellipses (or portions of them) are encountered, no reflections are present. In this case, the whole  $\tau - p$  gather is dominated by noise generated linear elements and no velocity information can be deduced. Figure 4 is an example for a  $\tau - p$  gather from an azimuth range without reflections, instead of ellipses straight lines are visible ( $30^\circ - 90^\circ$ ). Only between  $30$  and  $60^\circ$  against the inline direction (east-west) the corresponding  $\tau - p$  gather shows reflection ellipses between 0 and 6 s two-way traveltime (Figure 5). Due to the limited offset range of the data and the relatively wide velocity pass band of the hyperbolic velocity filter, reflections map only into the beginning of ellipses (small  $p$ -values, see Figure 3). The rest of the  $\tau - p$  gather is still dominated by straight lines. The NMO velocity as a function of two-way traveltime (Figure 6), was estimated from this data by elliptical correction in a range of constant velocities. The function graph shows a velocity reduction at about 2 s two-way traveltime. The deduction of interval velocities from NMO velocities requires the correction of 3D effects, i.e. the knowledge of dip angle and strike direction of the reflector planes. This is especially necessary in crystalline environment with mainly steep reflectors. For the extraction of these parameters, the NMO velocity has to be estimated in at least three independent azimuth

ranges. Here, the data enabled the estimation of NMO velocities in just one azimuth range. Thus the computation of interval velocities was not possible.

### Directional Dependency of the Velocities at the Top of the Crystalline

The velocities of the direct waves depend on azimuth, as shown in Figure 7 a) for a macro bin at the KTB site. The mean value is 5400 m/s. The maximum velocity exists for an angle of approximately 40° against inline direction, i.e. east-west. Changes in lithology and/or anisotropy may be one cause for the azimuthal dependency of the velocities. Velocities of the refractor at the base of the weathering zone are used to eliminate lithology effects (LENGELING, 1991). These refractor velocities result from the evaluation of first breaks in the 3D data and from short refraction lines carried out to determine static corrections and refer mainly to the inline direction. This two-dimensional data set allows the determination of traveltimes and average refractor velocities for defined source-receiver locations. Figure 7 b) displays the average refractor velocities for source and receiver located on a circle with a diameter of 8000 m, centered around the KTB site. The 40° angle for the maximum velocity corresponds to the direction of the maximum derived from the ESP measurements.

The next step is the correction of the measured ESP traveltimes  $t_{\text{ESP}}$  to eliminate the effects of lithology along the ray path. To this traveltimes, static corrections has been applied. Due to the applied method of corrections, in the case of no anisotropy the whole raypath of the direct waves should be completely explained by the traveltime  $t_{\text{Ref}}$ , computed from the refractor velocities by

$$t_{\text{Ref}} = \sum_{i=1}^N \frac{\Delta x_i}{v_{\text{Ref},i}}$$

with the corresponding source-receiver distance

$$x = \sum_{i=1}^N \Delta x_i.$$

$\Delta x_i$  is a segment along the ray and  $v_{\text{Ref},i}$  is the refractor velocity for this segment.

Residuals  $\Delta t$  between  $t_{\text{ESP}}$  and  $t_{\text{Ref}}$  are hints for anisotropy:

$$t_{\text{ESP}} = t_{\text{Ref}} + \Delta t.$$

To make  $t_{\text{ESP}}$  independant from lithology and consequently independant from azimuth,  $t_{\text{Ref}}$  is substituted by the lithology and azimuth independent

$t_{\text{Ref},c} = x/v_c$  with  $v_c = 5400$  m/s as mean velocity of the direct waves. This results in a new travel time of the direct waves,

$$t_{\text{ESP},c} = t_{\text{Ref},c} + \Delta t,$$

and a velocity

$$v_{\text{ESP},c} = \frac{x}{t_{\text{Ref},c} + \Delta t},$$

the azimuthal variation of which is only determined by the lithology independent  $\Delta t$ , containing however possible effects of anisotropy.

Even after this correction an azimuth dependency of the ESP-derived velocities is observed, as shown in Figure 7c). A least-mean-squares anisotropy-velocity ellipse was fitted to this data with  $18^\circ$  (WSW) as the direction of the maximum velocity and a velocity contrast of about 6%. Comparison with Figure 7a) shows, that only the  $40^\circ$ -maximum can be explained by lithological effects, whereas the minimum in the north-south direction (around  $120^\circ$ ) must obviously be explained by anisotropy. The main velocity axes show a  $60^\circ$  rotation relative to the seismic anisotropy in southern Germany, as derived from  $P_n$  measurements (BAMFORD, 1976). However, these axes correspond to the seismological results obtained by VINNIK et al. (1989) from *SKS* waves. It must be kept in mind, however, that we are dealing with completely different depth ranges. Therefore, it can be inferred that the particular anisotropy effects must have different causes.

Because of the good offset and azimuth coverage, the first breaks have been investigated for a velocity gradient at the top of the crystalline. Assuming a linear gradient, the travel times of the first breaks have been fitted to the travel time curve of diving waves (GAMBURZEW, 1965). After eliminating the angle dependency of the velocity caused by lithology and anisotropy, there was no evidence left for a velocity gradient at the top of the crystalline. Thus, the penetration depth of the direct waves is relative to the top of the crystalline zero.

## References

- BAMFORD, D., 1976. An Updated Time-Term Interpretation of  $P_n$  Data from Quarry Blasts and Explosions in Western Germany. In: *Explosion Seismology in Central Europe*, P. GIESE, C. PRODEHL, A. STEIN (eds.). Berlin, Heidelberg: Springer-Verlag, 215–220.
- BÖNNEMANN, C., BUTTKUS, B., 1990. Velocity Analysis of Deep Seismic Reflections in the  $p - \tau$  domain. Paper read at the 4th International Symposium on Deep Seismic Reflection Profiling of the Continental Lithosphere, Bayreuth/Germany.

- GAMBURZEW, G.A., 1965. Grundlagen seismischer Erkundung. *Verlag Otto Sagner, München, 430 pp.*
- LENGELING, R., 1991. Bewertung eines Inversionsverfahrens zur Berechnung statischer Korrekturen in der 3D-Seismik und seine Anwendung auf reflexionsseismische DEKORP-Messungen in der Oberpfalz 1989. *Dissertation, Universität Karlsruhe, 178 pp.*
- TATHAM, R.H., KEENEY, J.W., NOPONEN, I., 1983. Application of the  $\tau - p$  transform (slant-stack) in processing seismic reflection data. *Bull. Aust. Soc. Explor. Geophys.*, **14**, 163-172.
- VINNIK, L.P., KIND, R., KOSAREV, G.L., MAKAYEVA, L.I., 1989. Azimuthal Anisotropy in the Lithosphere from Observations of Long Period S-Waves. *Geophys. J. Int.*, **99**, 549-559.
- WIEDERHOLD, H., 1990. 3D-ESP-Experiment of the Integrated Seismics Oberpfalz 1989. In: *KTB-Report 90-6b* H.J. DÜRBAUM, REICHERT, C., BRAM, K. (eds.).

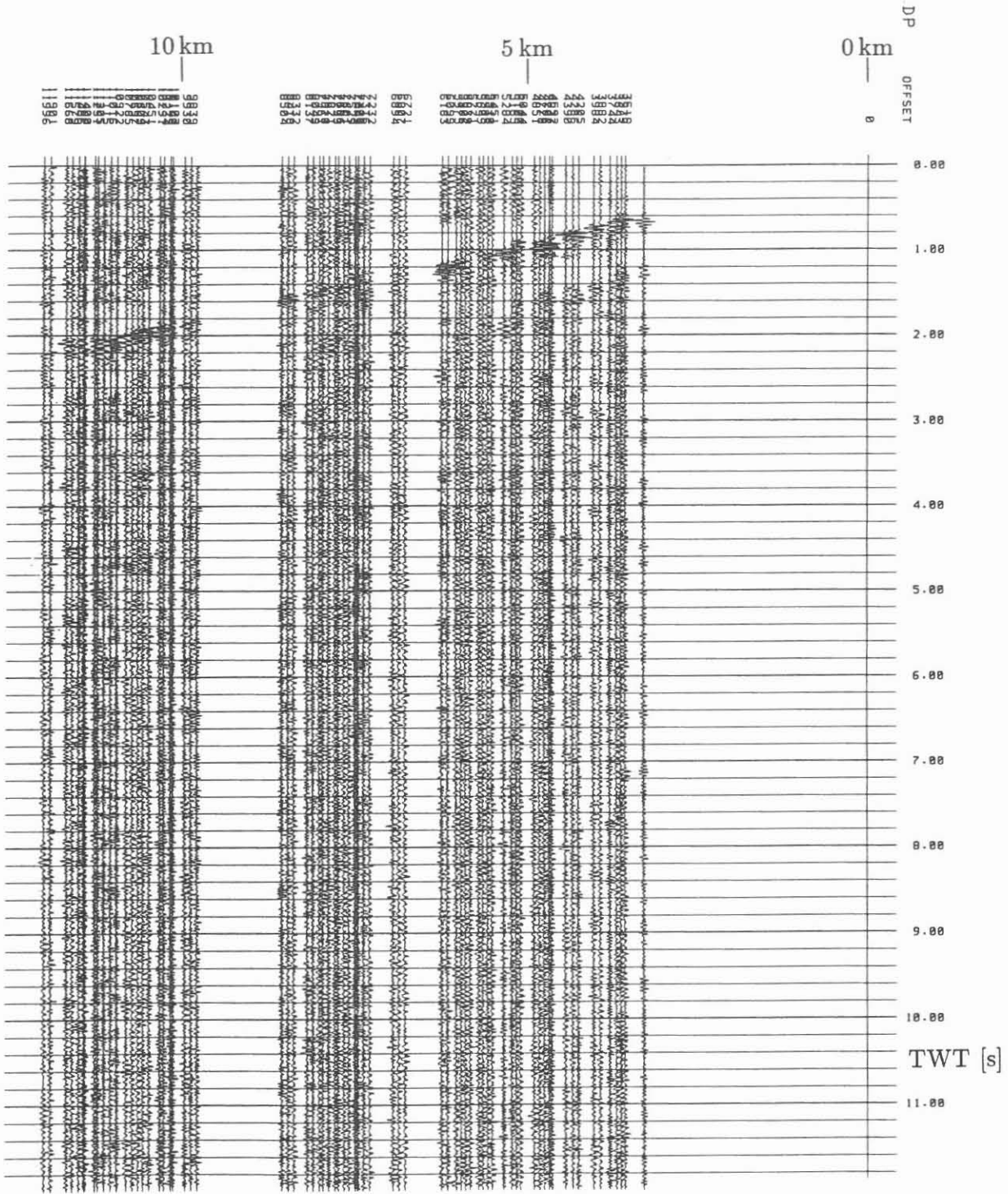


Figure 1: Offset dependent plot of the 3×3 macro bin around the KTB-location with all traces from the whole azimuth range and stacking of all traces in 50 m offset ranges, offset 0 - 12 km.



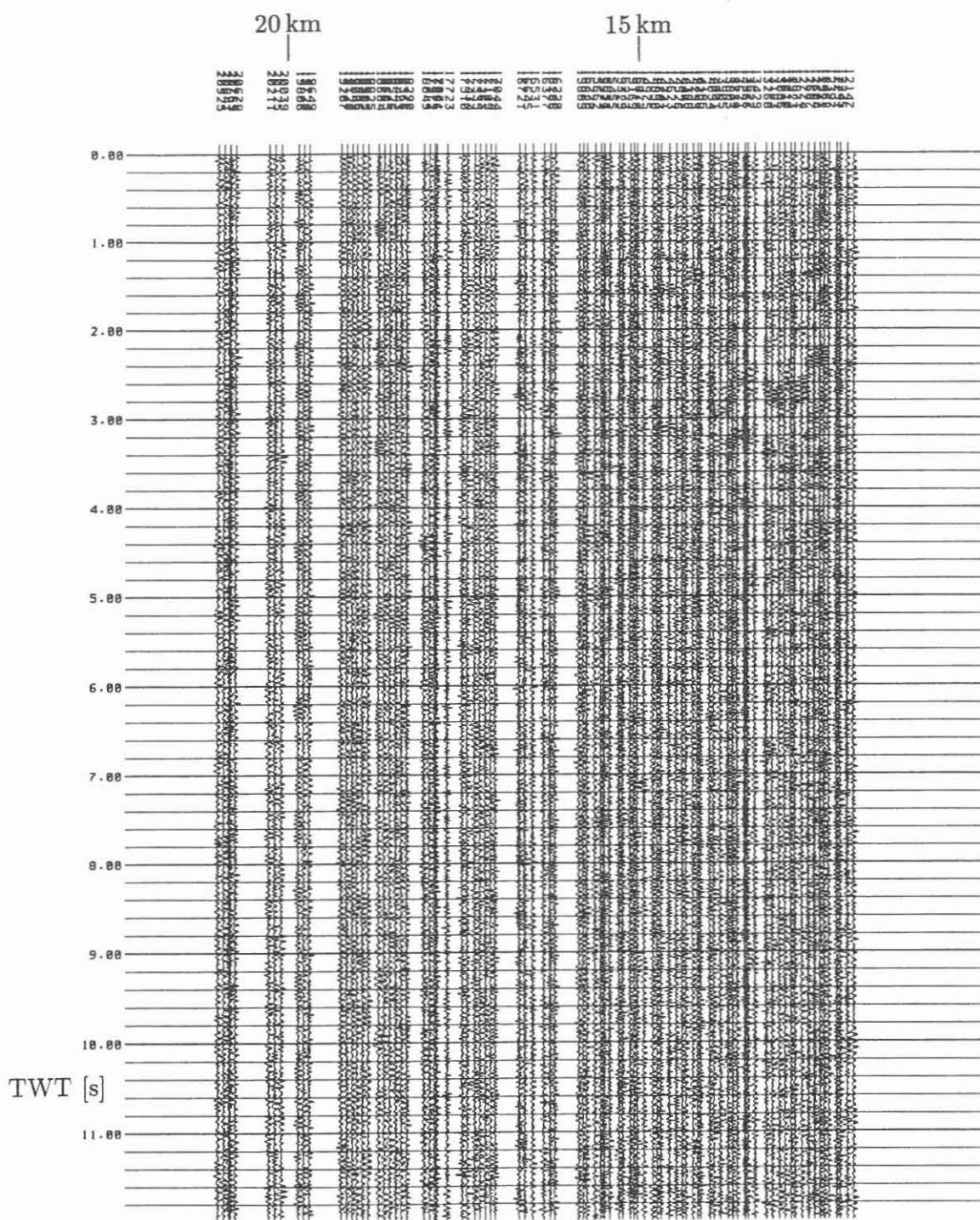
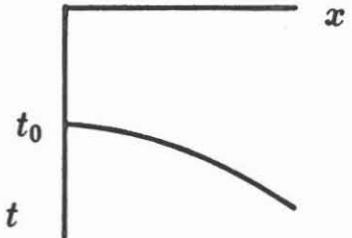
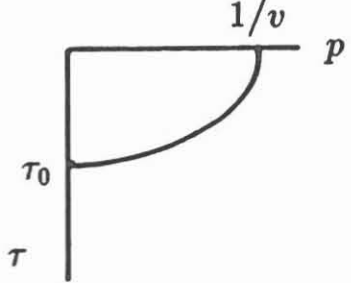
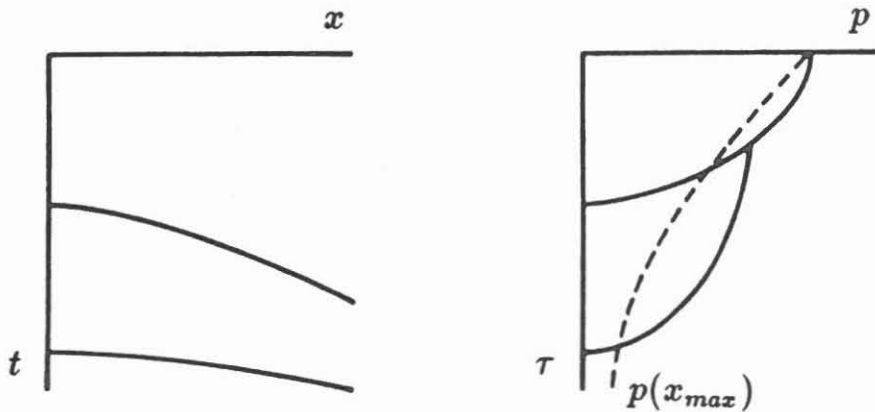


Figure 2: Offset dependent plot of the 3x3 macro bin around the KTB-location with all traces from the whole azimuth range and stacking of all traces in 50 m offset ranges, offset 12 - 24 km.

$x - t$ domain	$p - \tau$ domain
$t^2 = t_0^2 + \frac{x^2}{v^2}$  <p>NMO correction of hyperbolas</p>	$\tau^2 = \tau_0^2(1 - p^2v^2)$  <p>NMO correction of ellipses</p>

The maximum ray parameter  $p(x_{max})$  of a reflection ellipse, that can be measured, depends on the offset  $x_{max}$ ,  $t_0$ , and  $v$ :

$$p(x_{max}) = \frac{dt}{dx} \Big|_{x=x_{max}} = \frac{x_{max}}{v\sqrt{t_0^2v^2 + x_{max}^2}}$$



In the case of long traveltimes the hyperbolas are compressed to a few ray parameter traces.

Figure 3: Principle of the velocity analysis in the  $\tau - p$  domain.

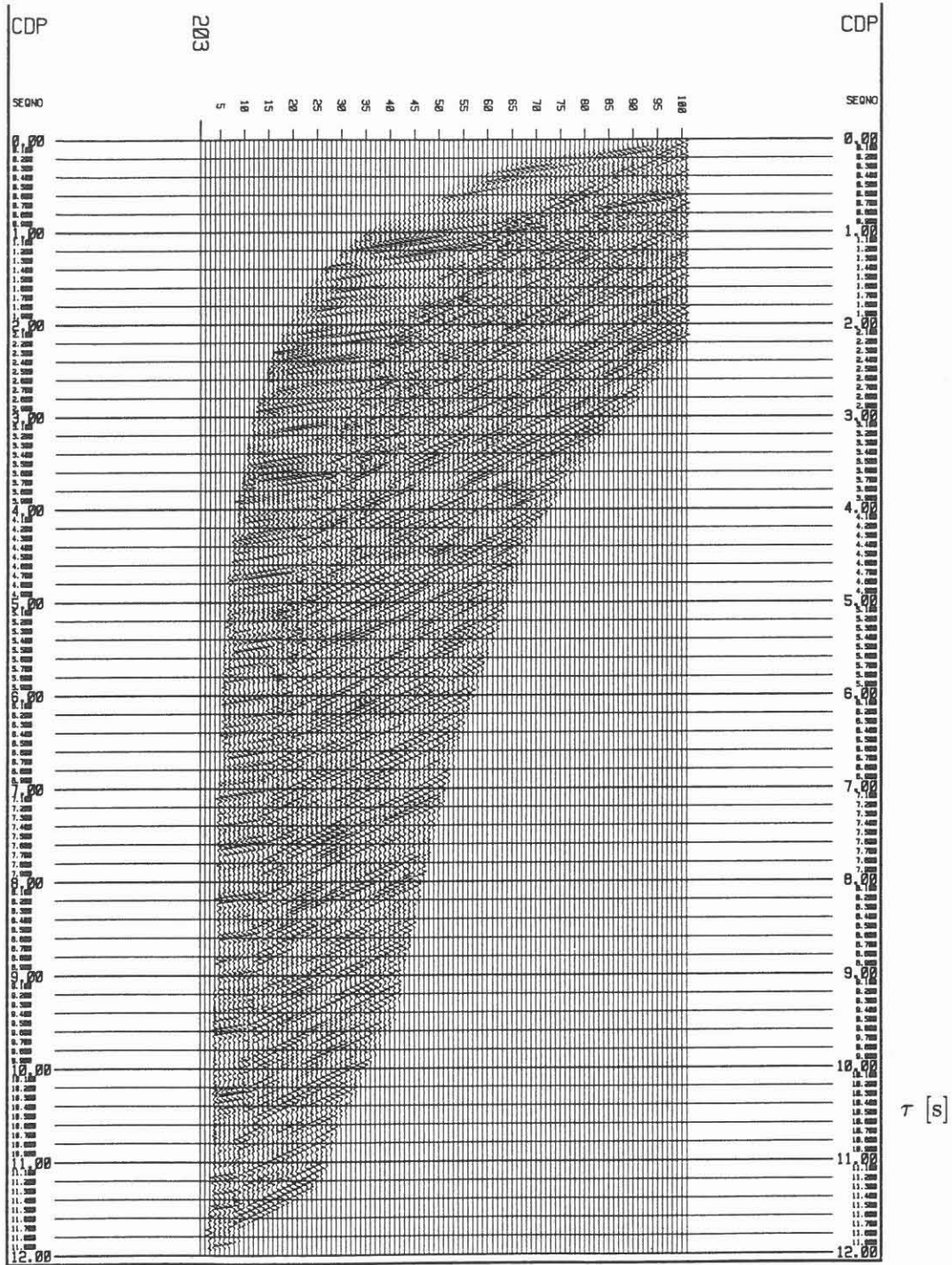


Figure 4:  $\tau - p$  transform of the data from Figure 1 and 2, restricted to  $60^\circ - 90^\circ$  azimuth range (SEQNO 1:  $p = 0 \mu\text{s}/\text{m}$ , SEQNO 100:  $p = 166 \mu\text{s}/\text{m}$ ).

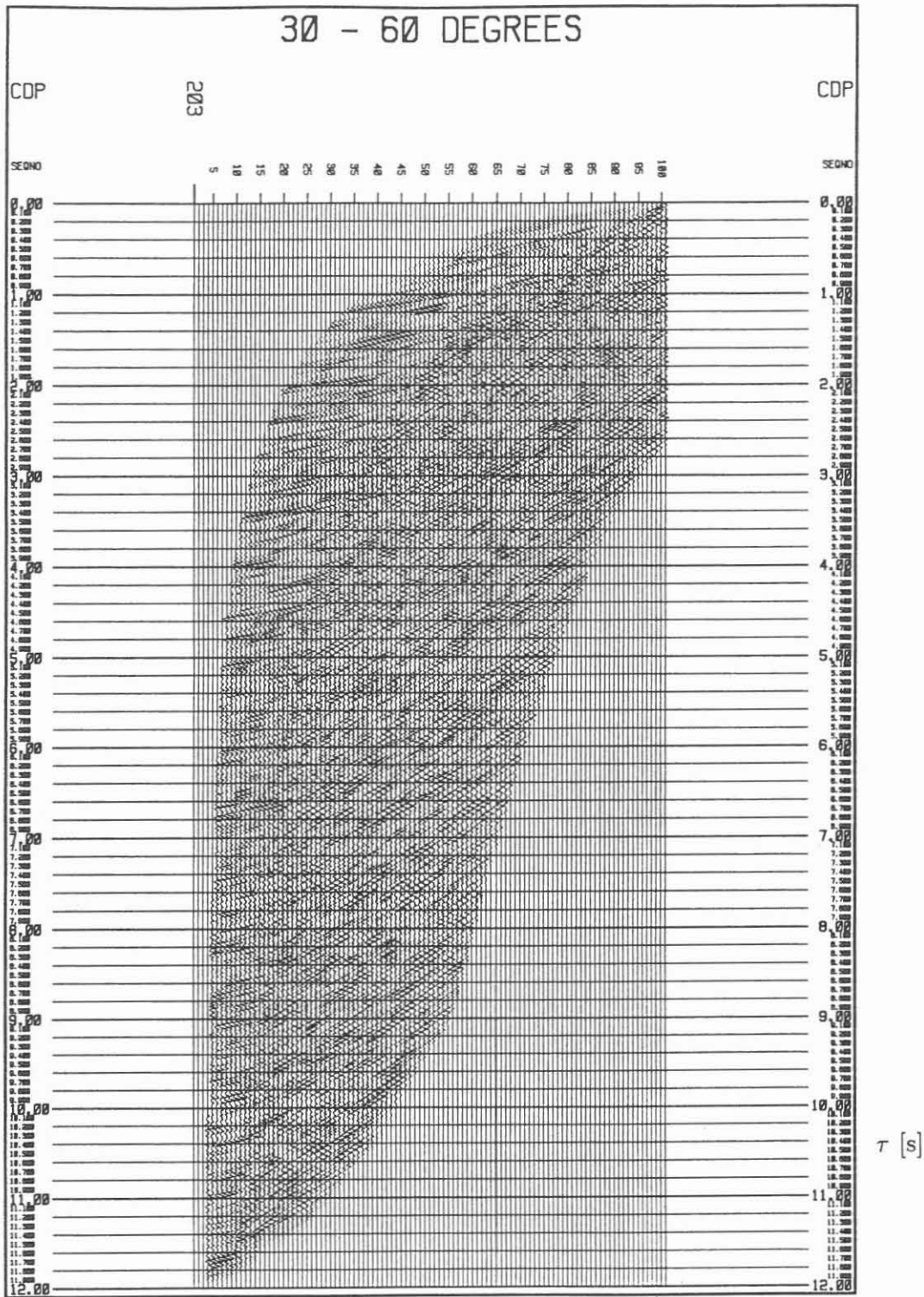


Figure 5:  $\tau - p$  transform of the data from Figure 1 and 2 restricted to 30° - 60° azimuth range (SEQNO 1:  $p = 0 \mu\text{s}/\text{m}$ , SEQNO 100:  $p = 166 \mu\text{s}/\text{m}$ ).

3D-ESP, KTB Location, 30° - 60°

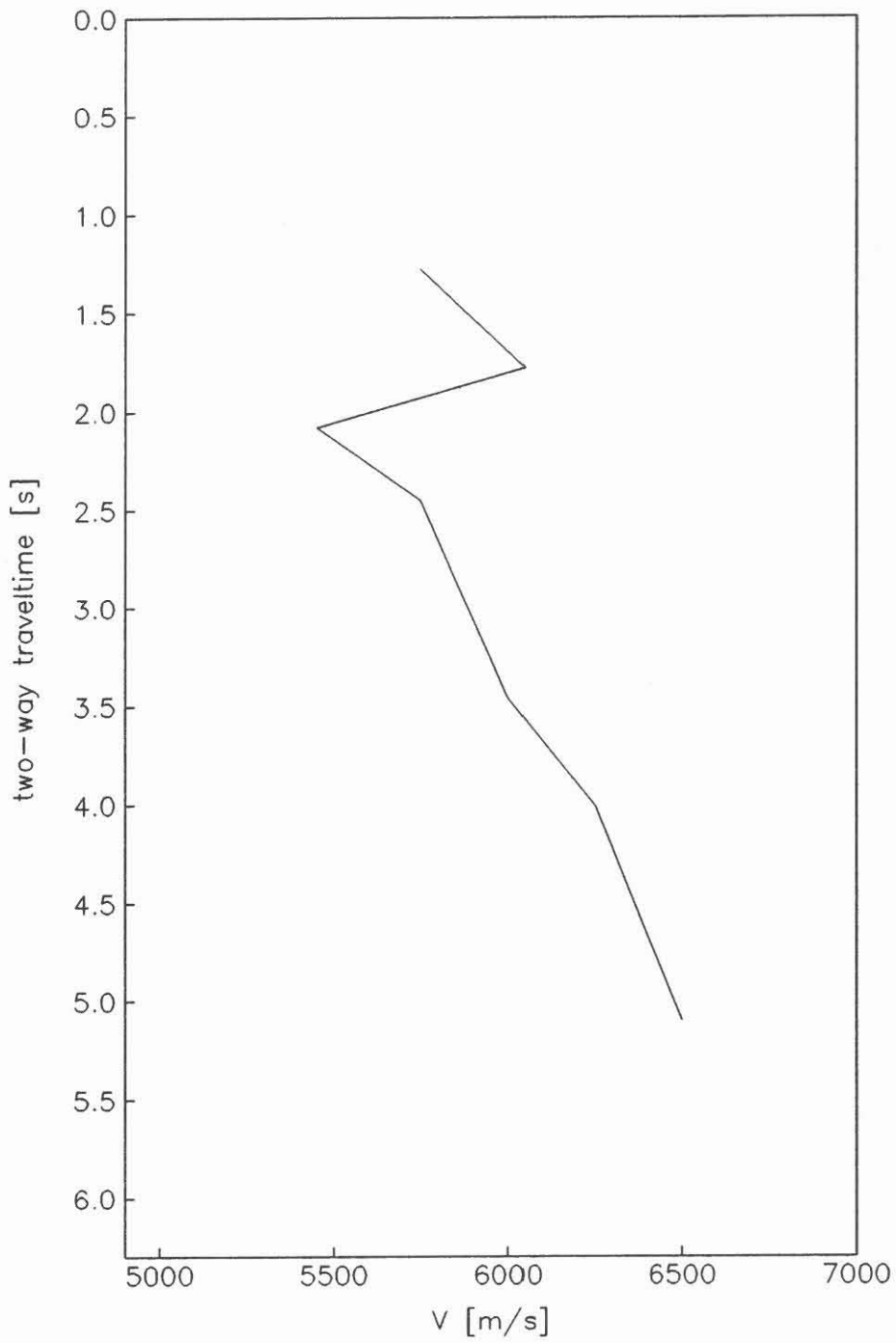


Figure 6: NMO velocity determined from 3-D ESP as a function of two-way traveltimes for the azimuth range of 30° - 60°.

0 - 12000 m

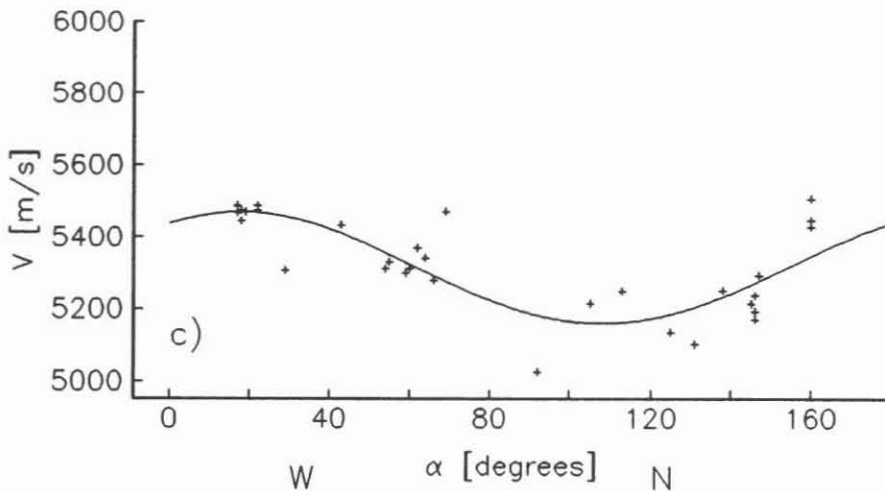
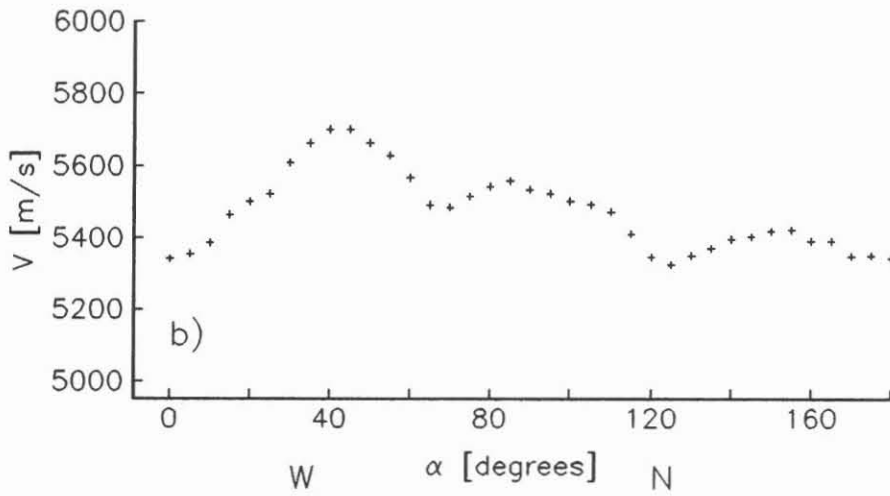
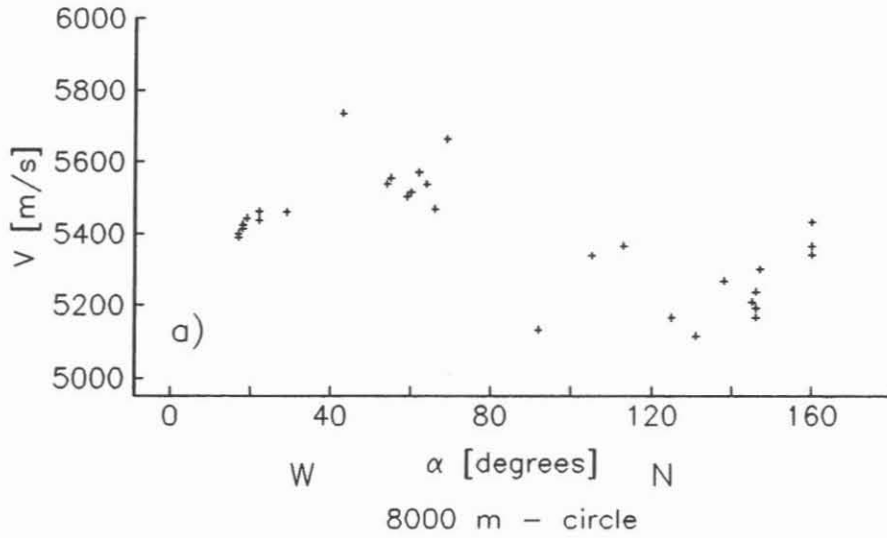


Figure 7: a) Velocity of the direct waves as a function of azimuth;  
b) average refractor velocity for a circle with a diameter of 8000 m around the KTB site;  
c) velocity of the direct waves after correction for varying refractor velocities, i.e. setting the refractor velocities to a constant value; the RMS-fitted anisotropy function is included (values of the largest and smallest velocity axis: 5470 and 5160 m/s, respectively).

**Results of the ISO'89 experiment "Durchschallung": Recording of the vibrator sweeps of the 3D-seismics in the KTB borehole**

Nils Martini, Manfred Stiller

Abstract

The determination of 3D-static corrections usually is possible only with the exact knowledge of thickness and velocity of the superficial layers. In order to determine these parameters extensive additional measurements are necessary, e.g. refraction seismics. These measurements can be reduced considerably if there is already a borehole in the survey area; the shots generated for the seismic survey can be recorded with a borehole geophone chain. The direct traveltimes determined from these records are lying on a 2nd-order plane (ideally a hyperboloid). If these traveltimes are influenced by e.g. differences in the elevations of the source location or velocity inhomogeneities, the first arrival traveltimes scatter around such a hyperboloid. The static corrections can be determined from the difference between the measured traveltime and the ideal hyperboloid. Further measurements are not required, because a precise knowledge of the parameters of the weathered layer is not necessary. In the following a method is presented (developed by Albrecht (1991) and Teichert (1991)) to determine the theoretical hyperboloid.

Another method, described at the end of this report, is the determination of average velocities from picked and corrected first arrival traveltimes.

Authors' address: DEKORP Processing Center, Institut für Geophysik der Technischen Universität Clausthal, Arnold-Sommerfeld-Str. 1, D-3392 Clausthal-Zellerfeld

Theory

If there is a geophone within a borehole in a depth  $z_e$ , the travel-time  $t_i$  from the source location  $(x_i, y_i)$  to the geophone yields

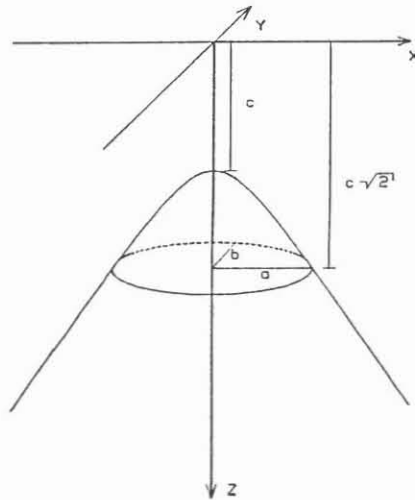
$$t_i = \frac{1}{V} \sqrt{x_i^2 + y_i^2 + z_e^2}$$

with  $V$  as velocity in an isotropic homogeneous halfspace. This equation describes a hyperboloid, which can be represented generally as

$$b_{11} \cdot x^2 + b_{22} \cdot y^2 + b_{33} \cdot z^2 + 2 b_{12} \cdot x y + 2 b_{13} \cdot x z + 2 b_{23} \cdot y z + 2 b_1 \cdot x + 2 b_2 \cdot y + 2 b_3 \cdot z = 0$$

or in another form

$$\frac{c^2}{a^2} x^2 + \frac{c^2}{b^2} y^2 + c^2 = z^2$$



Subsequently, the theoretical travelttime  $t_{i, theor}$  of the  $i$ -th source results in the following expression

$$t_{i, theor}^2 = a_1 \cdot x^2 + a_2 \cdot y^2 + a_3 \cdot x y + a_4 \cdot x + a_5 \cdot y + a_6$$

in which the coefficients  $a_i$  include the constants  $a, b, c$ ; in addition, displacements and torsions of the coordinate system are taken into account. To compute the coefficients  $a_1$  through  $a_6$  the real traveltimes  $t$  have to be determined precisely from the first arri-



vals; a suitable method is described already by Albrecht and Teichert (1990).

The measured traveltimes are not lying on such a hyperboloid, but depart of it, because of strong velocity inhomogeneities within the weathered layer and topographic influences depending on the source location. It is the aim to calculate the coefficients  $a_1$  through  $a_6$  of that hyperboloid, which results from the theoretical traveltime. Thus, six unknown variables are to be derived from  $n$  equations ( $n > 6$ ), which leads to the following system of equations

$$\begin{vmatrix} x_1^2 & y_1^2 & x_1 y_1 & x_1 & y_1 & 1 \\ x_2^2 & y_2^2 & x_2 y_2 & x_2 & y_2 & 1 \\ \vdots & & & & & \vdots \\ \vdots & & & & & \vdots \\ x_n^2 & y_n^2 & x_n y_n & x_n & y_n & 1 \end{vmatrix} \cdot \begin{vmatrix} a_1 \\ \vdots \\ a_6 \end{vmatrix} = \begin{vmatrix} t_1^2 \\ t_2^2 \\ \vdots \\ t_n^2 \end{vmatrix}$$

(Albrecht, 1991).

Such an overdetermined system of equations yields generally inconsistent solutions. With the least-mean-square solution the hyperboloid is determined, for that the sum of all distances between measured values and the theoretical hyperboloid becomes a minimum

$$\sum_{i=1}^n (t_i - t_{i, \text{theor}})^2 = \min$$

with  $t_i$  as the measured traveltime of the source location  $(x_i, y_i)$ . The overdetermined system of equations can be solved with the so-called Householder algorithm (Teichert, 1991). The difference between the measured traveltime and the traveltime on the hyperboloid yields the value of the static correction, in which the angle of incidence  $\alpha$  still has to be taken into account

$$\Delta t = (t_i - t_{i, \text{theor}}) \cdot \cos \alpha$$

## Results

The advantage of this method is the determination of all static corrections in the whole survey area with a single borehole geophone, whereas other methods require extensive additional measurements. A disadvantage is, that not only the weathered layer affects the traveltime, but also all further layers. The effect of refraction cannot be neglected, because there are large angles of refraction at the boundary between weathered layer and consolidated layer, due to the almost very strong velocity contrasts. These disturbing influences should be as small as possible. Therefore, it is not efficient to determine only a single theoretical hyperboloid. It is more suitable to compute the traveltimes for smaller sections of the survey area, because then the influence of the refraction and the geological effects is not very important. The single planes of traveltime have to be combined in order to determine the static corrections for the whole survey area; this happens by means of weighting factors, not described further here. The subplanes are not allowed to be too small, because otherwise only short-wavy parts of static corrections can be derived; long-wavy parts of statics (e.g. spacious topography) are only to be determined with greater subplanes, but than the above-mentioned disturbing influences become noticeable.

The traveltimes on the theoretical hyperboloid and the values for the static corrections derived from this can be determined by a computer program developed by Albrecht (1991) and Teichert (1991). Only the coordinates and the ground level at the source location, the station number of the source and the corresponding traveltime of the first arrival have to be specified. As mentioned before, the most important task is the precise picking of the first arrivals. The size of the subplanes and the size of the areas of overlapping between the subplanes are to be fixed with the help of test series. The number of the traverses and vibrator points used respectively results from the size of the planes. In the examples shown here there are 3-11 traverses (9-41 vibrator points), thereby sizes of the planes from 1.6 km x 1.6 km to 8 km x 8 km follow with a distance between the traverses of 800 m .

Figure 1 shows the results for subplanes 1.6 km x 1.6 km (continuous line: static corrections of the experiment "Durchschallung"; vertical bars: static corrections of the contractor (PRAKLA)); the values disperse around zero, because only short-wavy statics can be recorded. In Figures 2 and 3 larger subplanes are used (Figure 2: 4.8 km x 4.8 km, 7 traverses x 25 vibrator points; Figure 3: 8 km x 8 km, 11 traverses x 41 vibrator points), long-wavy statics are clearly recognizable; the area of overlapping between the subplanes is 2 traverses and 5 vibrator points, respectively. The differences between the results with the smaller (Figure 2) and the larger (Figure 3) subplane are not relevant; slight differences exist, because some of the larger subplanes embrace both the sedimentary and the crystalline area of the survey area.

There were no good circumstances in order to test the computer program according to the complicated geological conditions (folded and steep structures) of the survey area. In this connection, especially the Franconian Line is to be mentioned. The traveltimes of the first arrivals are influenced not only by the upper "static layers", but also by the deeper sedimentary layers. There are, i.e. not the same conditions on the ray paths, what would be an assumption for this method. In addition, the signal-to-noise ratio was partly insufficient in the seismograms of the experiment "Durchschallung", therefore a precise picking of the first breaks was not possible in all records. All these interference factors may effect that the determined values for the static corrections are not directly comparable with the results of PRAKLA.

With this method, static corrections can be determined principally by the measurement of the traveltimes of the first arrivals at a borehole geophone. Under easier geological conditions in the consolidated layers, modeling calculations show very good results for determining static corrections. The interpretation is relatively easy. It consists of the picking of the first arrivals and the determination of the theoretical plane of traveltime. The expense of additional conventional measurements can be reduced, if a borehole already exists in a survey area.

At present another attempt is made with regard to the 3D-data processing. With the measurements of the experiment "Durchschallung"

average velocities between surface and borehole geophone shall be determined.

As mentioned above it was presumed for the determination of static corrections, that differences between measured and theoretical traveltimes are caused mainly by lateral inhomogeneities in the weathered layers and by varying ground levels of the source locations; inhomogeneities, anisotropies and various geological structures within the consolidated layers are assumed negligible or symmetrical to the borehole. In contrast to these assumptions it has to be assumed, that such effects in the survey area still influence the traveltimes. A hint at the correctness of these assumptions derives already from the relatively large differences between the static corrections of the experiment "Durchschallung" and the static corrections of PRAKLA.

Now an attempt is made, to determine a field of average velocities from traveltimes of first arrivals for different offsets and azimuths. For that purpose, the static corrections found out by PRAKLA are assumed correct and are applied to the picked traveltimes of the experiment "Durchschallung", in order to avoid near-surface influences on the traveltimes and to introduce a uniform datum plane (500 m). The length of the ray paths can be determined easily from the known depth of the geophone and the source locations. Together with the corrected traveltimes average velocities can be calculated. The deflection of the vertical plumbline of the borehole and the distance from the datum plane were taken into consideration. Figures 4 and 5 show the picked first arrival traveltimes for each source location after spatial interpolation as isoline maps for both depths of geophones. A homogeneous medium would yield concentric circles for the traveltimes in the isoline map. Especially anisotropies should appear as deformations of the circles. A slight tendency to this is noticeable. However, for such an interpretation the picked traveltimes have to be verified, because single values are eventually incorrect, which appear as "islands" and strong inlets in the isolines. If such mispicks are removed, better smoothing functions can be applied, whereby the interpretation becomes more easily. Now an average velocity for each source location can be calculated from the first arrival traveltimes and from the length of the respective ray path. These velocities can also be figured in isoline maps (Figure 6: depth of geophone 3420 m; Figure

7: 3220 m). In both figures the Franconian Line is clearly perceptible by a strong jump of the average velocities. In addition the velocities decrease slightly towards north-east with increasing distance from the borehole. The mentioned sources of errors should be taken into account at the interpretation of these results. As already at the determination of the static corrections the influence of the refraction is to estimate hardly, especially at the boundary between weathered layer and consolidated layers. It is possible, that the actual rays paths are somewhat longer than the pure geometrical ray paths, thus higher velocities would follow. A specified interpretation of the results will follow. It depends on the precision of the static corrections, the measurement of the ground level and the picking of the first arrival traveltimes, in what respect slight anomalies of velocities are interpretable.

#### References

Albrecht, J., Teichert, D., 1990: Calculations of static corrections from seismic borehole records using the vibrator signals of the 3D seismic reflection survey within ISO89. KTB-report 90-6b, pp. 57-64

Albrecht, J., 1991: Beschreibung der Meßanordnung und der Datenbearbeitung bei der Bestimmung statischer Korrekturen aus dem Durchschallungsexperiment ISO'89. Diplomarbeit, TU Clausthal

Teichert, D., 1991: Entwicklung, Überprüfung und Anwendung eines Programmes zur Bestimmung statischer Korrekturen aus den Daten des Durchschallungsexperimentes der ISO'89. Diplomarbeit, TU Clausthal

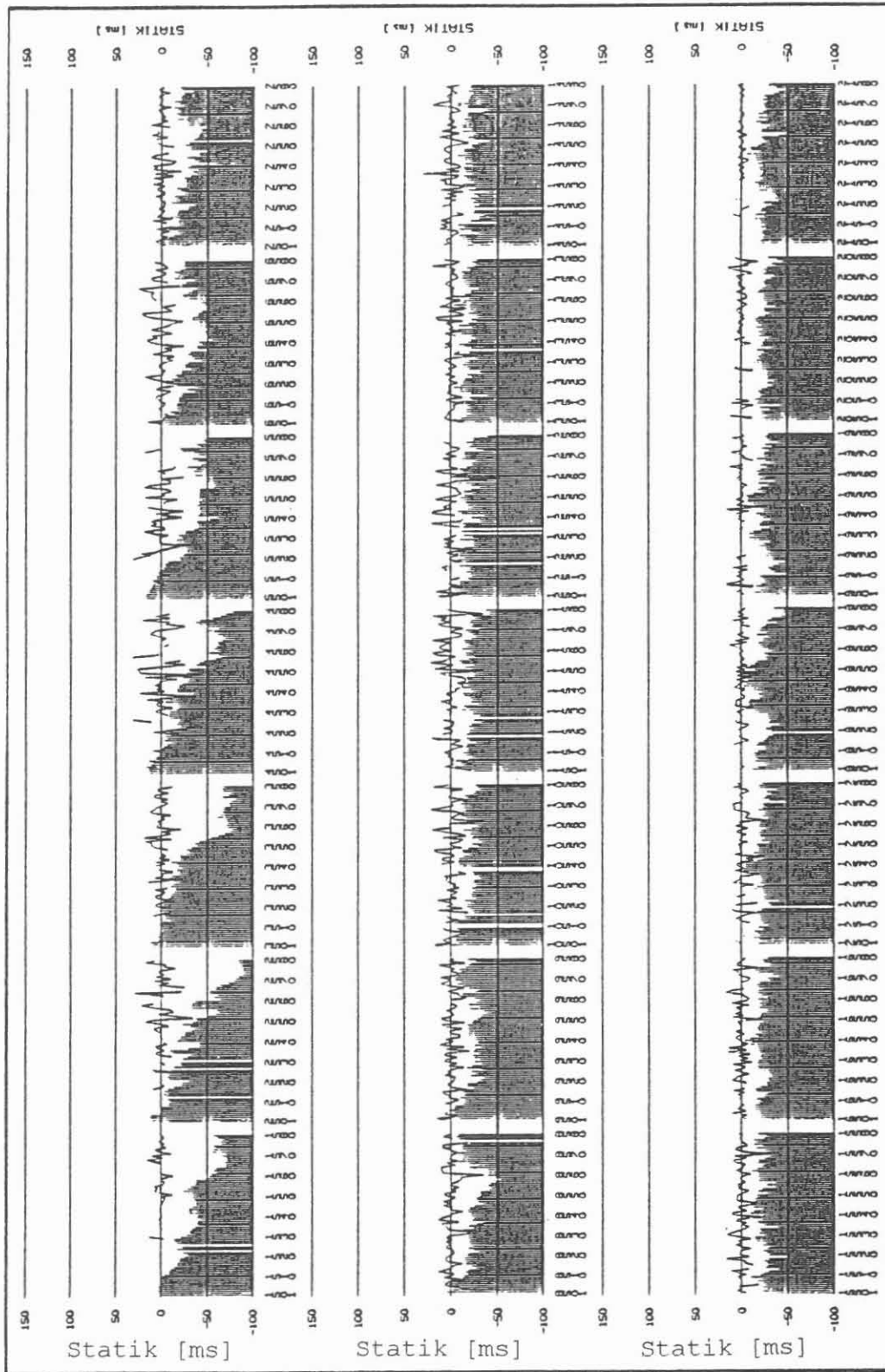


Figure 1: Static corrections of vibrator points of swath 1 and 3 (continuous lines; vertical bars: statics of PRAKLA); subplanes 3 traverses x 9 vibrator points

(Albrecht, 1991)

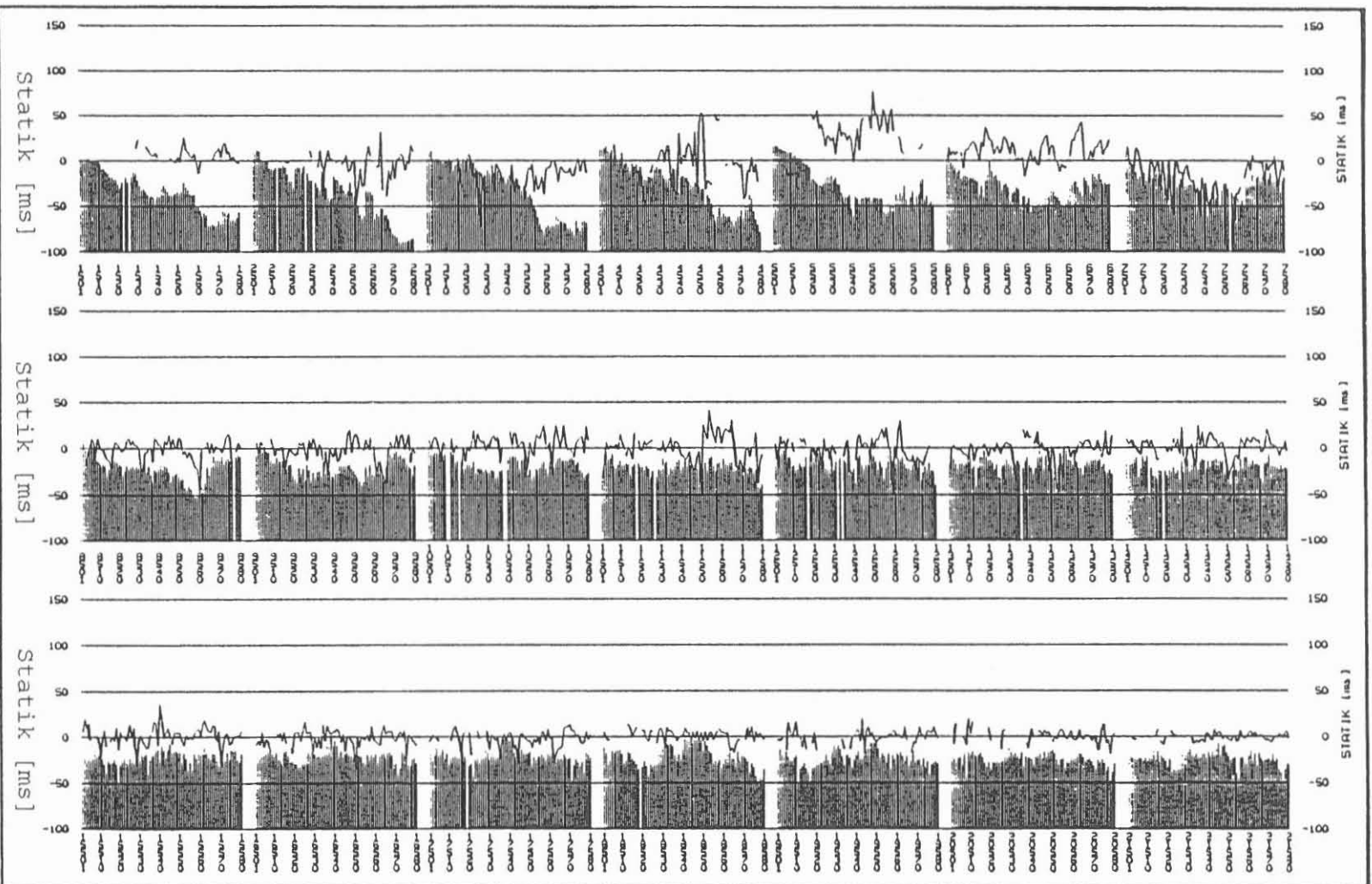


Figure 2: Static corrections of vibrator points of swath 1 and 3 (continuous lines; vertical bars: statics of PRAKLA); subplanes 7 traverses x 25 vibrator points

(Albrecht, 1991)

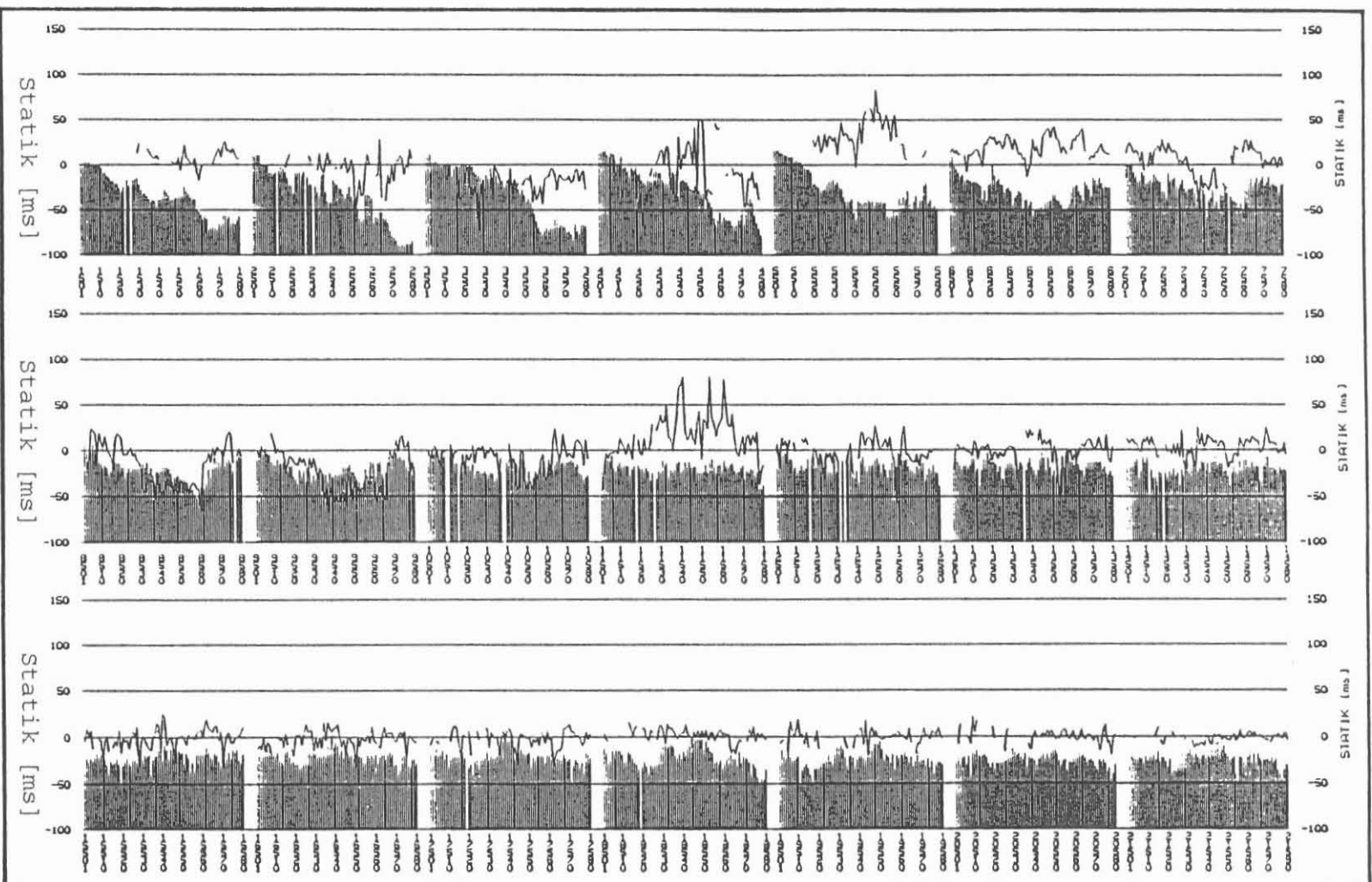


Figure 3: Static corrections of vibrator points of swath 1 and 3 (continuous lines; vertical bars: statics of PRAKIA); subplanes 11 traverses x 41 vibrator points

(Albrecht, 1991)



LAUFZEIT13, Z=3420m, XBIN=190..541, YBIN=163..484

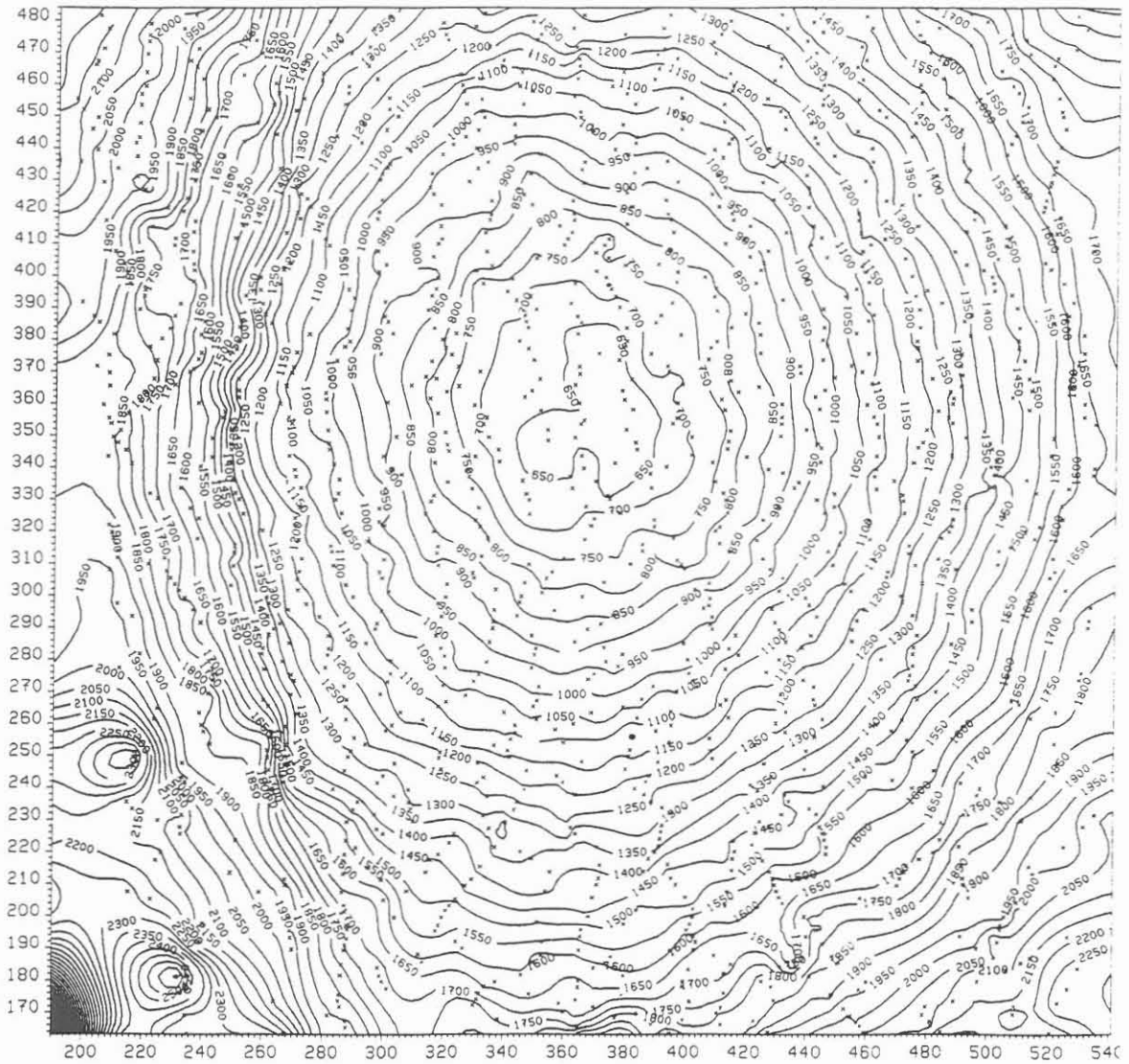


Figure 4: Isoline map of the traveltimes; depth of geophone 3420 m

LF0F2E.124; LF022011; ABIN=190.1071; IDIN=241.1002

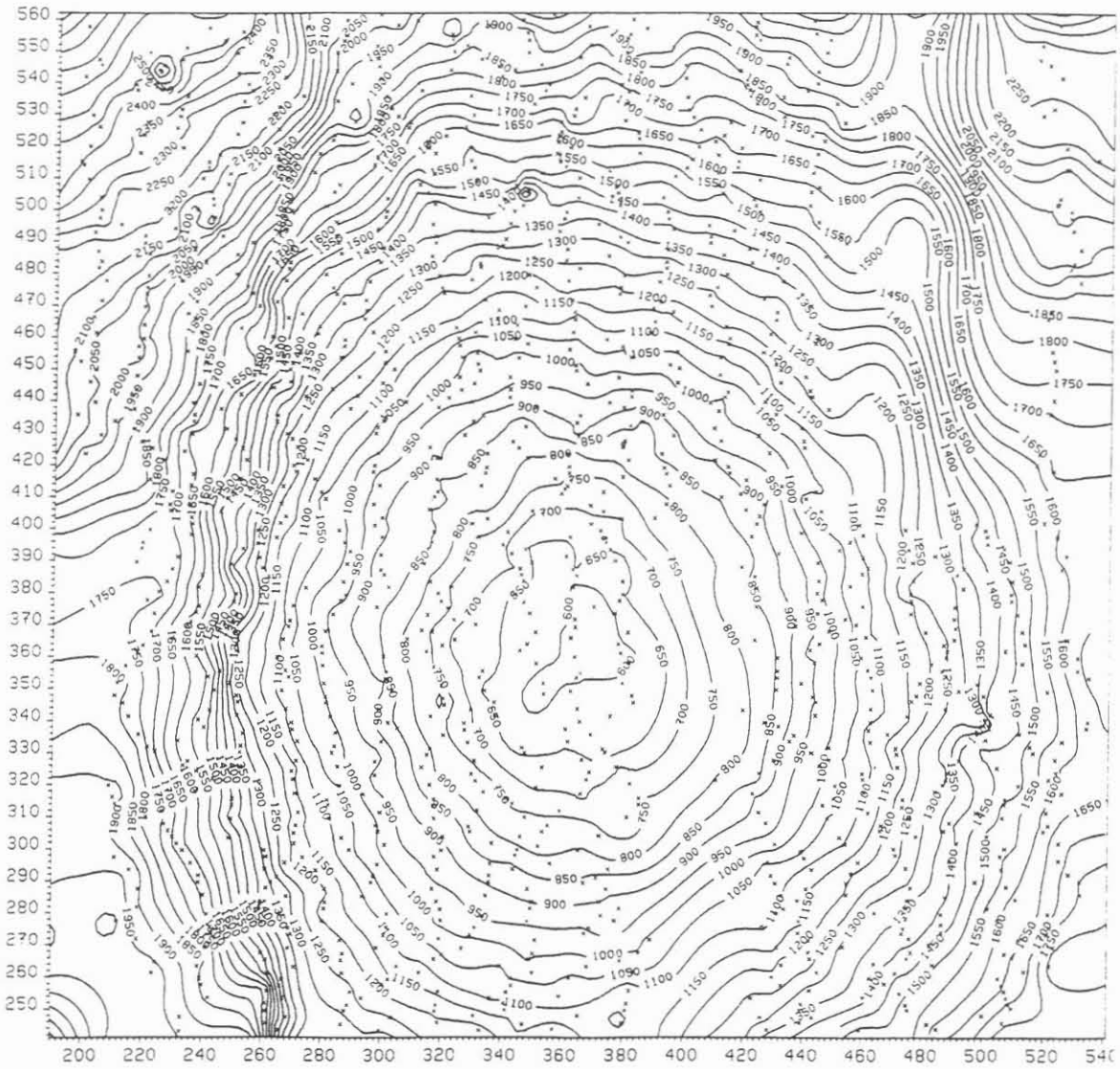


Figure 5: Isoline map of the traveltimes; depth of geophone 3220 m

GEBCOHW13, Z=3420m, XBIN=190..541, YBIN=163..484

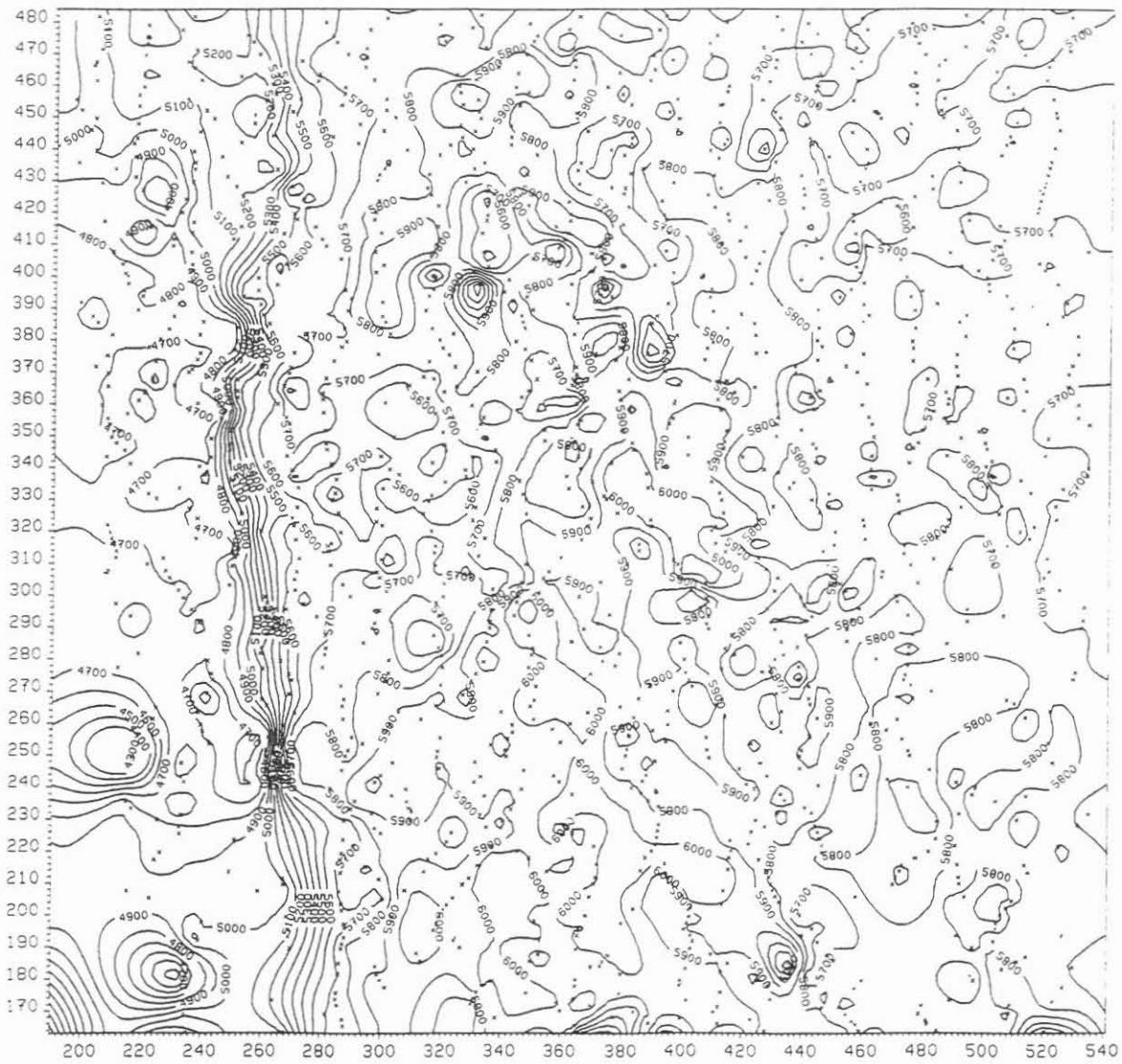


Figure 6: Isoline map of the average velocities; depth of geophone 3420 m

GESCHW24, Z=3220m, XBIN=190..541, YBIN=241..562

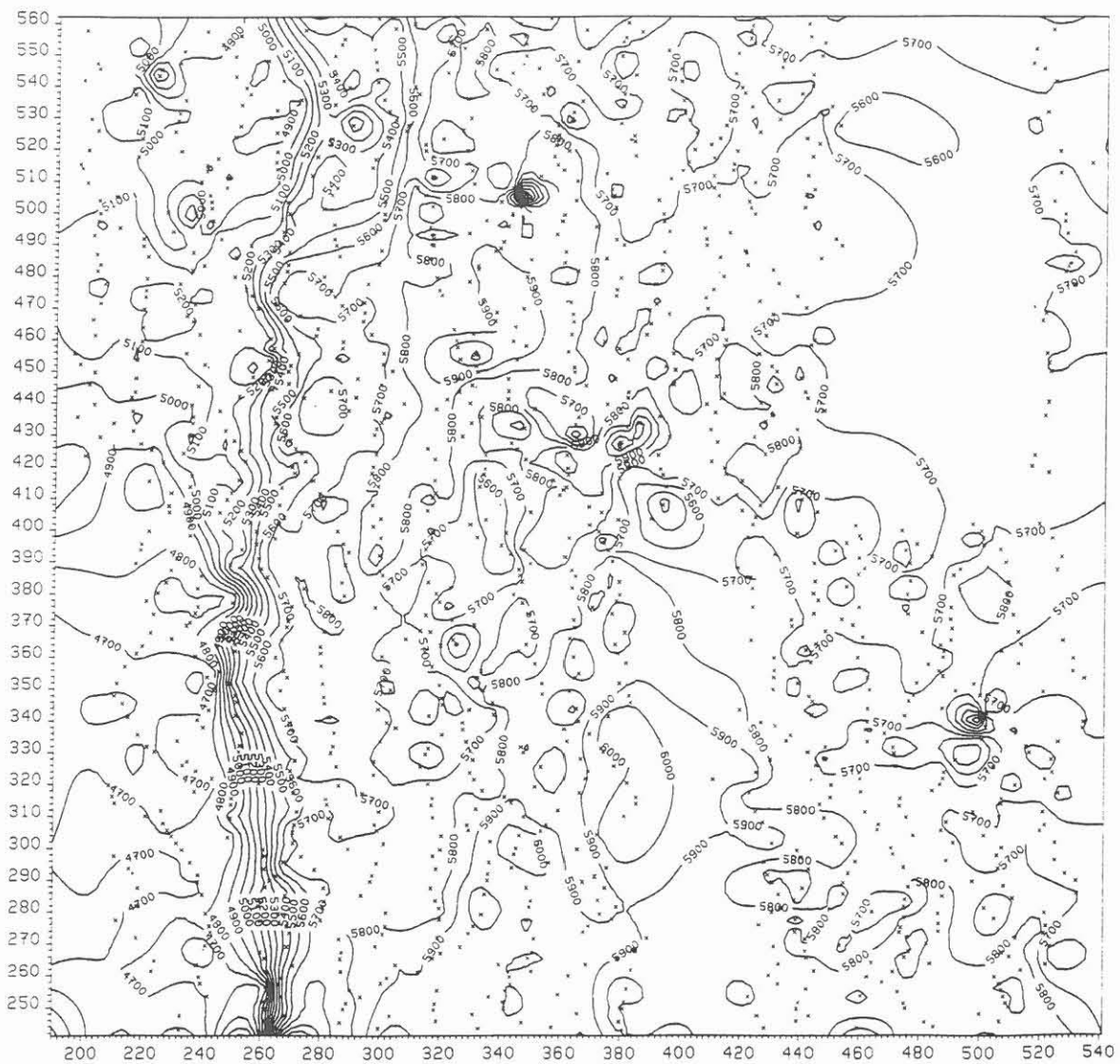


Figure 7: Isoline map of the average velocities; depth of geophone 3220 m

## FLUID/GAS INDICATIONS IN 8 KM DEPTH BENEATH THE KTB AND ROCK ANISOTROPY FROM SHEAR-WAVE REFLECTION SURVEYS

Ewald Lüschen and Ulrich Werner

### *Abstract*

A reflection survey using shear-wave sources and 3-component receivers has been performed on two orthogonal lines across the KTB-deep drilling site in the Oberpfalz area (Bohemian crystalline Massif). A combination of surface-consistent statics and automatic residual statics proved to be of crucial importance to obtain good coherency and a good signal/noise ratio for deep crustal shear-wave reflections after CMP-stacking.

Direct comparisons with previously processed standard P-wave CMP stack sections exhibit deep structures ('Erbendorf-body', 10-12 km depth) which reflect equally strong in P- and S-waves indicating normal lithological variations. In contrast to this, in 8 km depth a bright reflection is seen only on the P-wave section. It is absent on the S-wave section. This behaviour can be explained by two alternative geological models. The first one is an accumulation of fluid or gas under still unknown reservoir conditions. The alternative, purely compositional model is a crystalline body with an anomalously low  $V_p/V_s$ -ratio. A rock mass with a high amount of quartz could also produce impedance contrasts for P-waves but not for S-waves.

Pronounced S-wave splitting, observed for the 'Erbendorf'-reflections, indicates that the symmetry system of the rock anisotropy is rotated by 90 degrees below 3 km against the one which was detected above 3 km by S-wave vertical seismic profiles.

### **Introduction**

Evidence for the possible presence of a fluid/gas reservoir under the KTB (German Continental Deep Drilling Project) Hauptbohrung at a depth of approx. 8 km is provided in this paper. Lithological models and depth prediction will be tested by drilling and direct probing in early 1993. In-situ testing of the interpretation of geophysical observations obtained at the surface is one of the major goals of deep continental drilling.

-----  
Authors' address: Geophysical Institute, University of Karlsruhe, Hertzstrasse 16,  
D-7500 Karlsruhe 21, Germany

Lithological and structural problems in deep seismic exploration can be addressed advantageously by the integrated use of compressional (P) and shear-wave (S) data, as indicated by numerous laboratory and field studies. Although often considered as noise in standard P-wave surveys, the S-waves, if appropriately generated and recorded, hold the promise to obtain additional information on rock anisotropy (e.g. Helbig and Mesdag, 1982; Crampin, 1987) by means of their polarization and on lithology by means of the Vp/Vs-ratio (Pickett, 1963; Tatham, 1982). The latter effect is in the context of porous hydrocarbon reservoirs caused by the fact that the effective shear modulus ( $\mu$ ) of the rock is less sensitive to the fluid content of the pores than the effective bulk modulus ( $k$ ), resulting in a higher Vp/Vs ratio than in dry rock. Laboratory experiments on rock samples show that the Vp/Vs ratio is a good indicator of the quartz content (Kern, 1982) or the porosity of a sedimentary medium (e.g. Tatham, 1982).

Several industrial reflection surveys with shear-wave sources and horizontally orientated receivers were successful in identifying 'bright spots' as caused by gas reservoirs (Ensley, 1984; Garotta, 1985; Frasier and Winterstein, 1990; Tatham and McCormack, 1991), which were verified by exploration drilling. Such studies motivated us to apply controlled shear-wave experiments also in deep crustal studies. Pilot studies, focussed on the strongly reflective lower crust in SW-Germany (Lüschen et al., 1990a) and in northern England (Ward et al., 1991), showed that significant shear-wave signal/noise ratio can be achieved for deep reflections using horizontal vibrators and even single explosive sources. Shear-wave generation from explosive sources in boreholes can be caused by mode conversion from P- to S-waves at the free surface (Fertig, 1984) or at heterogeneities adjacent to the source. Horizontal vibrators offer a better control on the source polarization.

After completing the pilot hole of the KTB-project at 4000 m depth in 1989, integrated P- and S-wave experiments were performed under the auspices of the DEKORP program (German Continental Seismic Reflection Program). First results of this program, consisting of 1) S-wave common midpoint reflection profiling (SCMP), 2) S-wave moving source profiling (S-MSP), 3) P- and S-wave multiple offset vertical seismic profiling (VSP), and 4) multiple azimuth S-wave observations (MASE), covering the same area where a DEKORP 3-D reflection survey was conducted, were published by Lüschen et al. (1990b, 1991). The S-wave VSPs revealed evidence for rock anisotropy by direct observation of S-wave splitting and orthogonal polarizations. This particular rock anisotropy is mainly related to the rock foliation showing preferred NW strike directions (particle motion of the fast S-wave phase) and subvertical dip from the surface to about 3 km depth. Its amount of approximately 10 % is in accordance with corresponding laboratory experiments on core samples.

The data quality of the reflection survey SCMP was hampered by insufficient static corrections at the very beginning of the CMP-processing, although the non-

stacked sourcepoint gathers immediately showed significant energy of deep reflections. The present paper describes the discovery of a 'bright spot'-phenomenon, a bright reflector present in the P-wave section, but absent in the S-wave section, after optimizing the S-wave static corrections. This may be indicative for a fluid or gas trap in porous or fractured crystalline rocks, located at approx. 8 km depth. It is expected to be drilled through until the beginning of 1993. Similar bright P-wave reflections in an otherwise transparent middle crust, i.e. the COCORP Surrency Bright Spot (Pratt et al., 1990) were subject for testing whether fluids are candidates for their explanation.

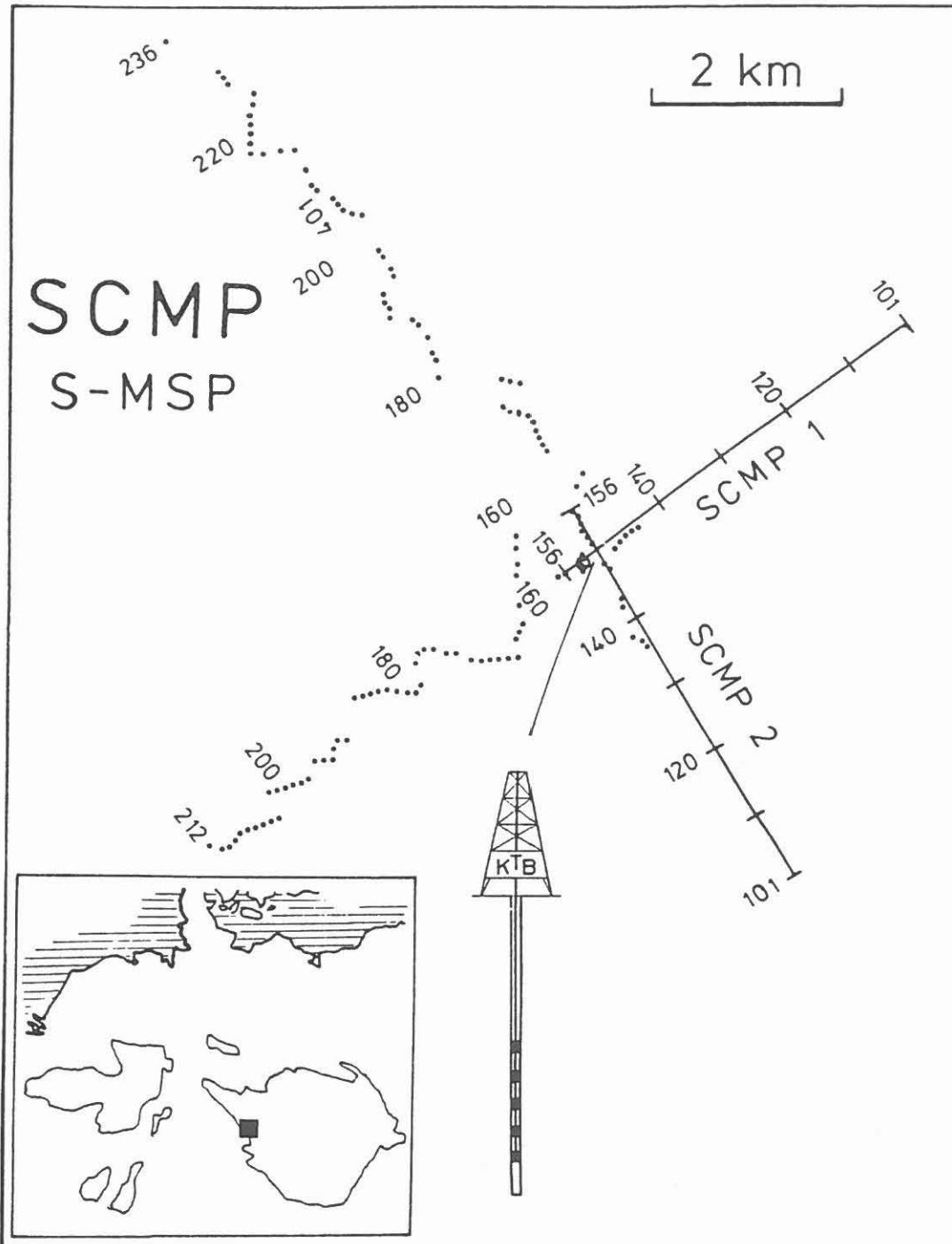
Apart from the lithological prediction, the precise location based on three-dimensional control by orthogonal surface profiles and a recent downward extension of the VSP to 6 km depth is a special incentive for looking ahead of the drillbit.

### **The Experiment: Data Acquisition**

The field configuration of the experiment was closely tied to a standard P-wave reflection survey conducted during the presite investigations in 1985 (DEKORP Research Group, 1988). Figure 1 shows the base map of the field configuration for the two orthogonal lines which have been described in more detail by Lüschen et al. (1990b, 1991). They are located normally (SCMP1) and parallelly (SCMP2) to the strike direction of the general geological trend, in particular the strike of the southwest border of the Bohemian crystalline massif (Franconian Line).

Both lines consisted of moving sources and a fixed 3-component receiver spread (56 stations, each with strings of 12 geophones for the vertical (Z), horizontal in-line (X) and horizontal cross-line (Y) component, in order to avoid frequent changes in geophone coupling and orientation. As the primary source for S-waves, two horizontal vibrators (Type VVCS, Prakla-Seismos, 170 kN Peak Force) were used. After a startup test, an upsweep of 9-43 Hz with 30 s length was used for vibrator control (with phase-locked force control). Recording was done with two DFS-V systems (168 channels) with 5-fold vertical stacking and two uncorrelated records for each vibratorpoint. The spacing of vibratorpoints as well as receiverpoints was 80 m.

Additionally, explosives were used for a check-shotpoint on each line, providing a shot-gather with the KTB location in the centre of its subground coverage. Receiver spread and vibrator sourcepoints were asymmetric in order to achieve the largest mean offset. This enables better velocity control for greater moveouts. More importantly, it also provided a better balance between the energy of the first arrivals and late reflections, which is of crucial importance when using the Vibroseis technique. The vibrator points were located along a crooked line.



**Fig. 1:** Field configuration of the SCMP experiment (shear-wave common midpoint reflection profile), reduced from scale 1:25000. Line SCMP1: locations 101-212 (NE-SW), line SCMP2: locations 101-250 (SE-NW), dots indicate vibrator points, solid lines stationary 3-component receiver spreads. Location interval is 80 m. All vibrator points were recorded also with a downhole 5-unit 3-C chain (Shear-wave moving source profile S-MSP). Modified from Lüschen et al. (1990, 1991). Inlet shows Variscan basement outcrops in Middle Europe.



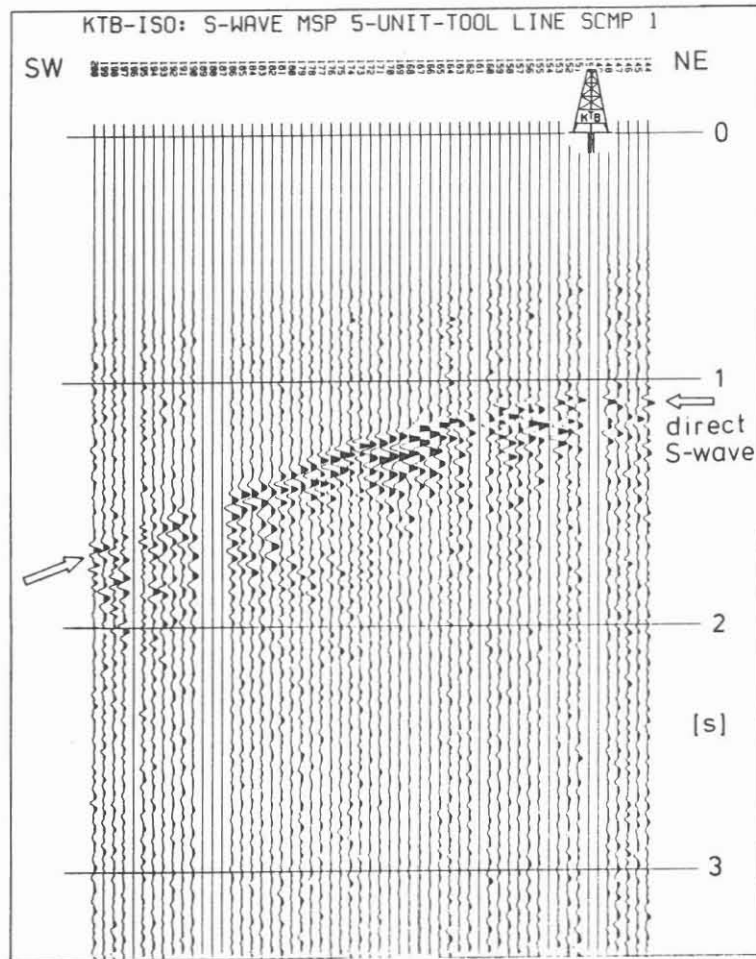
Priority was given to a careful selection of the points in order to provide an optimum ground coupling for the wedge-shaped vibrator baseplates. Orientation of the horizontal sources was cross-line (Y), on a fewer number of points also orientations of Y+45 and Y-45 degree were used.

The purpose of the field configuration was not to resolve lateral structure variations, but to achieve the highest CMP coverage (50-fold) for enhancement of the signal/noise ratio on shorter segments with the KTB drillhole in their centre. In contrast to explosive sources, vibroseis offers the possibility to apply well-defined stresses to the ground regarding their frequency and orientation. On the other hand, the energy of shear-wave generation is not always equal to explosive sources and sometimes not predictable. This may be caused by non-optimum ground coupling and by a variety of effects occurring within the weathering zone, e.g. scattering, mode conversion and multiples. This drawback was expected to be compensated during multiple vertical and horizontal (CMP) stacking.

The dynamite shotpoints were expected to provide a direct comparison with the P-wave image recorded by the vertical receiver components, additionally to the previously collected P-wave vibrator profiles in 1985 (DEKORP Research Group, 1988). Actually they consisted of five shots in distinct drillholes, recorded separately to enable application of the three-hole technique (or Camouflet method, Edelmann, 1985) for enhancement of the shear-waves. A comparison of these different source types with a more detailed technical description will be given elsewhere (Lüschen, 1992).

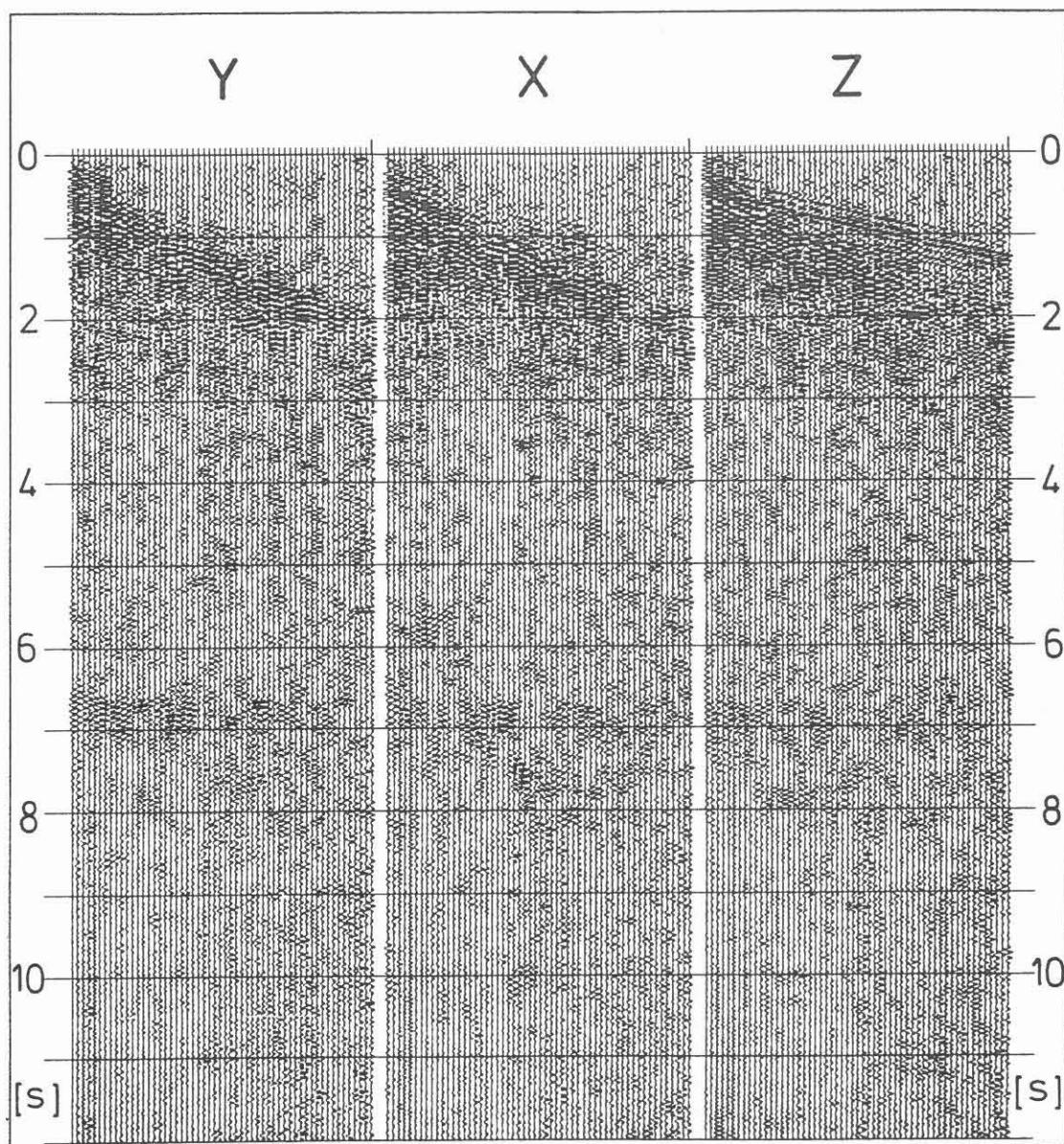
All sourcepoints were also recorded in the borehole by a digital 5-unit geophone chain with 3 components each, placed between 3690 m and 3590 m with a spacing of 25 m. This measurement provides a S-wave MSP or walkaway survey. Figure 2 shows such a common downhole receiver gather with all recorded vibratorpoints on line SCMP 1. The shear-wave direct arrivals can be clearly recognized on a hyperbolic curve. Undulations in traveltimes from trace to trace are caused by the topography and by near-surface delays in a weathering layer varying in thickness and velocity.

Figure 3 presents a typical example for single-fold gathers from a surface vibratorpoint with three components. Extended Vibroseis correlation with the 30 s long pilot sweeps has been applied for the 33 s long field records (filled up with zeros to 40 s length). The traces have been bandpass filtered with 8-18 Hz where filter tests located the main energy of the S-waves. The plot displays true observed amplitudes. The vertical component shows only little P-wave energy. The arrivals of the direct P-wave, however, are much better aligned than those of the S-waves, indicating stronger influence of the weathering layer to the S-waves. Although source orientation in this case was cross-line, the energy of the direct shear-waves is distributed over all receiver components. This is indicative



**Fig. 2:** Moving source profile (or walkaway survey) with the shear-wave sources of the SCMP1 line. The traces are recorded with a horizontal component (H1) located in 3665 m depth (selected from 5 units with a spacing of 25 m and 3 components each). True amplitudes (after demultiplexing and vibroseis correlation) are displayed without any special processing.

of scattering due to strong lateral heterogeneities and/or rotation of the signal polarization due to seismic anisotropy. Lüschen et al. (1991) noted remarkable differences of P- and S-wave velocities of the direct waves between the two lines, which favours an explanation by seismic anisotropy. At about 7 s TWT one of the key targets, the 'Erbendorf-body', already known from P-wave profiling (DEKORP Research Group, 1988), can be recognized by clear S-wave reflections.



**Fig. 3:** Single vibratorpoint gather of VP 170 of line SCMP 1. 56 stationary channels for each component, X (in-line), Y (cross-line) and Z (vertical). Source orientation was cross-line (Y). Offset range is from 1 to 5.5 km. Data were demultiplexed, correlated (extended correlation), 10-fold vertically stacked (5-fold in the field), bandpass filtered 8-18 Hz. True observed amplitudes. Note strong direct S-wave on all three components and good signal/noise ratio for deeper reflections ('Erbendorf-body') near 7 s TWT.

## Processing

First CMP stacking tests using topography-derived statics were highly discouraging. Therefore, special efforts were made in order to optimize the S-wave static corrections. General experience from shallow seismic profiling is that S-wave velocities in the uppermost layers are often very low and unpredictable. S-waves in this case are more sensitive to lithological changes than P-waves, but complicate the situation for imaging of the deeper structures. In Figure 2 this effect is clearly demonstrated by undulations from trace to trace (80 m spacing) of the order of 50-100 ms which is more than the dominant S-wave period. We made therefore an attempt to use such undulations for a first estimate of the static effects (Werner, 1992).

The recordings of the downhole units represent the equivalent of gathering the surface traces into a common-depth-point (CDP) gather, the CDP being at the position of the borehole geophone. A normal move-out analysis was performed and the difference of the arrival times against the best approximating hyperbolic move-out curve were plotted (Figure 4). The deviations can be considered as static effects (they do not depend on recording time) caused by near-source velocity variations (e.g. weathering layer) and topography. The same approach including statistical evaluation was used for the arrivals of the direct shear-waves in the surface recordings, the common shot gathers (example in Figure 3) providing receiver statics, the common receiver gathers after resorting providing another set of sourcepoint statics. The direct wave was approximated by a straight line. All static corrections are plotted in Figure 4 for comparison. It is obvious that static corrections are usually greater than the dominant period of the S-wave signal and therefore of crucial importance for S-wave CMP-stacking. The influence of static corrections and the degree of multifold coverage is demonstrated in Figure 5 using the S-MSP data. From this test it can be concluded that, if static corrections cannot be controlled optimally (the static corrections from the SMSP are optimum), the CMP-coverage must be very high in order to compensate for many destructive traces.

After applying the statics using the above described approach - we used actually the S-MSP derived set for sourcepoint statics because of better quality - we decided to try automatic residual statics. This approach uses correlation techniques and can be focussed on good reflectors seen in single-fold gathers (compare Figure 3). It is particularly successful if such residual statics are lower than half of the dominant signal period. In this respect, the surface-consistent static corrections described above and the residual statics complement each other. Figure 6 shows a stacking test using the X-component of the line SCMP 1 with different stages of static corrections. Considering the deepest S-wave reflection between 6 and 7 s TWT, the stacking test demonstrates convincingly the efficiency of optimum static corrections. A smooth coherency filter has been used at the end of the processing, enhancing the stacking quality furthermore.

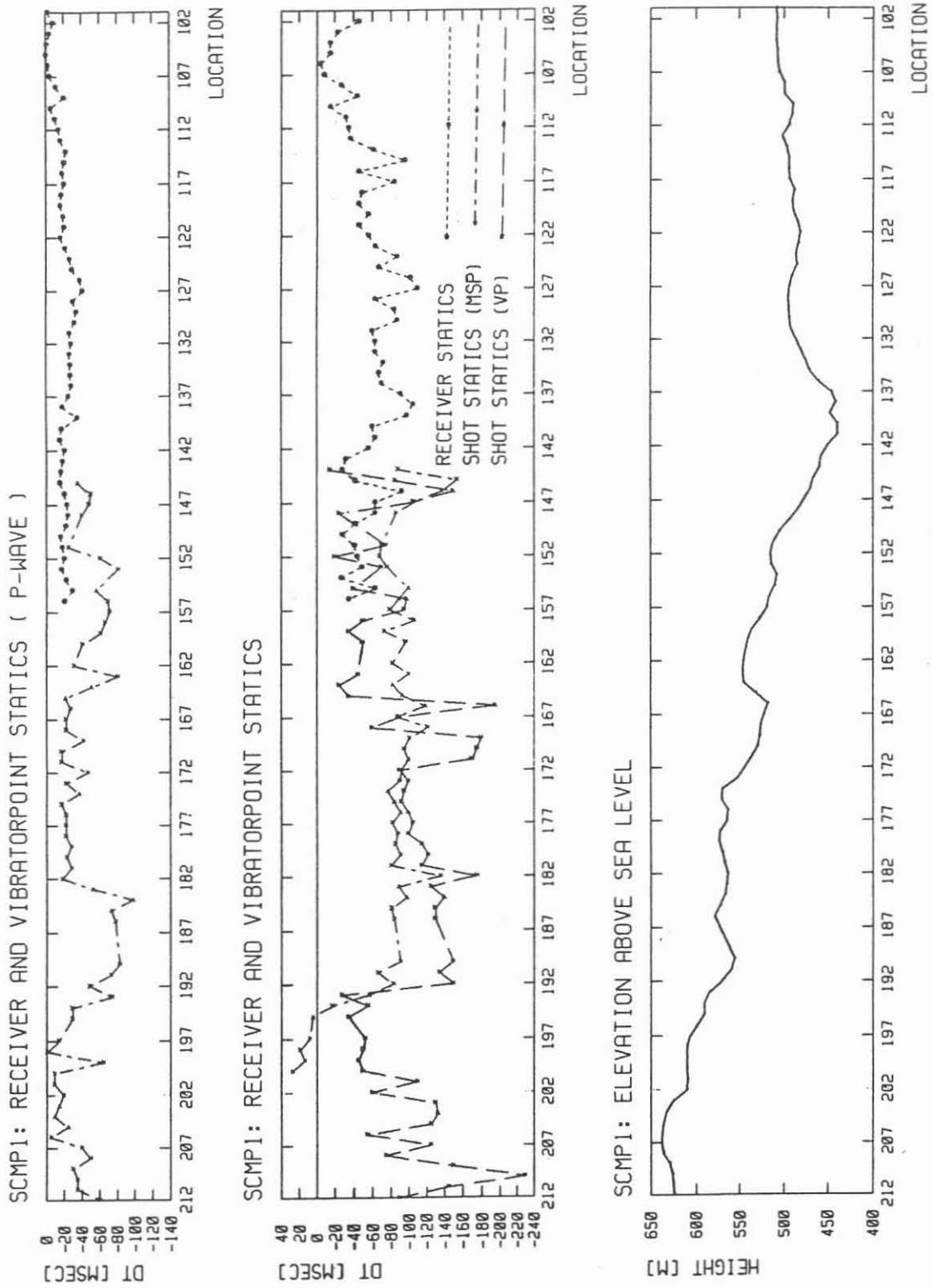


Fig. 4: Static corrections obtained by alignment of first arrivals for P-waves (top) and S-waves (middle). Topography is shown with 8:1 vertical exaggeration at the bottom. Statics are derived separately from common vibrator gathers of the SCMP reflection survey (labelled receiver statics) and common receiver gathers of the SCMP reflection and the S-MSP walkaway survey (labelled as shot statics VP and MSP). Statics are relative to an arbitrary datum level.

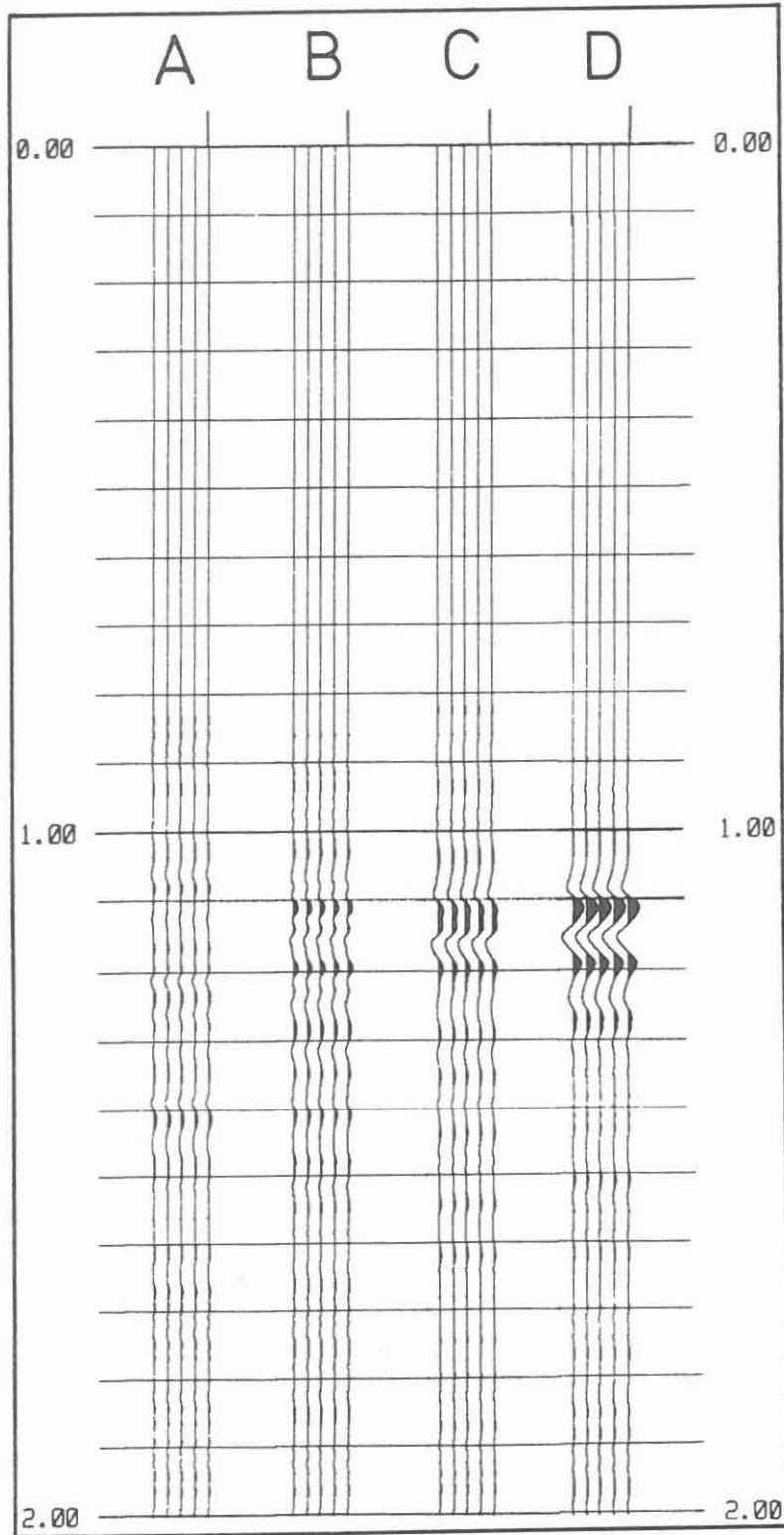
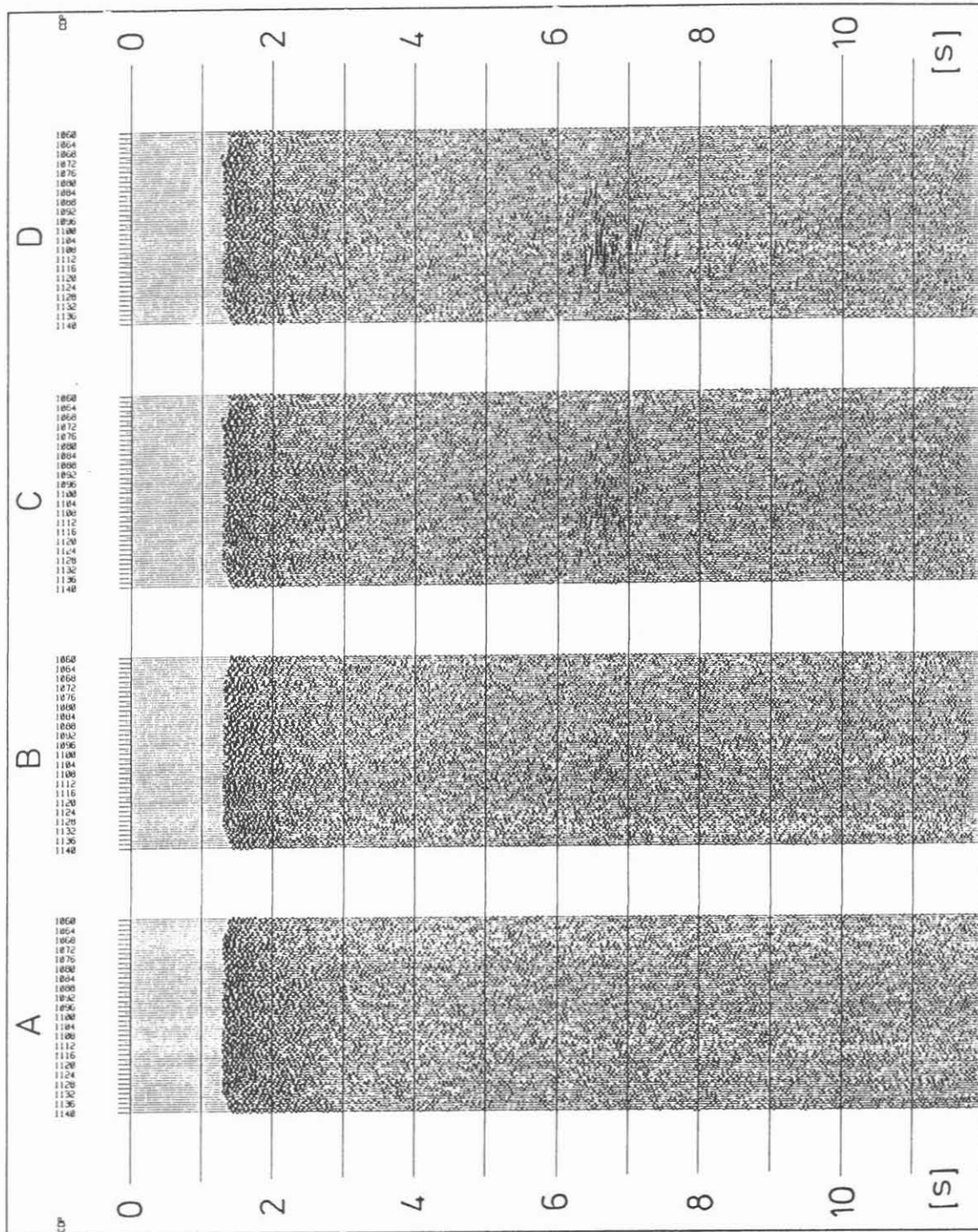


Fig. 5: Stacking test with the S-MSP traces from Figure 2. Traces are stacked after normal move-out correction and then repeatedly plotted for better visual inspection. A: 10 traces stacked (10-fold), B: 25 traces, C: 49 traces (all), D: 49 traces stacked with optimum statics.



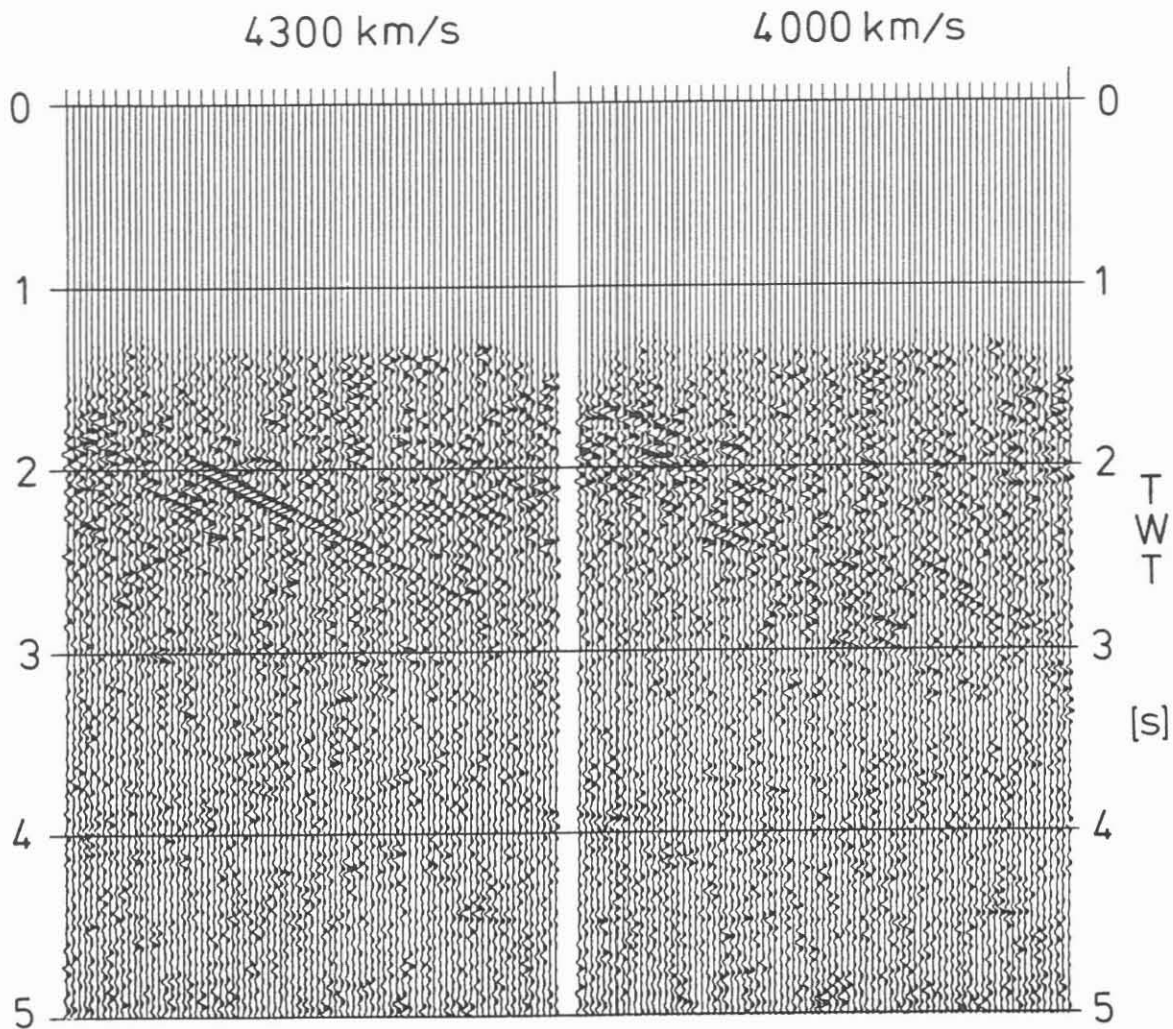
**Fig. 6:** CMP-stacking test with X-component (in-line) of line SCMP 1. Maximum coverage is 50-fold. True amplitudes are plotted, 8-18 Hz bandpass filtering before stacking. A: without any static correction, B: with surface-consistent statics, C: surface-consistent plus residual statics, D: with coherency filter. Stacking velocity after constant-velocity-stack analysis: increasing from 3600 m/s at 0 s to 3800 m/s at 12 s. Note that 'Erbendorf' reflections are enhanced significantly from panel A to D.

The static correction has been proved to be the most critical processing step. All the other steps can be regarded as rather standard. Editing of bad traces and despiking was done before correlation (extended correlation). Two records, each one with 5-fold field vertical stack, were stacked together. After CMP-sorting, all traces were bandpass-filtered (8-18 Hz) according to filtertests, horizontally balanced and then CMP-stacked (max. 50-fold). Analysis of stacking velocities did not reveal any strong variation in vertical direction, since the 'Erbendorf'-body at about 7 s is the only remarkable target for such analysis. Thus, a rather simple velocity-depth function was chosen, increasing from 3600 m/s at the surface to 3800 m/s at 12 s. The static correction described above and muting of the first S-wave breaks were applied after CMP-sorting. The amplitudes after this procedure can be regarded as true recorded amplitudes, no time-dependent scaling was applied. The whole processing sequence has been applied independently for the X (in-line) and the Y (cross-line) receiver component, the source orientation being in Y direction.

The velocity analysis (testing constant velocity stacks) revealed an anomalous feature in the upper part of the section (Figure 7). If anomalously high stacking velocities are used, here 4300 m/s for shear-waves, a steeply dipping reflector is imaged. This element was obtained previously by a similar approach using the P-wave 3-D reflection data and subsequently by reprocessing the former 2-D data (reflector 'SE 1', DEKORP Research Group, this volume; Wiederhold, this volume; Hluchy et al., this volume). It can be traced to and is presumably related to the Franconian Line, which is the SW-border of the Bohemian crystalline massif against Mesozoic sediments. This element could thus be interpreted as a major fault zone. On the other hand, inspection of single-fold data shows that there is an indication of direct waves reflected at a steeply dipping discontinuity in P-wave as well as S-wave sections. If it is a real structure, this element would exhibit after migration a dip of approx. 55 degrees and would be drilled through in 7 km depth by the KTB-borehole.

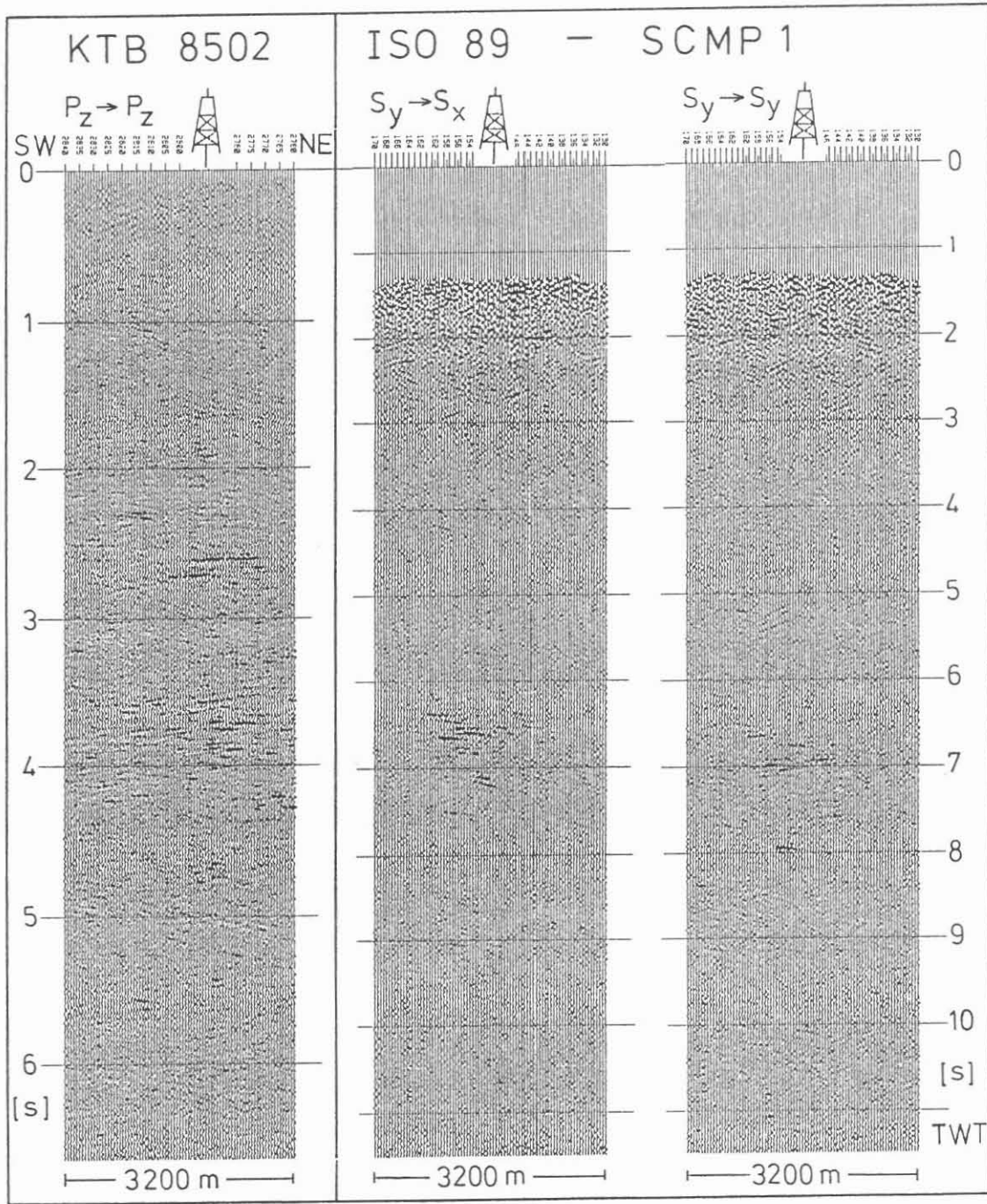
The processing sequence described above resulted in a 3.2 km long stack section for each receiver component and for each line. A corresponding P-wave section (KTB 8502) was selected from the former presite survey, processed by the DEKORP Processing Center, Clausthal (DEKORP Research Group, 1988). The only difference in processing consists of 1) amplitudes are not true observed amplitudes (AGC before stacking) and 2) CMP-coverage was 70-fold (50-fold in the S-wave sections). In Figures 8 and 9 a direct comparison is presented between P-wave and S-wave sections. The time scale of the S-wave sections has been compressed by the factor of 1.73 (the average  $V_p/V_s$  ratio) in order to enable correlations between P- and S-sections in horizontal direction.



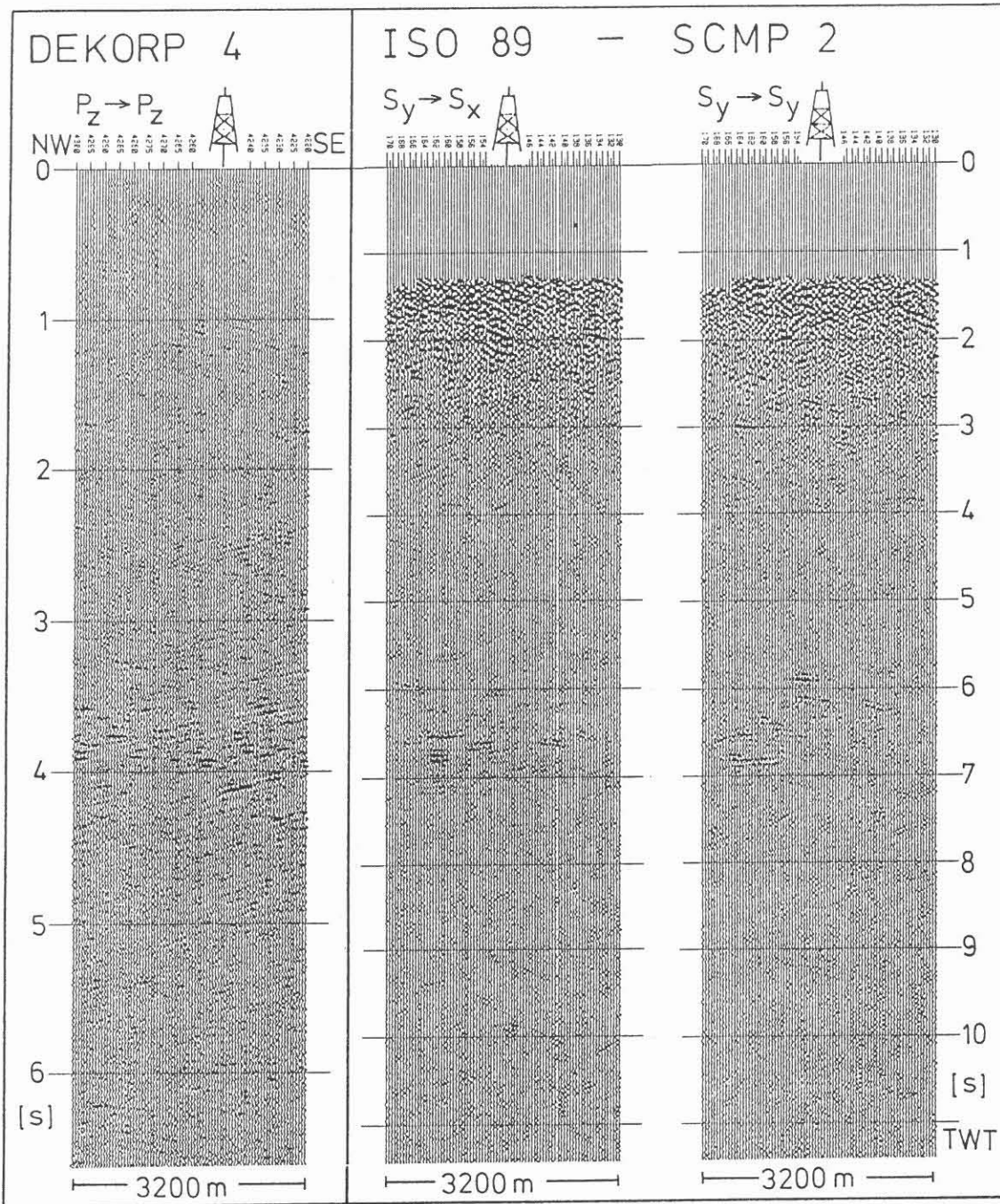


**Fig. 7:** Constant-velocity-stacking test of line SCMP 1 (left panel: 4300 m/s, right panel: 4000 m/s) showing a bright reflecting element between 2 and 3 s TWT when anomalously high stacking velocities (4300 m/s) are used. It vanishes at lower velocities.

There is a remarkable correspondence in P- and S-wave reflections from the 'Erbendorf'-body at 3.5-4 s P-wave TWT and 6-7 s S-wave TWT. Although slightly different images are discernable, in particular between the X and Y S-wave sections, the signal/noise ratio is quite similar. In remarkable contrast, at 2.6 s P-wave TWT there is a bright reflector, which is completely absent in the



**Fig. 8:** Comparison of P- and S-wave stack sections. Left: Part of line KTB 8502 (courtesy DEKORP Processing Center, compare DEKORP Research Group, 1988), Vibroseis source, 70-fold coverage. Middle: line SCMP 1, X receiver component, Y source component, 50-fold, Right: line SCMP 1, Y receiver component. Length of sections 3.2 km. Ratio of P- and S-wave time scales is 1.73. VSP data are available to 6000 m depth (2 s P-wave TWT).



**Fig. 9:** Comparison of P- and S-wave stack sections (cross lines). **Left:** Part of line DEKORP 4 (courtesy DEKORP Processing Center, compare DEKORP Research Group, 1988) Vibroseis source, 70-fold coverage. **Middle:** line SCMP 2, X receiver component, Y source component, 50-fold, **Right:** line SCMP 2, Y receiver component. Length of sections 3.2 km. Ratio of P- and S-wave time scales is 1.73. VSP data are available to 6000 m depth (2 s P-wave TWT).

S-sections. This observation we consider as a qualitative indication for a fluid/gas accumulation or for an alternative model as discussed below. At 1-2 s P-wave TWT and 2-3 s S-wave TWT there is the steeply dipping feature being equally imaged by P- and S-waves (compare Figure 7), only if anomalously high stacking velocities are used. These correlations between P- and S-sections, which are positive in two cases and negative in one case, indicate that the missing S-wave reflector at 4-5 s TWT is not an artefact of a lower signal/noise ratio or of the processing.

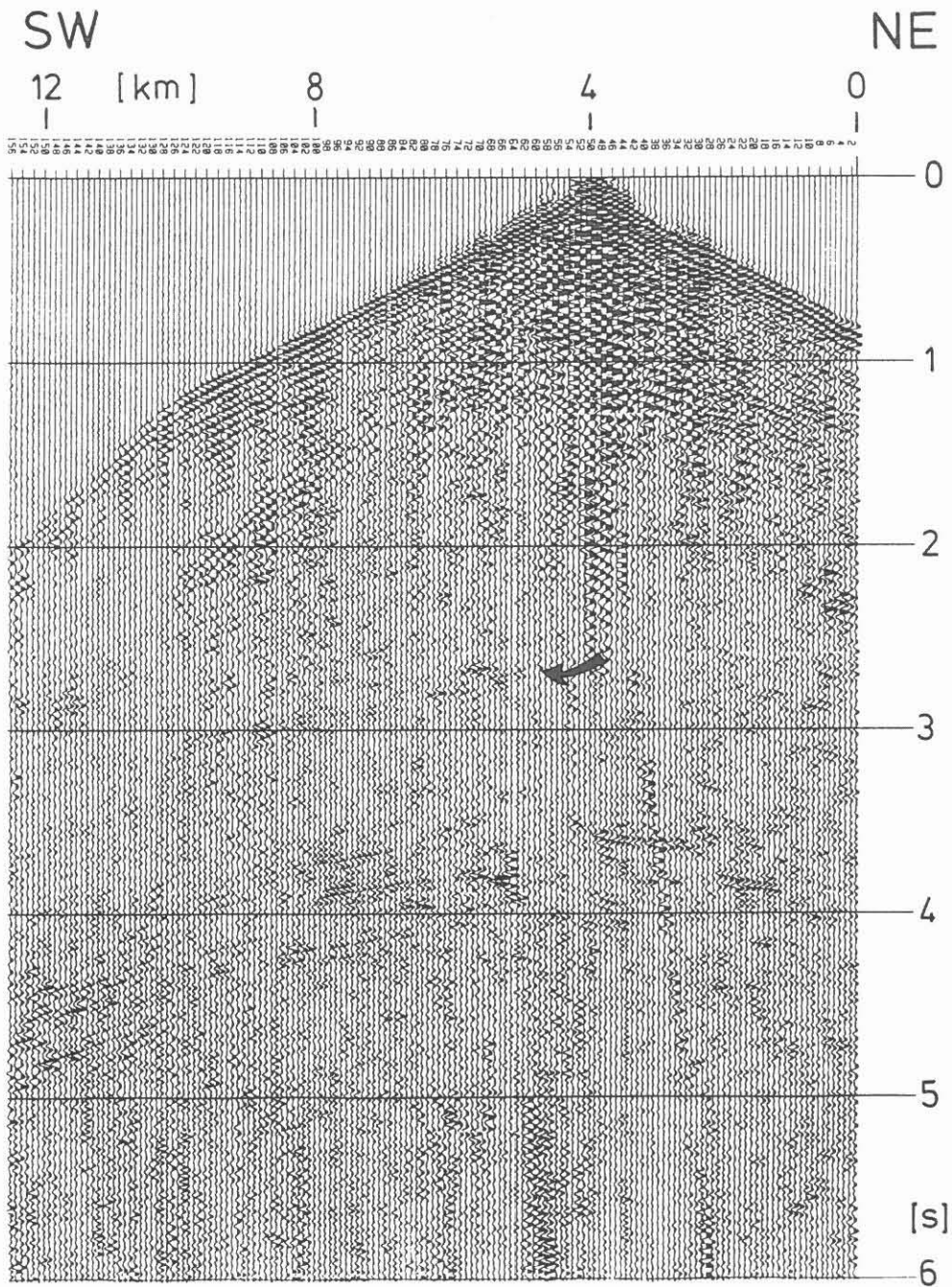
The key observation of this paper is an obviously missing S-wave reflection at a depth where a bright P-reflector appears.

### **Reality of Absence of the S-Wave Reflector**

The apparent dominance of the P-reflector (Figs. 8,9, left panel) relative to its surroundings could be the result of signal enhancing effects of the CMP stacking. On the other hand, single-coverage sections (shot records) of the standard P-wave survey in 1985, as well as such sections of the present SCMP survey (explosive shots, see previous chapter), clearly reveal the same relative dominance of the reflector and confirm the stacking result (Fig. 10). In contrast, recent efforts in 3-D processing and in reprocessing of the KTB 8502 profile did not show such a dominant P-wave feature (M. Stiller, pers. communication). We argue that this is mainly due to the fact that the recent processing has been focussed on steeply dipping events. Horizontal and subhorizontal reflections would have been weakened in this case. Independent confirmation of the bright reflector arises from evaluation of a P-wave walkaway survey (Janik and Harjes, 1992) and from recently accomplished VSP measurements to 6000 m depth.

The following effects, partly artificial, could impede the recording of S-wave reflections. Differences in resolution are ruled out, since P- and S- wavelengths are approximately equal (200-450 m). The difference in frequency compensates the difference in wave velocities. Strong signal/noise ratio at a deeper event ('Erbendorf'-body, Figs. 8,9) as well as at a shallower event (dipping reflector, Fig. 7) argue against any disturbing effect of stronger S-wave noise and scattering. Dipping interfaces and seismic anisotropy would lead to a distribution of the S-wave energy among the different source and receiver components. On none of them any indication of reflections is recognizable.

Another effect that could lead to false interpretations in case of positive impedance contrasts equal for P- and S-waves, follows directly from calculation of the reflection coefficients for S-waves as a function of the offset or angle of incidence (amplitude-versus-offset) according to the Zoeppritz amplitude equations. SV-waves (polarization oblique to the reflecting interface) as well as SH-waves (polarization in plane of the reflecting interface) show a polarity



**Fig. 10:** Unstacked vibratorpoint gather (200 channels) of the 1985 presite survey. Target reflector at 2.6 s is marked.

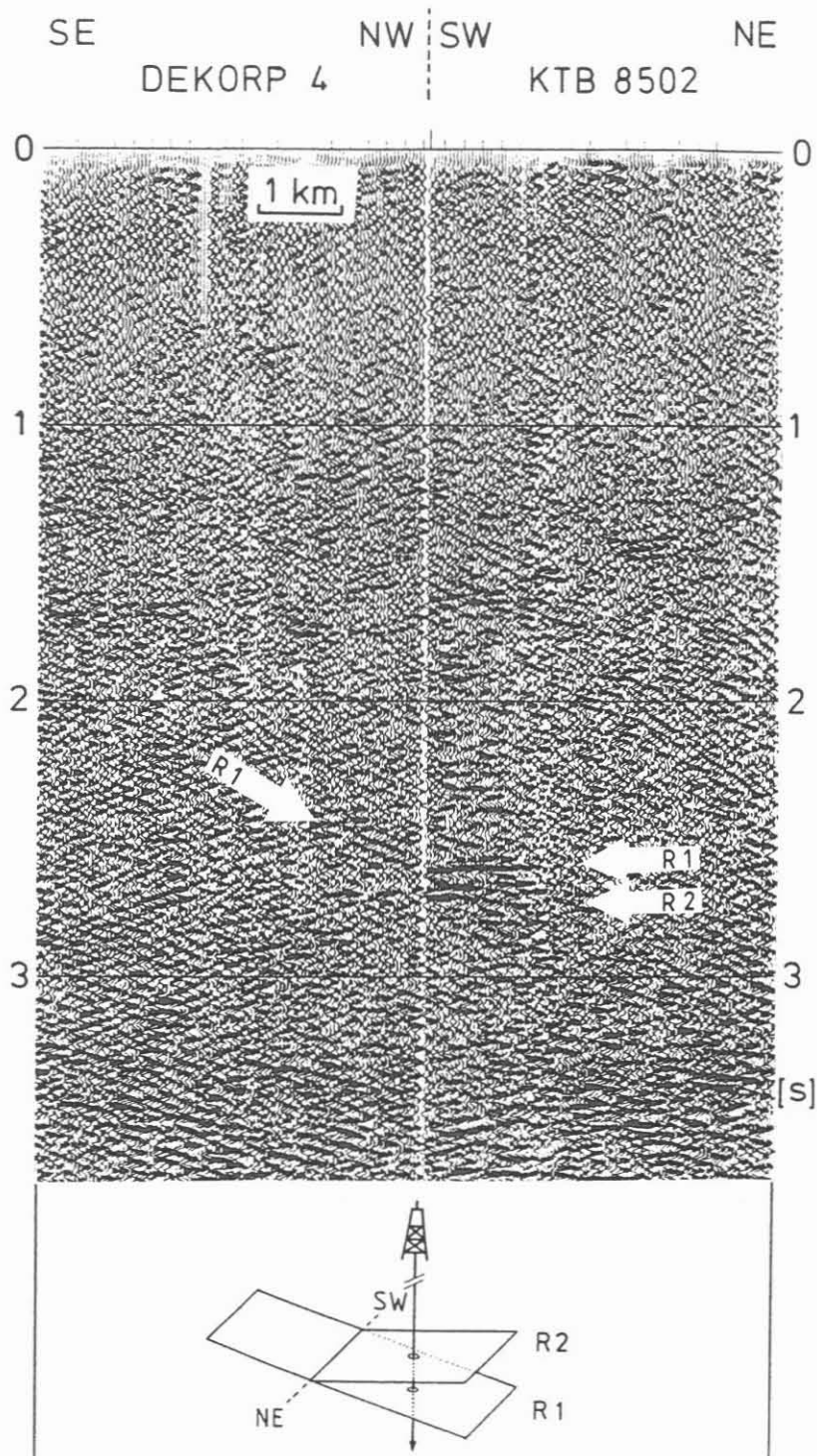
reversal significantly below the critical angle for normal impedance contrasts (Liu et al, 1990; Winterstein and Hanten, 1985). At that angle, which is different for SV- and SH-waves, the reflected S-wave amplitude crosses zero and its polarity is reversed. Although this situation may apply to the present case (maximum offset 9 km, target depth 8 km), it would appear at only one particular offset range. Therefore, the potential reflector should be visible at other offsets in unstacked data (compare Fig. 3). In CMP-gathers the traces are stacked with

offsets ranging from 0 to 9 km. A possible mixing of reversed reflected amplitudes would result in a degraded reflection. On the other hand, the residual statics would tend to compensate for this effect. This effect can be ruled out for explaining the missing S-wave reflector, but it may contribute to a slightly different image of the 'Erbendorf'-body between P- and S-wave reflections (Figs. 8,9).

### Prediction of Reflector Depth

Three-dimensional control by the two intersecting lines KTB 8502 and DEKORP 4 (DEKORP Research Group, 1988) and recently (April 1992) accomplished VSP recordings down to 6000 m depth provide the present base for predictions of the target depth. Figure 11 shows the two P-wave stack time sections tied together. The tiepoint is close to the target reflector location. From this figure it can be concluded that the target actually consists of two distinct reflectors. The upper one is dipping northwestwards with strike direction in-line of KTB 8502 (SW-NE). After seismic migration it moves away from the drilling location. If at all penetrated by the drillhole then this could only be at a deeper level. The lower element, as indicated in Fig. 11 is nearly horizontal and therefore does not migrate away. It is expected to be penetrated by the borehole at its center. Its length in the stack section (as well as in unstacked shotgathers) is of the order of 1 km. Considering that its edges are diffractions rather than reflections, it focusses in a migration section to a considerably shorter element (of the order of 500 m). The reality as well as the location of these reflections is independently confirmed by interpretations based on a P-wave moving source profile (Janik and Harjes, 1992).

Picking the arrival time of the central peak of the zero-phase Vibroseis signal gives a travelttime of 2.69 s with a bias of  $\pm 0.02$  s if the two side lobes are taken to denote the error bar in identifying the reflectors. The recently measured VSP gives a total travelttime of 0.975 s at 6013 m depth (that is two-way travelttime of 1.95 s). This travelttime is indicated in Fig. 11 at the tiepoint (note that the drillhole is 400 m off the tiepoint) and can be used for calibration of the target depth. If measured in travelttime, the target is located  $0.74 \pm 0.02$  s ( $\pm 2.7$  %) below the maximum VSP depth. The average P-wave velocity at 6 km depth calculated from the VSP is  $6.16$  km/s  $\pm 1$  % (average from surface to 6 km), the error being determined from the difference in time between the two Vibroseis side lobes. Hence, the marked target in Fig. 11 is located in 8280 m depth  $\pm 80$  m beneath the KTB mouth, the error bounds being estimated rather conservatively, assuming that the average velocity does not vary significantly between 6 and 8 km depth.



**Fig. 11:** Intersection of P-wave stack sections DEKORP 4 (left) and KTB 8502 (right) (courtesy DEKORP Processing Center, DEKORP Research Group, 1988). Gap marks the tieline, which is viewed from the east. Note that the upper part of the bright reflection is dipping to the NW, the lower one is nearly horizontal. KTB-location is 400 m out of plane of both sections. The lower sketch shows position of the reflections R1 and R2 after migration and three-dimensional control by the intersecting lines relative to the projection of the drillhole into the section (not to scale).

## Lithological models

### *Fluid/gas reservoir*

Experimental studies in oil- and gas exploration during the eighties, as well as corresponding modelling results established the significance of comparisons of P-wave and S-wave velocities and reflection characteristics for detecting layers or media with higher porosity and the type and saturation of pore content (eg. Tatham, 1982; Meissner and Hegazy, 1981; Ensley, 1984; Garotta, 1985; Frasier and Winterstein, 1990; Tatham and McCormack, 1991).

These experimental studies provide a heuristic approach to interpret the discrepancy in P- and S-wave reflectivity qualitatively in terms of a fluid/gas trap within porous or fractured rocks. P-wave velocity ( $V_p$ ) depends largely on rock bulk modulus, the shear modulus and rock density, whereas, the S-wave velocity ( $V_s$ ) is solely a function of the shear modulus and rock density:

$$V_p = \left( \frac{k + 4\mu / 3}{\rho} \right)^{\frac{1}{2}}$$

$k$  bulk modulus  
 $\mu$  shear modulus

$$V_s = \left( \frac{\mu}{\rho} \right)^{\frac{1}{2}}$$

$\rho$  density

Fluids have no shear strength, therefore S-waves should propagate only through the rock matrix, but not through the fluid material within pores or cracks. Practically, the most pronounced differences in P- and S-wave characteristics in porous media are attributed to the type of pore content. Gases are more compressible than liquids,  $V_p$  for gas saturated pores is therefore much lower than for liquid filled pores. There is only a slight change in  $V_s$  due to the presence of fluid/gas filled pores, which is attributed alone to the difference in density. The gas/water transition in hydrocarbon reservoirs is thought to be responsible for P-wave hydrocarbon indicators defining the classical 'bright spot', e.g. amplitude anomalies, flat reflections, polarity changes, edge diffractions, time sags, shadow zones and frequency changes (e.g. Ensley, 1984). Since hydrocarbon reservoirs may not be the only causes for such P-wave bright spots, the S-wave response (if resolution characteristics are equal) can be used to verify the presence of gas as suggested by modelling results of Meissner and Hegazy (1981) and Ensley (1984). If P-wave reflections and their amplitude and phase



anomalies along a formation boundary are caused by a gas reservoir, there are no corresponding S-wave impedance contrasts. The S-waves in this case image only the lithological change in rock matrix if any.

In the present study we are dealing with crystalline rocks (paragneisses and metabasites), which are even exposed at the surface. Here reflections are not caused by continuous formation boundaries, but rather by complex and discontinuous structures like faulting and folding, randomly distributed impedance and velocity contrasts and by interference and focussing effects of multiple and concave or convex structures. Moreover, reflected seismic energy very often shows indications of diffractions. There are two reasons why the bright spot concept is not applicable for evaluation in its original sense: 1) there are no continuous formation boundaries in the present case, 2) the P-wave amplitudes cannot be evaluated quantitatively, because relative amplitudes have not been preserved during CMP processing, as pointed out in the previous chapter. The reflecting element is relatively short (approx. 1 km) and shows diffractions at its ends. Since the polarity and hence the sign of the P-wave reflection coefficient can hardly be determined, and the S-wave reflection coefficient is presumably zero (the physical cause of the reflector absence), the  $V_p/V_s$  ratio of the medium beneath the interface can be both, anomalously high or low.

In addition to studies in exploration industry on clastic oil- and gas bearing sedimentary rocks (see review by Tatham and McCormack, 1991), the influence of fluids in a porous or fractured medium has been subject for measuring and modelling seismic velocities and the  $V_p/V_s$ -ratio for a long time. These studies were originally motivated by the dilatancy model for earthquake precursors (e.g. Nur and Simmons, 1969; Nur, 1972; O'Connell and Budiansky, 1974; Spencer and Nur, 1976). Several factors play an important and sometimes opposing role: elasticity of the dry crystalline rock matrix, porosity, permeability (or connectivity), pore content (e.g. liquids or gas), pore and crack geometry (e.g. aspect ratio), crack density, saturation (dry or wet), pore pressure, confining pressure and temperature.

Without a-priori information, it remains ambiguous to predict velocities and impedance contrasts from these complex interrelationships. Spencer and Nur (1976) found from measurements on low-porosity rocks (Westerly granite), that in samples with low pressure pore water  $V_p$  decreases with increasing temperature, while  $V_s$  is much less affected. Under high pore pressure, this relationship is reversed. O'Connell and Budiansky (1974) find from modelling the elastic moduli, that both seismic velocities decrease with increasing crack density, the  $V_p/V_s$ -ratio decreases for dry cracks and increases for saturated cracks.

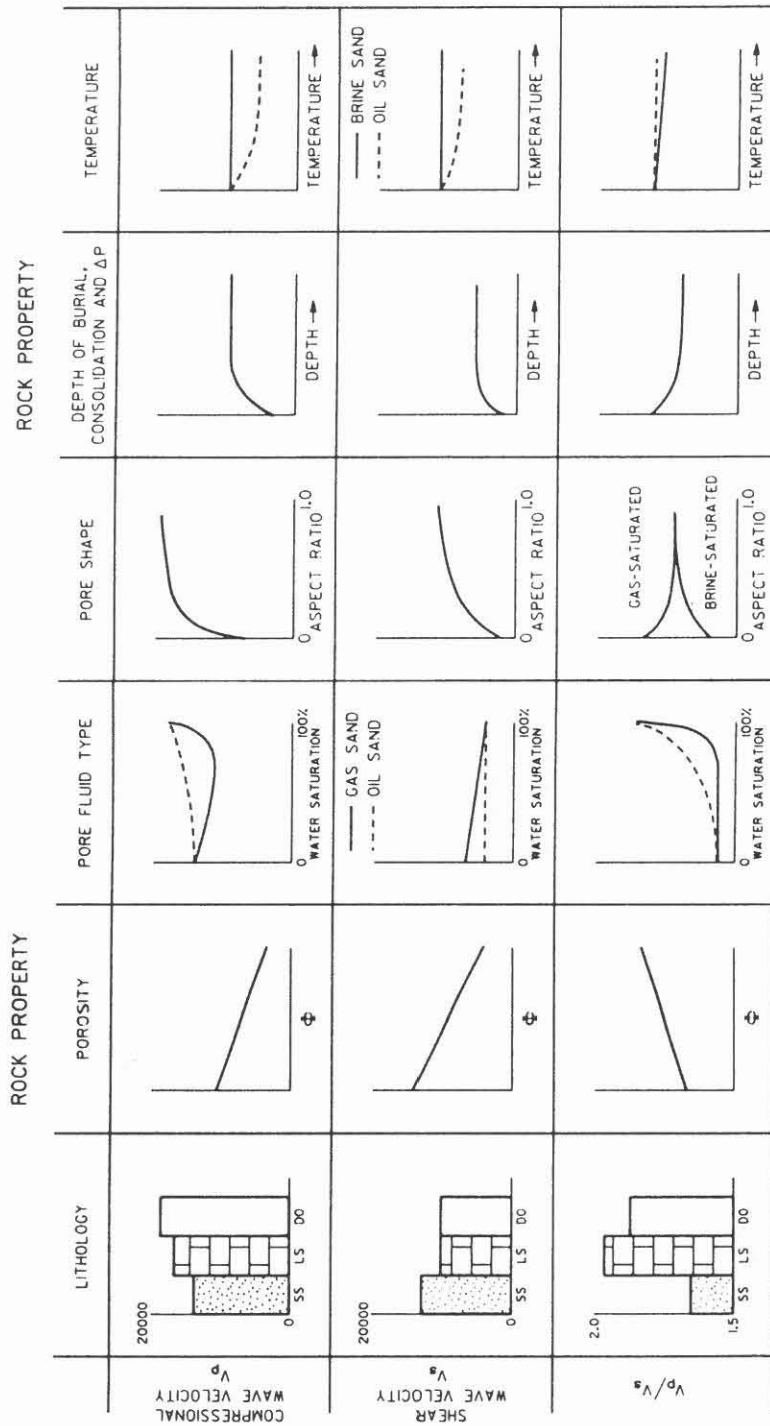


Fig. 12: Summary of the effect of different rock properties on the seismic P- and S-wave velocities, and on the velocity ratio  $V_p/V_s$  (from Tatham and McCormack, 1991, reproduced with permission of the Society of Exploration Geophysicists). Rock types in column for lithology: ss sandstone, ls limestone, do dolomite. Note the effects of the porosity, pore fluid type and differential pressure ( $\Delta p$ ) discussed in the text.

Tatham and McCormack (1991) presented a summary of the various effects of the different rock properties on P- and S-wave velocities and the  $V_p/V_s$  ratio (Fig. 12). We may use this compilation for seeking the appropriate conditions that produce impedance contrasts for P-waves but not so pronounced for S-waves. The pure effect of a porous medium saturated with saline water under presumably high pore pressure cannot account for the observation, since it produces both anomalously low P- and S-wave velocities according to laboratory experiments of Nur and Simmons (1969). Searching in the parameter space according to the theory of O'Connell and Budiansky (1974), conditions can be found that affect P-wave velocities more than S-wave velocities (St. Sobolev, pers. communication). If the fluid concept applies at all, then the effect of porosity must be overcompensated by the parameters pore shape (thickening of cracks) and fluid type (interfaces between liquids and gases) and others.

The question arises why is lithostatic pressure not closing the pores or cracks and why fluids can be trapped at that depth. There is considerable significance and growing evidence of the role of fluid and corresponding heat transport in the context of crust-mantle boundary interactions, in particular in tectonically active regions (e.g. Oliver, 1986; Bailey, 1990; Hyndman and Shearer, 1989; Marquis and Hyndman, 1992). Petrological considerations require metamorphic dehydration processes in the lower crust. Compilations and modelling of geophysical data, in particular magnetotelluric and seismic data, show that low electrical resistivity often correlates with low seismic velocities at deeper crustal levels and may be well explained by porosity models with few percent of free saline fluids (Hyndman and Shearer, 1989; Marquis and Hyndman, 1992). The mechanism of trapping aqueous fluids is discussed by Bailey (1990). If not consumed by retrograde metamorphic reactions, they migrate upwards. In the ductile deeper crust, thermal activation of ductility is considered to be strong enough to facilitate evolution of porosity (of the order of 0.1 %) and rapid fluid transport. Above the brittle-ductile transition this mechanism vanishes giving rise to fluid overpressure and hydraulic fracturing at midcrustal levels. The orientation of cracks depends on the state of stress at this depth. Fluids can accumulate in such horizontally extensive reservoirs near the brittle-ductile transition. Pore pressure reaches the lithostatic pressure or may exceed it slightly (see discussion by Bailey, 1990).

### *Rock composition*

The model which competes with the porous fluid-filled medium is a medium which varies purely in terms of rock composition. Such a case has been considered to fit strong wide-angle reflections from the lower crust in the Black Forest in SW Germany seen in P-wave sections, but absent in S-wave sections. Sandmeier and Wenzel (1990) modelled this discrepancy in terms of petrological

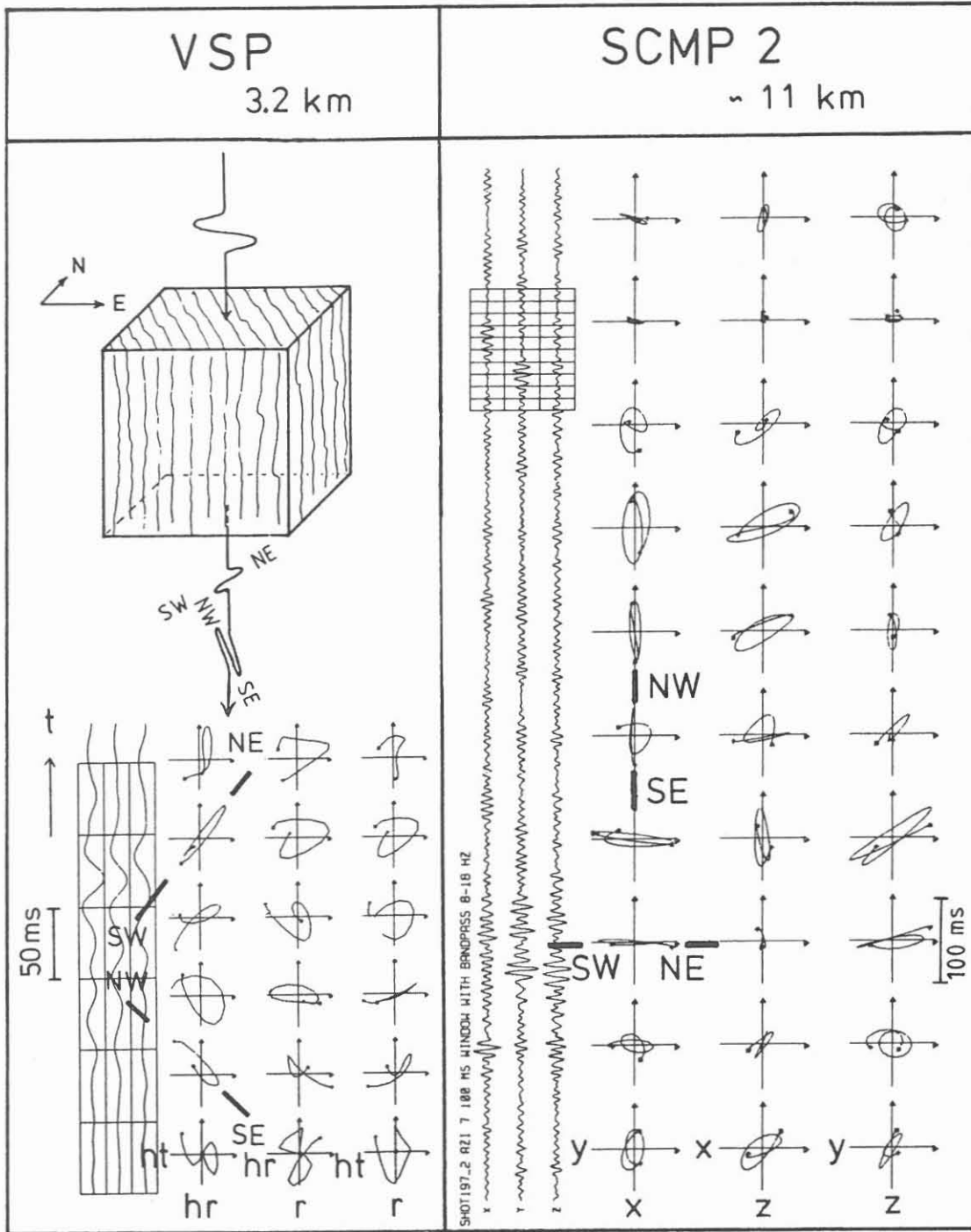


Fig. 13: Hodograms (particle motion diagrams) for windows from S-wave direct arrivals of the VSP 'VP101S' (Lüschen et al., 1991) in comparison with windows from S-wave reflections (non-stacked) of the line SCMP1. Time is increasing upward. Note the nearly perfect linear polarizations of two orthogonally polarized phases. The two preferred directions are the same in both observations, but the fast and the slow phases changed their polarization. Upper left panel shows schematically the average foliation in the depth range of 1-3 km explaining the observed polarizations in the S-wave VSP.

layering expressed in variation of the quartz content (high quartz content: low  $V_p$ , low Poisson's ratio), in accordance with corresponding laboratory measurements (Kern, 1982). In the Black Forest model the multiple layering (of the order of 100 m thickness) contributes significantly to the modelled reflectivity. If the model of high quartz content applies to the present situation, the amount of quartz within a thin layer (thickness much less than the wavelength) should be higher than in the lower crust model of Sandmeier and Wenzel (1990). Otherwise we would not observe such a discrete reflector. The  $\alpha$ - $\beta$  phase transition of quartz occurring at a temperature of about 600 degree could be considered for deeper crustal levels. It produces a decrease in  $V_p$  but not in  $V_s$  (Kern, 1982).

Juhlin (1990) reports a similar situation from the Siljan impact crater in Sweden, where bright P-wave reflections have been verified through drilling to be caused by dolerite sills. Laboratory measurements on core samples showed that these dolerites could produce relevant impedance contrasts for P-waves but not for S-waves.

### Seismic Anisotropy:

The two horizontal receiver components displayed in Figs. 8 and 9 do not image the 'Erbendorf'- body equally at approx. 6 to 7 s TWT. This behaviour might be related to the polarity reversals of the SV- and SH-waves occurring at different angles in the subcritical range, as mentioned above. Comparing both crossing lines, a striking systematic difference in traveltimes is discernible. The arrivals on the SW-NE receiver component (SCMP1:X; SCMP2:Y) tend to earlier traveltimes. We argue that this might be an effect of S-wave velocity anisotropy in the upper medium. Such anisotropy has been observed for vertical raypaths in S-wave VSPs between 1 and 3 km depth and interpreted in accordance with laboratory measurements as anisotropy due to the rock microstructure (foliation), which shows a mean strike direction in NW direction and a subvertical dip (Lüschen et al., 1991).

Fig. 13 shows an extract of particle motion diagrams of the 'Erbendorf'-reflections, based on unstacked data. These hodograms show two nearly optimum linearly and orthogonally polarized S-wave phases. These features are typical for S-wave splitting due to seismic anisotropy, although the effect of heterogeneities cannot be excluded. Compared to the hodograms of the VSP (Fig. 13), it is obvious that the same preferred directions are displayed, but fast and slow S-waves have interchanged their particle directions. This behaviour is compatible with a symmetry system displayed in the figure, but rotated by 90 degrees along the vertical axis. This might indicate that the folding axis and foliation change their directions somewhere between 3 and 11 km, possibly at the above discussed target reflector at about 8 km depth. This could provide another mechanism for

forming fractures and fluid traps. Furthermore, the VSP-derived S-wave anisotropy provides a hint that the absence of a S-wave reflector should not be an effect of a possibly anisotropic reflection coefficient. At least one of the two split S-wave phases would have been observed on at least one horizontal component section.

### **Acknowledgements.**

We acknowledge financial support by the Federal Ministry of Research and Technology (BMFT, Bonn) through grants RG 8801 and RG 9207, and the German Science Foundation (DFG, Bonn) through grant Hu-413/3. We are grateful to the DEKORP and KTB management at the NLFb, Hannover, in particular K. Bram, H.-J. Dürbaum, G. Dohr, J. Schmoll, C. Reichert, H. Wiederhold, and P. Sadowiak for continuous support and for administrative services. We thank W. Söllner and M. Widmaier (Karlsruhe) for their assistance and M. Stiller (Clausthal), K. Fuchs, P. Hubral, St. Sobolev (Karlsruhe) and H. Gebrande (München) for constructive discussions.

### **References**

- Crampin, S., 1987. Geological and industrial implications of extensive-dilatancy anisotropy. *Nature*, 328, 491-496.
- Bailey, R.C., 1990. Trapping of aqueous fluids in the deep crust. *Geophysical Research Letters*, 17, 1129-1132.
- DEKORP Research Group, 1988. Results of the DEKORP4-KTB Oberpfalz deep seismic reflection investigations. *J. Geophys.*, 62, 69-101.
- Edelmann, H.A.K., 1985. Shear-wave energy sources. in: *Seismic Shear Waves, Part B: Applications*, G. Dohr (ed.), Handbook of Geophysical Exploration, Vol. 15B, Geophysical Press, London, 134-177.
- Ensley, R.A., 1984. Comparison of P- and S-wave seismic data: a new method for detecting gas reservoirs. *Geophysics*, 49, 1420-1431.
- Fertig, J., 1984. Shear waves by an explosive point-source: the earth surface as a generator of converted P-S waves. *Geophysical Prospecting*, 32, 1-17.
- Frasier, C. and Winterstein, D., 1990. Analysis of conventional and converted mode reflections at Putah sink, California using three-component data. *Geophysics*, 55, 646-659.
- Garotta, R., 1985. Observation of shear waves and correlation with P events. in: *Seismic Shear Waves, Part B: Applications*, G. Dohr (ed.), Handbook of Geophysical Exploration, Vol. 15B, Geophysical Press, London, 1-86.
- Helbig, K. and Mesdag, C.S., 1982. The potential of shear-wave observations. *Geophysical Prospecting*, 30, 413-431.

- Hyndman, R.D. and Shearer, P.M., 1989. Water in the lower continental crust: modelling magnetotelluric and seismic reflection results. *Geophys. J. Int.*, 98, 343-365.
- Janik, M. and Harjes, H.-P., 1992. Structural interpretation of the MSP-experiment. in: KTB Report, this volume.
- Juhlin, C., 1990. Interpretation of the reflections in the Siljan Ring area based on results from the Gravberg-1 borehole. in: *Seismic Probing of Continents and their Margins*, J.H. Leven et al. (eds.), *Tectonophysics*, 173, 345-360.
- Kern, H., 1982. P- and S-wave velocities in crustal and mantle rocks under the simultaneous action of high confining pressure and high temperature and the effect of the rock microstructure. in: *High-Pressure Researches in Geoscience*, W. Schreyer (ed.), Schweizerbart'sche Verlagsbuchhandlung, Stuttgart, 15-45.
- Liu, E., Crampin, S. and Yardley, G., 1990. Polarizations of reflected shear waves. *Geophysical Research Letters*, 17, 1137-1140.
- Lüschen, E., Nolte, B. and Fuchs, K., 1990a. Shear-wave evidence for an anisotropic lower crust beneath the Black Forest, southwest Germany. in: *Seismic Probing of Continents and their Margins*, J.H. Leven et al. (eds.), *Tectonophysics*, 173: 483-493.
- Lüschen, E., Söllner, W., Hohrath, A., Rabbel, W., 1990b. Integrated P- and S-wave borehole experiments at the KTB-deep drilling site. in: *KTB Report 90-6b : DEKORP Report*, H.-J. Dürbaum et al. (eds.), Niedersächsisches Landesamt für Bodenforschung, Hannover, 85-134.
- Lüschen, E., Söllner, W., Hohrath, A., Rabbel, W., 1991. Integrated P- and S-wave borehole experiments at the KTB-deep drilling site in the Oberpfalz area (SE Germany). in: *Continental Lithosphere: Deep Seismic Reflections*, R. Meissner et al. (eds.), *Geodynamics Series Vol. 22*, AGU, Washington D.C., 121-133.
- Lüschen, E., 1992. Comparison of shear-wave source techniques applied in crustal seismology. In preparation.
- Marquis, G. and Hyndman, R.D., 1992. Geophysical support for aqueous fluids in the deep crust: seismic and electrical relationships. *Geophys. J. Int.*, 110, 91-105.
- Meissner, R. and Hegazy, M.A., 1981. The ratio of the PP- to the SS-reflection coefficient as a possible future method to estimate oil and gas reservoirs. *Geophysical Prospecting*, 29, 533-540.
- Nur, A., 1972. Dilatancy, pore fluids, and premonitory variations of  $t_s/t_p$  travel times. *Bull. Seis. Soc. Am.*, 62, 1217-1222.
- Nur, A. and Simmons, G., 1969. The effect of saturation on velocity in low porosity rocks, *Earth Planet. Sci. Lett.*, 7, 183-193.
- O'Connell, R.J. and Budiansky, B., 1974. Seismic velocities in dry and saturated cracked solids. *J. Geophys. Res.*, 79, 5412-5426.
- Oliver, J.E., 1986. Fluids expelled tectonically from orogenic belts: Their role in hydrocarbon migration and other geologic phenomena. *Geology*, 14, 99-102.

- Pickett, G.R., 1963. Acoustic character logs and their applications in formation evaluation. *J. Petr. Tech.*, 15: 569-667.
- Pratt, T., Hauser, E., Hearn, T., Reston, T., 1990. COCORP Seismic Investigations of the Surrency Bright Spot beneath the Southern Appalachians, USA, in: *Continental Lithosphere: Deep Seismic Reflections*, R. Meissner, L. Brown, H.-J. Dürbaum, W. Franke, K. Fuchs, F. Seifert (eds.), *Geodynamics Series*, 22, American Geophysical Union, Washington, D.C., 1-7.
- Sandmeier, K.-J. and Wenzel, F., 1990. Lower crustal petrology from wide-angle P- and S-wave measurements in the Black Forest. in: *Seismic Probing of Continents and their Margins*, J.H. Leven et al (eds.), *Tectonophysics*, 173, 495-505.
- Spencer, J.W. and Nur, A.M., 1976. The effects of pressure, temperature, and pore water on velocities in Westerly granite. *J. Geophys. Res.*, 81, 899-904.
- Tatham, R.H., 1982. Vp/Vs and lithology. *Geophysics*, 47, 336-344.
- Tatham, R.H. and McCormack, M.D., 1991. Multicomponent Seismology in Petroleum Exploration. *Investigations in Geophysics Series*, Vol 6., Society of Exploration Geophysicists, Tulsa, pp. 248
- Ward G., Warner, M., and the BIRP Syndicate, 1991. Lower crustal lithology from shear wave reflection data. in: *Continental Lithosphere: Deep Seismic Reflections*, R. Meissner, et al. (eds.), *Geodynamics Series Vol. 22*, AGU, Washington D.C., 343-349.
- Werner, U., 1992. Auswertung von Scherwellen-Reflexionsprofilen am KTB. Diplomarbeit, Universität Karlsruhe.
- Winterstein, D.F. and Hanten, J.B., 1985. Supercritical reflections observed in P- and S-wave data. *Geophysics*, 50, 185-195.



## Seismic Anisotropy at the KTB Deep Drilling Site

Wolfgang Rabbel

### ABSTRACT

Based on the DEKORP ISO 89 borehole experiments, the question of the existence of "seismic anisotropy at the KTB deep drilling site" has to be answered unambiguously with "yes". The anisotropy could be quantified in situ for a gneiss packet where it is apparently influenced by both rock foliation and cracks. The values obtained in the direct vicinity of the KTB pilot hole, however, cannot be extrapolated into its surroundings without modification: While the general trend of anisotropy with high velocity values towards SE-ESE is conserved, the amount of anisotropy shows smaller average values. This seems to reflect the inhomogeneous distribution of metamorphic rocks and granite in the target area. The direction of high seismic velocities (ESE) coincides approximately with the postulated direction of maximum horizontal tectonic stress in the Oberpfalz region.

### INTRODUCTION

The DEKORP ISO 89 field campaign was designed to obtain a most detailed description of the KTB deep drilling site from a seismic point of view. While structural information was obtained from reflection seismic methods an additional set of experiments was carried out in order to characterize the seismic material properties of at least the uppermost part of the crust.

In this context the existence of seismic anisotropy which indicates the either ordered or disordered state of a medium plays a major part. Seismic anisotropy may be caused for example by anisotropic minerals

---

Author's address: Institute of Geophysics, University of Kiel  
Olshausenstr. 40-60, D-2300 Kiel 1

or cracks if they are oriented in a preferred direction within larger rock packets. In the latter case seismic anisotropy can be related to the regional tectonic stress system which controls closure and opening of microfractures.

## FIELD EXPERIMENTS

From traveltimes considerations alone it is rather difficult to distinguish between effects of isotropic inhomogeneity and anisotropy. Therefore, the most reliable method for identifying seismic anisotropy is the analysis of shearwaves with regard to S-wave birefringence ("shear wave splitting": orthogonally polarized shear waves travelling with different velocities).

In this regard various seismic borehole experiments with special emphasis on generation and recording of S-waves were included in DEKORP's ISO 89 campaign; in particular: (1) vertical seismic profiling ("VSP") with different source offsets and -azimuths and geophone depth up to 3600 m and (2) a "multiple azimuth shearwave experiment" (MASE). In the latter case the geophones were fixed at a depth of 3300 m while the source was moved along two half circles of 4 and 8 km radius, respectively. Explosives as well as vertical and horizontal vibrators served as seismic sources for the VSPs. All data were recorded with 3-component-geophones.

The field configuration and a documentation of the data are presented in detail in Lüschen et al. (1990) and will, for brevity, not be repeated here.

## RESULTS

The data were analyzed with respect to the following topics:

- (1) diagnosis (is the subsoil anisotropic at all for seismic wavelengths?),
- (2) local quantification of anisotropy at the KTB pilot hole and (3) extrapolation (are the local results also valid for the vicinity area of the KTB).

Examples will now be given for each item.

## (1) DIAGNOSIS OF SEISMIC ANISOTROPY

Since arrival times of seismic signals are influenced by both structural inhomogeneities and anisotropy of the subsoil, an interpretation of traveltimes curves in terms of anisotropy is ambiguous in most cases. Therefore, the occurrence of split shearwaves, which reflect the intrinsic structure of media on scales at a small fraction of a wavelength, is commonly regarded as the most reliable indicator of seismic anisotropy. Orthogonally polarized shearwave arrivals were indeed identified already at an early stage of interpretation for the near offset VSPs. For example, Fig.1 displays records of a vertical vibrator VSP; the different wavetrains (qP-, qS1-, qS2- waves) are indicated.

From a diagnostic point of view it is important to show that the polarization of the observed S-waves does not depend upon the initial source polarization, as it is expected for anisotropic media. For proving this a horizontal vibrator source at a distance of 50 m off the KTB pilot hole was rotated in steps of 45 deg while a borehole geophone was fixed at 2900 m depth (Fig.2). The corresponding particle motion diagrams (Fig.3) show that the polarization of the split shearwaves stays indeed constant. The polarization direction of the faster S-wave (qS1) is nearly SE correlating with the strike of rock foliation at that depth: a result which holds approximately for the whole depth range of the KTB pilot hole.

## (2) IN SITU QUANTIFICATION OF SEISMIC ANISOTROPY

The rock composition along the KTB pilot hole is dominated by biotite gneiss with mostly steep but varying dip and strike of foliation. For investigating in situ values of gneiss anisotropy the variation of velocity for the direct P- and both split S-waves was picked from the near offset VSP VP101 shown in Fig.1. Most interesting is the depth interval of 2 - 3 km where the dip of rock foliation changes slowly from 80 to 30 deg. The corresponding seismic velocity values as well as a smoothed distribution of macroscopic fractures versus depth are shown in Fig.4. The information on both rock foliation and fractures were obtained by an analysis of core samples from the KTB pilot hole by the KTB Feldlabor (Röhr et al., 1990).

Seismic phase velocities of a weakly anisotropic homogeneous medium of hexagonal symmetry (transverse isotropy) can be approximated by the following equations:

$$\begin{aligned}qVP^2 &= C_0 + C_1 \sin^2(a) - C_3 \sin^2(a)\cos^2(a) \\qVS1^2 &= C_2 + C_4 \sin^2(a) \\qVS2^2 &= C_2 + C_3 \sin^2(a)\cos^2(a)\end{aligned}$$

where  $qVP$ ,  $qVS1$  and  $qVS2$  are the velocities of the P-wave and the two orthogonally polarized S-waves, respectively;  $a$  is the angle between the direction of wave propagation and the normal to the plane of rock foliation. The coefficients  $C_i$  ( $i=0,\dots,4$ ) are functions of the respective elastic constants. They can be obtained e.g. by a least squares fit if values of the seismic velocities and the respective angles of wavepropagation are known.

Based on the data of seismic velocity and dip of foliation shown in Fig.4 the equations above were used for estimating the average seismic anisotropy of the gneiss packet between 2 and 3 km depth. The procedure yields an estimate of 2.5%, 14% and 5% average anisotropy for  $qP$ -,  $qS1$ - and  $qS2$ -waves, respectively (see Fig.5).

The additional consideration of the fracture distribution (Fig.4) as a velocity influencing variable leads to an improved fit of the measured velocity data (Fig.6). In this case a linear relationship between the above coefficients  $C_i$  and the number of fractures at the respective dip angles or depths was assumed. The result gives evidence that there are variations of in situ anisotropy caused by locally varying crack densities within the gneiss packet: The intrinsic background anisotropy of the solid rock seems to be locally modified by fracture induced anisotropy.

### (3) AVERAGE ANISOTROPY OF THE SURROUNDING AREA

Seismic anisotropy in terms of S-wave splitting was observed as well for vertical seismic profiles with larger shot-borehole offsets. As an example, Fig.7 shows the shearwave arrivals for shotpoint SP402 located 4 km SE of the KTB . The travelttime difference of about 100 ms between both S-arrivals (Figs.7a, b, resectively), however, is less than expected from the measurements in the direct vicinity of the KTB pilot hole. The latter estimate of anisotropy (Figs.5,6) would imply a travelttime difference of about 180 ms between the arrivals of the direct  $qS1$ - and  $qS2$ -waves for 4 km source offset .  $qS1$ - and  $qS2$ -waves are polarized +/- in the vertical and horizontal directions within the plane of the wavefront, respectively (Fig.7). This observation is in agreement with the dip and strike direction of rock foliation found at the KTB pilot hole.

Fig.8 (dark dots) shows the azimuthal distribution of average shearwave velocities ( $qS_1$ ) around the KTB within circles of 4 and 8 km radius, respectively. The data were obtained from the above mentioned experiment "MASE". The sinus shape of the data graph (Fig.8, dark dots) is typical for an azimuthally anisotropic subsoil (compare the above equation for  $qS_1$ -velocities).

Regarding the geological map of the KTB surroundings (see e.g. Röhr et al., 1990), however, one has to consider the possible additional influence of regional scale structural inhomogeneities on the measured average velocities. Unfortunately, no reliable information about the extent of the involved gneiss, amphibolite and granit units at shallow depths is available until now. Therefore, the following procedure was applied for estimating inhomogeneity effects: (1) The geological map was projected vertically to depth for getting a structural model of the KTB surroundings, (2) the azimuthal S-wave traveltimes were used as input for a velocity inversion procedure yielding (3) optimum isotropic S-wave velocities for the respective gneiss, amphibolite and granite units in a least squares sense. Both the obtained isotropic S-wave velocities and the corresponding average velocities regarding the MASE experiment are shown in Fig.8 (light dots). Compared to the "optimum" inhomogeneous isotropic model (light dots) the real velocity values (dark dots) are lower to the N and higher around N110E deg. This result is in accordance with the P-wave observations of Bönnemann and Buttkus (this volume).

In conclusion, both vertical seismic profiling and MASE data support the assumption of a more or less NW-SE striking anisotropy system. The direction of high seismic velocities (ESE) coincides approximately with the postulated direction of maximum horizontal tectonic stress at the Oberpfalz region (see e.g. Hänel, 1989).

## REFERENCES

- Bönnemann, C., and B. Buttkus (1992): Results of the 3D expanding spread experiment. KTB report 92-5, DEKORP Report, this volume.
- Hänel, R. (1989): Abschätzungen zum Spannungsfeld aus Bohrlochaufzeichnungen. KTB report 89-1, 73-90.
- Lüschen, E., W. Söllner, A. Horath and W. Rabbel (1990): Integrated P- and S-wave borehole experiments at the KTB deep drilling site. KTB report 90-6b, 85-136.
- Röhr, C., J. Kohl, W. Hacker, S. Keyssner, H. Müller, J. Sigmund, A. Stroh and G. Zulauf (1990): German Continental Deep Drilling Program (KTB) - geological survey of the pilot hole "KTB Oberpfalz VB". KTB report 90-8, B1-B55.

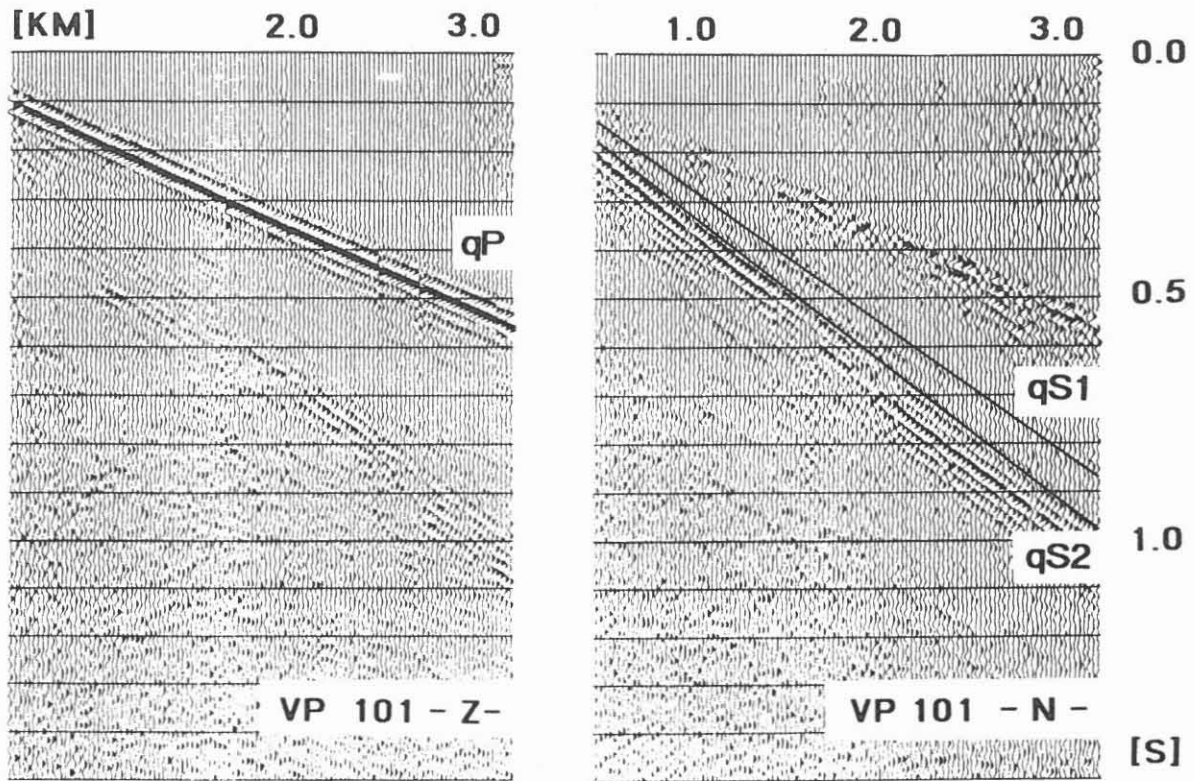


FIG.1 : Seismic sections of the vertical (Z) and one horizontal (N) geophone component for a near offset VSP. Source: Vertical vibrator. Arrivals of the direct P- and split S-waves are indicated.

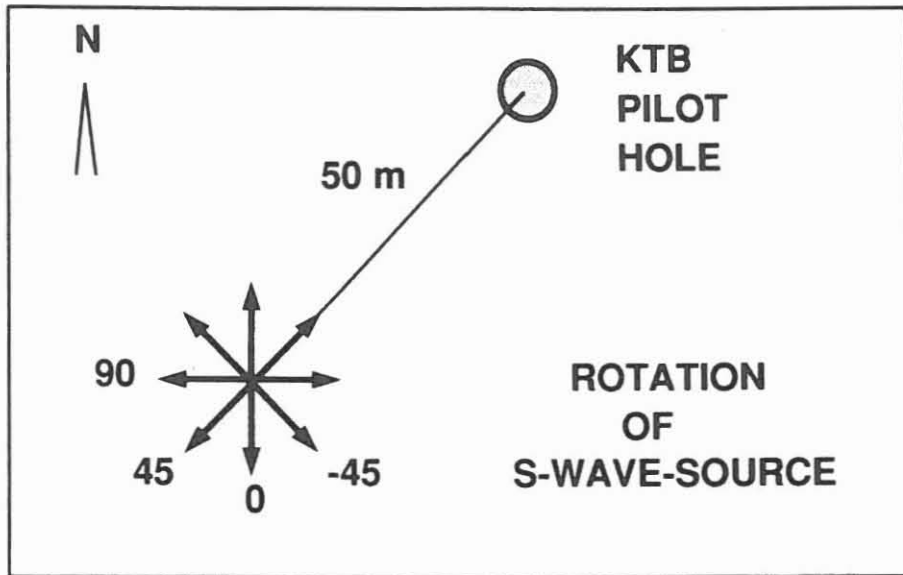
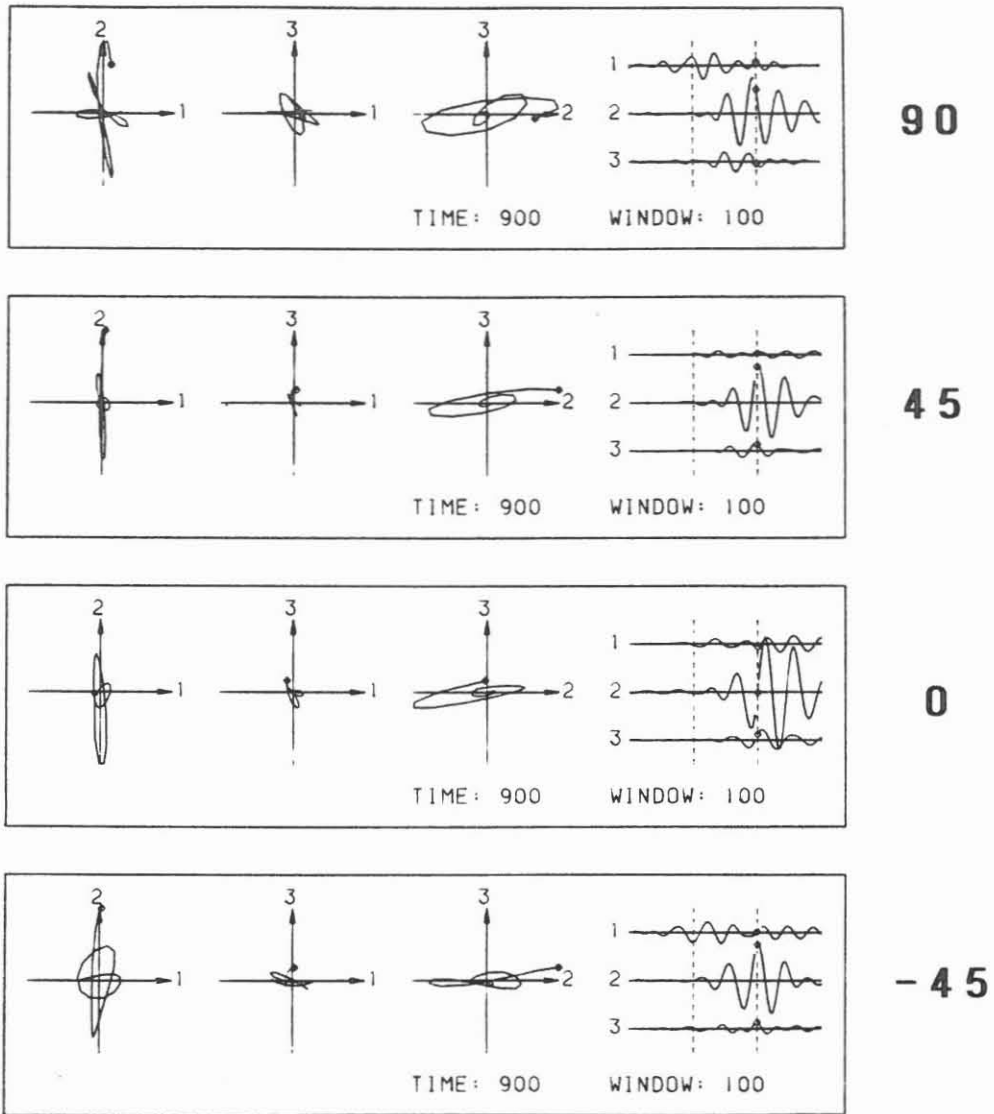


FIG.2 : Rotation of the S-wave-source. For confirming the diagnosis of seismic anisotropy a horizontal vibrator source was rotated in steps of 45 deg while the borehole geophone stayed fixed at 2900 m depth.





### Rotation of S-wave-source

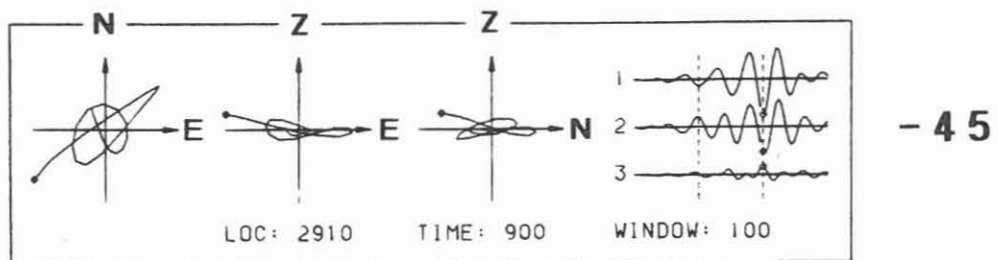


FIG.3 : Particle motion diagrams of split S-waves for the source rotation experiment (Fig.2). Source orientation indicated. TOP: ray coordinate system (1-,2-,3-axis corresponding to the polarization direction of the qS1-,qS2- and P-wave, respectively). BOTTOM: geographic coordinate system. Note the constant polarization direction of qS1- and qS2-waves.

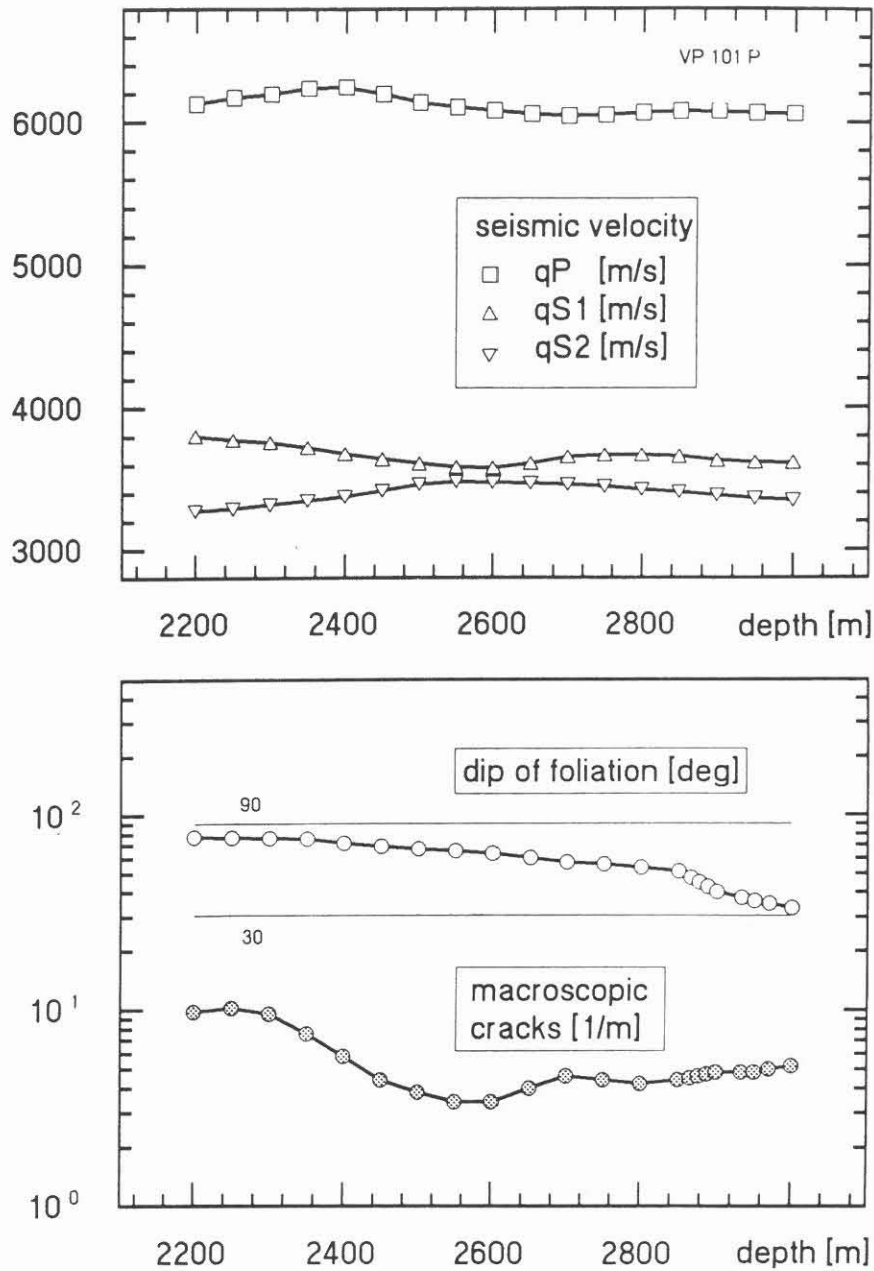


FIG.4 : TOP: Velocity vs. depth profile for qP-, qS1- and qS2-waves for the depth interval of 2-3 km of the KTB pilot hole picked from a near offset VSP (VP 101 P, see Fig.1). BOTTOM: Corresponding dip of gneiss foliation and distribution of macroscopic fractures for the same depth interval (smoothed data, after Röhr et al., 1990).

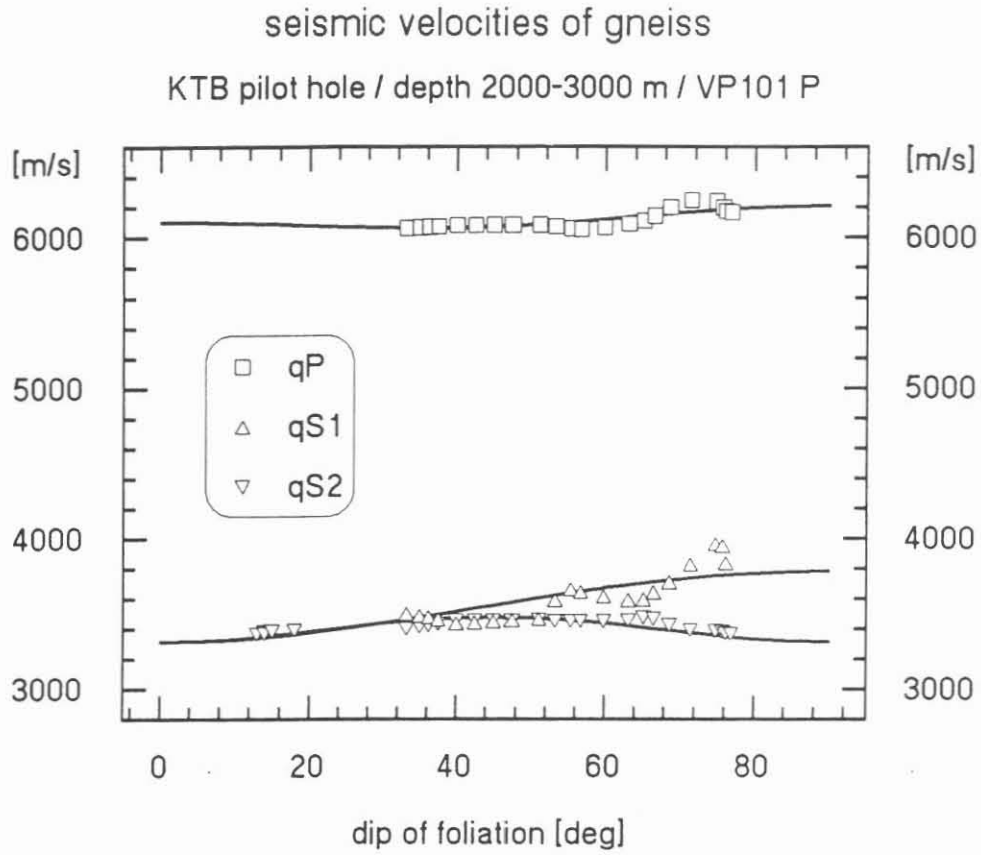


FIG.5 : Least squares fitting of seismic velocities to dip of foliation in terms of hexagonal anisotropy. Same data as in Fig.4.

seismic velocities of gneiss  
~ foliation and macroscopic cracks

KTB pilot hole / depth 2000-3000 m / VP 101 P

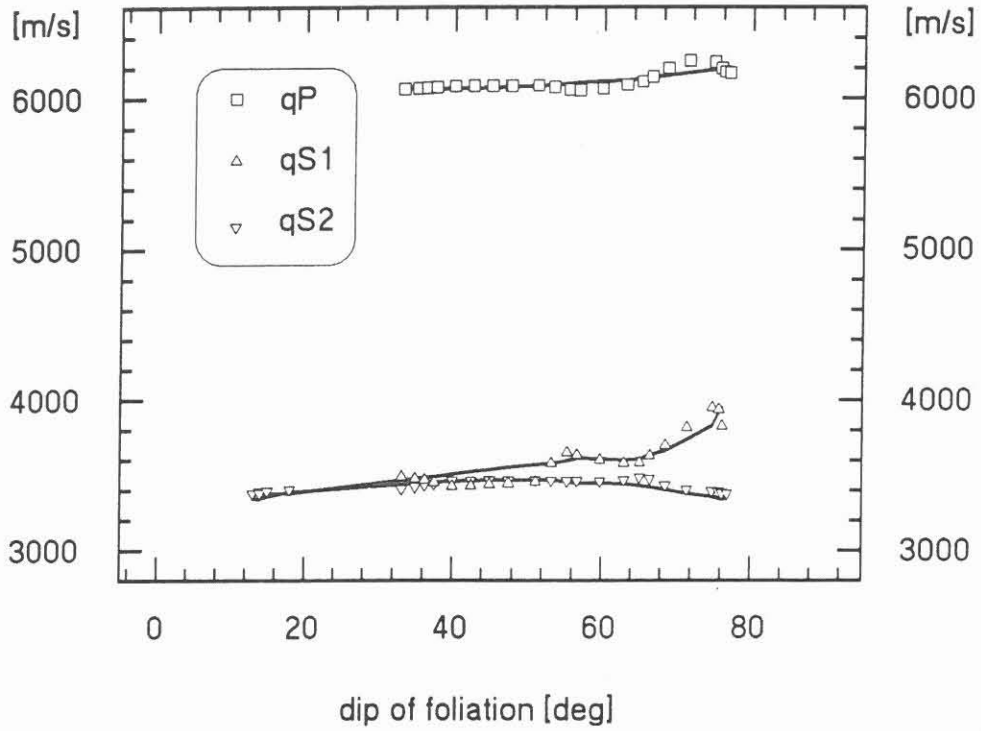


FIG.6 : Least squares fitting of seismic velocities to both dip of foliation and crack distribution in terms of hexagonal anisotropy. Data see Fig.4.

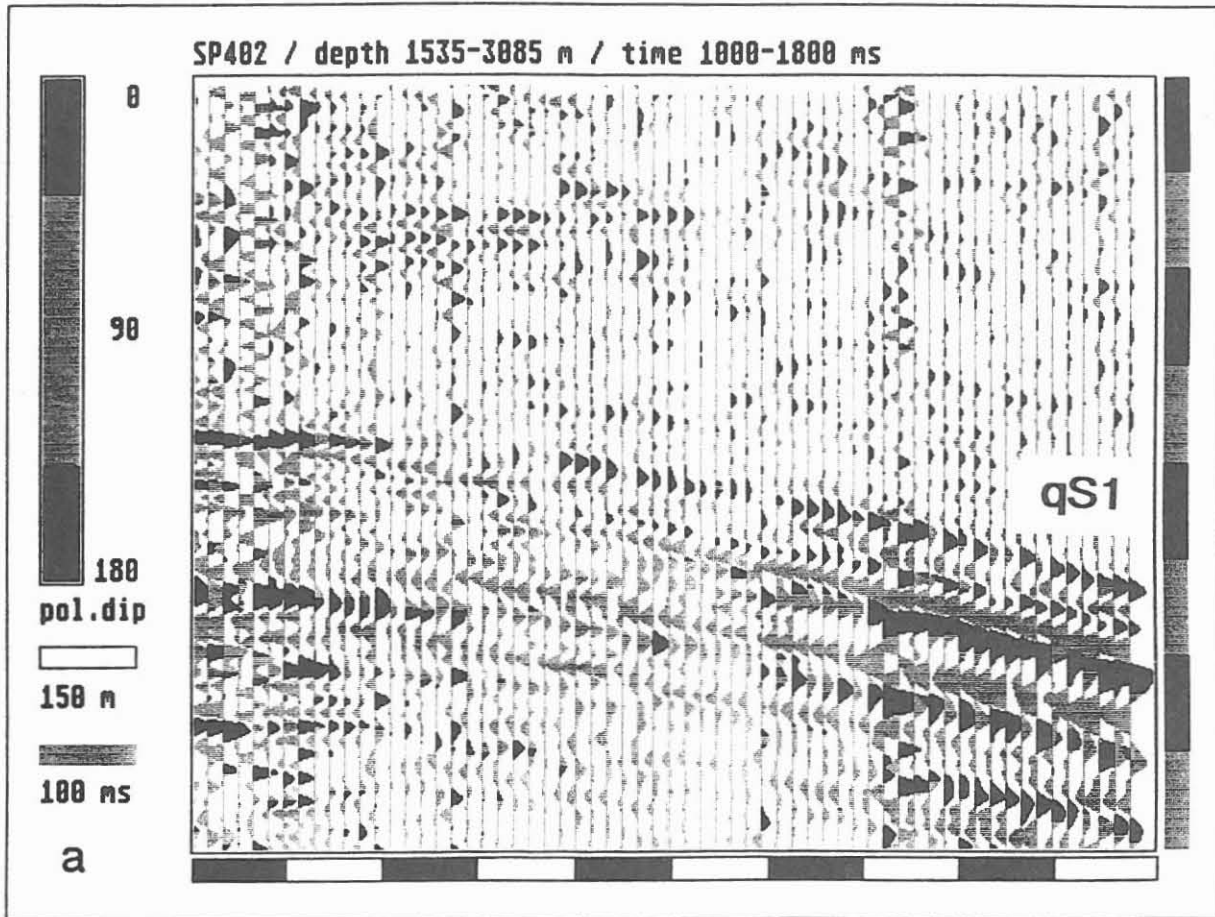


FIG.7a: Direct shearwave arrivals for an offset VSP. Shot location 4 km SE of the KTB pilot hole (SP402). Particle motion components tangential to the wavefront are shown: (a) in the vertical plane corresponding to the faster S-wave (qS1) The direction of polarization within the plane of the wavefront is attributed in black for the positive parts of oscillation (0, 90, 180 deg are the vertical, horizontal, vertical directions, respectively).

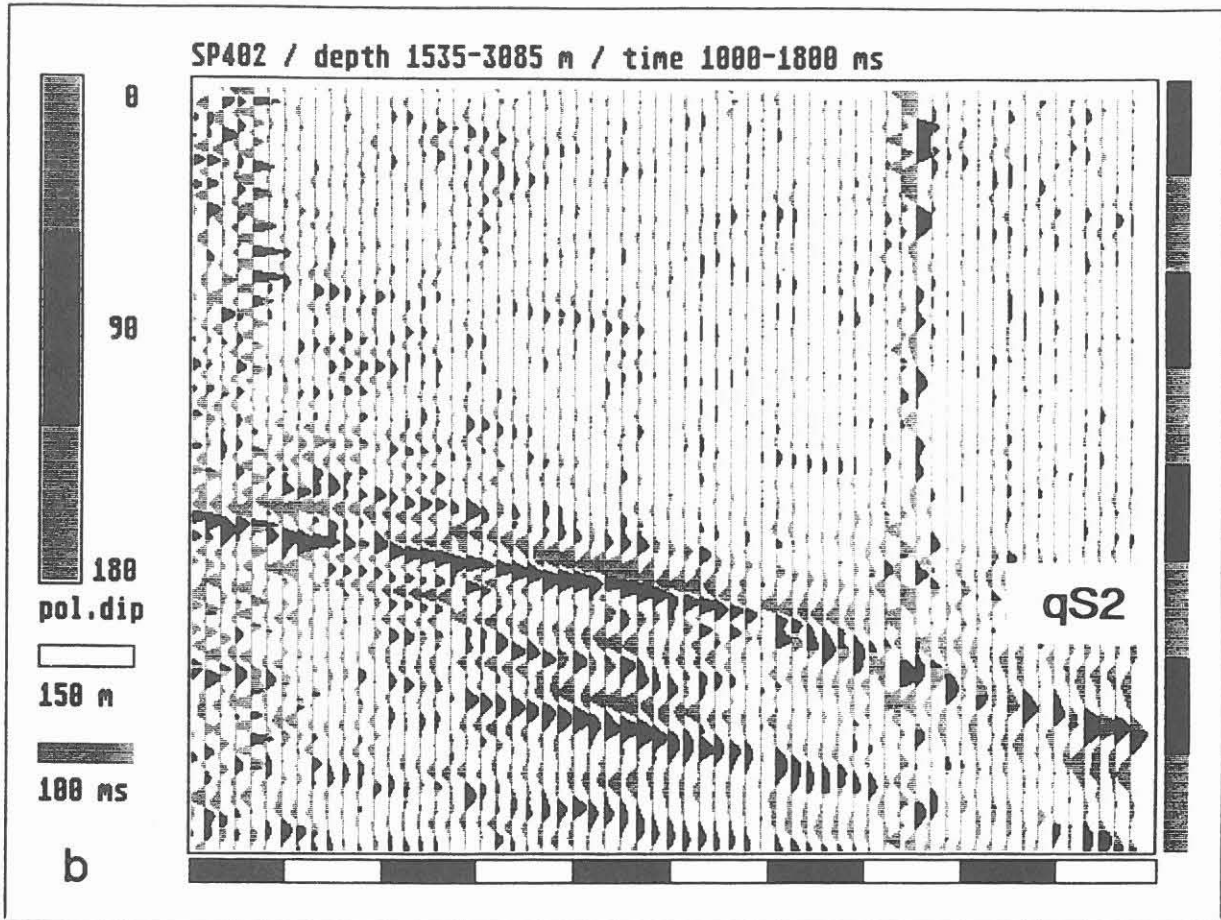


FIG.7b: Direct shearwave arrivals for an offset VSP. Shot location 4 km SE of the KTB pilot hole (SP402). Particle motion components tangential to the wavefront are shown in the horizontal plane corresponding to the slower S-wave (qS2). The direction of polarization within the plane of the wavefront is attributed in black for the positive parts of oscillation (0, 90, 180 deg are the vertical, horizontal, vertical directions, respectively).

### MASE / average velocities

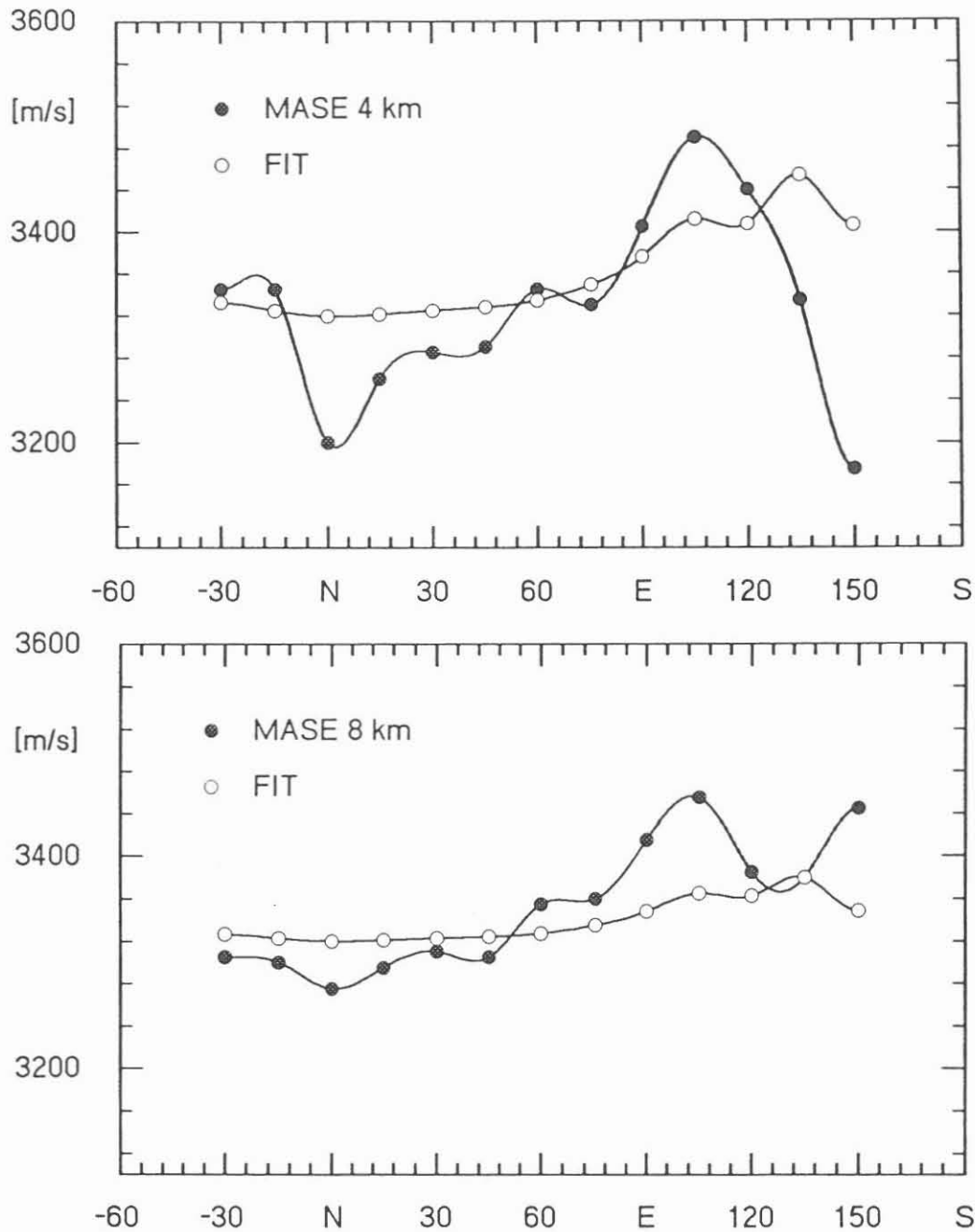


FIG.8 : Variation of average S-wave velocities with azimuth (Multiple Azimuth Shearwave Experiment MASE). Source positions were located at radii of 4 and 8 km , respectively, from the KTB pilot hole (top and bottom figure, respectively), geophones at 3300 m depth. Dark dots show the observed average velocities. Light dots represent average velocities for an optimum isotropic inhomogeneous model based on the geological map of the KTB surroundings (for details see text). The corresponding isotropic S-wave velocities are 3200, 3750 and 3400 m/s for granite, amphibolite and gneiss areas, respectively.





## More reliable shear-wave data from VSP by using CIPHER-technique

T.W. GUT\*, W. SOELLNER\*, E. LUESCHEN\* and  
H.A.K. EDELMANN†

It has been recognized for a long time that fracture systems in rocks can significantly influence the flow of fluids in the subsurface. Geophysical fracture characterization techniques based on seismic anisotropy and related shear-wave splitting have been under investigation for many years. It is now established as an observable effect. To keep rig time costs low, a 3-C multilevel downhole sonde has been introduced many years ago. Additional horizontal vibrators and additional survey time and processing costs for shear-wave data, however, are still important constraints. The CIPHER-method (Edelmann, 1992) described below aims both at the reduction of costs and at an improvement of VSP shear-wave data.

Fig. 1 shows schematically the basic concept of shear-wave splitting of a circularly polarized shear-wave in a fractured medium. The incident wave illustrated by a spiral is split into a fast component polarized parallel to the fracture direction and a slow component perpendicular to this direction when travelling through the medium.

Circularly polarized shear-waves can only be generated by using controlled sources, such as horizontal vibrators. Fig. 2 shows two vibrators, positioned orthogonally radiating two sweep signals differing in phase by 90 degrees. The resulting signal is recorded by a 3-C sonde in the KTB pilot hole over a depth range between 2800 and 3400 m. An upsweep signal of 30 s length and a frequency range between 9 and 43 Hz was used. The hole was drilled in crystalline rocks (gneisses, amphibolites) of the Bohemian Massif. The CIPHER-experiment (Circularly Polarized Horizontal Extension Radiation) was part of a more comprehensive P- and S-wave survey (Lueschen et al., 1991).

Fig. 3 shows the two horizontal components of the wavefield after being rotated into the natural coordinate system, which was determined from the polarization analysis described below. This coordinate system is assumed to coincide with the preferred strike direction of fractures. In this way the fast and the slow shear-wave events as marked in the figure can clearly be separated. The average shear-wave anisotropy (ratio of time delay to travel time of the first arrival) for the overburden is about 10% (Lueschen et al., 1991).

---

\*Geophysical Institute, University of Karlsruhe, Hertzstr. 16, W-7500 Karlsruhe 21,  
F.R. Germany

†Pirolweg 6, W-3000 Hannover 61, F.R. Germany

The horizontal polarization of shear-waves at different depths is determined by calculating the direction of the main axis of the polarization ellipse within a moving window. Fig. 4 shows the result of this analysis for eight different recording depths. The azimuth of the first arrival (fast event) is approximately N 140° E. After about 100 ms the azimuth switches over to about N 50° E the orientation of the second arrival (slow component) as can be seen from the curves.

The advantages of the CIPHER technique compared to the conventional technique are:

- No a-priori knowledge about optimum vibrator orientation needed,
- Only half the number of shear-wave recordings at the well necessary,
- Better quality of data so that less expensive processing is needed to achieve more reliable results.

#### References:

- Lueschen , E.; Soellner, W.; Hohrath, A.; Rabbel, W.: Integrated P- and S-wave Borehole Experiments at the KTB - Deep Drilling Site. In: Continental Lithosphere: Deep Seismic Reflections. Washington, D.C.. 1991
- Edelmann , H.A.K., Circularly Polarised Shear - Waves used for VSP: Geophysics, Vol.57., April 1992: P.643-646

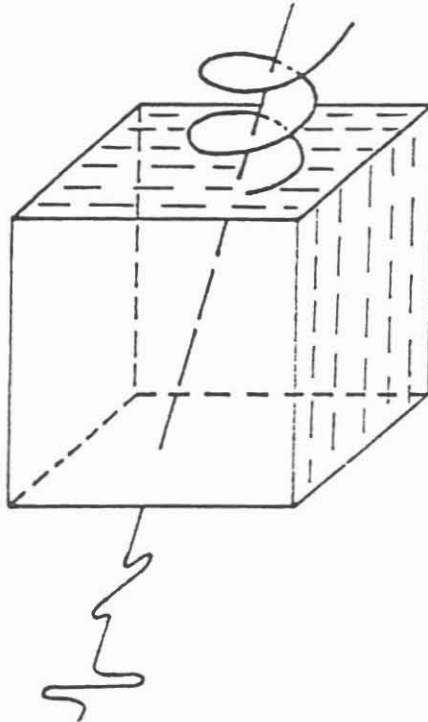


Figure 1: Schematic illustration of shear-wave splitting using circularly polarized shear-waves

## CIPHER field configuration

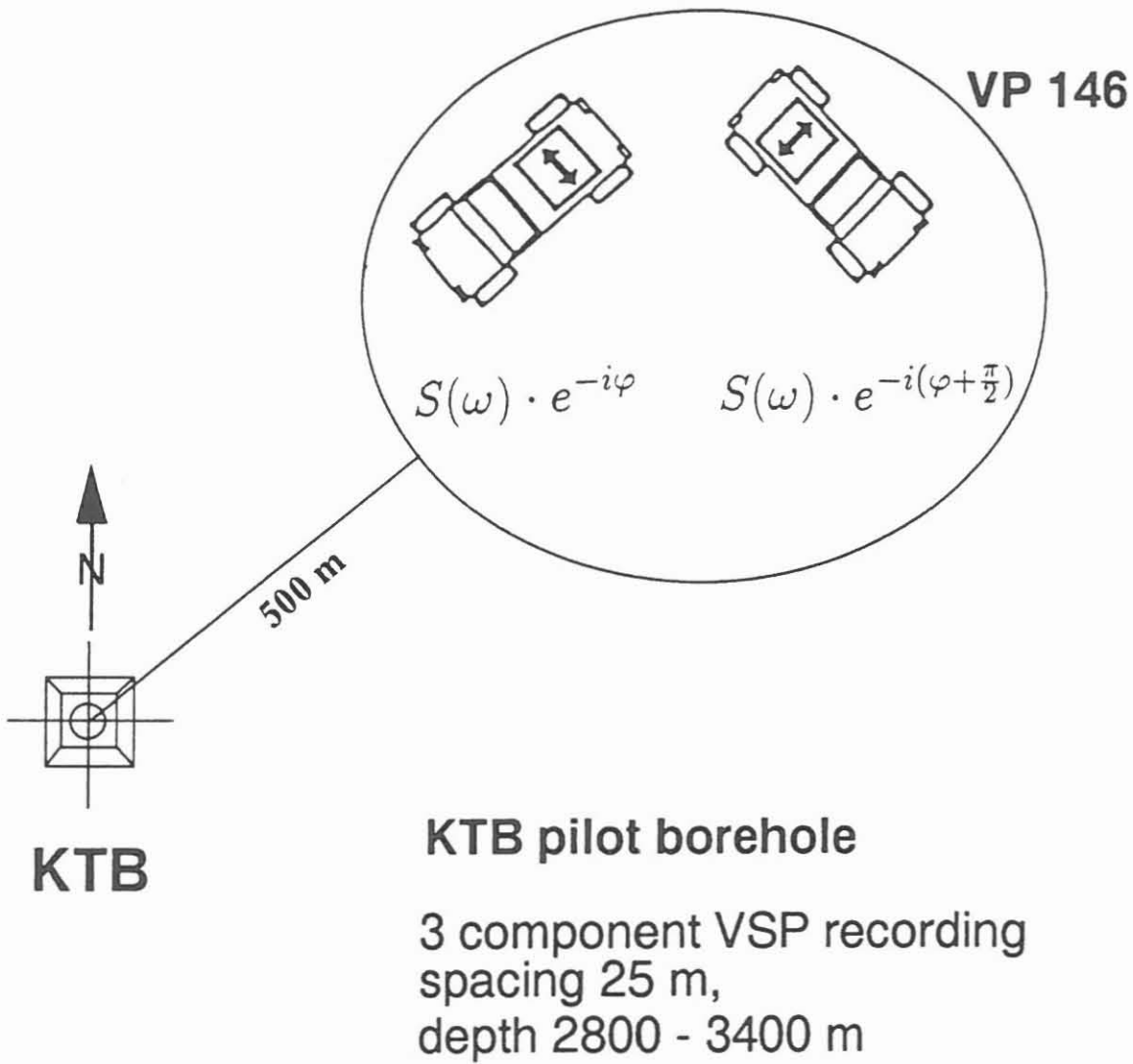


Figure 2: Vibrator arrangement for CIPHER VSP at the KTB pilot hole (CIPHER= Circularly Polarized Horizontal Extension Radiation, KTB= Kontinentales Tiefbohrprogramm)

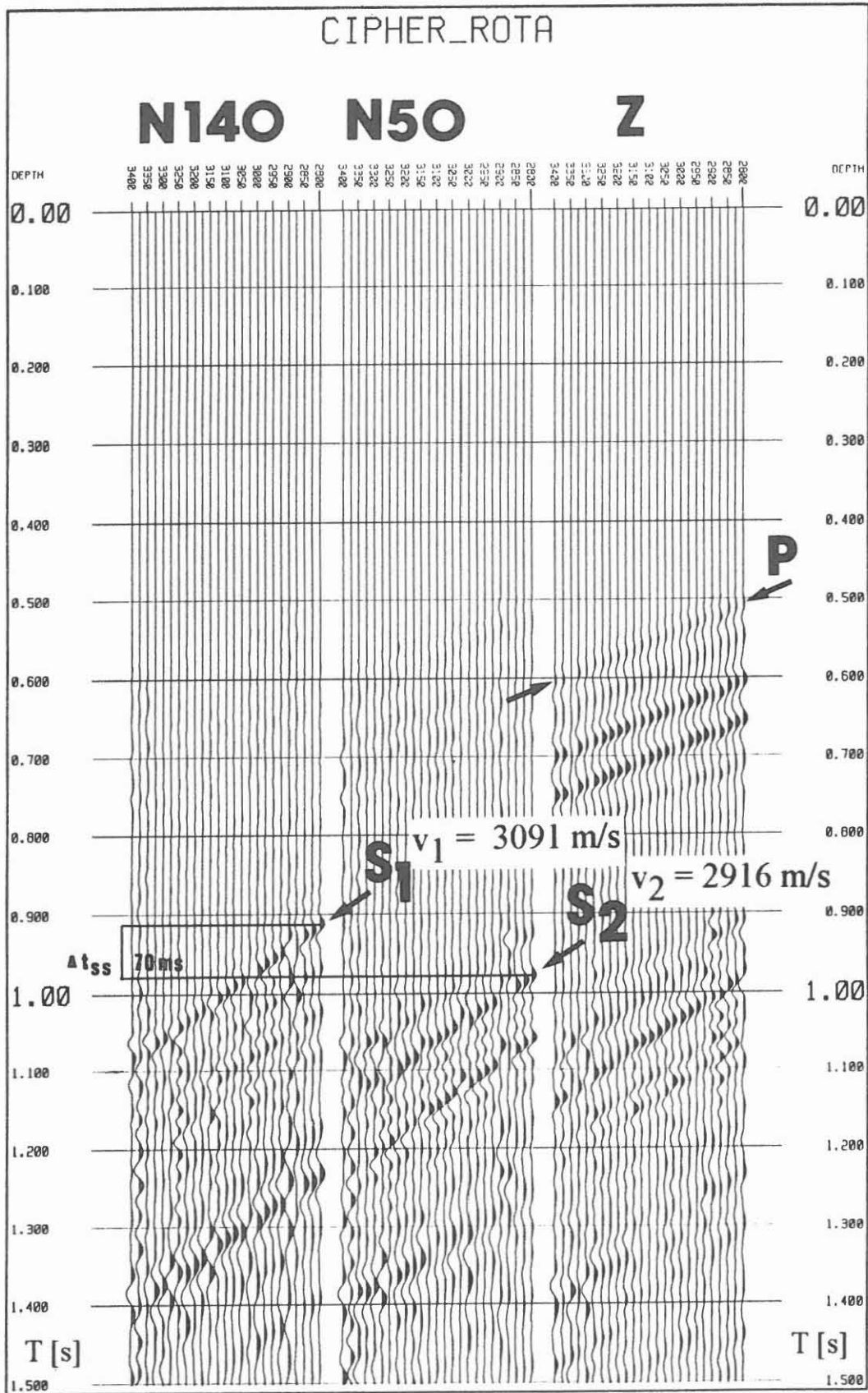


Figure 3: Horizontal component recording after being rotated into a natural coordinate system

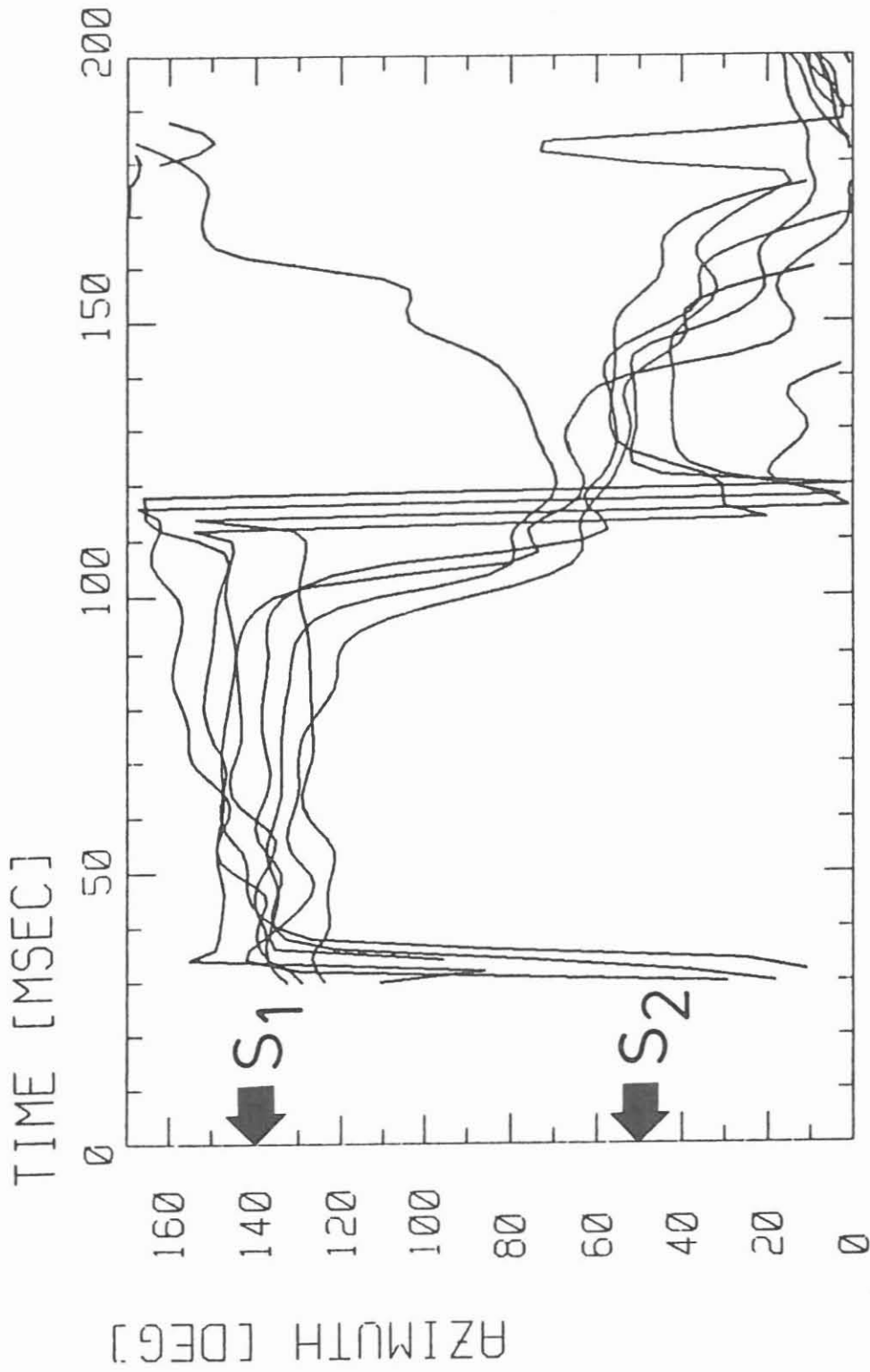
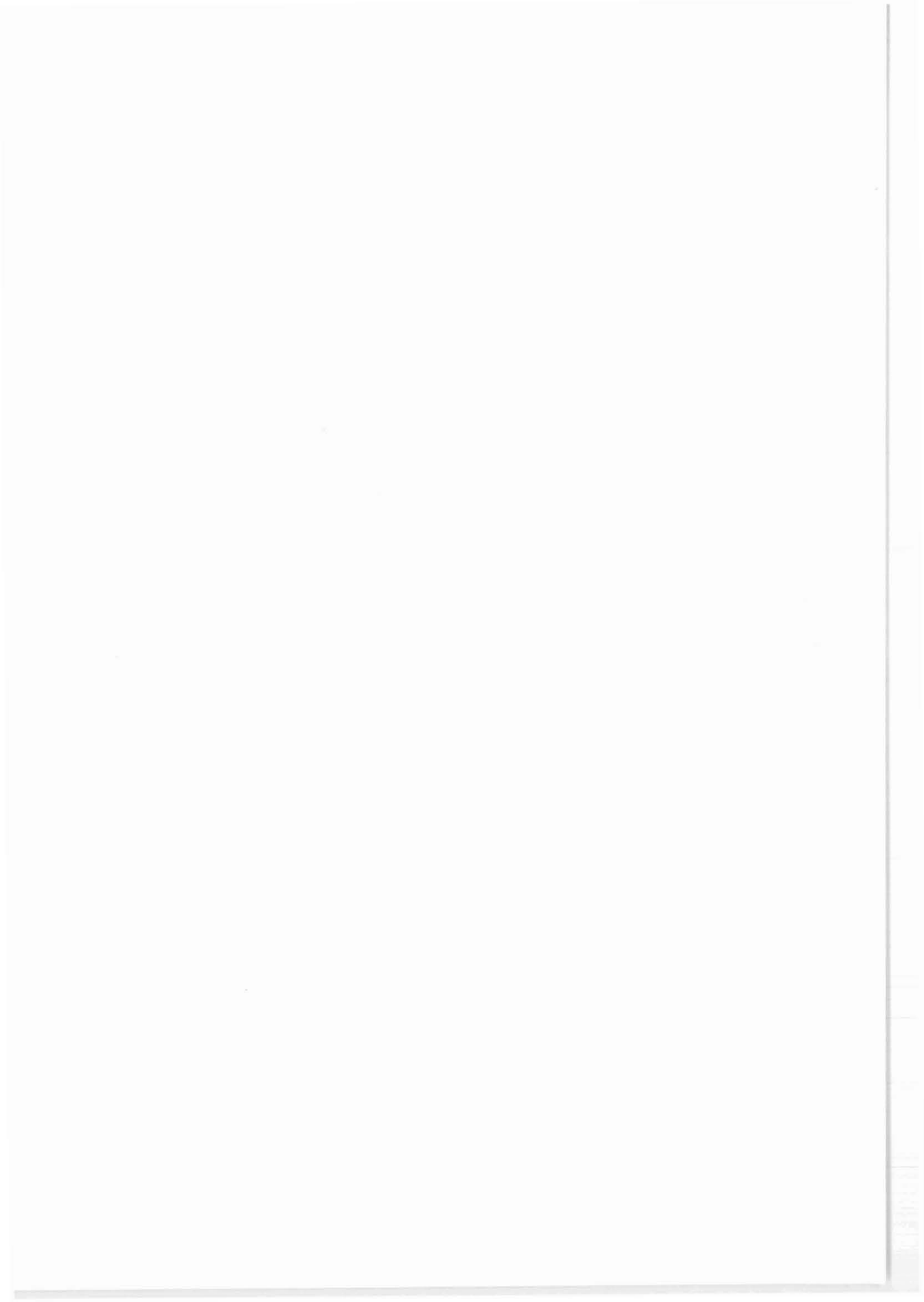


Figure 4: Results of azimuth angle determination as a function of recording time



## Shear-Wave Splitting Observed by Wide-Angle Measurement

Michael Bopp \*)

### Summary

The recordings of the wide-angle shots by 3-component geophones in the KTB pilot hole exhibit the effect of shear-wave splitting, that is the most diagnostic evidence of seismic anisotropy (Crampin, 1989). The possible reasons for seismic anisotropy will be discussed and the lateral extension of the anisotropic region will be estimated.

### Shear-wave observations in the KTB pilot hole

Shear-wave splitting has been observed for Vogtland earthquakes, recorded at seismological stations NE of the KTB location (Schmedes, 1987). By recording the wide-angle shots of the IS089

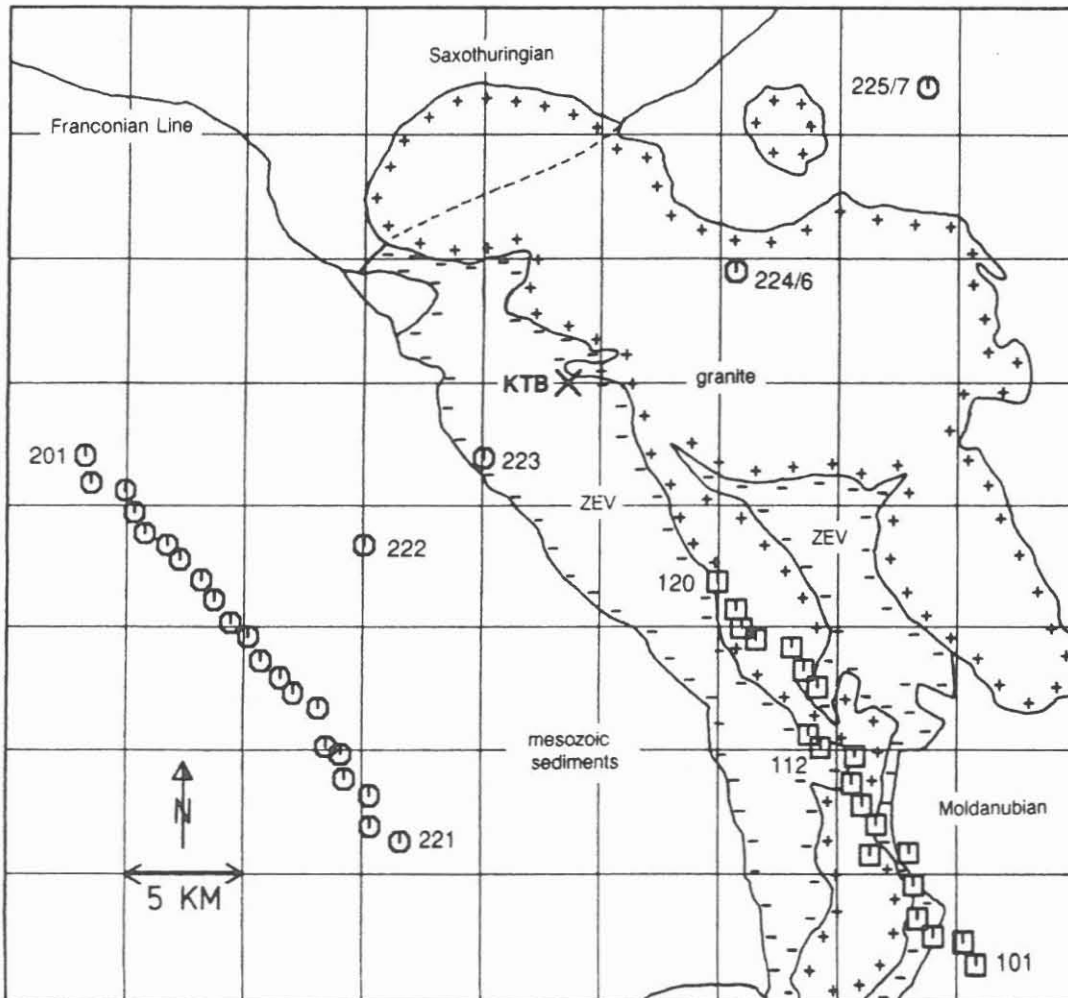


Fig. 1: Location map of IS089 wide-angle measurement superimposed with a simplified geology (after Stettner, 1981) of the KTB surrounding. ZEV is the Zone of Erbdorf Vohenstrauß; numbers indicate shots.

\*) Institut f. Allg. u. Angew. Geophysik, Theresienstr. 41/IV, D-8000 München 2, FRG

survey (Fig. 1; Gebrande et al., 1990) with 3-component geophones in the KTB pilot hole an independent check of the splitting effect became possible. Borehole recordings have the special advantage of being free from the usual distortions by the earth's surface, e.g. non-orthogonality of P- and S-polarization directions and non-linearity of S-polarization.

Decomposition of the 3-component recordings into mutually orthogonal components parallel and normal to P-wave polarization provides an almost perfect separation of P- and S-waves. Fig. 2 shows the seismogram section for the shotpoints 101-120 in the SE of the KTB location, recorded in 3270 m depth. The traveltime,  $\sqrt{3}$ -times greater than for P-waves, and the lower frequency content of the shear-waves indicate primary radiation from the source and no P-S conversions. Most likely, anisotropy and local heterogeneities of the crystalline source environment are responsible for the S-wave radiation. The shear-wave is not of pure SV- or SH-type, since it can be seen on the vertical and transverse horizontal component in Fig. 2. Its polarization is in the plane normal to P-wave polarization, proving shear-wave propagation parallel to the P-wave.

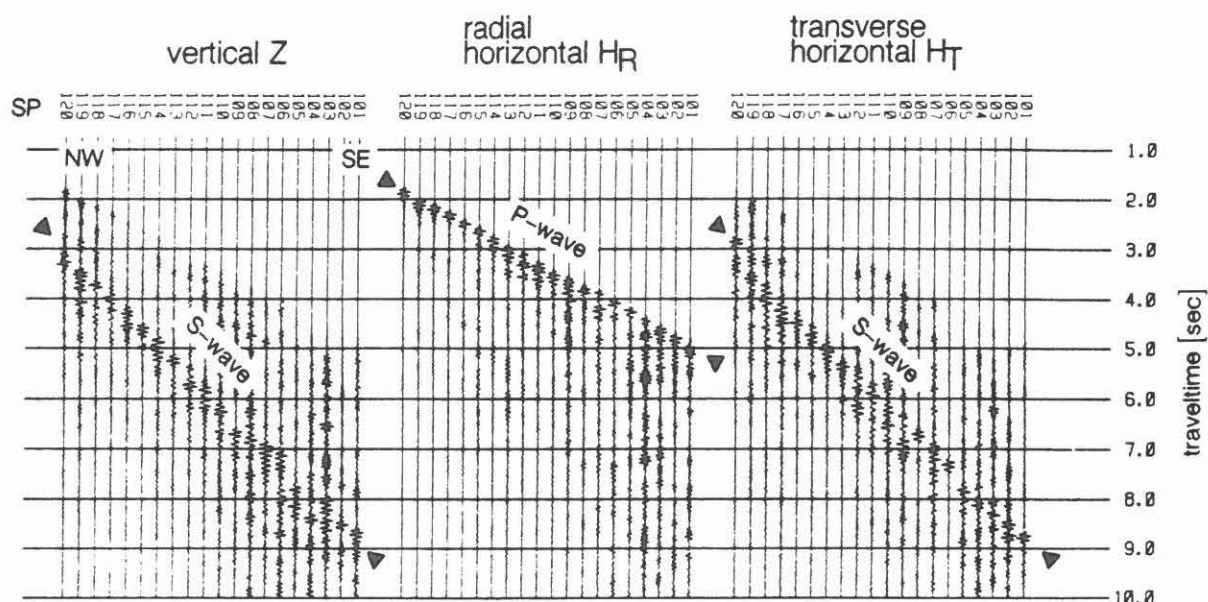
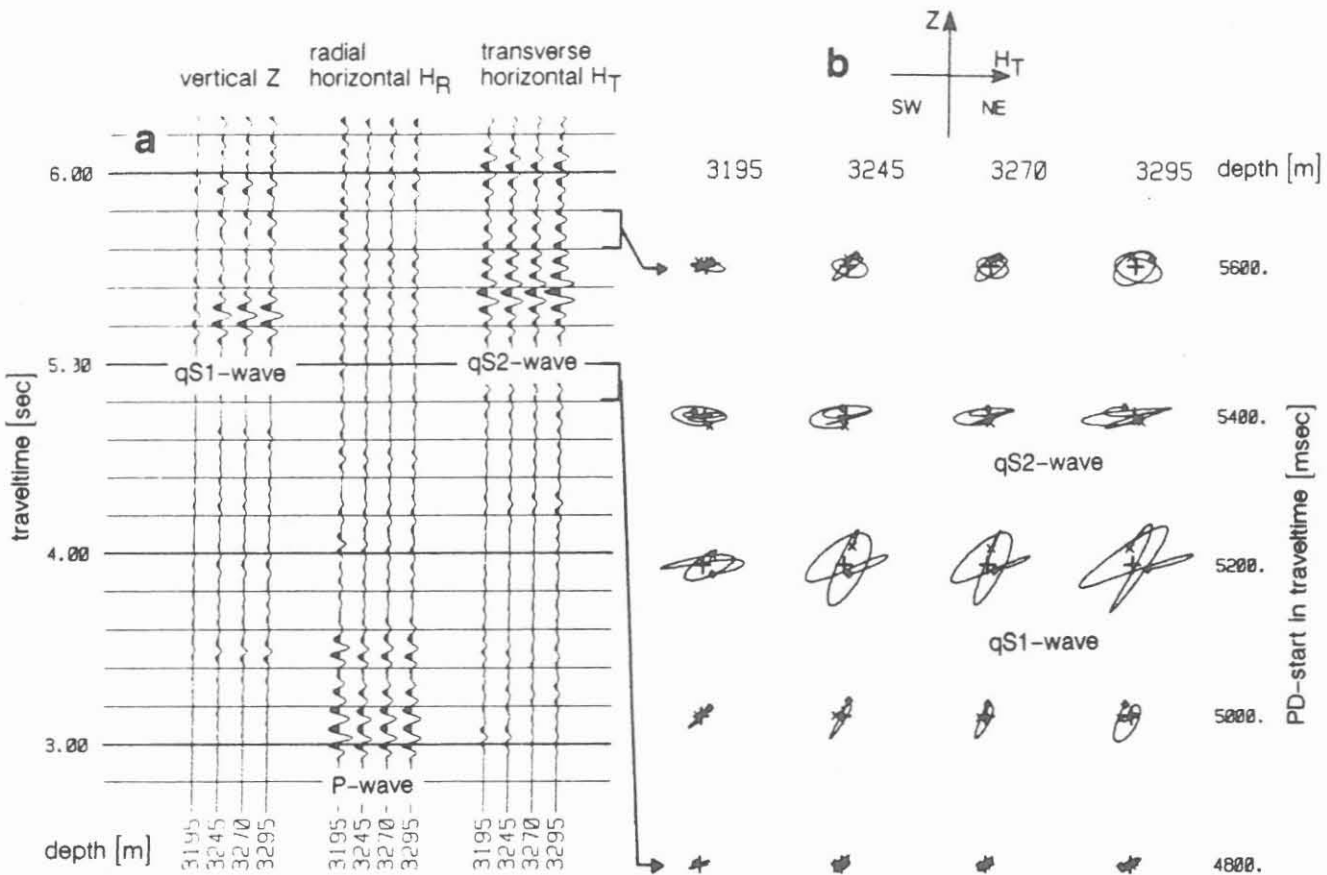


Fig. 2: Seismogram sections of SPs 101-120 for the 3-component receiver in 3270 m depth. A 6-15 Hz band-pass filter was applied to improve the appearance of shear-waves. Each trace is normalized to its maximum amplitude.

The recordings of SP 113 (Fig. 3a) show two shear-wave onsets with a time delay of nearly 0.2 s. The fast quasi shear-wave qS1 (terminology after Crampin, 1989) with linear polarization dipping steeply to SW is followed by the slow quasi shear-wave qS2 with more elliptical horizontal polarization. These properties can be seen from the polarization diagrams (PD) in the plane normal to P-wave polarization (Fig. 3b). It's a characteristic effect of S-wave propagation through an anisotropic medium. The fast qS1-wave is expected to be polarized in a preferred direction of anisotropy and the slow qS2-wave is perpendicular to this. A strict orthogonality is, however, not observed in the real data and possible reasons will be discussed later.





**Fig. 3:** Unscaled seismograms (a) and polarization diagrams (PD, b) in the plane normal to P-wave polarization showing shear-wave splitting for SP 113. All PDs are plotted with the same gain.

### Causes for seismic anisotropy

Seismic anisotropy in the continental crust is mainly due to the following reasons (Crampin et al., 1984):

- a) Parallel (micro-)cracks, occasionally filled with fluids (Extensive Dilatancy Anisotropy).
- b) Interbedding of rocks (foliation) that can be isotropic itself (Periodic Thin-Layer Anisotropy).

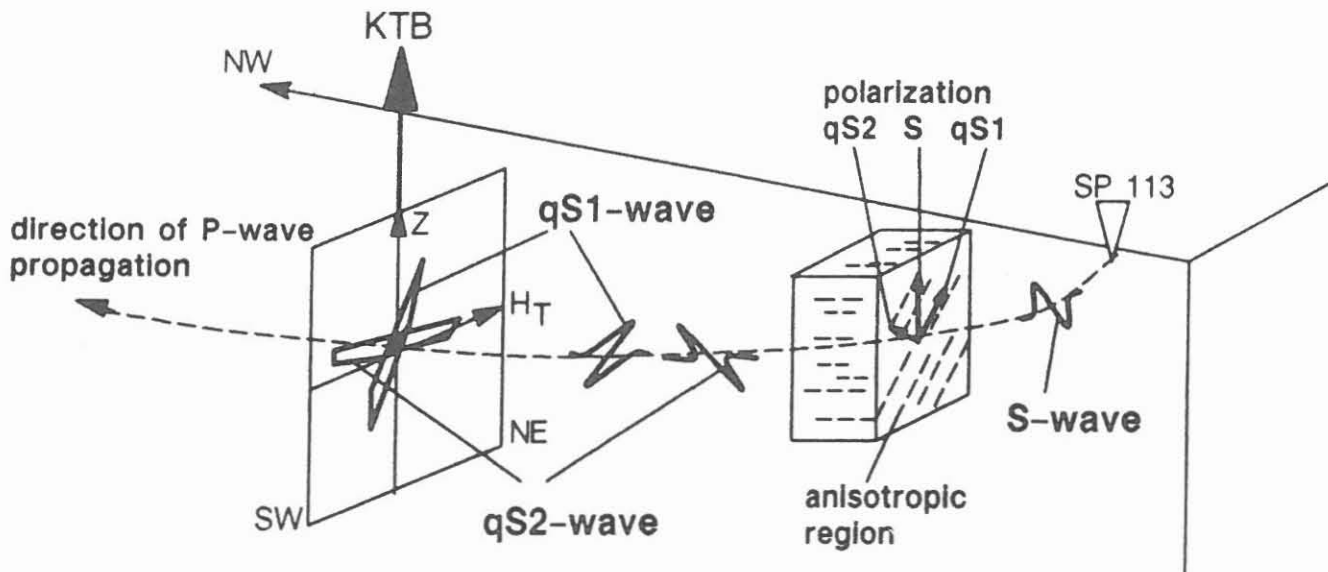
After Crampin (1989) EDA-anisotropy caused by vertically aligned cracks, that are generally orientated normal to the minimum compressive stress, should be wide-spread over the crust. Field observations have been interpreted in either way. Ahmed (1990) estimated the axis of maximum horizontal compressive stress from splitted shear-waves observed in a VSP-survey by identifying the polarization of the fast qS1-wave with the orientation of open micro-cracks (case a). On the other hand Brocher and Christensen (1990) observed maximum P-wave velocity in a seismic survey in the direction perpendicular to the axis of maximum compressive stress, but parallel to rock foliation, and explained this result by PTL-anisotropy and mineral orientation (case b).

Comparison with laboratory investigations on KTB cores should elucidate, whether case a and/or b is responsible for the observed shear-wave splitting in Fig. 3b.

Significant velocity anisotropy is present in most KTB core samples (Lippmann et al., 1989; Zang et al., 1989; Kern et al.,

1991). Their maximum P-wave velocity is generally observed parallel to foliation in gneisses. A larger part of this anisotropy is caused by micro-cracks aligned parallel to the foliation, because it diminishes with increasing pressure (case a; Zang et al., 1989, Kern et al., 1991). The remaining intrinsic anisotropy of about 10% in gneisses is a textural one (case b) and is caused by preferred orientation of anisotropic minerals as, e.g., micas in gneisses and hornblende in amphibolites (Kern et al., 1991). Crack and textural anisotropy interfere constructively, because the orientation of the cracks is coupled to the foliation. At in-situ conditions the textural cause is expected to dominate.

Ultrasonic measurements of shear-wave splitting in core samples (Kern et al., 1991) are even more important for the interpretation of the field data. In gneisses it is most pronounced for S-wave propagation parallel to the foliation with the fast qS1- and the slow qS2-wave being polarized parallel and normal to the foliation plane. Velocity differences up to 15% due to shear-wave splitting are expected at in situ pressures in gneisses.



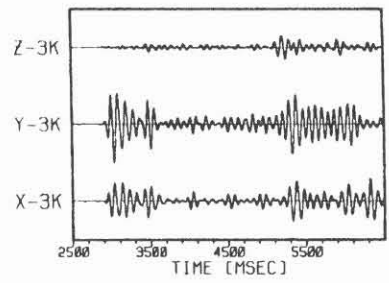
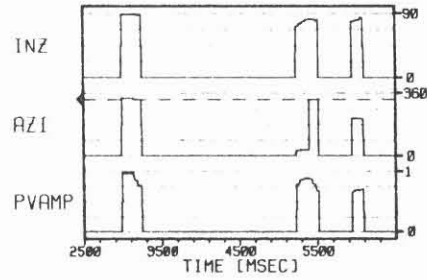
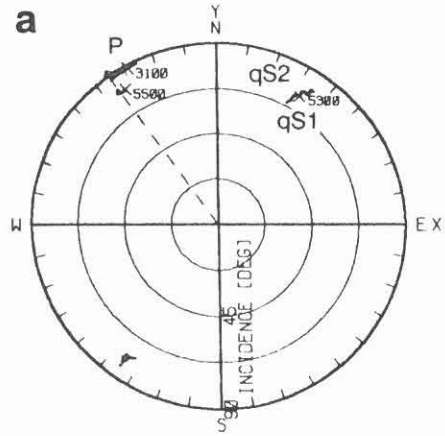
**Fig. 4:** Schematic illustration (modified after Crampin, 1989) that combines the observed shear-wave splitting with the results from ultrasonic measurements. A primary generated S-wave propagates through a region with foliation dipping steeply to SW and splits up into a fast qS1- and a slow qS2-wave.

In **Fig. 4** the simplified observation from the PDs in **Fig 3b** is combined with the results from laboratory investigations. The shear-wave generated e.g. by SP 113 propagates through a region with foliation dipping steeply to SW. The shear-wave splitting must be related to both effects, **a** (micro-cracks), and **b**

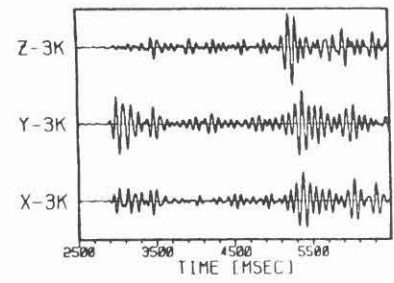
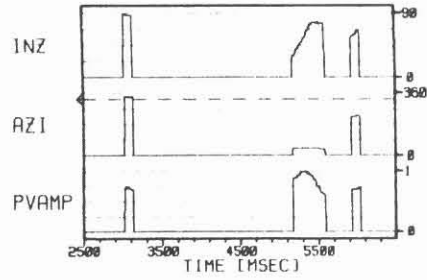
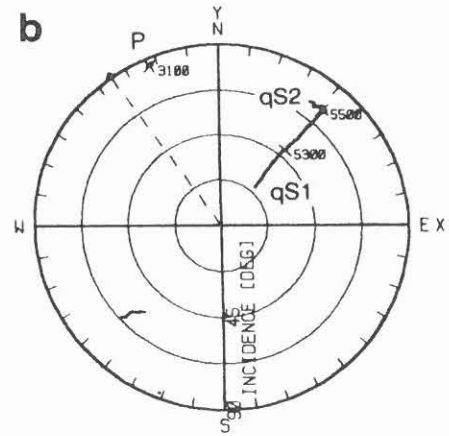
on right page:

**Fig. 5:** Results of polarization analyses of the 4 down-hole 3-component recordings (**a** to **d**) of SP 113. For each receiver position 3 plots are presented: 3-component seismograms on the lower right side, polarization parameters to the left as a Schmidt diagram and on the upper right side as functions of time. The P-wave polarization is almost horizontal and close to the shot-to-receiver azimuth. The shear-wave splitting is most pronounced for geophones at 3245 m (**b**), 3270 m (**c**) and 3295 m depth (**d**) with steep dipping qS1-polarization and almost horizontal qS2-polarization under the same azimuth.

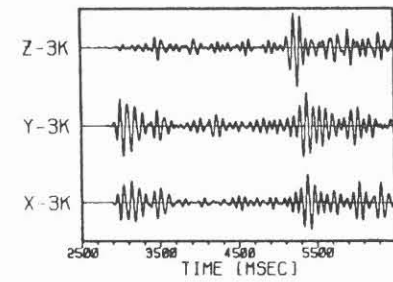
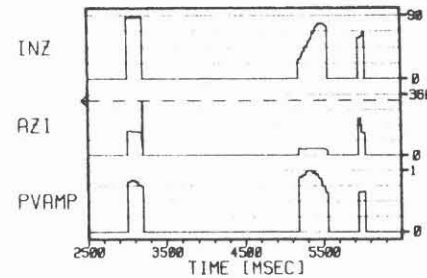
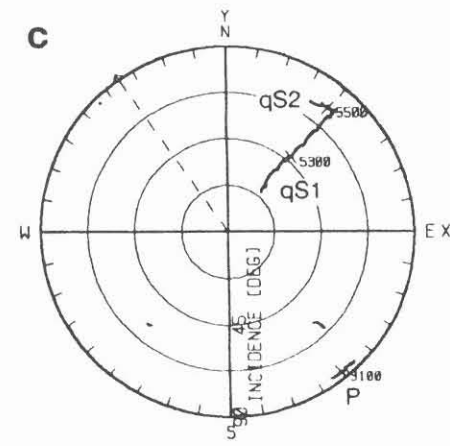
POLARIZATION VECTOR  
 FOR SHOT 113 AND DEPTH 3195  
 ↗ SHOT TO RECEIVER AZIMUTH 325.0 [DEG]



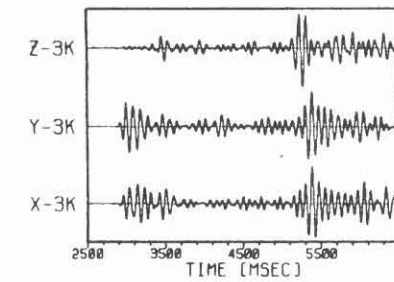
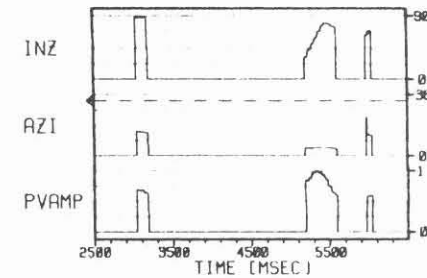
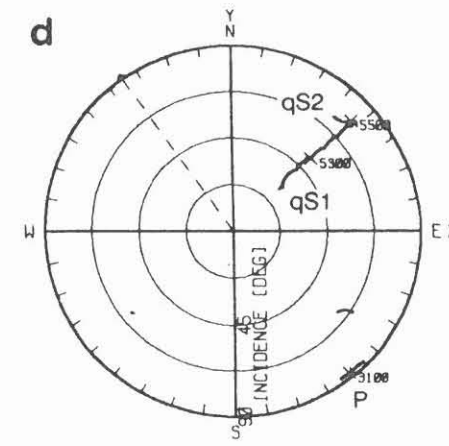
POLARIZATION VECTOR  
 FOR SHOT 113 AND DEPTH 3245  
 ↗ SHOT TO RECEIVER AZIMUTH 325.0 [DEG]



POLARIZATION VECTOR  
 FOR SHOT 113 AND DEPTH 3270  
 ↗ SHOT TO RECEIVER AZIMUTH 325.0 [DEG]



POLARIZATION VECTOR  
 FOR SHOT 113 AND DEPTH 3295  
 ↗ SHOT TO RECEIVER AZIMUTH 325.0 [DEG]



(texture). Cracks are not necessarily closed in the depth range of wave propagation as indicated by an open joint found at 3447 m depth (Stroh et al., 1990).

According to this model the dip of foliation can be obtained by the polarization of the fast qS1-wave (Crampin, 1985) assuming homogeneous anisotropy and wave propagation parallel to the strike of foliation. Figs. 5a-d show the results of polarization analysis for SP 113 using the so-called polarization vector (Bopp, 1992). The polarization parameters, azimuth (AZI) and angle of incidence (INZ), measured from the vertical, are calculated in sliding time windows of 200 ms. They are plotted as time dependent traces in a Schmidt diagram (left side in Figs. 5a-d). The "trace" of the polarization vector amplitude (PVAMP) is plotted together with the polarization parameters as function of time (upper right side). The magnitude of PVAMP is used to define a valid polarization result (s. chapter 3.2 in Bopp, 1992).

The P-wave (at 3100 ms) is almost horizontally polarized ( $INZ \approx 90^\circ$ ) close to the shot-to-receiver azimuth at all geophone depths (Figs. 5a-d). The estimated azimuth may be in the opposite direction (s. Fig. 5c and 5d) for inclined polarization, because it changes by  $180^\circ$  when the inclination crosses the horizontal plane ( $INZ = 90^\circ$ ).

At the deeper-located geophones (Figs. 5b-d) the angle from vertical to the qS1-polarization (before 5300 ms) amounts to  $\approx 30^\circ$  whereas the qS1-polarization at 3195 m depth (Fig. 5a) shows small dip ( $INZ \approx 70^\circ$ ). While instrumental effects should be excluded this observation fits to almost horizontal foliation at 3100 m depth and a fault zone at 3200 m depth (Röhr et al., 1990).

The qS2-polarization is almost horizontally polarized ( $INZ \approx 80^\circ$ ) at all depths. Because the azimuthal direction ( $\approx 40^\circ$  N°E) is the same for qS1- and qS2-polarization, it can be assumed that the splitted shear-waves are propagating in the same direction. From the qS1-polarization in 3245-3295 m depth it appears that the dip of foliation SE of the KTB location is about  $60^\circ$  to SW.

#### Lateral extension of the anisotropic region SE of KTB

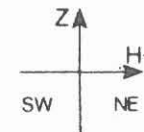
Fig. 6 shows the PDs recorded in 3245 m depth for all SP 101-120 SE of the KTB location. The plane of the PDs normal to P-wave polarization is individually adjusted for each shot. The amplitudes in the vertically arranged PDs are scaled to the maximum trace amplitude within this shot.

SP 113 exhibits the most pronounced shear-wave splitting. It is less distinct for the adjacent SP 111-116. The observed S-wave from SP 106 seems to be of pure SH-type. In general only the SP 112-120 nearest the KTB location exhibit the steep dipping qS1-polarization. Averaging these dip angles, measured from the horizontal and calculated with a polarization analysis by solving the 2D-covariance matrix for eigenvalues and -vectors (Kanasewich, 1973), leads to the results demonstrated in Tab. 1.



PD-start in reduced time [msec]

Fig. 6: Polarization diagrams in the plane normal to P-wave polarization for the recordings of the whole shot series SE of the KTB location at the geophon in 3245 m depth. The time reduction is carried out by 3.5 km/sec for the lateral offset (s. Fig. 7).

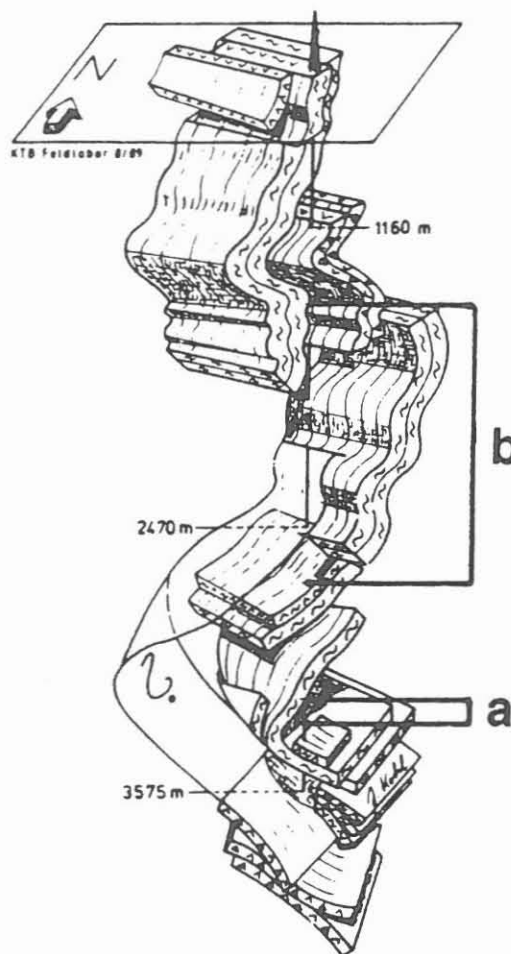


**Table 1:** Comparison between the qS1-polarization obtained by averaging the results of polarization analysis for SPs 112-120 and the dip of rock foliation determined at KTB core samples. Dip angles are measured from the horizontal.

geophone depth [m]	3195	3245	3270	3295
Dip of polarization to SW [°] (mean value with standard deviation)	37 ± 13	68 ± 10	68 ± 10	65 ± 10
Dip of foliation in the borehole [°]	35	30	35	40

The difference in the polarization angles between the uppermost and the deeper-seated geophones is about 30°. These polarization dips are compared in Tab. 1 with the dip of rock foliation (moving average over 25 m; from Fig. 4 in Lippmann et al., 1989). In the depth interval of the geophones (Fig. 7a) azimuth and dip of rock foliation are not uniform (Kohl et al., 1991). This implies that the immediate surrounding of the down-hole geophones can't be responsible for the observed shear-wave splitting with qS1-polarization dipping to SW.

The VSP-surveys of IS089 provided complementary observations of shear-wave splitting for vertical wave propagation (Lüschen et al., 1990) with the fast qS1-wave being polarized NW-SE. According to the authors this may be due to the uniform NW-SE striking and steeply SW-dipping foliation in the depth range 1500 to 2700 m (Fig. 7b). If this zone extends further to the SE, it could consistently also explain the wide-angle observations, since the ray-paths for the wide-angle shots, calculated by raytracing (Gebrande et al., 1990), are nearly horizontal in this depth range.



**Fig. 7:** Schematic sketch of the geological section in the KTB pilot hole (Röhr et al., 1990) marked in the depth ranges of: geophone locations (a); uniform dipping foliation, mentioned in the text (b).

**Fig. 8** shows record sections of the decomposed fast qS1- and slow qS2-wave for the total shot series recorded at 3245 m depth. As well as in Fig. 6 the shear-wave splitting is most evident for SPs 111-119. Surprisingly, the time difference between the qS1- and qS2-waves, marked by arrows (►) in Fig. 8a and 8b, does not increase with distance but remains constant about 0.2 s. This indicates that the anisotropy producing the splitting effect cannot be homogeneous between the borehole and the shotpoints. Homogeneity seems to be confined to a common segment of the

raypaths somewhere between the KTB location and shotpoint 120. From the geology (Fig. 1) this is, indeed, not surprising, since the shotpoints 112 to 120 are situated in probably isotropic granites, but the complementary wave paths cross foliated metamorphic rocks of the ZEV (Zone of Erbdorf-Vohenstrauß).

Assuming a splitting coefficient  $A=(V_{qS1}-V_{qS2})/V_{qS1}$  of 10% (Kern et al., 1991) and a velocity of 3.5 km/s for the qS1-wave, the diameter  $L$  of the anisotropic source area can be estimated from the observed qS2 to qS1 delay time  $dT$  (0.2 s from Fig. 8) by the equation:  $L = (V_{qS2} \cdot dT) / A$  giving  $L = 6.3$  km/s. This is less than the distance from SP 120 to the borehole.

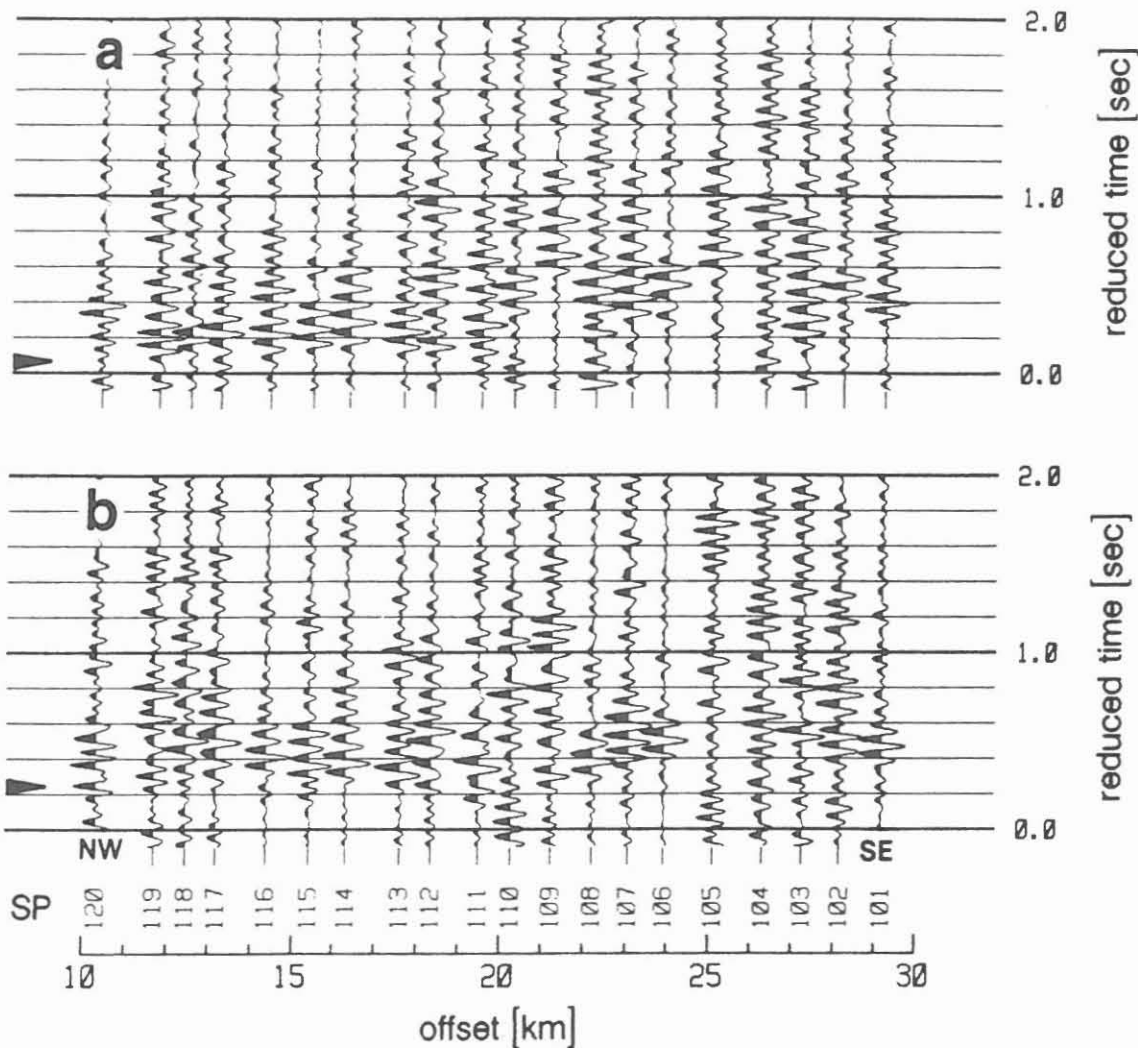


Fig. 8: Comparison of the separated fast qS1- (a) and slow qS2-wave (b) for all shotpoints recorded at 3245 m depth. The trace-normalized seismograms are plotted versus the lateral offset reduced by 3.5 km/s. The time delay between the onsets marked by (▶) of the fast qS1- and slow qS2-wave is almost 0.2 s.

### Discussion

The question arises, why shear-wave splitting is not observed for the more distant shotpoints 101 to 110 (Fig. 6) in spite of at least partially the same raypaths. Several reasons may be responsible for this. First of all the polarization direction of

the primary generated S-wave is accidental in contrast to the Vibroseis VSP-survey mentioned above, because the shooting technique has not been designed for S-wave radiation. Both polarization directions, qS1 and qS2, must be excited to observe shear-wave splitting. SP 106 in Fig. 6 may represent this case, where only one polarization direction is stimulated, because the primary S-wave polarization is parallel or normal to the foliation.

An extreme case for accidental or absent S-wave radiation is shown in Fig. 9 for the shotpoints situated in the sediments SW of KTB (s. Fig. 1). In spite of the same shooting technique and preprocessing parameters there are no significant onsets beside the direct P-wave compared with Fig. 2 and it seems that no shear-waves have been radiated. Shear-wave generation is related to heterogeneities in the immediate source surrounding and fractures that contribute to this heterogeneity in crystalline rocks are absent in sedimentary rocks.

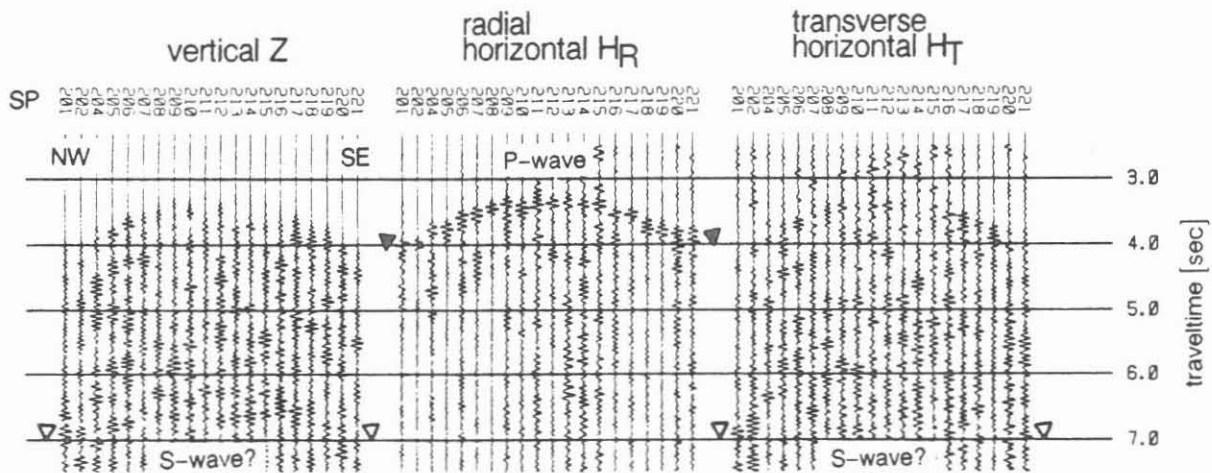


Fig. 9: Seismogram sections of SPs 201-221 for the 3-component receiver in 3220 m depth. The 6-15 Hz band-pass filtered seismograms are normalized to maximum amplitude within each trace. There are no significant S-wave onsets at this traveltime (open triangles) where they should appear for a  $V_p/V_s$ -ratio of  $\sqrt{3}$  (s. Fig. 2).

Other reasons for the extinction of splitting effects can be due to reflection and refraction. As an extreme case suppose a splitted shear-wave with orthogonally polarized components hits an interface at the Brewster angle of SH-waves. Then only the SV-components of the qS1- and qS2-waves are reflected and both waves will have the same polarization.

Finally the effect of heterogeneous anisotropy should be considered. For simplicity a sequence of homogeneous anisotropic layers as in Fig. 4 with constant strike but different dip angles of foliation is assumed. The qS1- and qS2-wave generated in the first medium will be generally split further. This results in a stretched shear-wavetrain and it is uncertain whether single shear-wavelets can be separated. Because the amplitude of the leading qS1-wave is generally diminished during each change in foliation and its time lead may presumably be less than the duration of the primary source generated S-wavelet, it becomes successively more unlikely that it can be resolved at all.



## Conclusions

Summarizing the results of wide-angle recordings in the KTB pilot hole it can be stated:

- Seismic anisotropy in the crystalline KTB surrounding is proved by the observed shear-wave splitting.
- From comparison with laboratory investigations rock foliation is expected to be the main cause of anisotropy.
- The observed qS1-polarization and the time difference between the split shear-waves can be explained in the simplest way by assuming foliated rocks with an average foliation dip of 60-70° and a NW-SE extension of  $\approx 6$  km at about 3 km depth in the ZEV south-east of KTB.

## References

- Ahmed, H., 1990. Investigation of azimuthal anisotropy from offset VSP data - a case study, *First Break*, **8**, 449-457.
- Bopp, M., 1992. Kombinierte Polarisations- und Arrayanalyse seismischer Daten im KTB-Umfeld, Diss. Ludwig-Maximilians-Universität München, in preparation.
- Brocher, T.M., Christensen, N.I., 1990. Seismic anisotropy due to preferred mineral orientation observed in shallow crustal rocks in southern Alaska, *Geology*, **18**, 737-740.
- Crampin, S., 1985. Evaluation of anisotropy by shear-wave splitting, *Geophysics*, **50**, 142-152.
- Crampin, S., 1989. Suggestions for a consistent terminology for seismic anisotropy, *Geophysical Prospecting*, **37**, 753-770.
- Crampin, S., Chesnokov, E.M., Hipkin, R.G., 1984. Seismic anisotropy - the state of the art: II, *Geophys. J. R. astr. Soc.*, **76**, 1-16.
- Gebrande, H., Bopp, M., Meichelböck, M. and Neurieder, P., 1990. 3-D Wide-Angle Investigations in the KTB Surroundings as part of the "Integrated Seismics Oberpfalz 1989 (ISO89)", KTB-Report **90-6b**, NLFb Hannover, 183-208.
- Kanasewich, E.R., 1973. Time Sequence Analysis in Geophysics, The University of Alberta press, pp. 352.
- Kern, H., Schmidt, R. and Popp, T., 1991. The velocity and density structure of the 4000m crustal segment at the KTB drilling site and their relationship to lithological and microstructural characteristics of the rocks: an experimental approach, *Scientific Drilling*, **2**, 130-145.
- Kohl, J., Kück, J., Sigmund, J., Wöhrle, Th., 1991. Bohrkernorientierung und Teufenkorrelation der KTB Vorbohrung, KTB-Report **91-3**, NLFb Hannover, F1-F22.
- Lippmann, E., Bucker, Ch., Huenges, E., Rauen, A., Wienand, J., Wolter, K. and Soffel, H.C., 1989. Rock physical properties: first results of the KTB-field-laboratory, *Scientific Drilling*, **1**, 143-149.
- Lüschen, E., Söllner, W., Hohrath, A. and Rabbel, W., 1990. Integrated P- and S-Wave Borehole Experiments at the KTB-Deep Drilling Site, KTB-Report **90-6b**, NLFb Hannover, 85-136.
- Röhr, C., Kohl, J., Hacker, W., Keyssner, S., Müller, H., Sigmund, J., Stroh, A., Zulauf, G., 1990. German Continental Deep Drilling Program (KTB) - Geological survey of the pilot hole "KTB Oberpfalz VB", KTB-Report **90-8**, NLFb Hannover, B1-B55.

- Schmedes, E., 1987. Some results from digital recording with 4 nearby stations, in: Earthquake swarm 1985/86 in Western Bohemia - Proc. of workshop in Mariánské Lázně, December 1986, D. Procházková (ed.), Praha, 124-129.
- Stettner, G., 1981. Geologische Karte 1:200000 C 6334 Bayreuth, BGR Hannover.
- Stroh, A., Hansmann, J., Heinschild, H.-J., Homann, K.D., Tapfer, M., Wittenbecher, M., Zimmer, M., 1990. Drill Hole KTB Oberpfalz VB, Geoscientific Investigations in the KTB-Field-Laboratory, Depth interval 0 - 4000.1 m, KTB-Report 90-8, NLFb Hannover, C1-C37.
- Zang, A., Wolter, K. and Berckhemer, H., 1989. Strain recovery, microcracks and elastic anisotropy of drill cores from KTB deep well, Scientific Drilling, 1, 115-126.

# Detection of permeable fracture zones by tube waves in the KTB pilot hole

C. Hanitzsch\*, T. Rühl† and B.B. Heinemann‡

## Abstract

The detection of permeable fractures is one of the research objectives of the KTB-project. Among seismic methods the tube wave survey is suggested for this purpose. Open permeable fractures intersecting the borehole may generate secondary tube waves which show up as V-shaped traveltime patterns (Chevron pattern) in sonograms. We investigated tube waves transmitted and recorded by the VAL-(Variable Acoustic Logging)-tool technique. The depths of tube wave generation were determined. 85 percent of them correlate with planar structures seen in acoustic borehole televiewer (BHTV) logs. BHTV data reveal many structures. One third of these coincide with tube wave events in the VAL data. To verify the hypothesis that the occurrence of a structure in both, traveltime and amplitude displays of BHTV data indicates an open fracture, we compared this dataset with stronger tube wave events assuming that the latter can be correlated to open fractures. We found no evidence for the correctness of the hypothesis. We compared tube wave events with caliper logs, temperature and mud conductivity anomalies during hydraulic tests, temperature anomalies during heat exchange test, core sample observations and gas-geochemical anomalies. The comparison between these various borehole data is not as satisfactory as to ensure the reliability of tube wave analysis to determine open fractures. Earlier investigations suggest that amplitudes of tube wave events are related to hydraulic permeabilities. Deficiencies of the present tube wave dataset (VAL) and missing fluid logging for calibration purposes prevents us from quantitative analysis.

---

\*Geophysikalisches Institut, Universität Karlsruhe, Hertzstr. 16, W 7500 Karlsruhe 21, Germany; now at: ELF UK, Geoscience Research Centre, 114A Cromwell Road, London SW7 4EU, UK

†Geophysikalisches Institut, Universität Karlsruhe; now at: GEOMAR, Wischofstr. 1-3, W 2300 Kiel 21, Germany

‡Geophysikalisches Institut, Universität Karlsruhe; now at: GTC, Kappelmeyer GmbH, Technologiefabrik, Haid- und Neu-Str. 7-9, W 7500 Karlsruhe 1, Germany

# 1 Introduction

One of the main research objectives within the KTB-project is to learn as much as possible about fluids in and their migration through the crystalline crust [Emmermann, 1986]. Migration of fluids has important implications for the understanding of zones of high electrical conductivities and low seismic velocities. Fluids are also important for heat- and mass transport processes in the crust.

Because of extremely low porosity of crystalline rocks the matrix permeability plays a minor role, whereas fracture permeability is of great importance. Thus, the main question is the detection of fracture zones. Not only the location of fractures but also their classification is desirable. Once determined where the borehole intersects a fracture zone, we want to get information whether it is a closed, mineralized or an open, fluid-filled fracture.

Nearly all logging tools (radioactive, electrical and seismic) can yield indications for fracture locations [Burkhardt and Müller, 1987, Fig. 8]. Concerning the classification of fractures the authors conclude that optical and seismic measurements are indispensable in this regard.

It is often suggested to use the energy of the direct tube wave generated and recorded by a usual borehole compensated sonic tool (see e.g. Draxler and Hänel [1988, p.86]). The proposed method is to determine the normalized differential energies of tube waves between adjacent receivers of the tool. The sum of all these differences (8 receivers available in the tool) should indicate permeable fractures. On this basis, Hänel [1989] presented his investigation of tube wave energies. He stated that most of the locations of assumed fractures correlate well with borehole inhomogeneities indicated by caliper logs. Probably the observed energy anomalies of tube waves are caused by strong attenuation in the vicinity of borehole inhomogeneities.

In contrast to common sonic measurements the tube wave method suggests to observe the tube wave, reflected by an open fracture, in greater offsets from the fracture location. This can be done by a vertical seismic profile where the source is at the surface of the earth [Huang and Hunter, 1981; Beydoun et al., 1985; Lüschen et al., 1990; Nagra, 1985]. In vertical seismic profile experiments at the KTB location no convincing example of tube waves appropriate to fracture analysis was observed. Another possibility is to use a type of sonic tool where source and receiver coincide. The transmitter generates a tube wave and body waves in the formation. These are reflected at the location of fractures and recorded by the receiver in the vicinity of the transmitter. A tube wave echolog survey was commissioned by KTB project management to Petrodata AG, Switzerland, and carried out in April 1989, using the VAL ("Variable Acoustic Low Frequency System"). Results of the analysis concerning fractures are presented in this report.

The second chapter describes in detail the method of tube wave survey which is proposed for detection of permeable fractures.

The third chapter gives a comparison between the tube wave method and other borehole measurements which are relevant for fracture detection. These are acoustic borehole televiewer (BHTV), caliper log, hydraulic conductivity and temperature profiles as well as other geological and geochemical evidences.

The fourth chapter comprises a discussion of the comparison and estimates the reliability of the tube wave method. We suggest some recommendations concerning the question how to get the most reliable information about permeable fracture zones in the KTB main hole.

Nearly all results of our investigation are summarized in one plot at the end of this volume. We refer to this figure as 'figure in the appendix'. The figure caption is appended to this paper in the chapter titled 'Appendix'.

## 2 Detection of permeable fractures by the tube wave method

### 2.1 Tube wave generation

Tube waves are often encountered in vertical seismic profiles (VSP) where the seismic source is at the earth's surface. Usually they are considered as coherent noise disturbing the downgoing and upgoing wavefield of body waves [Balch and Lee, 1984].

Tube waves are generated by direct waves at the top of the mud column from where they propagate down the hole [White, 1983; Balch and Lee, 1984]. They can be reflected at the bottom of the hole as well as at major lithological changes and borehole inhomogeneities like washouts. At these locations tube waves can additionally be converted into body waves again. An permeable fracture which intersects the borehole, can also generate secondary tube waves. The widely accepted mechanism assumes a P-wave impinging on a subsurface fracture or permeable zone. The fracture is compressed and a fluid pulse is injected into the borehole. The amplitude of tube waves depends on the permeability and length of the fracture and the frequency [Beydoun et al., 1985]. Huang and Hunter [1981] suggest to use tube waves as an indicator for open fractures. They carried out three tube wave surveys using an array of hydrophones. Likewise other investigators tried to use tube waves as desired signal [Beydoun et al., 1985; Nagra, 1985].

A tube wave survey can also be realized by a downhole source, e.g. a kind of sonic tool, with low offset between transmitter and receiver. The acoustic signal travels as a P-wave through the drilling fluid. When impinging on the borehole wall, part of the energy penetrates into the surrounding formation as a P-wave, another part converts into S-waves. In addition, tube waves are generated propagating along the borehole axis. Pressure waves travelling through the surrounding formation interact with permeable zones such as fractures and faults which intersect the borehole. They cause oscillations of the fluid within the permeable zone, generating a secondary tube wave as described above. Fig. 1 shows the generation of secondary tube waves illustrated by ray paths. In a downhole logging operation with moving tool upward at constant speed while recording, the receiver will first pick up a weak signal from a permeable zone when it is still some distance away. Approaching the intersecting point, signal strength will increase and travel time decrease. From here on, the picture will be reversed resulting in a V-shaped pattern (called "Chevron pattern") in the sonogram (Fig. 2).

### 2.2 Variable Acoustic Logging tool

The Variable Acoustic Logging (VAL)-system consists of two elements, the "echolog" for the detection of permeable fractures and faults, and the "selective velocity log", which permits a separate recording of P-, S- and tube wave signals. Low frequency acoustic signals (0.2–8 kHz) are generated by a downhole transmitter and recorded by eight receivers. The recordings of the nearest receiver are used for the "echolog". Six of the other receivers operate as two 3-component receivers. All receivers are used for the "selective velocity log" to determine travel times of P-, S- and tube waves. The transmitter and all receivers can be run either in monopole- or in quadrupole mode [Petrodata, 1987; Kurkjian and Chang, 1986].

There are three characteristics of the VAL-system: low frequency signals, minimum spacing between transmitter and echolog-receiver and long recording time (up to 0.25 s). Because wave lengths reach multiple borehole diameters, the advantage of low frequency is, that S- and tube waves can be recorded without disturbing P-wave fore-runner [Chang et al., 1988]. The P- and tube wave log is run in monopole mode, the S-log in quadrupole mode. The echolog is run in both modes. In common sonic logs a long spacing is required to determine

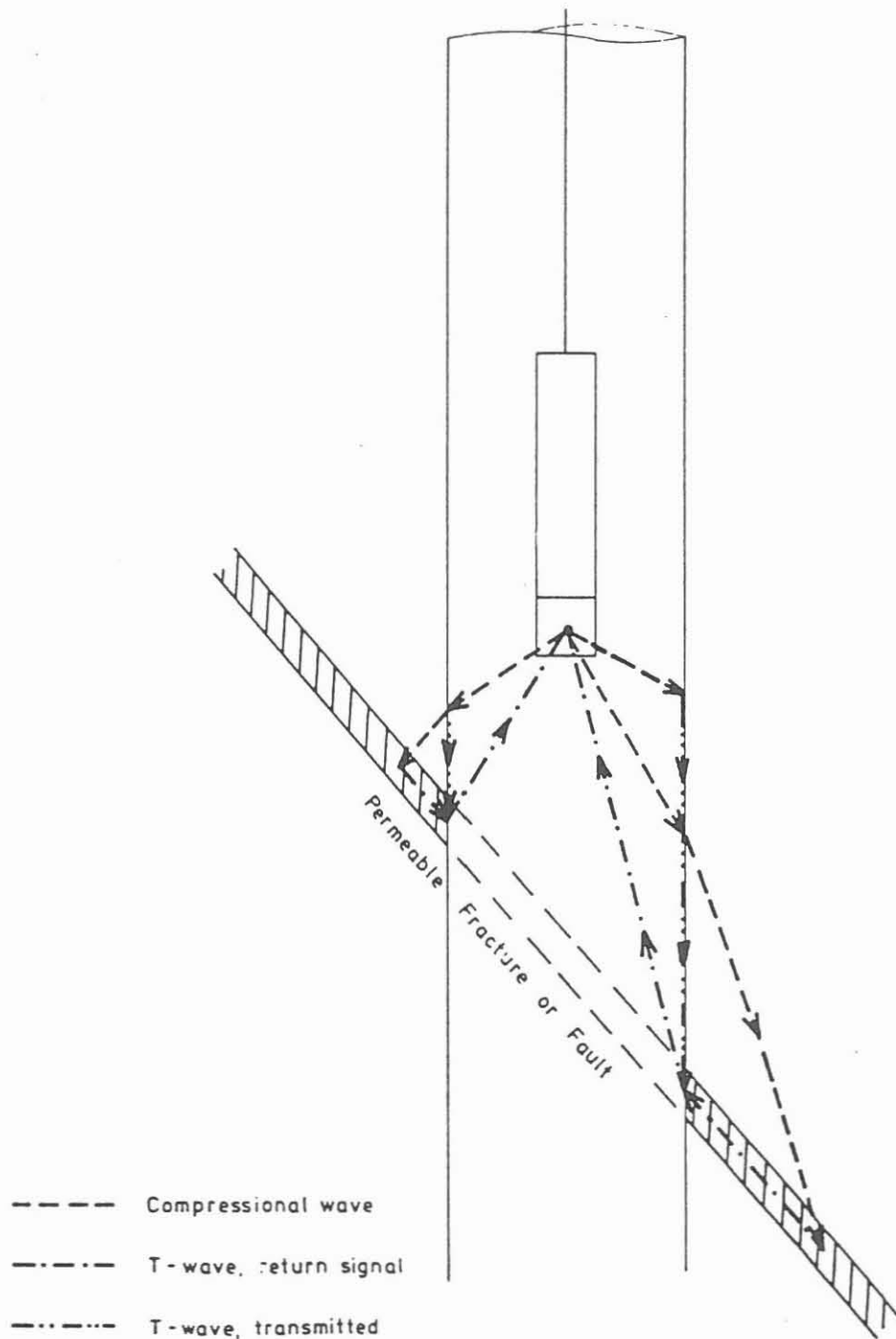


Figure 1: Generation of secondary tube waves by a downhole source illustrated by ray paths (from Petrodata [1987]).

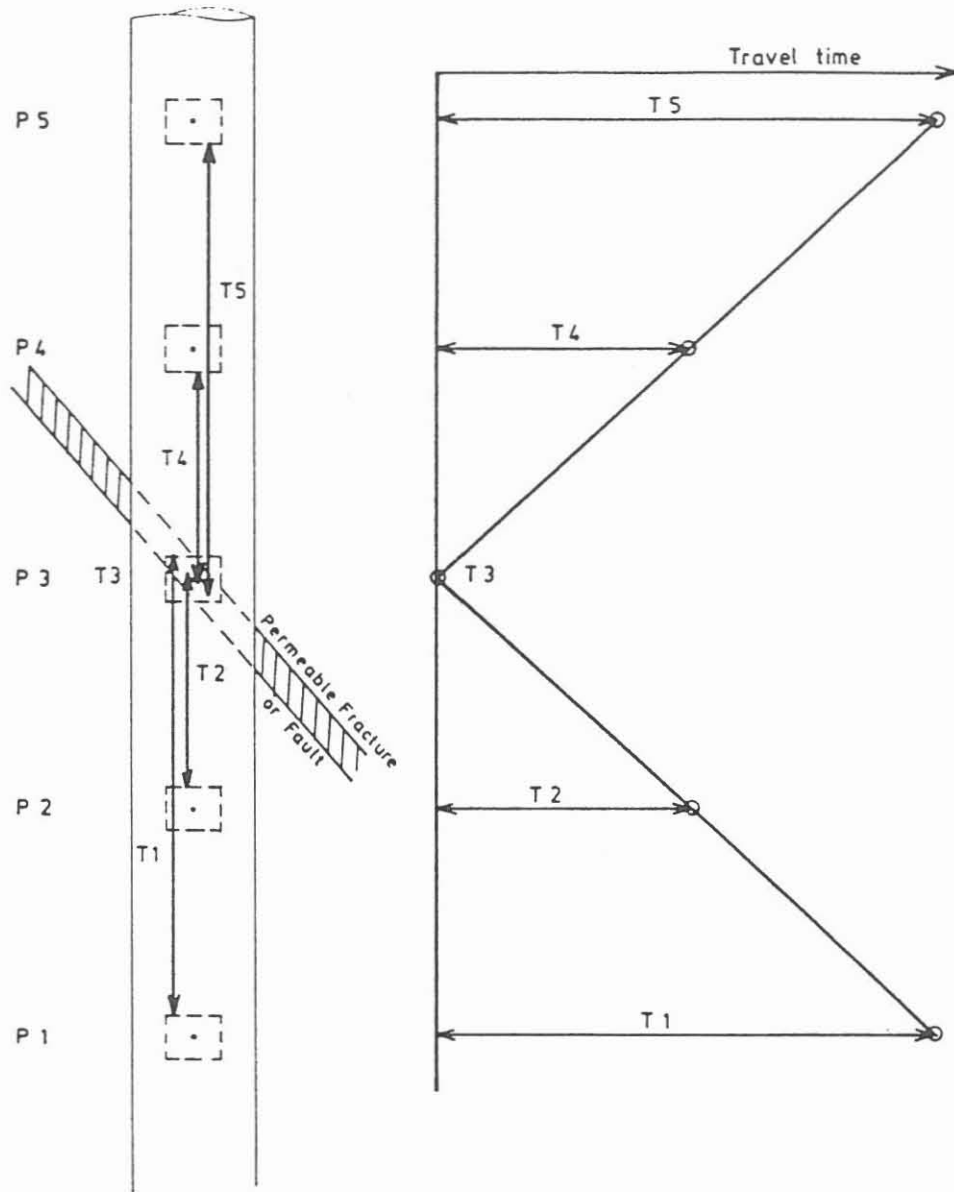


Figure 2: Tube wave V-shaped-pattern ("Chevron pattern"). Consecutive logging tool positions are denoted by P1-P5. The traveltimes (T1-T5) of tube wave signals increase starting from the intersection point of the fracture with the borehole (from Petrodata [1987]).

P-, S- and tube wave velocities. For echologs a minimum spacing between source and receiver is recommended. In fact, the VAL-echolog receiver has a 47 cm spacing. In common sonic logs the recording time is of only several milliseconds, e.g. 4.34 ms and 10.24 ms recording time in the KTB pilot hole. The recording time of VAL echolog at KTB was 64 ms at a sampling rate of 6  $\mu$ s. A long recording time is necessary to recognize V-shaped pattern. If the recording time is of only a few milliseconds, it is almost impossible to recognize these pattern, because of interactions of P-, S- and tube wave signals. Fig. 3 shows a sonogram of a sonic tool (SDT) with a plotted time axis of 3 ms, only the time axis of the VAL example comprises 64 ms (Fig. 4). Both examples were chosen for a depth interval including 3447.5 m depth, where a 1 cm wide open fracture is present. The different characteristics of both data sets are clearly seen.

### 2.3 Analysis of the VAL-echolog sonograms

We analysed the VAL-echolog sonograms as mentioned above looking for V-shaped pattern ("Chevron pattern") which would indicate possible open fractures. A bandpass filtered version (1-6 kHz) of the sonograms on paper was available for interpretation. Fig. 4 shows an example of the VAL-echolog sonogram in the depth range of 3419-3491 m. The pronounced V-shaped pattern clearly visualizes the open fracture at 3447.5 m depth.

It was not possible for us to get VAL-echolog data on tape for quantitative studies. Our analysis had to be based on paper readings. Without knowledge of plotting parameters we had no control of signal amplitudes. Therefore the analysis was restricted to the determination of the generating points of secondary tube waves. By subjective criteria we classified them into weak, intermediate and strong events. In column F of the figure in the appendix the length of lines corresponds to estimated relative amplitudes of the generated tube waves. Intermediate and strong events are listed in Tab. 1.

Another handicap concerning the data is the fact that no gamma-ray log was run together with the VAL tool. Therefore an exact depth control is not possible. Comparing some typical features in different logs with the VAL echolog, systematic depth errors were encountered. Especially between about 1600 and 3860 m, depths in VAL tend to be too low. The systematic error reveals to be superimposed by statistically varying depth errors. This can be due to variations in logging velocities of the tool. In the comparison, presented below, we added 6 m to all depths between 1600 m and 3860 m. But this correction was not applied in any table or figure presented in this report.

The data examples of Figs. 4 and 5 show that the signature of tube waves is not a simple pulse but a long complicated wavelet. One reason for this phenomenon could be multiples originated at nearby borehole inhomogeneities. At certain depth ranges where several weak V-shaped pattern are observed, it is difficult to differ between single tube wave events. Therefore, our analysis is somewhat subjective, especially for weak events. Some of the weak events show only one branch of V-shaped pattern, in most cases the ascending one. Sometimes both branches have different amplitudes. Having no other explanation, it might be a tool-effect.

There are some regions (marked by unfilled rectangles in column G of the figure in the appendix), where the amplitudes of the wavefield are very low (see the example in Fig. 5). Comparison with caliper logs shows that these are zones of increased diameter of the borehole.

Fig. 6 shows the distribution of tube wave events per depth interval of 100 m. Between 500 and 1200 m depth only very few and weak events are observed. Below 1200 m depth up to 4000 m depth there is a nearly constant distribution of events per depth interval. This is surprising because we expected a decrease of open fractures with depth.



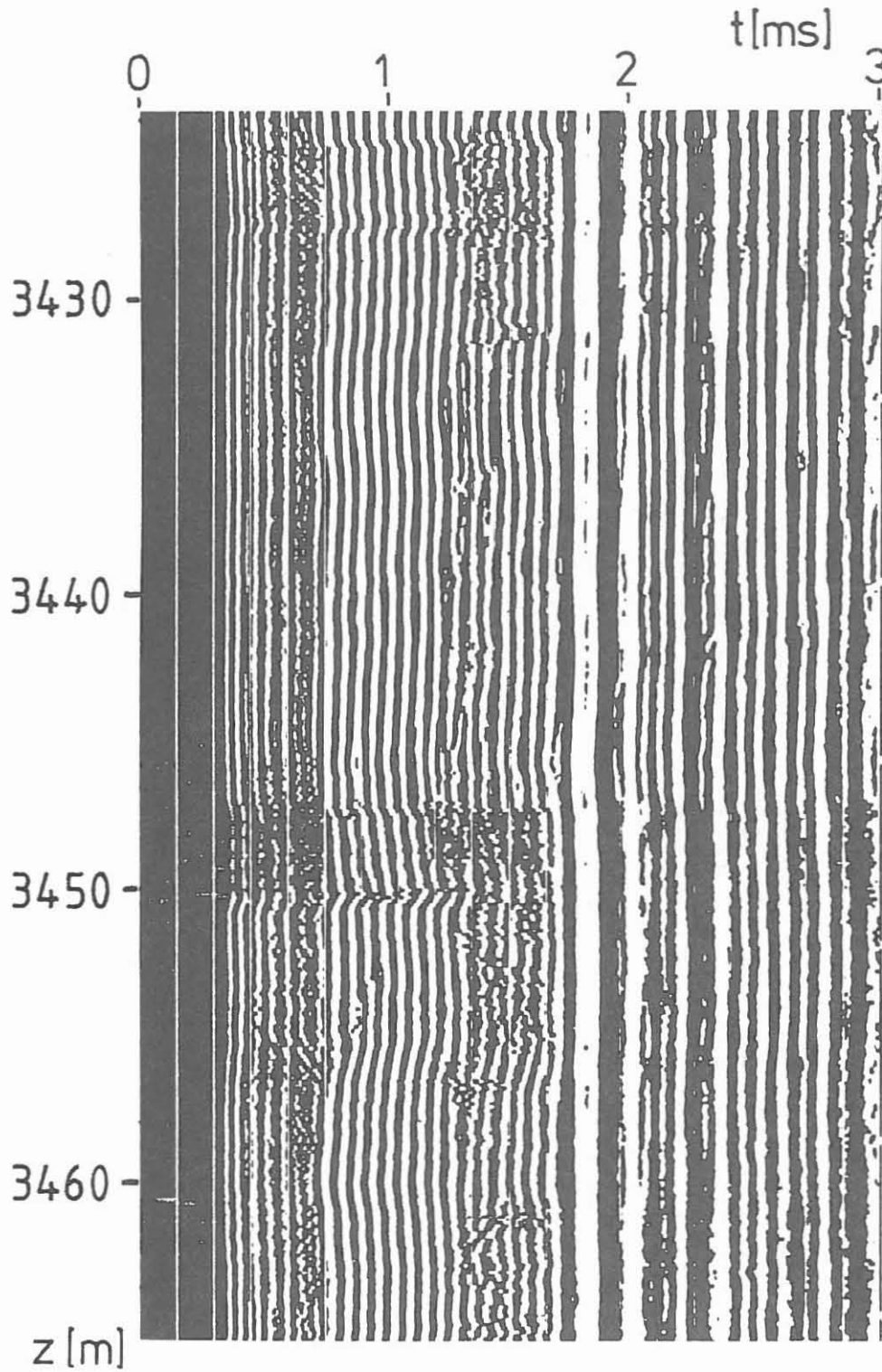


Figure 3: Sonic Digital Tool (SDT) sonogram example of the 1 cm wide open fracture at 3447.5 m depth. The plotted time axis is 3 ms long. The depth range is 3424–3466 m. No V-shaped pattern resulting from a tube wave is recognizable.

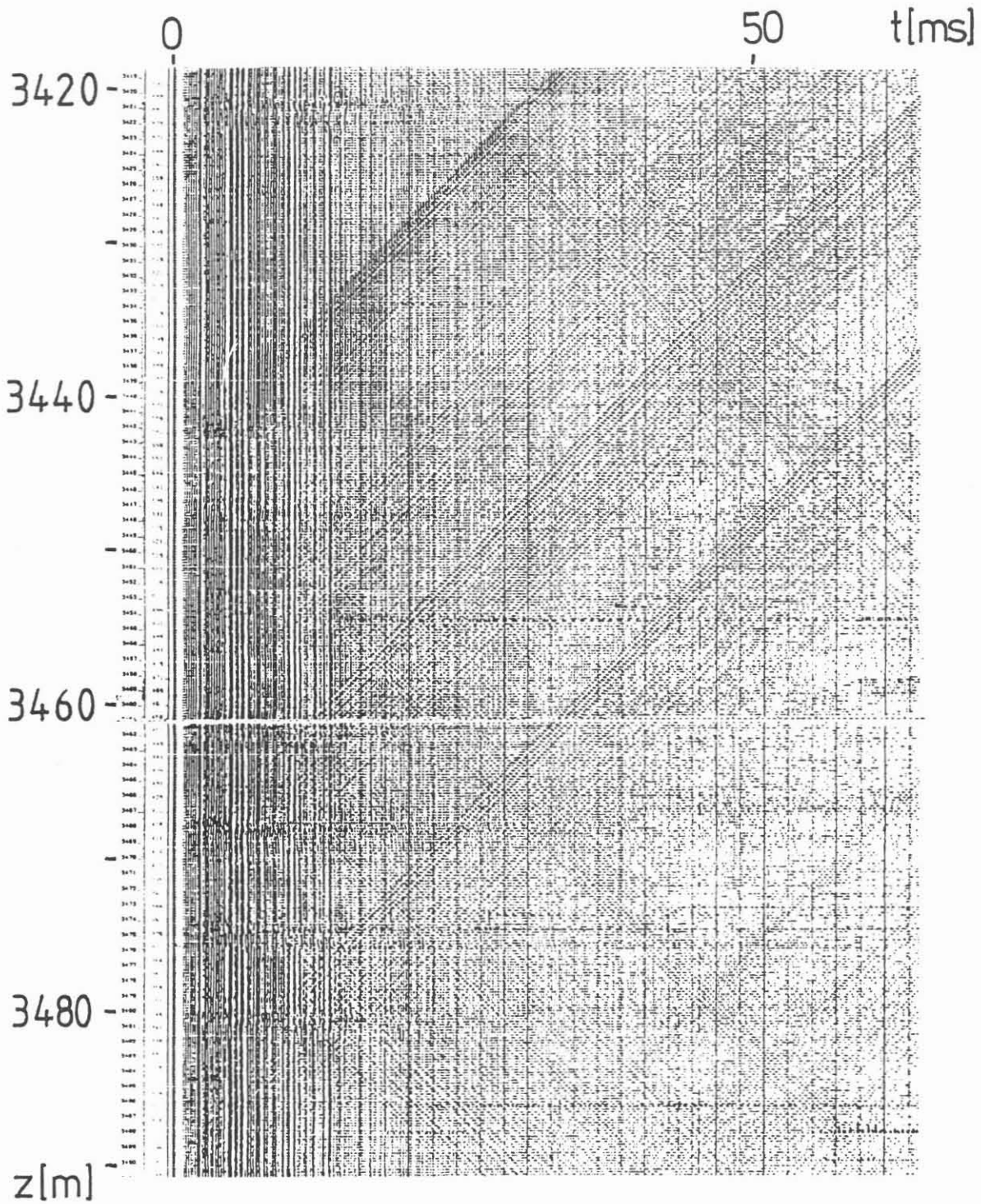


Figure 4: Variable Acoustic Logging (VAL) - echolog sonogram example of the 1 cm wide open fracture at 3447.5 m depth (the same as in Fig. 3). The plotted time axis is 64 ms long. The depth range is 3419–3491 m (depths are not corrected). Because of long recording time, V-shaped pattern of tube waves are clearly recognizable.

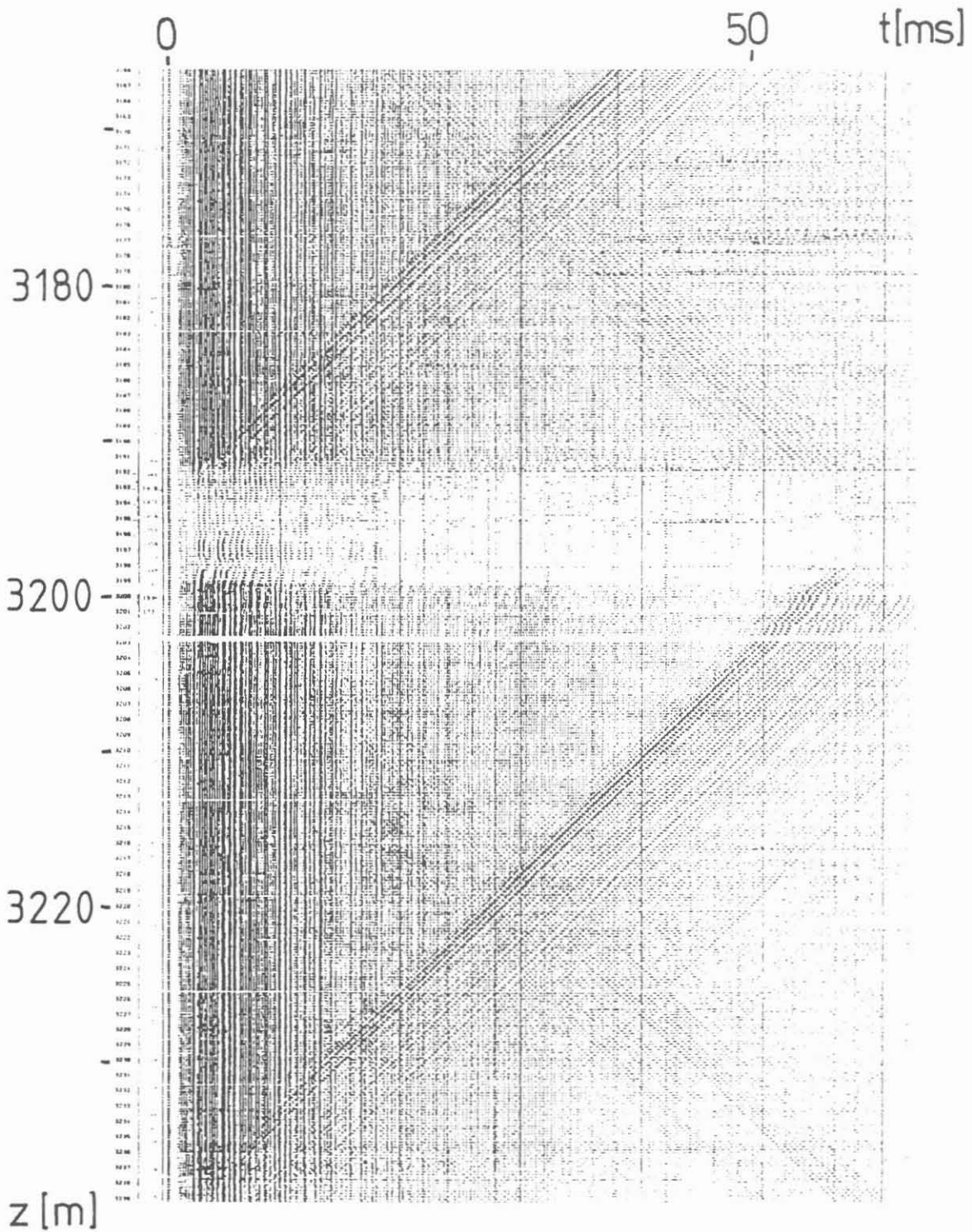


Figure 5: Example of a Variable Acoustic Logging (VAL) - echolog sonogram in the depth range of 3166–3239 m (depths are not corrected). A tube wave is generated at a fault zone at 3200 m depth. Reduced amplitudes in that zone could be explained by lower energy transfer into formation because of increased borehole diameter or by strong attenuation.

Table 1: List of intermediate (2) and strong (3) tube wave events, picked from VAL echolog sonograms.

Depth [m]	*	Depth [m]	*	Depth [m]	*	Depth [m]	*	Depth [m]	*
1235.5	2	1826	2	2298	3	2894	3	3470.5	3
1248.5	3	1891	2	2384.5	2	2915	2	3486.5	2
1335.5	2	1928	2	2397	2	2933.5	2	3577.5	3
1381	3	1964	2	2423	2	3049.5	2	3598	2
1410	2	1990	2	2440	2	3102	2	3649.5	3
1454.5	3	2099	3	2498	2	3154	3	3663	2
1457.5	2	2130	2	2541.5	3	3195.5	3	3716	3
1498.5	3	2200.5	2	2592	2	3240	3	3751.5	2
1517.5	2	2207.5	2	2639.5	3	3343	2	3772	2
1519.5	3	2225	3	2644.5	2	3357.5	2	3815	2
1550.5	3	2244.5	3	2660	3	3444.5	3	3905.5	3
1614	2	2284	2	2865.5	2	3459	2	3926.5	2
								4001	3

\* Strength of tube wave

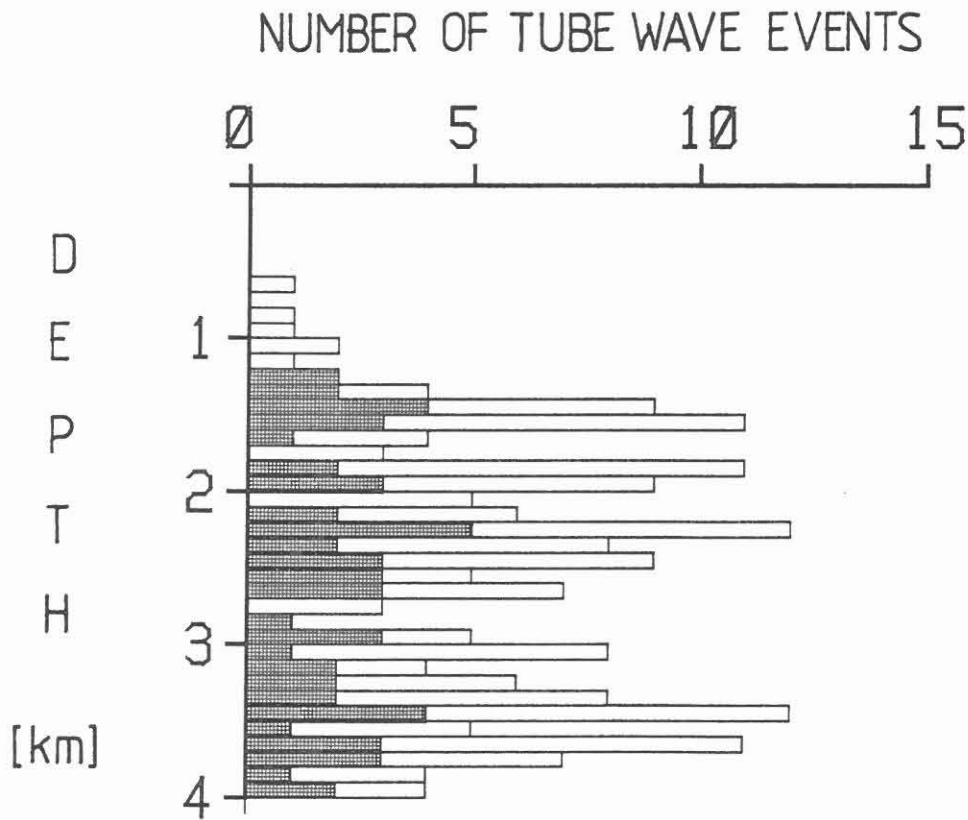


Figure 6: Histogram of tube wave events. The depth interval is 100 m. The shaded (unshaded) columns represent the number of intermediate and strong (of all) events.

### 3 Comparison between tube wave survey and other borehole measurements

In this chapter tube wave events, found in VAL echolog sonograms, are compared with results of other borehole measurements. The aim of this comparison is to verify whether tube waves are generated by open fluid-filled fracture zones or by other causes. Our comparison is mainly based on acoustic borehole televiewer (BHTV) data. The televiewer gives a high-resolution image of the borehole wall. Open fractures should be detected in these data. To calibrate the results of the VAL echolog another independent method for the determination of open fracture zones and influx horizons is desirable. In this regard, Hänel [1989] suggested to use hydraulic (packer) tests, the fluid logging method and the thermal flowmeter. The packer tests carried out in the KTB pilot hole yield information about hydraulic parameters of relatively large depth intervals. They miss the higher resolution required for fracture detection, and therefore, are not useful for this comparison. Fluid logging and thermal flowmeter were not run in the KTB pilot hole.

Further a comparison with caliper logs was performed to detect anomalies in borehole diameter which could be responsible for tube wave generation. Some open fractures are known from core observations. Results of mud and gas analyses as well as temperature and mud conductivity anomalies may indicate fluid-filled fractures. Therefore, these data were used for comparison.

The first section describes the different methods. The second section contains a compilation and detailed comparison between results of these methods and the tube wave survey.

#### 3.1 Borehole measurements relevant for fracture detection

##### 3.1.1 Acoustic borehole televiewer

The borehole televiewer (BHTV) is an acoustic tool which operates in the 0.2–2 MHz range. The measurement results in an image of the surface of the borehole wall. The televiewer spirally scans the borehole wall with a rotating high frequency acoustic beam [Hänel, 1987, p.109-112]. The amplitude of the reflected signal allows the analysis of the condition and quality of the borehole wall, e.g. of oriented planar structure elements intersecting the borehole like fractures, faults and rough texture. The traveltime of the signal yields a high resolution caliper. Computational processes result in an image of the unwrapped cylindrical borehole wall. Values of traveltimes and amplitudes are printed in colours or shadings. The image of an inclined fracture is a sinusoidal structure. As an example, the open fracture at 3447.5 m depth is shown in Fig. 7.

We analysed BHTV data from logging companies Schlumberger and WBK (Bochum, FRG), now DMT. Recognizable structures in traveltimes and/or amplitudes were evaluated according to subjective criteria. Column D of the figure in the appendix presents all structures in the same way as was done for the VAL-echolog results. The longest lines correspond to most easily discernible structures. A line on the left indicates a structure found in traveltime displays, a line on the right the corresponding one in amplitude displays.

The resolution of Schlumberger data is better as the one of WBK data. Schlumberger also used variable shadings in different regions, which makes it easier to recognize structures. So we used Schlumberger data where available. In depth intervals with bad data quality, existing structures are likely to be undetected and identified structures are questionable. In column C of the figure in the appendix, we specify measured depth ranges, indicating their data quality and the measuring company.

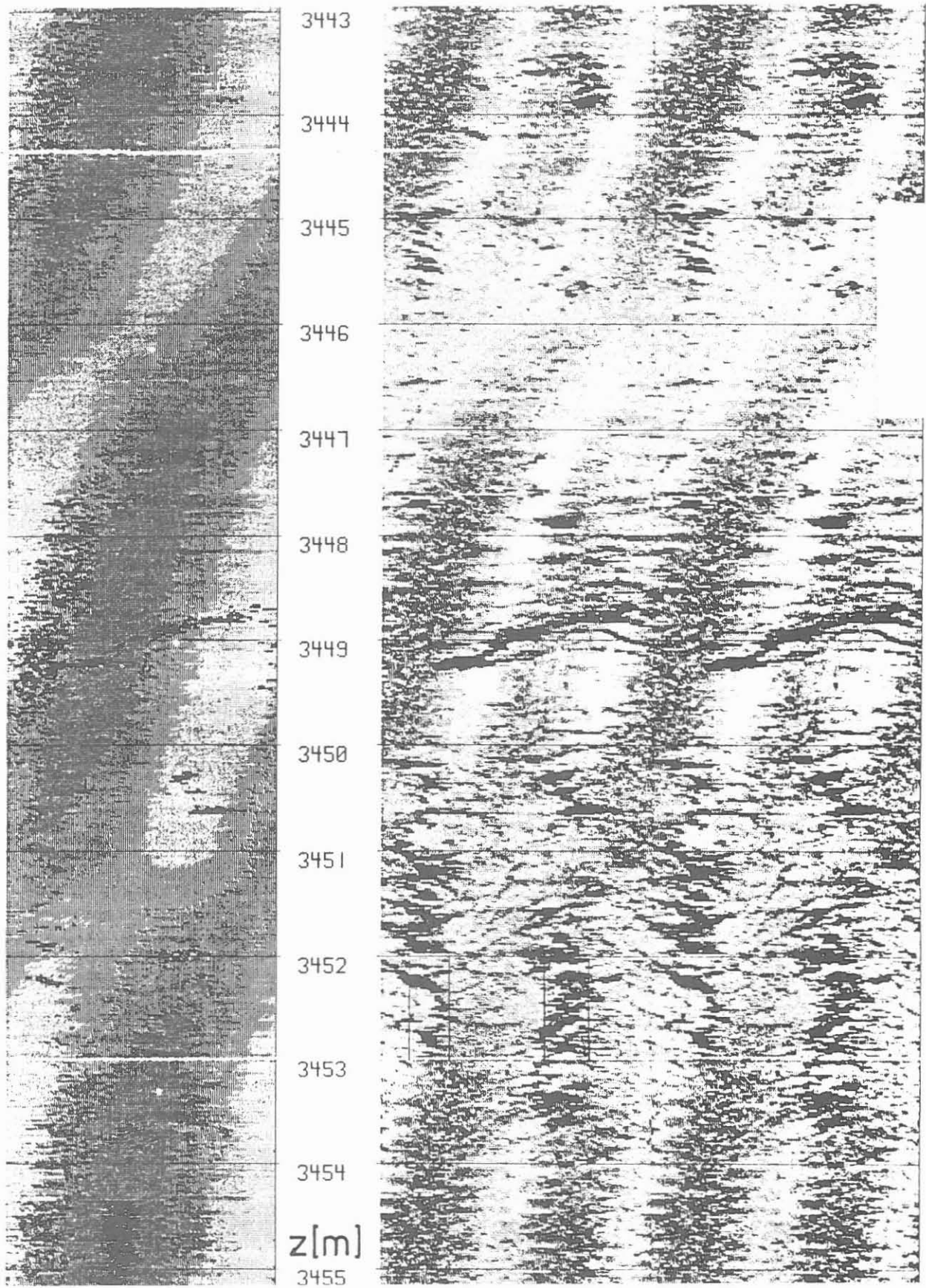


Figure 7: Example of an image of the acoustic borehole televiering (BHTV): the 1 cm wide open fracture at 3447.5 m depth (at 3449 m in the figure, depths are not corrected). The left display shows the traveltimes, the right display twice the amplitudes in shadings. The depth range is 3443–3455 m.

Table 2: Compilation of geochemical data and open fractures known from core observations. The second column gives the existence ('X') or wideness of an open fracture known from observations on core samples. The third and fourth column show the depths of influx of formation waters and of increased content of methane and helium gases (data compiled from Emmermann et al. [1988; 1989; 1990] and Erzinger et al. [1989]).

Depth [m]	Fracture	Influx	Gas
2000-2200	-	X	X
2508.9	1 mm	-	-
2532	1 mm	-	-
2542	1 mm	-	-
2545	1 mm	-	-
2546	1 mm	-	-
2554	X	-	-
3198-3208	-	-	X
3447	1 cm	X	X
3491.3	X	-	-
3587.5	X	-	-
3602	3 mm	-	-
3607.7	X	-	-
3733.4	X	-	-
3798.2	X	-	-
3817.2	5 mm	X	X
3860-3880	(3861 m)	(3875 m)	X
3980-4000		X	X

Both tools were combined with a gamma-ray-tool, but the data we used were not depth corrected. Schlumberger data reveal a depth error of the order of  $\pm 1.8$  m, which occurred because of differences in tool velocity. Comparing different overlapping WBK logs of same depths we found differences in the order of  $\pm 3$  m.

### 3.1.2 Caliper log

In caliper logs, three, four or six arms mechanically scan the borehole wall and determine the diameter [Heinemann and Mastin, 1989]. Two perpendicular arms of a caliper log are plotted in column B of the figure in the appendix. It is possible to distinguish between "washouts" and "breakout"-regions.

We use the definition, that "washouts" are zones with both diameters larger than size of the drill bit, and "breakout"-regions are zones, where only one diameter is larger than bitsize meaning that the borehole has an elliptical cross-section.

### 3.1.3 Geological and gas-geochemical data

The lithological profile in column A of the figure in the appendix was determined from observations on core samples and results of geochemical analyses by the KTB field laboratory. With increasing depth a difference between logging-depth and core-depth up to 4 m appears.

From core observations some open fractures are known. Analyses of drilling fluid showed some influx of saline waters. Analyses of gases released from drilling fluids yielded increased methane and helium content at certain depths [Emmermann et al., 1988; 1989; 1990; Erzinger et al., 1989]. These data are represented in Tab. 2 and in the figure in the appendix (in column L and M). Disadvantages of core sample observations are that not the entire depth range of the KTB pilot hole was cored and that fractures are not studied under in-situ conditions.

#### 3.1.4 Hydraulic tests and mud conductivity logs

Hydraulic tests represent the only method to get direct information of fluids in the formation and fluid flow into a borehole. They should be carried out in order to calibrate results of the tube wave method.

Only a few hydraulic measurements were performed in the KTB pilot hole. Below 500 m depth, two drill stem tests (DST) were carried out in the depth ranges of 813–839 m and 3442.9–3486.9 m respectively. These tests yield integrated hydraulic parameters in the mentioned depth intervals and therefore are not relevant for our investigations.

The thermal flowmeter was not applied in the KTB pilot hole. It was suggested [Hänel, 1989] to use the conductivity fluid logging method [Tsang, 1987; Tsang and Hufschmied, 1988] in the KTB pilot hole. Unfortunately this was not possible due to various reasons.

In May 1989 a hydraulic withdrawal slug test and an injection test were performed [Reifenstahl and Stober, 1990; Jobmann, 1990]. During the withdrawal slug test several mud conductivity logs were run. The quality of data is not satisfactory but results demonstrate that conductivity logs are a reliable and low-cost method for the detection of water-filled fractures. An evaluation based on principles of the conductivity fluid logging method was not possible [Reifenstahl and Stober, 1990]. During the injection test several temperature logs were run. Tab. 3 shows a compilation of detected fracture zones derived from temperature logs during injection-test and from conductivity logs during the withdrawal slug test (from Reifenstahl and Stober [1990]). In the figure of the appendix these zones are represented in columns J and K.

In some cases conductivity logs indicate permeable fractures, which are not revealed by temperature logs. The reason could be a low permeable fracture system, yielding a small but highly saline fluid volume during production. Because of low permeability the thermal effect of fluid injection cannot be measured. Another explanation of missing temperature anomalies could be a chemical solution process in the formation [Reifenstahl and Stober, 1990].

At some depths temperature logs indicate permeable fractures which are not seen in conductivity logs. One reason could be that under-pressure during withdrawal slug test or over-pressure during injection test will close or open fractures, respectively. A missing contrast in conductivity of mud and fluid in the fracture presents another explanation. This is the case when mud fluid is pressed into the fracture during injection and drawn out into the borehole again [Reifenstahl and Stober, 1990].

#### 3.1.5 Temperature logs

Temperature anomalies can also indicate fracture zones with incoming fluids. In March 1990 a heat exchange experiment was performed in the KTB pilot hole [Stiefel, 1990]. The mud was circulated for 97 hours and afterwards, 13 temperature-depth profiles were logged. During the temperature adjustment phase temperature anomalies of about 0.1 K over a depth range of several meters should be explained in context with other related measurements [Stiefel, 1990]. Fig. 8 shows temperature anomalies with amplitudes greater than 50 mK, derived from



Table 3: Compilation of detected fracture zones derived from temperature logs during injection test and mud conductivity logs during withdrawal slug test (from Reifenstahl and Stober [1990]).

Depths (in meters) of indications of fracture zones in the logs of temperature (injection test) | mud conductivity (withdrawal slug test)

490 - 513	450 - 500
553	-
1104	-
-	1170
-	1202 - 1250
1370 - 1385	1325 - 1400
1445 - 1460	1420 - 1480
1538	1530
1600 - 1640	-
1692 - 1703	-
1738 - 1740	1710 - 1738
1780 - 1785	-
1924 - 1936	-
2146 - 2178	-
2232 - 2256	-
2433 - 2446	-
2595	2580 - 2610
2640 - 2680	-
2780	2785 - 2815
2980 - 3000	-
3030 - 3035	-
-	3157
-	3190
3200 - 3206	-
-	3340
-	3365
3396 - 3409	3375 - 3430
3438 - 3447	3445
3472 - 3476	-
3478 - 3484	-
3492 - 3512	-
3533 - 3541	-
3557 - 3573	-
-	3600 - 3700
3768 - 3780	-
-	3817
3840 - 3855	-
3890 - 3895	-

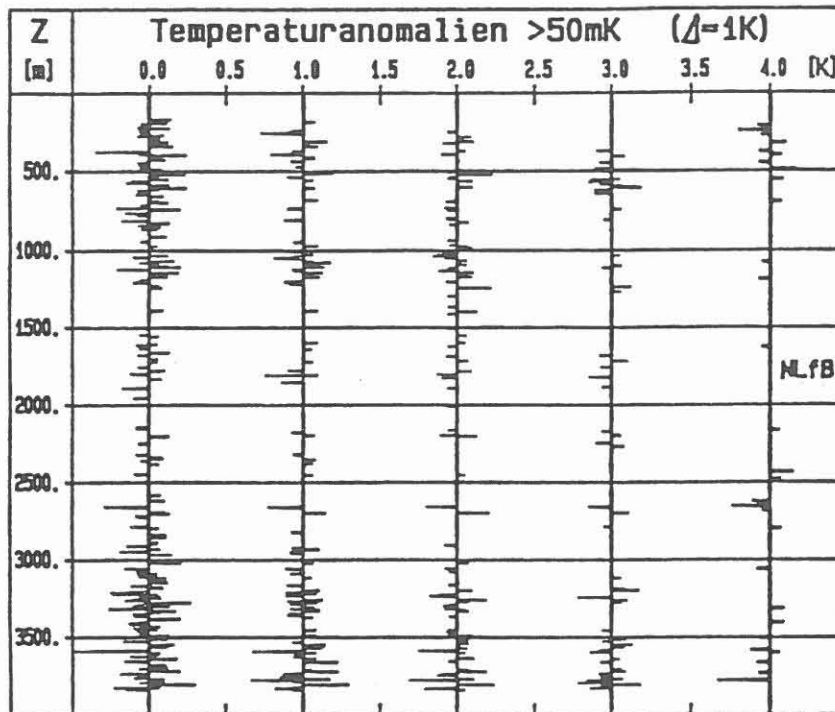


Figure 8: Picked temperature anomalies (from heat exchange experiment) with amplitudes greater than 50 mK, derived from reduced temperature logs. For one profile three subsequent measurements were averaged and plotted with a displacement of 1 K. The right log (NLfB) shows anomalies of the stationary temperature distribution (from Stiefel [1990]).

reduced temperature logs. For one profile three subsequent measurements were averaged. The data were corrected with the depth varying temperature gradient, computed within moving depth intervals, which means a high-pass-filtering. The right profile shows anomalies of the stationary temperature distribution.

Temperature anomalies can be caused by several effects [Stiefel, 1990]:

- different thermal conductivity in the formation,
- a convectively accelerated temperature adjustment because of back-flowing mud out of fracture zones which are in contact with the borehole,
- a convective propagation of energy in fracture-systems which are not in contact with the borehole,
- varying caliper which causes a different accumulation of energy via the thermal capacity of the mud and
- different conditions of the borehole wall.

Technical problems related to temperature measurements cannot be excluded as possible reasons for temperature anomalies. Therefore temperature logs are not a unique indicator of open fractures and must be evaluated with care.

In case of convective heat flow from fracture zones into the borehole, a temperature profile will show a narrow anomaly at a time just after cessation of mud circulation, assuming that

the influx has different temperature from the mud in the borehole. With increasing time the anomaly will decrease. Therefore, the anomaly will be recognizable in the first but not in later temperature profiles. In case of a continuous influx, the anomaly will generally remain as a peak recognizable in all profiles.

The profile of temperature anomalies after the heat exchange test (column I of the figure in the appendix) shows anomalies recognizable either only in the first or in all profiles of Fig. 8. The accuracy of depth is  $\pm 2.5$  m (personal communication, Stiefel).

### 3.2 Compilation of results

Results of different research groups which contain various sources of errors are compared. The most important problem is the accuracy of different depth readings. The VAL data reveal both a depth-varying statistical error due to a non constant measuring speed of the sonde and a systematic error in the depth range of 1600-3850 m. By means of comparison with other typical features we argue that 6 m must be added to VAL-depth readings at these depths. In all tables and figures no depth correction was applied but in the following comparison we chose a corresponding depth tolerance window. BHTV data contain a statistical depth error, too. With increasing depth the difference between core-depth, which was used for determination of the lithological profile, and logging-depth, used for all log data (VAL, BHTV,...), can run up to 4 m. Logging-depth is always greater than core-depth. Some thermal anomalies (e.g. at open fractures at 3447 m and 3817 m depth) show that the depths of temperature anomalies after the heat exchange test are too low and must be shifted upwards by 5-10 m.

Firstly we compare VAL data (tube wave events, abbreviated TWE in the following) with structures visible in BHTV data (see the figure in the appendix A, columns D, E and F). Considering a depth tolerance of  $\pm 3$  m, we try to correlate each TWE with structures in BHTV. Up to 85% of all TWE coincide with structures in BHTV. There are seven intermediate and strong TWE without corresponding structure in BHTV data, at 2244.5 m, 2639.5 m, 2644.5 m, 2660 m, 3459 m, 3470.5 m and 4001 m depth. The TWE at 4001 m is caused by the bottom of hole. Enlarging the depth tolerance to  $\pm 3.5$  m, the TWE at 2644.5 m and 2660 m depth correlate with washout structures in BHTV. The remaining TWEs are situated in breakout-zones (with elliptical cross-section) where structures can hardly be identified because of bad data quality.

Secondly we try to correlate each BHTV structure with a TWE. Nearly 30% of all BHTV structures coincide with a TWE. Due to higher resolution of BHTV it is obvious that several BHTV structures are correlatable to the same TWE. We try to verify the assumptions, that strong TWE are related to clearly recognizable structures in BHTV and, that strong TWE are related with structures simultaneously seen in traveltime- and amplitude displays of BHTV. Both assumptions are not evident. But a final confirmation must be postponed to a quantitative comparison of amplitudes of events in tube wave survey and BHTV.

Finally, we perform a comparison where we start from known open fractures (core observations) or anomalies in geochemical analyses, conductivity or temperature profiles to test whether these anomalies are indicated by TWEs.

- There are only two fractures (3447.5 m, 1 cm wide; 3817 m, 0.5 cm wide) which are correlated with influx of formation water and high helium and methane content. At both depths a strong or intermediate TWE is generated. The conductivity logs, run during the withdrawal slug test, indicate these fractures as well. In temperature logs, run during the injection test, only the fracture at 3447 m depth is seen. Probably the second fracture is too narrow to be recognized as temperature anomaly. Temperature

profiles after the heat exchange test show both anomalies, the fracture at 3817 m depth shows a permanent temperature peak opposite to the fracture at 3447 m depth.

- The circumstances are difficult in the depth interval of 3860–3880 m. In this depth range two different segments of the pilot hole called VB1a and VB1b were drilled due to drilling problems. In hole VB1a a porous, epidote-rich zone was found at 3861 m depth. The parallel hole VB1b was not cored. Influx of formation water only occurred into hole VB1a at 3875 m depth. In both holes the gas analysis showed increased methane and helium content in the respective range. All logs were run in hole VB1b. At 3876 m depth a weak TWE was generated.
- Other open fractures, known from core observations, do not coincide with geochemical anomalies. The fractures in the range of 2500–2600 m and at 3491 m, 3587.5 m and 3798 m depth do not appear in the temperature and conductivity logs. The strong TWE at 2541.5 m depth (in BHTV only a weak structure at 2546.5 m) obviously corresponds to open fractures at 2542 m, 2545 m and 2546 m depth. The open fracture at 3491 m correlates with a TWE at 3486.5 m, the one at 3798 m to a TWE at 3793 m. It is possible that the TWE at 2498 m and 3577.5 m depth are correlated with open fractures at 2509 m and 3587.5 m depth, respectively.
- The zone of 3600–3700 m depth was classified as anomalous in the conductivity log. Two open fractures were found at 3602 and 3608 m depth, but no temperature anomaly is present. An intermediate TWE (at 3598 m, only a weak structure in BHTV) is probably caused by the fracture at 3602 m.
- The open fracture at 3733 m depth causes only a weak TWE at 3726.5 m in spite of a permanent anomaly in the temperature log after the heat exchange test.
- Some of the open fractures known from core observations do not appear to correlate with TWE (2509 m, 2532 m, 2554 m and 3608 m depth). Hydraulic and geochemical tests do not reveal any anomaly at these locations. Probably those fractures are too impermeable or do not contain any fluids.
- Another helium and methane increase was recorded between 3198 and 3208 m depth. At 3199.7 m depth a several-centimeters wide steep fault was recognized. Between 3201.2 and 3203.2 m depth no core could be drilled. But because of a minimum in the gamma-ray log and of a small “washout” (known from caliper logs) it is probable that another fault exists. It is believed that the high helium and methane content is due to a cataclasite horizon [Emmermann et al., 1988; 1989; 1990]. A temperature anomaly during injection is observed. A TWE at 3199.5 m depth can be generated by the washout or by a permeable zone.
- Mud analysis detected the strongest influx zone of the entire borehole between 3980 and 4000.1 m depth. In VAL there is an extremely weak TWE at 3991 m. A strong TWE at 4001 m depth is generated by the borehole bottom or by a permeable fracture zone responsible for the high gas content.
- The temperature logs after the heat exchange test accentuate four distinguished anomalies seen in all temperature profiles. We already discussed two of them, at 3725 m and 3810 m depth which correlate with open fractures at 3733 m and 3817 m. The third anomaly at 3775 m depth is seen as temperature peak during injection, as intermediate

structure in BHTV, as a small washout in caliper log and as an intermediate TWE at 3772 m depth. The fourth temperature anomaly at 3835 m depth corresponds to an intermediate structure in BHTV, but not to a TWE.

- Conductivity logs, run during the withdrawal slug test, reveal an anomaly between 2580 m and 2610 m depth. Other measurements detect anomalies at 2595 m (event in BHTV, temperature, TWE, fault in lithological profile). It is not clear whether a strong breakout zone (maximum at 2599 m depth) is partly responsible for these anomalies.

Balch and Lee [1984] state that TWE are also generated at borehole inhomogeneities like bottom of hole, strong variations of caliper (washouts), or strong lithological contrasts. As mentioned earlier in section 2.3, some zones of strongly reduced amplitudes are visible in VAL sonograms (see an example in Fig. 5). Comparison with caliper log indicates washout zones. In one third of these zones tube waves are generated. It is possible that fractures are present in these washouts causing a TWE. But the majority of existing washout zones in the KTB pilot hole do not generate tube waves.

There are many borehole inhomogeneities and lithological contrasts which do not produce a TWE. It cannot be excluded that some of the TWE are generated by such structures, but we do not find a convincing example in our investigation.

## 4 Discussion and conclusions

In this paper the detection of permeable fracture zones in the KTB pilot hole by the tube wave method is investigated. Data of a special acoustic borehole tool, the VAL-sonde, is used, which records in the echolog-mode mainly tube waves.

The tube wave survey still is a widely unknown method for detection of permeable fractures, especially in crystalline rocks. It has been used for the first time during the AECL radioactive waste disposal program in Canada [Huang and Hunter, 1981]. Another application of this method is reported from the Böttstein hole [Nagra, 1985]. These early investigations perform a qualitative evaluation of tube wave amplitudes.

The intention at the beginning of this investigation was to check the efficiency and reliability of the tube wave method and to proceed to a quantitative evaluation. It was not possible for us to get digital data of the VAL. Therefore the investigation relied extensively on paper readings. Without control of amplitudes we classified tube wave events into three classes (weak, intermediate and strong events) by subjective criteria. In addition there was an inaccuracy in depth. No gamma-ray log was run together with the VAL tool as usually done. We found an obvious systematic error in a certain depth interval superimposed on a probable statistical error. Without a gamma-ray log there is no chance to carry out a depth correction.

Tube wave events nearly regularly occur over the total depth range of the pilot hole except above 1200 m depth where only a few weak events exist. Above 1000 m depth the data quality was bad [Bram et al., 1990, p.224]. The regular occurrence is surprising because we expected a decrease of open fractures with depth. Essentially we compared locations of tube wave generation with data of BHTV, because it is widely accepted that BHTV reliably detects structures indicating fractures. The BHTV data also were not depth-corrected and available as gray scaled paper logs.

Taking into account a depth tolerance of  $\pm 3$  m we compared tube wave events with corresponding structures in BHTV. 85% of the tube wave events in VAL are associated with structures in BHTV. The remaining tube wave events were probably hidden within breakout

regions because of bad quality of BHTV data. Comparing BHTV with VAL, one third of all BHTV structures are observed as tube wave events. Thus, we conclude that in BHTV images many structures are observable which are not necessarily permeable fracture zones. Open fractures exist which are not detected as planar structures in BHTV data probably because of bad data quality. The same result was found by Huang and Hunter [1981]. They report from some open fractures which are not observed by the BHTV method but can be detected by both tube wave analysis and by hydrogeological studies.

The hypothesis is suggested that the simultaneous occurrence of a structure in traveltimes and amplitude display of BHTV data indicates an open fracture. To verify this we compared the BHTV dataset with stronger tube wave events, assuming that the latter can be correlated to open fractures. We found no evidence for the correctness of the hypothesis. Additionally we could not confirm the assumption that more clearly recognizable structures in BHTV data are correlated with stronger tube wave events.

One characteristic of the VAL echolog is the low frequency range of 0.2–8 kHz. A greater penetration depth is achieved than by the BHTV tool. Therefore greater fractures which are likely to extend into the formation are detected. Because of its small wavelength (about 1.4 MHz), the BHTV detects small fissures and fractures in the immediate vicinity of the borehole wall.

In case of the KTB the most suitable borehole measurement in order to test and calibrate the tube wave method is the conductivity fluid logging method [Tsang, 1987; Tsang and Hufschmied, 1988]. This comparison was favoured by Nagra [1985] in the Böttstein borehole. Unfortunately the method was not applied at KTB pilot hole. Thus, we chose the following borehole measurements for comparison: temperature anomalies during heat exchange test [Stiefel, 1990], temperature and conductivity anomalies during hydraulic injection and withdrawal slug test [Reifenstahl and Stober, 1990], data of open fractures known from core observations and gas-geochemical data [Emmermann et al., 1988; 1989; 1990; Erzinger et al., 1989].

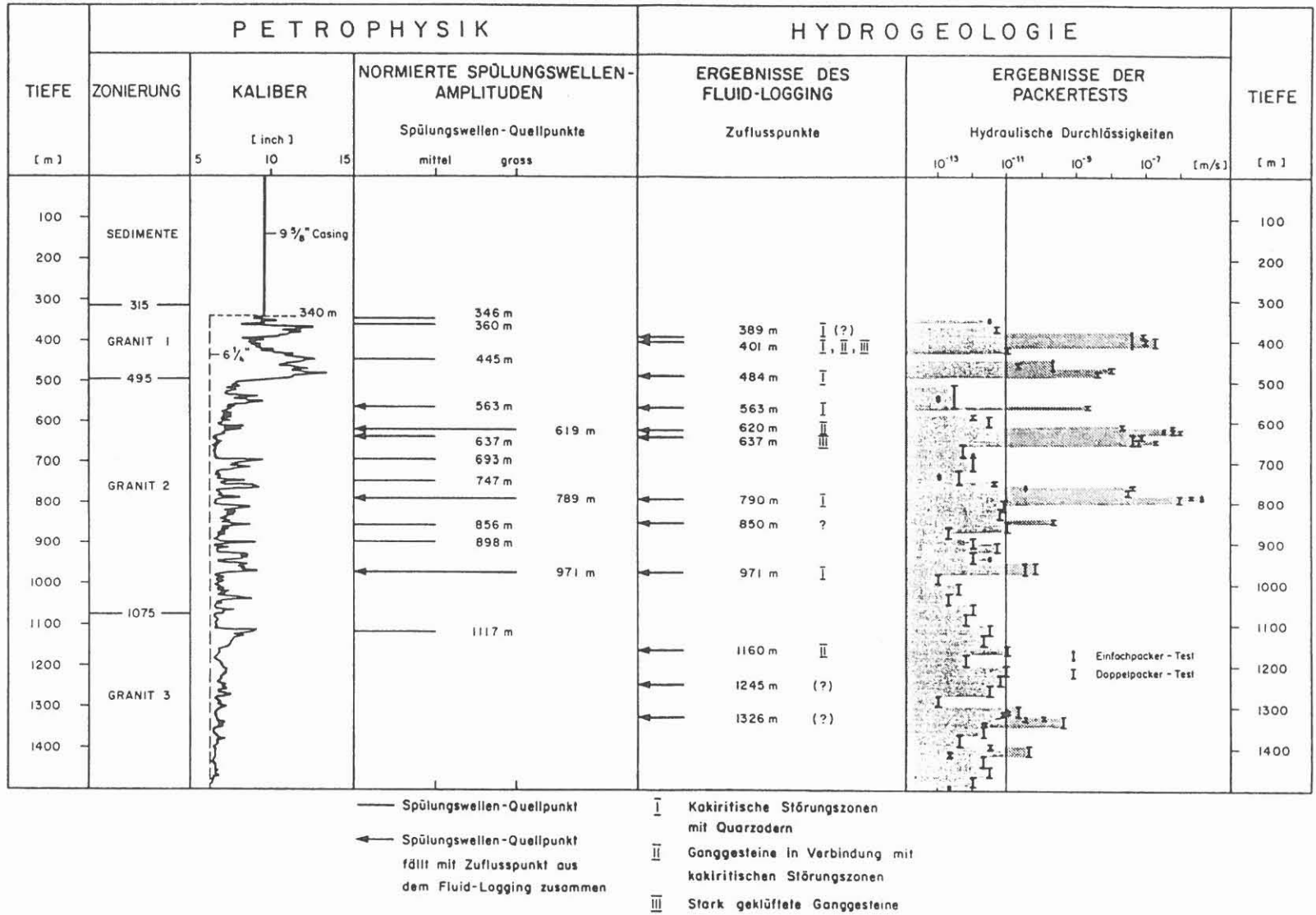
Compilation of core and geochemical data reveal the existence of open fractures with influx at 3447 m and 3817 m depth. These fractures and other geochemical anomalies indicating influx correlate with tube wave events. Contrarily, four open fractures seen on core samples do not generate tube waves. Disadvantages of core sample observations are that coring could not be done continuously over the entire depth of 4 km at KTB pilot hole and that fractures cannot be studied under in-situ conditions.

Temperature anomalies are also not unique and reliable indicators of open fractures. Temperature anomalies are caused by many circumstances. Fluid-filled fractures without temperature difference between formation fluid and mud cannot be indicated.

It is possible that tube waves are generated at borehole inhomogeneities like strong variations in caliper diameters. In data from the KTB pilot hole we did not find convincing evidence for this. There are some tube waves situated in strongly varying caliper regions, contrarily many strong caliper anomalies do not produce any tube wave.

Nagra [1985] applied the tube wave method in the Böttstein borehole (see Fig. 9). They concluded that this method is in general not reliable for fracture detection, mainly because they observed that some tube waves are generated at thin, deep washouts and borehole inhomogeneities. But the degree of correspondance is changing with depth. Within a special type of granite (495–1075 m) the correspondance between tube wave event and location of fluid influx or increased permeability is very good. Therefore the reliability of the tube wave analysis seems to be dependent on the conditions of the borehole and the surrounding formation.

Figure 9: Tube wave measurements at the Böttstein borehole, Switzerland: Comparison with results of hydraulic packer tests and conductivity fluid logging (from Nagra [1985]).



Considering all available experiences with the tube wave method, the reliability as a method for detection of open permeable fracture zones cannot be quantified. It is suggested that there is a relation between tube wave amplitudes and permeability of a fracture zone. It is a still open question whether borehole inhomogeneities in caliper or changes in lithology can generate tube wave events.

In order to test the tube wave method and to get reliable information about fractures, a tube wave survey should be carried out with the following requirements:

- The tube wave survey can be carried out by a tool similar to the VAL sonde or by a usual sonic log tool if a recording time of at least 30 ms is realized. A third possibility is a VSP-survey with an array of hydrophones not clamped to the borehole wall. The offset of the shots at the surface should be as small as possible and the fluid column in the hole as high as possible in order to get a good generation of tube waves.
- The frequency should be low to get a large penetration depth.
- A gamma-ray log in combination with the VAL sonde is indispensable to get depth control.
- A reliable independent method to calibrate the tube wave analysis is needed. In our opinion, the conductivity fluid logging method is qualified for this purpose. It is necessary to perform such a measurement at least in a defined depth interval.
- Other borehole observations should be available like e.g. core sample analysis, mud and gas analytic data and electrical measurements.
- Very convenient for a quantitative comparison with tube wave data are borehole televiewer (BHTV) measurements.

## Acknowledgements

We benefit from many discussions with our colleagues at the Geophysical Institute at Karlsruhe. We like to thank B. Müller, A. Krammer and L. Mastin from the borehole geophysics group. A. Stiefel (geothermal group) and F. Reifensahl (geohydraulic group) gave us their data and preprints of their reports. They permit us to present one of their figures. We thank I. Bush and E. Lüschen for reading the manuscript, J. Draxler and K. Bram (NLF, Hannover) for providing the data and discussions. Eventually we like to thank K. Fuchs and P. Hubral who stimulate this interdisciplinary investigation and take part with helpful discussions. We are grateful to the Deutsche Forschungsgemeinschaft (DFG, Bonn) for funding through grant No. HU 313/2-1 within the KTB priority program.

## 5 Appendix

In this appendix we give a description of the figure at the end of this report which shows a comparison between tube wave events found in VAL echolog data and other borehole measurements relevant for fracture detection. The figure is divided into two parts, representing a depth range of 0–2100 m and 1900–4000 m respectively.

The columns are explained from left to right. In **column A** the lithological profile is shown, its legend is in the lower part of the figure. In **column B** the caliper log is presented. The two curves give the diameter of the borehole in two perpendicular directions. The left



margin corresponds to a value of 10 cm. The spacing between two vertical gridlines represents 10 cm.

The evaluation of visible planar structures in the acoustic borehole televiewer (BHTV) (**columns C–E**) and tube wave events in VAL-(Variable Acoustic Logging tool of Petrodata AG)-echolog data (**columns F–H**) are presented as lines, its length representing subjectively estimated amplitudes of the events. Three categories were used: weak, intermediate, strong. Planar structures in BHTV are seen in traveltime displays (**column D**) and/or in amplitude displays (**column E**). **Column C** indicates the company and the achieved data quality. Locations where tube waves are generated which are detected by characteristic V-shaped pattern in VAL-echolog data are given in **column F**. Zones of reduced amplitudes are indicated in **column G**. **Column H** shows in which depth range data were available.

BHTV and VAL are the main subject of this investigation. We compare their results with other borehole measurements relevant and available for fracture detection. Temperature anomalies after the heat exchange test [Stiefel, 1990] are shown in **column I**. During a hydraulic injection test [Reifenstahl and Stober, 1990] temperature anomalies were recorded (**column J**). During a hydraulic withdrawal slug test [Reifenstahl and Stober, 1990] conductivity anomalies of the mud were measured (**column K**). In **column L** geochemical anomalies (high helium and methane contents, influx of saline fluids) [Erzinger et al., 1989] are indicated. In **column M** we show the locations of open and permeable fractures (zones) derived from core samples in the KTB field laboratory.

Depths in VAL data are not corrected for the systematic error (see section 2.3). In comparison, 6 m have to be added to all depths in the depth interval 1600–3860 m.

## References

- Balch, A.H. and Lee, M.W., 1984, Vertical Seismic Profiling: Technique, applications and case histories: D. Reidel Publishing Comp.
- Beydoun, W.B., Cheng, C.H., and Toksöz, M.N., 1985, Detection of open fractures with vertical seismic profiling: *Journal of Geophysical Research*, **90**, 4557–4566.
- Bram, K., Draxler, J.K., Kessels, W., and Zoth, G., 1990, Grundlagenforschung und Bohrlochgeophysik (Bericht 10): KTB-Report 90-6a.
- Burkhardt, H. and Müller, K., 1987, Forschungsvorhaben: Untersuchungen zur Übertragbarkeit der Bohrloch-Meß- und -Auswerteverfahren in Sedimentgesteinen zur Bestimmung der Porosität und Permeabilität im Kristallin (nichtelektrische Verfahren): Endbericht Bu 298/11, available at the KTB project management.
- Chang, S.K., Liu, H.L., and Johnson, D.L., 1988, Low-frequency tube waves in permeable rocks: *Geophysics*, **53**, 519–527.
- Draxler, J.K. and Hänel, R., 1988, Grundlagenforschung und Bohrlochgeophysik (Bericht 4): KTB-Report 88-4.
- Emmermann, R., 1986, Das Deutsche Kontinentale Tiefbohrprogramm, Forschungskonzeption und Zielsetzungen: Deutsche Forschungsgemeinschaft, Bonn, 147–166.
- Emmermann, R., Dietrich, H.G., Heinisch, M., and Wöhrl, T., 1988, Tiefbohrung KTB-Oberpfalz VB, Ergebnisse der geowissenschaftlichen Bohrbearbeitung im KTB-Feldlabor: Geologie, Geochemie: KTB-Report 88-1, 88-2, 88-6, and 88-9.

- Emmermann, R., Dietrich, H.G., Heinisch, M., and Wöhl, T., 1989, Tiefbohrung KTB-Oberpfalz VB, Ergebnisse der geowissenschaftlichen Bohrbearbeitung im KTB-Feldlabor: Geologie, Geochemie: KTB-Report 89-4 and 89-5.
- Emmermann, R., Dietrich, H.G., Lauterjung, J., and Wöhl, T., 1990, Tiefbohrung KTB-Oberpfalz VB, Ergebnisse der geowissenschaftlichen Bohrbearbeitung im KTB-Feldlabor: Geologie, Geochemie: KTB-Report 90-2.
- Erzinger, J., Heinschild, H.-J., Figgemeier, C., and Samer, M., 1989, Ergebnisse der Gasanalytik in der KTB-Vorbohrung: 2. KTB Kolloquium, KTB-Report 89-3, 42-45.
- Hänel, R., 1987, Grundlagenforschung und Bohrlochgeophysik (Bericht 2): KTB-Report 87-3.
- Hänel, R., 1989, Versuch zur Ermittlung von permeablen Klüften in der Pilotbohrung KTB-Oberpfalz VB mittels Stonely-Wellen: KTB-Report 89-1, 123-134.
- Heinemann, B.B. and Mastin, L., 1989, First evaluation of Four-arm-caliper and borehole televiewer measurements in the KTB pilot hole below 500 m depth: 2. KTB Kolloquium, KTB-Report 89-3, 243-244.
- Huang, C.F. and Hunter, J.A., 1981, The correlation of "tube wave" events with open fractures in fluid-filled boreholes, *in* Current research, Part A, Paper 81-1A: Geological Survey of Canada, 361-376.
- Jobmann, M., 1990, Thermischer Injektionstest und Temperaturmessung nach sechsmonatiger Standzeit in der KTB-Oberpfalz VB: KTB-Report 90-6a, 229-243.
- Kurkjian, A.L. and Chang, S.K., 1986, Acoustic multipole sources in fluid-filled boreholes: *Geophysics*, **51**, 148-163.
- Lüschen, E., Söllner, W., Hohrath, A., and Rabbel, W., 1990, Integrated P- and S-wave borehole experiments at the KTB-deep drilling site: KTB-Report 90-6b, 85-136.
- Nagra, 1985, Sondierbohrung Böttstein - Untersuchungsbericht: Technical Report 85-01, Nagra.
- Petrodata, 1987. Variable Acoustic Logging - A new acoustic logging tool generation: Company brochure.
- Reifenstahl, F. and Stober, I., 1990, Absenk-/Injektionstests und Leitfähigkeits- Fluid-Logging in der KTB Oberpfalz VB: KTB-Report 90-6a, 285-313.
- Stiefel, A., 1990, Gegenstrom-Wärmetauscher-Experiment und Temperaturangleich in der KTB-Oberpfalz VB vom 9. bis 19. März 1990: KTB-Report 90-6a, 259-281.
- Tsang, C.F., 1987. A borehole fluid conductivity logging method for the determination of fracture inflow parameters: NDC-1, Earth Sciences Division, Lawrence Berkeley Laboratory, University of California.
- Tsang, C.F. and Hufschmied, P., 1988. A borehole fluid conductivity method for the determination of fracture inflow parameters: NTB-88-13, Nagra.
- White, J.E., 1983, *Underground sound*: Elsevier Science Publishers B.V.

# Migration of steeply dipping reflectors at the KTB site: Depth errors caused by inaccurate velocity models

C. Hanitzsch\*, P. Hubral†, T. Rühl‡ and W. Söllner†

## Abstract

A depth migration is very sensitive to the velocity model especially in the case of steeply dipping reflectors like the so-called SE reflectors at the KTB site. Velocity models derived from first breaks in *vertical seismic profiling (VSP)* experiments were used and compared with velocity data at the top of the crystalline refractor derived by short range measurements. Because of high picking errors, the possibility to compare seismic events with information of the upper part of the KTB HB hole allows only a very limited calibration of the velocity model. Based on the cutting profile, we assume that the reflectors SE-2 and SE-3 represent faults at 3600–3660 m depth and 5440–5560 m depth (or a lithological contrast at 5540–5610 m depth).

We suppose that the velocity of an average model starts at about 5.2 km/s at the surface, reaches a value of 6.0 km/s in about 2.5 km depth and remains approximately constant below. In that case, the reflector SE-1 will be hit at a depth of 7.0 km. Because of the steep dip of reflector SE-1 which increases the size of the error range (from inaccurate velocity models and picking errors), the tolerance of about  $\pm 0.4$  km is very high.

---

\*Geophysikalisches Institut, Universität Karlsruhe; now at: ELF UK, Geoscience Research Centre, 114A Cromwell Road, London SW7 4EU, UK

†Geophysikalisches Institut, Universität Karlsruhe, Hertzstr. 16, W 7500 Karlsruhe 21, Germany

‡Geophysikalisches Institut, Universität Karlsruhe; now at: GEOMAR, Wischofstr. 1-3, W 2300 Kiel 21, Germany.

## Introduction

The depth migration of surface seismic data needs an accurate velocity model in order to get reliable results of the position of reflector elements especially in case of steeply dipping events. This short report investigates the order of magnitude of the errors caused by the use of an inaccurate velocity model and some trials how to get a more accurate model. In particular, the results of the 2D depth migration of the events SE-1, SE-2 and SE-3 are presented and discussed.

## Velocity models derived from first breaks in *VSPs*

One possibility to get a velocity-depth model is to pick the first breaks from *vertical seismic profiling (VSP)* experiments and to compute interval velocities. This was done in Rühl and Hanitzsch (this volume) for different *VSPs* performed at the KTB site. Based on this investigation we established three (laterally homogeneous) velocity models which are represented in Fig. 1. Model V1 (starting with 5.4 km/s at the surface and a constant velocity of 6.0 km/s below 2.5 km) seems to be a good approximation of the real complicated situation. We consider model V0 (a constant velocity of 6.0 km/s) and model V2 (starting with 4.0 km/s at the surface and a constant velocity of 6.0 km/s below 2.5 km) to be extreme cases and use them to estimate maximum errors.

In *VSP* experiments, a vertical velocity gradient in the formation, a refractor near the hole or velocity anisotropy can produce shorter traveltimes than direct waves. In that case the derived velocities are higher than sonic-log velocities.

In a new investigation, Söllner et al. (this volume) use the *VSP6000* of the main hole and show that the velocity increases to 6.15 km/s below 4 km depth.

## Migration depth errors

### Theoretical considerations

As a first investigation, synthetic traveltimes were calculated: a steeply dipping reflector (40-60 degrees) was modelled (in 2D) using velocity models V1 and V2. The computed traveltime curve was migrated using the constant velocity model V0. The conclusions are:

- The dip of a reflector is hardly changed.
- Reflector elements are shifted mainly in horizontal direction by several hundred meters.
- The vertical displacement between two points at the same horizontal coordinate can be as large as 1100 m.

The results of this more theoretical consideration show us that we must be aware of large errors resulting from the use of inaccurate velocity models in a depth migration.

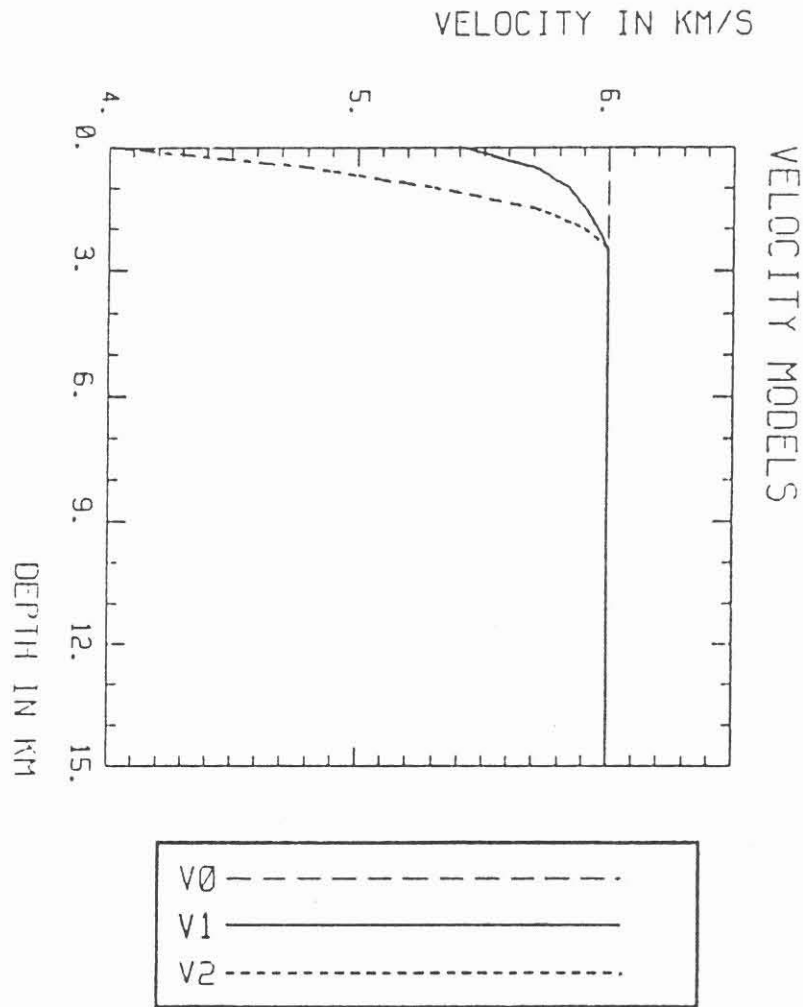


Figure 1: Representation of the three velocity models V0 (6.0 km/s), V1 (5.4-6.0 km/s) and V2 (4.0-6.0 km/s) as a function of depth.

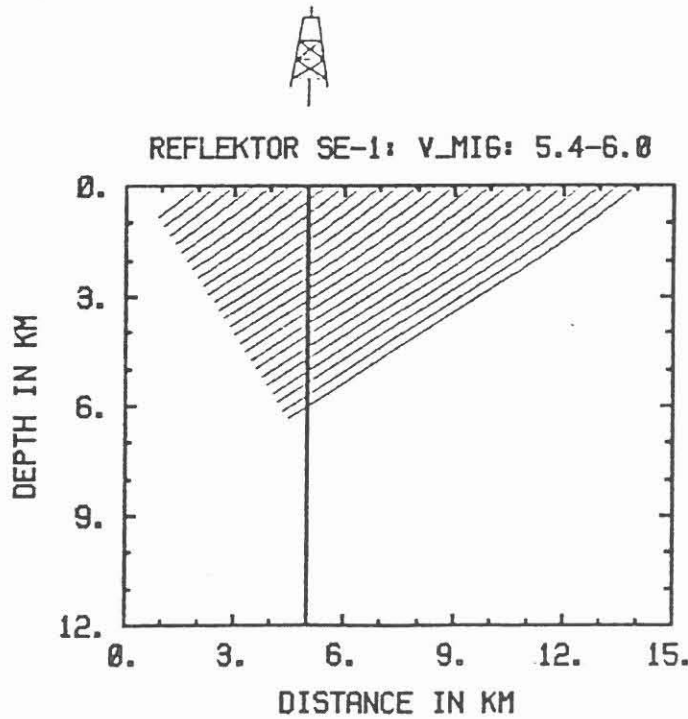


Figure 2: Ray paths from receivers to reflector SE-1. The receivers cover an area which is marked in Fig. 5.

Table 1: Depth of intersection of the SE reflectors with the KTB HB hole, depending on the velocity models V0, V1 and V2 used for migration, and the approximate dip of the reflectors.

	SE-1	SE-2	SE-3
V0 (6.0 km/s)	7.4 km	3.8 km	5.8 km
V1 (5.4-6.0 km/s)	7.2 km	3.7 km	5.5 km
V2 (4.0-6.0 km/s)	6.4 km	3.2 km	4.9 km
Approximate dip	57°	45°	55°

## Migration of SE-horizons using different velocity models

As a second investigation, the real 3D surface seismic near offset data were used. The traveltimes surfaces of several reflectors have been picked from envelope stacks at the DEKORP center, University of Clausthal. The reflectors SE-1, SE-2 and SE-3 form approximately a plane dipping parallel to the inline profiles. Therefore, it was possible to perform a 2D migration.

The used migration algorithm traces rays from the receiver points using a starting angle which is determined by the local derivative of the traveltimes curve  $\tau$

$$\frac{d\tau}{dx} = \frac{\sin \alpha}{v}. \quad (1)$$

The rays are traced backward in time from  $t = \tau(x)$  to  $t = 0$ . As an example, Fig. 2 shows the traced rays for reflector SE-1 and velocity model V1.

Each traveltimes surface was migrated three times using the velocity models V0, V1 and V2. The resulting reflectors are represented in Fig. 3 and 4. The depth of intersection with the KTB HB hole are given in Table 1. The depth tolerances run up to 1000 m.

## Picking error propagation

The picking of events in seismograms always includes statistical errors. In case of the plane SE reflectors, the size of this time error can be estimated by computing the standard deviation. Wiederhold (this volume) determines the time errors and the resulting vertical depth errors: SE-2:  $\pm 200$  m, SE-3:  $\pm 110$  m, SE-1:  $\pm 140$  m. These high values result from the large dip and from the fact, that the envelope-stacked seismic data was used for the interpretation.

## Discussion

In the case of steeply dipping reflectors ( $>40$  degrees), a depth migration is very sensitive to the velocity model. Especially the velocity close to the surface is important because it determines the starting angle of rays to the reflector. To improve the depth tolerances (up to 1000 m) we require better information about the velocity distribution.

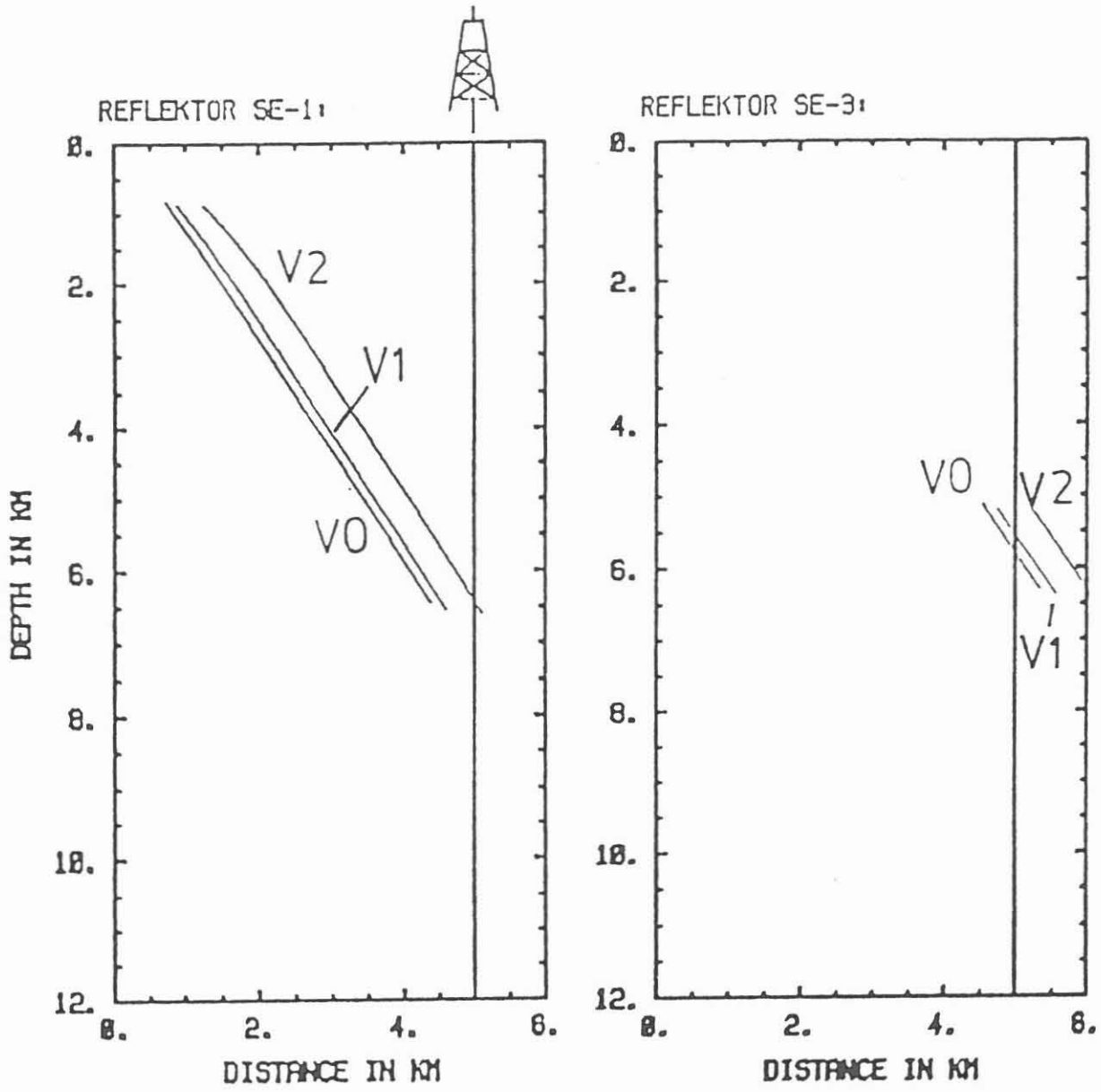


Figure 3: Reflectors SE-1 (left) and SE-3 (right), after migration using three velocity models: V0 (6.0 km/s), V1 (5.4-6.0 km/s) and V2 (4.0-6.0 km/s).

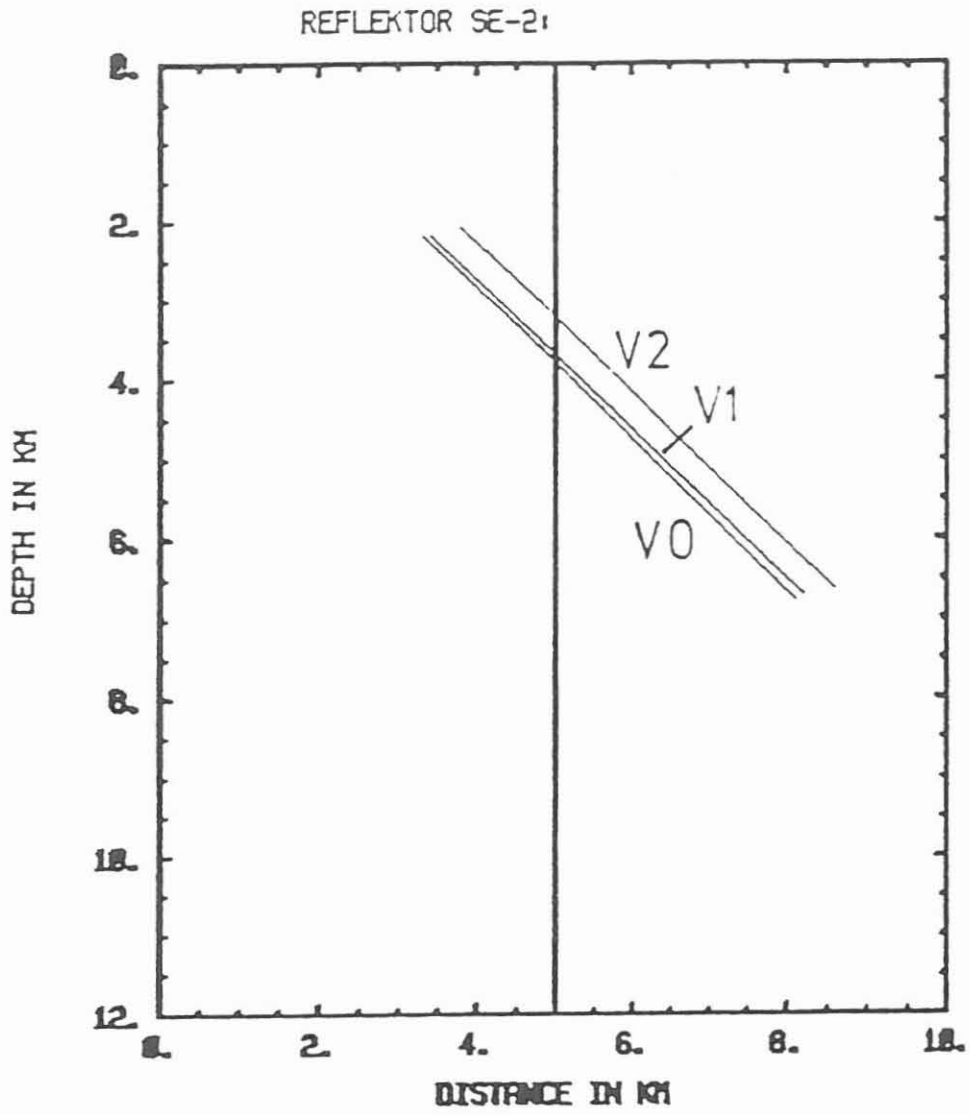


Figure 4: Reflector SE-2, after migration using three velocity models: V0 (6.0 km/s), V1 (5.4-6.0 km/s) and V2 (4.0-6.0 km/s).



Lengeling (1991) computed velocities at the top of the crystalline refractor at the KTB site using short range measurements. He found velocities in the range of 4900-6150 km/s. In the migration process, those rays which hit the reflectors close to the hole start in the northeast of the measurement area (marked in Fig. 5). There, Lengeling found velocities in the range of 4933-5420 m/s, concentrated at 5.1-5.3 km/s.

When the investigations for this report were performed, the drilling of the KTB HB hole was already in work. This fact could open the possibility to use first information from the upper part of the hole to calibrate the velocity model. If a discontinuity in the hole can be identified as a seismic reflector and if the picking error of the identified reflector does not result in a too big depth error, information about the velocity distribution could be derived and the migration error for the deeper events would decrease.

The depth errors which result from picking errors in envelope stacked data were determined by Wiederhold (this volume). The large values (up to  $\pm 200$  m) allow, however, only a very limited calibration of the velocity model.

The question of the nature of seismic reflections in crystalline environments is one of the research objectives of the KTB project, but cannot be answered here. At the surface, the reflector SE-1 is related with the Franconian Line, a geologic contrast between crystalline rocks in the east and sediments in the west. In the subsurface, seismic reflectors can represent mayor lithological contrasts, faults or other discontinuities.

The depth, where the reflector SE-2 hits the hole, was predicted by us between 3.2 km and 3.8 km with an expectation value at 3.65 km depth. The cutting profile (Lich et al., 1992) indicates lithological contrasts at 3425 m (amphibolite-gneiss) and at 3530 m (gneiss-amphibolite) and faults at 3420 m and 3600-3660 m depth. The focus of a small earthquake in April 1991 correlates well with the SE-2 event in that area (Wiederhold, this volume). This is an indication, that faults are responsible for the SE-2 reflection, presumably in the range 3600-3660 m depth.

The reflector SE-3 should hit the hole between 4.9 km and 5.8 km depth with an expectation value at 5.5 km depth. The lithology in that range is predominated by amphibolite, with zones of gneiss at 5230-5320 m and 5540-5610 m depth. Faults are found at 5250-5300 m, 5370 m, 5400 m and 5440-5560 m depth. We assume the SE-3 event to represent a fault at 5440-5560 m depth or a lithological contrast at 5540-5610 m.

We expected more information from the *vertical seismic profiling (VSP)* experiment which was carried out in the KTB HB hole between 3 km and 6 km depth in March 1992. The first investigations (Söllner et al., this volume) show that the SE reflectors (strong in surface seismic data) do not strongly show up in *VSP* data. A correlation seems to be difficult.

## Summary

Both error sources (picking errors and inaccurate velocity models) result in large depth error ranges in the case of the steeply dipping reflectors SE-1, SE-2 and SE-3. The independance of both allows only a very limited calibration of the velocity model on

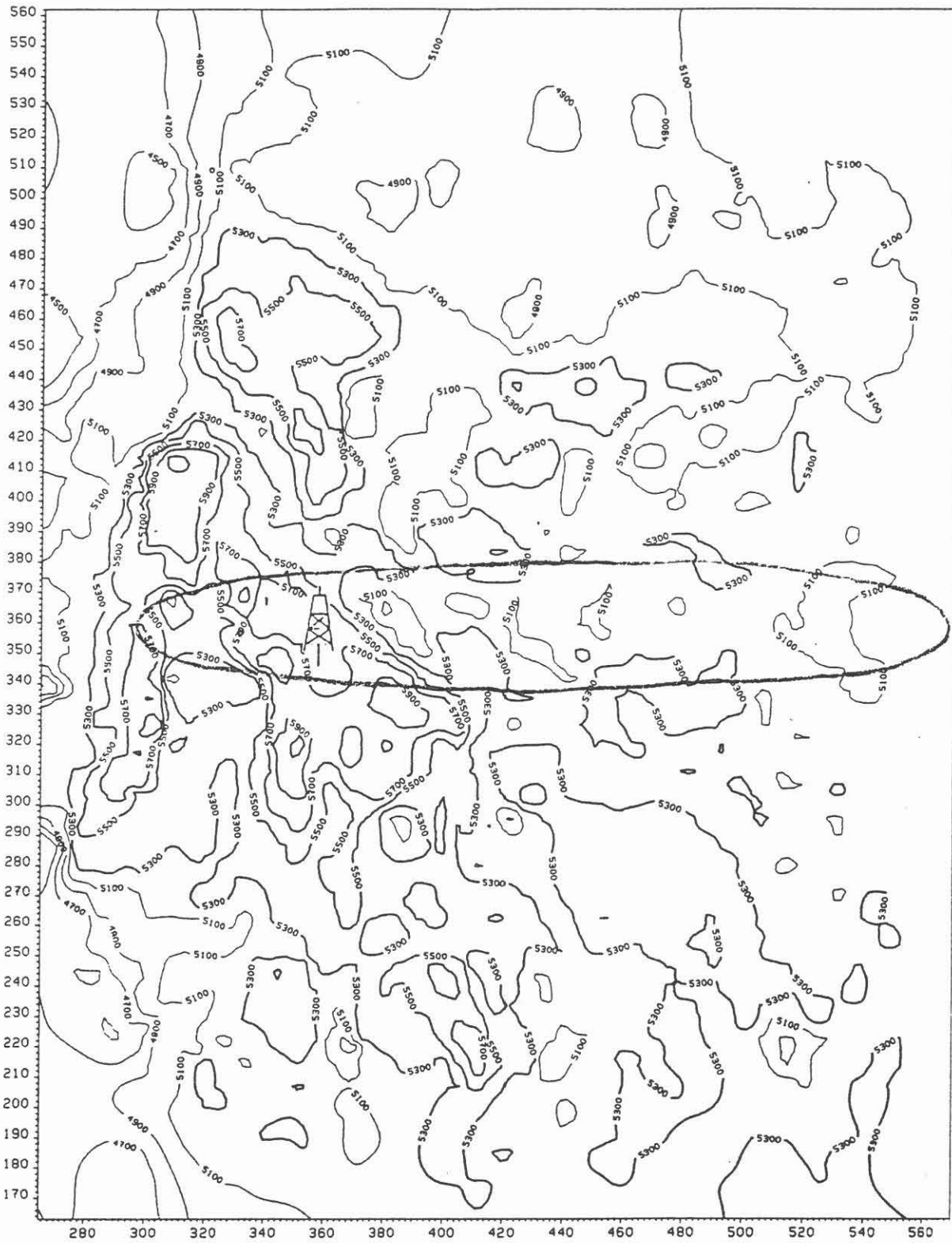


Figure 5: Velocities at the top of the crystalline refractor at the KTB site derived by using short range measurements (from Lengeling, 1991, provided by the DEKORP processing center, Clausthal). The marked area in the northeast (on the right) denote the zone of points which are connected with the SE reflectors by normal incidence rays. These rays and the velocity at these points must be used for migration.

events in the upper part of the hole. Based on the cutting profile (Lich et al., 1992), we assume the SE-2 and SE-3 reflectors to represent faults at 3600–3660 m depth and at 5440–5560 m depth (or a lithological contrast at 5540–5610 m depth).

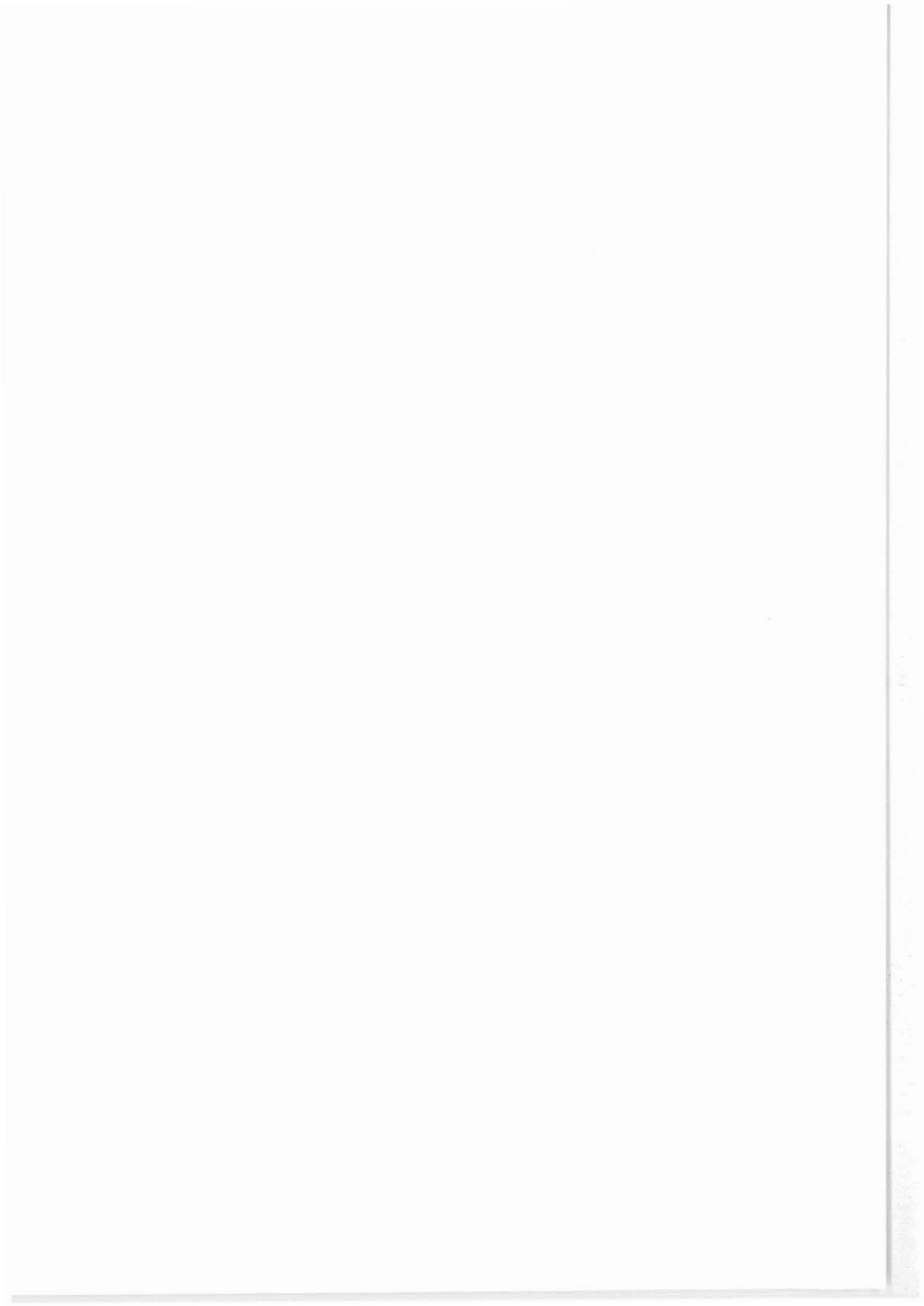
We suppose – in accordance with Lengeling's velocity values and the velocity models derived from *VSP* experiments – that the velocity of an average model starts at about 5.2 km/s ( $\pm 0.2$  km/s) at the surface and reaches 6.0 km/s in about 2.5 km depth. This value remains approximately constant below. A new investigation using the *VSP6000* of the main hole (Söllner et al., this volume) shows that the velocity increases to about 6.15 km/s at 6 km depth. We predict the reflector SE-1 to be hit at a depth of 7.0 km ( $\pm 0.4$  km). The large error range consists of about  $\pm 300$  m (from inaccurate velocity model) and about  $\pm 140$  m (from picking error, Wiederhold, this volume).

## Acknowledgements

We like to thank H. Wiederhold for discussions and the DEKORP center in Clausthal for providing the envelope stacked data on paper and the map of velocities which is used in Fig. 5. We are grateful to the Deutsche Forschungsgemeinschaft (DFG, Bonn) for funding through grant No. HU 413/3-1 within the KTB priority program.

## References

- Lengeling, R., 1991, Bewertung eines Inversionsverfahrens zur Berechnung statischer Korrekturen in der 3D-Seismik und seine Anwendung auf reflexionsseismische DEKORP-Messungen in der Oberpfalz 1989: Dissertation, Geophysikalisches Institut, Universität Karlsruhe.
- Lich, S., Duyester, J., Godizart, G., Keyssner, S., and de Wall, H., 1992, German Continental Deep Drilling programme (KTB) - geological survey of the main hole 0-6000 m: KTB-Report 92-2, B1–B83.
- Rühl, T. and Hanitzsch, C., 1992, Average and interval velocities derived from first breaks of vertical seismic profiles at the KTB pilot hole: KTB-Report 92-5, DEKORP Report.
- Söllner, W., Lüschen, E., Li, X., Hubral, P., Gut, T., Werner, U., and Widmaier, M., 1992, A link between reflection seismic profiling and lithology: KTB-Report 92-5, DEKORP Report.
- Wiederhold, H., 1992, Interpretation of envelope stacked 3d seismic data and its migration - another approach: KTB-Report 92-5, DEKORP-Report.



## Zur Korrelation des tektonischen Baues mit den seismischen Strukturen im Raum KTB-Oberpfalz – Münchberger Gneismasse

GERHARD STETTNER\*

### Zusammenfassung

In der folgenden Darstellung wird davon ausgegangen, daß bei der reflexionsseismischen Erkundung von Krustenstrukturen ältere orogentektonische Strukturen wahrscheinlich nur bei günstiger Geometrie und Tiefenlage erfaßt werden können. Eine grobe lithologische Differenzierung mit ausreichenden Elastizitätsunterschieden ist im fraglichen Raum auf einen bestimmten Krustentyp, das Bohemikum, beschränkt. Dessen größte Mobilität ist wahrscheinlich mit der spätkaledonischen Tektogenese nach Ablauf des Silurs verbunden. Das Bohemikum beinhaltet mächtige und lateral aushaltende Metabasite und liegt in größeren Abschnitten relativ flach. Dies gilt vor allem für subduzierte Bereiche des Bohemikums. In dieser Aussage kommt eine Modellvorstellung zum Ausdruck (STETTNER 1990, 1992), welche eine Deutung und Korrelation der seismischen Strukturen ermöglicht. So können im oberpfälzer Grundgebirge die in etwa 7 bis 12 km Tiefe liegenden seismischen Reflexionen mit dem höheren Abschnitt des subduzierten Bohemikums korreliert werden. Im Fichtelgebirge entspricht dem der Bereich zwischen 9 und 15 km Tiefe. Von den spätkaledonisch in höhere Krustenbereiche aufgeschobenen Bohemikumkomplexen sind nur jene durch seismische Reflexionen registriert, welche relativ flach liegen (der Schwerestörkörper des Frankenwaldes).

Variskische Relativbewegungen zeichnen sich nur in räumlich begrenzten Bereichen ab. Junge, wahrscheinlich tertiäre Störungen, werden seismisch – auch bei mittelsteilem Einfallen – auffallend deutlich abgebildet. Die mit diesen Störungen verbundenen Gefügelockerungen (Porositäten) und dadurch bedingte Geschwindigkeitserniedrigungen werden anscheinend seismisch besser registriert als die Geschwindigkeitsunterschiede einer mächtigen Gneis-Metabasit-Wechsellagerung.

### Einleitung

Die KOLA-Tiefbohrung hat die Bedeutung von Porositäten, sei es in tektonischen Bruchzonen oder in allgemein fluidbedingten subhorizontalen Strukturen für das reflexionsseismische Bild in besonderer Weise deutlich gemacht (KOZLOVSKY 1982). Auch unter den von reflexionsseismischen Untersuchungen im näheren KTB-Bereich (ISO 89-3D-Seismik) herausgearbeiteten deutlichen Reflexionen befinden sich Strukturen dieser Art. Um solche von primär lithologischen (z.B. Metabasiteinlagerungen) abzutrennen, bedarf es jeweils der Kontrolle durch ein Geschwindigkeitsprofil des jeweiligen Krustenabschnittes. Andererseits kann den bisherigen Auswertungen von ISO89 (HLUCHY et al., this volume) entnommen werden, daß sich lithologische Unterschiede von Gneis/Metabasit-Wechsellagerungen bei ungünstiger Geometrie kaum erfassen lassen (z.B. wechselndes und steiles Einfallen, Faltung, geringe Ausdehnung). Unter diesen Aspekten erscheint die Aufhellung eines älteren prävariskischen und variskischen Strukturbaues durch reflexionsseismische Untersuchungen allein kaum möglich zu sein. Es ist deshalb notwendig, unter Zuhilfenahme von Modellvorstellungen nach lithologischen und strukturellen Eigenschaften zu suchen, welche Aussicht auf reflexionsseismische Erfassung bieten.

---

\* Author's adress: Dr. Gerhard Stettner, Roßsteinstr. 8, D-8150 Holzkirchen

### **Voraussetzungen der reflexionsseismischen Erfassung geologischer Vorzeichnungen**

Es ist hier zu fragen: Welche Einheiten des Grundgebirges bieten folgende Bedingungen:

- größere E-Modul-Unterschiede zwischen Gesteinen ausreichender Mächtigkeit, etwa in Gestalt einer günstig dimensionierten Wechsellagerung (z.B. von schiefrigen Metasedimenten mit massigen Metabasiten)
- ausreichende laterale Erstreckung und möglichst flache Lagerung.

Derartige Eigenschaften können in der westlichen Böhmisches Masse lediglich im Bohemikum-Krustentyp und im Lithotyp der Münchberger Gneismasse (Hangendserie) gefunden werden. Mit gewissen Vorbehalten kann man die Münchberger Gneismasse, vor allem deren Hangendserie, ebenfalls der Bohemikum-Kruste zuordnen. Letztere umfaßt stratigraphisch Oberproterozoikum briooverischer Fazies (wie im Teplá-Barrandium) sowie eine altpaläozoische Auflagerung, welche ich hier mit dem Silur enden lassen möchte. Besonders die vielfältige Wechsellagerung in der Hangendserie der Münchberger Gneismasse (Hornblendebändergneise, Amphibolite und Eklogite) dürften bei relativ flacher Lagerung günstige Voraussetzungen für die Ausbildung seismischer Reflektoren bieten. Darüber hinaus dürften die Metabasite der Grünschiefereinheit und die ordovizischen Diabasdecken bei relativ flacher oder nur wenig geneigter Lagerung als deutliche Reflexionen im seismischen Bild in Erscheinung treten.

### **Deutung seismischer Reflexionen im Rahmen des Modells "spätkaledonische Bohemikum-Subduktion"**

Das Modell einer spätkaledonischen Subduktion von Bohemikum-Kruste unter das Moldanubikum (und das südliche Saxothuringikum) bietet die Möglichkeit eine Gruppe von seismische Reflektoren zu erklären (Abb.1). In diesem Modell (STETTNER 1990, 1992) wird die nach Südwesten subduzierte Bohemikumkruste teilweise durch Aufschiebungen nach Nordosten wieder in höhere Krustenpositionen gebracht.

Ausgangspunkt in diesen Vorstellungen sind die mit einer spätkaledonischen Prägung verbundenen Metamorphoseverhältnisse im heutigen Westteil des Teplá-Barrandiums (Westböhmisches Metamorphe Zone oder Zone von Teplá-Domazlice). Hier ist der Eingangsbereich der Subduktion östlich des Böhmisches Pfahls wieder herausgehoben und der Beobachtung zugänglich. Im Bereich des westlich anschließenden Moldanubikums befindet sich das subduzierte Bohemikum infolge der unterschiedlichen zwischenzeitlichen Hebungsvorgänge in entsprechend unterschiedlichen Tiefen. Diese spiegeln sich auch im unterschiedlichen Anschnittniveau des Moldanubikums. Danach sollte im Bereich des hochmetamorphen Moldanubikums östlich von Tirschenreuth der Grenzbereich Moldanubikum/ Bohemikum in etwa 7 km Tiefe liegen und nach Südosten und Südwesten zu stufenweise absinken. Es ist durchaus denkbar, daß der "Erbendorfkörper" (GEBRANDE in KTB 1986) Teil dieses Systems ist. Zu den direkten Hinweisen für eine Unterlagerung des Moldanubikums durch Bohemikumkruste gehören die Vorkommen von Metabasiten in Störungszonen innerhalb des hochmetamorphen Moldanubikums (tiefen Anschnittes) östlich Tirschenreuth. Mit reliktschen Merkmalen von Hochdruck-Prägung können sie als Einschuppungen aus dem unterlagernden Bohemikum-Subduktionsstockwerk aufgefaßt werden. Ähnliche Verhältnisse im moldanubischen Block Böhmens, wie auch die südböhmischen Granulite, können analog gedeutet werden.

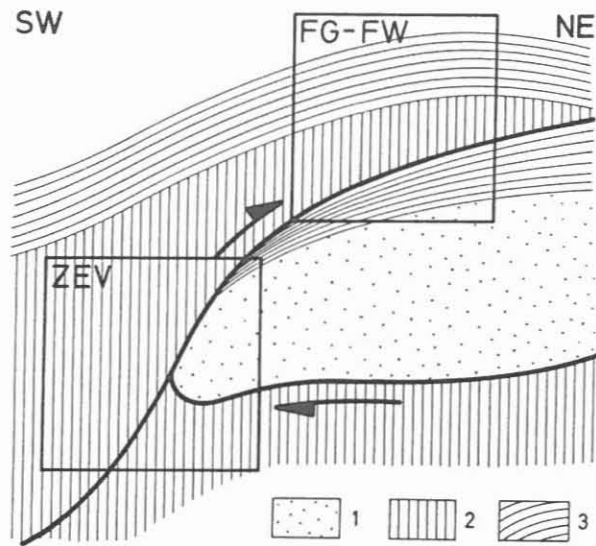


Abb.1. Modell der spätkaledonischen, nachsilurischen Subduktion von Bohemikumkruste nach Südwesten unter Moldanubikum und der entgegengesetzten Aufschiebungen am Westrand der Böhmisches Masse.- ZEV = Abschnittbereich der Zone von Erbdorf-Vohenstrauß mit dem Aufschiebungskomplex der Neustädter Scholle. FW-FG = Abschnittbereich im Abschnitt Fichtelgebirge-Frankenwald. 1 = Moldanubikum, 2 = Bohemikum, 3 = prädevonische altpaläozoische Auflagerung.

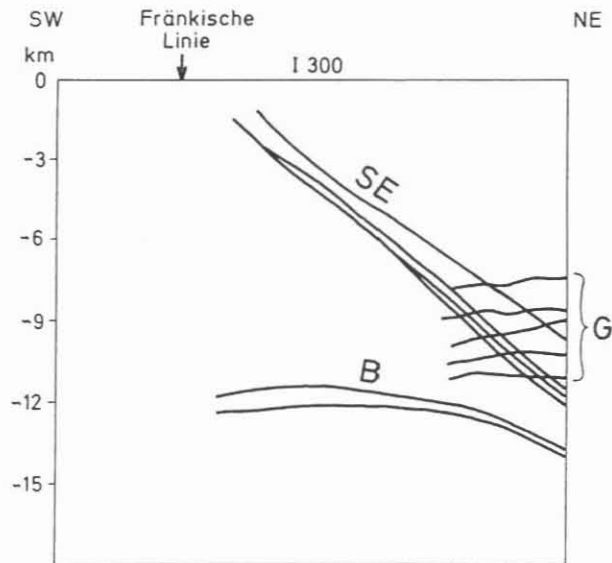


Abb.2. Reflexionshorizonte der Gruppen "SE", "B" und "G" im Bereich der ISO 89 - 3D-Seismik im KTB-Umfeld. Aus der inline 300 - Darstellung der Enveloppenstapelung (unmigriert), SW-NE-Profileschnitt etwa 2,5 km SE der KTB-Lokation. Nach HLUCHY et al., this volume.

Die in der ISO89 – 3D–Seismik (HLUCHY et al., this volume) im KTB–Umfeld deutlich gemachten, relativ flach liegenden Reflexionen der Gruppe "G" in etwa 8 bis 11 km Tiefe und die der Gruppe "B" in etwa 12 km Tiefe, können mit gleichorientierten Gesteinsverbänden des subduzierten Bohemikums in Beziehung gebracht werden (Abb.2).

Im Saxothuringikum haben diese im Geschwindigkeitsprofil mit Komplexen höherer Geschwindigkeit verknüpften Reflektoren eine andere Position, was mit den variskischen Relativverschiebungen zwischen Fichtelgebirge und Moldanubischer Region einerseits sowie zwischen dem Fichtelgebirge und dem Frankenwald andererseits zusammenhängt.

Im Fichtelgebirge sind nach den bisherigen seismischen Untersuchungen (DEKORP 4 – BORTFELD et al. 1988) sowohl in etwa 9 km Tiefe relativ höhere Geschwindigkeiten in Verbindung mit Reflektoren–Häufung erkennbar, als auch ausgeprägtere Bereiche höherer Geschwindigkeit in 12–15 km Tiefe. Möglicherweise gehören beide zum Subduktionsstockwerk des unterlagernden Bohemikums.

Im Krustenabschnitt des Frankenwaldes, welcher vordevonisch mit dem Fichtelgebirge eine wahrscheinlich nicht differenzierte Einheit gebildet hat, ist das Subduktionsstockwerk in einer größeren Tiefe zu suchen. Verschiedene Gründe geben Anlaß zur Annahme, daß infolge der jungvariskischen Heraushebung der Fichtelgebirgsschwelle um 6 bis 8 km der Grenzbereich zum Subduktionsstockwerk im Frankenwald in etwa 18 bis 23 km Tiefe zu suchen ist. Es ist zu fragen, ob dafür im reflexionsseismischen Profil Münchberger Gneismasse – Vogtland – Erzgebirge (MVE) Hinweise vorhanden sind. Nach dem schematischen Profil in Abbildung 2 ist das nicht der Fall. Denn es ist anzunehmen, daß die Haupt–Relativbewegungsfläche zwischen dem Muldenbereich des Frankenwaldes und der Fichtelgebirgsschwelle nach Nordwesten einschiebt und den MVE–Profilschnitt in einem mittleren Tiefenbereich um 10 km schneidet. Darunter befindet sich Fichtelgebirgskruste mit einem auffälligen Reflexionsbereich unterhalb 11 km. Im Westen des seismischen Profils besteht hier eine auffällige Diskordanz zum höheren Profilabschnitt (Abb.4).

Im Abschnitt des Frankenwaldes sind durch das reflexionsseismische DEKORP 4–Profil zwar auffallende Reflexionen in bestimmten Tiefenbereichen festgestellt worden, es fehlen bislang jedoch noch nähere Überlegungen zum Geschwindigkeitsprofil (mündliche Mitt. GEBRANDE), um eine lithologische Korrelation vorzunehmen.

### **Die Aufschiebungsstrukturen im westlichen Randbereich der Böhmisches Masse**

Der Westrand der Böhmisches Masse ist dadurch ausgezeichnet, daß im weiteren Verlauf der spätkaledonischen Tektogenese subduziertes Bohemikum durch gegenläufige, nach Nordosten gerichtete Aufschiebungen in höhere Krustenpositionen gelangt ist (Abb.1).

In der Neustädter Scholle (oder Zone von Erbdorf–Vohenstrauß = ZEV) ist ein solcher nach Nordosten aufgeschobener Abschnitt des Bohemikums von der Oberfläche angeschnitten und in der KTB–Tiefbohrung "Oberpfalz" erfaßt. Bei einem überwiegenden Einfallen mit 40 bis 60° scheint nach den bisher vorliegenden Auswertungsergebnissen der Seismik eine klare Dokumentation des tektonischen Baues durch diese Methode nicht gegeben zu sein.



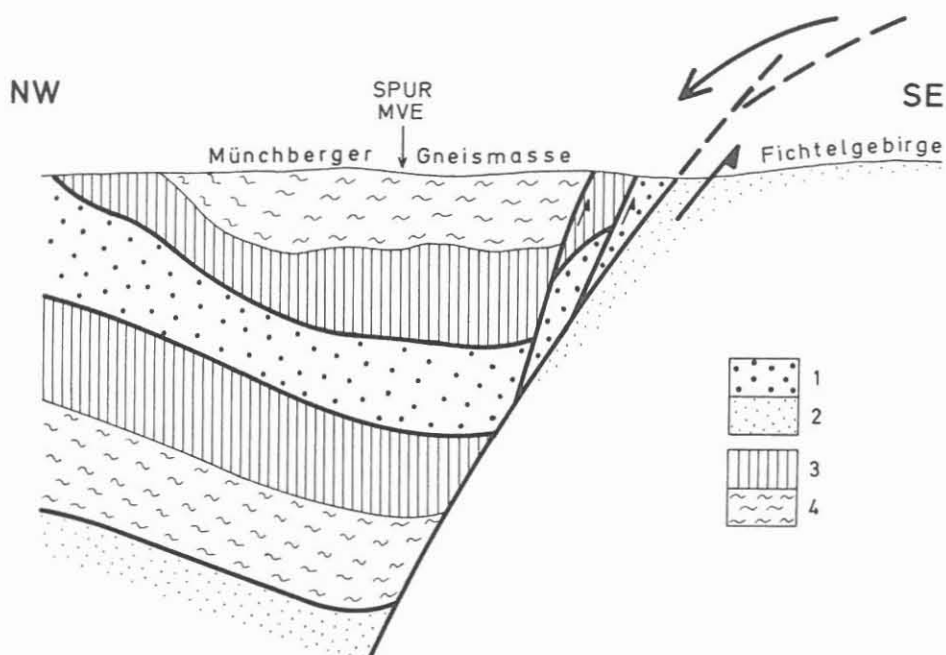


Abb.3. Schematischer SE-NW-Querschnitt Frankenwald – Münchberger Gneismasse – Fichtelgebirge (etwa durch den Ostteil der Münchberger Gneismasse), mit der Spur der DEKORP`90- (MVE-)Meßlinie. Zur Verdeutlichung des komplexen Untergrundes (vgl. Abb.4).- 1 = devonisch-unterkarbonische Sedimente der Thüringischen Faziesreihe, 2 = prädevonisches Altpaläozoikum der Thür.Faziesreihe, 3 = prädevonisches Altpaläozoikum der Bayer.Faziesreihe und Grünschiefereinheit im Münchberger Deckenstapel und in der spätkaledonischen Aufschiebungs-masse, 4 = Gneise und Metabasite der Münchberger Gneismasse und des spätkaledonischen Aufschiebungs-komplexes (Frankenwald-Schwerestörkörper).

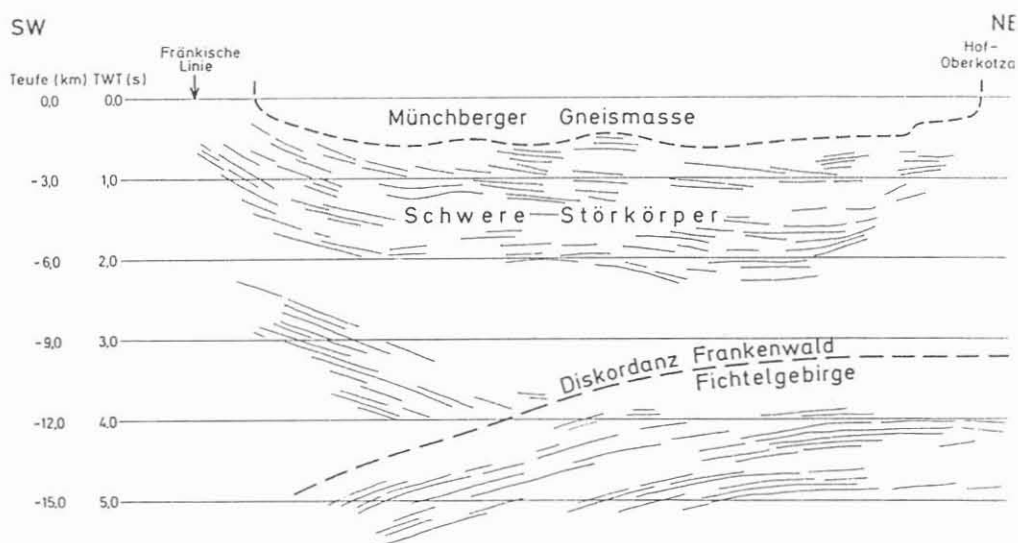


Abb.4. Line drawing des reflexionsseismischen Profils DEKORP `90 (MVE) im Abschnitt der Münchberger Gneismasse (unmigriert), mit einer schematischen Kennzeichnung der allochthonen geologischen Einheiten (Münchberger Gneismasse und Frankenwald-Schwerestörkörper). Im unteren Abschnitt ist die mutmaßliche Diskordanz Fichtelgebirgsschwelle/Frankenwälder Muldenzone eingezeichnet, welche – nach NW einschiebend – das südliche Frankenwälder Paläozoikum unterteuft (vgl. Abb.3).

Im Profil der KTB-Vorbohrung liegt unterhalb 3000 m offensichtlich ein anderer Strukturabschnitt. Hier wird das generelle Südwest-Einfallen des Lagenbaues der Neustädter Scholle (ZEV) durch ein überwiegendes Nordostfallen abgelöst. Eine strukturell vergleichbare Einheit ist an der Oberfläche nicht angeschnitten, sieht man von Schollenrotationen geringen Ausmaßes in der südlichen Neustädter Scholle ab. Der Abschnitt unterhalb 3000 m kann als hochgeschlepptes Bohemikum des Subduktionsstockwerkes angesehen werden. Gleiches gilt für diesen Teufenbereich in der Hauptbohrung.

Im angrenzenden Fichtelgebirge ist der spätkaledonisch aufgeschobene Komplex jungvariskisch herausgehoben und als Decke abgeglichen (Münchberger Gneismasse). Im Bereich des Frankenwaldes ist die aufgeschobene ehemals subduzierte Kruste von Devon, Unterkarbon und zum Teil vom Münchberger Deckenstapel überdeckt (Abb.3). Soweit es die Metabasite betrifft, ist dieser Komplex mit dem Schwerestörkörper PLAUMANN'S (1982) identisch.

Das höchste Bohemikum-Stockwerk in Gestalt der Münchberger Gneismasse (Hangendserie) ist von der Erdoberfläche angeschnitten und braucht deshalb nicht seismisch identifiziert werden. Der hier sichtbare lithologische Bau gibt eine Vorstellung vom Aufbau der analogen tieferliegenden Bohemikumabschnitte.

Im reflexionsseismischen Profil MVE sind im Abschnitt der Münchberger Gneismasse (Abb.4) die kräftigen Reflexionen bis in etwa 7 km Tiefe hauptsächlich dem aufgeschobenen Bohemikum-Komplex zuzuordnen. Bei der schüsselartigen Form ist zu berücksichtigen, daß der spätkaledonische Aufschiebungsbau durch spätere, variskische bis saxonische Relativbewegungen beeinflußt worden ist. Hierzu gehört die Heraushebung am Westrand der Böhmisches Masse, welche sich im südwestlichen Randbereich der Münchberger Gneismasse und im westlichen Frankenwald in der Geologie deutlich zeigt. Die seismischen Strukturen bilden diese Hebung ab. Am Ostrand der Gneismasse, im Bereich der Frankenwälder Querzone, ist ebenfalls ein deutliches Hochsteigen der seismischen Strukturen mit dem geologischen Verteilungsbild an der Oberfläche in Einklang zu bringen.

Im ISO 89-Bereich ist die jüngere Tektonik in den bisherigen Auswertungen durch die mittelsteil nach Nordosten einfallenden "SE"- Reflexionen belegt (Abb.2). Es ist hier anzunehmen, daß die an diesen Störungen erfolgte Gefügeauflockerung zu erhöhter Porosität geführt hat. Da die im gleichen Raum gegenläufig nach Südwesten einfallenden Gneis-Metabasit-Verbände seismisch nicht dokumentiert sind, scheint es, daß die mit den Störungsporositäten verbundenen Geschwindigkeitserniedrigungen seismisch deutlicher zum Ausdruck kommen.

## Literatur

- BORTFELD, R.K. et al. (1988): Results of the DEKORP 4/KTB Oberpfalz deep seismic reflection investigations. DEKORP Research Group. - J. Geophys., **62**: 69-101.
- GEBRANDE, H. (1986): Beitrag in KTB, Ergebnisse der Vorerkundungsarbeiten Lokation Oberpfalz. 2. KTB-Kolloquium Seeheim/Odenwald.

HLUCHY, P., KÖRBE, M., THOMAS, R. (1992): Preliminary Results of the Interpretation of the 3-D-Seismic Survey at the KTB-Location. KTB-Report 92-5: DEKORP-Report, this volume.

KOZLOVSKY, Y.A. (1982): Kola Super-Deep: Interim Results and Prospects.- EPISODES, Vol.1982, No.4:9-11.

PLAUMANN, S. (1982): Die Schwereanomalie im Bereich der Münchberger Gneismasse und ihre Interpretation.- Z.dt.geol.Ges., 133: 649-665, Hannover.

STETTNER, G. (1990): KTB-Umfeldgeologie.- 31 S., Bayerisches Geologisches Landesamt, München.

(1992): Geologie im Umfeld der Kontinentalen Tiefbohrung Oberpfalz. Einführung und Exkursionen.- 240 S., Bayer.Geologisches Landesamt München.



On the Geological Interpretation of the 3-D Seismic Data with  
Special Regard to the Information from the KTB Boreholes

Gottfried Hirschmann \*)

**Abstract**

A preliminary interpretation of the major 3-D reflectors is given by correlation with the surface geology and the drilled sections of the KTB Vorbohrung and the Hauptbohrung. Possible explanations for the reflections are discussed: lithological boundaries, cataclastic fault zones (partly filled with fluids) and other structural properties (e.g. foliation). Flat reflectors near the surface (MF1 - 4) can be correlated with Permocarboneous and Mesozoic sediments of the South German Platform. Special attention is drawn to a group of steeply NE-dipping reflectors (SE1, SE2, SE3) which are, obviously, produced by en-echelon fault structures of the Franconian Lineament. In the boreholes, SE2 can be identified as a bundle of faults near 3600 m. The calculated depth of the most prominent reflector SE1 in the Hauptbohrung is between 6600 and 7100 m. It represents, probably, a deep-reaching reverse fault zone which produces an offset of the reflections of the midcrustal "Erbendorf body" (B1 - B2/G4 - G1).

**Introduction**

During the pre-site studies in 1985, the KTB target area in the Oberpfalz had been investigated by a net of seven 2-D seismic reflection lines (DEKORP Research Group 1988). The results of the geophysical investigation combined with the knowledge of the surface geology as well as petrological and structural studies supported the relatively simple model of underthrusting of Saxothuringian units under Moldanubian units and of supracrustal nappe units (Münchberg, Zone Erbendorf-Vohenstrauss - ZEV) overlying the suture zone. Midcrustal reflections in connection with a high velocity zone ("Erbendorf Body") were interpreted as wedge-type structures generated by compressional tectonics during the Variscan collision.

The results of reflection seismics in connection with other geophysical data (P-wave velocities, VSP, electrical resistivity) and especially results from

---

\*) Niedersächsisches Landesamt für Bodenforschung, Stilleweg 2,  
D-3000 Hannover 51

the KTB Vorbohrung (KTB-VB) which had reached in 1989 a depth of 4000 m were used to establish a more detailed prediction for the Hauptbohrung (KTB-HB). As shown in Fig.1 it was expected at that time to meet the lower boundary of the ZEV at a depth of approximately 6 km and the "Erbendorf body" (EB) at 10.5 km. Metamorphic Saxothuringian and/or Moldanubian units were assumed to build the interval between these boundaries. Reflections between 7.5 and 8 km were interpreted as imbricated parts of the Erbendorf body. The interpretation of the Erbendorf body which is, possibly, subdivided into a highly reflective zone and a high-velocity zone (HVZ) and of the neighbouring highly conductive interval (graphite? saline fluids?) remained unsolved. With

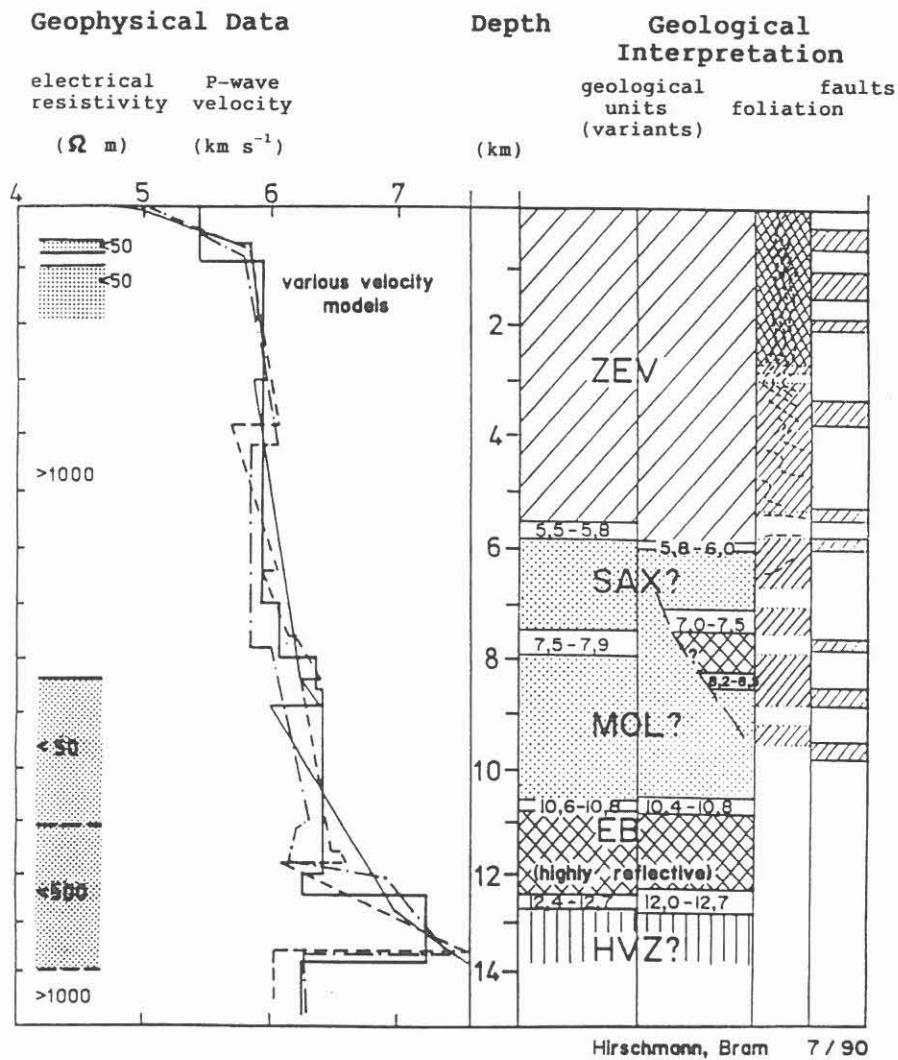


Fig.1 Prediction for the KTB main borehole (HB) regarding the results of the KTB pilot hole (VB), 1990

increasing depth, a gradual transition from steeply to gently inclined foliation seemed to be probable though the existence of fold structures down to at least the lower boundary of the ZEV had to be taken into consideration.

### Major 3-D reflectors

The 3-D seismic survey carried out in 1989 should provide a more precise structural resolution and the correct spatial arrangement of reflectors in the surroundings of the KTB drill site as well as an improved prediction for the KTB Hauptbohrung. The processing and interpretation of the abundant seismic data has not been finished. So far, only major reflectors were mapped and migrated. In the following, the position and nature of these reflectors with respect to the prediction of structures and/or geological units in the deeper parts of the main borehole will be discussed by comparison and correlation with the surface geology and the drilled section.

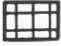



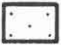

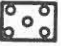
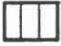

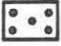
Figs.2 - 6 illustrate the position of selected Inline and Crossline sections with respect to the surface geology. These (unmigrated) sections give first information on the structural or stratigraphic interpretation of some of the reflectors. The Permocarboniferous, Triassic and Cretaceous sediments W of the Franconian Lineament are characterized by horizontal or gently dipping reflectors (0.5 - 1.3 s TWT, Crossline 230: MF1 - 4, Inlines: reflectors in the upper left). Time-slices show the distribution of sediments clearly by their characteristic reflectivity pattern (e.g. time-slice 1240 ms, near the SW-edge - Fig.7). At the surface, the Permocarboniferous and Mesozoic sediments are separated from the basement rocks of the ZEV and the Saxothuringicum by the Franconian Lineament. The Inline sections show that SE1, SE2 and some parallel elements are steeply NE-dipping structures belonging to this lineament. Since the SE1 strikes NW-SE it appears in Crossline 365 (Fig.6) as a flat structure. The different orientation of SE4 which dips NNE becomes evident by comparing Inlines (Figs.3 and 4), Crosslines (Fig.6) and time-slices (Fig.7). A group of steeply SE-dipping reflectors (ES1, ES2) is clearly visible in the area W of the Franconian Lineament (Crossline 230 - Fig.5). These reflectors have not been migrated so far.

SE12 is a gently NE-dipping element without clear connection to the surface geology. The nearly horizontal mid-crustal Erbendorf reflectors B1 and B2 were mapped in the central parts of the 3-D area whereas the reflectors G4 - G1 are restricted to the NE-part of the area.

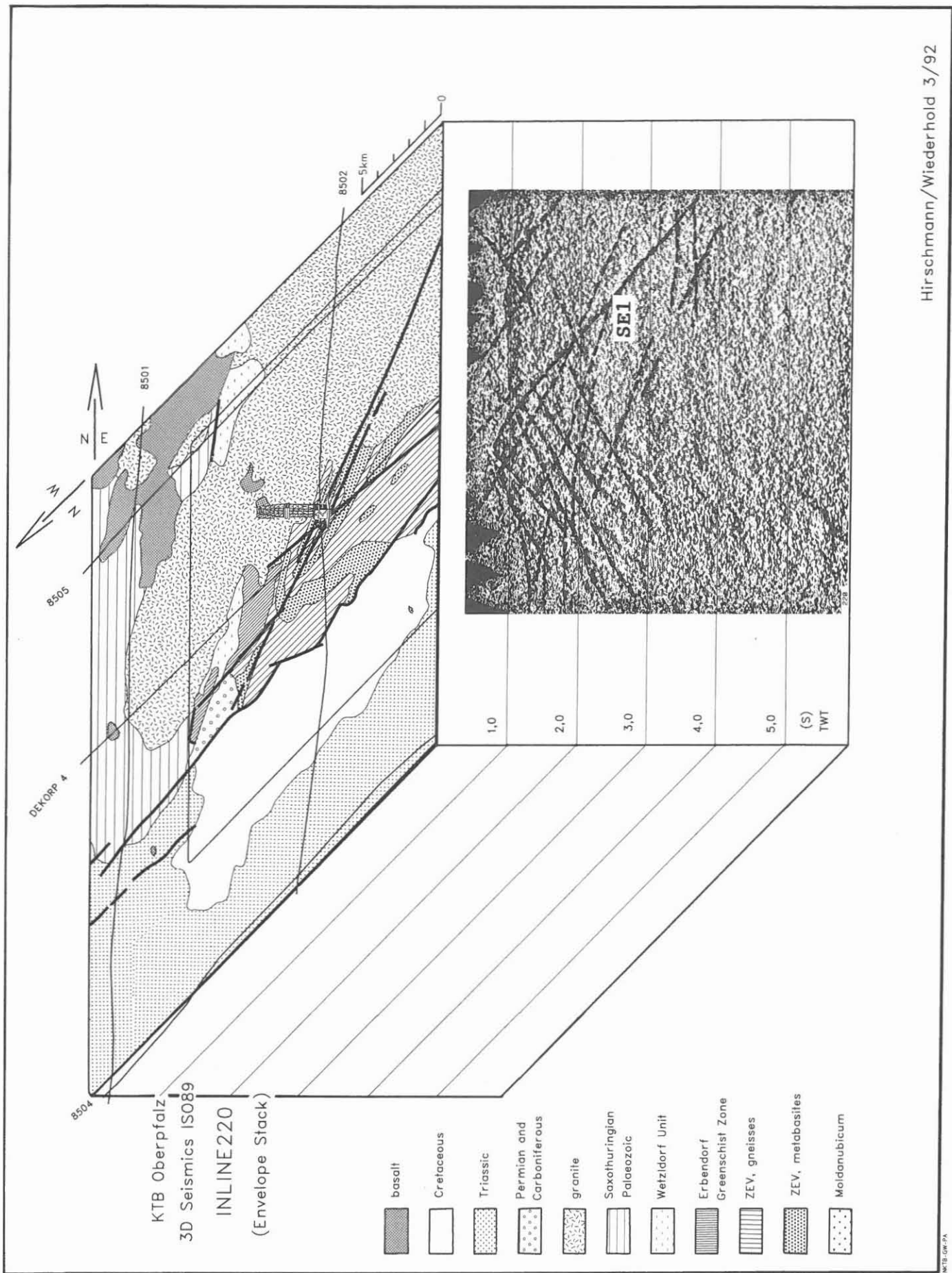
Figs.8 - 11 show depth contour maps of the migrated reflectors SE1, SE2, SE12 and SE4 (WIEDERHOLD this volume) combined with the simplified map of the surface geology. The intersection with the KTB drill site gives the depth (km below surface) of the reflections in the borehole. The resulting depth values according to WIEDERHOLD (this volume), HLUCHY et al. (this volume) are listed below:

	depth	dip	azimuth of dip
SE2	3700-4000 ±200 m	40-45°	50°
SE12	4700-4900 ±190 m	20°	60°
SE3	5500-5800 ±110 m	50°	60°
SE1	6500-7100 ±140 m	55°	50°
B1	10600-10700 ±200 m	-	-
B2	11400-11600 ±200 m	-	-

Explanation to Fig.7 - 11:

	basalt (Tertiary)		Saxothuringian Palaeozoic
	Cretaceous		Wetzldorf unit
	Triassic		Erbendorf Greenschist Zone
	Permian and Carboniferous		Zone of Erbendorf- Vohenstraus
	granite		Moldanubicum





Hirschmann/Wiederhold 3/92

Fig.2

KTB Oberpfalz  
 3D Seismics IS089  
 INLINE 357  
 (Envelope Stack)

-  basalt
-  Cretaceous
-  Triassic
-  Permian and Carboniferous
-  granite
-  Saxothuringian Palaeozoic
-  Wetzldorf Unit
-  Erbendorf Greenschist Zone
-  ZEV, gneisses
-  ZEV, metabasites
-  Moldanubicum

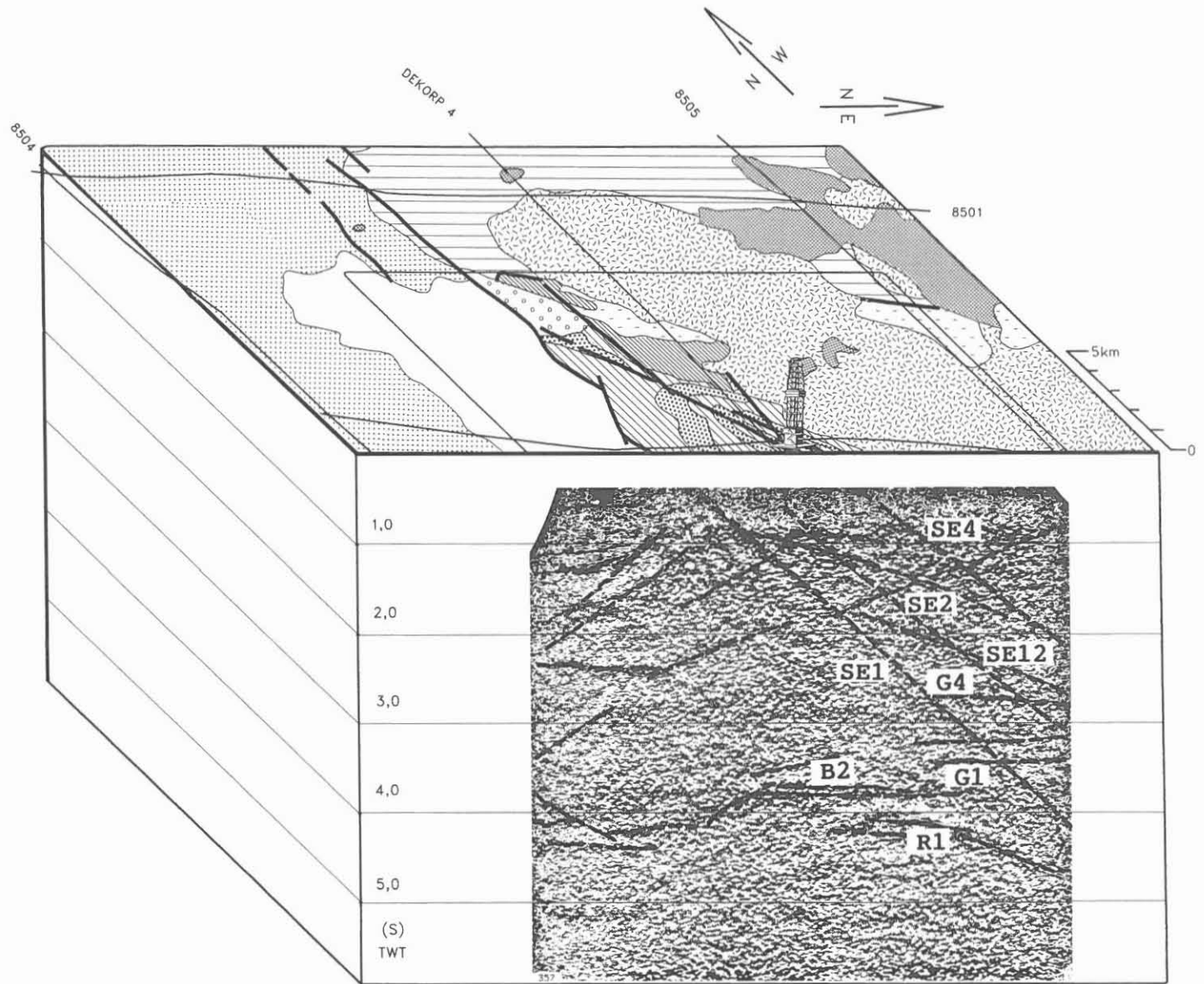


Fig. 3

KTB Oberpfalz  
 3D Seismics IS089  
 INLINE 400  
 (Envelope Stack)

-  basalt
-  Cretaceous
-  Triassic
-  Permian and Carboniferous
-  granite
-  Saxothuringian Palaeozoic
-  Wetzlendorf Unit
-  Erbendorf Greenschist Zone
-  ZEV, gneisses
-  ZEV, metabasites
-  Moldanubicum

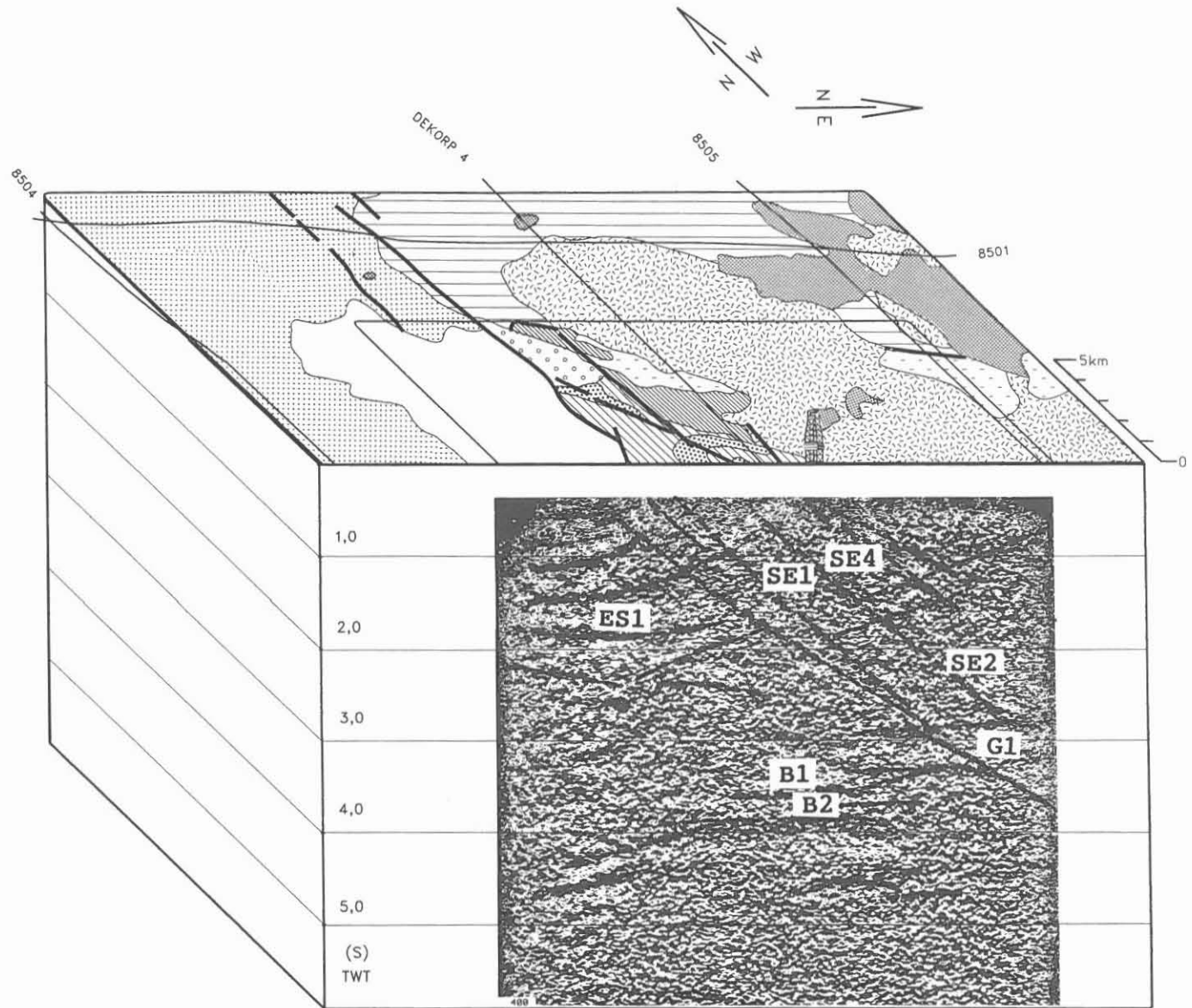


Fig. 4

Hirschmann/Wiederhold 3/92

KTB Oberpfalz  
3D Seismics IS089  
CROSSLINE 230  
(Envelope Stack)

-  basalt
-  Cretaceous
-  Triassic
-  Permian and Carboniferous
-  granite
-  Saxothuringian Palaeozoic
-  Wetzeldorf Unit
-  Erbendorf Greenschist Zone
-  ZEV, gneisses
-  ZEV, metabasites
-  Moldanubicum

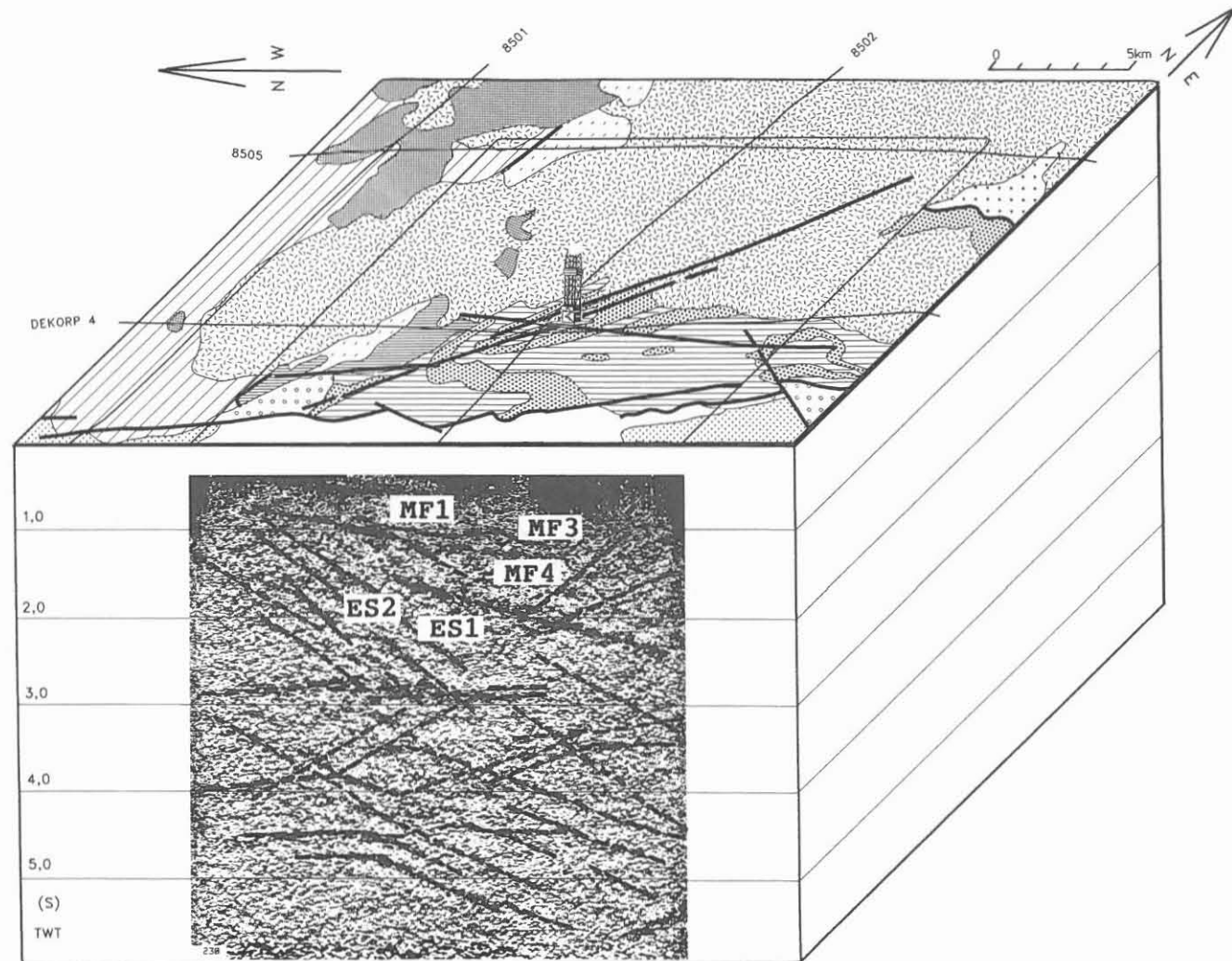


Fig. 5

KTB-OW-PA

Hirschmann/Wiederhold 3/92

KTB Oberpfalz  
3D Seismics IS089  
CROSSLINE 365  
(Envelope Stack)

-  basalt
-  Cretaceous
-  Triassic
-  Permian and Carboniferous
-  granite
-  Saxothuringian Palaeozoic
-  Wetzeldorf Unit
-  Erbdorf Greenschist Zone
-  ZEV, gneisses
-  ZEV, metabasites
-  Moldanubicum

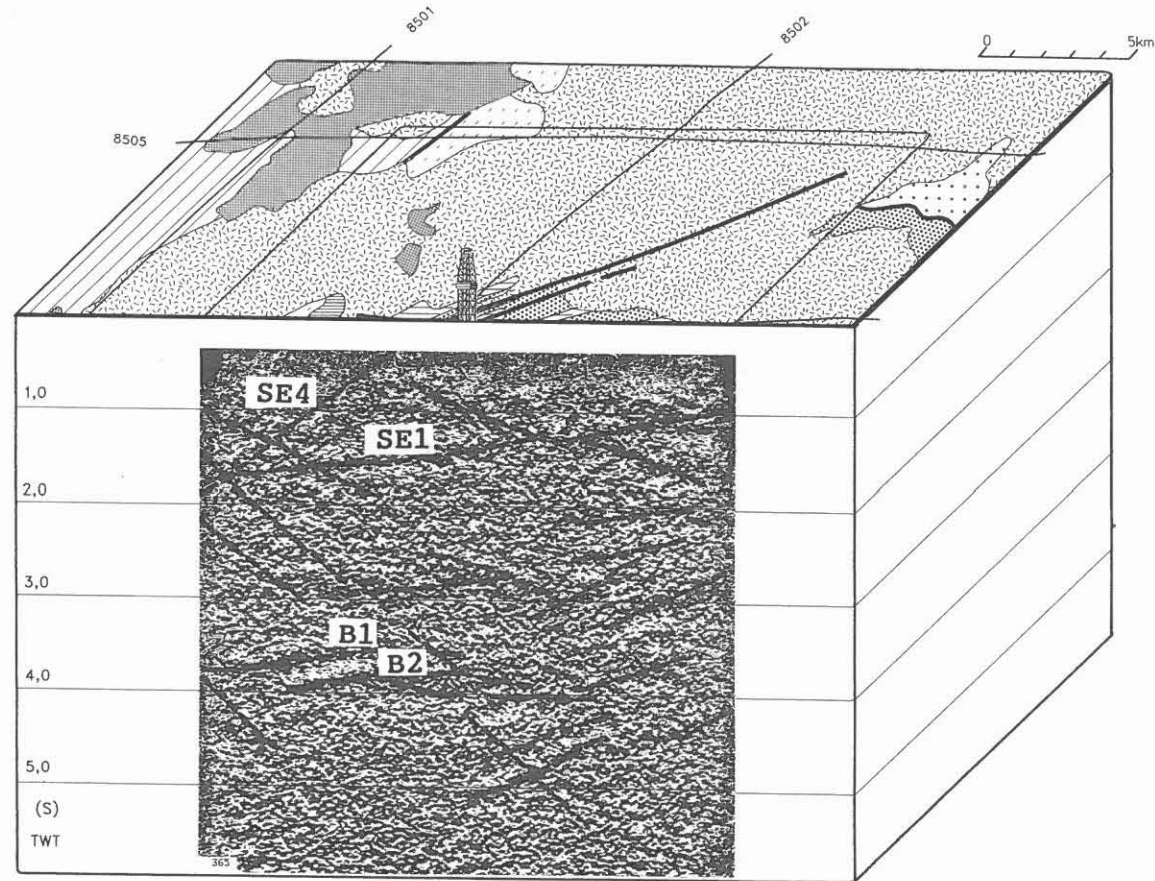


Fig. 6

M7B-GW-PA

Hirschmann/Wiederhold 3/92



Fig.7 Simplified geological map (explanation next page) and time-slice 1240 ms. Linear structures in the area of crystalline rocks, broad reflections in the area of sedimentary cover

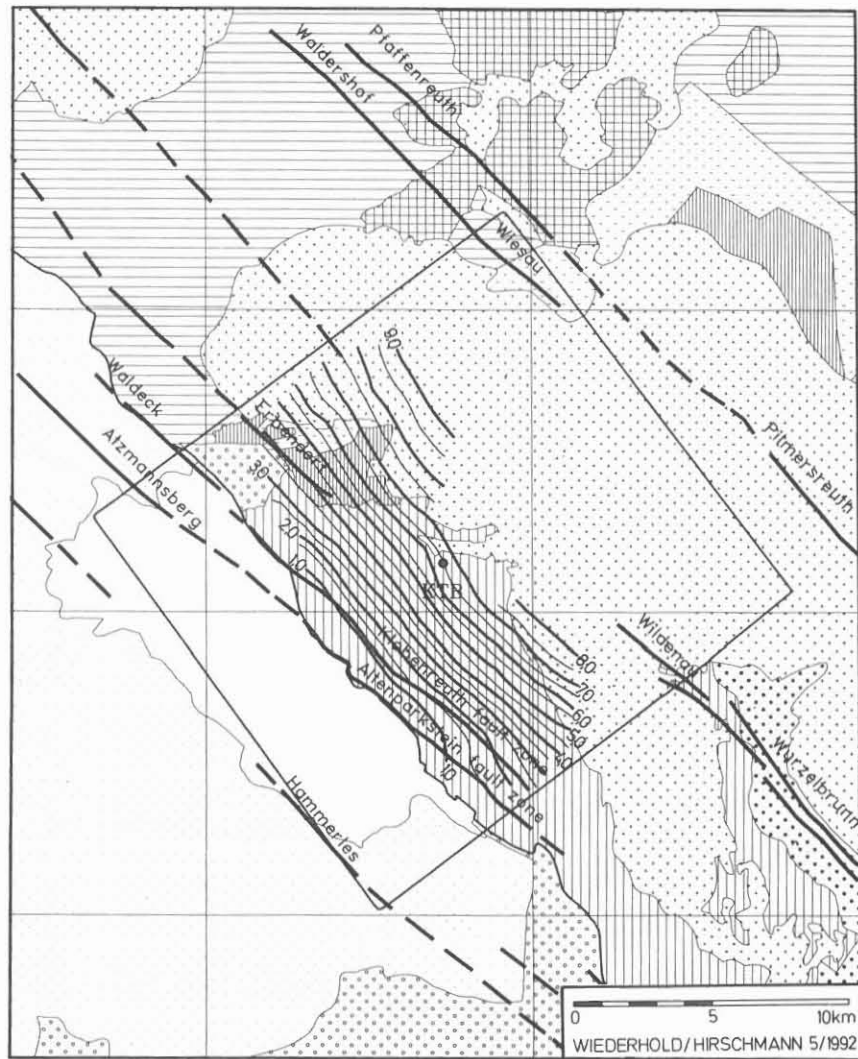


Fig.8 Depth contour map of SE1 related to the surface geology and NW-SE fault zones (depth in km below surface)

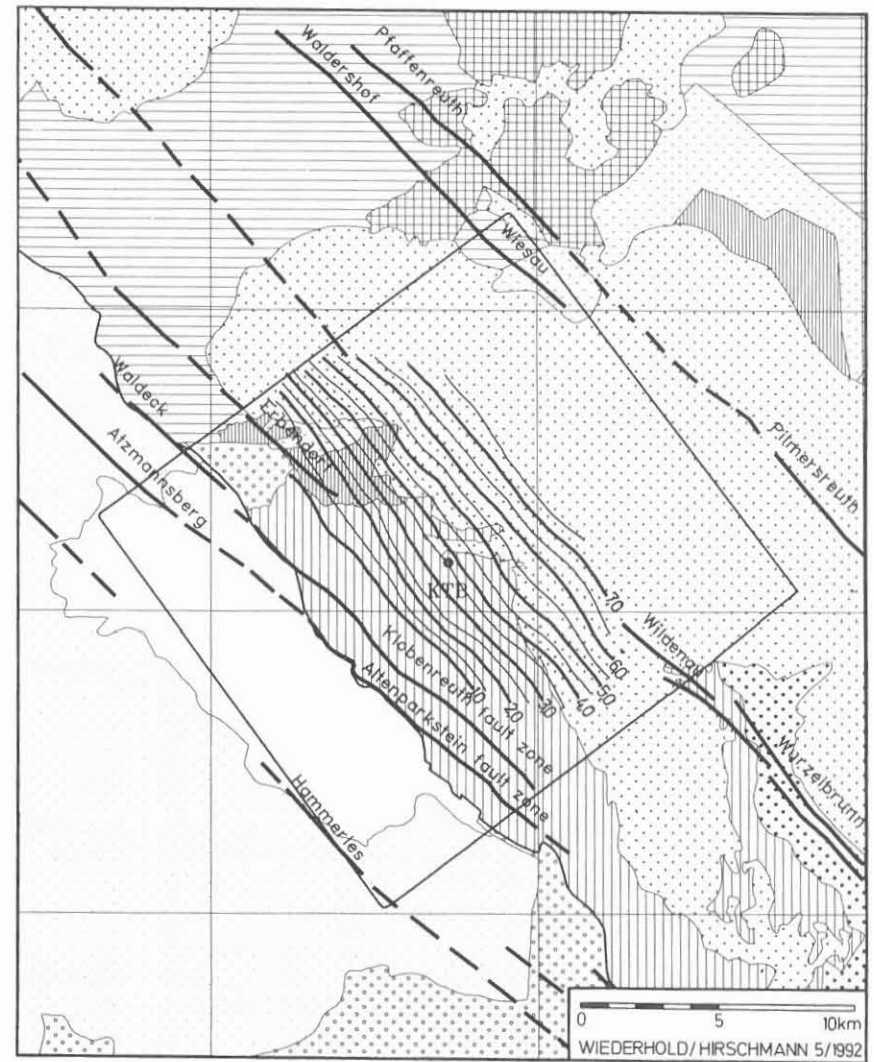


Fig.9 Depth contour map of SE2 related to the surface geology and NW-SE fault zones (depth in km below surface)

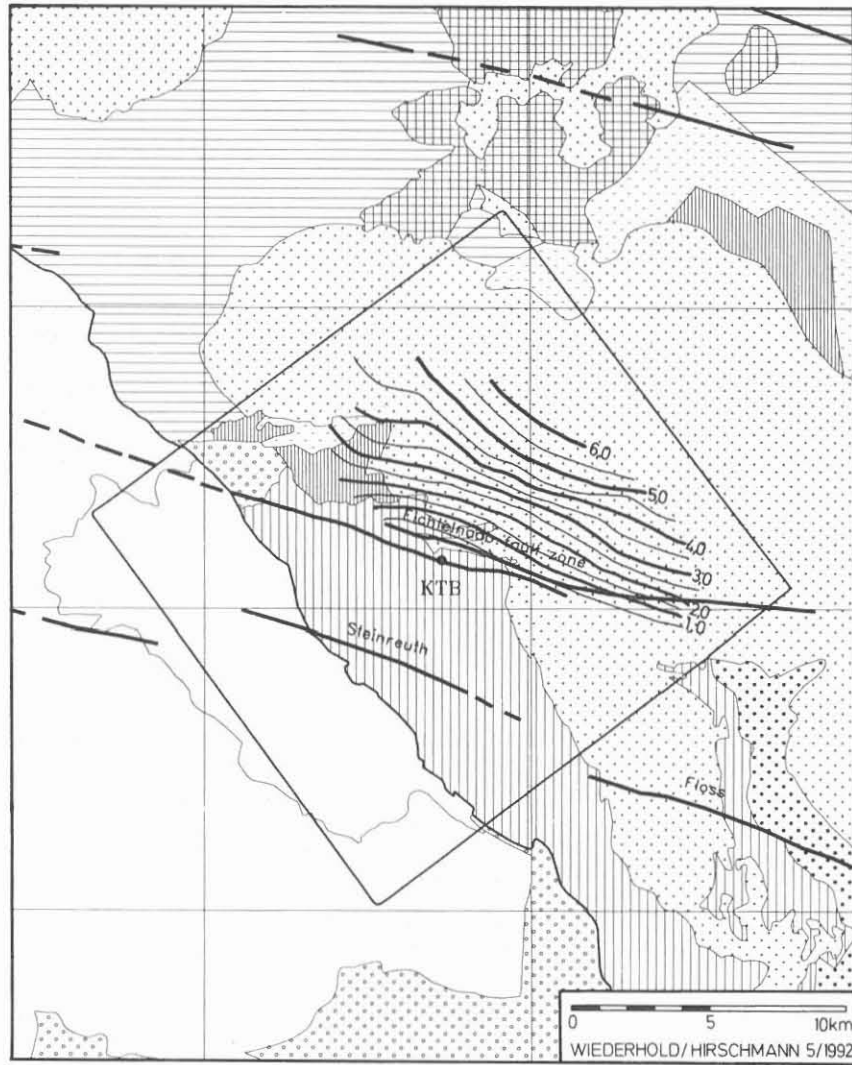


Fig.10 Depth contour map of SE4 related to the surface geology and WNW-ESE fault zones (depth in km below surface)

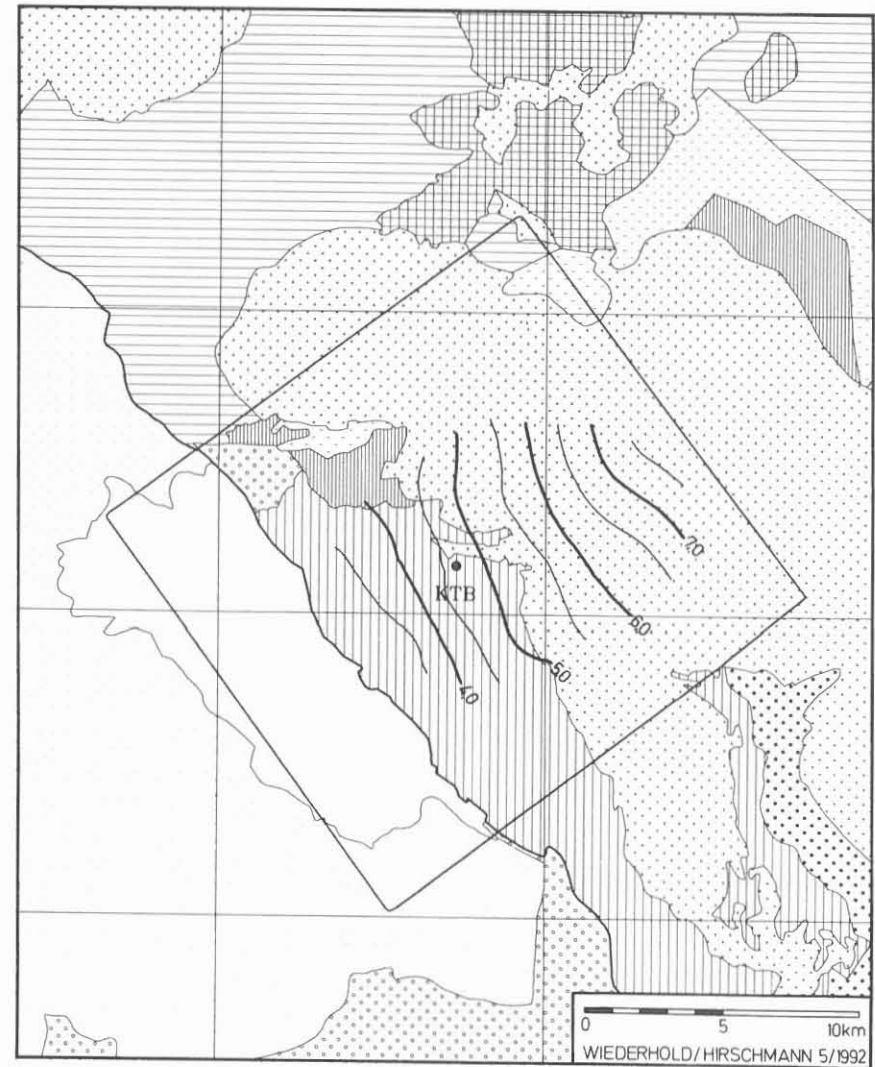


Fig.11 Depth contour map of SE12 related to the surface geology (depth in km below surface)



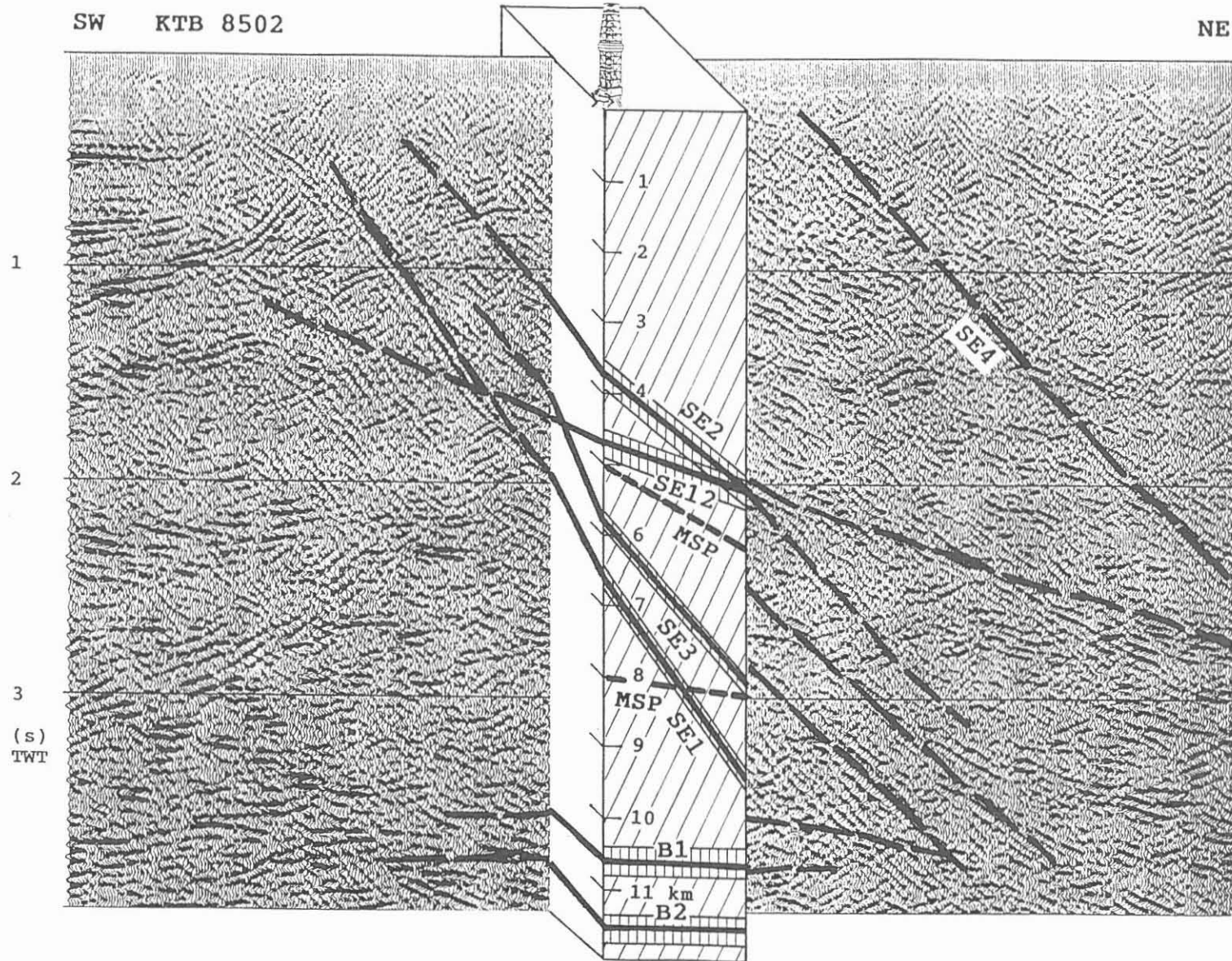


Fig.12 3-D and MSP reflectors at the drilling site (central column) and correlation with the migrated 2-D section KTB 8502

Fig.12 shows the position and orientation of the 3-D reflectors at the drill site (central column). Two MSP-reflections (JANIK & HARJES this volume) are marked additionally. The correlation with reflections in the migrated section KTB 8502 which runs about 500 m NW of the drill site is rather good. In general, the mapped and migrated reflectors are planar structures. They are of great lateral extent and the inclined reflectors reach at least to the middle crust.

#### **Correlation with the drilled section**

One of the most important questions is how the reflectors may be recognized and explained in the drilled section. Fig.13 shows a simplified geological section of the KTB Vorbohrung (VB) and Hauptbohrung (HB). Both profiles are very similar and they can be characterized by the alternation of metabasic units (b1 - b5) and paragneisses of the ZEV, by large-scale folding and numerous faults and cataclastic zones. Some of the major faults can be correlated with structures of the surface fault pattern (HIRSCHMANN 1992a and b).

Principal possibilities to explain the reflectors are seen as follows:

- **Lithological boundaries:** In contrast to the metabasites below 3.5 km (b5) which contain only very small gneissic intercalations the upper parts of the drilled section are built up of alternating paragneisses and metabasic complexes (b1 - b4). However, due to intense folding and faulting the structural pattern is very complex so that in general lithological boundaries are unlikely to cause regionally extended reflectors.

- **Cataclastic faults and fault systems:** There are abundant faults of variable geometry and character distributed over the total depth range of more than 6700 m. Major fault zones may be recognized by concentrations of narrow-spaced faults in the drilled section. Apparently, they represent structures of considerable regional extension. Some of them can be correlated with fault zones at the surface (e.g. Nottersdorf Fault Zone). Such fault zones offer the best prerequisites to produce seismic reflections. Enhanced reflectivity may be expected in cases when lithological changes are connected with faults. In many cases, fault zones, cataclastic zones and zones

with open fissures are filled with fluids and thus may display specific seismic properties.

In the following, the correlation of reflectors and faults in the drilled section will be discussed. Fig.14 shows the simplified lithological and structural section of the Hauptbohrung between 2500 and 6000 m. SE2, SE12 and SE3 are marked in their calculated positions (left). These reflectors are dipping between  $20^{\circ}$  and  $50^{\circ}$  to the NE. Therefore, only faults with a dip (up to  $70^{\circ}$ ) in this direction (azimuth  $30-80^{\circ}$ ) are taken from the total of all measured faults (plot in the upper right, hatched obliquely) for the correlation with the reflectors. In the central column, these faults are plotted against the depth and compared with the depth positions and dip ranges of the reflectors (hatched vertically). Probably, the SE2 is caused by a group of faults between 3530 and 3580 m. In the pilot hole, the correlation of SE2 can be shown in more detail (Fig.15). As is demonstrated by the depth contour map (lower part, right) the SE2 can be expected in a similar depth interval as in the main borehole. Most of the measured faults in the depth interval 3500-4000 m dip to the NE (upper part, right - hatched obliquely). Faults dipping similar as SE2 ( $35 - 45^{\circ}$ ) are concentrated near the gneiss-amphibolite

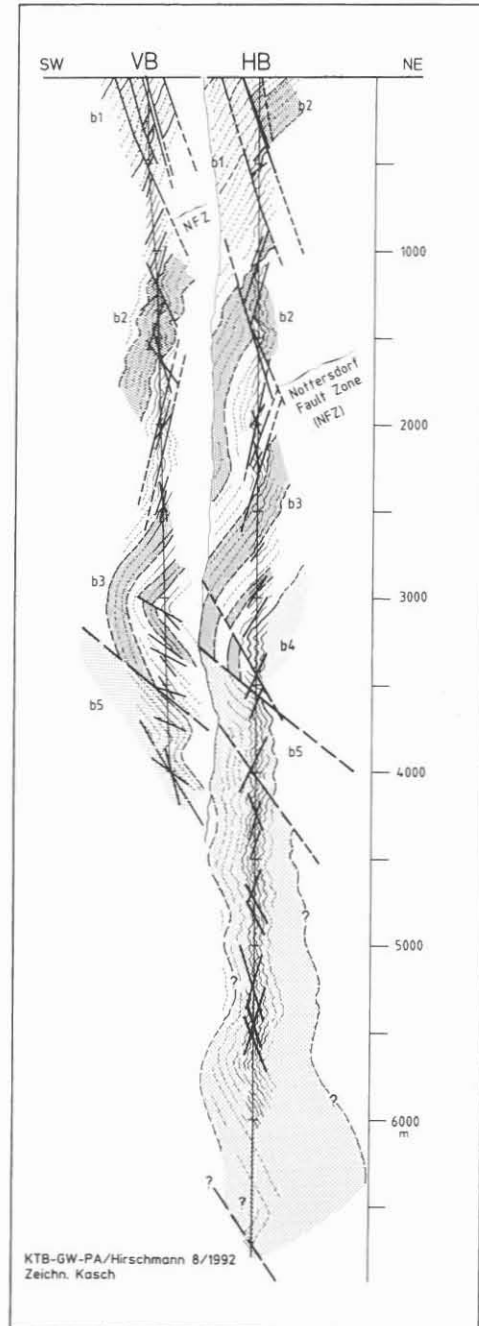


Fig.13 Simplified geological section of KTB-VB and KTB-HB. White: paragneisses, shaded: metabasites (b1 - b5)

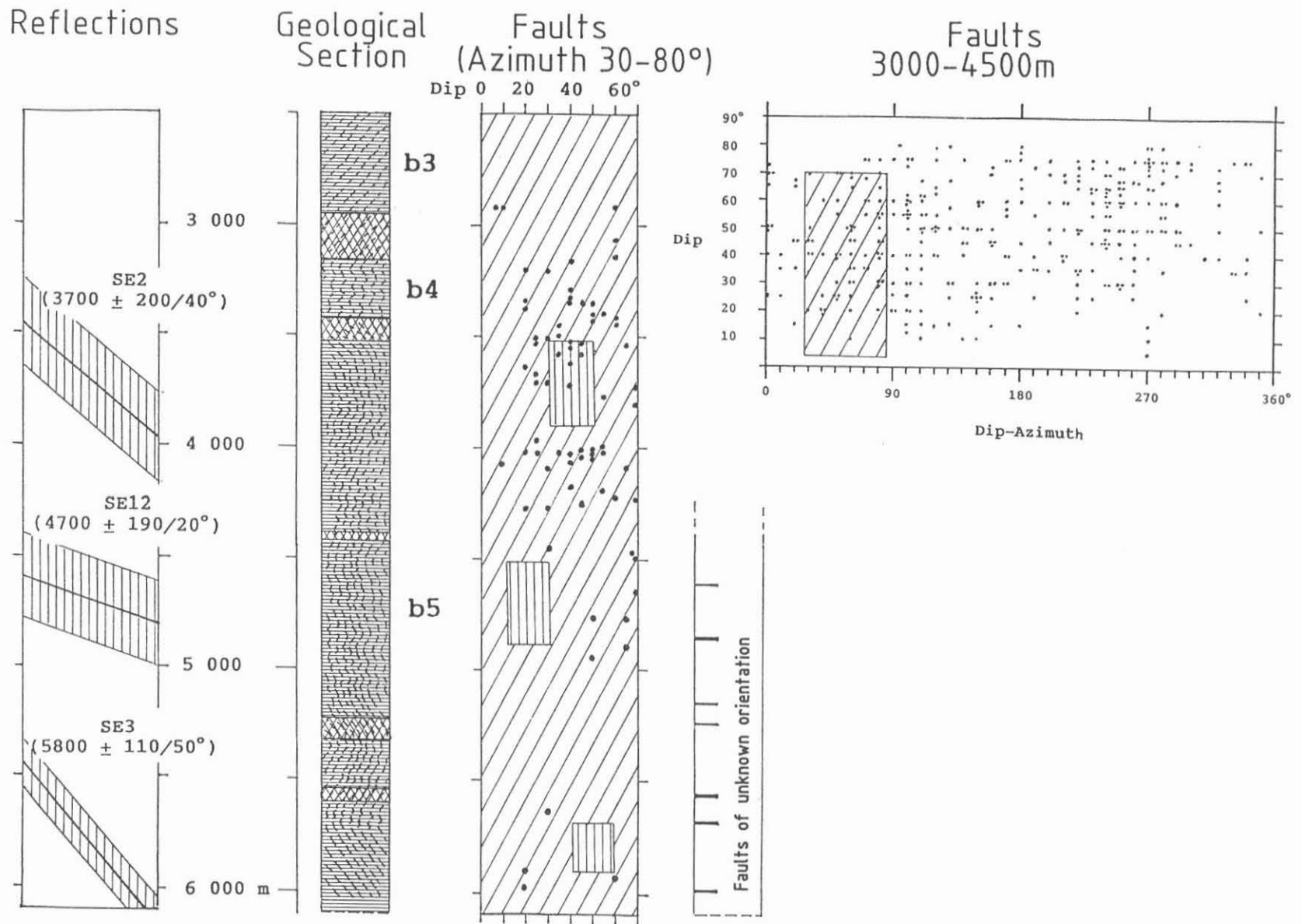


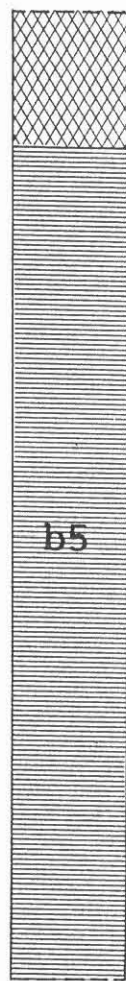
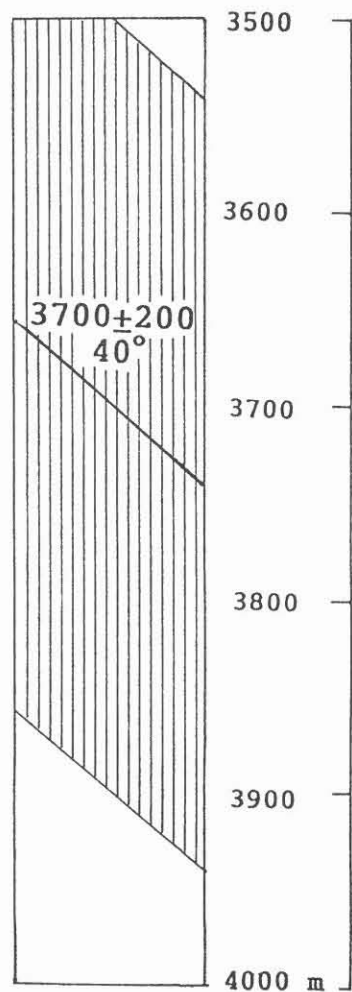
Fig.14 KTB Hauptbohrung (HB): correlation of seismic reflectors (SE2, SE12, SE3) with faults (according to Formation Microimager interpretation)

Reflection  
SE 2

Geological  
Section

Faults  
(Azimuth 30-80°)

Faults  
3500 - 4000m



Dip 0 20 40 60°

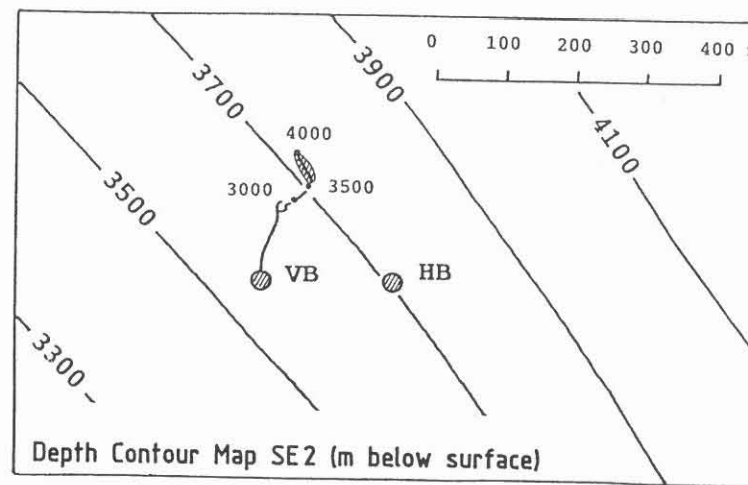
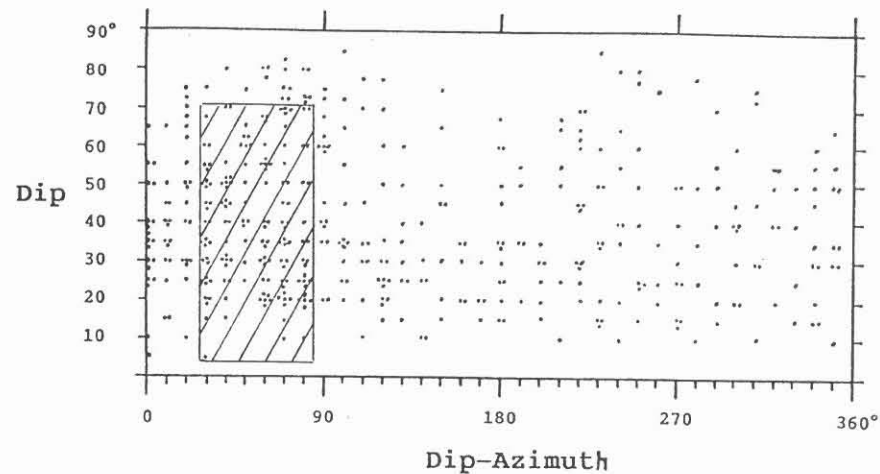
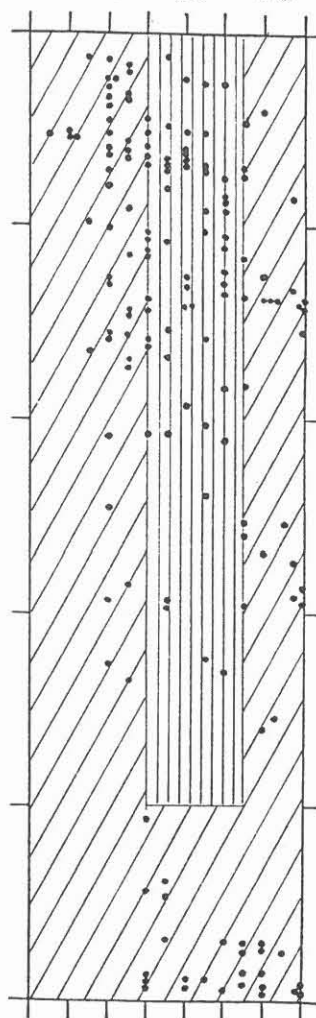


Fig.15 KTB Vorbohrung (VB): correlation of SE2 with faults  
(according to Formation Microscanner Interpretation)

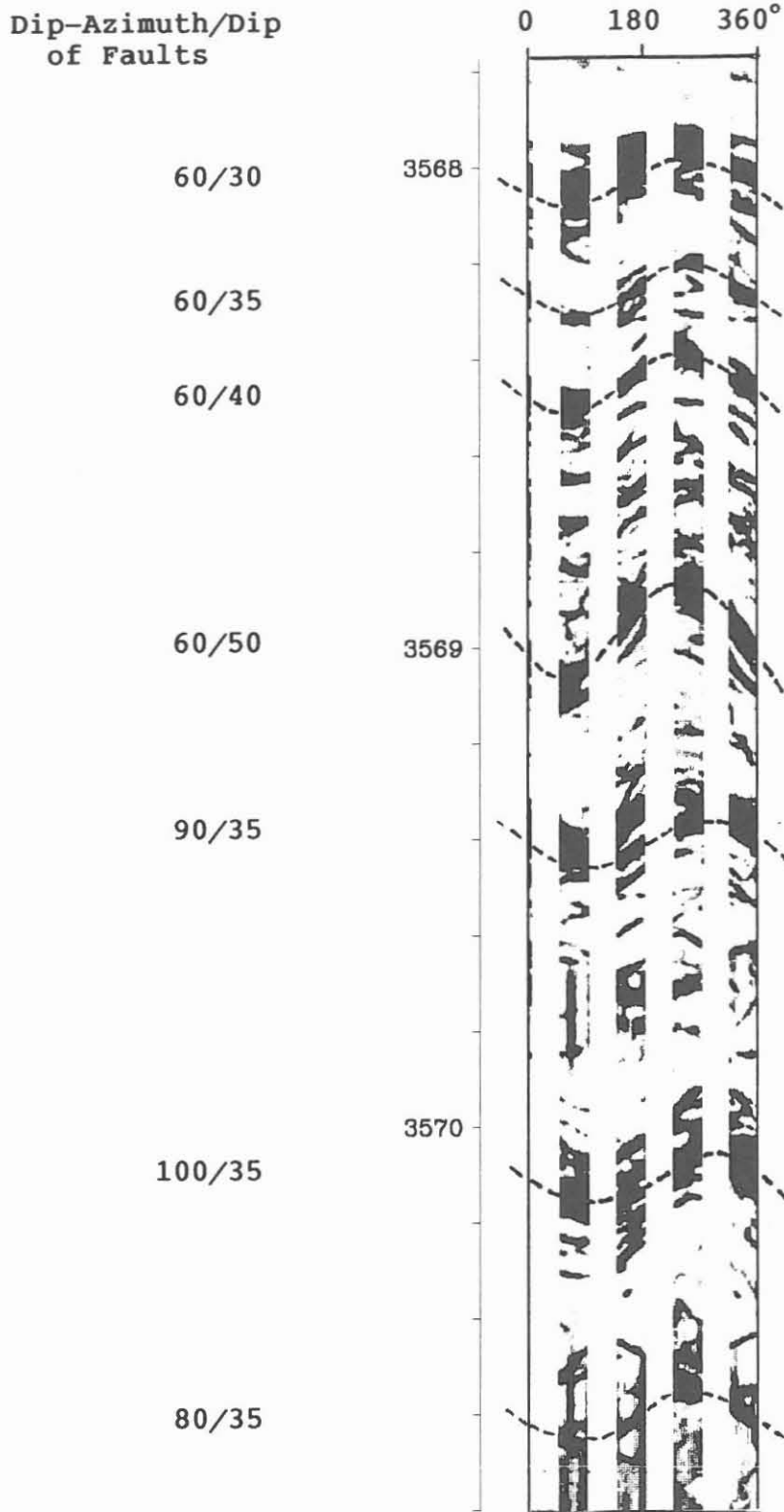


Fig.16 Formation Microscanner (FMS) Borehole Imaging (Schlumberger). KTB-VB, fault zone 3568-3570 m

boundary (upper boundary of b5) between 3550 and 3580 m. The central part of this fault zone can be well seen in the Formation Microscanner imaging (FMS) between 3568 and 3570 m (Fig.16).

The positions of SE12 and SE3 do not coincide with faults of known orientation. However, in the main borehole especially the depth interval below 5000 m is characterized by large borehole breakouts. Therefore, the accurate orientation of several fault zones cannot be determined by log interpretation. It is difficult to judge whether these fault zones correspond to SE12 and SE3 or not.

**- Structural properties, e.g. changes in anisotropy or in attitude of foliation:** Changes in anisotropy are, in general, identical with changes of lithology (metabasites/gneisses). Therefore it is probable that they do not produce broad reflections. Changes in attitude of foliation are due to fold structures. In general, they may be responsible only for minor or local reflectors (e.g. flattening of foliation near 3000 m?). However, it seems possible that the SE3 reflection is caused by the more or less uniform dip of foliation to the NE or E below 5680 m.

## Results

At present, the connections between the reflectors, the drilled section and the surface geology can be summarized as follows (Fig.17):

Flat reflectors between 0.5 s and 1.3 s TWT in the area W of the Franconian Lineament correspond to the Permocarboniferous, Triassic and Cretaceous sediments covering the basement of the South German Platform.

Most remarkable are NE-dipping reflectors (SE2, SE3, SE1) representing en-echelon fault zones of the Franconian Lineament. Near the drill site, they separate the crystalline rocks of the Bohemian Massif from the South German Platform.

SE2 dips  $40-45^\circ$  to the NE (Fig.9). Probably, at the surface it can be correlated with the Waldeck-Klobenreuth Fault Zone. In the KTB Vorbohrung as

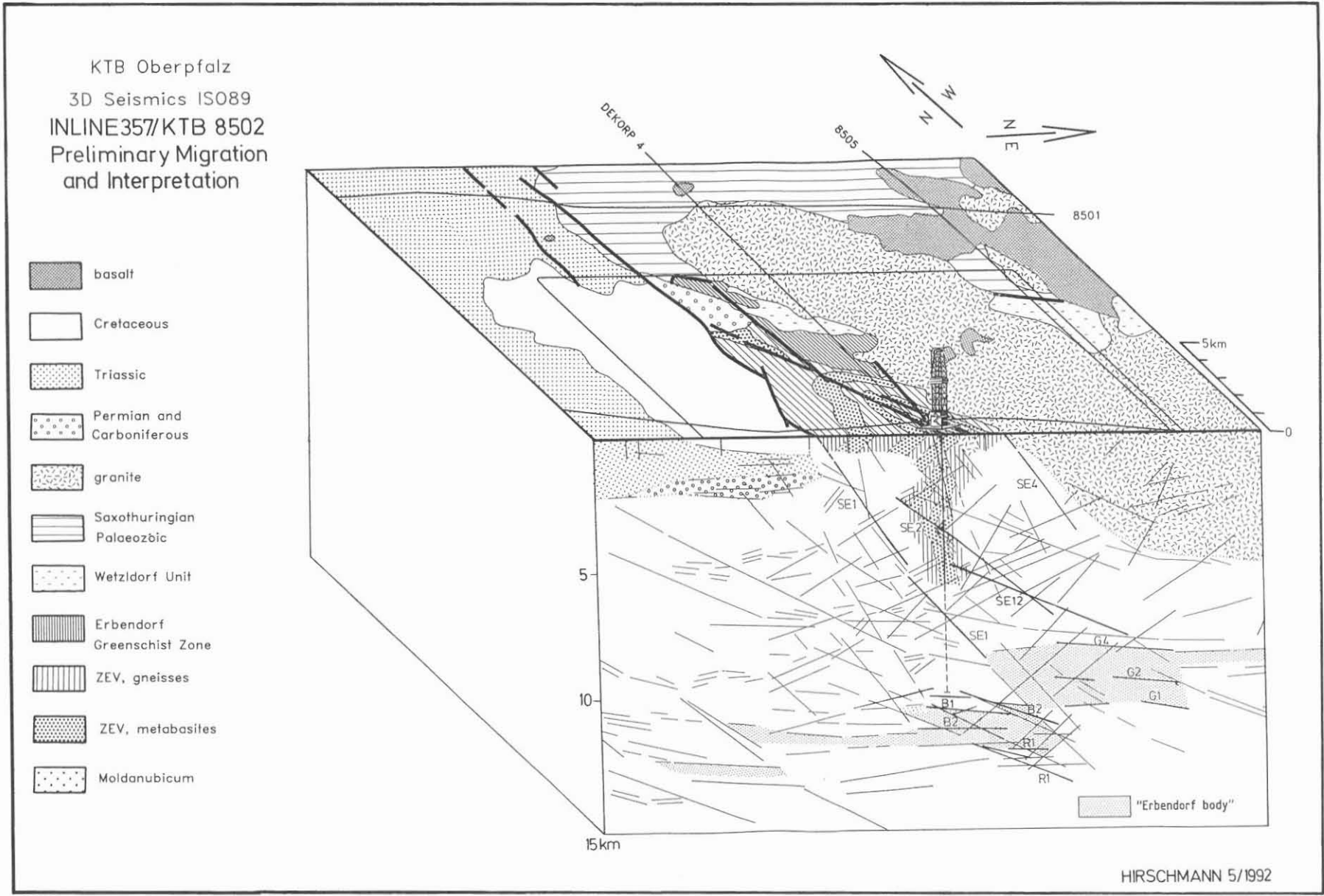


Fig.17 Connections between the surface geology, the geological section of the KTB boreholes and seismic reflections in a SW-NE section across the drilling site



well as in the KTB Hauptbohrung it can be identified as a bundle of faults near 3600 m, i.e. in the vicinity of the upper boundary of metabasite b5.

SE3 (between SE2 and SE1) dips  $50^{\circ}$  to the NE and, apparently, represents a structure nearly parallel to SE1. The expected depth in the main borehole is 5500 and 5800 m. However, the correlation with structural elements in the drilled section is not sufficiently clear (fault zones of undetermined orientation? NE- to E-dipping foliation?).

SE1 is the most important structure among the steeply inclined reflectors. It dips about  $55^{\circ}$  to the NE (Fig.8). At the surface, it can be correlated with the Altenparkstein Fault Zone which represents the most important fault zone of the Franconian Lineament in the vicinity of the drill site. In the Hauptbohrung the reflector, probably, will be represented by a bundle of parallel (cataclastic?) faults in the depth interval between the present drilling depth of 6700 and 7100 m.

Contrary to these steeply inclined reflectors the SE12 (Fig.11) is a structure dipping  $20^{\circ}$  to the NE. The correlation with structures at the surface is unknown. Until now, attempts to correlate this reflector with structures in the drilled section were not successful. However, there are reflectors parallel with SE12 which, until now, are not mapped in detail, e.g. a reflector intersecting the borehole near 3000 m. Probably these reflectors can be correlated with faults or shear planes of a corresponding orientation which were observed in the pilot hole as well as in the main borehole.

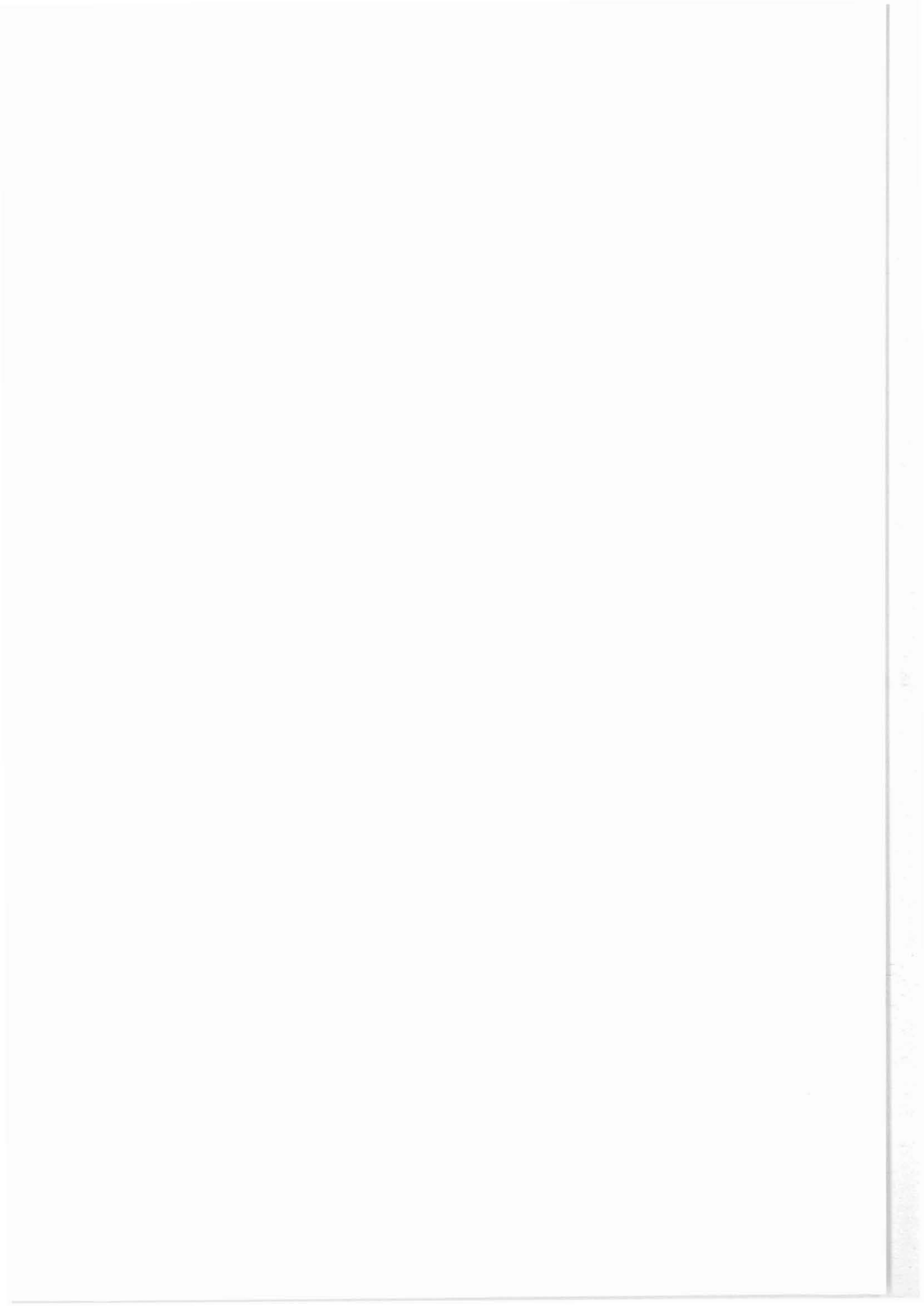
Further reflectors of different strike and dip are known both from Inline and Crossline sections. With a few exceptions they have not been mapped and migrated until now. SE4 (Fig.10) dips about  $50^{\circ}$  to the NNE. It is connected to the Fichtelnaab Fault Zone immediately N of the drill site with an estimated vertical offset of geological units of several kilometers. The interpretation of the steeply SE-dipping reflectors (ES1, ES2 - Fig. 5) is still unclear. They may represent either structures of the tectonic boundary between ZEV/Moldanubicum and Saxothuringicum or structures of the Cenozoic Ohre Rift. Similarly the role of gently SW-dipping reflections (Figs.2 - 4) is still unknown.

Apparently, the Erbendorf reflectors B1 and B2 in the central part of the 3-D area represent equivalents of the reflectors G4 - G1 in the NE-part. The depth offset (2.5 - 3 km) is, probably, produced by the tectonic structure of SE1. Therefore, the latter can be interpreted as a reverse fault zone which produces an important offset of geological units of the upper crust as well as of the mid-crustal "Erbendorf Body". Therefore, it seems possible that below the SE1 the borehole will meet further parts of the ZEV. On the other hand, the Franconian Lineament may be an old crustal boundary separating different basement units. It is still unclear whether the "Erbendorf Body" may be explained by lithological contrasts or structural properties. Nevertheless, these reflections in connection with the seismic high velocity zone and the accompanying zone of high conductivity represent an important object for the further research.

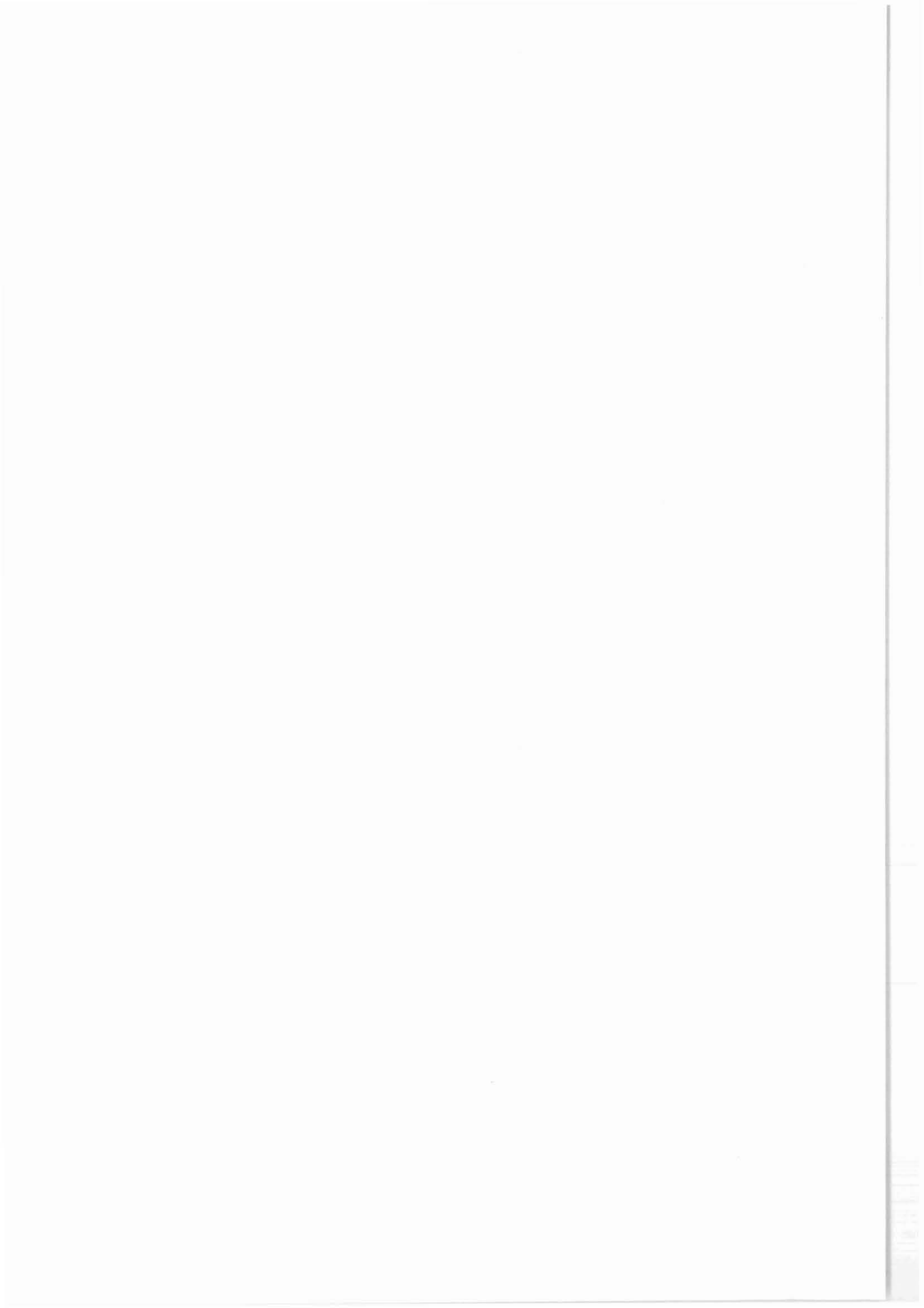
## References

- DEKORP Research Group (1988): Results of the DEKORP 4/KTB Oberpfalz deep seismic reflection investigations. - J.Geophys. 62: 69-101
- EMMERMANN,R., DIETRICH,H.G., LAUTERJUNG,J. & WÖHRL,TH. (eds.)(1990): KTB Pilot Hole, Results of Geoscientific Investigation in the KTB Field Laboratory, 0 - 4000,1 m. - KTB Report 90-8,
- HIRSCHMANN,G. (1992): Das Bruchstörungsmuster im KTB-Umfeld. - KTB Report 92-3: 85 - 124 (1992a)
- (1992): Vorläufige strukturelle Interpretation von KTB-Vor- und Hauptbohrung. - KTB Report 92-4: 3-6 (1992b)
- HLUCHY,P., KÖRBE,M. & THOMAS,R. (1992): Preliminary Results of the Interpretation of the 3D-Seismic Survey at the KTB Location. - KTB Report 92-5: DEKORP Report
- JANIK,M. & HARJES,H.P. (1992): Structural interpretation of the MSP experiment. - KTB Report 92-5: DEKORP Report

- LICH,S., DUYSER,J., GODIZART,G., KEYSSNER,S. & DE WALL,H. (1992): German Continental Deep Drilling Program (KTB) - Geological Survey of the Hauptbohrung 0 - 6000 m. - KTB Report 92-2: B1-42
- STETTNER,G., BARDUA,J. & SCHRÖDER,B. mit Beiträgen weiterer Autoren (1990): Geologische Karte des KTB-Umfeldes Oberpfalz 1:10 000. - Hannover
- WIEDERHOLD,H. (1992): Interpretation of Envelope-Stacked 3D-Seismic Data and its Migration - Another Approach. - KTB Report 92-5: DEKORP Report



## Annex



**K T B R E P O R T S** related to Borehole Measurements  
already published:

**KTB Report 87-2 (1987)**

Grundlagenforschung und Bohrlochgeophysik. Beiträge zur Tagung der Deutschen Geophysikalischen Gesellschaft in Clausthal-Zellerfeld (31.03.-04.04.1987). Hsg.: R. Hänel und R. Schopper

**KTB Report 87-3 (1987)**

Grundlagenforschung und Bohrlochgeophysik (Bericht 2). Arbeitsprogramm KTB-Bohrlochgeophysik sowie Bohrlochmeßprogramm KTB-Oberpfalz VB (01.09.1987). Hsg.: R. Hänel

**KTB Report 87-4 (1987)**

Grundlagenforschung und Bohrlochgeophysik (Bericht 3). Bohrlochmessungen in der KTB-Oberpfalz VB - Intervall 0-478,5 m -. Hsg.: J.K. Draxler und R. Hänel

**KTB Report 88-4 (1988)**

Grundlagenforschung und Bohrlochgeophysik (Bericht 4). Bohrlochmessungen in der KTB-Oberpfalz VB - Intervall 478,5-1529,4 m. Hsg.: J. K. Draxler und R. Hänel

**KTB Report 88-7 (1988)**

Grundlagenforschung und Bohrlochgeophysik (Bericht 5). Bohrlochmessungen in der KTB-Oberpfalz VB Intervall 1529,4-3009,7 m. Hsg.: J. Draxler und R. Hänel

**KTB Report 88-11 (1988)**

Grundlagenforschung und Bohrlochgeophysik (Bericht 6). Forschung und Entwicklung - Berichte laufender und abgeschlossener Vorhaben. Hsg.: P. Kehrer und W. Kessels.

**KTB Report 89-1 (1989)**

Grundlagenforschung und Bohrlochgeophysik (Bericht 7). Auswertung von Bohrlochmessungen der KTB-Oberpfalz VB. Hsg.: R. Hänel

**KTB Report 90-1 (1990)**

Grundlagenforschung und Bohrlochgeophysik (Bericht 8). Auswertung von Bohrlochmessungen der KTB-Oberpfalz VB. Hsg.: J.K. Draxler

**KTB Report 90-5 (1990)**

Grundlagenforschung und Bohrlochgeophysik (Bericht 9). Hydraulische Untersuchungen in der Bohrung KTB-Oberpfalz VB. Hsg.: W. Kessels

**KTB Report 90-6a (1990)**

Grundlagenforschung und Bohrlochgeophysik (Bericht 10). Langzeitmeß- und Testprogramm in der KTB-Oberpfalz VB. Hsg.: K. Bram, J.K. Draxler, W. Kessels und G. Zoth

**KTB Report 90-6b (1990)**

DEKORP REPORT. Integrated Seismics Oberpfalz 1989. Longterm Logging and Testing Programme of the KTB-Oberpfalz VB. Hsg.: H.-J. Dürbaum, Ch. Reichert, K. Bram

**KTB Report 91-2 (1991)**

Grundlagenforschung und Bohrlochgeophysik (Bericht 11). Bohrlochmessungen in der KTB-Oberpfalz HB - Intervall 0-1720,0 m Hsg.: K. Bram, J.K. Draxler, G. Zoth

**KTB Report 91-4 (1991)**

Grundlagenforschung und Bohrlochgeophysik (Bericht 12). Forschung und Entwicklung. EFA-LOG - Rekonstruktion kristalliner Lithologie anhand von bohrlochgeophysikalischen Messungen für die Bohrungen URACH 3 und KTB-Oberpfalz VB

**KTB Report 92-1 (1992)**

Grundlagenforschung und Bohrlochgeophysik (Bericht 13). Bohrlochmessungen in der KTB-Oberpfalz HB - Intervall 1720,0 - 4512,0 m -. Hsg.: K. Bram, J. Draxler



ISSN 0939-8732  
ISBN 3-928559-08-7